Table of Contents

Abstract

Lung disease and lung injury are responsible for 20% of deaths of the Irish population every year, and the country has the 2nd highest death rate in Europe for respiratory diseases. Conditions related to the respiratory system are the second largest long term illness by young adults. Lung cancer is the largest cause of cancer related death in Europe as a whole.

New and refined mechanisms of drug delivery for the prevention, cure or delayed progression of disease, represents a pathway for the delivery of novel style therapies and for the targeted delivery of different of more toxic drugs to the airways in order to increase efficiency of both the delivery mechanism and of the drug utilised. Here we looked at the use of a number of different mechanisms, which can be used as stand-alone devices/delivery agents and/or in conjunction with other devices and delivery agents to optimise targeted delivery to the lung, and to the specific areas required.

We examined the use of a direct delivery mechanism, particle bombardment, for the delivery of various molecules to human and murine cells lines, and to mouse primary cell isolates, MAECs, to examine the potential of the mechanism for adaption to a clinical mechanism for delivery. An aerosol delivery system was developed to utilise a current aerosol generator for the delivery of aerosol to mice *in vivo*. This was done with the aim of creating a more efficacious and ergonomic mechanism for the delivery of aerosols to mice in vivo and also to investigate the effects of aerosolistation on various drug compound molecules.

We also looked for BMP4 disregulation in a number of different animal models to help ascertain the role of the pathway in the progression of disease and damage in the lung. BMP4 has been shown to have a role in the induction of EMT in MAECS (E.Molloy) and to play a role in both lung cancer and allergic Rhinitis. Here we looked at its role in a number of different models. It was firstly examined in vitro in mouse cell lines and primary cell isolates and the effect of pathway stimulation and deregulation examined. The role of the pathway was then examined in both a murine Elastase model of emphysema, where it was determined to be inactive, and a murine OVA model of asthma where deregulation of the active pathway was evident. The pathway was also shown to be activated in a deregulated fashion in an Ozone/HDMA model of allergic asthma in Rhesus Macaques.

In vitro models of mouse, human and primate cells lines were used to examine the role of BMP4 in more detail. Mouse cell lines and primary isolates were used both in normal culture and in an air liquid interface (ALI), stimulated with BMP4 and

examined. An air liquid interface enables the culturing of cells in a system consistent with that of the in vivo environment, where the nutrition is provided through the basal surface of the cells and the dorsal surfaces of the cells are exposed to air. Murine model of OVA induced asthma in vivo was also stimulated with exogenous BMP4 and the effects monitored. Human primary cells and primate primary cell isolates were also grown in ALI and were treated with either BMP4 or EGTA and BMP4 in order to help determine more information about the cells involved in the pathway and the other pathways that are recruited by BMP activation.

Abbreviations

µg	Microgram
µl	Microlitre
µm	Micrometers
AEC	Airway Epithelial cell
ALI	Air Liquid Interface
API	Active Pharmaceutical Ingredient
ATCC	American Type Culture Collection
Av	Accumulated Volume
BALF	Broncho Alveolar Lavage Fluid
BEAS	Bronchial Epithelial Airway cell
BME	β-mercaptoethanol
BMP	Bone Morphogenetic Protein
BMPR	BMP Receptor
bp	base pair
bpm	Breaths per Minute
CC10	Clara Cell 10, also known as CCSP
CCSP	Clara Cell Secretary Protein
cDNA	complimentary DNA
COPD	Chronic Obstructive Pulmonary Disease
DAPI	4',6-diamadino-2-phenylindole
Depc	diethylenepyrocarbonate
DMEM	Dulbecco's modified Eagles Medium
DMEM:F12	DMEM and Ham sF12
DMSO	Dimethyl sulphoxide
DNA	Deoxyribonucleic acid
dNTP	Deoxynucleoside tri-phosphate
DSFM	Defined Serum Free Medium
dV	Change in Volume
E7.5	Embryonic Day 7.5
EBAO	Ethidium Bromide Acridine Orange
EEP	End Expiratory Pause
EF50	Tidal mid-expiratory flow

EGF	Epidermal Growth Factor
EGTA	Ethylene Glycol Tetra acetic Acid
EIP	End Inspiratory Pause
EMT	Epithelial-Mesenchymal transition
EtOH	Ethanol
f	Frequency
FACS	Fluorescent Activated Cell Sorting
FBS	Fetal Bovine Serum
FPF	Fine Particle Fraction
g	Gravity
GAPDH	Glyceraldehyde 3-phosphate dehydrogenase
GFP	Green Fluorescent Protein
HDMA	House Dust Mite Allergen
HLH	Helix-Loop-Helix
hr	Hour
HRP	Horseradish Peroxidase
Id	Inhibitor of Differentiation
IgE	Immunoglobulin E
IL	Interleukin
I-Smad	Inhibitory Smad
Kb	Kilobase
kDa	Kilo Daltons
L	Litre
LDH	Lactate Dehydrogenase
MAECs	Murine Airway Epithelial Cells
MAPK	mitogen activated protein kinase
MeOH	Methanol
$MgCl_2$	Magnesium Chloride
Min	Minute
Ml	millilitre
MMAD	Mean Mass Aerodynamic diameter
mRNA	messenger RNA
MTS	3-(4,5-dimethylthiazol-2-yl)-5-(3-carboxymethoxyphenyl)-2-(4-sulfophenyl)-2H-tetrazolium
Mv	Minute Volume

NaCl	Sodium Chloride
Neb	Nebulised
Ng	nanogram
Nm	nanometres
O.D.	Optical Density
O_3	Ozone
OVA	Ovalbumin
PAGE	Poly Acrylamide Gel Electrophoresis
PAH	Pulmonary Arterial Hypertension
PBS	phosphate buffered saline
PCNA	Proliferating Cell Nuclear Antigen
PCR	Polymerase Chain Reaction
PEF	Peak Expiratory Flow
PFA	Paraformaldehyde
PIF	Peak Inspiratory Flow
pSmad	Phosphorylated Smad
QPCR	Quantitative PCR
RNA	Ribonucleic acid
RNAi	RNA interference
R-Smad	Receptor Smad
Rt	Relaxation Time
rtPCR	reverse transcriptase PCR
SDS	Sodium Dodecyl Sulphate
SE	Standard Error
Sec	Second
siRNA	short interfering RNA
Smad	Mothers Against Decapentaplegic Homology
TBS	Tris Buffered Saline
Te	Expiratory Time
TGF	Transforming Growth Factor
Ti	Inspiratory Time
UV	Ultraviolet
VMD	Volume Median Diameter

Acknowledgments

"...it used to be so simple, once upon a time. Because the universe was full of ignorance all around and the scientist panned through it like a prospector crouched over a mountain stream, looking for the gold of knowledge among the gravel of unreason, the sand of uncertainty and the little whiskery eight-legged swimming things of superstition"- Terry Pratchett

1 Introduction

1.1 The Lungs

The human lungs are responsible for the gaseous exchange of O_2 into the vascular system, and the removal of CO_2 from it. They do this through a network of capillary lined epithelial cells responsible for respiration, which in the average adult human, covers some $70m^2$, and at an average overall thickness of just 1µm. In order to fit this much functional respiratory surface area into a space the size of a human chest cavity, with expansion limited by a ribcage in an area shared with the central cardiac system, the human lung has evolved a complex entwined vascular and respiratory system, divided into 5 lobes, 3 on the right and 2 on the left. The inhalation of air into the human respiratory system typically starts in the nasal cavity, especially in infants, though inhalation through the buccal cavity becomes more common (Shannon and Hyatt, 2004; Warburton and Bellusci, 2004) The nasal cavity however leads to optimal deep lung inhalation, and conditions the air before encountering the respiratory bronchioles. It serves to humidify, warm and filter particulate matter from the inhaled air which inhalation through the buccal cavity does not offer (Harkema et al., 2006). The buccal and nasal cavity join at the top of the trachea which in turns brings inhaled oxygen through to the bronchus, bronchioli and into the alveolar region where the majority of gas exchange occurs. There is a series of 23 generations of dichotomous branching in the human lung, the first 16 of which are stereotypically reproducible and the remaining 7 are random, and in total there is estimated to be more than 40 different cell types in this system. Of the in excess of 40 types present, to date 8 have been identified in the epithelium of the tracheobronchial airways, though the location, type and number of cells can differ between species (Crapo et al., 1982; Pinkerton and Joad, 2000).

Although the human lung has many similarities with other mammalian lungs, with the use of animal models it is vital to understand various discrete differences. In common with primates, humans have a relatively simple nasal passageway, but many commonly used animal models such as mice are obligate nasal breathers with more complex nasal structures, especially important with regard to the delivery of inhaled particulates. Humans have near dichotomous branching of the tracheobronchial tree, in common with primates, but this is much more branched than evidenced in common rodent models such as mice. Human and primates also have a gradual transition from ciliated only to alveolar only lined ducts with a number of generations of combined bronchiolar epithelium and alveolar gaseous exchange that form respiratory bronchioles making up this transitional area. Mice however lack in entirety the

respiratory bronchiole system present in humans. In terms of delivery this results in much faster alveolar clearance of inhaled particles than seen in humans and primates. The changes in structure come from underlying differences in developmental regulation of the respiratory system (Plopper et al., 1992; Phalen et al., 2008).

1.1.1   Development

Development of the respiratory system begins during gestation, and although it is capable of functional gaseous exchange by week 40, it is by no means fully developed. An understanding of the development of the lung system, and how its development is regulated, helps further the understanding of how disease and damage can induce long term damage to the system, and help us discover means to help control the system, either by subjectively switching it off where deregulated, or trying to turn it back on where tissue or cell regeneration may be beneficial.

Development of the lung begins with evagination of an avascularised epithelial cell into the mesenchyma finishes with a multicellular, vascularised, innervated and ventilated region comprising of over 25000 distinct terminations and 300million alveoli. The bronchiolar region undergoes completion between weeks 5 and 25 gestation, whit the development of the alveolar units beginning at week 20, with development continuing on for many years afterwards, as far as year 7, allowing for the fact that as the mass of the body increases, its demand for greater oxygen exchange capacity also increases. Over 80% of the alveoli mass in the adult human is formed postnatally. This process of development is a carefully regulated by a highly conserved set of developmental genes whose function in the generation of airways and modelling of the respiratory and entwined vasculature system, also play a role in the repairing of the lung after insult or injury in order to maintain optimal function in the lung. As will be seen however, deregulated or inappropriate activation of the genes during repair can lead to further complications and disease within the lung.

Post embryogenesis, and common to all mammalian lung systems, there are 5 stages of lung development. The main central stages of development on average last 10 to 12 weeks each and can slightly overlap. They can be divided as follows:

a) Embryonic- Humans weeks 0-7, mice embryonic (E) 0-9.5

b) Pseudo-glandular - Humans weeks 7-17, mice E9.5-16.6. This is the beginning of development of the lung structure and is the duration during which branching of the airways develops. During this stage both the tubular epithelium, lined internally with as yet underdeveloped respiratory cells not capable of gaseous exchange, and

externally with arterial blood vessels, as well as the development of the vein system through the mesenchyme, occurs. This process helps to assign borders for later lung segmentation. The branching epithelial tubules are heavily interwoven with the mesenchyme and the interaction between these two regions is vital in the guidance of further development of the lungs

c) Canicular- Humans weeks 17-27, mice E16.6-17.4. This period sees enlargement of the tracheobronchial tree, with epithelial tubules growing wider in diameter and longer, and accompanied by capillarisation of the respiratory units. It also marks the period during which respiratory bronchioles and alveolar airways undergo development, and the synthesis of lung surfactants begins. During this stage of development the type I and type II pneumocytes start to differentiate and lamellar bodies such as start to appear in the type II pneumocytes. This occurs before the production of surfactant can begin. It is also the period of development that sees the creation of the blood-gas or alveolar-capillary barrier.

d) Sacular- Humans weeks 28-36, mice E17 post natal day 5 (P5). This stage marks the further development of the peripheral regions. Peripheral airways from terminal saccules which further enlarge the respiratory surface through an increase in generations. This process is especially influenced by regulating factors from the mesenchyme. Vascular growth is ongoing also throughout this stage, and capillary influx throughout the alveolar mesenchyme is greatly increased in order to be capable of sufficient diffusion of gas. In combination with this the cells of the respiratory system start to differentiate. Fibroblasts differentiate cells producing extracellular matrix, elastin and collagen; while alveolar epithelial cells fully differentiate into type I mature squamous cells and type II secretory cells. Type I cells surfactant levels increase, vital to the capability of the lung to sustain gas exchange without collapsing. A final and key factor to this stage is the switching of the system from a chloride ion driven fluid secretion into the airway with a sodium ion uptake into the airway induced by the cutting of the umbilical cord upon delivery.

e) Alveolar/postnatal- Humans week 36 prenatal to postnatal year 7/8, mice P5-P30. The development of the alveoli regions of the lungs continue. This period of growth is fastest in the first 1.5-2 years post natal and sees the number of alveoli in the lungs increase from approximately 50 million to approximately 300million plus, the exact number varies between an estimated 300 and 800 million, matching the increase in demand from a still growing body. It also sees an increase in capillarisation again, "shortly after birth the secondary septation begins in the terminal saccules", increasing the capacity of the lungs for gaseous exchange. Males will also have larger

lungs than females at any given age or body length, a possible factor for consideration where therapeutic delivery is concerned, as males will have a larger alveolar surface and a higher number of alveoli than females. Also it has been reported that the deposition of particles inhaled could be 6 times greater in resting infants than seen in resting adults, a concern for both potential inhaled therapeutics and also for exposure to inhaled toxins in the developing lung (Pinkerton and Joad, 2000; Shi et al., 2009).

The majority of the gaseous exchange sites therefore are undergoing development during this final postnatal stage, during which time the lungs will be exposed to external factors that will influence and possibly impede or deregulate development, such as exposure to stand alone toxins or exposure to toxins in combination with underlying genetic predisposition factors as can be seen in childhood asthma. The human airways actively inhale to complete gaseous exchange, and as they do they are responsible for ensuring that the sterility of the body is maintained. The lungs are a primary route of infection for numerous viruses and micro-organisms, and are also exposed to particulate matter and toxins. In order to deal with this the lungs have developed a highly efficient set of systems to maintain sterility and rid the lungs of pathogens, toxins and inhaled particulates. At birth, the immune system is active but underdeveloped and exposures to challenges are an essential part of its development into a fully functioning system capable of helping protect the body. The immune defences of the lung comprise of both innate and adaptive mechanisms

1.1.2 Lung defence and immunity

The cells lining the airways contribute to the lung defences. The goblet and Clara cells, discussed later, of the conducting airways as well as the submucosal glands and the type II alveolar cells, form the mucous secretory apparatus of the lungs and are as a result vital parts of the lung defence mechanism, coating the airways in a thin layer of mucous or airway surface liquid. In combination with ciliated cells, the secreted mucus and cilia form a muco-cilliary ladder which propels the mucus and any trapped particle to the top of the trachea for expulsion.

Due to the nature of operation of the lung, it is exposed to a large number of inhaled micro-organism, pathogens and toxins. In order to protect against damage resulting from this a number of innate and adaptive immune responses are in place.

With regards to the innate immunity, there are a number of defence mechanisms in place. They include the physical barrier provided by the epithelial cells, the muco-cilliary clearance mechanism, antimicrobial production by way of active and

inducible chemical production, chemotactic signalling for the induction of immune cells response such as macrophages and dendritic cells, as well as protease activity (Bivas-Benita et al., 2005). The muco-cilliary clearance ladder is perhaps one of the main lines of defence and recruits cells from throughout the airways in its operation. The function of the muco-cilliary ladder is to trap inhaled particles and by ciliary action propel the particles up out of the airways to be cleared. The mucous is secreted by secretory cells such as type-II alveolar cells, Clara cells, goblet cells and ciliated cells line the airways. This pseudo-stratified airway is a mainstay in the protective function of the lung. The secretory cells are also responsible for the secreting anti-microbials into the Airway Surface Liquid (ASL), also known as the perciliary or sol layer. This lines the respiratory airways and its height affects the muco-cilliary clearance capabilities as differences in height can affect the ability of the cilia and the overlying mucus to effectively work in tandem. This periciliary layer also contains defensins, lactoferrin and lysosyme that have potent anti microbial properties that help prevent damage or insult to the underlying epithelium (Cowley et al., 2000). The attraction of immune cells by the release of cytokines can induce a localised inflammatory response, which if properly regulated and occurs in tissue that has not been badly injured, can stay contained. However deregulation of this inflammatory process or its occurrence in pathologically damaged tissues can see the cytokine release spread to undamaged tissue and exacerbate any local problems, causing either potentially damaging inflammation occurring throughout the organ or even systemically. However this process is tightly regulated and usually is well managed with the exception of major insult of underlying pathological or genetic problems. Chemotactic cytokines recruited during this inflammatory process include granulocyte macrophage–colony stimulating factor (GM-CSF) and lymphocyte chemo attractant factor which attract inflammatory cells to the sites required, as well as pluriepotent chemokines such as IL-1, IL-5, IL-6, IL-8 and tumour necrosis factor-α (TNF-α) which have effects on numerous different cell types and are responsible for the activation of B lymphocytes and monocytes (Mills et al., 1999). Pulmonary macrophages work by phagocytosis of any potential pathogen followed by the release of anti microbial enzymes as well as T-cell stimulatory and pro inflammatory cytokines. Regulation of macrophage activity prevents a constant state of inflammation, and resultant organ damage, from occurring. Dendritic cells are also part of the innate immune system, but are a vital link to the adaptive immune response of the lung. They are key antigen presenting cells, with the greatest populations located in the conducting airways of the lungs. During inflammation the concentration

of dendritic cells in greatly increased. Transforming growth factors such as TGF-β, secreted by bronchial epithelial cells help play a role in the suppression of the inflammatory response.

1.1.3 Clara cells

Clara cells are non ciliated type II undifferentiated lung epithelial cells. They are progenitor cells for type I ciliated cells and are regarded as the lung stem cell. They are heavily involved in injury repair in the lung. In both human and primates Clara cells undergo cytodifferentiation both pre and post natally and this changes see a move from glycogen filled non ciliated cell to a ciliated, low glycogen containing multi organelle cell (Plopper et al., 1992). Experimentally in rodents Clara cells have been shown to play a vital role in the repair and regeneration of epithelium after injury or disease. In hamsters exposed to inhaled NO2and O3 which negatively affects the epithelium, the proliferative response that follows on from exposure has been shown to be primarily a result of Clara cell division. In rabbits heavily enriched Clara cell populations grafted onto a denuded trachea have been shown to resolve the lack of epithelium, with the Clara cells differentiating to leave both non ciliated Clara cells and ciliated type I cells forming an epithelial layer.

The importance of Clara cells to the process of development regeneration and resolution of injury can be seen in their locations throughout the lungs, as determined by the analysis of 7 histologically normal lungs in autopsy. The lungs showed Clara cells to be almost absent from the proximal airways, but in the terminal bronchioles they formed 11±3% of the cell population and 22±5% of the total cell population of the respiratory bronchioles. In the regions of proliferation of the airways, determined to be on average 0.83±47% of the total airways, Clara cell population was 9%, with 15% showing in the terminal bronchioles and a 44% share of total cell population in the more proliferative regions of the respiratory bronchioles. This high percentage of Clara cell location in the proliferative regions of the lungs shows the vital role they play in the maintenance of healthy epithelial organisation in the lung (Boers et al., 1999).

1.1.4 Repair responses of the lungs

Where damage and insult has occurred to the lungs a wide number of pathways linked to repair are activated. However this can in certain cases lead to chronic inflammatory responses or pathological changes in the structure of the lung. Growth factors

involved in the process of development outlined above, play a vital role in the direction of repair in the lungs and can guide in undifferentiated or partially differentiated lung cells to a damaged area in order to regenerate the denuded or damaged epithelium. One of the major pathways involved in guiding the repair of lung surface epithelium is part of the TGF-β super pathway, the BMP pathway. The BMP pathway is a pleiotropic signalling pathway heavily involved in both lung development and lung repair, and its deregulation linked to various lung diseases and cancer.

1.2 Diseases Of the lungs

The lungs are susceptible to many different types of infection and disease, as a result of genetic defects, protein abnormalities, environmental stimuli or various combinations thereof. The initial aim of this project was to assess the role of the BMP pathway, cell cycle and differentiation markers as well as markers of EMT in the progression and development of some of these diseases. Following on from this the aim was to then identify and target for potential aerosol delivery of therapeutics, some of the underlying causes of these problems. Some of the main diseases examined included genetic diseases such as cystic fibrosis (CF), pulmonary hypertension (PAH), chronic inflammatory diseases linked to both genetic and environmental causes such as asthma, and diseases of the lung resulting from prolonged environmental insult, such as emphysema.

1.2.1 Cystic Fibrosis

Cystic Fibrosis (CF) gene therapy has been long held as a major milestone on the road to the development of successful gene therapy. The reason for this is that the cause of the disease lies in the mutation of a single gene, CFTR, first identified in 1989. It is thought that correction of this mutation by the expression of a non mutated gene and its subsequent protein in just 5% of the airways would be sufficient to result in a healthy airway epithelium. CF is a particularly pertinent problem in Ireland, with over 1100 CF patients in the population, significantly the highest concentration of CF patients per head of population in the world. The occurrence in Ireland is 2.98 patients per 10,000 head of population, vs. 0.737/10,000 in the rest of Europe and 0.797 in the United States. CF is also the most common lethal autosomal recessive disease in European and US populations (Farrell, 2008). The disease is caused by a mutation of the ΔF508 gene in 60-70% of cases, where a deletion of 3 nucleotides results in the loss of the amino acid phenylalanine. This results in erroneous synthesis of the protein

and incorrect folding and structure and prevents the protein from embedding and functioning in the cell membrane. All told however there are an estimated 1400 mutations in the gene in total that can result in CF pathogenesis. The CFTR gene functions as a cyclin-AMP-dependent low conductance chloride channel (Legssyer et al., 2006). When this is defective in the epithelium, it is most commonly a result of incorrect quaternary structure due deletion of three nucleotides at the 508 position on the protein, leading to the incorrect formation of the amino acid phenylalanine. This leads to incorrect processing of the chloride channels and results in a thickening of mucus and the formation of mucus plugs. This thickened mucus is too viscous for clearance by the muco-cilliary ladder, leading to a build-up of mucus in the airways. This leads not only to restrictive breathing, but to reduced surface area and most importantly, to increased residency times for infectious microbes leading to infection, inflammation and airway obstruction. Cystic Fibrosis is not just a disease of the lungs, affecting all the mucous membranes of the body, however it is the manifestation of disease in the lungs that is the most life threatening. This particular disease is a strong target for gene therapy advocates as only one gene needs to be corrected for and a relatively low level of correction will have a high benefit. It will then pave the way for the development and delivery of other gene therapies for different more complex genetic diseases. The mode of delivery of gene therapies to the lungs is covered later.

Mice, though commonly used for CF studies, are not necessarily the most ideal model for the study of CF treatments. ΔF508 mice show little CF pathogenesis without repeated exposure to bacterial infection. This is in part due to the low salt environment of their ASL, allowing the salt sensitive lung defences to function normally and clear low levels of infection (McCray et al., 1999). In humans the alteration of the Chloride transport channels is purported to affect the ionic concentration of the ASL, increasing it sufficiently to impair the ability of epithelial cells to stave off excessive bacterial infections and colonisation of the lungs (Cowley et al., 2000). Porcine models of CF provide a better mechanism for the study of CF, due to the similarities of anatomy, biochemistry, physiology size and genetics (Rogers et al., 2008). All told there a number of different large mammal models of CF including sheep, ferrets and monkeys which all have unique advantages as a model of the disease (Rogers et al., 2008).

Aside from being a model for gene therapy, CF is also a major target for inhaled therapeutics such as anti-inflammatories and anti-bacterials. Inhaled delivery of therapeutics to the CF lung has numerous advantages including the direct targeting of active compounds on the infected site, limited systemic activity, fast onset of action,

and no first pass metabolism to bypass. Also due to the fact that CF morbidity ultimately results from the inflammation and resulting destruction of the lung parenchyma, it is possible that combined delivery of both therapeutics such as anti bacterials in combination with drugs that have the ability to modulate the response of pathways such as the BMP pathway, EMT and cell cycle could have a positive effect in limiting the destructive inflammatory response and help ensure epithelial survival. Currently being heavily investigated are anti-bacterials delivered via inhalation targeting pseudomonas aeruginosa, which is found in approximately 80% of all CF patients between the ages of 25 and 34 years of age (Heijerman et al., 2009)

It has been shown that aerosol delivery of tobramyin, the only aerosol therapeutic currently licensed for treatment of P.aeruginosa in CF patients, is more effective than systemic dosing as a treatment regime (Sabet et al., 2009).

1.2.2 Asthma

Asthma is a disease resulting from a combination of genetic and environmental factors. Allergic asthma is a major health and social burden. According to the Irish thoracic society report, as of 2006 approximately €92.56 million was the cost to the Irish state as a result of the state covered prescriptions, of which there were approximately 3.083 million. The total number of items prescribed for asthma in the state (Public and Private) was put at approx. 806.3 million. Epidemiological studies show Ireland with a population of approximately 470,000 asthmatics, the 4th largest in the world (O'Connor, 2008). Asthma is also a concern globally, in the US 9% of all children, or approximately 6.7million children, are diagnosed as having asthma (Bloom et al., 2009). As a result asthmatic patients form a huge percentage of the market in relation to inhaled therapies where direct delivery of steroids is regularly use to control or alleviate asthmatic response. This means that the patients are largely educated as to the correct use of inhaler and/or nebuliser type devices and so novel therapeutics dependent upon inhalation delivery are likely to be more readily accepted will not require a steep learning curve from a patient standpoint.

Asthma is a chronic inflammatory disease that is characterised by intermittent onset of symptoms and variable airflow obstruction that can occur spontaneously or as a result of environmental or non specific stimuli that results in eosinophil influx and inflammation, mucus hyper secretion, bronchial hyper reactivity, alterations to the smooth muscle lining the airways and extensive remodelling of the airways themselves. These are all components of the pathophysiology in adult humans. Remodelling of the airways results in thickening of both sides of the airway wall,

making the bore of the airways smaller and affecting mechanical properties of the lung and has been directly associated to hyper responsiveness. The remodelling aspects of the disease in the airway wall include increase in smooth muscle, increased capillarisation, goblet cell hyperplasia, epithelial cell disruption and an increase in the amount of collagen deposition on the basement membrane (McKay and Hogg, 2002; Lambrecht and Hammad, 2003).

Dendritic cells play a major role in the onset of asthma as they are an essential component in the recruitment of eosinophils to the lung and the resultant inflammation. It has been consistently shown that asthmatic patients have a high amount of eosinophilic infiltrate as well as increased lymphocytes and neutrophil populations. This inflammatory milieu adds to the mucus on the surface of the epithelial cells and accumulation of the inflammatory exudate in mucus can lead to characteristic mucus plugging of the asthmatic airways.

1.2.2.1 Animal Models of Asthma

Mice are the most commonly utilised animal model in the study of asthma with the methods of bringing around asthma like disease varying greatly between labs. One of the most common means of inducing chronic inflammation of the lung in mice that closely resembles the pathology of asthma is by using OVA as an antigen. Delivery of the antigen via subcutaneous injection in the presence of the Th2 inducing adjuvant Alum over the period of 10-14 days followed by inhalation exposure to the OVA antigen induces increased levels of OVA specific IgE. There is much inter lab and experimental variation between timing of dosages and the routes of administration. However there are problems associated with this model of disease in mice. Primarily short term exposure to OVA as described inhibits the examinations of the effects of long-term damage from asthma. Attempts to extend the sensitisation period have resulted in either widespread inflammation of lung parenchyma or a down regulation of airway inflammation and hyper reactivity responses (Kumar and Foster, 2002). The manifestations of the disease do not directly correlate with asthma seen in humans however such as 1) mice display less eosinophilic granulation than observed in humans 2) mice develop transient airway hyper reactivity as opposed to persistent hyperactivity 3) no defined role for IgE and Mast cells, differences in anatomy and eosinophil function between the two species (Epstein, 2006). In spite of these differences however and the lack of a long term chronic inflammatory model in mice, mice provide a valuable model in the initial testing of therapeutics targeting asthma and chronic inflammation of the lung.

One of the best models available for the studying asthma is the primate model. In 2001 Schelegle et al. reported that they had created a model of allergic asthma in Rhesus macaques using a protocol of repeated exposure to a known human allergen, house dust mite (HDMA). The rhesus model provides a better model for human asthma for a number of reasons: 1) rhesus monkeys share a common ancestor with humans from 25 million years ago (versus 70million years for rodents) and show greater similarity to human genetics, physiology, neurobiology and susceptibility to human infectious diseases (Gibbs et al., 2007), 2) the immune systems are very similar, 3) all the components of the lung that are altered in human asthma are present in the rhesus monkeys and 4) the rhesus monkey undergoes similar levels of extensive postnatal lung development as the human lung (Schelegle et al., 2001). The HDMA model of asthma in rhesus monkeys that was established met the criteria for asthma as defined by the 1997 national heart, lung and blood institutes' national education and prevention program clinical guidelines. In common with humans the majority of the cells in the asthmatic primates BAL after aerosol challenge were found to be ciliated cells. They also demonstrated a similar immediate bronchorestrictive response to inhaled allergen as seen in humans. An important feature of the bronchorestrictive response is that it is triggered by histamine and histamine was seen to be produced as an early response to type I hypersensitivity in both the human patient and the HDMA primate model. Rhesus primates also share the distribution profile of inflammatory cells with humans as well as the same type of allergen mediated response. Pathologically the HDMA model of asthma in primates underwent the same extensive remodelling of the airway walls as well as mucus hypersecretion seen in the human disease. Extensive hyperplasia and thickening of the basement membrane was also shared between the primate model and the human occurrence of the disease. (Schelegle et al., 2001). This model of HDMA induced asthma was then improved upon to help more closely mimic the onset of the disease in humans.

Ozone is a known environmental toxin and acute inhalation of it damages the entire lung parenchyma, and initiates an inflammatory response that subsides as repair is carried out on the damaged cells (Schelegle et al., 2003). Cyclic exposure to Ozone occurs in humans as the levels in the atmosphere can be seasonally dependent. It has been shown in primates that cyclic exposure to Ozone resulted in repetitive cycles of injury and repair that lead to altered development of the lung in the primate as well as decreased lung function and increased chronic airway diseases ((Fanucchi et al., 2006). It was shown that by combining the HDMA model of allergen exposure to a common human allergen with a cyclic dose of a common environmental toxin such as

Ozone led to a stronger model of naturally occurring human allergic asthma. It resulted in a marked increase in serum IgE and histamine levels as well as airway eosinophilia. It led to more extensive remodelling of the airways and lung resistance as well as increased reactivity (Schelegle et al., 2003).

These models of asthma in both mice and primates as well as what is seen in human pathology, shows the process of remodelling and inflammation to be strong contributory factors in the prevalence of the disease in the human body. Targeting the pathways that control remodelling by means of BMP antagonism therefore provides a potential means of alleviating not only the symptoms of asthma as achieved with steroidal drugs, but in the blocking of the cycle of injury and repair that leads to progressive inflammation, constriction and damage to the lung tissue. Targeting delivery to the lungs directly via inhalation reduces the systemic impact of the drugs and increases the bioavailability for the targeted region than could other wise be achieved.

1.2.3 Emphysema

Emphysema is a major disease of the lung. It is closely associated with COPD and it generally results from exposure of the lungs to tobacco smoke. Emphysema results in enlargement of the alveolar spaces through destruction of the lung parenchyma and it is clinically diagnosed through a loss of elastic recoil in the lung and an increase in lung volume. It has also been shown that emphysema, independent of cigarette smoking predisposes the individual to lung cancer (Houghton et al., 2008). There are a number of different types of emphysema with different pathogenesis, believed to result from different genetic markers in the individuals but the root of these differences are not fully understood. The different types of pathogenesis include centriacinar, which includes centrilobur as seen in tobacco smokers which begins in the respiratory bronchioles and primarily affects the upper half of the lungs, panacinar which is the most commonly seen in patients suffering from α1-protease inhibitor deficiency that begins with the alveolar ducts in a secondary lobe of the lung and primarily affects the base of the lung, paraseptal which initiates in alveoli adjacent to the fibrous planes and is mostly located in the peripheral regions of the lung and adjacent to the septa, and airspace enlargement with fibrosis which is associated with scarring in the lungs(Snider et al., 1991; Lucey et al., 2002). It is possible that underlying genetic differences are also the reason that smoking cessation does not slow the progression of emphysema in some patients as much as it does in others. As

with COPD there is no current cure for emphysema with smoking cessation being the biggest contributory fact to the prolonging of disease advancement in patients.

Numerous mice models have been established to examine emphysema and are generally of the genetic variety using over expression or knockout to induce damage or the exposure variety based on the delivery of damage inducing agents such as elastase or tobacco smoke to the lung to bring about the onset of the disease (Taraseviciene-Stewart and Voelkel, 2008). The most common model is based on the delivery of elastase to the mouse lung. It is the direct action of elastolytic enzymes such as elastase that brings about the emphysema phenotype, delivery of other proteases do not bring about the same pathology (Snider et al., 1991). As it stands there is no clinically relevant method for promoting recovery of the lung from emphysema. Data in rats had appeared to indicate that treatment of the lungs with all-*trans*-retinoic acid aided recovery however it has not proven effective in other models of the disease such as mouse and guinea pig and is possibly a species specific result (Fujita et al., 2004). Elastase induced emphysema has also been shown to be decreased in severity in TNF-α and Il-1β receptor deficient mice indicating a role for the pro-inflammatory cytokines in the onset of the disease (Lucey et al., 2002). Another characteristic of elastase induced damage in mice is the loss of body weight in exposed animals where the control animals gain or maintain weight and also show decreased ability to exercise as is the pattern in the human disease (Luthje et al., 2009).

1.2.4 Pulmonary Arterial Hypertension (PAH)

PAH occurs in approximately 2-3 cases per million and atypically affects young females. It is a severe and fatal disease with an average survival period of 2.5yrs from the time of diagnosis. Death begins with obstruction of the small pulmonary blood vessels that leads to a continuous increase in pulmonary vascular resistance. This gives rise to an increase in pulmonary arterial pressure that eventually brings on the failure of the right heart wall (Davies and Morrell, 2008). Current therapies include the use of anticoagulants which can double the average survival length and calcium channel blockers which in patients in which they are effective sees a 95% survival rate at the 5year mark after diagnosis (Rubin, 1997). The disease is a result of extensive remodelling of the small blood vessels found surrounding the lung. Specifically what defines this disease is the fact that it is limited to the pulmonary bed with no pathology occurring in the vasculature of any other area of the body (Stewart,

2005). The pathology encompasses thrombus formation, vascular remodelling due to unregulated proliferation and inflammation.

There is a strong link between the onset of PAH and a defective BMPR-II gene. Mutated BMPR-II gene expression leads to the deregulation of responses to BMP and TGF-β signalling in the vasculature (Stewart, 2005; Morrell, 2006; Teichert-Kuliszewska et al., 2006). In animal model studies it has been shown that if the ratio of expression of normal gene to mutated gene is as low as 1:9 the mice will survive, though vasculature deformities will arise. Beppu et al. reported that in BMPR-II$^{+/-}$ heterozygous mice there was an increased pulmonary arterial pressure and pulmonary vasculature remodelling compared to wild type BMPR-II$^{+/+}$ mice, though the following year Song et al. reported that BMPR-II$^{+/-}$ mice enjoyed the same lifespan and right ventricular systolic pressure and histology as the wildtypes in the absence of any stressing conditions. However under inflammatory stress the BMPR-II$^{+/-}$ increased right ventricular systolic pressure and an increased level of vascular remodelling then the wildtype animals subjected to the same stresses (Beppu et al., 2004; Song et al., 2005b). When dominant negative BMPR-II$^{-/-}$ expression located specifically in the smooth muscle however was switched on after birth utilising a tetracycline gene switch, mice developed pulmonary specific arterial hypertension, an increase in right ventricular systolic pressure and muscularisation of the arteries in the absence of an inflammatory stimuli (West et al., 2004). These experiments seem to suggest that total loss of BMPR-II can induce PAH, and where an individual is heterozygous for the gene inflammatory stimuli leads to disease progression.

Due to the major involvement of BMPR-II in the onset and prognosis of disease numerous means of trying to improve function have been postulated. Of particular relevance is the fact that in cell culture experiments, the use of a recombinant BMP ligand to increase the available concentration of the ligand to the cells has been shown to overcome the defects in BMP signalling (Davies and Morrell, 2008). As such it is foreseeable that direct delivery of BMPs to the targeted vasculature by using the lung surface as an entry point for the protein could potentially provide a means for alleviating the issues associated with PAH remodelling by, for example, supplying a constant low dose of protein to the system and increasing amounts over periods of inflammation, or by targeting plasmid induced over expression of BMP4 to the vasculature of the lungs.

1.3 BMPs

Bone Morphogenetic Proteins (BMPs) are so named as they were first discovered for the ability to induce the formation of bone and cartilage (Urist, 1965). They are now known to be part of the much larger family of TGF-Beta superfamily of signalling molecules. Erroneous triggering or inhibition of members of this superfamily of cytokines is responsible for giving rise to the majority of human diseases including various forms of cancer, developmental disorders and vascular diseases (Gordon and Blobe, 2008). They are found at different stages and to different extents in nearly every organ and tissue throughout the body. The extent of their importance can not only be seen in the number of roles they play in critical stages of development and repair, with TGF beta family signalling being one of the most ubiquitously expressed regulators of prenatal development, but also in how evolutionarily conserved they remain. (Massague, 1998).

Embryogenesis and prenatal development sees the involvement of the BMP pathway in left-right asymmetry, mesodermal patterning, bone and cartilage formation and repair, organogenesis as observed in the lung, amnion, gut, teeth, kidneys and testis, neurogenesis, and epithelial mesenchymal interactions in the developing organs such as lungs (Wozney et al., 1988; Massague, 1998; Balemans and Van Hul, 2002; Herpin and Cunningham, 2007; Zhu et al., 2007). In the post natal period and all through adult hood BMPs continue to play a role in growth, proliferation, differentiation apoptosis as well as chemotaxis in cells throughout the body (Massague, 1998). It is this continued role throughout adulthood that has linked BMPs to inflammatory responses in fibroblasts, myocytes and other cells linked with or undergoing an inflammatory response. For example, Rosendahl et al reported phosphorylation of the downstream effectors of BMP signalling, the Smads, particularly Smads 1 and 5, in response to OVA induced inflammation of the bronchi in mice, confirming BMP pathway activation involvement in the inflammatory response (Rosendahl et al., 2002).

The pathway itself can be activated in one of two main ways; the canonical, or Smad dependent pathway, or alternatively if the pathway activation is not Smad dependent, the MAP Kinase pathway. The predominant interest in the role of the effect of the BMP pathway in inflammation and disease in the human lung has focused on the canonical Smad dependent pathway (Figure 1.1). The Smad molecules are the signalling effector molecules of the BMP pathway.

1.3.1 The BMP pathway

The canonical Smad dependent pathway operates as follows. Secreted BMP ligand binds to a type I or type II ser/thr kinase receptor, also known as a BMP receptor (BMPR-I or BMPR-II). BMP ligands typically bind to BMPR-II when both receptors are expressed together before recruiting a type I receptor. The binding affinity of the receptors for BMP is greatly increased when both are present. However BMP ligands will also bind weakly to type II receptors expressed alone on the cell surface and to type I receptors expressed either alone or in solution. In the typical scenario, once the type II BMPR has bound the BMP ligand it recruits a type I receptor and then goes on to form a hetero-tetra BMPR complex by recruiting another type I and type II receptor to the complex. When the complex is formed the type II receptors phosphorylate the glycine-serine (GS) activation domain of the type I receptors, activating the complex. The now active complex can phosphorylate the effectors modules, the Smads. The group of Smads activated in this fashion are known as the regulatory Smads. Once they are phosphorylated they are capable of binding to Co-Smad, Smad4, which is responsible for trafficking of Smad complex into the nucleus. Once in the nucleus, the Smad complex links with a DNA binding protein such as FAST-1, before binding to the target gene and regulating its transcription (Heldin et al., 1997; Massague, 1998; Yu et al., 2005).

In the lung the Smad dependent BMP pathway is linked to ongoing repair and development of the lung tissue. In our lab it has already been established that the canonical BMP pathway is involved in the process of EMT in mouse airway epithelial cells (Molloy et al., 2008). The pathway has been shown to be involved in processes linked to certain types of lung cancer (Gilbert, J., unpublished data) and to Allergic Rhinitis (Molloy, E., unpublished data). A link has also been established between BMP signalling and airway regeneration (Masterson et al., 2010). This data, in conjunction with work such as from Rosendahl et al., suggest that the BMP pathway is a potential target in order to interfere with the onset of damage in certain disease models, particularly those linked to inflammatory responses and remodelling. As such it is important to have a good understanding of the make-up and functions of the different components of the pathway.
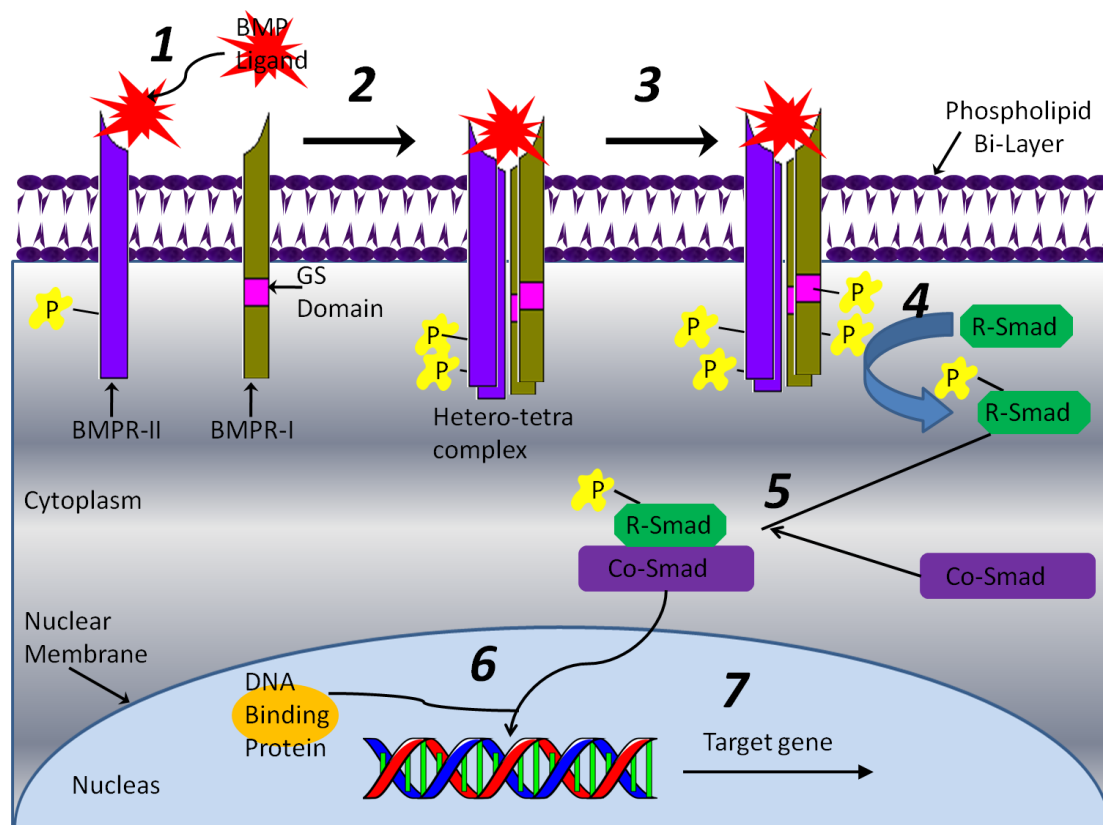
Figure 1.1 The BMP Pathway

The BMP pathway is activated by the binding of a BMP ligand to a BMP specific receptor (1). This receptor (Can be a type I but BMP preferentially binds type II) then recruits a type I receptor and this in turn leads to the formation of a hetero-tetra complex consisting of a total of four receptors (2) This leads to the activation of the type I receptors by phosphorylation of the GS domain (3). This activated receptor complex can now in turn phosphorylate a regulatory Smad (Smad 1/5/8) (4). Phosphorylated Smads are the intracellular mediators of BMP signalling. This phosphorylated Smad complex is now capable of binding the nuclear trafficking Smad, a.k.a. Co-Smad or Smad4 (5). Co-Smad then escorts the Smad complex into the cell nucleus where the activated Smads, in conjunction with a DNA binding protein (6) can now actively regulate the transcription of the target gene (7).

1.3.1.1 BMPs and Asthma

There is an established link between airway inflammatory disease in mice established via OVA induced asthma and the activation of the BMP pathway. Rosendahl et al investigated the involvement of the Smad proteins, notably phosphorylated Smad1 and Smad5 and found that with the onset of disease and in contrast to healthy models, animals undergoing airway inflammation saw increased signalling via the canonical, Smad dependent, BMP pathway. They also showed that the onset of disease in the model animals led to alterations in the expression profiles for various BMP ligand and protein and mRNA levels. In combination with the known effects of the BMP ligands this shed light on the possible role of activated BMP pathway involvement in the pathology associated with allergic airway inflammatory diseases (Rosendahl et al., 2002). Later studies examining the correlation between BMP pathway activation in asthma and the associated remodelling and pathophysiology was carried out in humans using bronchial biopsies from asthmatic patients with 'mild' asthma and non asthmatic patients (Kariyawasam et al., 2008). Findings showed that overall BMPR protein expression was down significantly in asthma patients, and that exposure to allergen caused a significant response in terms of increased BMP7 production. This increase in endogenous BMP7 was then linked to an increase in both pathway activation and BMPR expression levels. This contrasts somewhat with the earlier work by Rosendahl et al which had shown type I BMPR levels to be significantly upregulated after exposure to OVA allergen. The difference in profiles of the type 1 receptors could be due to a myriad of different reasons such as time after allergen exposure, differing immune responses to different allergens, the difference between the model and the clinical reality and the type of inflammation reaction present. Both models however demonstrate clearly the involvement of the BMP pathway in response to allergic inflammatory disease of the airways and the need for a better understanding of the underlying mechanisms and responses.

1.3.2 BMP proteins

BMP functional proteins are large dimeric molecules that are bound by hydrophobic interactions and an inter subunit disulphide bond which is a strong covalent bond that holds the subunits of the protein together. They are synthesised and undergo conformational folding in the cytoplasm. As they are secreted they are cleaved by proteases. The receptors are highly specific and the BMP molecules are highly conserved in order to ensure correct conformation for binding (Eimon and Harland, 1999; Danesh et al., 2009).

In total there are over 20 known BMP proteins. Of particular interest to our lab is BMP4.

1.3.3 BMP4

BMP4 is a secreted protein that plays a key role in morphogenesis in the local environment. It has been shown to have an active role throughout development and also in processes resulting from injury and repair within the human body. It is required for early mesoderm formation and is also expressed in the splanchnic mesoderm from which the lung buds will emerge (Molloy et al., 2008). After this it is shown to be active in areas of rapid division and growth such as the proximal regions of the developing lungs and in areas undergoing repair and proliferation (Shannon and Hyatt, 2004). In the developing lung the expression of BMP4 occurs with precise spatial and temporal specificity (Hogan, 1996; Zhu et al., 2007). The level of BMP4 activity is tightly linked to its role in development, with over expression of the protein resulting in lung hypoplasia and lower proliferation of the epithelial cells and has been linked to inhibition of epithelial proliferation in the lung and trachea also (Hyatt et al., 2002). The regulation of the levels of BMP4 is, in part, carried out by Fibroblastic Growth Factor (FGF) signals. FGFs are themselves pluripotent growth factors shown to have a vital role in development, with FGF10 and BMP4 shown to play opposite roles in lung bud morphogenesis and BMP4 shown to modulate FGF signals during branching lung bud formation in the developing lung (Weaver et al., 2000; Hyatt et al., 2002). In mouse embryos, BMP4 deletion specifically in the epithelium via Cre- induced silencing resulted in abnormal development of the lung. This shows that BMP4 has a pivotal role in the control of proliferation, survival differentiation of lung epithelial cells (Eblaghie et al., 2006).

BMP4 is also expressed throughout the adult lung. In adult cells our lab has shown that BMP4 induces an epithelial-to-mesenchymal-like transition in airway epithelial cells (Molloy et al., 2008). It is also a known inhibitor of myogenic formation, and studies in mice have shown that under hypoxic conditions it is upregulated. This is linked to the role that BMP4 plays in the direction of pulmonary vascular remodelling after hypoxic shock and also links BMP4 remodelling to pulmonary hypertension. As such, targeted silencing of BMP4 activity presents itself as a means to possibly prevent aberrant BMP4 induced remodelling of the pulmonary vascular system in patients who suffer from hypoxia induced in pulmonary hypertension (ten Dijke et al., 2003). Selective targeting of BMP4 however is required rather than full organ silencing. This can be seen in the case of idiopathic pulmonary fibrosis, where a

natural inhibitor of BMP4, Gremlin, is over expressed, causing an enhanced fibroblastic growth response in the lung and reduce epithelial regeneration (Koli et al., 2006). This over expression of a BMP4 antagonist is linked to the increased resistance of the myofibroblasts in the lung and therefore presents itself as a therapeutic target, or potentially, increased BMP4 as a possible means of therapeutic intervention into the disease (Koli et al., 2006). This report into the role of Gremlin and BMP4 in idiopathic pulmonary fibrosis both highlights the potential use in certain cases of BMP4 as a therapeutic, but also highlights the advantage of using specific, targeted antibodies against BMP4 rather than using a natural occurring antagonist such as Gremlin which could have more widespread and unknown consequences.

BMP4 activity in proliferation of cells is closely linked to its known inhibitory effect on cell cycle activity. As a result BMP4, if correctly utilised could play a potential role in the control of some lung cancers by inhibition of cell cycle machinery. This has been seen in cell lines where up-regulation of p21 and p27 as a result of BMP4 inhibited the growth of the cancer cell lines Ghosh (Ghosh-Choudhury et al., 2000; Buckley et al., 2004). BMP4 has also been shown by Su et al. to be involved in the mediation of adriamycin induced premature senescence in lung cancer cells, and over expression of the BMP4 protein induced premature senescence of the lung cancer cells (Su et al., 2009). The specific role of BMP4 in other diseases including allergic inflammatory type conditions such as asthma will be expanded upon later. However this serves to show that the BMP4 induced biological responses are dependent upon the development of disease scenario encountered. As such it shows itself to be a highly important target for therapeutic intervention in certain areas of developmental insult or aberrant injury remodelling, yet as a potential therapeutic in its own right in other areas of injury or deregulated cell cycling and growth.

1.3.4 BMP receptors

There are two types of BMP receptors, type I and type II. Type I receptors for BMP include BMPR-IA and BMPR-IB and they are approximately 55kDa. The Type II receptor involved in BMP signalling is known as BMPR-II and is approximately 70kDa. Both receptor types are glycoproteins consisting of core polypeptides of 500-570 amino acids with short extracellular regions that are N-glycosylated and contain 10 or more cysteines that determine the superstructure of the final folded protein (Massague, 1998). Neither the type I nor type II receptors have any discernable structural features in the transmembrane or cytoplasmic juxta-membrane regions. BMPR-IA and BMPR-IB however contain a type I specific amino acid region called

the GS domain, which plays a pivotal role in the activation and activities associated with the Type I receptor. Both Type I and Type I receptors have a kinase domain that is known to concur with the canonical sequence of serine/threonine protein kinase domain (Massague, 1998). This is seen in type I receptors ability to phosphorylate their target Smads on serine residues, whereas type II receptors self phosphorylate as well as have the ability to phosphorylate type I receptors. BMPR-II also has a short C-terminal extension, though in human a variant also exists with an extended C-terminal region of unknown function and type I receptors have no C-terminal extension (Massague, 1998).

BMPR-1A and –IB are structurally similar. They have an extracellular domain which contains two β-sheets and one α-helix that are a central part in the specificity of the type I receptors (Miyazono et al., 2010). It is thought that there is an element of redundancy in signalling between the BMPR-IA and –IB receptors with overlapping functionality; however both are required for bone formation *in vivo*. With regard to the lung, both the type I receptors are to be found in the central regions of lung epithelium, but BMPR-IA is the only one found in the distal regions of the lung. Mice in which BMPR-IA has been completely silenced die at E9.5 due to defects in mesoderm formation (Miyazono et al., 2010). Specific deletion of BMPR-1A in mouse embryos via Cre-mediated knockout results in death by P1 or P2 with major defects occurring in lung morphogenesis, and showing reduced epithelial proliferation, morphological differences to healthy lungs and higher rates of apoptosis than observed in normal lung (Eblaghie et al., 2006). BMPR-IA signalling has also been shown to be required for successful vessel and atrioventricular endocardial cushion formation (Park et al., 2006). Type I BMP receptors are also subject to selective inhibition. Dorsomorphin for example has been shown to be capable of blocking BMP induced Smad1/5/8 activation (Miyazono et al., 2010).

BMPR-II is the main instigator of typical BMP induced activation of the Smad signalling cascade (Figure 1.2). It is a constitutively expressed and active receptor and upon ligand binding it is responsible for the recruitment of a type I BMPR, the formation of the hetero tetra complex and the phosphorylation of the GS domain of the type I receptor that is responsible for Smad activation. Loss of function studies with BMPR-II have shown BMPR-II to be vital in development and to play a role in a number of different human diseases. Mice without BMPR-II die by E9.5 due to defects in mesoderm formation during gastrulation. Loss of function of BMPR-II has been linked to pulmonary arterial hypertension (PAH) as far back as 1997. The BMPR-II gene promotes survival of the arterial endothelial cells due to its role in

developmental and repair pathway regulation in processes including apoptosis and the inhibition of differentiation. Studies in mice have shown that BMP heterozygous mice develop normally under unstressed condition, but that under inflammatory stress, they are more susceptible to right ventricular systolic pressure increases and vascular remodelling than homozygous mice. This shows that BMPR-II loss of function on its own is not sufficient to trigger the onset of disease and other environmental effects may be required for pathology to occur (Song et al., 2005b; Miyazono et al., 2010). Studies of human cells where BMPR-II has been silenced also show a link between BMPR-II loss of function and PAH (Teichert-Kuliszewska et al., 2006). The role of BMPR-II in PAH is discussed above (section 1.2.4).

BMPR-IA, -IB and -II are regulated by processes such as dephosphorylation and ubiquitination amongst others. Dephosphorylation, or the removal of phosphate groups, can prevent activation of the of the pathway be inhibiting the formation of the hetero-tetra complex. Ubiquitination is a process by which ubiquitin, a small regulatory protein, binds to protein and signals it for destruction via proteosome degradation and can be used to control the amount of the BMPR proteins available in a cell..Use of regulators of BMPR activity by inhibitors such as dorsomorphin in the instance of type I receptors and BAMBI which is a pseudo receptor for serine threonine receptors that can interact with both type I and type II receptors to inhibit signalling is a potential means for therapeutic targeting of bmp activity. However as BMPs are pleiotropic signallers, the same issue with blocking receptors lies with the aforementioned problems of using BMP inhibitors as with BMPR inhibitors. Using such inhibitors either long term or by constitutive activation of expression in even defined areas is likely to lead not only the blocking of specific targeted BMP induced problems, but also to the creation of an array of other issues based on the other functions disabled. However correct and efficient targeting of the secreted ligands and the receptors with specific antibodies holds potential, especially due to the fact that BMP ligands are secreted and therefore can be 'mopped up' and receptors are expressed at the cell surface and so may be more readily targeted than the intracellular signallers such as the Smads which require entry of the therapeutic into the cell.
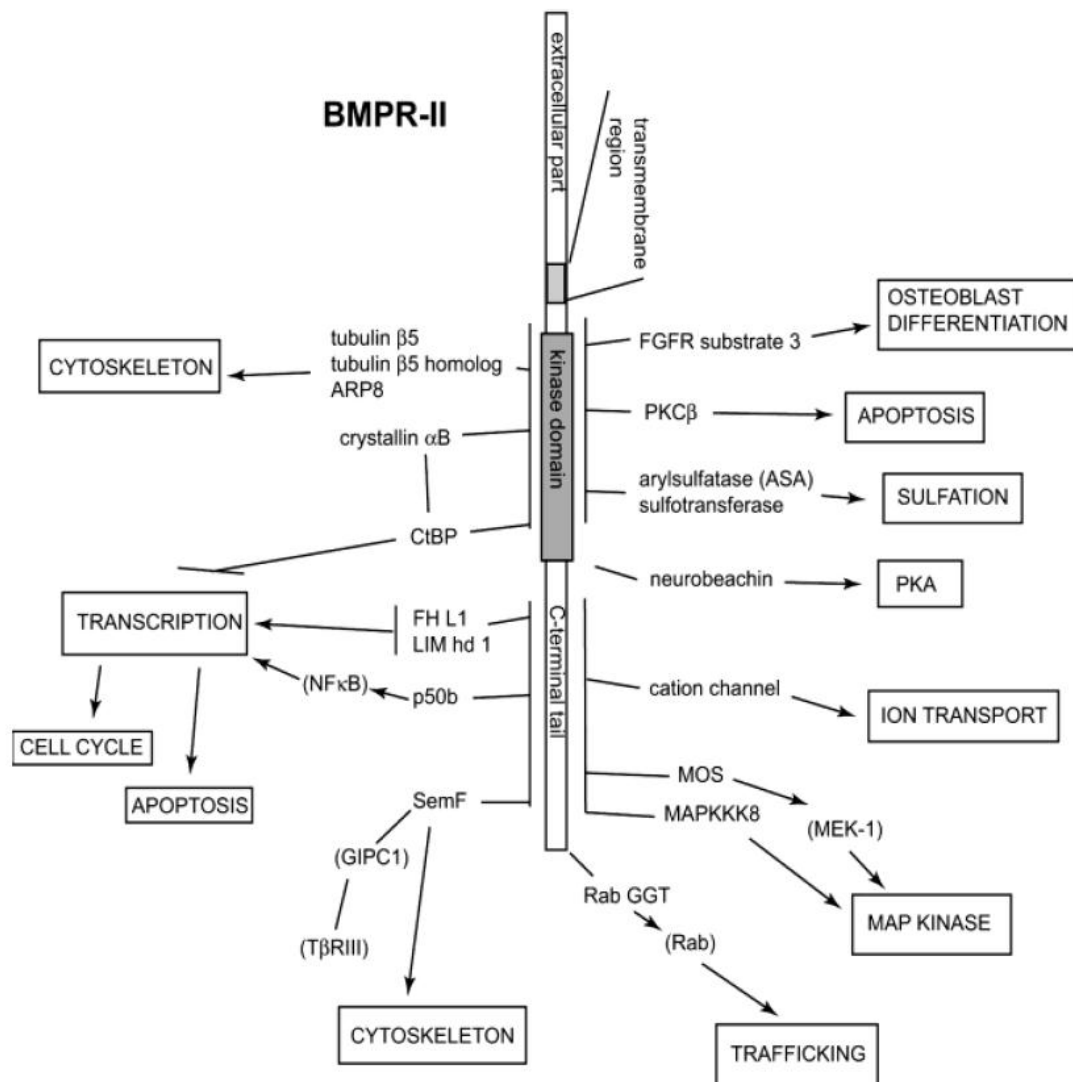
Figure 1.2 Strucure and regulatory mechanisms linked to BMPR-II and its ligands.

This figure shows both the structure and related functions of the BMPR-II, including regulation of differentiation, transcription, cell cycle regulation and apoptosis, trafficking, ion transport etc. The c-terminal region is not found on the type I receptor. Figure from (Hassel et al., 2004).

1.3.5 Smads

The Smads are the intracellular effector molecules of the BMP pathway and were originally described in Drosophila with identification of the protein Mad. In total there are 3 different functional classes of Smad protein and these are

1) Receptor mediated or Regulatory Smads (R-Smads) Smad1, Smad5 and Smad 8, which are activated by phosphorylated receptors and Smad2 and Smad 3 which are involved in TGF-β/activin signalling.

2) Inhibitor Smads (I-Smads) Smad6 and Smad7 which block the activity of R-Smads in the cytoplasm.

3) Co-Smad which is responsible for the ferrying of phosphorylated Smad complexes into the cell nucleus. There is only one member of the Co-Smad class known in mammals, Smad4.

(Kretzschmar and Massague, 1998; Massague, 1998; Karaulanov et al., 2004).

R-Smads are comprised of 2 domains, the N terminal and C terminal, also referred to as MH1 and MH2, which are joined together by a variable linker region and they play a vital role in mouse embryogenesis, eg Smad1 is essential for regulation of BMP mediated early lung development and Smad5 is required for endothelium-mesenchymal interactions that are necessary for survival of the epithelium (Yang et al., 1999). These domains are responsible for controlling the protein-protein or protein-DNA interactions of the Smad molecules. The MH1 domain is responsible for the DNA binding capacity of Smads and also plays a role in protein-protein interactions in the phosphorylated state. In the basal, or un-phosphorylated, state the MH1 domain is responsible for inhibition of the MH2 domains activities. It is also known that in Drosophila the MH2 domain can inhibit the DNA binding capacity of the MH1 domain, meaning that both domains are responsible for inhibiting each others function in the un-phosphorylated state (Massague, 1998). The highly conserved MH2 domain has the ability to activate transcription regulation but it does not bind DNA and plays a role more in the activation of the Smads by phosphorylation from type I receptors at the C-terminal SS(V/M)S motif, as well as binding to SARA and a number of nuclear receptors such as Fast, TGIF and Ski (transcription co-suppressors), CBP and MSG1 (transcription co-activators) (Massague, 1998; Wrana and Attisano, 2000). The linker region that joins the 2 domains can vary in both sequence and size. In the R-Smads it is the location of the

phosphorylation site for MAP Kinase. When phosphorylated here the R-Smad is no longer capable of entering the nucleus.

The R-Smads in their basal state are homo oligomers and are cytoplasmic. Upon ligand binding to the receptors they become phosphorylated and form heteromeric complexes with the Co-Smad, Smad 4. The afore-mentioned protein SARA (Smad Anchor for Receptor Activation) has been shown to play an important role in the phosphorylation process (Kretzschmar and Massague, 1998; Wrana and Attisano, 2000). The heteromeric complex is then transported into the nucleus where either alone, or in combination with a nuclear DNA binding protein, they regulate target genes through binding with specific elements. A DNA binding protein can be required due to the fact that due to the fact that the heteromeric complex can have a low binding affinity and low specificity on its own. The Smads can then positively regulate transcriptional activity through recruitment of co-activator molecules including CBP/p300 and MSG1 or negatively through recruitment of repressors including Ski and TGIF (Wrana and Attisano, 2000). In the nucleus R-Smads are subjected to continuous dephosphorylation which renders them inactive and leads to their transport out of the nucleus. They are also subject to ubiquitin-proteosome degradation that helps regulate the levels of R-Smads available in the cytoplasm at any particular time.

The Co-Smad, Smad4 is needed in most cases for trafficking of the R-Smad/Co-Smad complex into the nucleus. Smad4 can be found in both the nucleus and the cytoplasm of the cell and its stability can be selectively upgraded via sumoylation. It was initially reported that Smad1 does not require the presence of Smad4 to enter the nucleus, though Smad4 does require the presence of Smad1 or Smad2 in order to translocate (Massague, 1998) however subsequent work has shown Co-Smad can travel between the nucleus and cytoplasm due to a nuclear localisation signal in the N-terminal and a nuclear export signal in the linker region of the protein unit. It is thought that when the Co-Smad binds to the R-Smad complex in the cytoplasm that the nuclear export signal is blocked thereby facilitating transport into the nucleus (Derynck and Zhang, 2003). Smad4 also differs from R-Smads in that they are not susceptible to ubiquitin mediated degradation. As it is a highly important mediator of signalling, Smad4 is highly conserved and required for normal growth and development, e.g. specific knockout of Smad4 in heart tissue results in heart failure due to defects in cardiogenesis (Song et al., 2007).

The I-Smad proteins Smad 6 and Smad 7 are located in the cytoplasm of the cell. They play a major role in the inhibition of the BMP activated Smad pathway. Also,

they differ from R-Smads in that 1) they have no N-terminal domain and 2) their expression levels are highly regulated by external factors. Induction of these inhibitory Smads by BMP provides a negative feedback loop for inhibition of active BMP signalling (Derynck and Zhang, 2003). The I-Smads are not the only means of inhibiting the activity of the regulatory Smads. As an example, Smurf1 over expression is known to negatively regulate embryonic lung development through specific targeting of Smad1 and Smad 5 regulatory Smads for ubiquitination mediated degradation as a means to modulate the signals from BMP4 on the developing lung (Shi et al., 2004)

1.3.6 Id1

Id1 is a member of the Helix-Loop-Helix (HLH) protein family. There are 4 Id proteins, with Id1 being the original member of the family identified in 1990 by R.Benezra (Benezra et al., 1990). Originally Id1 was designated Id, and was named for both its functional properties as an **I**nhibitor of cell **D**ifferentiation and as an **I**nhibitor of **D**NA binding. HLH transcription factors have a vital function in regulating growth and differentiation in vertebrates and invertebrates and the entire family of proteins consists of over 240 family members, broken down into seven classes dependent on localisation, dimerisation ability and DNA binding specificities (Massari and Murre, 2000; Campuzano, 2001; Yokota, 2001). Id proteins constitute the Class V family and there are 4 distinct Id proteins, 1-4 respectively. All Id proteins share a highly homologous HLH region. Id proteins do not contain a basic motif region. With the exception of four small homology domains, which may indicate some other conserved functional commands, the Id sequences are predominantly unique. The HLH region is responsible for homo or hetero dimerisation but it is the basic region on basic HLH (bHLH) proteins that is in charge of sequence specific binding to 'E-box' DNA sequences. It is these E-box sequences that control the transcription of genes for terminal cell differentiation in a number of different cell lineages (Norton et al., 1998). The Ids function by binding to bHLH proteins by forming non-functional Id-bHLH heterodimers, as such they have the role of a dominant-negative regulator, removing the ability of the bHLHs to interact with E-box sequences. This was first evidence for a role in controlling differentiation was elucidated from studies in *Drosophila* by examining mutations in the *Drosophila emc* locus. *Drosophila emc* is a HLH protein that functions in the same manner as Id, binding to bHLH proteins to form heterodimers, preventing them from binding to

DNA and functioning transcriptionally. (Campuzano, 2001). Id1 has also been shown to have a much higher binding affinity for the ubiquitously expressed E protein family of HLH transcription factors than that of tissue specific HLH transcription factors. These E-proteins are themselves obligate binding partners for tissue specific bHLH factors. Therefore, by binding both ubiquitously expressed and cell type restricted bHLH transcription factors these it allows Id family members to regulate the transcriptional array of a vast number of cell types in different tissues and locations, while utilising the same basic mechanism. It has also hypothesised that E-box proteins chaperone Id proteins, which lack a nuclear localisation sequence, into the nucleus in order to increase the half life of the protein which is otherwise very short (Deed et al., 1996).

1.3.6.1   General Pathways associated with Id1 Protein

Id1 is associated with cell proliferation, cell cycle progression and invasiveness during tumorgenesis (Di et al., 2007). One pathway it has been shown to interact with in order to effect changes in these areas is the TGF-β pathway. Id1 has an ability to modulate a cells sensitivity to TGF-β: It was shown that Id1 disrupted the adherens junctions in TGF- β treated cells via down-regulation of E-cadherin, up-regulation of N-cadherin and redistribution of N-cadherin. This shows a role for Id1 in tumourgenesis via re organisation of the actin cytoskeleton and a breakdown of cell adhesion in response to TGF- β in human prostate epithelial cells, giving the hypothesis that intracellular Id1 levels might be the deciding factor in TGF- β going from growth factor to a tumour promoter during prostate carcinogenesis (Di et al., 2007). BMPs, members of the TGF superfamily, have also been shown to induce an Id1 response in a variety of cell lines and in embryonic stem cells. BMPS directly target and up-regulate Id as has been illustrated in various studies (Hollnagel et al., 1999; Ruzinova and Benezra, 2003). BMPs themselves are responsible for up-regulation of Id1 in epithelial cells, but TGF- β reduces levels of ID1 in epithelial cells.

Ids role in cancer progression is also well established (Fong et al., 2004). One of their major functions is regulation of epithelial cell phenotype, from differentiation through to proliferation through to cancer development (Coppe et al., 2003), and Id expression is concurrent with both cancer progression and prognosis. Examination of Id in cell lines has shown that as a general rule, it is strongly expressed in proliferating cells and is present at its lowest levels in non-differentiating and terminally differentiated cells. As well as strong induction by BMP proteins, generally mitogen and growth factor

stimulation has the same effect with the highest level of expression being recorded 1-3 hours after stimulation, as is the case with lots of other early response proteins (Norton et al., 1998).

1.3.6.2 Id1 in Embryogenesis and Cell Cycle

Id1 plays a major role in both embryogenesis and in normal cell cycle progression. It has been shown in mouse embryonic development to express unique and definite patterns of expression. It is present along with the three other Id proteins for neurogenesis in its own expression pattern and remains active after neuronal development. It is also expressed post-gastrulation in many different tissues which are experiencing morphogenic actions. After this it is also to be found in the endothelium surrounding the epithelium (Coppe et al., 2003). The Ids are known to play a role in cell cycling and differentiation. They are expressed at the beginning of cell cycle and peak again between G1 and S phase, before DNA synthesis begins to occur. Ids role in cell cycle has been observed experimentally by ectopic expression of MyoD and E47, bHLH proteins that function to stop proliferation, by causing a halt in the cell cycle at the G1 phase. Experiments have also shown that E2A (E12/E47) dependent transactivation of p21 is inhibited by Id1. It has furthermore been shown that an increased level of cell growth in the presence of ectopically expressed Id1 matches with inhibition of p21 expression (Norton et al., 1998). Additional studies, in keratinocytes and endothelial cells, have shown that Id over-expression is capable of delaying the senescence program (Nickoloff et al., 2000; Tang et al., 2002). Id1 levels have also been shown to be upregulated during differentiation, and have been shown to summit in alveolar cells that support the non-proliferating and well differentiated phenotype, which implies that they positively regulate alveolar cell differentiation (Liu et al., 2000). Furthermore Id1 was revealed to affect differentiation of Keratinocytes in epidermal wound healing, where it functions in transitioning sessile keratinocytes into mobile, migrating and proliferating keratinocytes during the repair of lesions and also during re-epithelialisation (Schaefer et al., 2001).

1.3.6.3 Id1 in Cancer

Id1 has been shown to play a major role in cancer progression. It is commonly over-expressed in tumour cells and is predominantly associated with aggressive, invasive and less differentiated tumour phenotypes. The level of Id1 proteins tracks with poor prospects and tendency to metastasize. (Langlands et al., 2000; Sikder et al., 2003; Di et al., 2007).

Of pertinent interest to our studies Id1s role in cancer has been linked to regulation of E-cadherin, as well as β-catenin, F-actin, EMT and fibrogenesis. Results show that E-cadherin switching in prostate carcinogenesis is promoted by Id1 over-expression. This is of note as adherens junctions are important in maintenance of cell to cell contact, with breakdown closely linked to tumour progression and metastasizing, as seen with the established link between prostate cancer and the down regulation of E-cadherin. The main proteins in adherens junctions include E-cadherin as well as β-catenin and α-catenin. Results suggest also that, in NPTX cells, Id1 over expression on its own didn't greatly affect the amounts of the adherens proteins present, but that when the cells with over expressing Id1 were also treated with TGF- β, there was a decrease in E-cadherin and α-catenin and an increase in β-catenin. Overall results imply that Id1 promotes cadherins switching which gives increased cell motility in TGF- β treated cells. The membranes of these cells were almost entirely devoid of the usual E-cadherin staining also; showing Id-1 over expression in response to TGF- β1 can bring about deconstruction of the Adherens junction complex (Di et al., 2007).

Id1 has also been purported to drive cancer survival in other ways (Figure 1.4). Id1 over expressing cells have been shown to resist TNF-α induced apoptosis by inactivating caspase 3 and Bax, along with up-regulation of NF-κB functional activity as well as that of Bcl-xL and ICAM-1 (Fong et al., 2004).

As a result Id1 is now demonstrating itself to be a promising candidate in targeted treatments of cancer. It therefore falls within our remit to evaluate its progression in growth factor induced damage in cells and its functional activity levels in order to help assess different pathways stimulated by addition of both transfection reagents and growth factors.
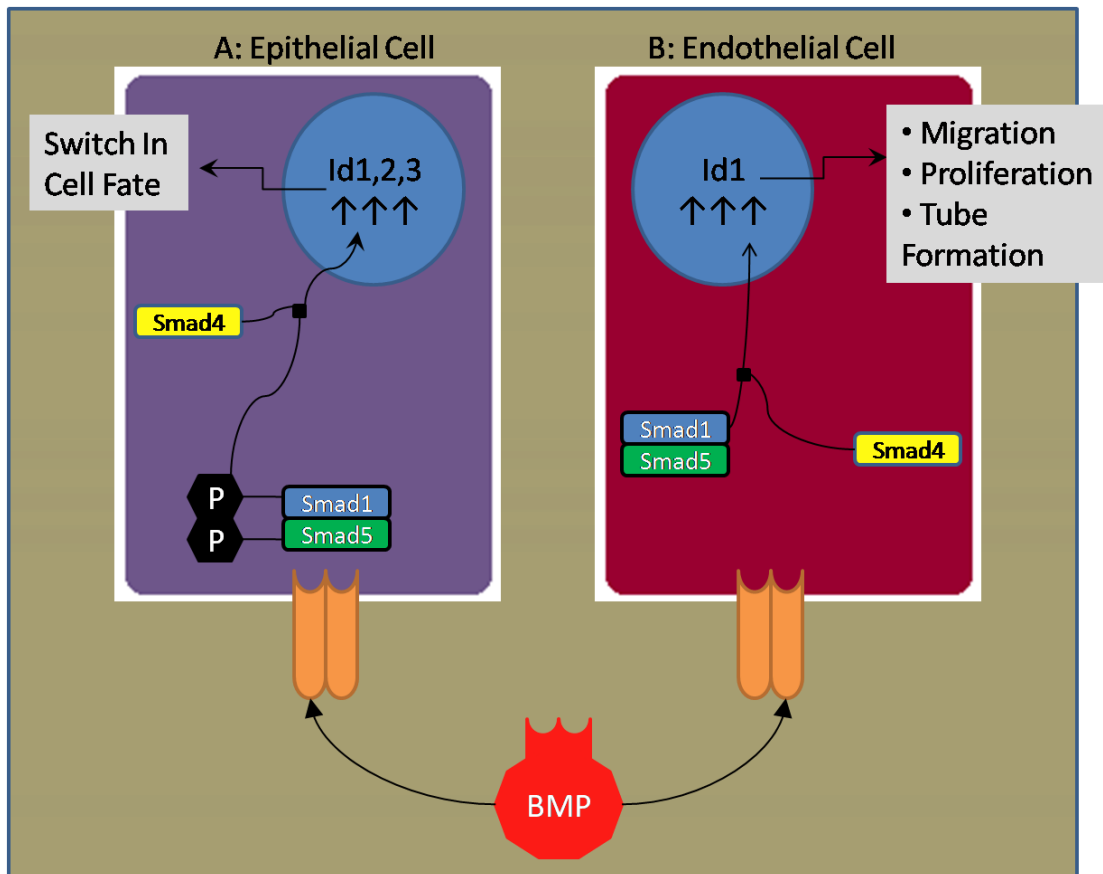
Figure 1.3 Id related BMP functions in epithelial and endothelial cells

In epithelial cells BMP triggers phosphorylation of Smad1/5 which bind to Smad responsive elements in the Id1 promoter and activate transcription which in turn leads to a switch in cell fate. In endothelial and epithelial cells it leads to cell migration, proliferation and tube formation. Figure adapted from (Ruzinova and Benezra, 2003).
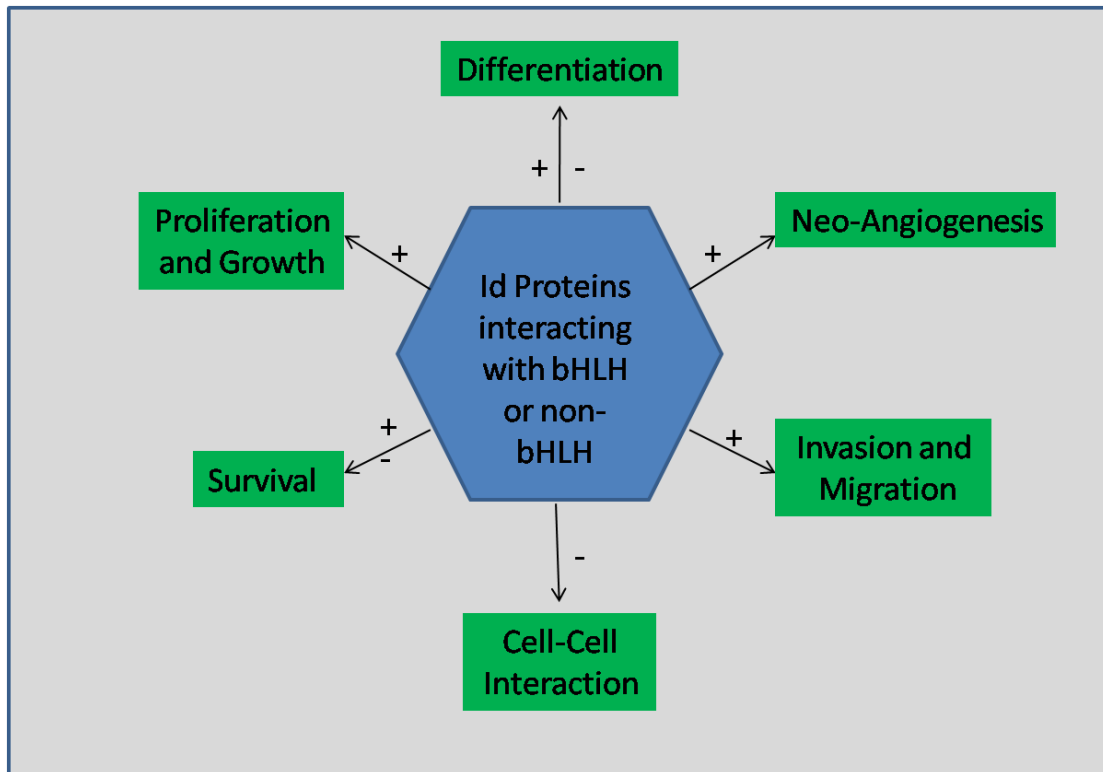
Figure 1.4 Id protein plays a major role in cancer metastatic progression.

Id proteins regulate pathways that are essential to the metastatic progression of cancer. Through an interaction with bHLH or non bHLH proteins, Id proteins have positive (+) or negative (-) regulatory roles in cellular pathways that are crucial to cancer metastasis. (Fong, S. et al. 2003).

1.4 E-cadherin and Snail1/Snail2

E-cadherin is the most extensively characterised molecular marker in epithelial cells. The full length protein is 124kD and it is an adherens junction protein found between epithelial cells that plays a major role in cell-cell adhesion (Masterson and O'Dea, 2007). It is located on the cell membrane and creates the tight junction by means of calcium dependent dimer interactions with E-cadherin molecules on adjacent cells. One of the major developmental roles of E-cadherin is embryogenesis epithelial to mesenchymal transition, or EMT. EMT allows tightly bound epithelial cells to dissociate from each other to differentiate into loosely bound mesenchymal cells. This function during embryogenesis plays an important role in developmental procedures such as gastrulation movement and neural crest formation (Katoh and Katoh, 2008). The process of EMT sees a class switch in the cadherin junction molecule form E-cadherin, which is associated with tightly bound adherens junction, to N-cadherin, which is found at the junctions of loosely bound mesenchymal cells. This sees the loss of the epithelial phenotype to a mesenchymal phenotype, and loss of cell-cell contact and polarity. Zinc fingered proteins Snail1 and Snail2 play a pivotal role in overseeing this class switch at the adherens junction during EMT through inhibition of the transcription of E-Cadherin (Schmidt et al., 2005; Tsuji et al., 2008). This is done by their binding of the proximal promoter region of the E-cadherin gene. E-cadherin function and EMT is also believed to play a role in a number of human diseases such as cancer where it has been linked to lung, breast, pancreatic and other cancers and inflammatory diseases (Schmidt et al., 2005). In tumourgenesis where E-Cadherin is down regulated by promoter methylation, and where upregulation of EMT inducers Snail1 and Snail 2 also occurs, it is characteristic of a invasive malignant cancer phenotype, as the loss tight junctions help tumour cells to proliferate and disseminate more rapidly, and associated with metastasis and a poorer prognosis (Masterson and O'Dea, 2007; Katoh and Katoh, 2008). As such when E-cadherin is present it is seen as a tumour suppressor and an indicator of tumour status. However the presence of E-cadherin inactivated via truncation as a result of tumourgenesis and the effect of this shortening of the full length functional protein on junction strength and stability is an important consideration when using E-cadherin as such a marker.

E-cadherin expression can also be affected during chronic inflammation resulting in loosely bound epithelial cells which can result increased cytokine signalling and an increase in the spread of inflammation to surrounding cells. EMT, discussed again later in certain diseases, where E-cadherin is down regulated and fibrosis occurs can

result in a pathological outcome in the lungs where epithelium is lost and replaced with fibrotic cells in what is essentially a faulty repair mechanism as seen in such as airway fibrosis resulting from lung transplant operations (Ward et al., 2005).

1.5 Delivery of therapeutics

Delivery of therapeutics can take many forms and can be practically related to the culture system, model or disease/damage targeted. Many forms of delivery are combined efforts. This consists of coupling one method of delivery, such as inhalation, with another system, such as a plasmid encoding a gene, in order to successfully target, deliver and achieve the desired therapeutic effect. While some forms of delivery are very specific as to the nature of the therapeutic they can deliver, others are capable of delivering numerous types of therapeutic compounds. Specifically this thesis is interested in the delivery of therapeutics to the lung and examines the feasibility of delivering DNA and protein based therapeutics *in vivo*. Delivering therapeutics to the lung *in vivo*, either for localised delivery and effect in the lung, or for systemic uptake, requires an understanding of the different methods for not only delivering compounds locally, but also the use of carrier compounds which can aid in the targeting, protection and dissemination of the drug as and if required. The benefits of targeting delivery to the drug to specific regions are outlaid in Figure 1.5. Some of the principle benefits include higher efficacy and lower drug loading leading to lower costs and less off target effects, improved deposition patterning and uptake.
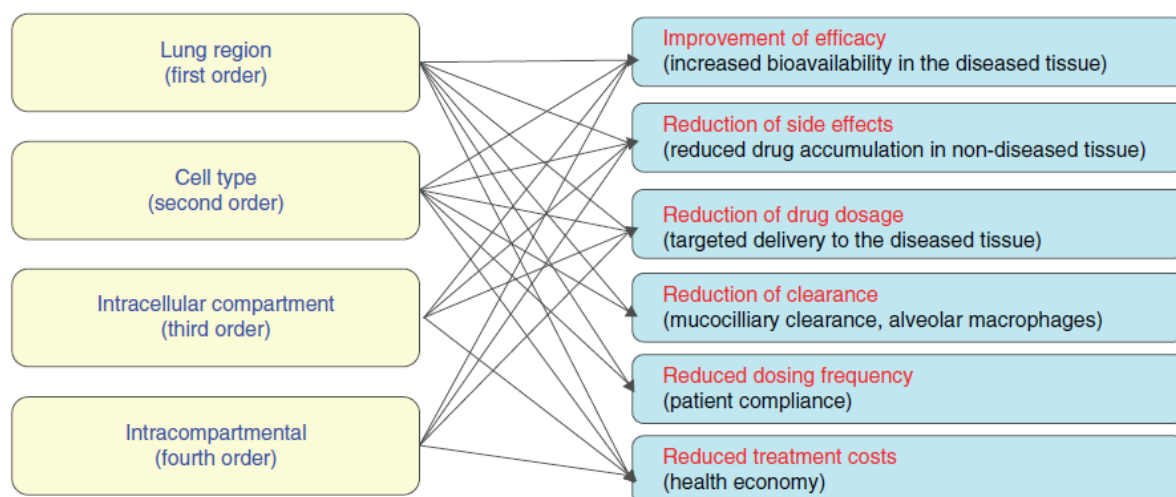
Figure 1.5 Order of targeting delivery to Lungs.

Targeted delivery of drugs to lungs, to specific cells within the lung, to inside the cells and finally to within the various specific compartments of the cells all add to the levels of complexity of targeted drug delivery. Depending on the requirement and the type of drug used not all orders need to be achieved. On one end of the scale certain drugs such as corticosteroids and bronchodilators need very little targeting with the lung, however genes therapies that require nuclear localisation within a certain cell type require a much higher level of targeting. The arrows in the above diagram show how achieving ever increasing levels of lung targeting from the lung region to specific cellular compartments within specific cells in the lungs increases the therapeutic and cost benefit of drug delivery (from (Aneja et al., 2009)).

The ways of introducing the therapeutics to the lungs are outlined also. For different therapeutics and different diseases, selective mechanisms can enhance the targeting of drugs *in vivo*. Some mechanisms are invasive and not suitable for repeat or frequent administration though for certain applications may be of relevance. Other methods require hospitalisation or physician direction. The ideal delivery system in most instances, however, would allow repeat, non invasive dosing by the patient.

1.5.1 Aerosol as a mode of delivery

Aerosols hold potential for the delivery of therapeutics to specific regions within the lungs, for systemic delivery throughout the body, and for targeted delivery of molecules to site specific regions within the body. The structure of the lung, as described earlier, lends itself to this method of delivery. It provides a target for delivery with an immense surface area designed for the exchange of solutes.

The development and assessment of drug molecules for the aerosol delivery to humans *in vivo* most commonly entails the delivery of the molecules to a small animal model in order to determine efficacy of aerosol delivery on the *in vivo* activity and stability of the delivered agent. Prior to the aerosol being available for inhalation to the animal it is first subjected to the flow dynamics of the chamber from which it is delivered. These characteristics can help determine the final Variable Mass Diameter (VMD) and over all Fine Particle Fraction (FPF) available for inhalation as its design must account for potential shear forces, aerosol collision and aerosol agglutination which can occur.

To this end a chamber system was designed for the delivery of aerosol to small animal models including, but not limited to, mice rats and guinea pigs. Our primary concern was to study effect of chamber dynamics on the aerosol that would be available for inhalation, in comparison to what was formed initially by the nebuliser on its own, that is, did we improve upon the nebuliser.

A design for a novel restraint was also included in this work. Most current restraints have remained largely unimproved upon over the period of the last 30 yrs. The basic model involves a cylindrical tube with space for the nose to exit at the top and a plunger behind to hold the animal in place. This results in an unnatural and restrictive position for the animal, with a potentially negative effect on the animals respiration in order to preserve nose only exposure. Animals can also become suffocated if they manage to struggle to turn around in the chamber. Aside from the ethical concern, the

loss of experimental animals can lead to statistical problems and can be costly depending on the treatment, cost of the animal and in experimental hours invested. As a result it was decided to design a novel restraint system that could more effectively and safely restrain the animal for the duration of any exposure procedure and that would be complimentary to the aerosol chamber.

1.5.1.1 Current Aerosol Generation Technology

There are a number of different types of chambers currently available, some with specific adaptations for the aerosol producing device. In choosing a device to produce an aerosol a number of different parameters need to be examined and ultimately one will provide the best answer to the delivery agent in question. In order to deal with clinical demands, aerosol devices should be aiming to decrease delivery time, deliver large doses and be capable of dealing with different viscosities and multiple drugs at the same time.

On the market at the moment there are a number of different types of aerosol producers. These include, amongst others, 1) Dry powder inhalers, 2) Pressurised metered dose inhalers and 3) Nebulisers.

1.5.1.1.1 Dry Powder Inhalers (DPIs):

These are amongst the newest members of the inhaler family on the market and include products such as the GlaxoSmithKline Diskus®. They are breath activated devices, requiring no propellant and are generally considered amongst patient groups as being easier to use than metered dose inhalers. DPIs vary in performance depending on manufacturer, operation techniques and drugs loading. They can be sold as single dose units where each individual dosage is loaded prior to inhalation, multiunit dose inhalers which contain multiple individually sealed units of drug dosages and reservoir multidose units which contain a large supply of the drug, of which a small amount is released upon each activation, with dose counters available on the multidose versions (Chrystyn, 2007). DPIs, due to the fact that they are breath actuated, require a relatively high inspiratory flow rate, thus precluding patients with severely limiting airflow restrictions, and they are generally also not recommended for use in patients under the age of 5 (Geller, 2005). Matching the correct DPI to the patient is also important as it will help improve patient compliance. Some DPIs utilise a higher airflow resistance than others against the inspirational flow in order to trigger device activation. This means that in a situation where a patient is using a number of

different devices, different deposition patters will emerge for the drugs dependent of the charge required to activate each one.

Other reasons for varying deposition patterns between DPIs are differences that occur in how different patients use the devices and also in the drug formulation (Martonen et al., 2005). Mid level to high resistance devices are generally more efficient at delivery than low resistance devices, but due to the requirement for high airflow, this can lead to greater inter and intra patient variations in deposition dependent on the exact way in which the intake manoeuvre was carried out. As regards to drug formulation, with or without excipient present, the powdered drug is formulated and engineered to present a specific aerodynamic profile or VMD. Where excipient is used, with the most common excipient being lactose, high shear mixing is used to blend the final powder. High shear blending results in the powders encountering a variety of different forces. The DPIs themselves also lend themselves towards being highly cohesive and adhesive in their release of the powder. Together this results in poor drug aerosolisation and less than optimal deposition patterning in the lung (Adi et al., 2008; Wagner et al., 2009).

Essentially DPIs provide a light, discreet and portable mechanism for the delivery of dry powdered therapeutics in patients who have a sufficiently competent inspiratory flow rate and have correct inhalation technique.

1.5.1.1.2 *Pressurised Meter Dose Inhalers (pMDIs)*

pMDIs consist of a small self-contained unit consisting of a canister containing propellent and drug formulation, a metering valve, an actuator and a mouthpiece. They are generally used by shaking the canister first to ensure good mixing of the drug and propellent before actuation of the canister to release the drug/propellent formulation through a carefully designed actuator nozzle. Aerodynamic forces within the nozzle disassociate the propelled mixture into an aerosol, while the propellent rapidly evaporates leaving only the drug formulation behind that is cooled by the evaporation of the propellant. The propellant used in pMDIs is hydrofloroalkane (HFA), which replaces CFCs out of environmental concerns. The change of propellent in the formulations has resulted different behaviour and deposition characteristics for different drugs, changing plume properties and particle size distribution profile of the generated aerosol (de Vries et al., 2009).

pMDIs are generally regarded as being the most difficult and inconsistent of the nebulisers, for a number of reasons. Delivery of therapeutics is carried out by the actuation of a charge, which in some pMDIs can be breath activated. This leads to a

high pressure release of the drug that requires careful timing and co-ordination on the part of the patient in order to ensure proper inspiration for the best deposition of the drug. In general the mode of actuation, whether breath or manual, and the accompanying high flow rate of the delivered aerosol has led pMDIs to being regarded as the least efficient and least consistent of the different available inhaler types. pMDIs generally do not come with incorporated dosage counters and so rely on patient tracking to count remaining dosages. They are generally over filled with drug, meaning that even if a patient count is slightly off, the individual should still be receiving medicine upon actuation. However comparative studies of different pMDIs with inhaled corticosteroids found that different pMDIs created significantly different VMD sized aerosol particles, with delivered dose quantity varying throughout the lifespan of the different devices (de Vries et al., 2009). This can in part be due to how the drug formulation and propellent are combined. If not correctly mixed prior to use, or in instances where inaccurate dose counting has been performed patients can receive an aerosol containing propellant only. The use of breath actuation can help improve the coordination of the patients' use of these devices, as does the use of a spacing chamber. However spacing chambers are not without issues, they are large and make the device both less discreet and less portable, therefore less likely to help with patient compliance. They are also prone to the build up of static charges and require cleaning in order to reduce this build up. They are also regarded as being very difficult to use successfully with young children (Geller, 2005).

However in spite of the problems associated with pMDIs they are still a highly utilised inhaler. They are, due to the nature of the concerns expressed above, restricted in their use to potent quick acting local drugs such as bronchodilators and corticosteroids. They are also unique in that pMDIs, unlike devices such as nebulisers, are required to be tested and approved as a joint drug-delivery system combination (Hess, 2008).

1.5.1.1.3 Nebulisers:

Nebulisers are clinically relevant devices capable of creating an aerosol suitable for inhalation for patients of all ages and sizes, for any disease severity and are actively recommended for patients on ventilation. Most of the modern devices for nebulisation are relatively small and portable and this facilitates their use both in clinical settings and in day to day life. The greater the level of convenience of use the greater the level of patient compliance with prescription protocols and an increase in the number of the devices in prescriptions. This greater convenience makes them more widely

acceptable to patients and therefore more likely to be prescribed for use with more and more medications. Another advantage with this nebuliser system is that it is possible to deliver a combination of drugs at the same time, reducing delivery time over all, and the amount of administrations a patient may have to make. In a laboratory setting this also allows for simultaneous delivery of different active agents to a particular system, such as a siRNA molecule in combination with an active protein molecule, reducing the amount of animal handling time and also reducing the amount of stress on the animal. Another advantage along this line is that it is possible with an inhaler to, in one sitting, deliver a very large dose of a therapeutic. This is due to the fact that a larger reservoir is all that is needed. DPIs for instance are limited in this fashion as although newer generations of devices are capable of delivering larger doses, they can require too many breath activations that have to be precisely co-ordinated to be an effective means of delivery. An example of this is inhaled tobramycin, which is a topical antibiotic for Pseudomonas endobronchial infections in cystic fibrosis. This antibiotic is delivered as a unit dose of 300 mgs which is impossible to deliver with a metered dose inhaler (Geller, 2005). As a lab delivery device also helpful is the fact that the therapeutic of interest can be delivered as a liquid or as a suspension, allowing a wide range of potential drugs to be examined without the need for reformulation.

There are a number of important reasons why a nebuliser was chosen as the most suitable instrument for the aerosolisation of therapeutics in this project. Chief amongst reasons is the fact that nebulisers are a clinical reality; they are used in hospitals and homes around the world with various different medications and meet most of the important characteristics of an ideal inhalation system as defined by Virchow et al in 2008 (Virchow et al., 2008);

Simple to handle-especially for children

Should possess control mechanisms which ensure:

-optimal respiratory flow at the time at which the dosage is triggered

-a correct inhalation manoeuvre

-allow the patient to verify successful completion of the inhalation manoeuvre

-Both the released active ingredient dosage and the deposition of the active ingredient in the lungs must be sufficiently high and reproducible.

-There is a need for a dosage encounter that counts not only the dosages but also the correctly executed inhalations which allow supervision of compliance

-Free of propellant gas and refillable

-Maintenance requirements should be minimal

The vibrating nebulisers overcome a lot of issues associated with other delivery devices. They have short nebulisation times, are easy to use and clean and are not overly expensive. They also avoid the problems of heating the drug or subjecting it to strenuous shear forces as seen in ultrasonic and jet nebulisers and as shown below, this makes them suitable for the delivery of liposomes and nucleic acids.

1.5.1.1.3.1   Important considerations and difficulties associated with Nebulisers.

Although there are many positive aspects associated with this technology, it is not perfect. While each nebuliser type on its own is characterised, there is highly variable performance efficiency between different types. This means that when a drug is being marketed as being suitable for nebulisation delivery, it should be tested in a single device which should then be paired with that drug to ensure consistency across doses and patients. This is because the amount of drug available for lung deposition will not be predictable unless the device has been studied with the drug of interest. Other factors such as fill volume for the reservoir all need to be considered. Another drawback with nebuliser technology is that nebulisers tend to be more time consuming than MDIs or DPIs, and therefore not necessarily always the best choice for certain types of treatment (Geller, 2005).

The specific drug formulation can also have a major impact on device performance, with it being reported for example, that nebulizer performance can be greatly improved by the addition of preservative to the drug formula as a result of its surface activity (MacNeish et al., 1997). Nebuliser efficiency is constantly being improved in efficiency in various different ways Figure 1.6.

The main types of nebuliser, ultrasonic, jet and vibrating membrane are discussed below.
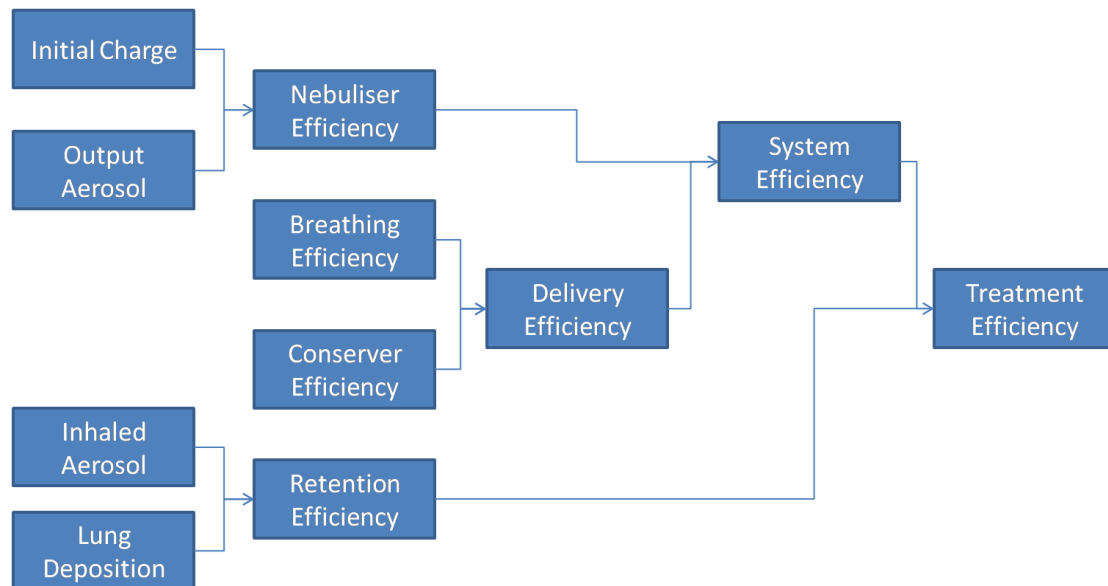
Fig1.6: Schematic of nebuliser performance efficiencies

Treatment Efficiency (TE) depends on system efficiency (SE) and Retention Efficiency (RE): TE=RE x SE. System Efficiency depends on Delivery Efficiency (DE) and Nebuliser Efficiency (NE): SE=DE x NE. Delivery efficiency (DE) depends on Conserver Efficiency (CE) and Breathing Efficiency (BE); DE=CE x BE. Nebuliser Efficiency is the ratio of output aerosol (OA) to Initial Charge (IA): NE=OA/IC. Retention efficiency (RE) is the ratio of lung deposition (LD) to Inhaled Aerosol (IA): (RE) =LD/IA (Chatburn and McPeck, 2007).

1.5.1.1.3.2 Ultrasonic Nebulisers

Ultrasonic nebulisers generate an aerosol through vibrating a piezoelectric crystal, converting electrical energy into ultrasonic waves. However a negative effect of these types of nebulisers is that they require 3.5-4 MHz vibration in order to sufficiently disrupt the liquid formulations into a respirable aerosol, generating a sufficient amount of heat that precludes the use of this system for the delivery of certain heat labile drugs proteins and liposomes, and are regarded as not suitable for the aerosolisation of suspensions (Ghazanfari et al., 2007; Shen, 2010) There is also a potential for the ultrasonic waves to deactivate drugs during nebulisation, though this has not seen with commonly used aerosol medications (Hess, 2008).

1.5.1.1.3.3 Jet Nebulisers

Jet nebulisers are powered by pressurised air travelling at high velocity through a venturi nozzle, generating an area of low pressure. Since the area of low pressure is less than that of the reservoir where the drug solution is stored, this drives the solution for aerosolisation to be incorporated into the jet stream where it is sheared into an unstable liquid film. The instability, due to large surface tensions, causes the film to disintegrate into droplet aerosol. This aerosol is then impacted upon a baffle driven by compressed air or oxygen that creates an aerosol of suitable size particles for inhalation (Lentz et al., 2005; Ghazanfari et al., 2007; Hess, 2008). The VMD of the particles reaching the lungs can be influenced by the humidity of the carrier gas being used. The use of solvent in the drug solution means that as the aerosol is created, the solvent evaporates, leading to a higher concentration of drug solute in the aerosol. The operation of a jet nebuliser requires a compressor, an air line and bottled gas and as such they are not overly portable. They also require equipment maintenance and cleaning in order to limit the opportunity for infection of the device. Jet nebulisers average a drug deposition of 5-25% of the given dose in the patients' lungs, with specific drug-device combinations being required to allow accurate gauging of drug dosing.

Due to the high pressures used to create the aerosol in jet nebulisers there is a risk of drug degradation linked to their use that may make them less desirable for certain applications. The use of the jet nebuliser for the delivery of 'naked' gene therapies results in sub-optimal dosing as a result of hydrodynamic shear. This necessitates the use of cationic lipids or other protective carriers to prevent the loss seen in DNA integrity. The breakdown in integrity is usually a result of a strand break in the phosphate backbone. This results in the conversion of supercoiled plasmid into an

open circle plasmid. Any subsequent breaks on the other double helix results in linearization of the plasmid which makes it more likely to end up as fragmented DNA by the time the aerosol is formed (Lentz et al., 2005). In comparison to the vibrating mesh nebuliser discussed below the jet nebuliser can be more destructive of nebulised drug. In a study looking at the effect on liposomes it was found that a vibrating mesh nebuliser Aeroneb Pro, in comparison to a jet nebuliser, the Pari-LC, had less negative impact on the stability of the liposomes examined and also that the vibrating mesh nebuliser liposomes retained more entrapped salbutamol than that of the jet nebuliser (Elhissi et al., 2007). It has also been shown in the delivery of rhDNase that although a jet nebuliser (Pari-LC) is comparable with the amount of active amount of Drug aerosolised, the vibrating mesh nebuliser (Omron Microair) was more efficient and required less time for nebulisation and delivery (Johnson et al., 2008).

1.5.1.1.3.4   Vibrating Mesh Nebulisers

Vibrating mesh nebulisers come in two main varieties, passive and active. An example of the active vibrating mesh nebuliser is Aerogens Aeroneb Pro, which is discussed in detail below. Aerosol droplet size, total aerosol output and FPF are all dependent on fluid physiochemical properties.

With vibrating mesh nebulisers, an increase in viscosity is desirable up to a certain limit but would not be recommended for delivery of liquids with a viscosity above 1,92cP. Nebulisers using Aeroneb Pro technology have previously been shown to have higher output rates than certain competitors such as the Omron Microair nebuliser which is a passively vibrating device, due to the higher energy input and the fact that the Aeroneb Pro mesh vibrations are active, permitting a more efficient ability to overcome the resistance of fluids to the shear forces applied. Compared specifically to the Omron Microair, the Aeroneb Pro was superior in terms of completing nebulisation in shorter times and producing higher aerosol output rates especially when viscosity was increased. Comparison studies found that increased viscosity of drug solution was more debilitating in the passive nebuliser and resulted in prolonged nebulisation times and poorer output compared to the Aeroneb Pro actively vibrating nebuliser (Ghazanfari et al., 2007).

1.5.1.2   Clinical and lab uses

The Aeroneb Pro is clinically operational, meaning the transfer of therapeutics from lab bench to bedside is easier as the therapeutics being tested will not have to be reconfigured, lyophilised or altered in any way by the addition of a propellant etc. to

allow use in a human *in vivo* setting. The advantage of an aerosol device like this, as previously mentioned, is that it allows for both targeted local and systemic delivery of a wide variety of therapeutics. The Aeroneb Pro has been used to successfully nebulise amorphous itraconazole (ITZ) as an antifungal agent in aspergillus infected mice, so as to directly target the affected region. Recombinant human DNase1(rhDNase) has also been nebulised using the Aeroneb Pro as means to evaluate the potential of aerosol delivery improving clearance of cisco-elastic secretins directly in the region affected in patients with cystic fibrosis (Johnson et al., 2008). The Aeroneb Pro has also been used for pulmonary drug delivery with aerosolisable nanoparticles in an ex-vivo model utilizing an isolated rabbit lung model. The nanoparticles used were investigated for stability and performance after aerosolisation where the results showed nebulisation as a potential mechanism for successful delivery targeting the lung tissue (Beck-Broichsitter et al., 2009). The Aeroneb Pro has also been utilized for the delivery of liposomes, where *in vitro* analysis found it to be a comparatively better than one of the main rivals, the Pari LC jet nebuliser, having a less disruptive effect on the liposomes and also having a higher rate of aerosol production (Elhissi et al., 2007).

Also, as stated, a major advantage of the Aeroneb Pro is its ability to deliver solutions where powders can be dispersed in water and delivered via nebulisation. Instances of such solutions that have been examined with this technology are solutions of nanoparticulate amorphous or crystalline tacrolimus-an immunosuppressive drug used in transplantation medicine. Current mechanisms of delivery include either oral or intravenous administration. The dosages needed for these mechanisms of delivery are poorly tolerated by patients and are not consistent in delivering an accurate dosage. This is due to either poor absorption of the drug in the gastro-intestinal tract and/or first pass metabolism, which varies from patient to patient. The solution of TAC comprising of TAC nano-crystals was shown to be successfully delivered to the lungs with the use of the Aeroneb Pro, and did so without the use of polymers, surfactants or propellants. Another example of an effective use of nebulisation to counter problems with other mechanisms of delivery, as mentioned earlier, is inhaled tobramycin, which is a topical antibiotic for Pseudomonas endobronchial infections in cystic fibrosis. Furthermore nebulisers can be used for a variety of drugs as effectively as other delivery mechanisms, case in point being studies by Cates et al that showed that short acting beta2 agonists delivered via either nebuliser or MDI/chamber are essentially equivalent in the treatment of acute asthma. Moreover, for outpatient COPD, 7 studies found that bronchodilator via nebulizer, MDI or MDI/chamber are

essentially equivalent (Geller, 2005). Another gain of the nebuliser system is that it can be used in combination with Heliox. This is a gas mixture of helium (60-80%) and oxygen, which is used to improve airflow in patients with partial airway obstruction. In patients with asthma, heliox has the potential benefit of being able to carry the nebulised medication further (than air or pure oxygen) into the distal airways during severe airway obstruction (Hess, 2008).

Hindi et al have also shown nebulised sustained release silver carbine complex loaded L-tyrosine polyphosphate nanoparticles as potentially translating into less frequent dosing of the antibiotic, which in a clinical setting would also help with patient compliance (Hindi et al., 2009).

1.5.1.2.1 *Systemic Delivery*

Aside from the localised delivery of therapeutics specifically combating lung related illnesses, the potential for systemic delivery of therapeutics is becoming clearer. The best example of this to date is the delivery of insulin via aerosol in order to remove the need for injections in diabetics. This particular project is covered in detail below.

1.5.1.3 **Mechanism of Action**

The Aeroneb Pro was the nebuliser unit all aerosolisation work was carried out with in this thesis. The Aeroneb Pro is referred to specifically as an actively vibrating nebuliser, as it contains a vibrating element which is activated by applying an electrical charge to it. Upon activation this vibrational plate responds by moving constantly, contracting and expanding. This creates a micro pumping action, propelling the domed aperture plate to move up and down. This domed aperture is the "Vibrating mesh" referred to. It consists of a small dome shaped plate with up to 1000 precision engineered holes which are tapered in shape, consisting of a larger diameter opening on the side acting as the medication reservoir, and a smaller diameter exit on the ventral surface where the aerosol is formed. It is the size of this exit diameter that determines the characteristics of the aerosol produced and the flow rate of the medication through the nebuliser, i.e., how quickly a fixed volume with specific characteristics can be nebulised. As the aperture plate moves up and down by a few micrometers, the tapered holes temporarily enlarge as the plate moves up, allowing liquid to enter, and then as it enters the downward motion the liquid is forced through the small exit on bottom of the plate beneath the reservoir, thus generating the aerosol and doing so without recourse to propellants or compressors which could interact or effect the aerosol. It also does this without producing heat, giving it a competitive

advantage over other types of nebulisers such as sonic nebuliser which do produce heat and are therefore unsuitable for certain applications where the therapeutic may be heat labile (J.B. Fink, 2001).

1.5.1.4 Aerosolisation chamber

The Chamber used in this project was designed especially for use in conjunction with the Aerogen Aeroneb pro. It was designed for use with nose only exposure restraints with mice, rats, guinea pigs and other small rodents. An important characteristic of the chamber is how it holds the aerosol in the time between the aerosols being generated and before it reaches the point of inhalation. There are a number of properties of the chamber which can affect this. One is to ensure that there are no dead spaces within the chamber where the aerosol can settle and not be reached by airflow through the chamber. Dead spaces can be caused by sharp angles or major intrusions into the chamber itself which would interrupt the circulation of air. The chamber design is symmetrical with 4 ports on the current design (vs. 8 on the original concept) for the delivery of aerosol (Chapter 5). Within the chamber there are a number of factors that will affect the behaviour of the aerosol. These are the rates of collision of aerosol droplets with each other, which can cause agglomeration and increase the FPF and MMAD and also result in the formation of droplets that fall out of the aerosol and deposit on the surfaces of the chamber, which can in turn trap more aerosol as it passes alongside these droplets. A way of controlling this is by monitoring the airflow within the chamber, which was a factor that we analysed. The positioning of the ports strategically centred vertically also helped ensure an even sized aerosol would be available for respiration without a bias for smaller or heavier aerosol particles. Due to the fact that the particles are in the chamber for a time period before being inhaled, the aerosol generated by the nebuliser was analysed for MMAD, FPF and respirable dose prior to being connected to the chamber, and subsequently the aerosol generated by the nebulisers was tested at the point of inhalation. Characterisation was carried out by laser diffraction using a Malvech Spraytech analyser. The chamber is a vital component in this aerosol delivery, proper characterisation enables the researcher to determine, in conjunction with plethysmography, not only the amount of aerosol available but the likely inhaled volume by the animal. The advantage of using a chamber system like this multifold, instead of a nebulised drug being only available to one animal in the case of a nebuliser with a spacer attached to the restraint, this allows for effective treatment of multiples of animals at the same time. It also ensures equal exposure to a dose. In the case of expensive proteins or other therapeutics this can

help reduce costs and also increases experimental repeatability. This also relates to the advantage of a nebuliser in a lab setting, such multiple exposures, reducing costs, time and drug expense are not possible with some other mechanism of delivery such as those associated with dry powder.

1.5.1.5 Restraint

The restraint is the perhaps one of the least prioritised components in relation to the restrained delivery of therapeutics to an animal model. Over time the generic restraint has remained largely unmodernised, and this appears to be more of a case of oversight than it reaching a finely tuned point in its evolution. Overall most restraints available to date had resembled a 50ml tube, with a small opening on the conical end for the protrusion of the animals nose, and a crude plunger system at the tail end to effectively squeeze the animal down to the bottom of the restraint so it could not back up the tube and negate the nose only element of the exposure. There are a number of serious design flaws in this design that we set out to address relating to the following areas:

1) Comfort

       A: Heat

       B: Positioning and Stress

       C: Animal Safety

2) Restraint

3) Ease of Handling for animal technicians

4) Guaranteeing nose only exposure

Comfort:

Heat-Restraints are generally made out of plexiglass type material that can be easily shaped to design for needs such as this. However, when an animal is restrained in a traditional restraint for a long period of time, the body heat given off by the animal has no vent through which it can dissipate away from the animal. This results in the animal quickly growing warmer in the chamber during exposure, which will affect plethysmograph readings such as rate of respiration and heart rate as it copes with this increase in heat. It can therefore affect how well it is exposed to the aerosol, as if the animal is increasing its rate of respiration in order to cool down, this can result in a shallower breathing pattern, effectively restricting aerosol deposition to only the upper regions of the airway. Due to the fact that the animal is breathing quicker, its inspiratory pause can be shortened, allowing less time for aerosol deposition in the lung. Although these changes can be quite small over a very short period or on a

single exposure, over the course of multiple or long aerosol exposure periods this could lead to a significant difference, further exacerbated in the case of animal models with a disease or damage induced in the lung already.

Positioning and Stress-Traditional restraints do not keep the animal (mice in particular), in a standard anatomical position. Due to the plunger like mechanism of keeping them in place they are tightly compressed in the restraint. This forces an unnatural breathing position on the animal, again potentially affecting the delivery of aerosol into the lungs as desired. This unnatural position can stress the animals, resulting again in increased heart rate and shallower heightened rate of respiration. Again in disease or damage models the effect of this may be amplified.

Animal safety- A problem with the generic restraint model is ensuring that the animal is effectively restrained in a position that is tight enough to ensure that the exposure remains nose only and that the animal cannot turn on itself, without applying to much pressure to the animal. If the animal manages to back up at all and turn on itself it can quite quickly suffocate itself, and if too much pressure is applied by the animal handler then the animal can either get limbs or tails trapped or damaged or may get crush injuries

Restraint-As addressed in the above points, the physical restraint of the animal is not in line with what like to be achieved. Most current models require a technician with a reasonable level of familiarity and competence with the restraints to rapidly and safely change over and restrain units. Also it was my belief that a more effective, technician and animal friendly, restraint was achievable that would be more effective at restraining the animal in a nose only exposure position without so many complications.

Ease of handling for animal technicians- Current restraints, though simple in design tend to be neither ergonomic or handler friendly. In instances where large numbers of animals need to be restrained for exposure or for other requirements, and especially in the case of disease bearing animals, safe ergonomic handling had potential to be greatly improved

Guaranteeing nose only exposure-This is vital for a number of reasons. In the case where plethysmography is taking place a tight seal is required in order to be able to gain the most accurate readings. It prevents loss of drug through the restraint. It averts deposition of aerosol in the eyes and on the fur of the animal. Rodents are habitual cleaners and will likely ingest any aerosol that lands on their bodies. It is also important to prevent deposition of aerosol in the eyes for a number of reasons. One is animal safety to prevent any potential drug interactions with the eye where exposure

has led to complications such as over dilated pupils (Brodie and Adalat, 2006) and the other is to ensure that any effect seen is due to the aerosol being inhaled and not due to absorption in through the eye, especially in instances where the therapeutic may be for systemic delivery.

As a result of this data I set about the design of such a restraint, keeping in mind other potential uses for such a system, such as injection and biopsy. In conjunction with designers from Buxco, we fabricated such a design that is now being considered for general production and sale (Chapter5).

1.5.2   EGTA

Ethylene **G**lycol-bis(β-aminoethyl ether)-N,N,N',N'- **T**etraacetic **A**cid (EGTA) is a chemical known for its ability to modify paracellular permeability and enhance gene and drug transfer to cells. It is a poly amino carboxylic acid and functions as a calcium chelating agent giving it the ability to open or loosen tight epithelial junctions in a transient and time dependent manner, and this has been well catalogued both *in vitro* (Martinez-Palomo et al., 1980; Denker and Nigam, 1998) and *in vivo* (Chu et al., 2001; Johnson et al., 2003). EGTA has the capacity to do this with minimal toxicity to the lungs, meaning that its toxicity need not be a rate limiting factor for delivery as can be seen with other chemical delivery aids (Chu et al., 1999; Johnson et al., 2003). It is very similar to EDTA, a more commonly known chelating agent, except that it has a higher affinity for Ca2+ molecules than $Mg2^{+}$ ions and has been shown to exhibit a less toxic profile (Ortega et al., 1989). EDTA, as well as being more toxic than EGTA, is also less effective at disrupting epithelial tight junctions (Chu et al., 2001). This is particularly of note as EDTA has previously been delivered *in vivo* to human normal and cystic fibrosis patient lungs which resulted in no significant differences noted in either lung function or in the growth of *pseudomonas* and no other determinable lung toxicity (Hillman and Twigley, 1984; Brown et al., 1985)

1.5.2.1 EGTA and Barriers to Drug and/or Gene Delivery

In damaged and diseased lungs, and even, in the situation where systemic delivery through the lung is being examined, in healthy lung, there are a number of general barriers to gene and drug delivery to the surface of the epithelium allowing for successful targeting of either the membrane or specific receptors. These barriers include indiscriminate barriers such as the glycocalyx, the airway luminal contents and the inflammatory response, and more specific defences such as cell type specific

barriers and barriers targeting specific sorts of vectors. In certain disease and damage models such as cystic fibrosis the expression of functioning apical membrane receptors can be greatly reduced or entirely eroded, reducing the number of binding sites for vectors dependent on receptor mediated endocytosis for successful integration into the target cells. Alongside this vectors or drugs can be met by a decreased capacity of the cell itself carry out endocytosis and also some vectors, especially in the case of retroviral, AdV and AAV, encounter post nuclear entry defects. Taken together in combination, these barriers provide a challenging problem to overcome in order to successfully carry out delivery to the Airways (Johnson et al., 2003).

In general most initiatives to target this defence involve 'designer vectors'-vector modification as a means to bypass the defence elements (Kreda et al., 2000; Kobinger et al., 2001). However EGTA shows another way to achieve the goal of bypassing elements of the defences. By opening and loosening tight epithelial junctions it exposes receptors located on the basement membrane of the epithelial cells and the cells below in the endothelium, opening up a far larger surface area with a greatly increased number of receptors available for targeting, and has also been shown to work *in vitro* and *in vivo* (Johnson et al., 1998; Chu et al., 2001).

1.5.2.2   EGTA Use In Vitro

A large number of studies have been carried out examining the effect of EGTA on cell lines and undifferentiated cells. A549 epithelial cells were utilised to examine whether or not EGTA increased the effectiveness of AdV transfer of a gene, in this instance a Luciferase reporter construct, into a cell line. The use of EGTA resulted in a 600% increase in the level of reporter detected in the cells treated with EGTA and then the AdV construct versus the cells treated with just the AdV construct (Myles et al., 2002). The same study also treated fetal distal lung epithelium cells and primary human airway epithelium cells ± EGTA with AdV *lacZ* and across the board it resulted in a significantly higher level of expression when EGTA was used to pre-treat the cells. In a more detailed look at the mechanism of action, it was concluded that while EGTA does loosen epithelial tight junctions, there may also be other mechanism at work. This was elucidated by growing airway epithelial cells on plastic at very sub-confluent levels. Again, EGTA pre-treatment significantly increased the level of Luciferase expression compared to the no EGTA controls. This means that in a situation where tight epithelial junctions were not a major obstacle to successful transfection, use of EGTA still enabled higher levels of transfection (Myles et al.,

2002). Of particular interest was a similar study carried out using NHBE cells, where EGTA pre-treatment was again determined to be capable of significantly increasing expression levels when the cells were subsequently treated with an AdV construct (Chu et al., 2001). Cells which had CA^{2+} free media added before treatment, which would result in a reduction of the overall available Ca^{2+} available to the cells, also resulted in increased levels of AdV transfection. The cells used were polarised NHBE cells grown in ALI, of the same type used in this study.

1.5.2.3 EGTA Use *In Vivo*

Due to EGTAs success in *in vitro* conditions a natural progression would be to consider it as s potential transfection reagent for human use *in vivo*. Prior to this it is important to study its effects in either *ex vivo* and/or animal models. As such a study was carried out (Johnson et al., 2003) examining the effects of EGTA compared to a PBS control and a number of Medium Chain Fatty Acid (MCFA) transfection reagents, Sodium Laurate (C12) and Sodium Caprate (C10) which act as non-ionic surfactants and have been shown to work *in vitro* by the redistribution of Claudin1 as a means to increase paracellular permeability (Coyne et al., 2000). Examination of the effects of EGTA showed that it triggered a significant neutrophil response and increase in pro-inflammatory cytokines (Table 1.1). It also led to a mild level of inflammation but did not affect airway responsiveness.(Johnson et al., 2003).

Pre-instillation into mouse trachea of EGTA prior to treatment with an AdV-β-Gal construct significantly increased reporter uptake into the airway epithelium (Chu et al., 2001). From studies on cells lining human airway epithelium it was determined that the increase of transfection by the AdV vector *in vivo* was due to an increase in availability of internalising receptors that were exposed on the basolateral surface of the cells lining the airway epithelium by the EGTA loosening the tight epithelial junction, thereby providing access to the vectors to these otherwise hidden receptors (Pickles et al., 1998; Walters et al., 1999). Myles et al also showed this successful increase in CD-1 mice *in vivo* by utilising EGTA prior to vector treatment (Myles et al., 2002). Studies of EGTA in Humans *in vitro* studies with EGTA have shown also that EGTA has the capacity to change the physiochemical properties of M1/MUC5AC, which compliment earlier canine studies *in vivo* which suggest that it can also alter the solubility of the respiratory mucous (Coles et al., 1982).

Toxicity Profile Of EGTA	
In vitro	
Histology	No change
LDH	No change
P. aeruginosa/IL-6	No change
P. aeruginosa/IL-8	Increased
In vivo	
Wet-to-dry ratios	No change
BAL fluid	
Murine Albumin	No change
LDH	No change
Cell count	Increased
MIP-2	Increased
mKC	Increased
mTNF-α	No change
mIL-6	Increased
mIL-1β	Increased
Histology	Mild
Airway Responsiveness	No change

Table 1.1 Toxicity profile of EGTA

(Adapted from Table2, (Johnson et al., 2003)). Summary data for toxicity induced by EGTA administration relative to vehicle (PBS) control.

1.5.3 Particle mediated gene transfer/Particle bombardment

Particle mediated gene transfer is a method for the delivery to cells of exogenous materials, such as proteins, DNA, RNA or chemicals. It is done by adsorbing the exogenous material onto inert metal particles and physically shooting them under high pressure through the cells surface and into the cytoplasm and/or nucleus of the targeted cells. The method was first derived in 1987 by Klein et al as a way to transfect plant cells with foreign DNA, specifically as a means to avoid the limitations of host-range restrictions found with *Agrobacterium Tumefaciens* (Klein et al., 1987), with *A. Tumefaciens* for example, only naturally able to transfect DNA in dicotyledons, and many of the main food plants and cereals mass produced such as grain crops are monocotyledons. *A. Tumifaciens* is a gram negative bacterium that naturally infects over 140 species of dicot plants and where no host restrictions were present, was successfully used to transfect plants with plasmids of interest since Schell J and Van Montagu M published their work on the Ti plasmid in 1977 (Schell and Van Montagu, 1977). It was also designed with the idea of bypassing problems associated with protoplast regeneration, which was both more timely and painstaking. Most crucially at the time it provided the potential for the successful transformation of important monocotyledons such as grasses and grains which hitherto had been impervious to other methods of genetic manipulation. Zelenin et al first demonstrated this successfully by showing transformation of *Hordeum vulgare* L. (Barley) by early 1989 (Zelenin et al., 1989). Utilizing chimearic constructs of Beta-glucuronidase (GUS) (Colour metric- transfected cells stain blue) and Neomycin phosphotransferase 11 (NPT2-confers resistance to a wide range of aminoglycoside antibiotics such Kanamycin and Geomycin and G418 by phosphorylating them) under the control of either the Agrobacterium T_R 1'2" promoter or the Cauliflower Mosaic Virus 35 S Promoter.

The method was initially published by Klein et al in 1987 (Klein et al., 1987) as a mechanism to transfer genetic material into epidermal cells of *Allium cepa* (Onion). It was a crude system involving a modified pistol, a vacuum and tungsten powder as the transfer material to carry the DNA to the target site. Essentially a firing pin was triggered, igniting gunpowder which then shot the bullet coated with DNA coated tungsten microparticles as far as a stopping screen, stopping the bullet but allowing the microparticles to continue. Though it destroyed the central region of the epidermal layers targeted, it was successful in transferring the genetic material into the halo of cells surrounding the blast site as shown by the expression of viral inclusion bodies

after transfection with Tobacco Mosaic Virus and of an increase in CAT (chloramphenicol acetyltransferase) activity after bombardment with p35S-CAT plasmid.

There were a number of serious limitations with this technique as regards its suitability for the transfection of mammalian cells and tissue. Though the force of the bullet carrying the DNA could be modified by altering the amount of explosive propellant used it was nonetheless not as controllable as desired. The tungsten particles used would also prove toxic to many cells types. As soon as late 1989 however the first reports were published with successful transfection of mammalian NIH 3T3 mouse cells by the pSV3neo plasmid (G418-resistant) (Zelenin et al., 1989). In this instance tungsten particles were again utilized as a microcarrier for the DNA. Stability of the transformed murine cells was analysed by culturing the cells in G418 containing medium for a period of 3 weeks.

Two years later the same group published data showing successful transfer of the CAT enzyme gene, under 3 different promoters, both into ex-vivo tissue samples of mouse and rat liver, kidney and mammary glands (Zelenin et al., 1991). They also showed successful transformation of liver cells *in vivo*. This was done by opening the abdomen, then exposing and elevating part of the liver with the use of surgical pads. The remainder of the animal was shielded from bombardment by means of plastic sheeting and the liver was then bombarded before being repositioned within the animal for 24 hrs before harvesting. In all of the tissue types, *in vivo* and *ex vivo*, CAT activity was detectable

As the technique advanced the basic principles remained the same, but the mechanisms were designed to be better regulated. One of the most significant modifications was the substitution of a helium blast mechanism in the place of the gunpowder discharges. Now inert helium gas is pumped into a chamber sealed with a rupture disk. These rupture discs are designed to withstand a certain defined pressure, after which they will give way and allow a sudden discharge of built up gas and subsequently project the macrocarrier. The macrocarrier is a disk that was incorporated to replace the bullets used in the earlier set up. This macrocarrier is itself coated with a suitable Microcarrier. Most of this was pioneered in 1991 (Williams et al., 1991) with successful expression of foreign genes in murine liver and skin cells. In this instance human Beta Actin promoter was paired with Firefly Luciferase to allow for visual detection of successful transformation. They also managed to modify the device so it could be handheld and used without vacuum so as to allow easier use in the bombardment of skin *in vivo*. In this study a non replicating promoter was used

and it was noted that for skin cells treated *in vivo* detection lasted approx 3 days, the brevity due to the natural cornification and sloughing of the cells as they matured. However they reported detection in the liver up to a period of 23 days. It also displayed very little damage to the soft internal organs targeted.

More modifications of the technique have taken place as requirements for more selective control have materialised and the technique itself has grown in use from just its envisioned use of transforming plants to gene-gun immunisation with DNA as a powerful mechanism of vaccination against infectious diseases and tumours (Seder et al 2000). It has also been employed in the biolistic delivery to live embryos initially using the PDS-1000/He system from Biorad (Zelenin et al., 1993) and later via a version which is a pneumatic capillary gun, using multiple plasmids targeting the same cells to both "knock in" and "knock down" specific genes leading to huge potential in animal models (Shefi et al., 2006). In 2005 it was shown that epidermal biolistic delivery help reduce allergic sensitivity, possibly as a means of controlling diseases such as asthma (Kendall et al., 2006).

Gold has now, especially in mammalian system, replaced tungsten as it exhibits less cellular toxicity than that of tungsten and is inert in mammalian systems. It also has a high chemical stability, is a dense material and has a high affinity to biomolecules. Gold molecules above 2nm in diameter have been shown, even in an inflammation stimulating environment, not to induce toxic or adverse effects, with particles smaller than this potentially interacting with DNA in the cell to cause adverse toxic effects (Brandenberger et al., 2010) However any unnecessary exogenous material can potentially lead to unforeseen stresses or complications and as result would be less desirable as a medical tool for targeted delivery. Work by Lian et al has shown that intracellular delivery can be achieved by bombarding cells or tissues with accelerated molecules or bacteria without the need for carrier particles and Bombardment has also been carried out using no carrier on cells in culture, including primary cells and tissue explants using PDS-1000/He system from Bio-Rad and used successfully in the delivery of plasmid DNA and protein (Lian et al., 2007).

This has lead to a progression whereby DNA can be projected into cells without the need for not only such a carrier but without the restrictions of vacuum and large fixed devices by utilizing a portable endoscope device (O'Dea et al., unpublished data).

The device utilized in our Lab was the commercially available Helios pds1000 from Bio-Rad. This particular system worked as follows. A disc macrocarrier is projected at force down a short barrel until a stopping screen is reached, this retards the progression of the macrocarrier disc, but the microparticles get dislodged from the

surface of the macrocarrier and continue on through a vacuum until they reach the target site (Figure 1.7). This mechanism allows for the control of several different variables allowing the optimisation of the technique between different cells types. One can control the pressure of the Helium blast, the size and type of microcarrier used, the vacuum pressure in the chamber and the length of distance from the stopping screen to the target site, all of which impact on the force with which the target cells are exposed and also on the surface area exposed.

The purpose of this work was multifold. We wanted to be able to quickly insert various plasmids into different cell lines that were present in the lab to analyse the effects of the encoded DNA. We also wanted to compare the technique directly with other methods of transfection which were commercially available for success rates. In particular we were interested in being able to successfully transfect primary cells with our plasmids of interest using a physical method and therefore not jeopardising their characteristics by using chemical or viral transfection methods or antibiotics. The last purpose was to gain a further understanding of the technique with a view to examining the potential for a different commercially viable and hospital friendly device that could be used for targeted drug, protein or DNA delivery.
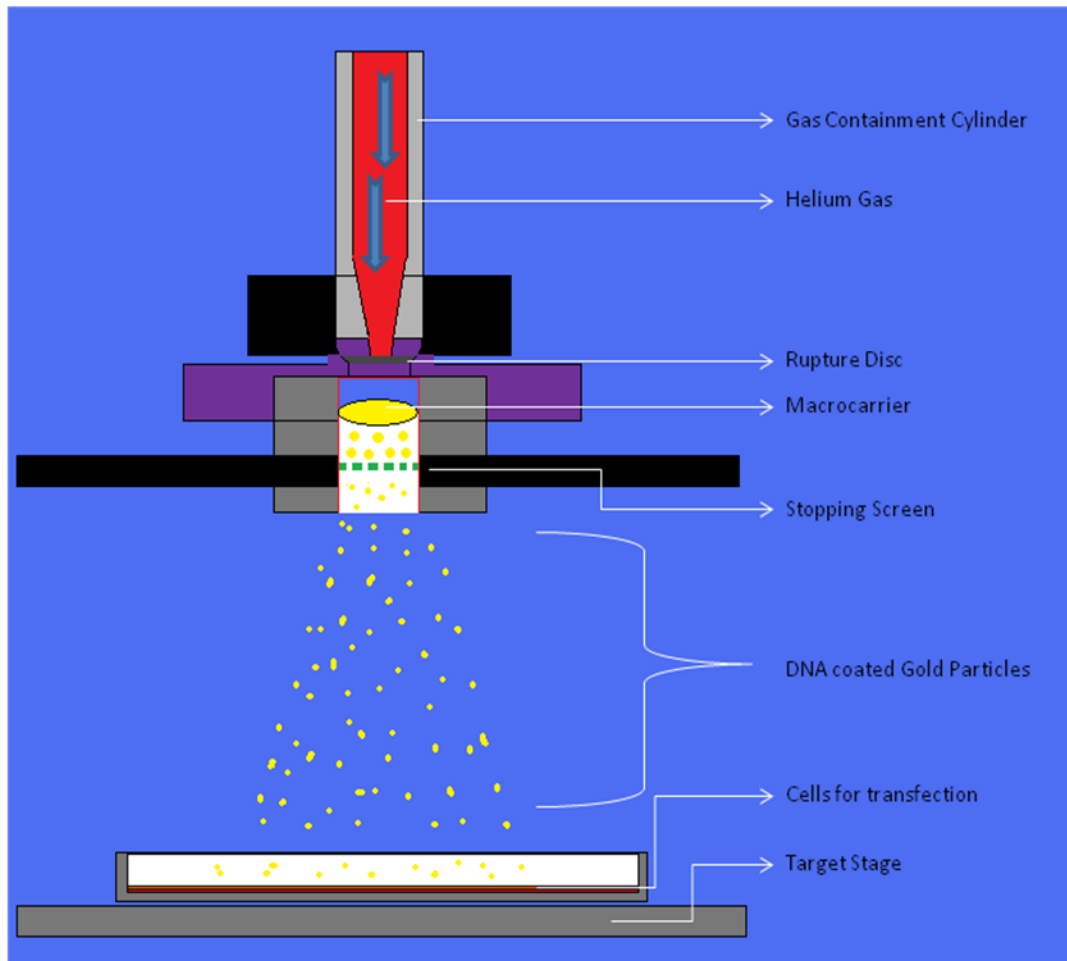
Figure 1.7 Helios pds1000 from Bio-Rad (top) and Schematic (below)

1.6 Insulin as an example of a model therapeutic for inhaled therapeutics.

Insulin is the best example to date of a protein based inhalation therapeutic brought to market. It is a 6kDa protein used for the treatment of type I and type II diabetes, with a growing market. Insulin is required by diabetics in order to control both their blood sugar levels and also the HbA1c, or glycemic control, levels. Insulin use for the treatment of diabetes dates back to the 1920's and its widespread use has led to its position as first amongst proteins on a number of fronts. It was the first protein molecule to have its primary structure fully analysed, the first to be fully synthesised, the first to have its 3D structure mapped and the first biotech product to be sold on a large scale.

Currently diabetics control their blood sugar levels via daily injection routines of insulin or by use of an insulin pump, which allow precise dosage levels to correct for food ingested and maintenance of blood sugar levels, down to fractions of $1/20^{th}$ of a unit in the case of pump users. The study of inhaled insulin being used as an inhaled therapeutic is not novel and dates back to experiments in 1924 (Heubner W, 1924). This has progressed to large scale human clinical trials by a number of companies in an effort to bring the aerosolised form to market, culminating in the launch of the inhaled insulin therapeutic Exubera® in the beginning of 2006, following approval by the FDA and the European Union Drug Advisory Board (Lenzer, 2006). It was brought to market by Pfizer, in partnership with Nectar. By the time it reached the market, inhaled insulin had become one of the most comprehensively tested drugs to be approved, and many other major biopharma companies such as Novo, Eli Lily and Mannkind amongst others, were also carrying out extensive clinical trials at different phases of development. However in little over a year and a half, in October 2007, Pfizer announced it was withdrawing the drug from the market and ceasing production due to unsuccessful uptake in the market (Siekmeier and Scheuch, 2008). This poor performance of what had been a highly anticipated "block buster" drug saw nearly all the other companies pursuing the inhaled insulin market cease all operations, trials and development related to the product. This meant that in less than 24 months inhaled insulin went from being potentially a major market force and paving the way for inhalation therapeutics to being one of the costliest exercises in failed drug marketing in history (Heinemann, 2008).

 There are a number of different reasons for the failure of Exubera as a drug product, and they are linked to both clinical concerns as well as poor marketing strategies.

Primary amongst these is that there was no perceived need for inhaled insulin, with s.c. insulin being an established and successful mechanism of disease control that is already in place and well understood by both clinicians and patients. This was a concern even amongst the members of the FDA advisory panel on the drug, with the acting chair of the Exubera review committee voting against the drug due to concerns over erratic absorption profiles and complex dosing conversions (Lenzer, 2006).

Erratic absorption of the drug was identified as a problem in patients with chronic lung diseases such as emphysema and asthma where reduced uptake of the drug was seen, and in smokers where tobaccos smoke induced damage saw more rapid uptake of the insulin into the system, contra indicating these groups of patients for the drug. Patients suffering period of lung infection and those exposed to even environmental tobacco smoke could also suffer altered absorption profiles, and exercise after inhalation of the insulin could result in increased absorption rates into the blood system from the lung and increase the risk of a hypoglycemia event. The dry powder formula the drug was released in offered certain advantages to patients in terms of drug stability, allowed for an uncomplicated inhaler device, and potentially the use of more complex formulations in the future. However a liquid drug would have allowed for more accurate dosing at the cost of requiring a more sophisticated nebuliser device.These issues are not just specific to the delivery of insulin and provide valuable information in dosing strategies for all drugs targeted for lung delivery for either local or systemic effect.

There were also a number of side effects associated with the inhaled insulin. Common were coughing, sore throats, shortness of breath and dry mouth after administration. Also seen throughout the clinical trials was a loss of FEV1, which members of the FDA advisory panel that voted against the initial approval of the drug voiced amongst their concerns, citing that reversals of decreased FEV1 in type I diabetics was not convincing (Lenzer, 2006). However over a two year period, although Exubera users did show a decrease of FEV1, it was on average only 20mls, measured against an average baseline of 3 litres. It was also shown to be a static, non progressive decrease that was reversible upon cessation of delivery of the drug product (Selam, 2008).

Also a potential issue with inhaled insulin was the risk of lipodystrophy occurring in the lung. Lipodystrophy occurs in over 30% of patients on s.c. insulin and is a result of insulin's anabolic activity at the site of injection, promoting protein and fat formation. Other issues with the drug involved the initial cost of the device and the training required for each patient to ensure that they were properly administering the insulin for maximum benefit. As there was no critical need for inhaled insulin the

additional costs over injections and lack of accuracy compared to pumps reduced the willingness of clinicians to prescribe Exubera, especially in line with the time and costs associated with the training of each patient. Inhaled insulin was also perceived as being more time consuming than injection, requiring blister insertion, air pump activation and inhalation of the standing cloud taking up to minutes to complete depending on the required dose.

After the launch and subsequent withdrawal of the drug a number of important considerations came to light with respect to the potential of inhaled insulin as a drug. One of the initial general concerns relating to the product was that the use and size of the inhaler would mean patients would be unreceptive to the product. However this proved to be unfounded amongst patients who were prescribed the device. The inhaler was also the first generation of mass market nebuliser for this type of purpose and was bulky, whereas technology has progressed and companies are now working on 5th and 6th generation inhalers, such as Mannkinds Technosphere palm size inhaler.

The failure of Exubera has left the future of delivery of proteins for systemic and/or frequent use on uncertain ground. After ceasing the marketing and sale of the drug, ongoing clinical trials of the drug with Pfizer revealed 6 patients, all of whom were former smokers, versus 1 control patient who remained on subcutaneous insulin, developed lung cancer. The number reported was not statistically significant, however in light of the revelations Nectar announced a cessation of all spending on all budgets associated with inhaled insulin. Currently the only remaining company developing insulin for inhalation is Mannkind with its Technosphere® insulin product. They are in the process of carrying out clinical trials, and to date have not reported increased incidences of lung cancer amongst any group of patients. Mannkind hopes to succeed where Pfizer has failed by providing a faster acting insulin formulation that will more effectively mimic the first phase insulin response seen in healthy individuals, providing patients with more effective control over HbA1c levels and clinicians with a product that offers pharmacological and clinical benefits over s.c. insulin (Heinemann, 2010). The Mannkind formulation utilises a pH sensitive protein carrier in its formulation to increase the rate of delivery. By better targeting select patient groups initially before rolling the drug out to larger populations of target users and by providing a clinical benefit with the product over currently available options, Mannkind could surmount the obstacles faced by Pfizer. Not only would this be of high value and importance for diabetics, but it would also provide a critical proof of principle for the large scale delivery of a whole raft of inhalation based therapeutics targeting different aspect of various diseases.

1.7 Mechanisms for improving delivery

Aside from the methods discussed throughout, there a number of methods available for improving the delivery of inhaled molecules. These methods can play a number of different roles, from aiding in specificity, to protecting the therapeutic molecule from degradation, providing timed release, increasing the spread of the molecule over a greater surface area, removing or temporarily disabling obstacles to delivery inherent in the lungs such as tight junctions or mucus build up. They can be availed of for a range of different delivery techniques, and of particular interest, they can be employed for use in combination with nebulisation and inhalation technologies.

Liposomes are commonly used *in vitro* for the application of gene therapy. When forming a complex with a nucleic acid, liposomes encapsulate it within a hydrophobic/philic bi-layer, depending on the liposomes chemical structure. This encapsulation not only serves to protect the cargo from degradation by internal defence mechanisms *in vivo* but also makes it more compact, making it less susceptible to damage resulting from the process of nebulisation. Liposomes can encapsulate hydrophilic molecules in their core and can contain hydrophobic molecules within the lipid bi-layer. The surface of the liposomes is structurally similar to that of the target cells membrane enabling the liposomes to keep the cargo encapsulated and protected until the cell contact is made, at which point the liposome can merge with the cell membrane and begin the release of its cargo into the cell. In addition to the protection of the therapeutic cargo, liposomes can be utilised as a system for time dependent drug release, allowing one delivery application to release a constant sustained supply of therapeutic over a definable time period (Siekmeier and Scheuch, 2008). Liposomes are particularly well suited to the delivery of nucleic acid cargos, such as seen in the delivery of siRNA and plasmid DNA in Chapter 5, but are also potential carrier molecules for drugs such as insulin where a constant slow 'background' release of the drug is required over a prolonged time period.

Also under development is the use of micro-spheres in the delivery of proteins in a controlled manner. Similar to liposomes they can facilitate a time dependent release profile of delivered drug and can protect the drug from degradation *in vivo* as well as ensuring the delivery method utilised has no untoward effects on the drug. By controlling the size, structure and chemical composition of the carriers it facilitates a prediction of the time release profile of the carrier and, in the case of aerosol delivery, the lung deposition profile. This allows for the development of carriers tailored to facilitate increased bioavailability and residency times in the lung (Cryan, 2005).

Small hydrophobic carriers are more rapidly absorbed than liposomes, so they can be more desirable for the delivery of therapeutics in situations where rapid onset of action is required such as bronchoconstriction or hypoglycemia. Their absorption times are in the range of seconds to minutes depending on composition. Hydrophilic compounds tend to be absorbed at a slower rate (Patton et al., 2004).

Chitosan is a prime example of an almost ideal delivery system that small microcarriers and liposomes for example strive to replicate in a number of areas. It is non toxic, biodegradable and does not induce a strong foreign body response by the host immune system. It also possesses its own antimicrobial activity against fungi and bacteria, favouring it for applications such as delivery to an infected lung. Chitosan also facilitates easy to form highly stable complexes with DNA (Shi et al., 2006).

Other means for the assisting in the delivery of therapeutics involves the use of chemicals such as surfactants to increase the surface area over which an inhaled therapeutic will spread and therefore increase the rate of uptake of the drug or the use of anti mucin drugs to break down build up of mucus in clogged airways enabling better transport of the drugs into the system. Complexing drugs with antibiotics can facilitate cell type specific delivery or enhanced transport through the epithelium. FcN receptor for example is present in the epithelium of the lung in human adults. It is a functional active transport mechanism that has been identified as a potential means for erythropoietin (EPO) delivery through the use of EPO-Fc monomers (Bitonti et al., 2004). EGTA (Section 1.5.2) is an example of a calcium chelating agent that can be utilised during drug delivery to temporarily disrupt tight junctions to facilitate better transport of therapeutics across the epithelial barrier. In situations where a viral transfer mechanism is used, such as rhinovirus, removal of calcium has been shown to significantly increase infection with the carrier virus (Jakiela et al., 2008). This type of pre-treatment prior to therapeutic delivery can be used in conjunction with other mechanisms of delivery such as liposomes or antibodies to ensure that not only does the therapeutic successfully cross the epithelial barriers but its release is better targeted and/or controlled.

1.8 Aims

The overall aim of this thesis was to establish *in vitro* and *in vivo* models of lung disease and methods to target BMP signalling in these models.

Specifically we aimed to:

- Further confirm the role of BMP signalling in animal lung disease models.
- Assess *in vitro* lung disease and treatment models.
- Assess *in vivo* lung disease and treatment models.
- Establish clinically relevant methods to target BMP signalling *in vivo*.
- To test the safety and efficacy of aerosolised therapeutic strategy in an animal model.

2 Materials And Methods

2.1 Materials

2.1.1 Reagents

Reagent	Company	Address
1.6µm Gold particles/Microcarriers	Bio-Rad	California, USA
100bp Ladder	Promega	Madison, WI, USA
1Kb DNA Ladder	Invitrogen	Paisley, UK
2X TGS Running Buffer	Invitrogen	Paisley, UK
30% Bis-Acrylamide	Bio-Rad	Herts, UK
ABC Lowry Protein Assay	Bio-Rad	California, USA
Acridine Orange	Sigma	Dublin, Ireland
Agarose	Sigma	Dublin, Ireland
Ammonium Persulphate	Sigma	Dublin, Ireland
Antigen Retrieval Solution	Vector Labs	Dublin, Ireland
BEGM Media	Lonza	Maryland, USA
Blocking Serums	Sigma	Dublin, Ireland
BMPR-II siRNAs	Qiagen	West Sussex, UK
Bradford Protein Assay	Bio-Rad	California, USA
BSA	Sigma	Dublin, Ireland
Calcium Chloride	Reidel-deHaen	Hanover, Germany
Carrier Free rhBMP4	R&D	Oxon, UK
Chloroform	Sigma	Dublin, Ireland
Collagen, Human Placental	Sigma	Dublin, Ireland
Complete Mini Protease Inhibitor Cocktail	Roche	Dublin, Ireland
Cryovial	NalgeNunc	USA
DAPI	Sigma	Dublin, Ireland
DEPC	Sigma	Dublin, Ireland
DMEM :F12	Gibco	Paisley, UK
DMSO	Sigma	Dublin, Ireland
Dnase (PCR)	Invitrogen	Paisley, UK
DNase1 (MAEC isolation)	Roche	Dublin, Ireland
dNTPs	Invitrogen	Paisley, UK

DPX Mountant	Sigma	Dublin, Ireland
ECL Kit	Amersham	Buckinghamshire, UK
Eclipse E200 UV microscope	Nikon	Surrey, UK
EDTA	Sigma	Dublin, Ireland
Elastase, pancreatic, Type IV porcine pancreas	Sigma	Dublin, Ireland
Eosin	Sigma	Dublin, Ireland
Ethidium Bromide	Sigma	Dublin, Ireland
EtOH	Sigma	Dublin, Ireland
Euthanal (Pentabarbitone)	Rhône Meriéux	Ireland
Faramount aqueous mounting medium	DAKO	Galway, Ireland
FBS	Gibco	Paisley, UK
Fibronectin	Sigma	Dublin, Ireland
Film Fixer and Developer	Kodak	Dublin, Ireland
Glyceine	Reidel-deHaen	Hanover, Germany
Glycerol	Sigma	Dublin, Ireland
Hams F12	Gibco	Paisley, UK
Harris' Modified Hemotoxylin	Sigma	Dublin, Ireland
Hydrocortisone	Sigma	Dublin, Ireland
Hyperfect Transfection Reagent	Qiagen	West Sussex, UK
Imject Alum Adjuvant	Thermo	Dublin, Ireland
Insulin-Transferrin-Selenium	Gibco	Paisley, UK
Isoflurane	TCD	Dublin, Ireland
Isopropanol	Sigma	Dublin, Ireland
L-Glutamine	Gibco	Paisley, UK
Lipofactamine 2000	Invitrogen	Paisley, UK
M199 Basal Media	Gibco	Paisley, UK
Macrocarriers	Bio-Rad	California, USA
Magic Mark XP Protein marker	Molecular Probes	Dublin, Ireland
MAPK1 siRNA	Qiagen	West Sussex, UK

Marvel non fat dried milk	Dunnes Stores	Maynooth, Ireland
Maxi Prep Kit	Qiagen	West Sussex, UK
MeOH	Sigma	Dublin, Ireland
Microcarriers	BioRad,	California, USA
Mini Prep Kit	Qiagen	West Sussex, UK
M-MLV reverse Transcriptase	Invitrogen	Paisley, UK
MTS/Cell Titer 96® Aqueous One Solution Proliferation Assay	Promega	Madison, WI, USA
Nitrocellulose membrane	Amersham	Buckinghamshire, UK
Oligo(12-18) dT Primers	Invitrogen	Paisley, UK
Optimem	Gibco	Dublin, Ireland
Ovalbumin	Sigma	Dublin, Ireland
Oxygen	BOC Gases	Dublin, Ireland
Paraformaldehyde	Sigma	Dublin, Ireland
PBS	Sigma	Dublin, Ireland
Penicillin-Streptomycin	Gibco	Paisley, UK
pMGFP	Promega	Dublin, Ireland
Poly Acryl Carrier	MRC	Ohio, USA
Precast 10% Polyacrylamide Tris-HCl Gel	Bio-Rad	California, USA
Qiashredder	Qiagen	West Sussex, UK
Quantitect 18S primer Kit	Qiagen	West Sussex, UK
Quantitect SYBR Green PCR Kit	Qiagen	California, USA
RIPA Buffer	Sigma	Dublin, Ireland
Rnase OUT	Invitrogen	Paisley, UK
RNeasy Mini Kit	Qiagen	California, USA
Rosse Cat Catheder	C&M Vetlink	Limerick, Ireland
See Blue Protein Molecular Weight Ladder	Invitrogen	Paisley, UK
Sodium Chloride	Sigma	Dublin, Ireland
Sodium Dodecyl Sulphate	Sigma	Dublin, Ireland
Speedy-Diff	Clin-Tech	Guildford, UK

Spermidine	Sigma	Dublin, Ireland
Stopping Screen	Bio-Rad	California, USA
SYBR Green 2Step PCR	Qiagen	West Sussex, UK
Taq polymerase-Go Taq Flexi	Promega	Madison, WI, USA
TEMED	Sigma	Dublin, Ireland
Tissue culture semipermeable inserts	Greiner Bio-One	Herts, UK
TMB	Sigma	Dublin, Ireland
Transblot Filter Paper	Bio-Rad	Herts, UK
Tris	BDH	Dublin, Ireland
TRIS Glyceine 10X Buffer	Bio-Rad	California, USA
TriZol	Invitrogen	Paisley, UK
Trypsin for MAEC isolation	Sigma	Dublin, Ireland
Trypsin-EDTA	Gibco	Paisley, UK
Tween-20	Sigma	Dublin, Ireland
Ultroser-G Serum	Gibco	Paisley, UK
XL-1 Blue E-Coli	Stratagene	Cork, Ireland
Xylene	BDH	Dublin, Ireland
β-Mercaptoethanol	Sigma	Dublin, Ireland

2.1.2 Instrumentation

Product	Company	Address
Aeroneb Pro Nebuliser + Nebuliser Units	Aerogen	Galway, Ireland
Aerosol Chamber	Buxco	Hampshire, UK
ABI PRISM® 7900HT	Applied Biosystems	California, USA
Airflow Regulator for nebulisation	Buxco	Hampshire, UK
Benchtop Centrifuge	Hettich	Germany
Citadel 1000	Shandon	Dublin, Ireland
CS3 Software	Adobe	California, USA
Cytospinner Rotafix 32	Hettich	Germany
Densitometer	Bio-Rad	Herts, UK
Desktop centrifuge	Eppendorf	Cambridge, UK
FACScan Flow Cytometer	BD Bioscience	Oxford, UK
Gradient Cycler- MyCycler	Bio-Rad	California, USA
Mouse Restraints	Buxco	Hampshire, UK
Nanodrop 1000 spectrophotometer	Thermo	Surrey, UK
New Brunswick E25 Excella Shaker	Eppendorf	Cambridge, UK
Olympus 1030µ Digital Camera	Olympus	Dublin, Ireland
Olympus IX61 Fluorescence Microscope	Olympus	California, USA
Olympus IX81 Fluorescence Microscope	Mason Technologies	Dublin, Ireland
Opticon thermal cycler	MJ Research	Massachusetts
Plethysmograph	Buxco	Hampshire, UK
Quantity One Software	Bio-Rad	Herts, UK
Spraytech Analyser	Malvern	Worcestershire, UK
Tecan Plate Reader	Unitech	Dublin, Ireland
Trans-Blot SD semi-dry transfer cell	Bio-Rad	Herts, UK
Western Blotting Electrophoresis Rig	Bio-Rad	Herts, UK
XA Software Package	Buxco	Hampshire, UK

2.1.3 Primers

2.1.3.1 Primers for QPCR

Primer Id	Species	Sequence (5'-3')	Annealing Temp.	Product size (base pairs)
Id1 For	hu/mon	CGTGCTGCTCTACGACAT	55°C	95bp
Id1 Rev		GAATCTCCACCTTGCTCACC		
P21 For	hu/mon	CTGCCCAAGCTCTACCTTCC	55°C	123bp
P21 Rev		CAGGTCCACATGGTCTTCCT		
BMP2 For	hu/mon	ATGGATTCGTGGTGGAAGTG	58°C	198bp
BMP2 Rev		GCTGTTTGTGTTTGGCTTGA		
PCNA For	hu/mon	AAGAAGGTGTTGGAGGCACT	58°C	195bp
PCNA Rev		TTTGGACATACTGGTGAGGTTC		
BMPR-IA For	hu/mon	TCGTGATTTGGAACAGGATG	58°C	98bp
BMPR-IA Rev		CCAGACCCACTACCAGAACTTT		
BMPR-IB For	hu/mon	ACTCAAGGCAAACCAGCAAT	58°C	204bp
BMPR-IB Rev		TCTGTTCAAGCTCTCGTCCA		
BMPR-II For	hu/mon	CAGAGACCCAAGTTCCCAGA	58°C	139bp
BMPR-II Rev		GTTCAGCCATCCTTTCCTCA		
Smad1 For	hu/mon	ATGTTCAGGCGGTTGCTTAT	58°C	148bp
Smad1 Rev		CGGTTCTTATTGTTGGAAGG		
Smad4 For	hu/mon	TTGATGACCTTCGTCGCTTA	58°C	84bp
Smad4 Rev		CTTTGATGCTCTGTCTTGGGTA		
Smad5 For	hu/mon	GGAGAGGTGTATGCGGAATG	58°C	93bp
Smad5 Rev		GACAGTGGTGGGATGAAAGC		
E-cadherin For	hu/mon	GGCTGGACCGAGAGAGTT	58°C	350bp
E-cadherin Rev		CTGCTTGGCCTCAAAATCC		
GAPDH For	hu/mon	CATCCATGACAACTTTGGTATCGT	55&58°C	74bp
GAPDH Rev		CAGTCTTCTGGGTGGCAGTGA		
Snail1 For	hu/mon	TTTACCTTCCAGCAGCCCTA	58°C	108bp
Snail1 Rev		GACAGAGTCCCAGATGAGCA		
Snail2 For	hu/mon	GCCAAACTACAGCGAACTGG	58°C	239bp
Snail2 Rev		AGGAGGTGTCAGATGGAGGA		
BMPR-II For	hu/ms	GGCACATAGGTCCCAAGAAA	54&56°C	88bp

71

BMPR-II Rev		TTCATGCTCATCAGGACTGG		
18S Ribosomal RNA (Rn18s)	ms	Quantitect primer kit for QPCR, sequence not available	54-60°C	169bp

2.1.3.2 Primers for rtPCR

Primer	Species	Sequence (5'-3')	Product size (Base Pairs)	Annealing Temp.
Smad3 For	ms	AGACGCCAGTTCTACCTCCA	466bp	58°C
Smad3 Rev		GTAAGTTCCACGGCTGCATT		
CC10 For	ms	ATCGCCATCACAATCACT	282bp	55°C
CC10 Rev		GAATCTTAAATCTTGCTTACACAGAGG		
BMPR-II For	hu/ms	GCCCGCTTTATAGTTGGAGA	144bp	55&58°C
BMPR-II Rev		AGCAAGACGGCAAGCGATTA		
GAPDH For	hu/ms	CTGCACCACCAACTGCTTAG	487bp	55°C
GAPDH Rev		CCAGGAAATGAGCTTGACAAA		

Key   hu: human

ms: mouse

mon: monkey

2.1.4 Antibodies

Antibody/Clone	Raised In	IF conc.	WB conc.	Company
E-Cadherin/36	Mouse	1/200	1/2000	BDB
Smad4/B8	Mouse	1/100	1/100	SC
Smad8/A-17	Goat	1/50	N/D	SC
BMPR-IA/H60	Rabbit	1/20	1/200	SC
BMPR-II/a	Rabbit	n/a	1/200	Abgent
BMPR-II	Goat	n/a	n/a	R&D
pSmad 1/5/8	Rabbit	1/50	1/1000	CST
CC10/S20	Goat	1/100	n/a	SC
Id1/Q11	Mouse	n/a	1/100	SC
PCNA/pc10	Mouse	1/3000	1/3000	Sigma
Smooth Muscle Actin/1A4		1/2000	n/a	Sigma
BMP4/N-16	Goat	n/a	1/100	SC
Actin/(20-33)	Rabbit	n/a	1/2000	Sigma
Key	SC: Santa Cruz			
	CST: Cell Signaling Technology			
	BDB: BD Biosciences			
	R&D: R&D Systems			

2.2 Methods

2.2.1 Cell culture

2.2.1.1 Cell Lines

BEAS-2B cells, an adherent SV-40 transformed human bronchial epithelial cell line, were obtained from the ATCC. They were cultured in tissue culture flasks in a 1:1 ratio of Dulbecco's modified Eagle's media and Hams F12 (DMEM:F12) supplemented with 5% fetal bovine serum (FBS) and 1% L-glutamine. MLE-12 cells, an adherent cell line derived from an adenoma tumour of an SP-C SV-40 transgenic mouse, were obtained from the ATCC. They were cultured in tissue culture flasks in a 1:1 ratio of DMEM:F12 supplemented with 5% FBS and 1% L-glutamine. LA4 cells, an adherent adenoma mouse lung derived cell line, were obtained from the ATCC. Cells were cultured in tissue culture flasks with Hams F12 media supplemented with 5% FBS and 1% L-glutamine. A549 cells, a human adenocarcinoma cell line, were obtained from the ECACC. Cells were cultured in tissue culture flasks in a 1:1 ratio of DMEM:F12 supplemented with 5% FBS and 1% L-glutamine. All cells were maintained in a 5% CO_2 incubator at 37°C.

2.2.1.2 Routine sub-culture

Cells were routinely subcultured upon reaching 80-90% confluency. Culture medium was removed from the flasks and the cells rinsed with pre-heated PBS at 37°C. Trypsin-EDTA was then added to the cells and the flask returned to 37°C for approximately 5-10min until all cells had detached. The cell suspension was then centrifuged at 219g for 5mins in a 30ml sterilin in a bench top centrifuge to pellet the cells. The pellet was then resuspended in a fixed volume of preheated media and depending upon requirements a percentage of cells would then be used to either reseed the flask or for experimental procedures. All routine subculture was carried out aseptically.

2.2.1.3 Freezing and thawing of cells in liquid nitrogen stock

Once received, cells would be cultured and a master stock of cells cultivated and frozen in liquid nitrogen. From this a working stock of cells would be grown and frozen in liquid nitrogen facilitating the repeating of all experiments within 5 cell passages of each other. In order to freeze down an aliquot of cells the cells would be first grown to logarithmic growth phase (approximately 50-70% confluent). They

were then trypsinised and pelleted as per routine sub-culture. Once the supernatant from the pellet had been removed, the pellets were resuspended in 500µl FBS. To this resuspended pellet, a 1:9 solution of DMSO:FBS was added dropwise, the suspension then transferred to a chilled cryovial, and held on ice to be frozen at -80°C. After approximately 5-7days the frozen cells were then transferred to liquid nitrogen for long-term storage.

Thawing of cells from liquid nitrogen was carried out by removal of the cryovial from storage and thawing in a 37°C water-bath. Once thawed the cell suspension added to 5mls of culture medium and then immediately spun in a bench-top centrifuge at 219g for 5min. The supernatant containing DMSO was then removed and the cell pellet resuspended in culture medium and seeded into an appropriate tissue culture flask. After allowing cells to adhere culture medium was again changed after no longer than 18hrs to ensure all DMSO was removed from the culture medium.

2.2.1.4 Isolation and culture of primary murine airway epithelial cells (MAECs).

2.2.1.4.1 Isolation

MAECs were isolated form the lungs of between 4 and 6 6-8week old female C3/Hen mice. Mice were sacrificed by i.p. injection of sodium pentabarbitone. The dorsal vein was exposed and cut to prevent pooling of blood in the lungs. Then the trachea was isolated and cannulated. At this point the lungs were perfused with saline via gravity feed of PBS through the heart to remove any remaining blood cells. The lungs were then excised and pre-warmed trypsin was added to the lungs via the cannula until the lungs were fully inflated. The lungs were then placed in a 50ml sterilin and placed at 37°C for 15mins to allow the trypsin to digest the epithelial cells from the lining of the lungs. The lungs were then manually diced using a curved scissors for approximately 1-2mins to allow the release of the now digested epithelial cells. 1ml FBS per mouse was then added to stop the enzymatic action of the trypsin. The diced lungs and FBS mixture was then transferred to a 50ml tube and DNase solution CONCENTRATION REQD was added. The suspension was then shaken vigorously by hand for 5minutes, after which it was passed through first a 100µm nylon filter and then a 40µm nylon filter to remove lung particulate. This cell suspension was then pelleted twice and resuspended in a second DNase solution both times. The cell suspension was then added to a 10cm^2 non tissue-culture Petri dish for 1hr at 37°C for a differential attachment phase. This allowed non airway epithelial cells to attach to

the Petri and helped enrich for MAECs. After the hour the cell suspension was removed from the Petri dish, taking care not to disrupt the attached cell layer. This MAEC enriched cell population was then pelleted and resuspended in defined serum free media (Section 1.4.1.4.2). Due to the nature of MAECs and the fact that they clump together it is not possible to determine cell number by cell counting. Therefore the Cell Titre 96®Aqueous One Solution Cell Proliferation Assay, also known as an MTS Assay, was used to determine seeding densities (Section 1.4.4.1). The cells were then seeded as required on fibronectin or collagen coated glass chamber slides, 96-well, 24-well, 6-well plates or tissue-culture graded Petri dishes as required.

2.2.1.4.2 *MAEC Media*

Defined serum free media (DSFM): DFSM consisted of 1:1 HamsF12:M199 basal media supplemented with 100ng/µl hydrocortisone, 10ng/µl EGF, 1% L-glutamine, 1% penicillin/streptomycin, 1% Insulin Selenium Transferrin.

Plating media: Plating or seeding media consisted of DMEM basal media supplemented with 5% FBS, 2mM L-Glutamine, 1% Penicillin/Streptomycin.

USG/DSFM plating medium: consisted of 1:1 DMEM:Hams F12, Penicillin/Streptomycin 100µg/ml, 2% Ultroser-G Serum (USG) (15950-017 Gibco)

2.2.1.5 Fibronectin coated of inserts for non-ALI culturing of MAECs

All work was carried out aseptically in a laminar flow cabinet. Fibronectin (FN) was reconstituted in basal medium to a stock concentration of 1mg/ml. This was then aliquoted into 100µl aliquots in sterile eppendorfs and stored at -20°C. This formed the stock from which the work was carried out. The stock FN was then diluted to a working concentration of 50µg/ml by adding 1900µl of basal medium to a 100µl aliquot of the stock. 200µl of FN was then added to the base of the tissue culture surface (enough to ensure that the fibronectin was adequately coating the entire base of the well/insert/Petri). The chamber slide was then carefully wrapped in parafilm and incubated at 4°C overnight. The next day the FN solution was aseptically removed and used immediately or the slides/plates were again wrapped in parafilm and stored at -20 until required for use.

2.2.2 Culturing MAECs in ALI

A volume of cells was used which gave an absorbance of 0.1 by MTS assay (Section 1.4.4.1). The inserts were pre-coated with type VI Human Placental Collagen (see below). The cells were then seeded onto the tissue culture insert and incubated at 37°C

in 5% CO_2 for 3 days. On Day4 the media on the apical surface of the cultured cells was removed along with any non-adherent cells and debris and the media outside the insert, bathing the basolateral surface was replaced with 600µl of USG Media. Once the cells have reached confluency the apical surface of the insert appeared dry, and is to be expected from Day4 onwards. Media bathing the basolateral surface was replaced twice weekly thereafter.

2.2.2.1 Collagen coating of semi-permeable membrane tissue culture insert for ALI

Collagen solution: type VI Human Placental Collagen, 0.5mg/ml in Distilled H_2O with 0.2% Glacial Acetic Acid. 100µl of the collagen solution was added to the semi permeable membrane in each tissue culture insert, the insert was then allowed to air-dry overnight. The inserts were then washed twice with sterile PBS before use. All work was performed in a laminar flow hood.

2.2.3 Culture of human NEHB primary cells and primary primate airway epithelial cells in ALI

Human NEHB and primate airway epithelial cells were provided by Dr Mark Avdolovich, Jodie Usachenko and Dr Dallas Hyde (California National Primate Research Centre, UC Davis, California, USA.). Cells were seeded into 24well semi-permeable inserts and were cultured submerged in BEGM media (Lonza) without retinoic acid until fully confluent (Day3-Day5) and media was changed every second day. Once confluency had been established, the media from the apical surface of the insert that coated the cells was removed and the media in the well surrounding the well was replaced with BEGM media with retinoic acid added. Cells were cultured until Day10 in ALI before treatment.

2.2.4 Cell Counts and Cell Viability

Cell counts were carried out using a haemocytometer. In order to ascertain cell viability, EBAO staining was used in conjunction with a haemocytometer under a UV microscope. Dead cells stained orange and live cells stained green. Other methods for determining cell quantity and viability included the MTS and the LDH assays below

2.2.4.1 MTS/Cell Titer 96® AQ$_{ueous}$ One Solution Cell Proliferation Assay

The assay uses the reduction of MTS by a dehydrogenase enzyme in cells to give a colour change by converting the MTS chemical into a purple formazan dye. The

resulting change in absorbance value or O.D. reading between a control well that contains only MTS and no cells and a the target wells containing both MTS and live cells could then be used to determine the appropriate seeding densities required. For experimental purposes cells were seeded at a constant O.D. per experiment to ensure consistent results. 20µl of reagent was pipetted into each well of a 96 well plate containing a 100µl MAEC cell aliquot and a no cell, media only, control well. The plate was incubated for 1hr at 37°C and 5% CO_2. Absorbance was recorded at 490nm.

2.2.4.2 LDH assay for cells in culture.

The lactose dehydrogenase (LDH) assay is based on the principle that there is an increase in the release of the cytosol enzyme, lactate dehydrogenase, from cells with damaged cellular membranes. Thus in cell culture the course of drug induced cytotoxicity can be followed quantitatively by measuring the activity of LDH in the supernatant. O.D.'s at 490 nm can be put on y-axis, concentrations on x-axis of different drug concentrations utilized, and this allows the interpolation of IC50 values. A cell count is performed and equal volumes of cells added to each well with culture media only added to a control well. Cells are then incubated for 45min at 37°C. To a 'max release well' a lysis solution is added 45 minutes prior to the end of the 4hr timepoint. The contents of all wells are then removed by pipette and added to eppendorfs and centrifuged at 250*g* for 4mins and 50µl of supernatant from each tube is added to a well of a 96well plate. 50µl of reconstituted substrate mix is then added (reconstituted substrate mix is reconstituted using Assay buffer provided with the Kit). Plate is covered and incubated for 30 mins away from light. 50µl stop solution is added to each well. Absorbance is recorded at 490nm.

2.2.5 Acquisition of brightfield images

Phase contrast images were captured on a light microscope using an Olympus 1030µ Digital Camera

2.2.6 Immunofluorescence

2.2.6.1 Fixation and preparation for immunofluorescence

2.2.6.1.1 Cells

Cells for analysis by immunofluorescence were grown on either glass bottomed microscope chamber slides or on coverslip inserts in 24well plates or 35mm^2 Petri

dishes. Prior to antibody detection the cells had first to be fixed. To achieve this media was removed from the wells containing the cells and the cells then rinsed x3 with PBS. Ice-cold methanol was then added to the cells and the cells placed in a 20°C freezer for 5min. Methanol was then removed and the cells allowed to air dry for 10-15min. The fixed cells could then be used immediately or stored at -20°C until required.

2.2.6.1.2 *Whole Lung*

Whole lung isolation and fixation was carried out as described in Section 1.4.17.1. Paraformaldehyde fixed paraffin embedded lungs were chilled on a cold plate and lungs sections of 3µm were sliced using a microtome tissue slicer. The sections were then mounted on poly-L-lysine coated microscope slides in a water bath and allowed to dry and adhere to the slide. The sections were then baked onto the glass slide by incubation of the slides in a 60°C oven for 20-25min. After this the slides could be stored indefinitely or prepared for use. To prepare for use the slides were first de-waxed. This was done by placing the slides in a xylene bath for 5min in a chemical fume hood, then sequentially rehydrating the slides in a series of EtOH to water stages, incubating the slides for 2min in 90%EtOH, 75%EtOH, 75% EtOH and finally tapwater for 2min. Antigen retrieval was then performed by boiling the slides in a commercially available citric acid solution (Vector Labs Antigen Retrieval solution) for 15min in a microwave. This was done in 5 min intervals with 2-3min between each step to allow steam to escape and to ensure that the slides did not dry out. The slides were then cooled by the addition of cold water to the citric acid solution. The samples were then removed from the solution and allowed to air-dry for 2-3min on the bench. To facilitate the staining of the tissue sections present on the slide for immunofluorescence analysis, the tissue sections were then encircled using a wax pen. This facilitated the use of a reduced volume of antibody for coating the relevant sections. The slides were now suitable for immediate use.

2.2.6.2 Indirect Immunofluorescence

Indirect immunofluorescence was carried out on prepared tissue or lung sections in the same fashion. Samples were incubated for 5min in 1X Tris Buffered Saline (TBS). They were then incubated with an appropriate serum for 20min to prevent non-specific binding from occurring. The serum was then removed and the primary antibody diluted as per Section 2.1.4, then added to the sample. The sample was then incubated at 4°C overnight. Following this any unbound primary antibody was

washed away by washing the samples with TBS containing 0.1% Tween-20 x3 over a total period of 10min. Alexa-488 (Green) or -568 (Red) secondary antibodies were then made up to the appropriate dilutions in a solution of 20% serum (same as used for initial blocking step) in TBS buffer. Secondary antibody was incubated with the sample for 30min at room temperature protected from light. The samples were then washed x3 for a total of 10min in TBS/0.1% Tween-20 to remove any unbound secondary antibody. Samples were then counterstained using DAPI nuclear stain diluted 1/200 in TBS in a 5min incubation at room temperature followed by a rinse in tap water. The samples were then mounted in Faramount aqueous mounting medium. Samples were kept protected from light to prevent degradation of the fluorescent signal. Fluorescently tagged antigens were then visualised and examined using an Olympus IX81 fluorescent microscope. The only exception was primate tissue sections which were imaged using an Olympus IX61 microscope system. Appropriate secondary control slides were included with every experimental set-up to ensure that no non-specific binding was occurring.

2.2.7 Protein harvest and analysis

2.2.7.1 Harvest of protein from cells in culture and whole tissue

Cells: Briefly, at a harvest time-point, any media or mucus present was carefully removed by pipette and ice-cold RIPA buffer containing a protease inhibitor cocktail was added to the well/insert. The cells were then scraped off of the bottom of the well into the RIPA buffer using a pipette tip. This solution was then all collected by pipette and placed into an appropriately labelled 1.5ml Eppendorf tube that had been stored on ice. The sample was then stored on ice before being placed into -80 storage until required. MORE DETAILS ON VOLUMES ETC

Tissue: Whole lung samples for protein analysis were isolated and snap frozen in liquid nitrogen before storing at -80°C until required. Once required the tissue was added to a solution of ice-cold RIPA buffer containing 1X Complete mini protease inhibitor cocktail (Roche). The tissue was then homogenised in this solution mechanically either by a glass/Teflon homogeniser or by use of an electric homogeniser. This was carried out on ice to prevent a build up of heat that could lead to protein destruction. Once fully homogenised, the sample was aliquoted into a Qiashredder eppendorf and centrifuged at 12000g for 5min at 4°C. This filtered out all the remaining non homogenised tissue remnants and broke down any DNA present

in the sample, providing a homogenous protein solution for analysis. This could either be used immediately or aliquoted and returned to -80°C storage.

2.2.7.2 Protein Quantification

Protein quantification was carried out on cells and tissue samples for the purposes of Western Blot analysis. It was also carried out on BALF samples to ascertain the quantity of free protein in the lungs. When ready, all the samples were quantified for protein concentration using either the Bio-Rad ABC Lowry assay protocol (used specifically for NEHB and primate airway cell based experiments) or the Bio-Rad Bradford assay and read at the appropriate wavelength in a plate reader.

For both the Bradford and Lowry assays, standards made from BSA were used to prepare a standard curve ranging from 0.2-1.4µg/ml (w/v).

2.2.7.2.1 *Bradford protein assay*

Standards were assayed in duplicate and samples were analysed in triplicate. A fresh standard curve was required each time the assay was performed. Samples and standards were prepared at the same time. Samples were diluted 1/10 in RIPA buffer and 4µl of both samples and standards were added to 200µl Bio-Rad Bradford reagent in a clean, labelled, 96well plate. When added to their individual wells, samples and standards were mixed well with the reagent by gentle pipetting and care was taken to ensure no bubbles formed as they would block accurate measurements of the wells. Absorbance was read in a plate reader at 620nm and the protein concentration calculated by fitting the samples to the standard curve

2.2.7.2.2 *Lowry protein assay*

Standards were assayed in duplicate and samples were analysed in triplicate. A fresh standard curve was required each time the assay was performed. Samples were diluted 1/10 before assaying. 5µl of samples and standards were aliquoted into a clean, labelled, 96well plate. 25µl of Reagent A was added to each well, followed by the addition of 200µl of Reagent B to each well. The wells were gently pipetted to ensure even mixing of the reagents using a clean dry pipetted for each well. The plate was then incubated at room temperature for 15min and read at 750nm. Absorbances are stable for one hour.

2.2.8 SDS-PAGE gel electrophoresis and Western blotting

2.2.8.1 SDS-PAGE

Sodium dodecyl sulphate polyacrylamide gel electrophoresis (SDS-PAGE) was performed according to the Bio-Rad mini-PROTEAN 3 cell protocol.

2.2.8.1.1 *Sample Preparation*

Samples for analysis were quantified and an equal quantity of protein from each sample was loaded per gel. Samples were combined with an equal volume of loading buffer containing β-Mercaptoethanol (BME) (25μl/500μl loading buffer) and heated to 95°C for 5min in a thermal cycler block. The combination of BME treatment and boiling reduced the disulphide bonds present and denatured the protein respectively. After heating the samples were cooled on ice and then centrifuged for 30sec at 12000g at 4°C. They were now ready for loading onto the gels for electrophoresis.

2.2.8.1.2 *Electrophoresis*

Gels for separation of the proteins were prepared as per section 2.2.18, with the resolving gel being poured first and allowed to polymerise for 30min with a layer of dH2O on the top to prevent the gel for drying out on the top and to help give an even surface. This was then followed by the pouring of the stacking gel, which was prepared as per section 2.2.8. Once the stacking gel had been poured well plates were added to allow the formation of loading wells for samples. Gels could be used immediately after the polymerisation of the stacking gel (approximately 45min) or stored overnight at 4°C in a solution of 1:4 1.5M Tris:dH$_2$O. For the primate and human primary protein samples pre-cast gels were used. The samples and a pair of molecular weight protein markers- a SeeBlue colour-metric ladder that allowed for visual tracking of the gel running and MagicMark ladder which was visible on the developed blots for confirmation of protein size-were then loaded and electrophoresed in 1X TGS buffer at 110V for 75-90mins until the protein front was detected to be near the bottom of the gel.

2.2.8.2 Western Blot Reagents

2.2.8.2.1 *SDS-PAGE gels*

Reagents	Resolving Gels		Stacking Gel
	10%	12%	4%
dH$_2$O	4.1ml	3.4ml	6.1ml

30% Bis Acrylamide	3.3ml	4.0ml	1.3ml
1.5M Tris-HCl (pH 8.8)	2.5ml	2.5ml	
0.5M Tris HCl (pH 6.8)			2.5ml
10% SDS	100µl	100µl	100µl
10% Ammonium Persulphate	50µl	50µl	50µl
Temed	5µl	5µl	5µl

2.2.8.2.2 1X TGS Buffer

100ml 10X TGS brought to 1L in dH$_2$O to provide a 1X working solution.

2.2.8.2.3 Towbin Transfer Buffer

Reagent	Quantity
Tris-HCl	1.515g
Glycine	7.2g
MeOH	100ml

2.2.8.3 Semi-Dry Transfer

After the gel had finished separating the proteins according to molecular weight, the protein was transferred to a nitro cellulose membrane via semi dry transfer as follows. The gel was removed from the gel rig apparatus and transferred to a weigh boat containing 1X TBS transfer buffer and allowed to equilibrate for 15min. Nitrocellulose membrane was equilibrated in TGS for 5 min and extra thick blotting paper for 10min. The 1X TBS transfer buffer was prepared fresh immediately before use while the gel was still running. After the equilibration step the gel was sandwiched in between blotting paper and membrane on the Transblot SD Semi-Dry Transfer Cell in the following order building up from the base; blot paper, nitrocellulose membrane, SDS-PAGE gel, blot paper. The proteins were then transferred onto the nitrocellulose membrane by electrophoresis at 25V for 45min.

2.2.8.4 Immunoblotting

The nitrocellulose membranes were incubated in a blocking buffer consisting of either 5% Marvel or 5% BSA (w/v) in TBS for 1hr at room temperature to prevent non-specific binding. After incubation primary antibodies diluted as per section 2.1.4 and were incubated with the membrane over night at 4°C. The blots were then washed x3 over 10min with TBSt (TBS buffer containing 0.1% Tween-20) wash solution. The

blot was then incubated with the appropriate secondary horseradish peroxidase (HRP) labelled secondary antibody for 1hr at room temperature. The blot was then washed as before, x3 over 10min with TBSt. After this wash the membrane was then treated with enhanced chemi-luminescence (ECL) Western blot detection reagent as per manufacturers' instructions. The protein was then detected and visualised by placing the ECL treated membrane in an x-ray film cassette and exposing them to chemi-luminescence film in a dark room using Hyperfilm™ ECL film. The film was then developed and fixed in Kodak developer and fixer reagents allowing visualisation of the protein bands and analysis of the protein by densitometry.

2.2.8.5 Densitometry

Densitometry was carried out using a Bio-Rad Quantity1 software package. An image of the gel was taken and opened in the operations window. Using (No.2) 'Tool'-'Zoom Box' the bands present in the image were centred and enlarged. The lanes were then selected and autoframed and the number of lanes present was entered. The autolanes were then centred to be located in the centre of the bands. This was done by selecting the lane, editing the frame and adding/adjusting the anchor. The lane background was then set to be even across all bands by selecting a lane, selecting the lane background and putting all lanes on the same level background threshold. Band selection was then carried out by selecting 'Band-Detect Bands' and increasing the band widths until the bar was just overlapping the ends of the band. The band quality, i.e. the information about the band to be recorded, was then selected, and the measurement used was 'Trace Quantity-Area under the curve'. Measurements were then given on screen and a report was obtained detailing each band and its corresponding trace quantity via selecting 'Report-All lanes report' which was then saved to file or printed as required.

2.2.9 Treatment of human NEHB and primate airway epithelial cells

24 well inserts were seeded with cells of interest and allowed form an ALI. After day 10 of ALI establishment the cells were then treated with EGTA or BMP4 or kept as no treatment controls. The cells were harvested along the following time-points, t=0, t= 6hr, t=12hr, t=24hr, t=48hr and t=72hr respectively. For harvest cells were removed from the 24 well plate and lysed using a Qiagen RNeasy Kit as per manufacturers instructions and the cell pellet was either frozen immediately at -70°C or immediately made into RNA as per manufacturers' protocol. RNA was then quantified using a nanodrop and cDNA prepared as per section 2.2.20. rtPCR using

GAPDH primers, as per Section 2.1.3.2, was carried out on all cDNA preparations to ensure that the cDNA was intact before proceeding to the qPCR stage.

2.2.10 EGTA Pre-treatment of ALI cells

In order to treat cells with EGTA it was first necessary to remove any trace amounts of media present on the apical surface of the membrane. Once this was done 100µl of 10mM EGTA was added to the cells 1hr prior to the additional treatment with BMP4. Both human and primate cells were treated in the exact same manner.

2.2.11 BMP4 treatment of cells

2.2.11.1 Cells in culture

Cells in culture in 24 well plates were treated with BMP4 as follows. Before treatment media coating the cells was replaced with defined serum free media. BMP4 at the desired concentration was then added to defined serum free media and added to the cell culture in place of serum containing media. The cells were then harvested or fixed as required at specific timepoints.

2.2.11.2 Cells in ALI

Cells in ALI were treated only when ALI was fully established and the cell layer on the insert fully confluent. For BMP4 treatment the BMP was diluted to the desired concentration in DMEM or HamsF12 basal media in a final volume of 50µl which was then added to the apical surface of the inserts to coat the cells. No BMP4 was added to the media coating the Basolateral surface of the inserts.

2.2.12 Plasmids

2.2.12.1 pCyclinD$_1$-GFP

pCyclinD$_1$-GFP vector had been generated in the lab previously by the sub cloning of the CyclinD$_1$ promoter upstream of the *Aequorea Victoria* enhanced GFP gene in the pEGFP-1 promoterless vector, giving rise to GFP expression resulting from the activation of the CyclinD$_1$ promoter which is involved in cell cycle progression. The plasmid was especially useful in dividing cells for confirmation of plasmid integration by FACS analysis or Immunofluorescence but was not as effective in the treatment of confluent cell layers as very little promoter activation would occur.

2.2.12.2 pMGFP

pMGFP plasmid is a commercially available plasmid and was sourced from Promega. Its GFP gene is derived from *Montastrae cavernosa* and the gene is under the control of the constitutively active promoter CMV that was tailored for use in eukaryotic cells. Due to the fact that this was constitutively active it meant that this plasmid when used for determining transfection efficiencies was particularly useful as it was not reliant on cell cycle for activation.

2.2.12.3 Plasmid preparation-Mini/Maxi preparations of plasmid from E-Coli

Small scale preparations of plasmid stocks were carried out using Qiagen mini prep kit, large scale plasmid preparations using Qiagens Maxi prep kit. Preparations were carried out as per manufacturers' recommendations.

2.2.12.4 Generation of plasmid stocks

E-Coli that had been transformed with plasmid was grown overnight at 37°C on a shaker in LB broth at 200rpm. 500µl of the bacteria was then diluted in a 1:1ratio of 30% glycerol before being stored at -80°C until required.

2.2.12.5 Antibiotic preparation

The two antibiotics required were Kanamycin and Ampicillin. Kanamycin was used at a final concentration of 30µg/ml and Ampicillan at 25µg/ml.

2.2.12.6 Transformation of *E-Coli*

XL-1 Blue are commercially available ultra competent bacterial cells and were transfected with the desired plasmid DNA according to the manufacturers' recommendations. This consisted of thawing the cells on ice, the addition of β-mercapthoethanol and the incubation of the cells on ice for 10min. The plasmid was then added to the cells and incubated on ice for a further 30min. The cells were then heat shocked by incubation in a 42°C water bath for 30sec and then added to SOC media and incubated at 37°C for 1hr on an orbital shaker at 300rpm. The cells were then plated onto antibiotic agar selection plates and incubated at 37°C in a bacterial incubator overnight.

2.2.12.7 Plasmid Transfection

Conditions for the transfection of epithelial cells with plasmid using commercially available Lipofectamine 2000 (Invitrogen) were as follows. Cells were seeded at a density of $9x10^4$ cells/well in a 24well tissue culture plate. After 48hr, DNA and

vector were mixed allowed to form a complex by incubation together at room temperature and then incubated with the cells by adding in a dropwise manner while constantly swirling the plate to ensure even distribution of the complex and to prevent toxic side effects. Cells were then analysed by FACS analysis and/or fluorescent microscopy to determine the level of successful transfection, with FACS analysis facilitating quantitative reporting of the efficiency levels.

2.2.13 Particle Bombardment

Cells were seeded into 35 mm^2 tissue culture dishes. Cells required for subsequent analysis by fluorescence microscopy were grown on glass coverslips placed in the culture dishes. MAECs were seeded at a density of 0.1 O.D per dish as determined by the MTS/Cell Titer 96® AQ$_{ueous}$ One Solution Cell Proliferation Assay. MLE-12 cells and BEAS-2B cells were seeded at densities of $1x10^6$ cells per dish. Bombardment was carried out 24 hr later. pMGFP was precipitated onto gold microcarriers as follows: Briefly, 50µl pMGFP (1 µg/µl), 50 µl 2.5 M-CaCl$_2$, 20 µl 0.1 M-spermidine and 3 mg 1.6µm gold particles were mixed then rinsed once with 70 % EtOH, once with 100 % EtOH and resuspended in 60 µl 100% EtOH. 6µl aliquots were transferred to microcarriers. The gene gun (PDS-1000/He System, Bio-Rad) was used for bombardment. Cells were then bombarded under various conditions by varying the stage level and psi used as appropriate.

2.2.13.1 Stock Solutions

2.2.13.1.1 Gold Stock solution

Gold was weighed out and added to Absolute EtOH where it was then sonicated for 2min. It was then centrifuged at 1400 *g* for 3sec in a micro-centrifuge. Supernatant was removed and the wash step was repeated x2. 1ml sterile dH$_2$O was then added and the suspension sonicated for a further 2min. the suspension was then centrifuged at 1400*g* for 3sec. The supernatant was removed and the wash step was then repeated x1. The gold pellet was then resuspended in sterile dH$_2$O and vortexed to ensure it was well mixed. The gold was then aliquoted, vortexing between each aliquot, and stored at -20°C until required.

2.2.13.1.2 Calcium Chloride CaCl2

1.84g of CaCl$_2$.2H$_2$O dissolved in 5ml dH$_2$O. Solution vortexed and filter sterilised trough 0.2µm filter and aliquoted into 100µl aliquots and frozen at -20°C or used fresh.

2.2.13.1.3 Spermidine

Stock solution; Spermidine supplied as 1g ampoule of powder in argon. Warmed in 37°C water bath until liquefied then aliquoted into 15.8μl aliquots and snap frozen instantly in liquid nitrogen before storage at -80°C. Working solution; 984.2μl of sterile dH$_2$O was added to a 15.8μl aliquot and the solution mixed well by vortexing. The solution was then aliquoted into 30μl aliquots and stored at -80°C until required.

2.2.14 Flow Cytometry

Flow cytometry analysis can be used to detect the fluorescent emissions of cells using specific narrow bandwidth lasers. This allows for specific detection of target fluorescent markers contained in or being expressed by analysed cells. The FACS Calibur uses an FL-1 designated laser for detection of fluorescence in the range of 450-500nm that is used for the acquisition of Alexa-488 tags and GFP expression. This narrow bandwidth reduces the levels of false positives and issues with auto-fluorescence that can be problematic with certain cell types. For analysis, cells were first trypsinised from their culture vessel. Cells were pelleted and then re-suspended in a fixed volume of 1ml ice-cold PBS containing 1% paraformaldehyde. Cells were then stored on ice prior to acquisition. Pipetting of the cells to disrupt any clumps and vortexing before acquisition was important in order to increase the quality of the reading and to prevent the blockages occurring. An untreated control group of cells with no GFP or Alexa-488 was present was used in order to set the background threshold for fluorescence. All cells expressing above this level, not including those within a 5% level of error, were then deemed to be positively expressing the GFP plasmid or Alexa-488 tag. Mean Fluorescent Intensity (MFI) of every cell positive for expression was also measured, which can be used to determine the level of plasmid or Alexa-488 expression per cell population.

2.2.15 Laser Diffraction characterisation

Laser diffraction characterisation was carried out in Aerogen facilities in Galway, Ireland. A Malvern™ Spraytech analyser and accompanying software was used to characterise both the aerosol chamber and the nebulisers using 0.9% PBS solution. PBS was used as it was the solute of choice for aerosol delivery of therapeutics. Further detail of the use and characterisation of laser diffraction is given in Section 5.1, 5.2.

2.2.16 Plethysmography

Plethysmography was carried out using a Buxco plethysmograph and accompanying Buxco XA software. In all experiments the device was first calibrated to the individual restraints as per manufacturers' instructions. In order to ensure accurate calibration, and to prevent a high noise to signal ratio from occurring during both calibration and readings, all the pressure sensitive equipment was isolated on a standalone heavy table in a sealed and noise free room. This was to prevent pressure changes from door openings and loud noises from interfering with readings. The mice were introduced into the restraints for 10min before any recording of measurements began. This was to allow the animal to acclimatise to its new environment before taking any readings. Measurements of lung function were then recorded using the Buxco XA software for a period of 20min. Up to four mice could be analysed at a time. All mice were individually identifiable by a combination of ear tagging and cage identifications. This allowed for each mouse to be analysed in the same restraint for each of multiple recordings and prevented any differences in pneumotachs or restraints from having an effect on any recorded differences in lung function.

2.2.17 Lung Histological analysis

2.2.17.1 Isolation, gravity perfusion, and fixing of lungs for histology

Lung Isolation: The mice are killed by lethal i.p. injection of pentabarbitone (Euthanal). The Abdominal cavity is then opened up as far as the throat exposing the intestinal cavity, ribcage and trachea. The dorsal vein is cut to prevent pooling of blood in the lungs and in the work space surrounding them. The diaphragm is then pierced, deflating the lungs in situ, and the front of the rib cage is then removed exposing the lungs beneath. The thyroid gland is then removed and the trachea is cannulated with a short length of cannula (2.5 - 3.5cms) which has a syringe needle inserted in the open end of the cannula protruding from the trachea. The lungs with cannula attached are then removed from the body cavity. The abdomen chest and throat were then opened, and the trachea was intubated with a cannula which was secured in place with thread. The entire lungs with trachea intact are then removed from the thoracic cavity.

Gravity perfusion and fixation: The Cannula is now attached to a 3 way valve system that is attached to a butterfly tab intravenous cannula (Figure 2.1). This is then attached to a 50ml syringe which is located 20cm above the lungs. The 50ml syringe has had its plunger removed and is filled with fixative. Once the lungs were attached

to the valve system they were then perfused with the fixative by gravity feed. Once the lungs are fully perfused and inflated with fixative the cannula is detached from the valve and the lungs are then stored in individual, labelled 50ml sterilins containing fixative at room temperature for a minimum of 48hr. The remainder of the embedding protocol is as follows;

Day1- Fix in 4% paraformaldehyde in PBS for 48hr at room temperature.

Day2- Store in 70% EtOH over night at room temperature.

Day3- The individual lobes of the lungs are separated and each is assigned to an individual labelled cassette which is then put through various final solutions in succession to prepare the lobes for embedding as outlined in Table 2.1 below. The lungs were then embedded in wax moulds which were placed on a pre-chilled coldplate and allowed to set slowly overnight prior to sectioning.
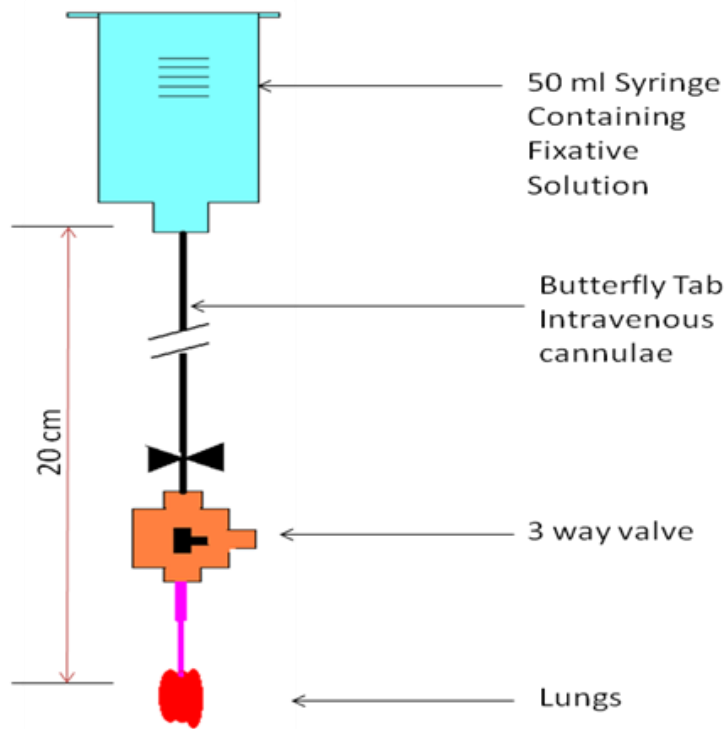
Figure 2.1 Gravity feed system for the perfusion of lungs

Duration	Solution	Temperature
60 minutes	70% EtOH	Room Temp.
60 minutes	80% EtOH	Room Temp.
60 minutes	95% EtOH (1)	Room Temp.
60 minutes	95% EtOH (2)	Room Temp.
60 minutes	100% EtOH (1)	Room Temp.
60 minutes	100% EtOH (2)	Room Temp.
60 minutes	100% EtOH (3)	Room Temp.
60 minutes	50:50 Xylene:100% EtOH	Room Temp.
60 minutes	100% Xylene (1)	Room Temp.
60 minutes	100% Xylene (2)	Room Temp.
60 minutes	Paraffin Wax	65°C
3-4hr	Paraffin Wax	65°C

Table 2.1 Succesion of treatments for parrafin embedding of lungs on Day3 of fixation

2.2.17.2 H&E staining of wax embedded tissue sections

Slides were placed in xylene for 3x3min, then 100% EtOH for 3x3min, 95% EtOH for 3x3min and then 75% EtOH for 3x3min before placing them in deionised H_2O for 1x5min. Slides were then placed in hematoxylin (Harris' Hematoxylin) for 1x3min. Slides were then rinsed in deionised H_2O and then dipped in tap water for 1x5min. Slides were then quickly dipped x8 into acid ethanol (1ml conc. HCl in 99ml EtOH) before rinsing the slides in tap water for 2x1min. Slides were then placed in d H_2O for 1x2min. Slides were then placed in Eosin Y (1g/100ml dH_2O) for 1x45sec. Slides were then rinsed in 95% EtOH for 3x5min and then 100% EtOH for 3x5min before being placed in Xylene for 1x10min. The slides were then allowed to dry and coverslips mounted using DPX mountant

2.2.17.3 Quantitative Histological Analysis

Lung sections were H&E stained and images of all sections were captured under the same magnification .Histological analysis was then carried out and scored in a blinded manner. Three different measurements were used to assess the effect of elastase-induced damage on the lungs:

(i) The mean interceptal distance for the alveoli was calculated. This was done by placing a 5 open square grid over a captured brightfield image of a section using Adobe CS3 software. This was done to three different sections for every set of lungs analysed. In a randomly determined fashion, in 3 of the squares of every section the mean interceptal distance (of all alveoli which were determined to be at least 50% inside the grid) was measured using a ruler tool available within the software. In combination with scale measurements from the original images it was possible to accurately convert pixels to µm measurements.

(ii) The number of alveoli present was determined. As per the interceptal distance, a grid was applied in Adobe CS3. The entire number of alveoli present was then counted using the counter tool available in the software and the results exported to excel for analysis.

(iii) The number of intersections present was determined. As per the interceptal distance, a grid was applied in Adobe CS3. The entire number of intersections present was then counted using the counter tool available in the software and the results exported to excel for analysis.

2.2.18 BALF isolation protocol

Mice were euthanized by i.p. injection of 0.3ml Euthanal pentabarbitone and subsequently weighed. The abdominal cavity was then opened as far as the throat exposing the intestinal cavity, ribcage and trachea. The dorsal vein was cut to prevent pooling of blood in the lungs and the surrounding tissue. The diaphragm was then pierced deflating the lungs in situ and the front of the ribcage removed, exposing the lungs beneath. The thyroid gland was then removed and the trachea cannulated and the cannula secured in place. The lungs with attached cannula were then removed from the body cavity. 200ml/100g bodyweight of the mouse of 37°C PBS was then instilled into the lungs via the cannula. After approximately 30 seconds the BALF was then removed from the lungs into a clean syringe, the volume retrieved noted and the solution placed in an eppendorf on ice. The BALF was then centrifuged at 259g for 15mins at 4°C on a desktop centrifuge. Supernatant was then removed and placed in a fresh clean eppendorf and the cell pellet resuspended in 200ul PBS. 50µl of the resuspended solution was utilised for performing a cell count with a haemocytometer and EBAO was used to determine percentage cell viability (Green cells were alive, Orange cells were dead). The remaining aliquot (150µl) was divided into two aliquots that were each used to prepare cytospins. From the supernatant 30µl was removed and stored at -80°C for a subsequent protein assay using the Bio-Rad Bradford protein assay. The remaining supernatant was also frozen at -80°C for any other analysis.

2.2.18.1 Cytospin preparations

A 75µl aliquot of resuspended cells from BALF as prepared above is used for each cytospin preparation. If the preparation turns out to be too high in cell number for accurate cytospin preparation, the second aliquot is diluted appropriately and used to prepare the sample. Briefly, glass slides are poly-L-lysine coated and placed in a cytospin slideholder. There is an absorbent layer placed on top of the slide leaving a clear circle of glass in the centre of the slide on which the cell sample is aliquoted. Using a cytospin centrifuge, the samples are then spun using a specially designed chamber onto the poly-L-lysine coated microscope slide. The cells adhere to the surface and any excess liquid is removed into the absorbent layer via centrifugation. The cells are now available suitable for further fixing and staining as required.

2.2.18.2 Speedy-Diff staining of BALF cytospin preparations

"Speedy-Diff" is a proprietary brand of a Romanowski stain, also known as Quick-Diff staining. It allows for colorimetric differentiation of cell types. Once the cytospin

preparation has been allowed to air-dry it can be subjected to Speedy-Diff staining. All solutions required are provided as part of the 'Speedy-Diff' kit and fixing and staining is carried out according to manufacturers recommended protocols. Once stained a coverslip is mounted using DPX mountant and the cells viewed by brightfield microscopy.

2.2.19 siRNA transfections

Pre-designed siRNA molecules were purchased along with Hiperfect transfection reagent from Qiagen. All siRNA transfections were carried out according to manufacturers' protocols

2.2.20 PCR

2.2.20.1 RNA Isolation

(i) Adherent cells were directly lysed with the addition of TriZol to the culture surface. For whole lung tissue RNA isolation, the lungs were homogenised using a glass/Teflon homogeniser or a mechanical homogeniser in a volume of TriZol equivalent to 1ml/g. Once lysed the cells/tissue were pipetted into a 1.5ml eppendorf and 5µl of Poly Acryl Carrier was added to each sample to help increase the final quantity of RNA isolated. The solution was then incubated at room temperature for 5min and at this point the cell solution could be stored at -20°C or used immediately. Phase separation of the mixture was carried out by the addition of 200µl chloroform followed by vigorous shaking of the tube for 15sec to ensure good mixing. The mixture was then incubated at room temperature for 3min before being centrifuged for 15min at 12000g, causing the solution to separate into 3 distinct phases, a lower, red, phenol phase, a central white interphase containing DNA and a clear aqueous upper phase containing RNA. The RNA phase was carefully removed from the eppendorf with care taken to ensure not to contaminate it with any of the DNA interphase, and transferred into a sterile 1.5ml eppendorf. 500µl of Isopropanol was then added to the aqueous RNA and mixed by inversion and left incubate at room temperature for 12min, causing the RNA to precipitate out of solution. The solution was then centrifuged for at 4°C for 8min at 12000g causing the RNA to pellet out of solution. The supernatant was then removed and the RNA pellet was washed x2 by the addition of 1ml 75% EtOH, vortexing and centrifugation at 4°C for 5min at 7500g. After the second wash all the supernatant was removed and the pellet allowed to air-dry for 2-3min until all residual EtOH had evaporated. The RNA pellet was then resuspended in

a fixed volume of DEPC water by gentle pipetting, followed by incubation at 60°C for 10min. The volume of water varied from 15-30µl DEPC depending on the expected concentration of the RNA. The RNA was then immediately put on ice and either stored at -80°C or quantified and used for cDNA synthesis.

(ii) RNA isolation from NEHB human primaries and primary airway epithelial cells was carried out by using a Qiagen RNeasy kit so as to help extract a sufficient quantity of high grade RNA for QPCR. RNA was isolated following manufacturers recommended protocols.

2.2.20.2 RNA Quantification

RNA was quantified using a nanodrop to ensure it was of sufficient purity and to determine the concentration by spectrophotometry. A 260:280 ratio of >1.8 was required for all RNA to be used in QPCR analysis.

2.2.20.3 cDNA synthesis

Two aliquots of RNA were DNase treated. Of these only one received reagents for cDNA synthesis, the other was used as a no-RT control for genomic contamination of the samples and received DPC water *in lieu* of cDNA synthesis reagents. To 1µg of RNA 1µl of 10X DNase Buffer and 1µl DNase were added and brought up to 10µl final volume with the addition of DEPC water. This was subsequently incubated at room temperature for 30mins. The DNase was then inactivated by the addition of 1µl of 25mM EDTA and incubated for 10min in a 65°C water bath.

For cDNA synthesis 1µl of Oligo $dT_{(12-18)}$ primers was added and incubated for 10min at 70°C. The samples were then immediately cooled on ice for at least one minute and in the order listed the following was then added to each sample; 4µl 5X First-Strand Buffer, 2µl DTT, 1µl RNase OUT, 1µl M-MLV Reverse Transcriptase and 1µl dNTP mix. The reaction was then carried out at 37°C for 1hr and then stopped by heating to 95°C for 2min. cDNA was then stored at 4°C for immediate use or at -20°C for up to a month for use later.

2.2.20.4 Primer design

Gene sequences were obtained from the NCBI *Entrez Nucleotide* database (http://www.ncbi.nlm.nih.gov/sites/entrez). Primers were designed using Primer3' software from the Whitehead Institute for Biomedical Research (http://frodo.wi.mit.edu/primer3/).

2.2.20.5 Reverse transcriptase PCR (rtPCR)

The conditions for standard rtPCR were as follows

5µl	10X Go Taq Flexi PCR Buffer
3-5µl	25mM MgCl2
8µl	1.25mM dNTP mix
1µl	Forward Primer
1µl	Reverse Primer
0.25µl	Go Taq Flexi Polymerase (5U/µl)
1µl	cDNA
to 50µl	DEPC Water

PCR mastermix was prepared on ice and as soon as samples were prepared they were transferred to a thermal cycler. This was then programmed to heat samples to 95°C for 2min to denature the cDNA. This was then followed by 35 cycles of 95°C for 45sec (denaturing step), 45sec at annealing temperature (primer specific) and1min at 72°C (extension step). The only exception to this was GAPDH which only had 30cycles carried out. Following this set of cycles there was a final extension step at 72°C for 10min before samples were cooled to 4°C at which temperature they were stored until required.

The temperature for annealing was determined by using a varying temperature gradient cycler and specific primer annealing temperatures are listed in Section2.1.3.

2.2.20.5.1 Agarose Gel Electrophoresis of PCR Products

0.8 - 2 % (w/v) agarose gels were made by dissolving 0.8 - 2 g agarose in 100 ml TAE buffer (40 mM Tris, 0.35 % v/v Acetic Acid, 0.5 mM EDTA). 3µl/100ml of ethidium bromide/gel was also added. This bound to the DNA and allowed visualization of the DNA product under UV light. The gel was then subjected to an electric current (electrophoreses) enabling the DNA to travel through the gel and separate according to size. A DNA ladder was also ran in all cases to allow for sizing of the DNA products present.

2.2.20.6 QPCR

2.2.20.6.1 QPCR in human and mouse cell lines

Quantitative Real-Time PCR (QPCR) enables the determination of the fold increases and decreases in RNA levels of specific targets. It allows for absolute quantification in terms of copy number or relative quantification in relation to a housekeeping gene. QPCR in human and mouse cell lines was carried out using Sybr Green. The relative

quantity of amplified product was calculated based on cycle threshold (CT) values and changes in expression levels of the gene of interest were compared to that of a housekeeper. The fold differences resulting from treatments were determined using $2^{-\Delta\Delta CT}$ calculations. Samples were set up in 8 well PCR strips and primers added to a concentration of 400nm. To each well was added 10µl Sybr Green and 1µl cDNA. The total colume was then brought to 20µl using DEPC and the samples were subjected to PCR on the Opticon thermal cycler. The first step was 10min at 95°C, followed by 40 cycles of 95°C for 45sec, 58°C for 45sec and 72°C for 1min.

2.2.20.6.2 QPCR in human and primate primary cells.

For qPCR the primer/cDNA mix was completed as follows: 12.5µl 2X Sybr Green, 0.5µl forward and reverse primer resectively, 0.5µl cDNA and brought to a final volume of 25µl with DEPC and added to 96well labelled plates. All reactions were carried out in triplicate for each 'n' number experiment, with the results being averaged and then compiled. All data was inspected for outliers within the triplicate for each reaction. Once the plates were made up they were coated with a plastic cover, spun briefly using a desktop centrifuge and then loaded into the ABI Taqman system for analysis. All data was exported from Taqman into excel format and compiled using Prism Software (Graphpad). Data was analysed as for 2.2.20.6.1 above. GAPDH was used as the qPCR house-keeping control.

2.2.21 Establishment of mouse lung damage models

2.2.21.1 OVA/Asthma models of allergic inflammation

2.2.21.1.1 Model establishment for the assessment of BMP pathway activity

Prior to treatment mice had their lung function analysed by plethysmography on Day0. Mice were then sensitized with 100µg of OVA (Sigma) emulsified in 2% Alhydrogel adjuvant administered i.p. on days 0, 7 and 14. The control group (Group 1) received PBS alone (i.p.). On Day14, approximately 6 hours following the i.p. administration, animals were anaesthetised and OVA was administered by i.n. delivery. Subsequently on Day25, 26, and 27, OVA-sensitized mice received 50µg of OVA intranasally (i.n.); control group mice received PBS alone. On day 28 half the animals from each group were sacrificed. Broncho alveolar lavage fluid (BALF) was obtained and analysed, or stored at −70 °C until time of analyses.

2.2.21.1.2 Model establishment for the assessment of therapeutic safety and effect.

The model was established in the same manner as above up as far as and including Day27. Animals were then exposed to an aerosol of 2.5µg of therapeutic protein in 10mls PBS until the solution was fully aerosolised at a flow rate of 4L/min on Day28. Also on Day28, prior to treatment, the mice had their lung function analysed by plethysmography, which was repeated again immediately prior to animal sacrifice at the appropriate time point.

2.2.21.1.3 OVA-specific IgE ELISA

96 well plate was coated with ovalbumin (5ug/ml) in alkaline buffer– 50ul/well and left overnight at 4°C. the plate was then washed with 1xPBS-Tween (0.05%) and blocked with 10% Marvel milk powder in PBS (300ul per well). The plate was then incubated for 2 hrs at room temperature. Plate was then washed with 1xPBS-Tween Add standards and sample dilutions of 1/50, 1/100, 1/200, 1/250 (50µl/well). Plate was then left overnight at 4°C or incubated at room temperature for 2 hours. Plate was then washed x3 with PBS-Tween-20 (1% Tween). Biotinylated anti-mouse IgE (1/250 dilution in PBS+2% BSA) was then added at 50µl/well and incubated at room temperature for 1hr. Plate was then washed with 1xPBS-Tween. Streptavidin-HRP was then added (50ul/well) and incubated at room temperature for 1hr. Plate was then washed with 1X PBS-Tween and TMB was then added (100µl) and incubated at room temperature for 30mins away from light. The reaction was then stopped with 1N H_2SO_4 and the results read at 450nm on a plate reader. Alkaline buffer: (a) =424mg Sodium carbonate (Na2CO3) in 40mls dH2O. (b) =840mg Sodium hydrogen carbonate (NaHCO3) in 100mls dH2O. 30mls of (a) added to 70mls of (b) and made up to 200mls with dH2O (Ph 9.6).

2.2.21.2 Elastase model in mice

Mice were anaesthetised via inhalation of isoflurane. 30Units of porcine pancreatic elastase (Type IV) were administered to each mouse (30µg in 0.1ml of sterile PBS) intranasally. This was repeated 3 times weekly for a duration of two weeks.

2.2.21.3 Anaesthetising mice for intranasal administration

Mice were removed from their cage and placed in a holding chamber connected to a gas scavenger unit. A connected isoflurane line was then opened and the oxygen flow rate was increased to 3L/min. The mouse was monitored carefully and once seen to have succumbed to the anaesthetic (after approximately 0.5-1min) it was scruffed and

removed from the holding chamber. The nasal administration was then carried out by pipetting a designated volume of solution into the nasal passages of the animal, which upon correct administration could be visibly confirmed to have been inhaled into the airway. Subsequently the animal is returned to its own cage where it is monitored carefully during recovery from the procedure. Animals were checked again one hour post anaesthetic and administration to ensure no adverse affects were to be observed.

2.2.22 Aerosolisation and delivery of potential therapeutics

All aerosolisation was carried out by means of an Aerogen Aeroneb Pro vibrating mesh nebuliser unit. This consisted of the Aeroneb Pro control unit and a detachable and replaceable nebuliser head which contained the reservoir and vibrating element.

2.2.22.1 Aerosolisation of therapeutics

Aerosolisation of therapeutics was carried out by aliquoting the solution into the reservoir on the nebuliser head. The device was then activated using the control unit and the resulting aerosol was captured in a pre-chilled sterilin sitting in an ice-bath. This helped rapid condensation of the aerosol, preventing a large cloud build-up in the sterilin from affecting the ability of the nebuliser to function correctly. Control solutions that were not being nebulised were aliquoted at the same time into ice-cold sterilins also. Once the nebulisation was complete and the aerosol cloud seen to have deposited on the inside of the sterilin, the nebuliser was removed from the top of the sterilin and the tube quickly capped. Both the control and nebulised solution were then centrifuged in order to facilitate recovery of the full amount of nebulised solution, the control was centrifuged also in order to make sure that centrifugation had no impact on the downstream analysis of the effects of the nebulisation.

2.2.22.2 Delivery to animals of nebulised therapeutics

Animals were restrained in specially designed whole body restraint, nose only exposure systems that were connected to a central aerosol chamber. The nebuliser head unit was attached to the top of this chamber. 2.5µg of therapeutic agent was dissolved in 10ml PBS and a Buxco Flow regulator was activated to provide a flow of dehumidified air through the chamber at a flow rate of 4L/min for 10min. The nebuliser control was interconnected with the airflow control to ensure that nebulisation only occurred when adequate airflow was established. The solution was then nebulised into the chamber and the mice exposed to a 2.5µg/10ml concentration of therapeutic for 10min at a flow rate of 4L/min dehumidified air though the central

chamber to facilitate the availability of optimal fine particle fraction and VMD of the nebulised therapeutic for inhalation to the animals. Immediately after nebulisation the animals were released from their restraints back into their cages and carefully monitored afterwards for any signs of toxicity or injury resulting from the aerosol exposure.

2.2.23 Animal Care and Ethical Approval

All mouse work was carried out on animals housed in NUIM Bio Resources Unit under licence from the Department of Health and Children and according to N.U.I. Maynooth institutional guidelines on animal care and experimentation. Ethical approval was sought and granted for all procedures. All Primate cells were harvested from Rhesus Macaques housed in the California National Primate Research Centre, Davis, California. All work was carried out under institutional guidelines on animal care and experimentation under licence.

2.2.24 Statistical Analysis

Unless otherwise confirmed, results are expressed as the mean +/- the standard error. Statistical analysis using Student T-test, one-way ANOVA, repeated measures ANOVA, two-way ANOVA, Tukeys post test and Bonferroni post test were all carried out utilising commercially available GraphPad Prism® software.

3 The BMP pathway *in vivo* in a primate model of asthma and the effect of BMP4 on human and primate airway epithelial cells *in vitro*

3.1 Introduction

For this project the effects of Ozone (O_3) and house dust mite allergen (HDMA) induced allergic asthma on the bone morphogenetic protein (BMP) pathway was assessed within the airways of neonatal Rhesus Macaques (*Macaca mulatta*) after exposure to O_3+HDMA over a 6month period (Section 2.1.2). It has been shown that these non human primates are suitable for research into the defining mechanisms underlying allergic airways disease in humans.(Plopper and Hyde, 2008). In our lab it has already been established that the BMP pathway is involved in the process of regeneration after injury (Masterson et al., 2010), and EMT in Mouse airway epithelial cells (Molloy et al., 2008) and has also been shown to be involved in the process linked to certain types of lung cancer and to Allergic Rhinitis (unpublished data). As such we hypothesised that the BMP pathway is a potential target for modulation in certain disease models.

In addition, ALI studies using primary human and primate airway cells were established to determine the effect of exogenous BMP4 in normal conditions and in an injury model. Injury was induced by pre-treatment of the cells with EGTA prior to exposure to BMP4 (Section 2.2.10). It helps evaluate the pathways differences in cells that are also contending with junction disruption in parallel with TGF pathway signals in the form of BMP4 as likely to be seen in an *in vivo* damage model.

3.1.1 Markers of lung injury

A number of important markers of injury were studied during the primate and human ALI studies and included p21 and PCNA.

p21, a cyclin/cyclin dependent kinase inhibitor, is a cell cycle regulator and is found to be upregulated in cell senescence, and over expression of the gene results in cell-cycle arrest. p21 regulates the cell cycle and proliferation through arrest at the G1/S transition (Steinman et al., 1994; Liu et al., 1996) and it is linked to both BMP4 and to PCNA and is shown to be increased in allergic asthma (Su et al., 2009).

Proliferating Cell Nuclear Antigen (PCNA), as mentioned above, is in part regulated by the activity of p21. It is a protein clamp that is has an essential role in the repair and replication of DNA and as such is vitally important in processes where injury or damage has resulted in DNA damage as may be seen in many airway inflammatory and pathological diseases.

3.1.2 Ozone and HDMA induced Asthma

The O_3 and HDMA induced asthma model was set up as described elsewhere (Schelegle et al., 2003). Briefly, primates were exposed to a combination of cyclic exposures to Ozone and house mite allergen that resulted in differences in airway morphology and in an increase in airway resistance combined with increased sensitivity to allergen. The study showed the combination of exposure to O_3 and HDMA produced an allergic inflammation phenotype similar to what is seen in human asthma.

3.1.3 Study Aims

Primate airway studies were designed as follows. Paraffin embedded sections of Rhesus trachea and airways levels 1, 2 and 6 from O_3+HDMA treated animals and control animals (Filtered Air) were evaluated by immunofluorescence analysis of PCNA, BMPR-IA and pSmad1/5/8 protein expression. The importance of the evaluation of the differing regions of the airways is that it can help define where the spatial remodelling is occurring within in the airways and to see if, as in vascular remodelling, airway response in terms of BMP activity is airway generation-specific (Avdalovic et al., 2006). In order to investigate the role of BMP signalling and to assess the level of damage response in the airways in this model the localisation and expression of three main proteins was examined, pSmad1/5/8 which is indicative of active BMP signalling; PCNA as a marker of proliferating cells used to identify areas undergoing regeneration and; BMPR-IA which indicates cells are responding to BMP ligands.

In addition to this analysis, ALI cultures of human and primate primary bronchial epithelial cells were examined in order to determine what effect activation of the BMP pathway had on cells. Pathway activation was achieved by the delivery of recombinant human BMP4 to the apical surface of the epithelial ALI cultures. A second study was also conducted with both human and primate ALI cultures that involved the pre-treatment of the ALI cultures with EGTA to create a disrupted epithelium, with the aim of modelling the disrupted and damaged environment characteristic of many diseases of the lung. In order to characterise the role of BMP4 in both a normal intact ALI culture and in an EGTA disrupted epithelium model culture, qPCR and Western Blot analysis of various markers was carried out. The following markers were analysed by qPCR: Id1, as an early responder to BMP4 signalling was used to evaluate whether or not the BMP4 delivery had induced

pathway activation; PCNA and p21 were examined to assess whether proliferation or quiescence respectively occurred in response to BMP4. BMP receptors BMPR-IA, BMPR-IB and BMPR-II were evaluated to determine the effect of pathway activation on their levels of production. The Smad signalling pathway was evaluated by examining the levels of R-Smads Smad1 and Smad5, and of co-Smad, Smad4. BMP2 was examined to see if BMP4 activity abrogated or stimulated its expression and E-cadherin was examined to help evaluate cell adhesion under pathway activity. The Snail family of genes play key roles in development, patterning and EMT. Western Blotting was used to analyse the levels of E-Cadherin, BMPR-IA, Smad4 and Id1.

3.2 Results

3.2.1 Ozone+HDMA Model in Rhesus Macaque primates

Expression of PCNA, BMPR-IA and pSMAD1/5/8 was examined by immuno-fluorescence in O3+HDMA treated animals and in control animals treated with Filtered Air. Tissue sections from trachea and airway levels 1, 2 and 6 were examined (n=3).

PCNA: PCNA expression appeared similar in the trachea of both control and O_3+HDMA animals with no difference in protein expression or localisation, with only low levels being detected in the trachea of both sets of animals (Figure 3.1). As the examination progressed down the airways however a marked change in expression between the two groups was noted. At airway level1, there was a marked difference in expression levels between the two treatment groups, with the epithelium lining the airways at level 1 showing elevated and abundant staining for PCNA in O_3+HDMA animals compared to that evident in the control animals (Figure 3.2). This trend became more pronounced at airway levels 2 and 6, with PCNA highly abundant throughout the epithelium of the O_3+HDMA animals and with no increase or change in expression from the control animals between any of the airway levels (Figure 3.3 and Figure 3.4).

BMPR-IA: In the trachea BMPR-IA expression was barely detectable in either group of animals (Figure 3.5). In level1 however in O_3+HDMA animals there was a marked increase in abundance of protein in the epithelium of the level1 airway (Figure 3.6). This was not apparent in the control animals where there was just a slight increase in the abundance levels to just above what was seen in the trachea. In the level2 and level6 airways this pattern was repeated for BMPR-IA expression with highly abundant BMPR-IA visible in the epithelium lining the airways of the O_3+HDMA animals and a low level of expression in the control animals (Figure 3.7 and Figure 3.8).

pSmad1/5/8: In airway level2, pSmad1/5/8 activity was significantly higher in O_3+HDMA treated animals than was apparent in the control animals, where no pSmad1/5/8 protein was detected. At airway level 6 there was pSmad1/5/8 activity detected in both groups of animals. The level detected increased in both groups compared to level2 airways. The level of expression in the control animals at airway

level6 was similar to that seen in the O_3+HDMA animals at airway level 2. The level of pSmad1/5/8 detected in the O_3+HDMA animals had increased expression far more abundant in at level 6 than observed at level2. The localisation of expression between the two treatment groups did not differ nor did it deviate between levels. Data was not obtainable for the trachea or level1 airways.

A summation of all results can be seen in Table 3.1.
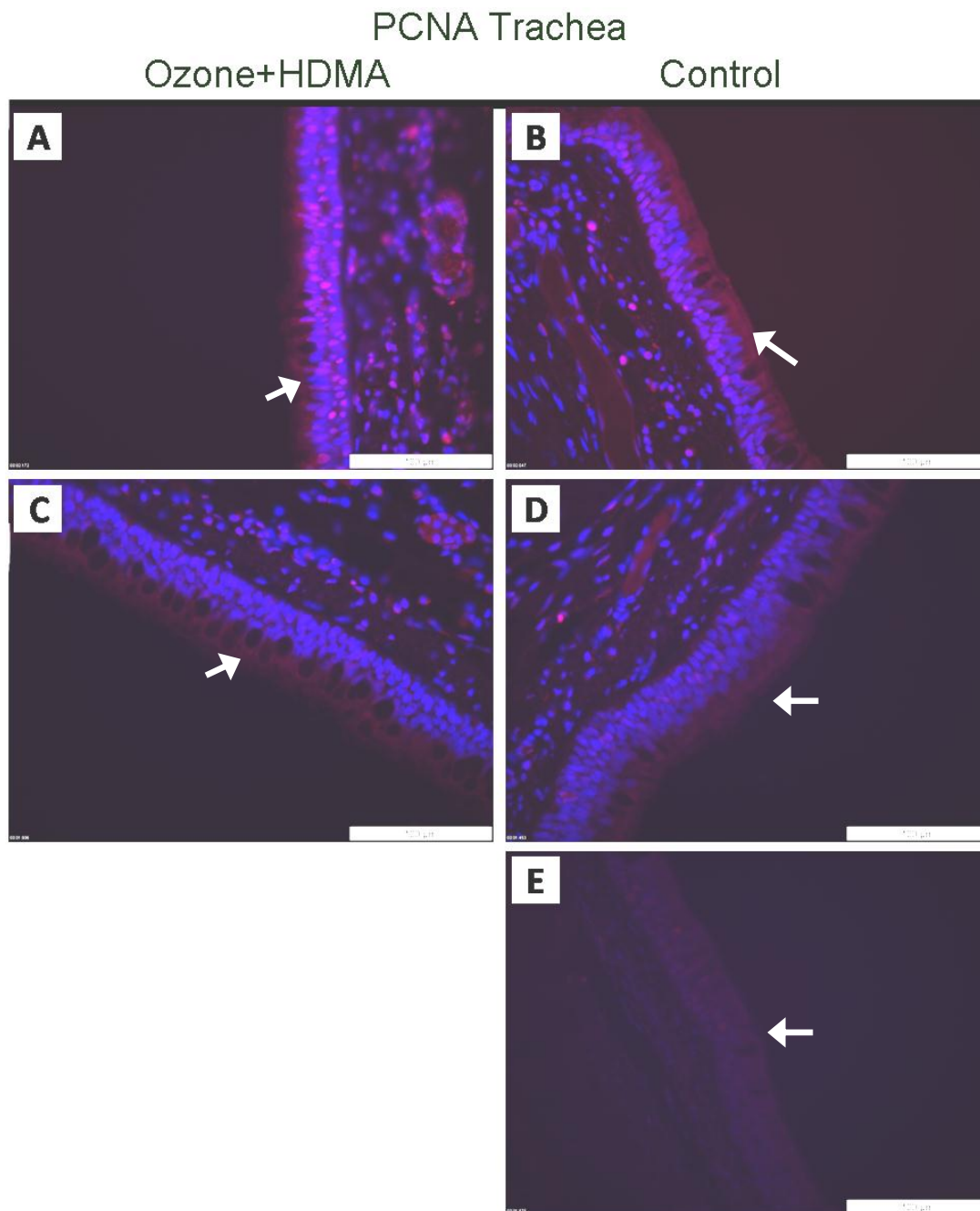
Figure 3.1 Expression of PCNA in the trachea of the primate lung

O_3+HDMA (A and C) compared to control lung (B, D and E). PCNA (568 Red) was present at very low levels in both O_3+HDMA and Control groups in the Trachea. (Blue = Dapi Nuclear stain).
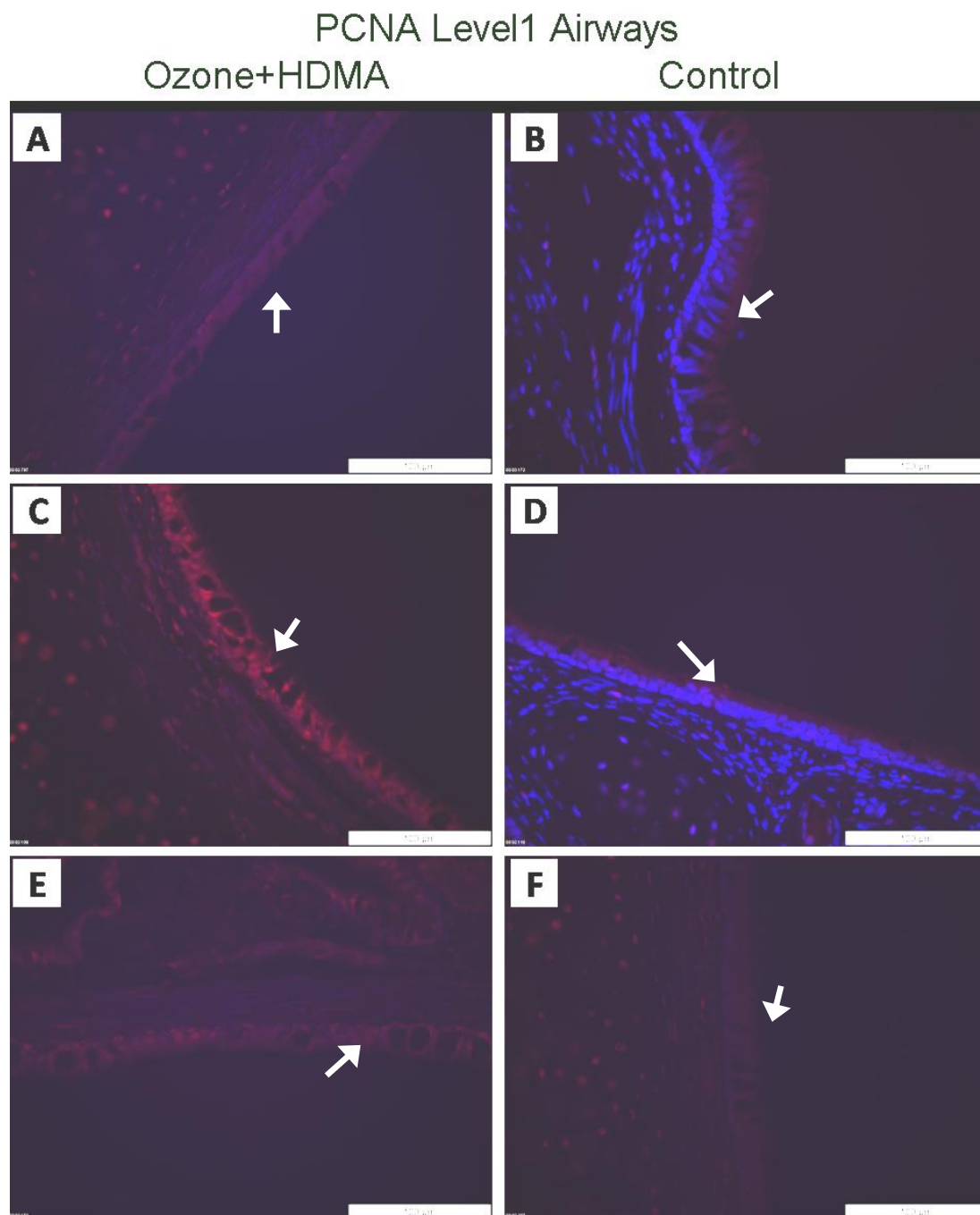
Figure 3.2 Expression of PCNA in airway level 1 of the primate lung

O_3+HDMA (A, C and E) compared to control lung (B, D and F). PCNA (568 Red) was observed at elevated levels in the O_3+HDMA which contrasted with level present in the Control group which was ranged from undetected to very low. (Blue = Dapi Nuclear stain).
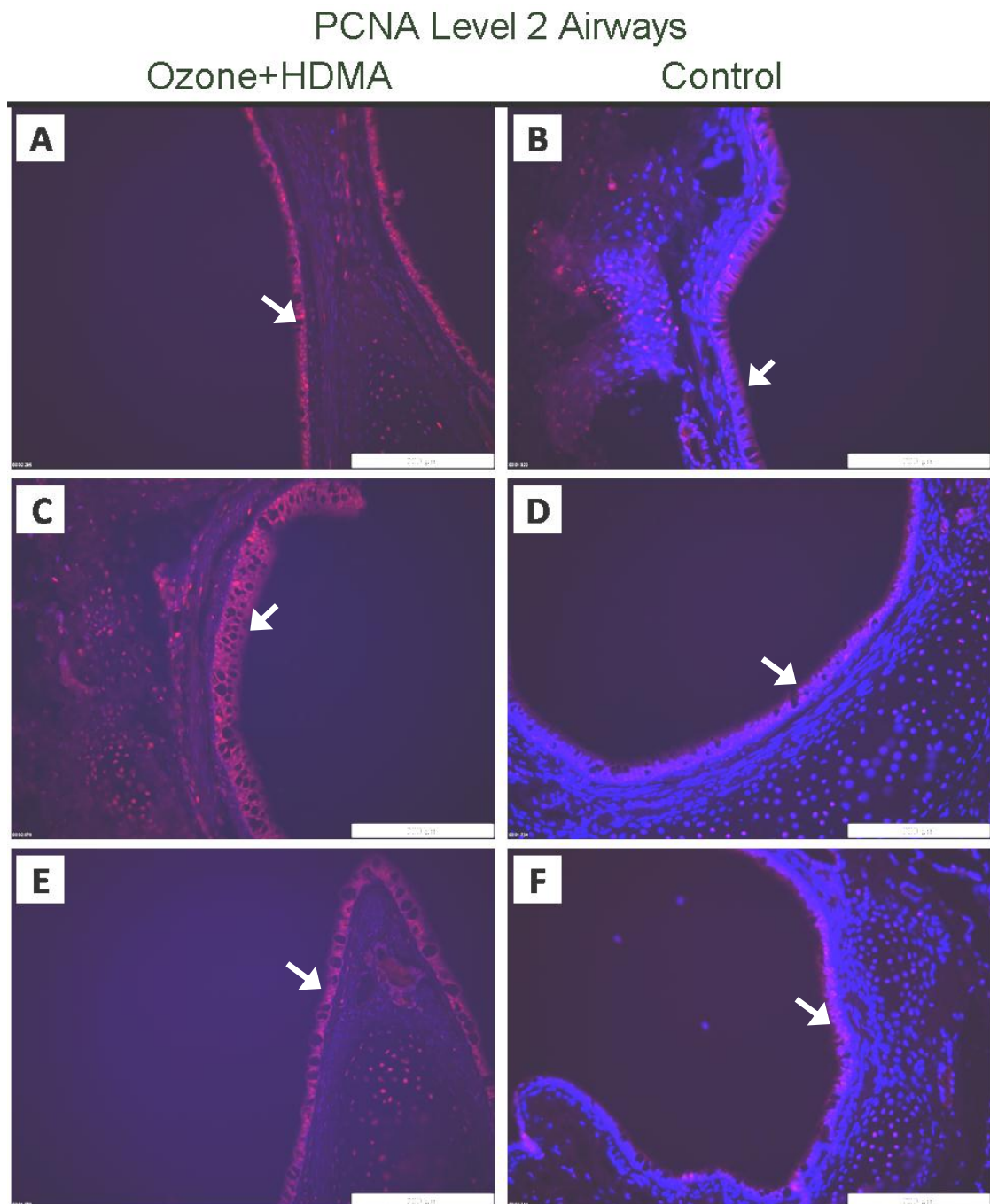
Figure 3.3 Expression of PCNA in airway level 2 of the primate lung

O_3+HDMA (A, C and E) compared to control lung (B, D and F). PCNA (568 Red) was detected at a level far in excess of that observed in the control lungs at this level in the O_3+HDMA group. (Blue = Dapi Nuclear stain).
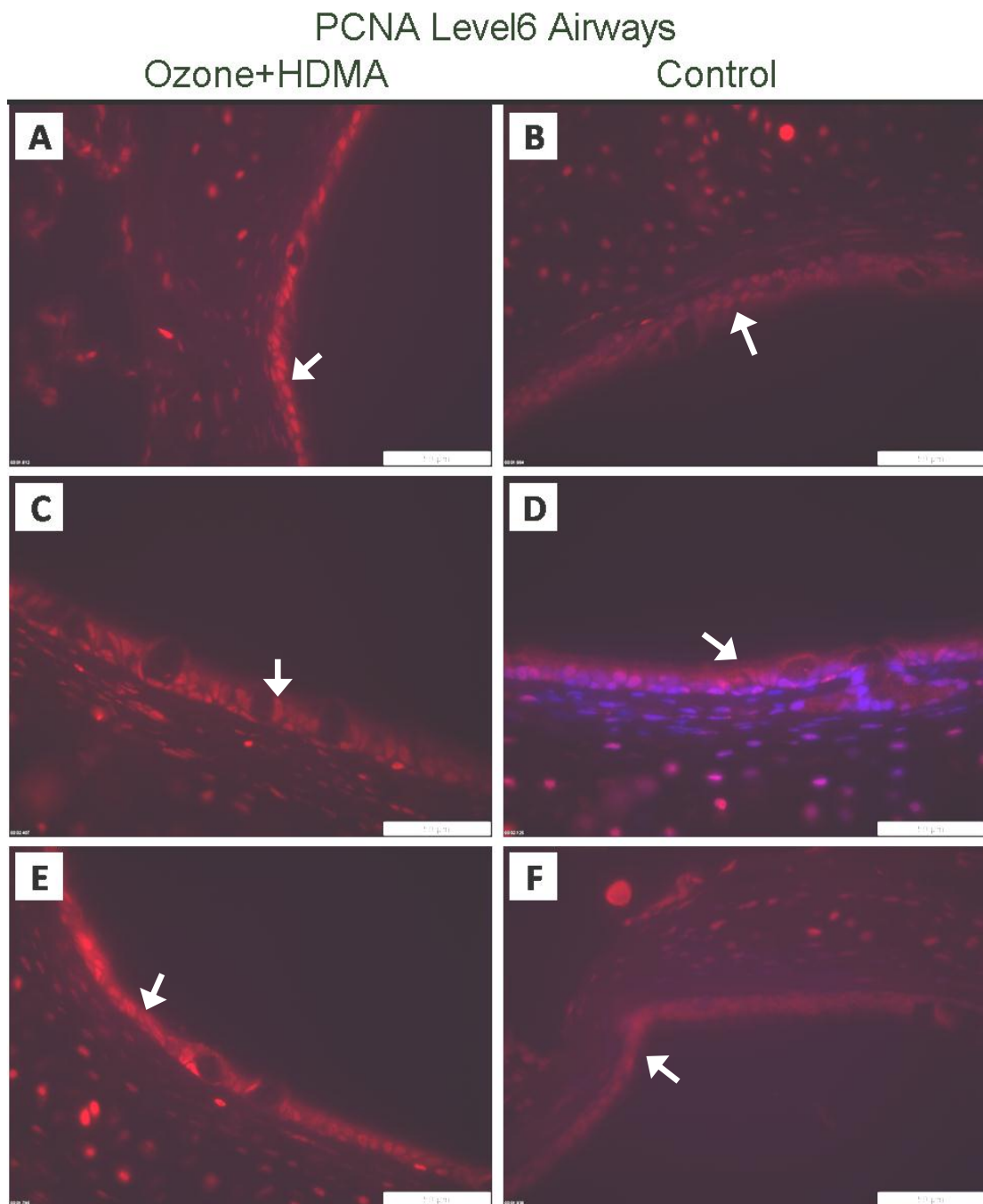
Figure 3.4 Expression of PCNA in airway level 6 of the primate lung

O₃+HDMA (A, C and E) compared to control lung (B, D and F). PCNA (568 Red) was here again detected at a level in excess of that observed in the control lungs at this level in the O₃+HDMA group. (Blue = Dapi Nuclear stain). The control lungs indicated the presence of PCNA at level barely exceeding that of the background (B, F) though one animal did display a moderate amount of flourescence (D).
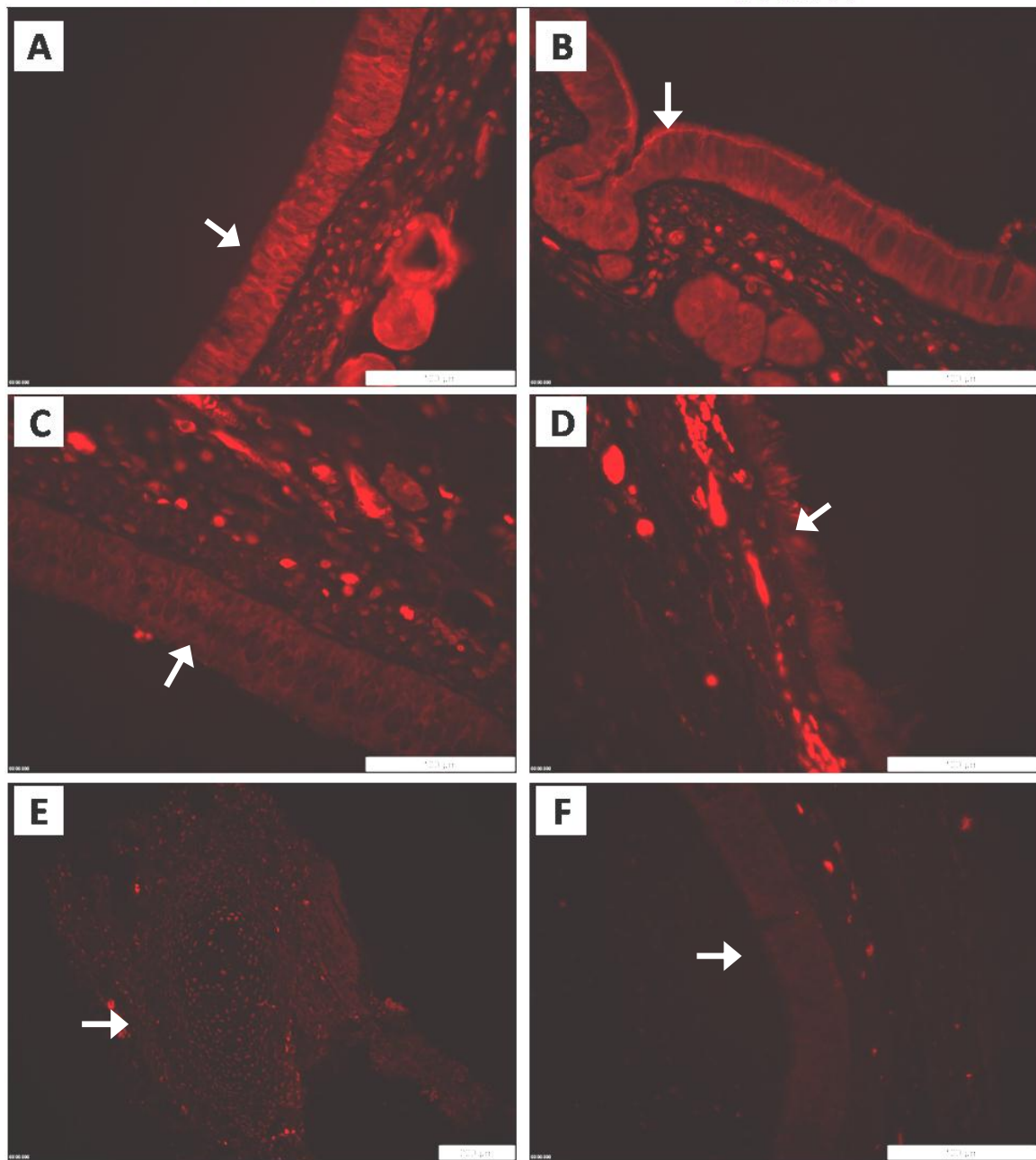
Figure 3.5: Expression of BMPR-IA in Trachea

O_3+HDMA (A, C and E) compared to control lung (B, D and F). BMPR-IA (568 Red) was detected at a low level in both O_3+HDMA and Treatment control groups in the trachea of the animals involved in this study. It was faintly present in airway cells in only one of each group (A and B) and not present n the remaining two animals in either group at the airway surface though levels could be etected in the basement memberane in both groups.
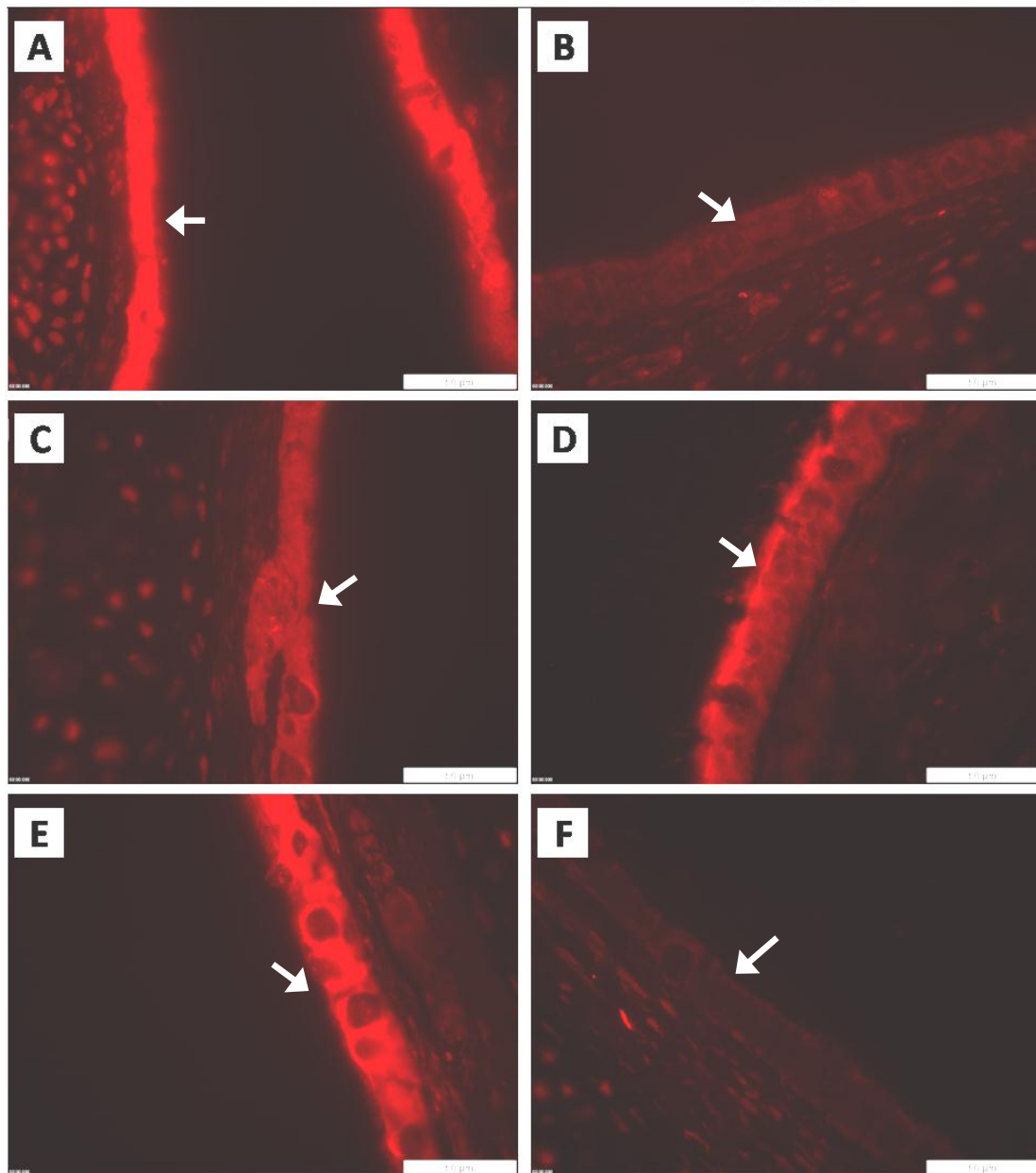
Figure 3.6 Expression of BMPR-IA in Airway level1

O_3+HDMA (A, C and E) compared to control lung (B, D and F). BMPR-IA (568 Red) was highly abundant in level1 of the airways in the O_3+HDMA treated group. This contrasted with the control group where only one animal displayed an abundance of the protein (D) while the remaining two animals, (B and F) had no detectable levels of BMPR-IA present.
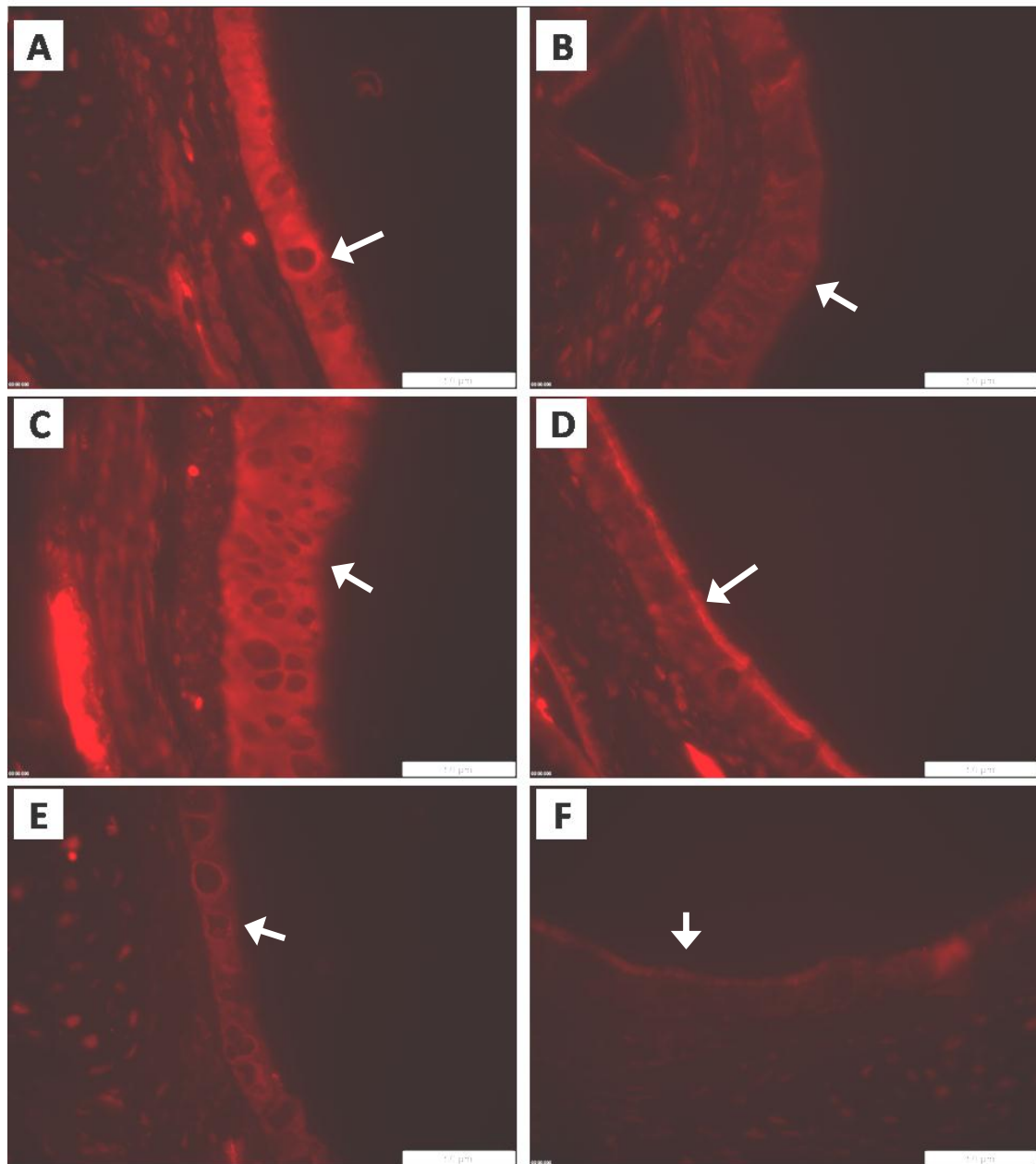
Figure 3.7 Expression of BMPR-IA in Airway level 2

O$_3$+HDMA (A, C and E) compared to control lung (B, D and F). BMPR-IA (568 Red) was highly abundant in level2 of the airways in the O$_3$+HDMA treated group. This again contrasted significantly with the control group as was seen in airway level 1 (Figure 3.6) where only one animal in the control group displayed an abundance of the protein (D). The other two animals in the control group displayed only faint amounts of the Protein.
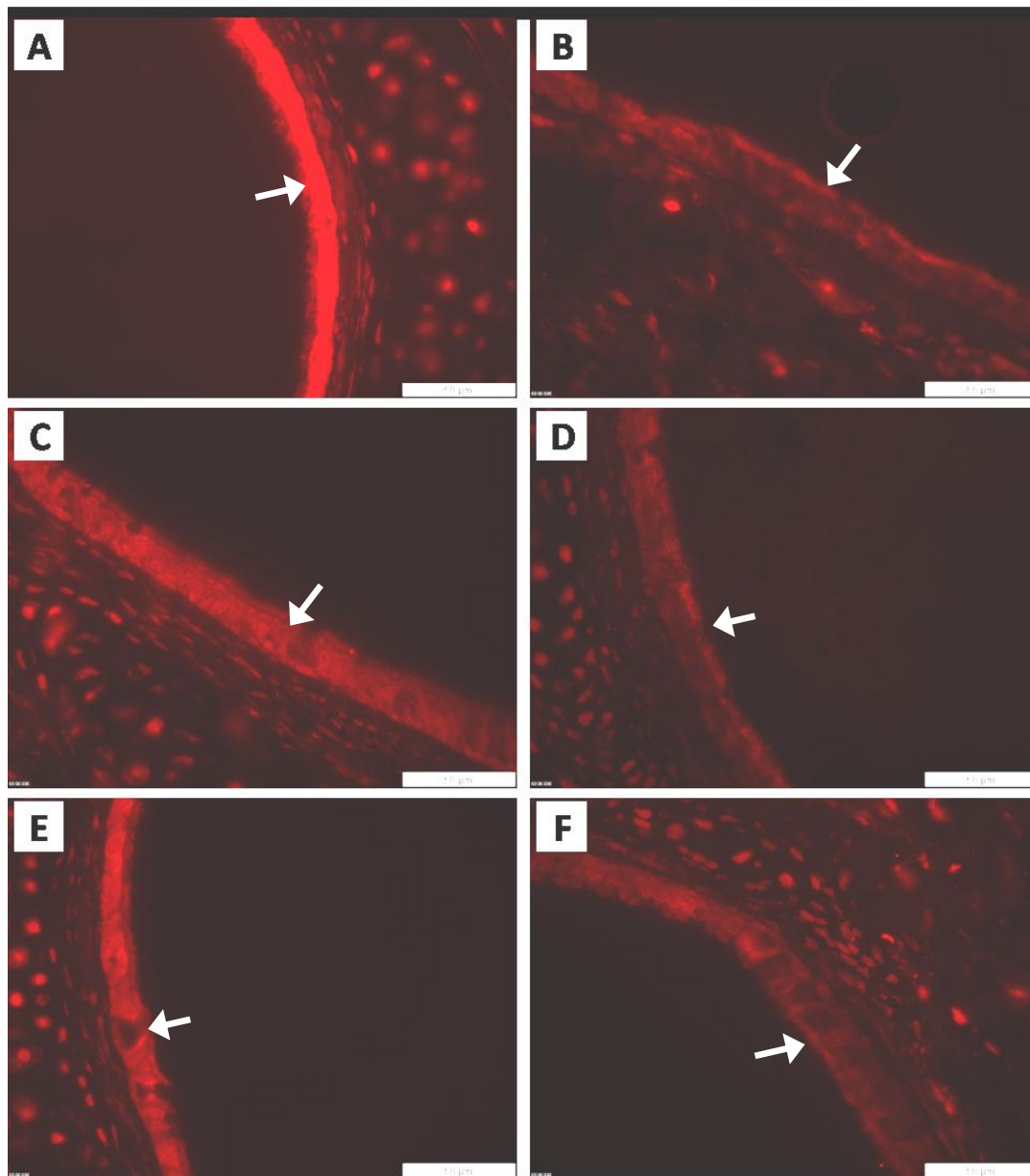
Figure 3.8 Expression of BMPR-IA in Airway level 6

O_3+HDMA (A, C and E) compared to control lung (B, D and F). BMPR-IA (568 Red) was highly abundant in level6 of the airways in the O_3+HDMA treated group. This was in contrast to the control group where BMPR- IA was deteced in the airways of the treated groups, though at a much lower level in all animals compared to the levels of the protein detected int he O_3+HDMA treated group.
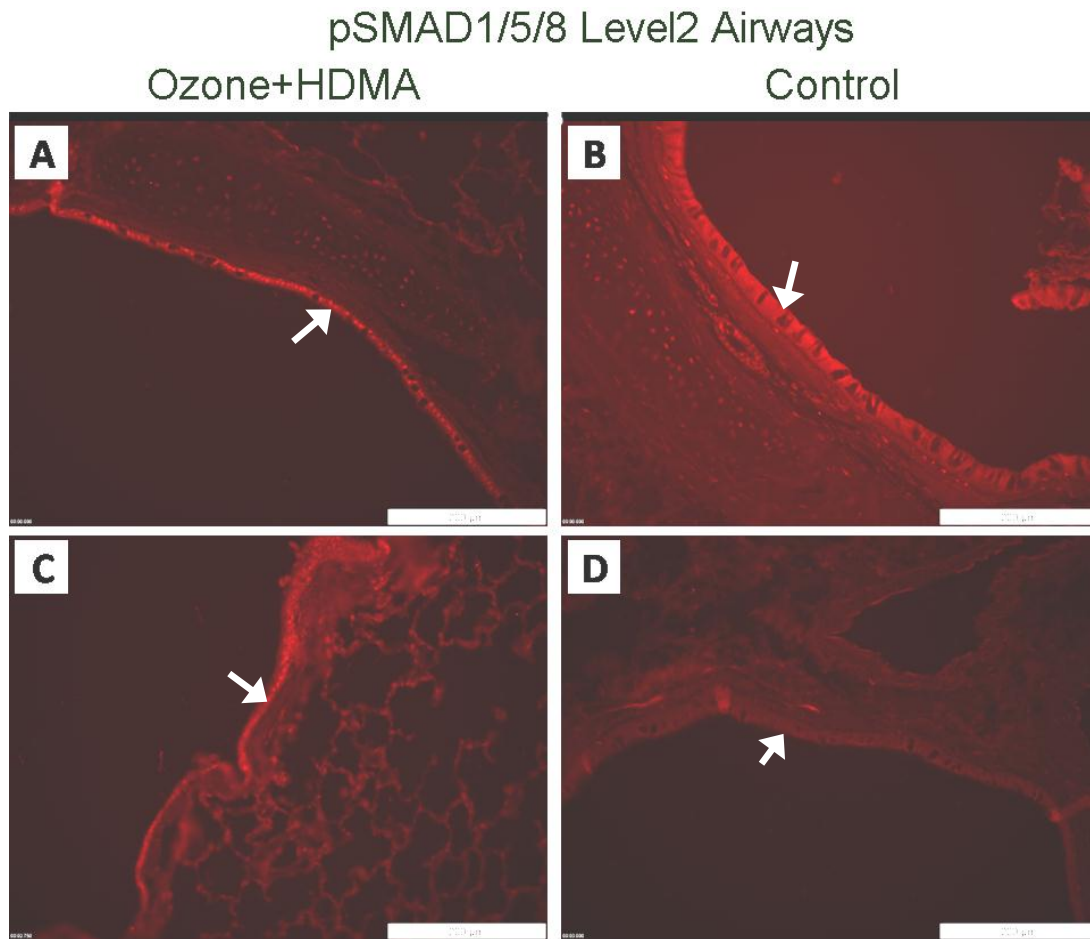
Figure 3.9: Expression of pSmad1/5/8 in Airway level2

O_3+HDMA (A and C) compared to control lung (B and D). pSmad1/5/8 can clearly be seen to be present in and staining the airways of the O_3+HDMA (A and C) treated animals. The staining present the control animals is non specific and is not present at a level higher than seen in the secondary controls (Figure 3.11 (C)).
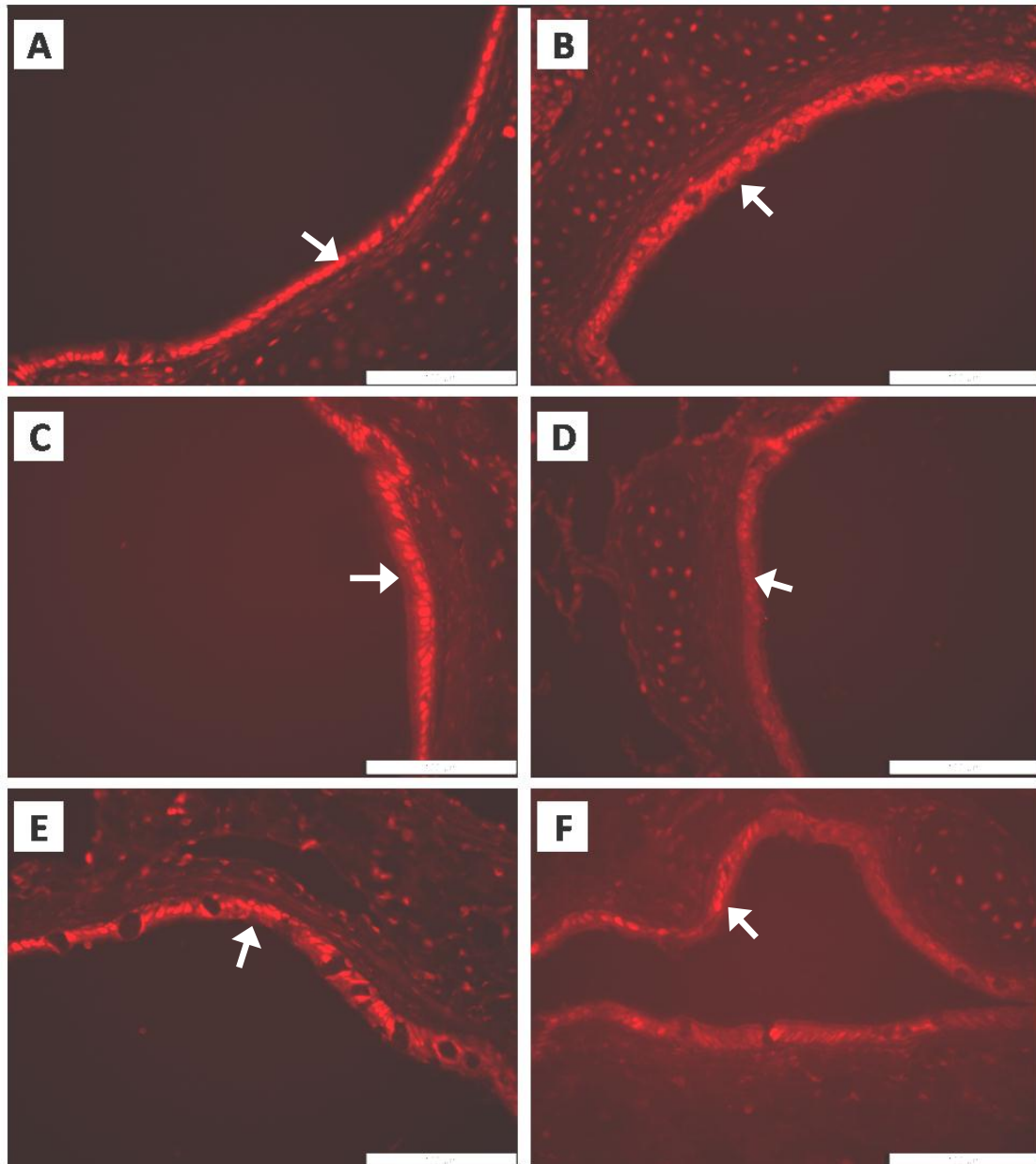
Figure 3.10 Expression of pSmad1/5/8 in Airway level 6

O_3+HDMA (A, C and E) compared to control lung (B, D and E). pSmad1/5/8 can clearly be seen to be present in and staining the airways of the O_3+HDMA (A, C and E) treated animals. The staining present the control animals (B, D and F) is not, overall, as definate or as abundant than the O_3+HDMA group though there is a detectable level of pSmad1/5/8 present.

Control Images
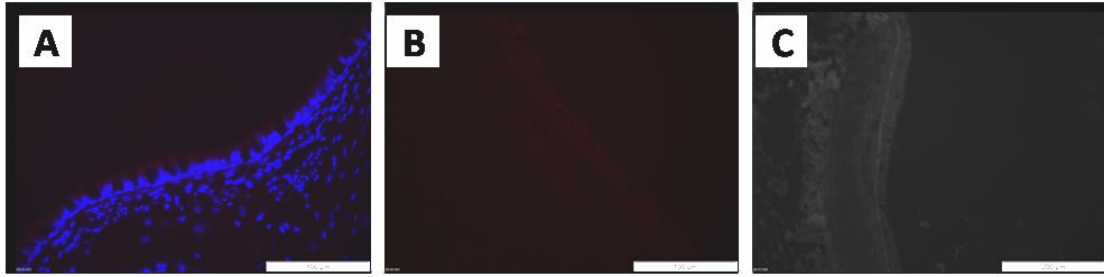
Figure 3.11: Secondary Controls

PCNA secondary control = (A), Blue = DAPI. BMPR-IA secondary control = (B).

pSmad1/5/8 secondary control = (C).

	PCNA		BMPR-IA		pSmad1/5/8	
	O$_3$+HDMA	Control	O$_3$+HDMA	Control	O$_3$+HDMA	Control
Trachea	0.5 (n=2)	0.5	.5	.5	n/a	n/a
Airway level 1	2	0.5	3	1	n/a	n/a
Airway level 2	3	0.5	2.5	1	2 (n=2)	0 (n=2)
Airway level 6	3	0.5	3	1	3	2

Table 3.1 Protein expression levels in the airways

A system of scoring was devised for the expression of a protein in an airway with n=3 in each airway and each group unless otherwise indicated in the table. In each animal, little to no protein presence was scored with a 0, an obvious presence of protein detected scored 0.5 and a highly abundant protein scored 1. This was compiled by examination of multiple sections of tissue from each animal in the study.

As can be seen from the table and in the immunofluorescence images the level of PCNA in the airways (Figures 3.1-3.4) in the O$_3$+HDMA models increased with decending airway level, whereas the control animals expressed a small amount in the trachea, but expression was not evident further down the airways. With regards to BMPR-IA, the level of protein present again increased from the trachea to the airways (1 in the trachea to 3 in the airway immediatly attached to it), and remained consistently high throughout the levels 1, 2 and 6 in the O$_3$+HDMA model. However the level in control animals increased slightly from the trachea to the airway but no difference in protein levels was noted down through the airway levels and it remained at a constant low level. The presence of pSmad1/5/8 was high in airway level 2, in the O$_3$+HDMA model (score=2), compared to no expression of the protein in the Control animals at this level (score=0). In airway level 6 there was an increased level of detection of pSmad1/5/8 in the control animals (score=1.5), though it was not as abundant as seen in the O$_3$+HDMA group (score=2.5).

3.2.2 ALI cultures

BMP4 treatment:

Both human and primate ALI systems were treated with BMP4 in the same manner. At Day0, t=0hr, BEGM media (+RA) in the well was replaced with 1.5ml fresh BEGM media (+RA). Cells to be treated with BMP4 had 50µl BMP4 at a concentration of 100ngs/ml DMEM applied to apical surface of the insert, while control cells had 50µl DMEM added.

EGTA treatment:

Both human and primate ALI systems were treated with EGTA in the same manner. EGTA was delivered at a dose of 10mM one hour before treatment or harvest (t=-1hr). At t=0hr the BMP4 media was added and subsequent time points were determined from this. EGTA treatment was administered to the apical surface of the insert and was removed after one hour by careful pipetting. It was not added in this instance to the media in the well below the insert as the media was Ca/Mg +ve and the chelating effect would be deteriorated prior to having an effect on the cells. In order to determine the level of EGTA to use and the dosage time a pilot experiment based on previous literature was carried out (data not shown). Cells were determined to have had their junctions disassembled and the cell layers beneath exposed after 1hr exposure to 10mM EGTA.

3.2.3 EGTA effect on cells:

The effect of EGTA alone on the expression profile of the cells was compared to that of control cells in both human and primate ALI systems. This was to determine the effect of EGTA alone. If agents such as EGTA are to be used *in vivo* these considerations are important as they could enhance or mitigate the effect of the treatment drug itself. It is conceivable that, by temporarily removing the calcium and thereby weakening adherens junctions, EGTA may promote generation or inhibition of certain proteins and protein channels. In this instance the profile of each of our pathway markers was examined after cells had been treated with EGTA and media had been added to the well that would coat the basal surface of the cells. It was of note that the profile of effect varied between the primate and human cells. Any fold increase/decrease or difference was considered significant for the purposes of this analysis if ≥0.5fold from the control at the corresponding time point. All results are displayed as (Mean±S.E).

Id1: Human cells treated with EGTA, most pronouncedly at the t=12hr and t=24hr time-points, showed a large decrease in the levels of Id1 mRNA (-3.497±1.947 fold at t=12hr and; -5.58±3.156 fold at t=24hr respectively) (Figure 3.12 (A, B)). After 48 hours this falls back in line with what is observed in the control cells (0.196 fold difference). This same pattern is largely repeated in the primate model, however in the primate cells, there is an increase in expression levels of Id1 after 48hours (t=48hr +2.132±0.426 fold and; t=72hr +2.397±1.463 fold respectively), whereas in the EGTA treated cells there continues to be a slight decrease (-1.250±1.285fold at t=48hr and -1.744 at t=72hr) compared to the initial t=0hr time-point. The most remarkable effect of the EGTA treatment in primate cells was observed at t=12hr post EGTA treatment where a -7.040±2.566 fold decrease in the level of Id1 mRNA was recorded. Primate control cells are the only group of cells analysed where an increase in the amount of Id1 mRNA was recorded at any time point.

p21: There was a sustained decrease in the amount of mRNA present in human in both EGTA and control cells over 72 hours (Figure 3.12 (C, D)). There is little difference in the profile expression and the fold levels of expression with the exception of t=24hr (control=-0.56±0.073 and EGTA = -4.236±3.335), though a large Standard Error has to be factored into account and the overall effect is not significant when analysed by two way ANOVA. In primate cells both the control and EGTA treated cells follow the same profile of expression levels across the time-course, with p21 mRNA being present at a relatively unchanged level at t=6hr and then a lower level at t=12hr and t=24hr before being up-regulated in both sets of cells after t=48hr.

PCNA: The levels of PCNA expressed in both human and primate ALI systems were comparable (Figure 3.13 (E, F)). A decrease compared to t=0hr at all timepoints in both sets of cell analysed with the exception of EGTA treated cells at t=48hr in both models, where a slight increase in expression compared to the t=0timepoint was noted (<0.5 fold). In the human cells this resulted in a difference in expression of Δ=0.95 fold between Control and EGTA treated, and in a Δ=1.54 fold difference in primate cells.

BMPR-IA: Control human cells showed no major alteration in BMPR-IA expression from the t=0hr control across the timeframe, but with a slight decrease of less than 1 fold at t=24hr (-0.559±0.264 fold). With the EGTA treated cells however there was a significant increase in the levels of BMPR-IA mRNA detected at t=6hr (0.85±1.53

fold) and t=12hr (1.36±1.866 fold), before a marked decrease to -0.973±0.578fold at t=24hr and increase again at t=48hr (+0.919±0.638 fold) before levelling off to a less significant difference at t=72hr between control and EGTA cells (0.022 fold difference at t=72hr). The control cells in the primate ALI largely matched this profile with a slight decrease in expression compared to t=0hr at all time points (Figure 3.13 (B)). This is matched by the EGTA treated cells for the first 12 hours of the time-course, but at t=24hr an increase in the level of BMPR-IA mRNA is observed against the t=0hr background (+0.309±0.143 fold) as opposed to a decrease in the control cells (-0.4±0.132 fold). This grows to a greater than 1fold increase at the t=48hr time-point (+1.32±0.204 fold), with a 1.84 fold difference observed between the control and EGTA treated cells profile. The increase, though less significant, is still observable at t=72hr (+0.688±0.282 fold).

BMPR-IB: BMPR-IB levels of mRNA in the Human ALI are largely similar between control and EGTA treated cells, with no major deviations from t=0hr levels or differences between control and EGTA of note (Figure 3.13 (C)). In the primate model however this is not the case (Figure 3.13 (D)). Though largely similar for the first 24 hours of the time-course, at t=48hr there is a marked increase in the level of BMPR-IB mRNA present in the EGTA treated cells compared to the t=0hr control (+1.87±0.464 fold), which gives an even larger discrepancy against the control cells (-1.07±0.26 fold) profile at the same time-point (2.94fold difference between the two). Though the difference drops at t=72hr time-point it is still a significant difference (1.608 fold) and the increased level of BMPR-IB in the EGTA treated cells is of note at 0.769±0.383 fold. It can be noted that EGTA treatment alone, at t=48hr, significantly changes the expression profile of BMPR-IB on its own accord.

BMPR-II: BMPR-II expression levels in the human ALI remain consistently close to the levels of the t=0hr time-point for the first 12 hours before a significant decrease in the level of expression can be seen at t=24hr (-1.412 fold) that remains largely unvaried through to the t=72hr time-point (-1.148±0.369 fold at t=48hr and -1.213 fold at t=72hr) (Figure 3.13 (E)). The EGTA treated cells however show a significant decrease in expression at t=6hr (-1.479±0.873 fold). This level however approaches to close to that of the t=0hr control over the time-course, with a barely discernable decrease in levels compared to the t=0hr control at t=24hr (-0.118±0.194 fold) followed by a significant increase over the t=48hr (+0.713±0.277fold) time point and a notable increase at the t=72hr (+0.383±0.392 fold) time-point. Though not largely

different from the t=0hr control for the EGTA treatments, they are quite different from the control cells, with over a fold level difference of expression between them (Δ=1.86 fold difference at t=48hr and Δ=1.596 fold difference at t=72hr). In the primate ALI system the level of BMPR-II in the control cells never varies significantly from the t=0hr control over the entire 72 hour time course (Figure 3.13 (F)). In the EGTA treated cells however it is noted that the levels remain consistent with those of the t=0hr time-point and the control cells for the first 24 hours, but that at the t=48hr time-point there is a notable increase in the levels of BMPR-II mRNA levels to +1.23±0.953 fold this increase can again be seen in the t=72hr time-point, though to a lesser extent (+0.903±0.841fold).

BMP2: mRNA levels of BMPR-II were generally reduced in both human and primate models compared to their controls, with the effect most pronounced in culture models pre-treated with EGTA prior to BMP4 treatment, most noticeably at t=24hr in humans (-2.217±1.604 fold) and t=12hr in primates (-2.021±1.174 fold) (Figure 3.14 (A, B)). Exceptions to this in human cells only occurred in BMP4 only treated cells where at the t=6hr time point there was a small increase in the amount of BMP2 mRNA detected compared to what was observed in the control cells. In primate cells both BMP4 (+0.637±0.201 fold increase) and EGTA+BMP4 (+1.19±1.181 fold increase) treated cells were significantly increased at t=6hr. It is possible it is noticeable in primates because of a slower response to the BMP4 stimulus whereas the peak may have been missed by t=6hr in human ALI cultures.

E-Cadherin: With regard to E-cadherin expression levels both control and EGTA treated cells in human ALI reacted in the same general pattern, both holding around the same level of expression down from t=0hr measurements with the exception of the t=72hr time-point (-0.129±0.415 fold in control cells vs. -1.441±1.84 fold EGTA treated) (Figure 3.14 (C)). In primate however there is a slight decrease in the control cells starting 12 hours from the t=0hr control of almost 1 fold difference (-0.895±1.121 fold) (Figure 3.14 (D)). In the EGTA treated primate cells however there is no significant change in expression at all over the first 24hr, but at t=48hr there is a marked up-regulation of E-cadherin mRNA contrasting with a decrease in expression in the control cells at this time point (1.914±1.138 fold EGTA vs. -1.537±0.316 fold Control).

Smad1: Smad1 levels in the human NEHB ALI system show a decrease in the level of mRNA compared to the t=0hr controls (Figure 3.15 (A)). At t=6hr there is a significant 0.617±0.634 fold decrease compared to control t=0hr cells. There is a decrease visible, though not surpassing -0.368fold at t=12, t=24 and t=48hr time points before another significant decrease in comparison to control t=0hrcontrol cells is again seen at t=72hr with a -0.66±0.422fold decrease. EGTA treated human cells show a greater decrease at t= 6hr than what was seen in control cells, with a -1.128±0.558 fold decrease. The level of mRNA by t=12hr is once again approaching the level of the t=0hr control (-0.123±0.198 fold) before another significant decrease is recorded of -1.237±0.638 fold at t=24hr. After this the level fluctuates within a half fold up (t=48hr) or down (t=72hr) of the level of the t=0hr control. The primate ALI profile of Smad1 expression varies from this (Figure 3.15 (B)). The control cells remain tethered to the t=0hr control level across the time-course, for the first 48hours (t=6hr -0.02±0.123 fold decrease; t=12hr +0.171±0.193 fold increase; t=24hr -0.261±0.177 fold decrease and; t=48hr -0.75±0.226fold decrease) with the only significant deviation away from the t=0hrcontrol occurring at t=72hr where there is a 0.568±0.134 fold deviation from the levels seen at t=0hr. However the EGTA levels, though also extremely close to both the t=0hr levels and also the control cells levels of expression, show a marked increase in the levels of Smad1 being expressed at t=48hr (+1.2±0.531 fold) and t=72hr (1.358±1.26 fold).

Smad4: Smad4 was briefly examined in the primate model (n=1 for control cells and n=2 for EGTA treated cells) but no major differences between levels of expression at the same time points was noted in either, though a significant drop in Smad4 mRNA expression was recorded in both in comparison to their respective t=0hr control at t=12hr (-0.636 fold in control cells and; -1.015±0.531 fold in EGTA treated cells) and t=24hr. (-0.523 fold in control cells and; -1.15±0.449 fold in EGTA treated cells) (Figure 3.15 (D)).

Smad5: Smad5 expression levels largely replicated the pattern of Smad1 with some notable exceptions. The human ALI control cells never deviated significantly from the level of expression to that of the t=0hr time-point (±0.115 fold difference at the most) (Figure 3.15 (E)). However EGTA treated cells showed a -0.775±0.323 fold decrease at t=6hr and a -2.14±1.453 fold decrease in the level of Smad5 mRNA expression at

t=24hr, before levelling out to the same level of expression as measured against the t=0hr time-point at t=48hr (-0.033±0.565 fold difference) and t=72hr (-0.019±0.550 fold difference). In the primate ALI system Smad5 profile more closely matched that of the Smad1 primate ALI profile (Figure 3.15 (F)). From t=6hr to t= 24hr there was very little difference in the level of Smad5 mRNA expressed between the t=0hr controls in either of the control or EGTA cells. This continues through to the 72hr time-point for the control cells. However with EGTA treated cells there was a significant increase at t=48hr (+2.241±0.863 fold) and t=72hr (+1.364±1.002 fold).

Snail1: Snail1 expression levels in the human ALI system didn't vary largely (Figure 3.16 (A)). Control cells mRNA levels averaged only a 0.134±0.474 fold deviation from the t=0hr control. EGTA treated cells however showed a greater variation from the t=0hr control over all time points (0.474±0.105 fold). The most significant changes as a result of EGTA treatment occurred with an increase of +0.57±0.537 fold at t=6hr and a decrease of -0.87±0.151 fold at t=24hr. In the primate ALI system however the same profile pattern was not to be found (Figure 3.16 (B)). Control cells showed a marked increase in the expression of Snail1 mRNA at t=6hr (+0.423±0.45 fold) and t=12hr (+1.103±1.148 fold). This was followed by a significant decrease in the level of expression compared to that seen in t=0hr control cells of -0.6±0.695 fold at t=24hr and -0.794±0.442 fold at t=48hr. The level of Snail1 mRNA was observed to have increased significantly relative to the t=0hr control again at t=72hr time point (+1.065±0.962 fold). This level of significant fluctuation far exceeded the level seen in the human control cells. EGTA treated primate cells also showed a much greater reaction in terms of the levels of Snail1 mRNA in the cells. At t=6hr a -1.674±0.859 fold decrease in the level of Snail1 was observed, with a 1 fold decrease (-0.999±1.15 fold) at t=12hr. This contrasted with a notable increase in expression at t=6hr for control cells (+0.423±0.45 fold), and a +1.103±1.148 fold increase in expression at t=12hr in the control cells At t=24hr both sets of cells exhibited a differing degree of decrease in the expression levels of Snail1 with EGTA treated cells recording a -1.131 fold greater decrease than that seen with the control cells (Control cells= -0.596±0.695 fold decrease vs.; EGTA treated cells =-1.727±0.915 fold decrease). The mRNA levels in EGTA treated cells continued to fluctuate significantly at t=48hr (+0.659±0.048 fold increase) and t=72hr (-0.814±1.279 fold decrease). This contrasts with the decrease seen in control cells at t=48hr and the increase seen in control cells at t=72hr.

Snail2: Snail2 expression profile in the human ALI treated cells showed a continuous decrease over time in the control cells versus t=0hr (Figure 3.16 (C)). There was a minor decrease by t=6hr (-0.043±0.302) followed by a notable decrease of -0.316±0.401 fold at t=12hr and this grew to a significant decrease of -0.78±0.47 fold by t=24hr It remained significantly decreased from control cells at t=48hr (-0.65±0.68 fold decrease) and t=72hr (-0.661±0.096 fold decrease). EGTA treated cells however showed a much more marked decline in Snail2 expression over the time-course, progressing continuously from a notable -0.416 fold difference at t=6hr straight to a significant decrease at t=12hr (-1.144±0.338fold decrease) to in excess of a 2.5fold decrease at t=72hr (t=24hr -2.09±0.518 fold decrease; t=48hr -2.231±1.264 fold decrease; t=72hr -2.678±1.625 fold decrease).

A similar pattern was observed this time in the primate ALI system (Figure 3.16 (D)). In the control cells at t=6hr there is a minor increase in the level of Snail2 expressed compared to the level seen in the cells at t=0hr (+0.183±0.555 fold increase). After this however there is a continuous decrease in the level of Snail2 mRNA in the cells. By t=6hr there is a significant decrease to -0.772±0.762 fold, before at t=24hr the level increases slightly to just -0.187±0.661 fold decrease below the t=0hr time point. t=48hr (-1.374±0.425 fold decrease) and t=72hr (-2.086±0.59) time points however both recorded significant decreases in the levels of Snail2 mRNA compared to what was quantified in the t=0hr controls. The EGTA treated cells had a much more profound decrease in expression levels compared to this. By t=6hr there was in excess of a 2.5 fold decrease (-2.666±0.341 fold decrease), at t=12hr, in excess of a 3 fold decrease (-3.891±0.496 fold decrease) and by t=24hr there is in excess of a 6 fold decrease (-6.786±2.856 fold decrease) in the expression of Snail 2 mRNA expression the in the primate ALI system. By t=48hr the level of decline compared to what was recorded in the t=0hr control cells appeared to level off at 4+fold decrease (t=48hr -4.386±0.857 fold decrease; t=72hr -4.609±1.081 fold decrease).

In both human and primate treated cells there was a significant effect decrease measured in control cells as time progressed. However in cells that were treated with EGTA the effect was much more significant with a multi-fold decrease in the quantity of Snail2 mRNA in cells compared to the t=0hr time point than seen in control cells.

Gene Of Interest	Human			Primate		
	EGTA	Time	Interaction	EGTA	Time	Interaction
BMP2	No	No	Yes (*)	No	No	No
E-cadherin	No	No	No	Yes (*)	No	No
Id1	No	No	No	Yes (**)	Yes (*)	No
p21	No	No	No	No	Yes (**)	No
PCNA	No	No	No	No	No	No
BMPR-IA	No	No	No	Yes (***)	Yes (*)	Yes (**)
BMPR-IB	No	No	No	Yes (***)	No	Yes (**)
BMPR-II	Yes (*)	No	No	No	No	No
Smad1	No	No	No	No	No	No
Smad4	No	No	No	No	No	No
Smad5	No	No	No	Yes (**)	No	No
Snail 1	No	No	No	No	No	No
Snail 2	Yes (*)	No	No	Yes(***)	No	No

Table 3.2 Two Way ANOVA analysis of effect of EGTA and time

Significance as analysed by Two Way ANOVA for each Gene of Interest (G.O.I) and whether or not the presence of EGTA, the passage of time, or the interaction of both had an effect on the level of expression of the G.O.I.
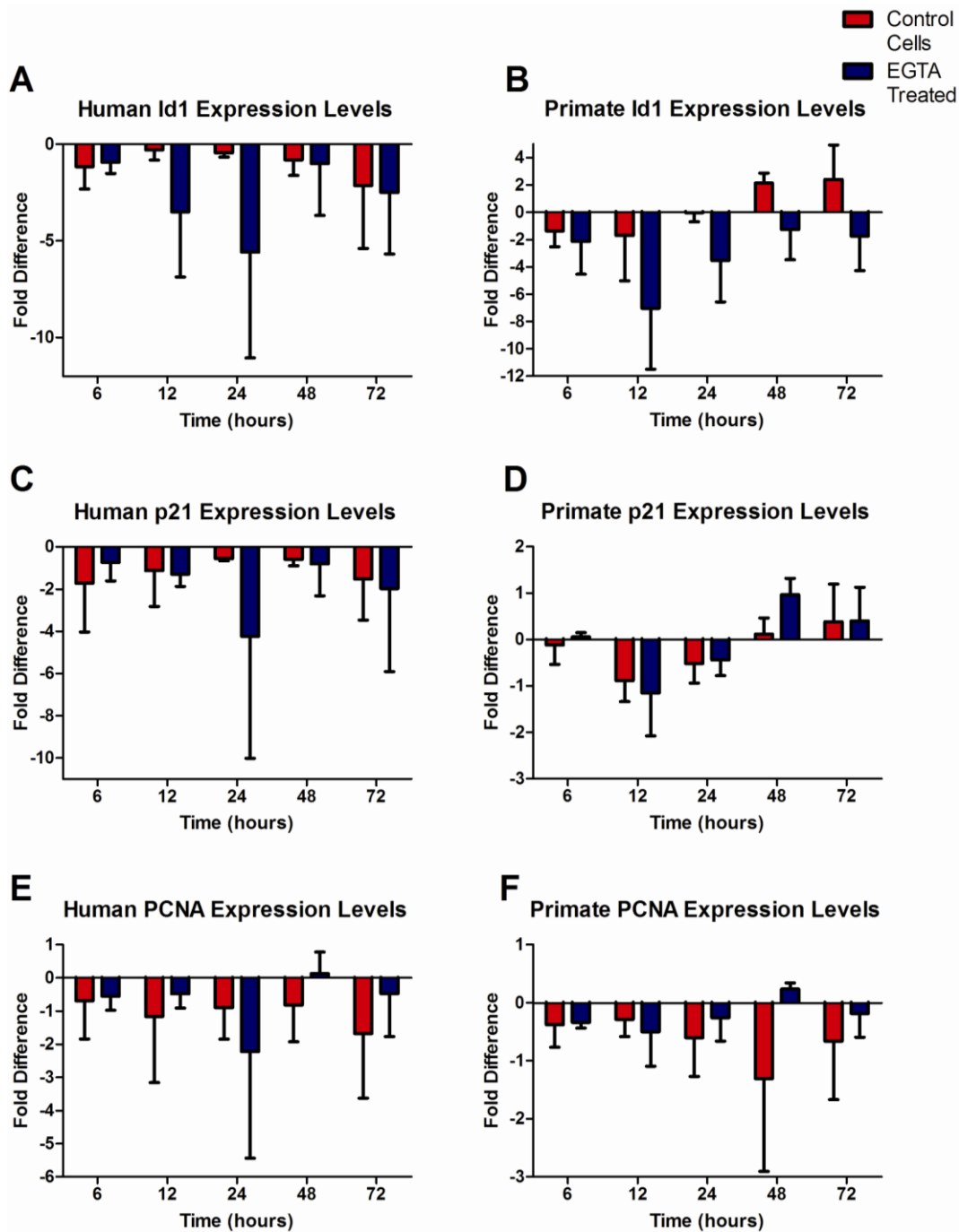
Figure 3.12 Quantification of Id1, p21 and PCNA mRNA expression levels

Id1 (A, B), p21 (C, D) and PCNA (E, F) mRNA expression levels in control and EGTA treated cells. Both control and EGTA mRNA expression levels are relative to the t=0hr control for each group.
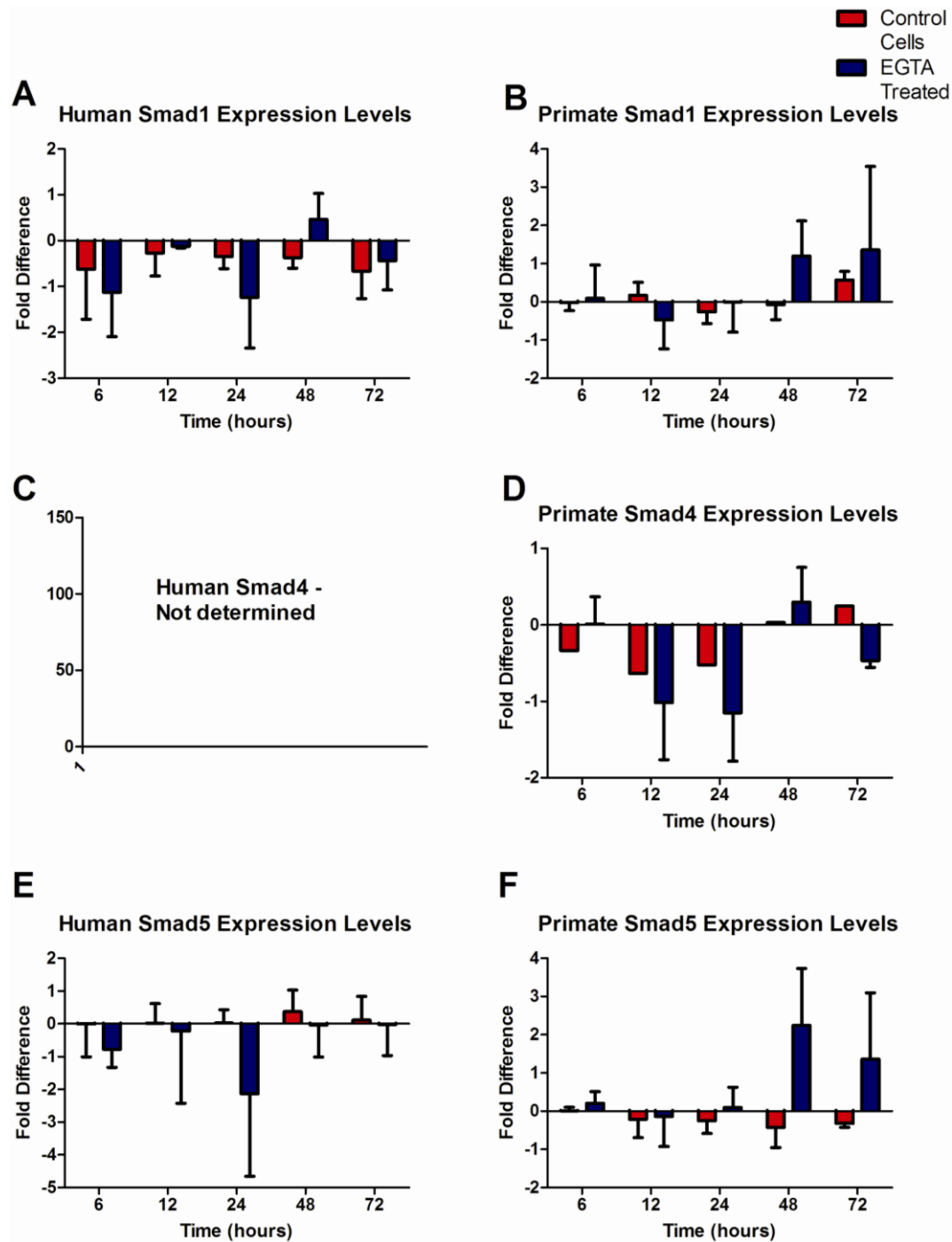
Id1: n=3† (†Human control cells; t=24hr n=2, t=72hr n=2).

P21: Human control n=3‡, Human EGTA n=3, Primate Control n=3, Primate EGTA n=2 (‡Human control cells; t=24hr n=2, t=72hr n=2).

PCNA: Human control n=3§, Human EGTA n=3, Primate Control n=3, Primate EGTA n=2 (§Human control cells; t=24hr n=2, t=72hr n=2).
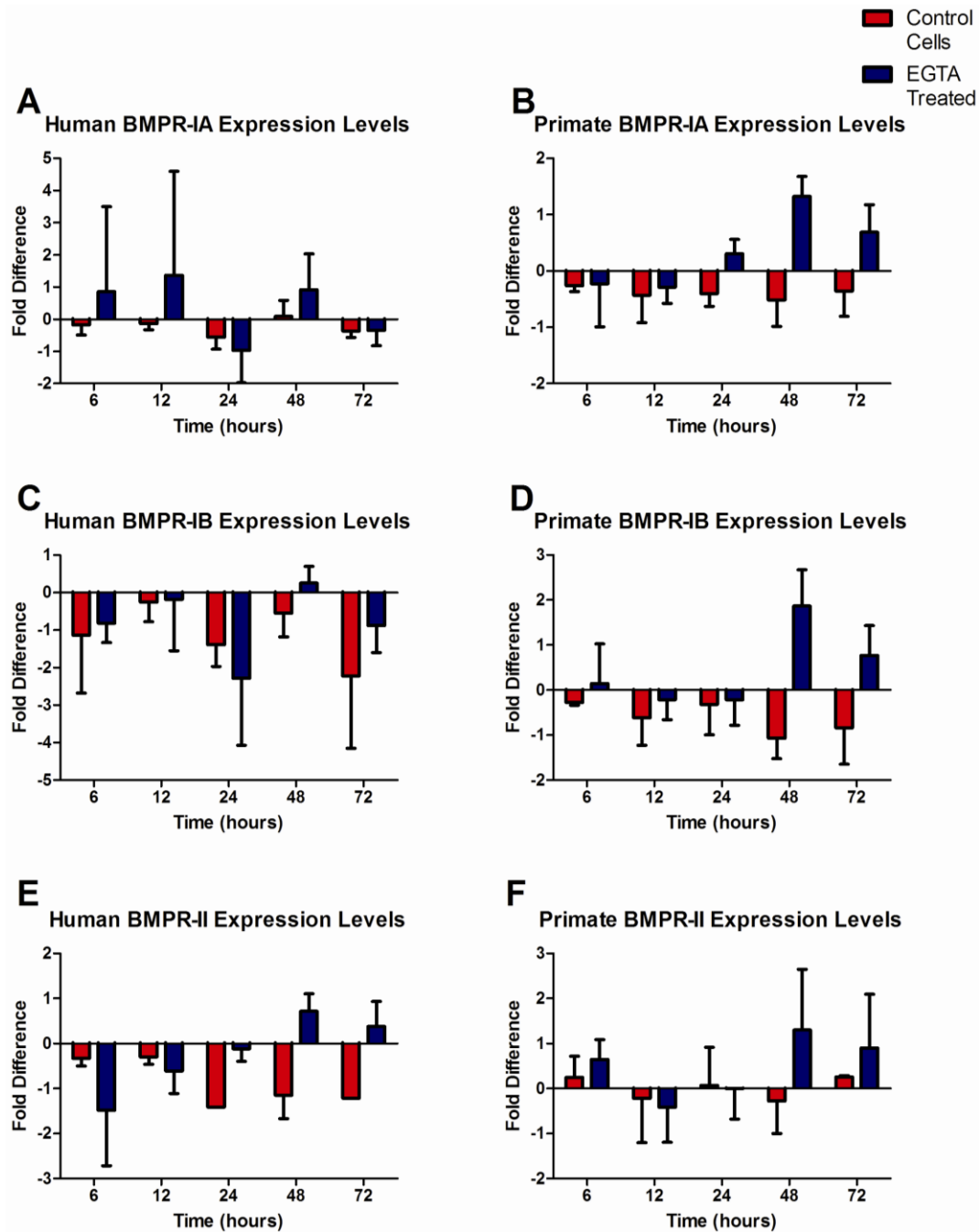
**Figure 3.13 Quantification of BMPR-IA, BMPR-IB and BMPR-II mRNA expression levels**

BMPR-IA (A, B), BMPR-IB (C, D) and BMPR-II (E, F) mRNA expression levels in control and EGTA treated cells. Both control and EGTA mRNA expression levels are relative to the t=0hr control for each group.

BMPR-IA: n=3† (†Human control cells; t=24hr n=2, t=72hr n=2).

BMPR-IB: n=3‡ (‡Human control cells; t=24hr n=2, t=72hr n=2).

BMPR-II: n=2§ (§Human control cells; t=24hr n=1, t=72hr n=1).
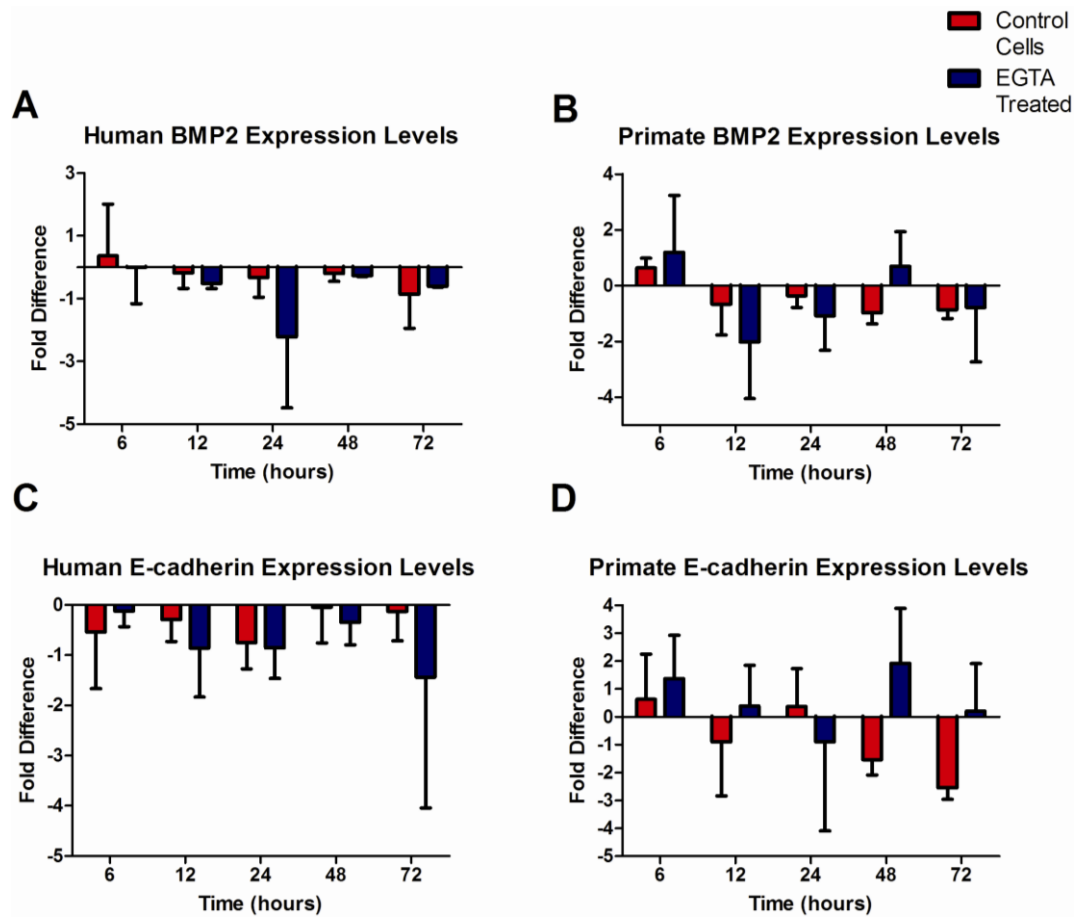
Figure 3.14 Quantification of BMP2 and E-cadherin mRNA expression levels

BMP2 (A, B) and E-cadherin (C, D) mRNA expression levels in control and EGTA treated cells. Both control and EGTA mRNA expression levels are relative to the t=0hr control for each group.

BMP2: Human control n=3†, Human EGTA n=2, Primate Control n=3, Primate EGTA n=3 (†Human control cells; t=24hr n=2, t=72hr n=2).

E-Cadherin: Human control n=3‡, Human EGTA n=2, Primate Control n=3, Primate EGTA n=3 (‡Human control cells; t=24hr n=2, t=72hr n=2).

Figure 3.15 Quantification of Smad1, Smad4 and Smad5 mRNA expression levels

Smad1 (A, B), Smad4 (C, D) and Smad5 (E, F) mRNA expression levels in control and EGTA treated cells. Both control and EGTA mRNA expression levels are relative to the t=0hr control for each group.

Smad1: n=3† (†Human control cells; t=24hr n=2, t=72hr n=2).

Smad4: Primate Control n=1, Primate EGTA n=2

Smad5: n=3‡ (‡Human control cells; t=24hr n=2, t=72hr n=2).
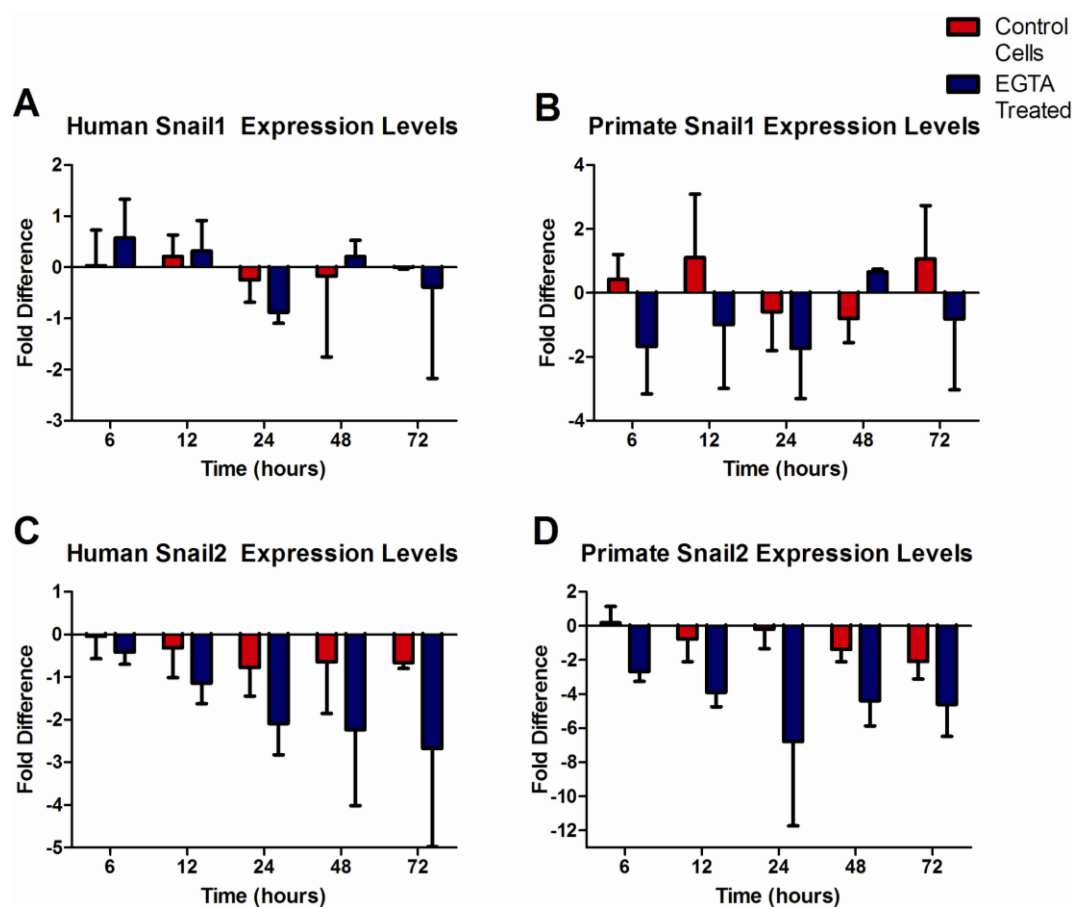
Figure 3.16 Quantification of Snail1 and Snail2 mRNA expression levels

Snail1 (A, B) and Snail2 (C, D) mRNA expression levels in control and EGTA treated cells. Both control and EGTA mRNA expression levels are relative to the t=0hr control for each group.

Snail1: n=3† (†Human control cells; t=24hr n=2, t=72hr n=2).

Snail2: n=3‡ (‡Human control cells; t=24hr n=2, t=72hr n=2).

3.2.4 Effect of BMP4 Treatment on Human and Primate ALI Cells:

The effect of BMP4 treatment on cells was analysed:

a) By examining the morphological effect of treatment on the cell morphology (Figure 3.17, Figure 3.18 and Figure 3.19). Human cells that received BMP4 with no EGTA pre-treatment exhibited morphological differences by at t=48hr and t=72hr. In primate cells that received BMP4 with no EGTA pre-treatment, morphological differences from the control cells were not detected until t=48hr and again at t=72hr, as was seen in human cells undergoing the same treatment conditions. In the case of primate cells which all received EGTA pre-treatment, cells that received no BMP4 treatment underwent no morphological changes until t=24hr. However BMP4 treated cells were responding with a morphological change by t=6hr.

b) By comparing the expression levels of various G.O.I in control cells which (i) received no exogenous BMP4 treatment, and treated cells which were apically treated with 100μl of 50ng/ml BMP4 protein and (ii) control cells which received EGTA treatment and treated cells that received EGTA treatment 1hr before commencement of BMP4 treatment at t=0hr with 100μl of 50ng/ml BMP4 apically. As will be seen one of the most striking set of results came from analysis of Id1 expression levels in BMP4 treated cells. mRNA expression levels were increased across the board, over all time points and both in cells treated with BMP4 alone and cells exposed to EGTA prior to BMP4 treatment. Any fold increase/decrease or difference was considered significant for the purposes of this analysis if ≥0.5fold from the control at the corresponding time point. All results are displayed as (Mean±SE).

A full breakdown of n number per group can be seen in Table 3.3.

Id1 mRNA levels were increased significantly at all time points in both human and primate BMP4 treated cells, with or without the presence of EGTA (Figure 3.20 (A,B)). Of note with regard to the human NEHB cells, at all time points, with the exception of t=24hr, cells treated with BMP4 alone that had not received EGTA pre-treatment showed a greater difference in fold expression of Id1 mRNA when compared to the EGTA+BMP4 treated cells (t=24hr; BMP4 = +7.642±2.018 and EGTA+BMP4 = +9.545±4.802 fold increase: Δ=1.902 fold)). It was therefore also of note that in treated primate cells, with the exception of the t=6hr time-point, the opposite is true and all cells pre-treated with EGTA had a greater difference in fold expression of Id1 compared to their respective controls (t=6hr; BMP4 = +18.591±6.265 fold and EGTA= +BMP4=8.964±5.108 fold: Δ=9.627 fold).

In human NEHB cells the greatest increase in expression was recorded at t=72hr for both BMP4 and EGTA+BMP4 treatment groups (46.585±38.161 fold in BMP4 treated and 17.911±0.271 fold in EGTA+BMP4 treated).

p21 mRNA expression in NEHB cells treated either with BMP4 or EGTA+BMP4 the most significant result was observed t=6hr in BMP4 only treated cells which recorded a significant 2.004±1.824 fold increase in fold expression of p21 mRNA (Figure 3.20 (C)). The corresponding time point in the EGTA+BMP4 treated cells recorded a -0.156±0.418 fold decrease, an insignificant difference from what is observed in the EGTA only treated control cells. The only other significant difference in quantity of p21mRNA present in NEHB BMP4 treated cells was recorded at t=72hr where a 1.216±1.173 fold increase was detected as a result of BMP4 treatment. The only two significant changes in that occurred in EGTA+BMP4 treated cells occurred at t=24hr with a 0.774±1.008 fold increase and at t=72hr with a 0.680±0.299 fold increase over respective controls resulted in no changes in expression in comparison to their controls.

With regard to primate cells p21 mRNA levels were initially decreased (-0.324±0.26 fold decrease) at t=6hr (Figure 3.20 (D)). However by t=12hr they were elevated to above that of the control cells and peaked at t=24hr with a significant +0.932±0.493 fold increase in expression levels compared to those found in control cells at the same time point. Over the next 48hr, at t=48hr and t=72hr, the levels of p21 were recorded as decreasing from this significant peak to still significant 0.747±0.493 fold increase at t=48hr and a not-significant 0.28±0.54 fold increase at t=72hr. In EGTA+BMP4 treated cells, p21 mRNA levels show increasing fold levels of expression from t=6hr to significantly higher at t=12hr and t=24hr (t=6hr; +0.005±0.078 fold increase: t=12hr; +0.793±0.014 fold increase: t=24hr; +0.97±0.006 fold increase) before returning to a level closer to that of the control cells at t=48hr (-0.203±0.08 fold less p21 mRNA than found in control) and t=72hr (+0.49±0.735 fold increase). p21 mRNA levels in both treatment groups showed an increase just shy of 1 fold in expression at t=24hr, a peak in expression deviation from respective controls for both groups.

It is also of note that in BMP4 treated cells in both human and primate, the level of expression change bears no major similarities in levels of p21 present in the respective cell types at corresponding times. However after if cells are first treated with EGTA and then BMP4 the profile pattern of both is more closely aligned between the two cell types.

PCNA mRNA in NEHB cells treated with BMP4 showed very little variation of note compared to the controls with significant exception at t=24hr (+1.213± fold increase) and t=72hr (+0.931±0.986 fold increase) (Figure 3.20 (E)). PCNA mRNA levels in cells treated with EGTA+BMP4 and EGTA controls were significantly increased at t=6hr with a 0.612±0.425 fold increase recorded (compared to a 0.352±0.224 fold increase in BMP4 only treated cells). The level exceeded that of control cells at t=12hr by only 0.037±0.08 fold but, as was seen in the BMP4 only treated cells, the most significant reaction to BMP4 treatment occurred at t=24hr with a 3.169±3.971 fold increase of PCNA mRNA recorded. After this peak no further increase in PCNA is recorded and levels drop to just below what was recorded in control cells at t=48hr (-0.24±0.325 fold decrease) and t=72hr (-0.005±0.34 fold decrease).

Expression of PCNA in primate cells showed a significant -0.567±0.16 fold decrease at t=6hr compared to control in BMP4 treated cells (Figure 3.20 (F)). The level of expression remained below that of controls again at t=12hr (-0.342±0.064 fold decrease) until t=24hr where a small increase in fold expression was detected (+0.115±0.369 fold), rising again at t=48hr (+0.31±0.148 fold) before returning to just below control levels again at t=72hr (-0.071±0.558 fold). The level of PCNA mRNA in EGTA and BMP4 treated cells did not significantly differ to that of control cells with the exception of t=24hr (+0.899±0.568 fold increase) and t=72hr (0.512±0.656 fold increase) where significant increases were recorded in comparison to the level of expression in control cells.

Of note in comparison between human and primate cell responses to BMP4 treatment is the decreased expression over the initial 12hours in primate cells in contrast with an increase in expression in human cells over this window. With regards to EGTA pre-treated cells, BMP4 doesn't result in such a significant decrease in primate cells as seen in BMP4 only treated cells and but human cells at this time point were recording a significantly increased level of expression at this time point. Both human and primate cells however, in response to EGTA pre-treatment followed by BMP4 treatment show the most significant increase in PCNA mRNA expression at t=24hr.

E-cadherin mRNA expression in NEHB human cells treated with BMP4 was increased at all time points, though not by significant levels, never exceeding a 0.25±0.172 fold difference from controls seen at t=12hr (Figure 3.21 (A)). However in EGTA + BMP4 treated cells, with the exception of t=12hr a decrease was noted

across all time points in the level of E-cadherin in mRNA expression, most notably at t=24hr (-0.207±0.143 fold decrease) and t=48hr (-0.342±0.023 fold decrease).

The effect on E-cadherin mRNA as a result of BMP4 treatments in primates was much more pronounced (Figure 3.21 (B)). In BMP4 only treatments, t=6hr saw a decrease in excess of 3fold (-3.199±2.772 fold decrease) in the level of E-cadherin mRNA. t=12hr saw almost no variation in expression levels from control (+0.171±0.221 fold increase), but t=24hr returned an in-excess of 2 fold decrease (-2.323±0.429 fold decrease) in E-cadherin mRNA also. At this point the level of E-cadherin mRNA was significantly increased, with t=48hr (+1.893±1.46 fold increase) and t=72hr (+2.926±2.33 fold increase) both showing significantly elevated levels of E-Cadherin mRNA. EGTA + BMP4 treated primate cells reacted almost exactly opposite to just BMP4 treated cells at every time-point, though the levels of variation from control were much less than that seen in just BMP4 treated cells. The most notable differences were a increase in expression of +0.844±1.056 fold increase at t=24hr (vs. a -2.323±0.429 fold decrease seen in BMP4 only treated cells against their No Treatment controls), a -0.816±0.482 fold decrease at t=48hr (vs. a +1.893±1.46 fold increase seen in BMP4 only treated cells against their No Treatment controls) and -0.536±0.423 fold decrease at t=72hr (vs. a +2.926±2.33 fold increase seen in BMP4 only treated cells against their No Treatment controls) compared to control cells. In human cells, BMP4 treatment resulted in a consistent, if small, increase in E-cadherin mRNA at all levels, however in primate, an on verge multi-fold knockdown in E-cadherin was noticed over the first 24hr period before a multi-fold increase was observed at t=48and t=72hr. With EGTA + BMP4 treated cells, in human as in primate, a small but consistent decrease in the expression of E-cadherin mRNA was noted across all time points, with exception of t=12hr in human and t=6hr and t=24hr in primate.

BMP2 analysis in the human NEHB cells showed that cells that were pre-treated with EGTA before BMP4 treatment showed a greater response in terms of BMP2 mRNA expression (Figure 3.21 (C)). BMP4 only treated cells responded at t=6hr with a significant 0.627±0.757 fold increase in the level of BMP2 mRNA over what was observed in control cells. The difference in expression compared to control cells decreased to less than significant values after this until the t=48hr time point when a significant (-1.235±1.38 fold decrease) was observed. This decrease was then followed by another increase in expression 24 hours later with another significant increase in BMP2 mRNA recorded (+0.847±0.397 fold increase). NEHB cells treated

with EGTA+BMP4, unlike BMP4 only treated cells, showed an increase in BMP2 expression over controls across all time-points. Most notably after 6 hours there was a +1.98±0.161 fold increase in expression, over a fold more than the difference observed between BMP4 only treated cells and their control (Δ= 1.353 fold). At t=12hr the level returned to closer to that of control cells (+0.327±0.199 fold increase), but at t=24hr the difference escalated to a significant +1.052±0.56 fold increase over the control cells, and to an even greater +2.356±3.447 fold difference over controls at t=48hr. A still significant increase in the amount of BMP2 mRNA compared to EGTA only treated cells was recorded at t=72hr with a 0.668±0.19 fold increase. With the exception of t=72hr, EGTA + BMP4 treated cells showed a greater increase in fold expression of BMP2 mRNA at all time-points.

In primate cells the level of response to treatment in fold of expression of BMP2 was not as great as observed in human cells, never achieving as much as a 1 fold difference from controls (Figure 3.21 (D)). In BMP4 treated cells the only significant difference in BMP2 mRNA levels occurred at t=6hr with a -0.898±0.631 fold decrease in the level of expression, after which mRNA levels at all other time-points remain do not significantly vary from controls. EGTA + BMP4 treated cells never exhibited a significant decrease in the level of expression of BMP2, they did however twice record a significant increase in expression levels, at t=12hr (+0.561±0.26 fold increase) and t=24hr (+0.705±0.349 fold increase). All other time-points showed decreases in mRNA expression (t=6hr -0.067±0.081 fold decrease; t=48hr -0.158±0.219 fold decrease and; t=72hr -0.283±0.648 fold decrease) remain. Comparison of human and primate shows the human and primate cells to have recorded increases of decreases opposite to each other at every time-point in response to BMP4 treatments, i.e. where a slight increase was seen in human a decrease was seen in primate at the corresponding time point. EGTA + BMP4 did not result in a identifiable pattern of expression between human and primate, though the difference in fold expression levels in primates cells was not as high as in human.

Smad1 mRNA expression in both treatment groups in NEHB human cells is increased significantly at t=6hr (+0.55±0.173 fold increase in BMP4 treated cells and; +0.941±0.425 fold increase in EGTA+BMP4 treated cells) (Figure 3.22 (A)). In BMP4 treated cells this returns to close to the control level expression constantly up through to the t=48hr time point (t=12hr +0.433±0.684 fold increase; t=24hr +0.077±0.11 fold increase and; t=48hr +0.038±0.571) fold increase). However at t=72hr a significant +1.206±0.565 fold increase in Smad1 expression was observed.

In EGTA + BMP4 treated cells however, while Smad1 mRNA levels also approached that of the control cells at t=12hr (+0.141±0.424 fold increase) and t=24 hr (t=0.29± 0.702 fold increase), the level in BMP4 treated cells pre-treated with EGTA fell to less than 1 fold below seen in control EGTA only treated cells (-1.038±0.944) fold decrease). Expression levels then again returned to close to those in the control cells at t=72hr (+0.144±0.242).

With regard to primate cells, expression levels of Smad1 never deviated significantly (by more than 0.5 fold) from control cells in BMP4 only treated cells until t=48hr when a significant +1.328±0.481 increase in expression was recorded (Figure 3.22 (B)). Levels again returned to those of control cells at t=72hr (+0.007±0.178 fold increase). With respect to EGTA + BMP4 treated cells the difference from control cells never varied to the same extent. However the increase in Smad1 levels in response to treatment began sooner, at t=12hr (+0.402±0.319 fold increase) and significantly at t=24hr (+0.713±0.259 fold increase). A return to control levels was observed at t=48hr (+0.006±0.395 fold increase) before a notable increase over controls was again seen at t=72hr (+0.461±0.753 fold increase).

Comparing human and primate responses it can be seen that the most significant response in terms of Smad1 mRNA expression was seen in primate cells, but that human cells, both BMP and EGTA+BMP4 produced significant responses to the presence of BMP4 quicker than primate cells (By t=6hr in both treatment groups in human cells vs. primate cells significant responses by t=24hr in EGTA+BMP4 treated cells and t=48hr in BMP4 treated cells.

Smad4 mRNA expression levels was only analysed in primate cells treated with EGTA + BMP4 (Figure 3.22 (D)). With the exception of the t=48hr time-point (-1.23±0.176 fold decrease) a steady increase across the experimental window can be seen from t=6hr to t=72hr, with the increase being significant at t=24hr (+0.872±0.459 fold increase) and t=72hr (+1.453±0.277 fold increase). One way ANOVA analysis showed the results to be significant, $p<0.05$.

Smad5 mRNA expression in human NEHB cells showed a similar profile for both BMP4 only and BMP4 with EGTA pre-treatment options; however the timing of the change in expression levels from controls differed (Figure 3.22 (E)). A response to treatment in BMP4 treated cells showing a significant decrease in mRNA levels was noted at t=48hr (-0.897±0.749 fold decrease) followed by a significant +1.65±0.664 fold increase 24hours later at t=72hr. However in EGTA + BMP4 treated cells a

significant decrease in expression was first noted at t=12hr (-1.577±1.387 fold decrease) with a notable increase in expression 12 hours later at t=24hr (+0.437±0.602 fold increase). Although the increase was not as great as seen in BMP4 treated cells it was still over twice the fold difference increase seen at any other time-point under these treatment conditions.

The effect on primate cells was not the same (Figure 3.22 (F)). With BMP4 treated cells a significant decrease in fold expression of Smad5 was noted at t=6hr (-0.797±0.306 fold decrease). This was followed by another significant decrease at t=12hr (-0.618±0.116 fold decrease) and a decrease of -0.201±0.162 at t=24hr, before a notable increase at t=48hr (+0.326±0.22 fold increase) and a return to control levels at t=72hr +0.048±0.276 fold increase). EGTA + BMP4 treated primate cells responded differently, a gradual increase was tracked over the first 24 hours to a significant peak of just over 0.5 fold more Smad5 mRNA than found in EGTA only treated cells (t=6hr +0.05±0.227 fold increase; t=12hr +0.163±0.165 fold increase; t=24hr +0.532±0.091). At t=48hr this increase in expression was stopped and a notable decrease was observed (-0.407±0.316 fold decrease) before returning to just above control levels again at t=24hr (+0.156±0.493 fold increase).

In comparison the human cells showed more significant responses to BMP4 treatment, both with and without EGTA pre-treatment than in primate cells. However primate cells showed a overall greater reaction to treatment, in the case of BMP4 only treated cells, primate showed an immediate reaction whereas no reaction was seen in until t=48hr.With EGTA pre-treatment however human cells showed a quicker response to BMP4 treatment at t=12hr vs. t=24hr in primate cells.

BMPR-IA in human cells treated with just BMP4 showed no response to treatment in terms of BMPR-IA expression levels until t=48hr, where a significant -1.889±2.417 fold decrease was recorded, followed by a significant +1.314±0.668 fold increase at t=72hr (Figure 3.23 (A)). EGTA + BMP4 treated cells however recorded a significant -3.606±3.542 fold decrease at t=6hr followed by another -1.362±1.413 fold decrease at t=12hr. By t=24hr there was no significant difference from control (+0.232±0.515 fold increase), however at t=48hr, as was seen at the corresponding time point in BMP4 treated NEHB human cells, there was another significant decrease in expression (-1.693±1.566) and a notable increase again observed in t=72hr analysed cells (+0.328±0.594 fold increase), though not to the same extent as seen in just BMP4 treated cells (+1.314±0.668 fold increase).

Primate BMPR-IA expression levels did not respond to the same extent as human cells (Figure 3.23 (B)). A notable decrease in expression was observed at t=6hr (-0.317±0.209 fold decrease) and t=12hr (-0.431±0.497 fold decrease). This returned almost to control level by t=24hr (-0.036±0.213) and then continued its trend of increasing the amount of expression in t=48hr and t=72hr with a significant fold increase in expression over controls in both (t=48hr +0.734±0.546 fold increase; t=72hr +0.676±0.776 fold increase). The primate EGTA + BMP4 treated cells did not vary in expression of BMPR-IA to the same extent as BMP4 treated. At t=6hr there was almost no difference in expression levels of BMPR-IA mRNA (-0.02±0.328 fold decrease). At t=12hr a notable increase in BMPR-IA mRNA of almost 0.5fold was observed (+0.432±0.376) decreasing over the remaining time-points to a level closer to that of the control cells.

In comparing the human and primate responses it can be observed that as a result of BMP4 treatment alone, both cells types only reacted with a significant change in BMPR-IA mRNA from their controls at t=48hr, however in human cells it was a significant decrease in expression following a constant small increase in levels, whereas in primates it was a significant increase, following a constant low level of decreased expression. The most significant effects were seen in human cells. In EGTA pre-treated cells then treated with BMP4 a much more significant and rapid response was seen in human cells compared to primates, with a significant decrease observed at t=6hr. Overall human cells with this treatment regime showed a greater decrease in BMPR-IA from their EGTA pre-treatment controls than was seen in primate cells from their EGTA pre-treatment controls.

BMPR-IB mRNA expression in NEHB human cells showed no major response to BMP4 either with or without EGTA pre-treatment until t=48hr (Figure 3.23 (C)). At t=48hr BMP4 treated cells exhibited a significant -3.651±3.751 fold decrease and BMP4+EGTA treated a -2.941±1.303 fold decrease in BMPR-IB mRNA. By t=72hr the expression returned to above control cell levels in both treatment groups, significantly so in BMP4 only treated cells (BMP4 only at t=72hr +1.556±1.261 fold increase; EGTA+BMP4 at t=72hr +0.303±0.251 fold increase). BMP4 treated cells showed a greater response than EGTA +BMP4 treated cells at these significant time points over the respective controls.

Primate cells did not exhibit the same level of response as humans, never exceeding or reaching a fold deviation from controls (Figure 3.23 (D)). For the first 24hr time period, BMP4 treated cells exhibited a significantly decreased level of expression of

BMPR-IB mRNA at every time-point (t=6hr -0.631±0.333 fold decrease; t=12hr -0.764±0.267 fold decrease and; t=24hr -0.688±0.728 fold decrease). The t=48hr time-point however showed an increase in expression levels to higher than these seen in the control cells (+0.372±0.443 fold increase), and t=72hr showed a return to just below control levels (0.062±0.777 fold decrease). In EGTA + BMP4 treated cells however the level of expression remained unchanged significantly up as far as t=12hr, before exhibiting a +0.546±0.373 fold increase at t=24hr followed by a significant decrease at t=48hr (-0.693±0.239 fold decrease) and t=72hr (-0.542±0.281 fold decrease) respectively. BMP4 only treated cells appeared to respond quicker in terms of reduced BMPR-IB expression to BMP4 treatment than cells pre-treated with EGTA.

Comparison between human and primate treatment shows no major correlations in results. Human cells showed more significant responses (seen at t=48hr) whereas primate cells differed more from each other with respect to treatment type than human cells did.

BMPR-II response to BMP4 treatment in NEHB human cells shows no significant deviation from control cell levels for the first 24hr period (Figure 3.23 (E)). However at t=48hr there is a +0.941±0.671 fold increase in the expression over control cells, seen again at t=72hr with a +1.164 fold increase over controls was recorded. This was markedly different from EGTA + BMP4 treated cells which exhibited an increase in BMPR-II mRNA levels of +0.798±0.103 0.5 fold was noted at t=6hr. The levels did not significantly vary from the control cells again until t=72hr where another significant increase in BMPR-II mRNA was recorded (+0.808±0.247 fold increase).

In primate cells the response to BMP4 treatment mirrored that of human cells (Figure 3.23 (F)). No significant differences to control BMPR-II mRNA expression levels for the first 24 hour period were observed. However at t=48hr a significant increase in expression of BMPR-II mRNA of +0.609±0.212 fold was observed and a notable increase of +0.387±0.482 fold again at t=72hr. The EGTA + BMP4 treatment did not mirror the response seen in human cells as closely. The response started later at t=12hr with a +0.727±0.017 fold increase in BMPR-II expression decreasing as in human over the next two time-points to a overall decrease in expression levels at t=48hr (-0.237±0.044 fold decrease), seen also at t=72hr (-0.172±0.244 fold decrease).

In human cells EGTA produced a significant response before one was observed in BMP4 only treated cells (t=6hr in EGTA+BMP4 vs. t=48hr in BMP4 only). In primate cells the EGTA+BMP4 treated cells also produced a significant response

before BMP4 only treated cells (t=12hr in EGTA+BMP4 vs. t=48hr in BMP4 only). Aside from the degree of significance BMP4 treated cells responded in much the same way in human and in primate cells, both establishing a significant deviation from their respective controls at t=48hr. EGTA+BMP4 treated cells in primates did not appear to react as quickly to BMP4 stimulation (t=12hr vs. t=6hr).

The response of Snail1 expression in human NEHB cells to BMP4 treatment shows a significant +0.604±0.41 fold increase in expression by t=6hr (Figure 3.24 (A)). However after this the level of variation from control decreases below a significant level. However at t=12hr there is a notable -0.437±0.415 fold decrease in expression. Time points at t=24hr and t=48hr were very close to control levels (+0.171±0.282 fold increase at t=24hr; -0.101±0.973 fold decrease at t=48hr) before there was another notable increase in the amount of Snail1 mRNA present compared to control cells at t=72hr (+0.494±0.536 fold increase). EGTA + BMP4 showed a more significant response overall. Treated cells showed a significant +1.232±1.14fold increase in Snail1 expression by t=6hr. This change in expression was followed by a small decrease by t=12hr (-0.246±1.077 fold decrease) but t=24 saw a notable increase of +0.411±0.18 fold, and t=48hr and t=7272hr continued this upward trend in expression with a 1.464±0.308 fold increase at t=48hr and a +1.719±1.579 fold increase at t=72hr.

Primate cells showed a much stronger response to treatment with BMP4 than was seen in human cells (Figure 3.24 (B)). BMP4 treatment resulted in an increase of Snail1 expression levels at all time points, and significantly so up to and including t=48hr. By t=6hr there was already a significant almost 2fold increase (+1.896±1.012 fold increase) in Snail1 mRNA. This was followed by a significant 1.184±1.753 fold increase at t=24hr and a significant 0.756±0.475 fold increase at t=48hr before levels returned to lose to that of control cells with only a 0.268±0.357 fold increase at t=72hr. EGTA+BMP4 treatment also exhibited a significant increase in Snail1 expression of +1.549±0.98 fold increase by t=6hr, slightly less than that seen in BMP4 treatment alone (Δ=0.347 fold). It retained this increase in expression over control cells for the first 24hr with a significant +0.59±0.398 fold increase at t=12hr and 1.672±0.735fold increase at t=24hr. Compared to the control the level decreases to a notable 0.442±0.647 fold decrease at t=48hr before another significant increase over the level in control cells of 0.91±0.17 fold is recorded at t=72hr. It is notable that with relation to Snail1 a bigger overall effect an increase in Snail1 mRNA production is observed in primate than in human cells with just BMP4 treatment, while a greater

response in terms of the expression levels of Snail 1 mRNA with BMP4 treatment following EGTA pre-treatment is seen in human cells.

Snail2 mRNA expression in human NEHB cells displays no significant deviations from the levels observed in control cells from t=6hr to t=24hr inclusive, however at t=48hr a significant decrease of -0.79±1.063 fold in expression compared to control cells was noted and at t=72hr this level was adjusted by a notable increase of +0.413±0.48 fold over control (Figure 3.24 (C)). EGTA + BMP4 treatment resulted in a small but steady increase in Snail2 mRNA from just in excess of the amount seen in control cells at t=6hr (+0.074±0.766 fold increase), steadily up to a significant +0.792±0.137 fold increase after 48 hours (t=12hr saw a +0.362±0.222 fold increase and t=24 hr recorded a significant +0.565±0.022 fold increase). The increase over controls reduced to below a significant level by t=72hr (+0.39±0.077 fold increase). With the exception of the t=48hr time-point (BMP4 only = -0.79±1.063 fold decrease and EGTA+BMP4= +0.792±0.137 fold increase) both treatments resulted in relatively similar profile of increased expression. Primate cells responded noticeably differently to treatments and with greater changes in expression levels to human cells (Figure 3.24 (D)). In relation to BMP4 treatment the levels fluctuated significantly between increased and deceased in comparison to the preceding time point measurement. There was an initial -0.533±0.496 fold decrease by t=6hr; this was followed by a notable increase at t=12hr of +0.427±0.242 fold (Δ=0.96 fold between t=6hr and t=12hr); t=24hr reported a significant decrease in comparison to control cells of -1.465±0.582 fold, followed by significant fold increases in expression of t=48hr (+1.178±0.573 fold increase) and t=72hr (+1.167±0.795) respectively.

EGTA+BMP4 treatment resulted in an almost exactly opposite profile. t=6hr and t=12hr saw a small increase and small decrease, neither of which were significant, in relation to control. However t=24hr saw a significant, +1.322±1.461 fold, increase in expression followed by a decrease at t=48hr (-0.327±0.653) and another, this time significant, decrease, -0.702±0.744 fold, at t=72hr time point.

In primate, as in human, the most significant results were recorded from t=24hr to t=72hr. It is also of note that the most significant results were in this instance recorded in primate cells in both BMP4 and EGTA+BMP4 treatment groups.
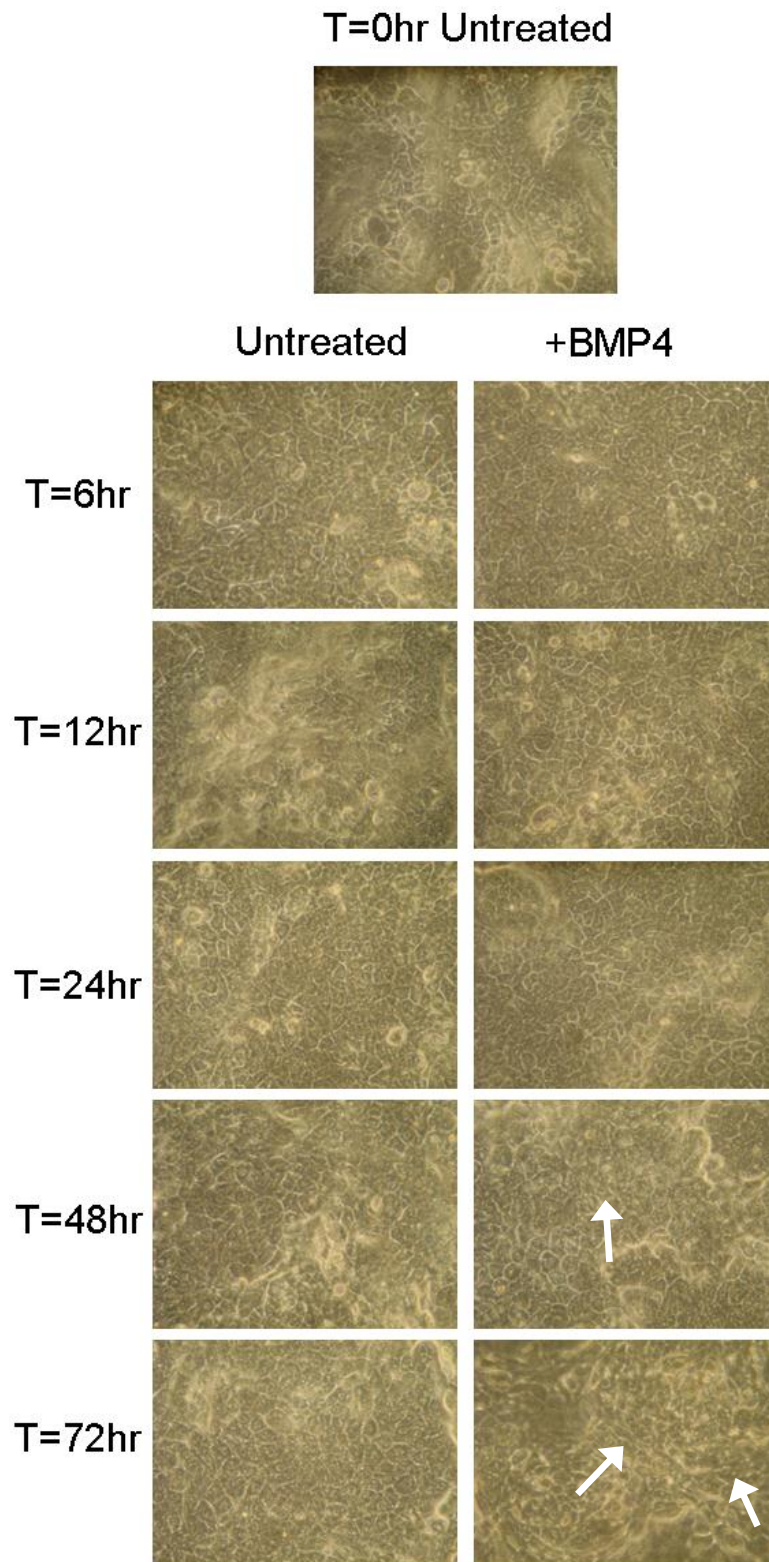
Figure 3.17 Human NEHB cells +/- BMP4 over a 72 hour time-frame.
Human NEHB cells with, (RHS) and without (LHS), BMP4 added over a 72 hour time-frame and imaged via brightfield microscopy. No major changes visible in BMP4 –ve cells, however cells receiving BMP4 by t=48hr and at t=72hr show a change in morphology as a result of BMP4 treatment as indicated by arrows.
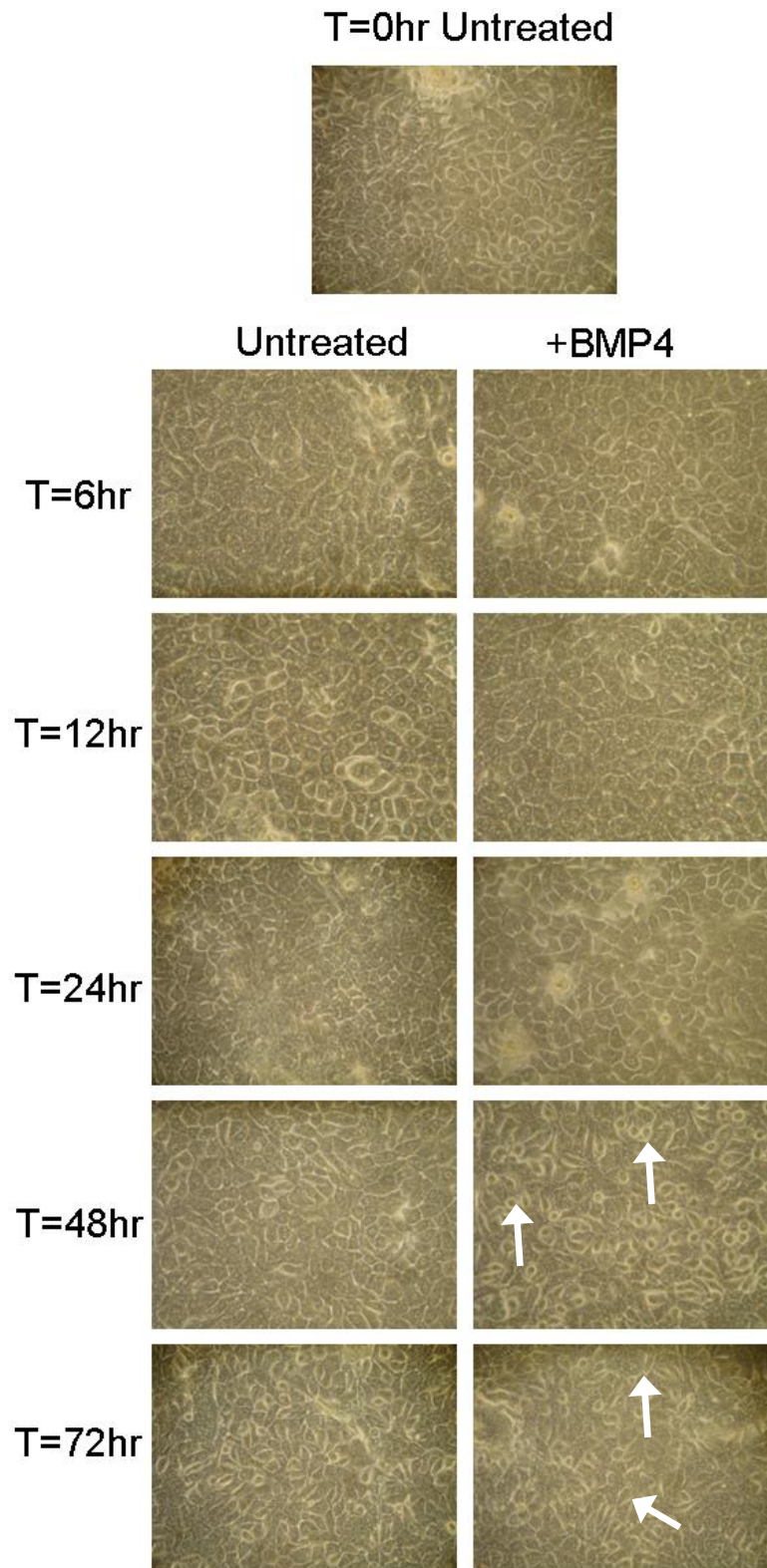
Figure 3.18 Primate cells +/- BMP4 over a 72 hour time-frame.

Primate cells with, (RHS) and without (LHS), BMP4 added over a 72 hour time-frame. No major changes visible in BMP4 –ve cells, however, cells receiving BMP4 by t=48hr and at t=72hr show a change in morphology as a result of BMP4 treatment as indicated by arrows
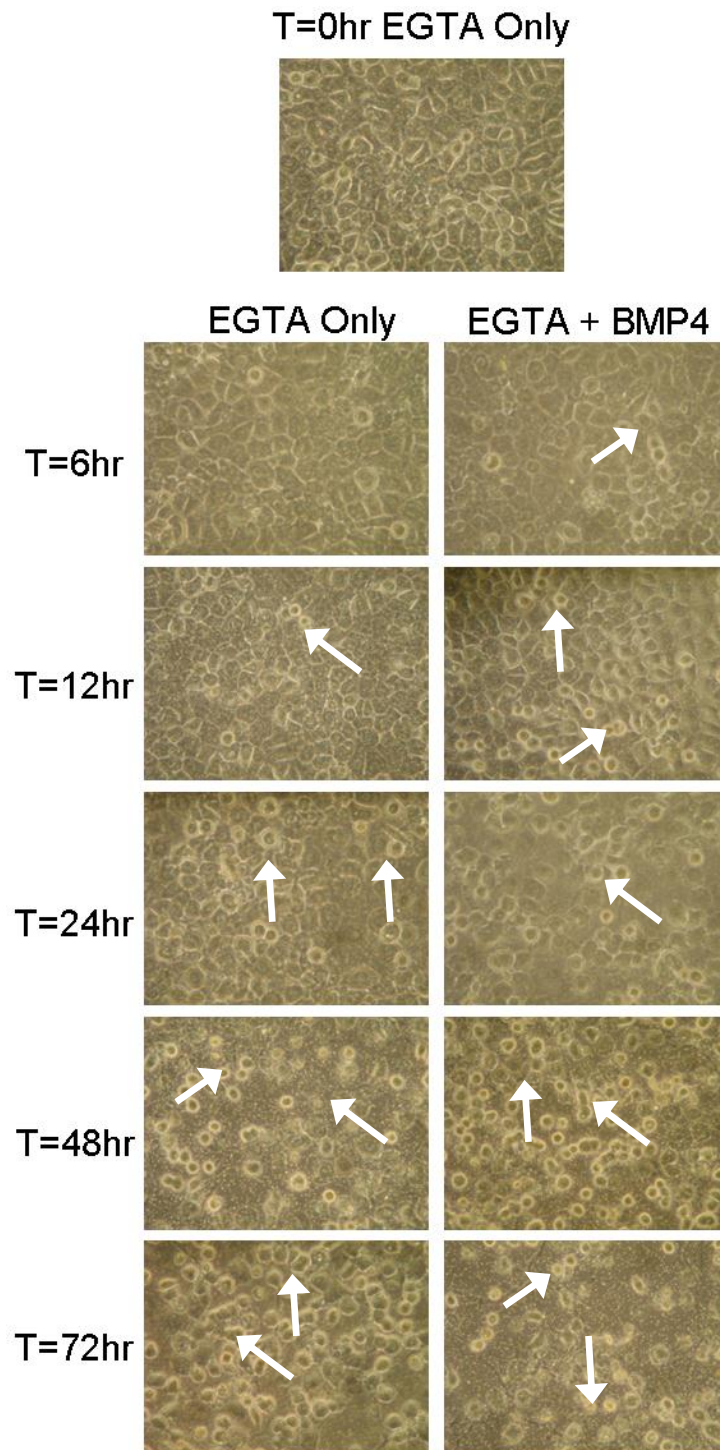
Figure 3.19 Primate cells with EGTA and +/-BMP4 over a 72 hour timeframe
Primate cells all treated with EGTA and with, (RHS) and without (LHS), BMP4 added over a 72 hour time-frame. No major changes visible in BMP4 –ve cells until t=24hr, however, cells receiving BMP4 by t=6hr show a change in morphology as a result of BMP4 treatment. Both sets of cells are markedly different from what was observed in non-EGTA treated primate cells (Figure 3.23). Arrows indicate mesenchymal like cells.
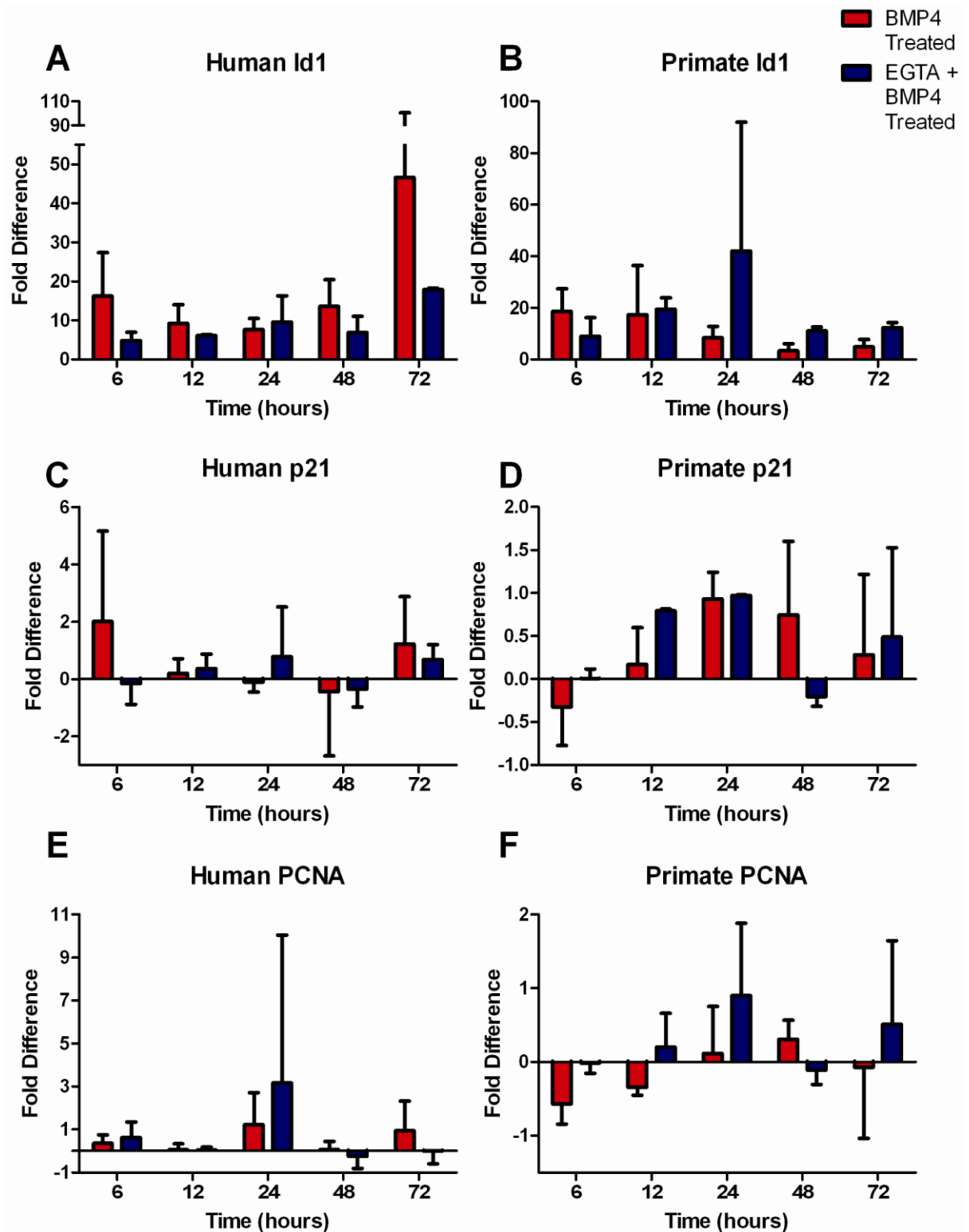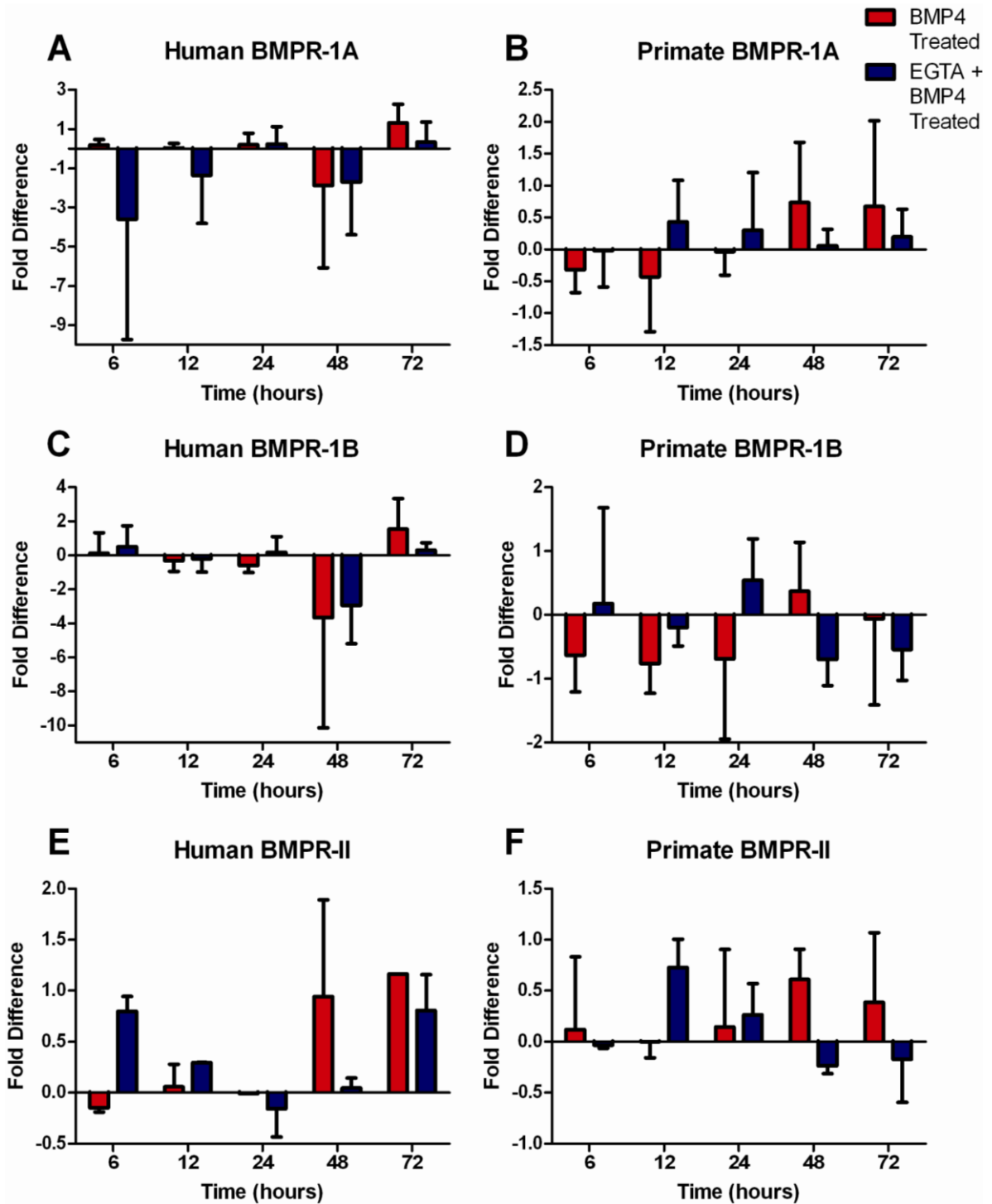
Figure 3.20 Quantification of Id1, p21 and PCNA mRNA expression levels

qPCR analysis of the change in expression of Id1 (A, B), p21 (C, D) and PCNA (E, F) mRNA expression in human and primate ALI bronchial epithelial cells (i) treated with BMP4 and compared to control cells treated with PBS and (ii) treated with EGTA and then with BMP4 compared to control cells treated with EGTA and PBS.
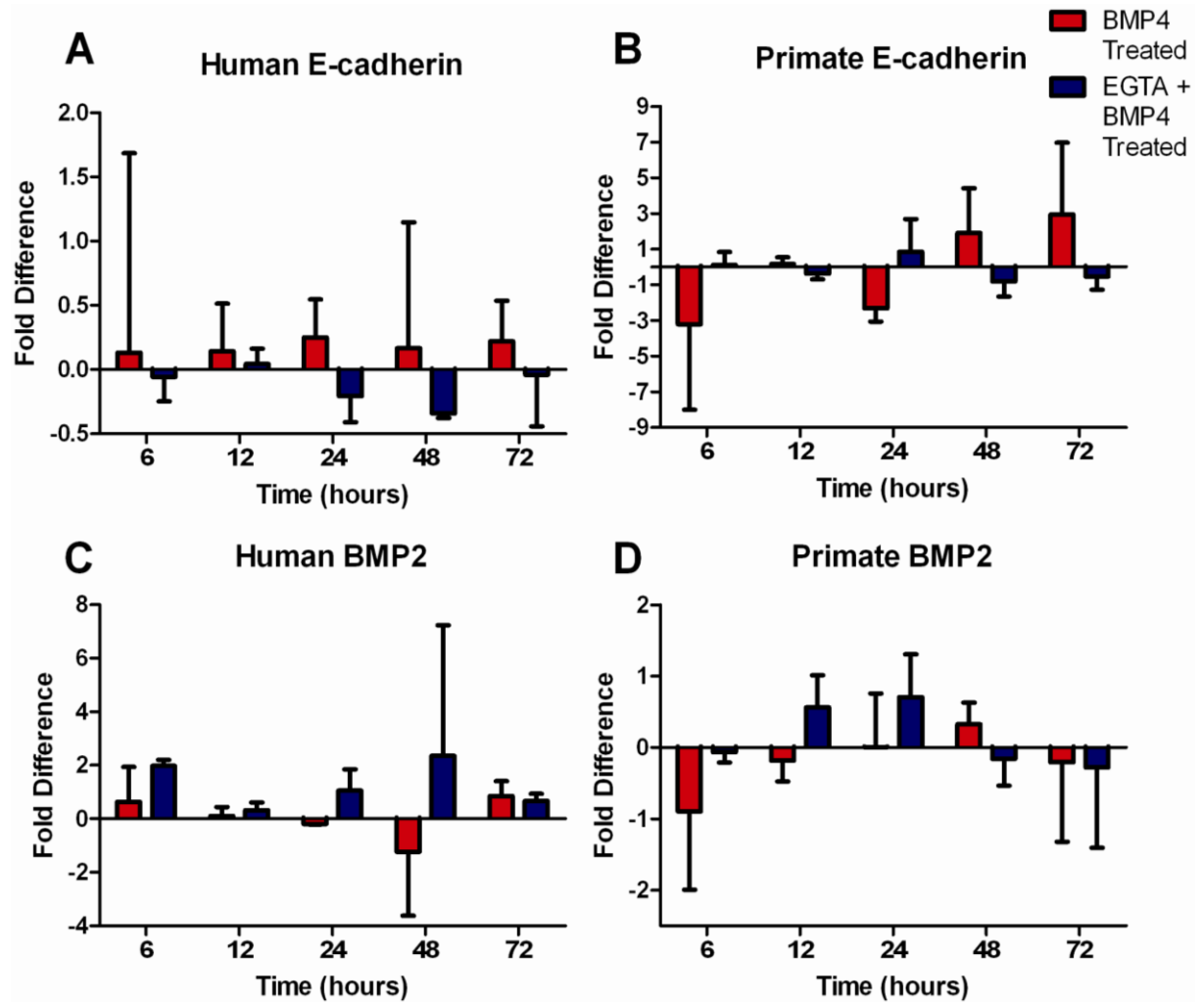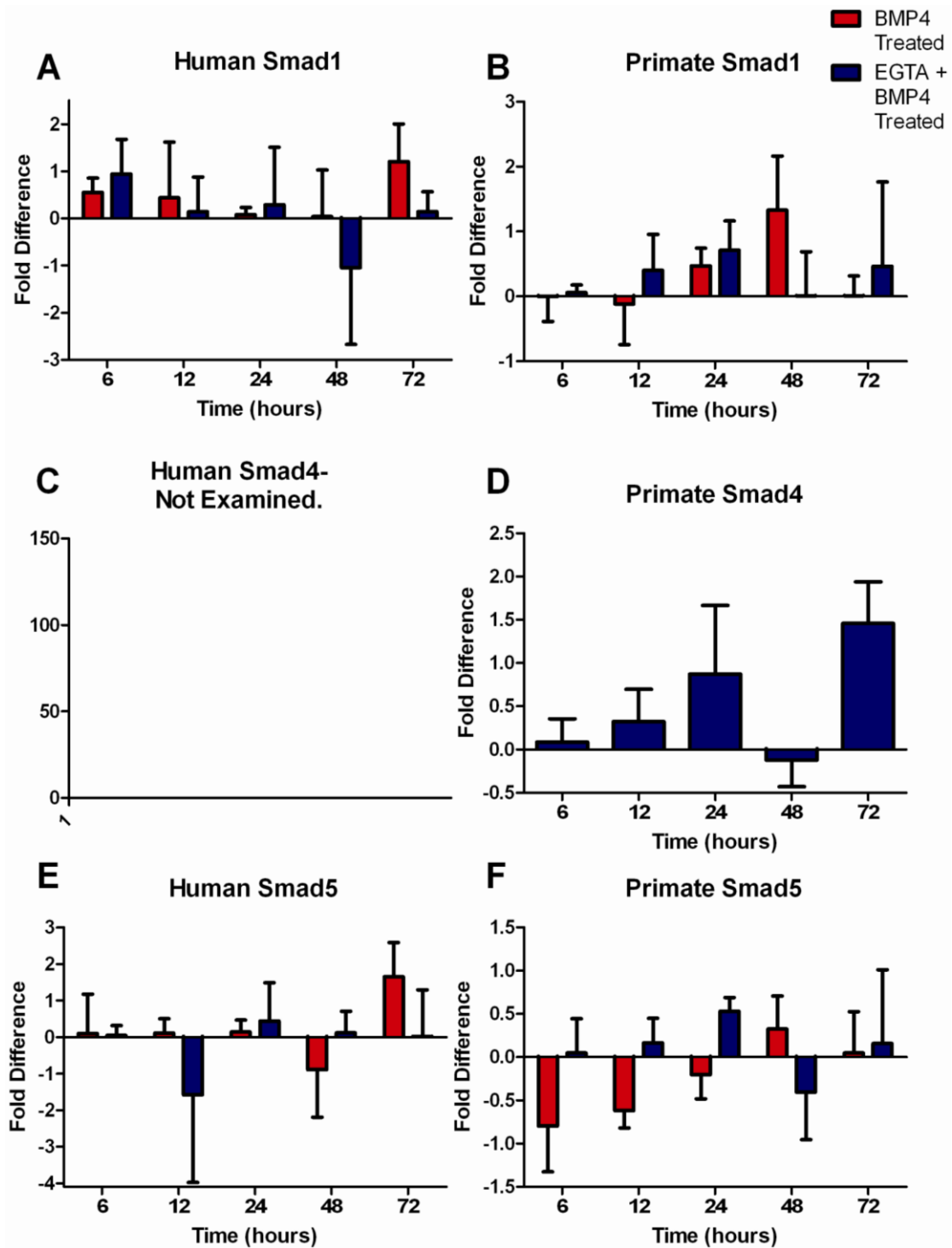
Figure 3.21 Quantification of E-cadherin and BMP2 mRNA expression levels

qPCR analysis of the change in expression of E-cadherin (A, B), and BMP2 (C, D) mRNA expression in human and primate ALI bronchial epithelial cells (i) treated with BMP4 and compared to control cells treated with PBS and (ii) treated with EGTA and then with BMP4 compared to control cells treated with EGTA and PBS.
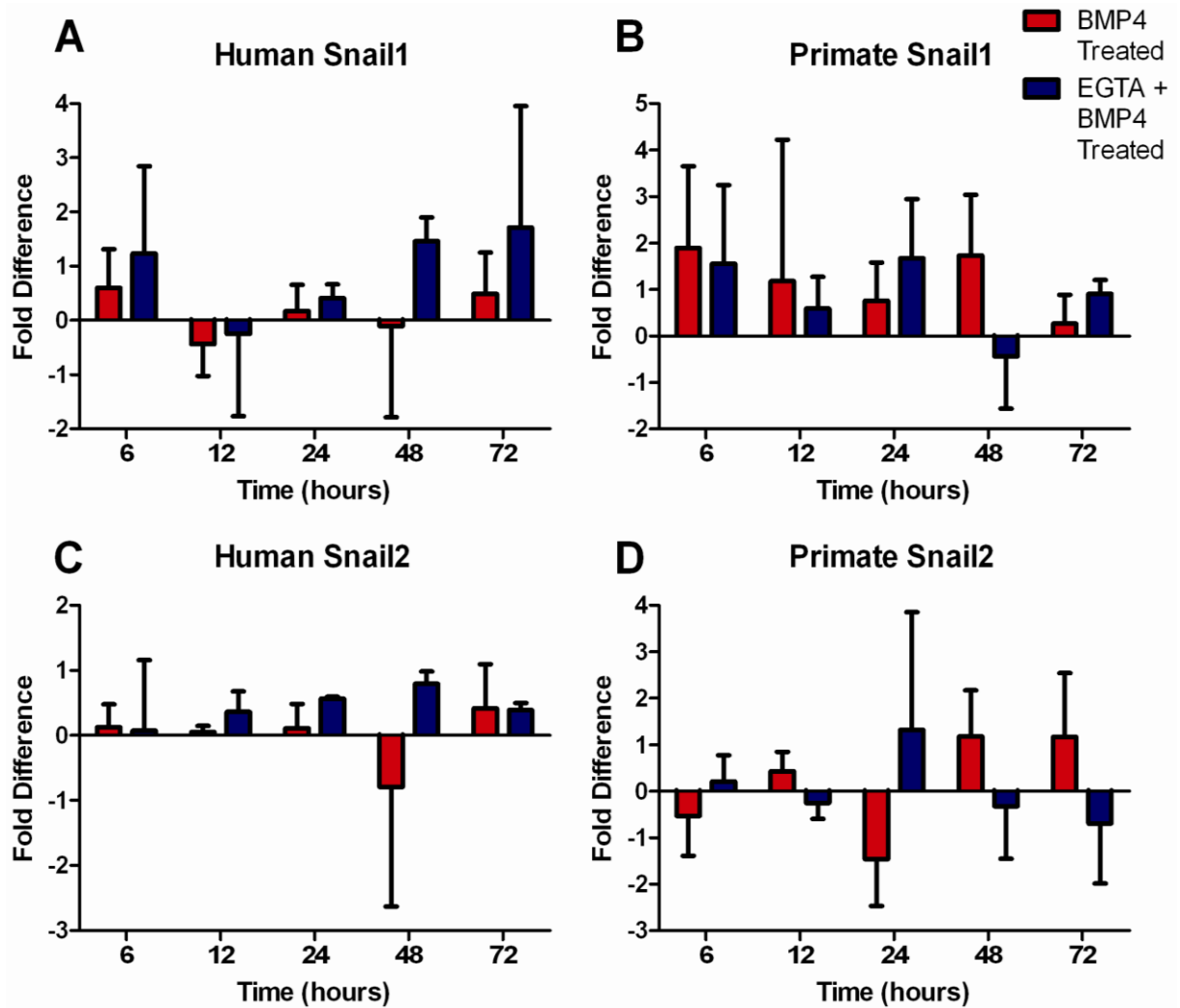
Figure 3.22 Quantification of BMPR-IA, BMPR-IB and BMPR-II mRNA expression levels

qPCR analysis of the change in expression of BMPR-IA (A, B), BMPR-IB (C, D) and BMPR-II (E, F) mRNA expression in human and primate ALI bronchial epithelial cells (i) treated with BMP4 and compared to control cells treated with PBS and (ii) treated with EGTA and then with BMP4 compared to control cells treated with EGTA and PBS.

Figure 3.23 Quantification of Smad1, Smad4 and Smad5 mRNA expression levels

qPCR analysis of the change in expression of Smad1 (A, B), Smad4 (C, D) and Smad5 (E, F) mRNA expression in human and primate ALI bronchial epithelial cells (i) treated with BMP4 and compared to control cells treated with PBS and (ii) treated with EGTA and then with BMP4 compared to control cells treated with EGTA and PBS.

Figure 3.24 Quantification of Snail1 and Snail2 mRNA expression levels

qPCR analysis of the change in expression of Snail1 (A, B), and Snail2 (C, D) mRNA expression in human and primate ALI bronchial epithelial cells (i) treated with BMP4 and compared to control cells treated with PBS and (ii) treated with EGTA and then with BMP4 compared to control cells treated with EGTA and PBS.

Gene	Species	Treatment	
		BMP4 (N)	EGTA+BMP4 (N)
Id1	Human	3†	2
	Primate	2	2
p21	Human	3†	3
	Primate	3	2
PCNA	Human	3†	3
	Primate	3	3§
E-cadherin	Human	3‡	2
	Primate	3	3
BMP2	Human	3†	2
	Primate	3	3
BMPR-IA	Human	3†	3
	Primate	3	3
BMPR-IB	Human	3†	3
	Primate	3	3
BMPR-II	Human	2*	2
	Primate	2	3
Smad1	Human	3†	3
	Primate	3	3
Smad4	Human	not examined	not examined
	Primate	not examined	3
Smad5	Human	3†	3
	Primate	3	3
Snail1	Human	3†	2
	Primate	3	3
Snail2	Human	3†	2
	Primate	3	3
† t=24hr n=2; t=72hr n=2			
‡ t=12hr n=2; t=24hr n=2; t=72hr n=2			
* t=24hr n=1; t=72hr n=1			
§ t=12hr n=2			

Table 3.3 qPCR n values

Table3.3 displays the n number for each qPCR experiment evaluating the effects of BMP4 and BMP4+EGTA on Human and Primate ALI.

3.2.5 Protein Expression:

Protein expression in both Human and Primate ALI was analysed by Western Blot and densitometry. The main proteins analysed were actin (housekeeper control), E-cadherin and Smad4 though others were also briefly examined including BMPR-IA and Id1.

E-cadherin was detected at two main levels by Western Blotting, at approx 124kDa, and again at approx 34kDa (Figure 3.25, Figure 3.26 and Figure 3.27). The higher band represents the full length protein and the 34kDa band appears to indicate the presence of a truncated protein molecule. These two bands were present in all samples, human and primate, under all treatment conditions and are the best indication of both the overall relative protein levels and the effects of the treatment upon the protein.

124kDa E-cadherin: With regard to the full length protein in NEHB BMP4 treated cells, treatment resulted in a small decrease at t=6hr (-11.47±17.57% decrease) (Figure 3.26 (A)). A much greater decrease was observed (-48.61±6.255%) at the same time point in the [EGTA+BMP4] treated cells (Figure 3.26 (B)). Both showed an increase in full length protein expression at t=12hr (significant in the case of BMP4 treated at +59.57±56.43% and; 28.97±14.89% on EGTA+BMP4 treated) over respective controls. The quantity of full length protein at t=24hr (-24.55±24.72% in BMP4 vs. +9.075±13.93% in [EGTA+BMP4]) and t=48hr (+139.9±84.02% in BMP4 vs. -26.67±14.47% in [EGTA+BMP4]) were at opposites between the BMP4 and [EGTA+BMP4] treated cells compared to their respective controls. Data was not available for t=72hr in BMP4 only treated cells but the [EGTA+BMP4] group recorded a notable increase in full length protein of 49.32±16.97% at t=72hr.

In the primate cells the profiles of the full length protein expression in the cells were similar to the expression profiles of the cleaved protein, with the exception in the [EGTA+BMP4] treated cells that the amount of full length protein present was higher at t=24hr compared to t=12hr for cleaved. The quantity of full length protein in the cells, as seen with the cleaved protein, decreased across all cell types and treatments compared to controls at t=6hr and increased over the amount seen in the controls by t=12hr. EGTA+BMP4 treated cells, both human and primate, showed the largest decreases in the amount of full length protein at t=6hr.

34kDa E-cadherin: In human NEHB cells the cleaved 34kDa protein quantity decreased slightly compared to control at t=6hr (-13.77±16.93% decrease) and subsequently increased as a result of BMP4 treatment from t=12hr to t=48hr (t=12hr +45.47±97.37% increase; t=24hr 115.2±133.4%; and t=48hr 72.28±50.02%) (Figure 3.27 (A)).

In the [EGTA+BMP4] treated cells the level of cleaved E-cadherin was also decreased slightly at t=6hr (-11.93±34.68%) and then notably increased at t=12hr (+39.28±55.91%), but unlike BMP4 only treated cells, dropped to that of the control cells again at t=24hr (-1.236±24.52% decrease) (Figure 3.27 (B)). t=48hr saw another, this time significant, increase in the amount of cleaved protein compared to control cells (+97.69±126.3%) before dropping again by t=72hr to a level lower than observed in controls (-14.56±26%).

Primate cells response to BMP4 also showed a slight decrease at t=6hr (-17.58±27.39%) and then a significantly elevated amount of cleaved E-cadherin protein at t=12hr (73.74%). However at t=24hr a significant decrease (-70.3±26.21%) compared to the level observed in control cells was recorded. By t=48hr the level of protein in treated cells had recovered to just above that of the controls (+8.186±0.988%) and is elevated once again to a notable level of 49.82±12.96% at t=72hr.

In primate [EGTA+BMP4] treated cells, t=6hr shows a notable decrease in expression of -40.43% (Figure 3.27 (D)). This is followed by a significant increase at t=12hr (123.5±95.36%) in relation to the amount of cleaved E-cadherin present in EGTA+BMP4 treated cells over EGTA only control cells. There is a steady decrease in its quantity in the cells to just below that of what was observed in the control cells at t=48hr (t=24hr +51.38±75.91% increase; t=48hr -10.05±36.17%) followed by another significant increase in the level of cleaved E-cadherin protein present at t=72hr of 197.2±164.2% over controls..

There were a number of observable traits throughout the different treatments and cells types. To varying degrees by t=6hr there was a decrease in the presence of cleaved protein in all cells within both treatment groups followed by a noticeable increase at t=12hr. Thereafter the responses of the cells to the various treatments are cell type and treatment specific.

Smad 4 was examined in human cells after treatment with BMP4 and [EGTA+BMP4] (Figure 3.28 (A, B)). In cells treated with solely BMP4, the level of Smad 4 protein expression in the cells was higher on average at every time-point recorded from t=0hr to t=72hr. This was not reflected in the [EGTA+BMP4] treatments however.

Compared to the control, delivery of BMP4 post EGTA treatment resulted in a decreased amount of BMP4 present in the cells compared to the controls at all time points with the exception of t=12hr (+48.65±26.75%).

BMPR-IA was detected at 66kDa and was briefly examined in human and primate BMP4 treatments (Figure 3.28 (C, D)). Over the period of 48hr from t=0hr the response to BMP4 treatment in both cell types was very similar. Both showed increased levels of BMPR-IA for the first 24hr post-treatment with BMP4 followed by a decrease at t=48hr.

Id1 was examined in primate BMP4 treated cells and was present at 34kDa (Figure 3.29). Id1 protein levels were elevated as a result of BMP4 treatment in primate cells at all time points recorded, with the most significant responses measured at t=6hr (+165.8±126% increase) and t=12hr (+149% increase).
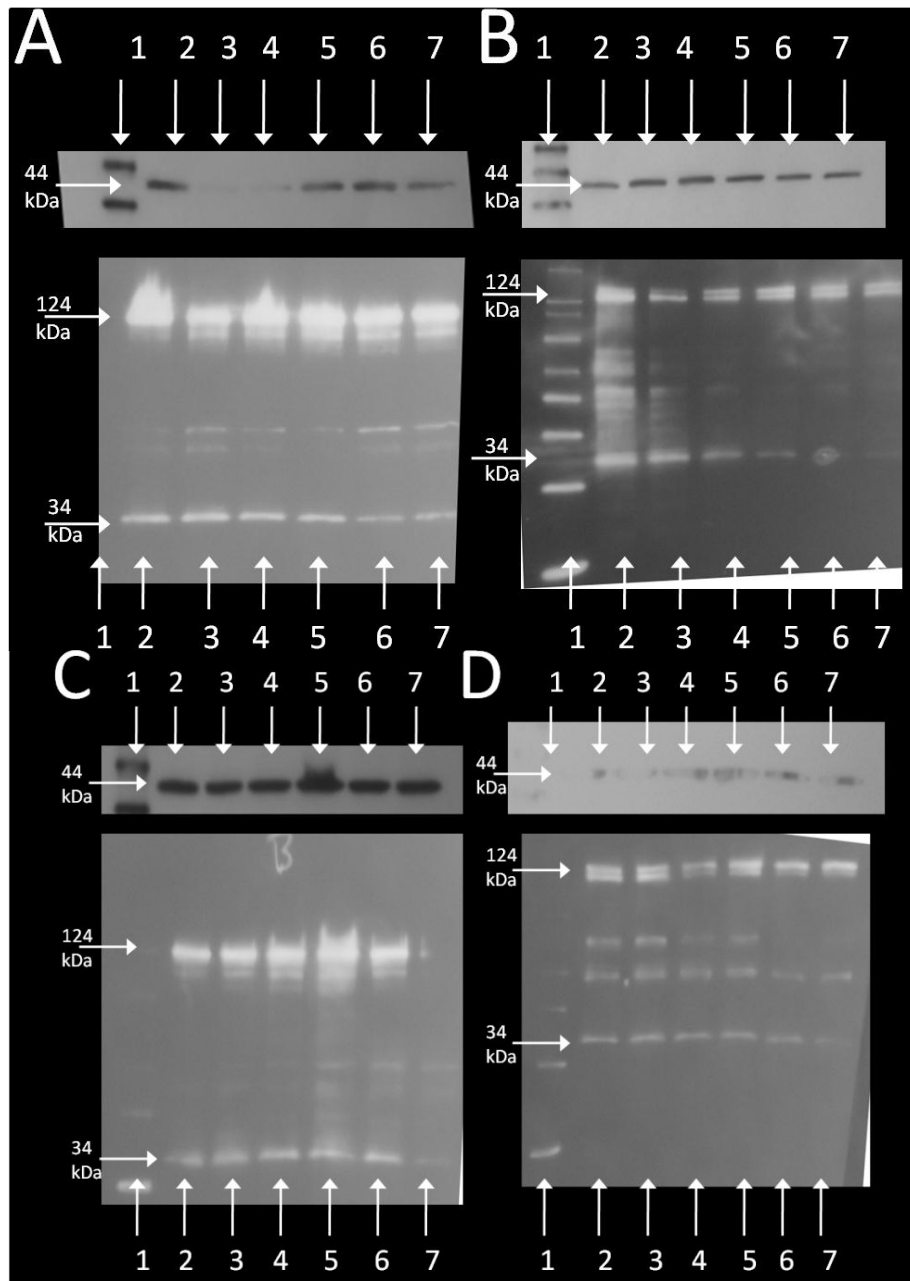
Figure 3.25 Western Blots Gels actin and E-cadherin detection in Human (A+B) and Primate (C+D) BMP4 (A+C) and BMP4+EGTA (B+D) treated cells

Human BMP4 (A) and EGTA+BMP4 (B) treated cells. The top gel shows actin detection (44kDa) and the lower gel shows E-cadherin detection at 124kDa and 34kDa respectively.

Primate BMP4 (C) and EGTA+BMP4 (D) treated cells. The top blot shows actin detection (44kDa) and the lower gel shows E-cadherin detection at 124kDa and 34kDa (truncated) respectively.

In all gels Lane 1 corresponds to the molecular weight marker with lane 2-7 inclusive containing protein sample from one repeat from each experiment as follows-

Lane2 t=24hr Treatment; Lane3 t=24hr Control; Lane 4 t=48hr Treatment; Lane5 t=48hr Control; Lane6 t=72hr Treatment; Lane 7 t=72hr Control.
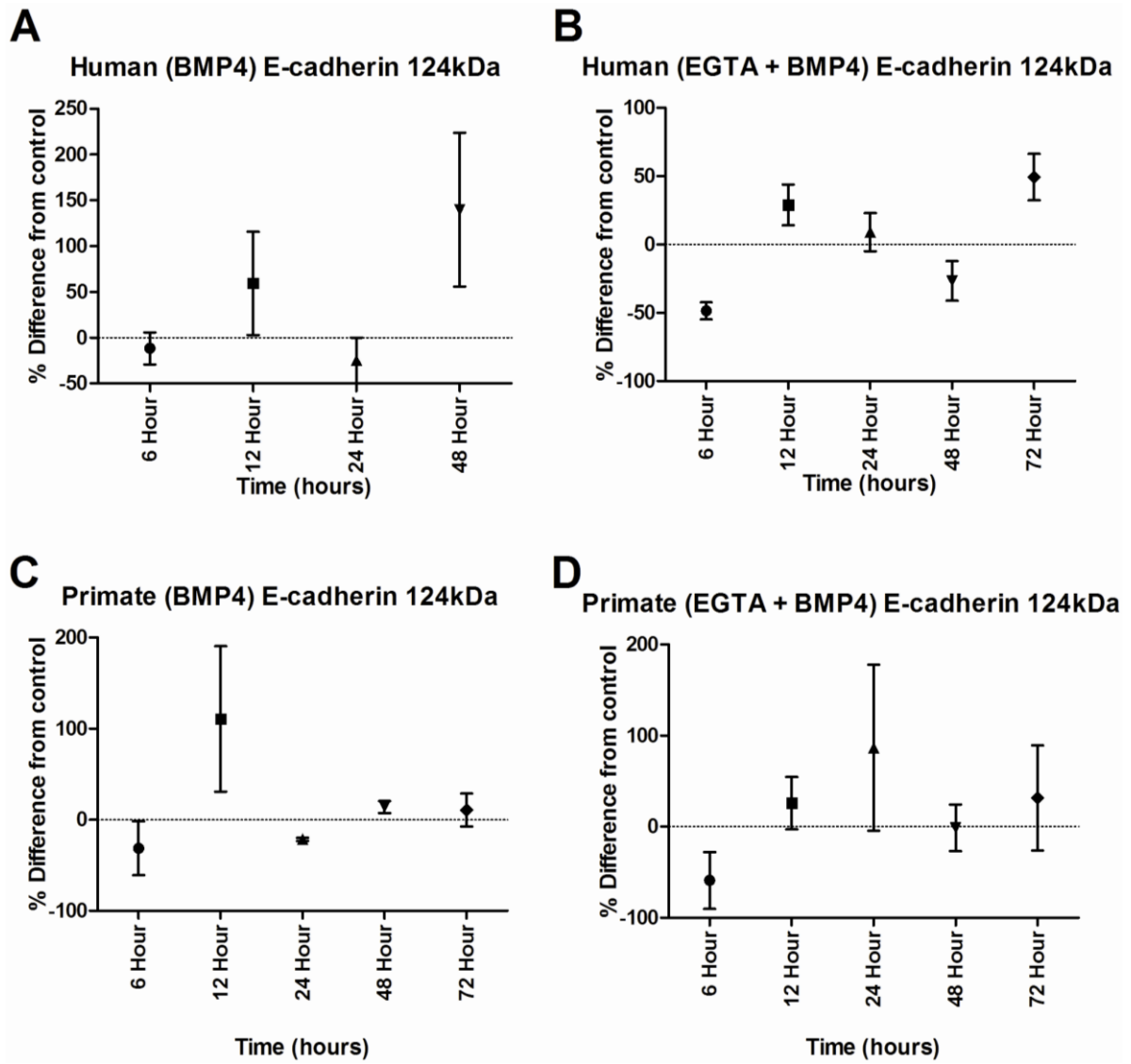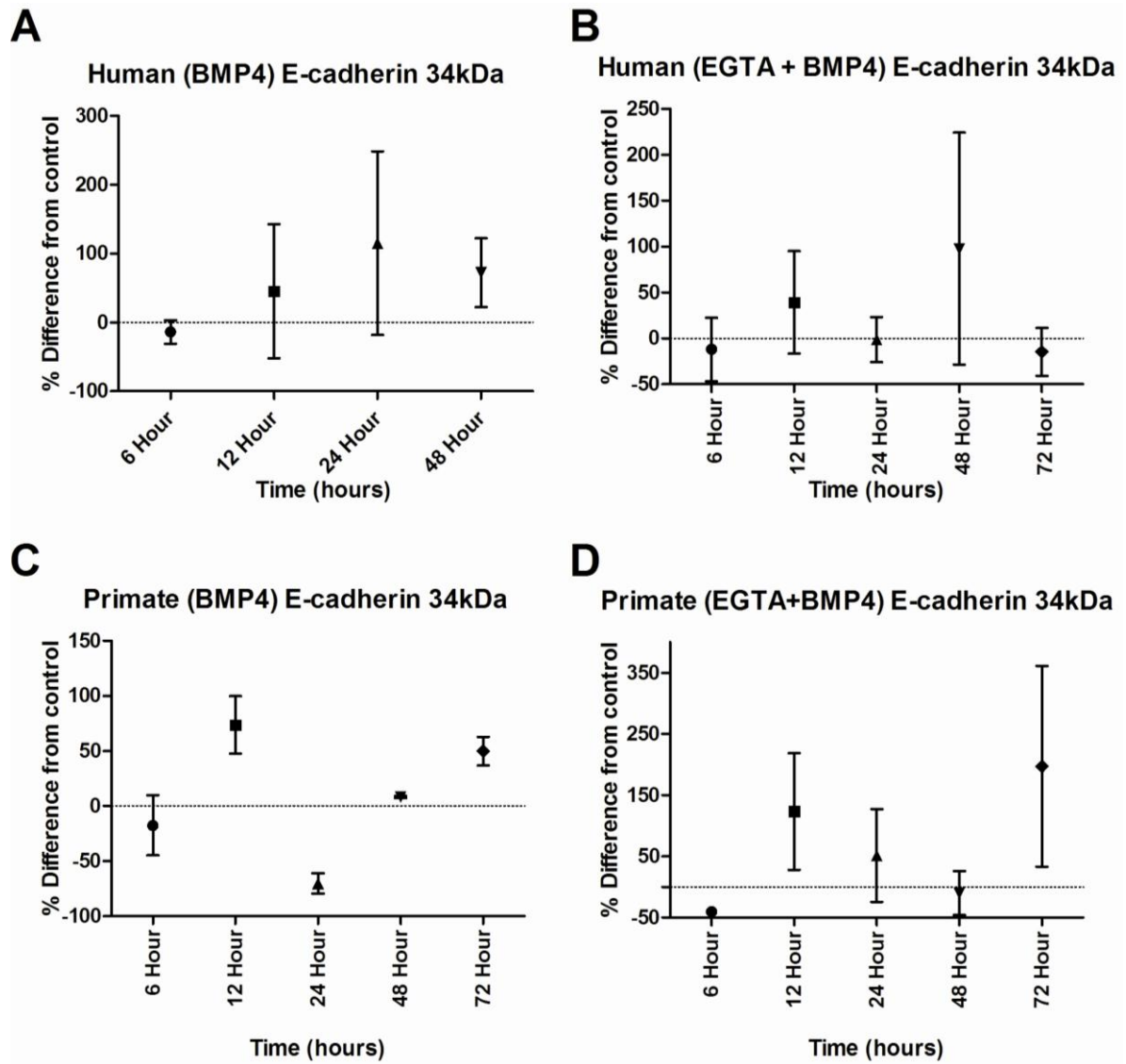
Figure 3.26 Full length E-cadherin (124kDa) protein levels

Percentage full-length (124kDa) E-cadherin present in human (A, B) and primate (C, D) BMP4 and [EGTA+BMP4] treated cells compared to either No Treatment or EGTA controls respectively over a 72hr timeframe. (n=3†)

†B: t=72hr n=2.

†C: t=24hr n=2; t=72hr n=2.

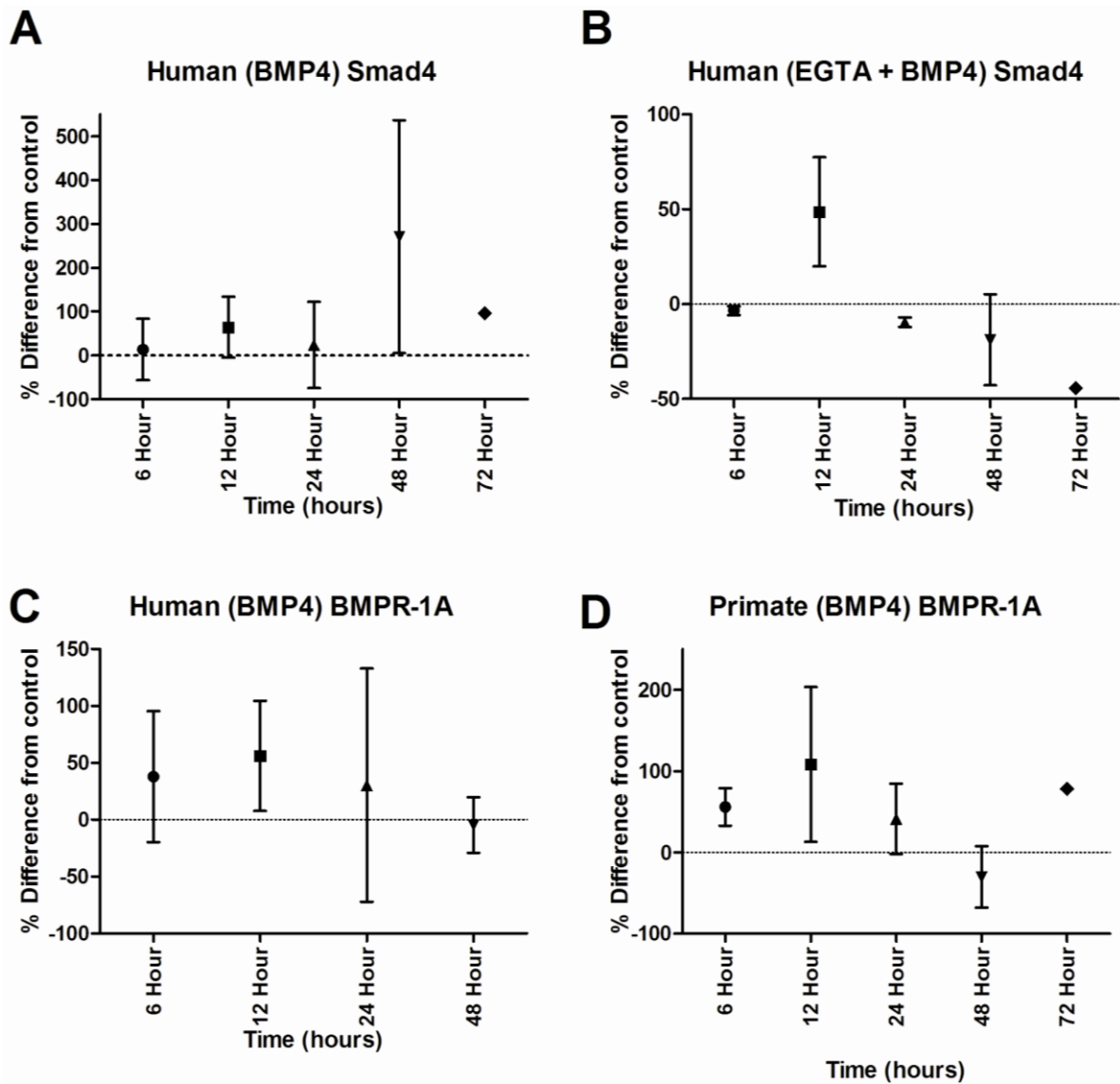†D: t=6hr n=2; t=12hr n=2; t=48hr n=2; t=72hr n=2

Figure 3.27 Truncated E-cadherin (34kDa) protein levels

Percentage cleaved (34kDa) E-cadherin present in human (A, B) and primate (C, D) BMP4 and [EGTA+BMP4] treated cells compared to either No Treatment or EGTA controls respectively over a 72hr timeframe. (n=3†)

†B: t=72hr n=2.

†C: t=72hr n=2.

†D: t=6hr n=1; t=12hr n=2; t=72hr n=2.

**Figure 3.28 Smad4 and BMPR-IA protein levels**

Percentage of

(i) Smad4 present in human cells, both BMP4 (A) and [EGTA+BMP4] (B) treated cells compared to either No Treatment or EGTA controls respectively over a 72hour timeframe (A: n=3†) (B: n=2‡).

(ii) BMPR-IA present in human (A) and primate (B) BMP4 treated cells compared to No Treatment control over a 72hr timeframe (A: n=3) (B: n=2).

† A: t=72hr n=1

‡ B: t=72hr n=1
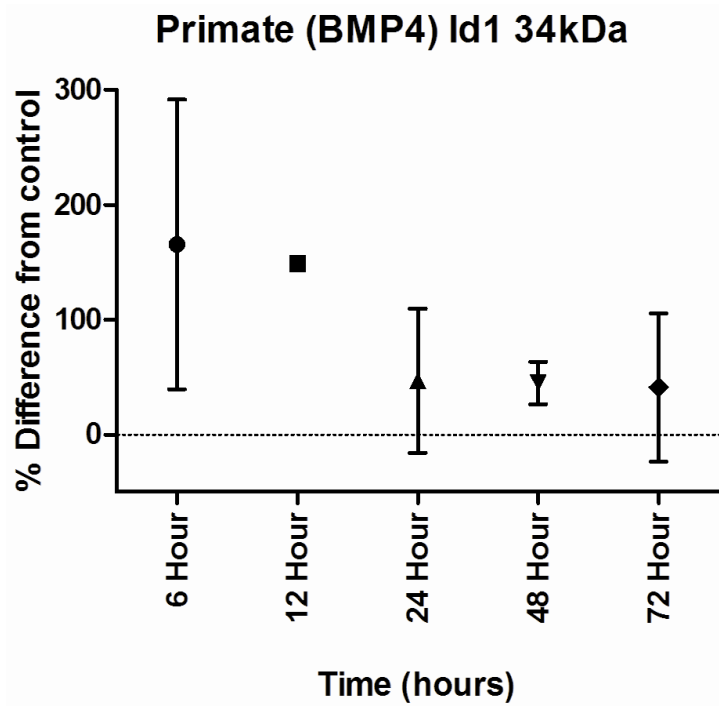
Figure 3.29 Id1 protein levels in primate

Percentage Id1 present in primate BMP4 treated cells compared to EGTA control over a 72hr timeframe (n=3†).

† t=12hr n=1; t=24hr n=2; t=48hr n=2; t=72hr n=2.

3.3 Discussion

3.3.1 Ozone + HDMA model in Rhesus Macaque Primates

To our knowledge this work represents the first report of BMP pathway expression in primate airways *in vivo*. Immunofluorescence analysis carried out on the comparison O_3+HDMA primates with filtered air control examined the expression of three proteins, PCNA, BMPR-IA and pSmad1/5/8. The expression profiles were evaluated at different layers in the airways, the trachea, airway level1, airway level2 and airway level6. In the two proteins examined in the trachea, neither PCNA nor BMPR-IA was present at anything above a low level. In comparing the same two proteins down through the airways however it can be seen that O_3+HDMA allergic asthma in primates triggered a large response with a substantially increased expression of the protein in the airway cells, while the level in the control animal never varied above a very low constant. BMPR-IA levels also increased dramatically in the airways of the O_3+HDMA group, again with no major increase in the control group lungs. pSmad1/5/8 was also analysed but results were only available in the level2 and level6 airways. At level2 airways in the treated animals there was a significant amount of pSmad1/5/8 activity, and there was none detected in the corresponding airways of the control animals. In the level 6 airways the level in the O_3+HDMA animals was higher than that seen in the controls. This means that the onset of allergic asthma in primates corresponds with an increased level of PCNA, BMPR-IA and pSmad1/5/8 activity, showing both the onset of genetic damage and the involvement of the BMP pathway in the process. The levels of pSmad1/5/8 detected in the control group level 6 airways require comment. The lungs being examined are 6month neonate primates and lung development is not arrested at this stage, therefore at the terminal ends of the bronchiolar regions development is still ongoing and would include BMP pathway activity.

The O_3+HDMA allergic asthma model clearly shows involvement of the BMP pathway. Therefore it provides a potential target for modification in attempting to moderate and suppress disease progression in the lung.

3.3.2 ALI Cultures-EGTA effect on cells.

EGTA treatment of the cells was used to disrupt tight epithelial junctions in the ALI, more closely resembling the airway state in a disease lung. In order to ensure that the results taken from the treatments of BMP4 were completely understood it was necessary to first determine the effect of the induction of this disease model on the

airway cells on the genetic markers to be examined. It was recorded that over the period of 72hours, mRNA levels for many of the genetic markers examined increased or decreased substantially more than was seen in non-EGTA treated cells. This was particularly noticeable in relation to the level of Id1 mRNA. Of particular note was the response of BMPR-IA and BMPR-IB at t=48hr and t=72hr where a reversal in expression levels occurred, i.e., in control animals, compared to their t=0hr control, there was a decrease in expression, whereas in EGTA treated animals there was a significant increase in expression levels. This was specific to primates and was not seen in the human models. The exact same pattern was also noted with E-cadherin mRNA levels in the primate model. The same reversal of expression levels was seen at t=48hr and t=72hr in BMPR-II mRNA levels in the human model between EGTA and control cells.

This illustrates that when examining the changes in the cells as a result of treatment it is important to have proper controls and to ensure comparison to like with like. It clearly demonstrates, through analysis of Id1 mRNA levels that no BMP pathway stimulation resulted from this pre-treatment damage. It illustrates that EGTA pre-treatment, of its own violation, can as result of its calcium chelating abilities, effect a significant level of change over a 72 hour period on the expression levels of various mRNA levels. It also further illustrated that although the primate model is regarded as being an exceptionally good model for the forecasting of responses in human cells, differences do occur.

3.3.3 ALI Cultures-Effect of BMP4 on healthy and damaged human and primate ALI models

BMP4 stimulated the activation of the BMP pathway in ALI cultures of primary human and primate airway epithelial cells and to the best of our knowledge is the first report to do so. This was clearly signalled by the response of cells with the levels of Id1 mRNA, in both human and primate models showing a significant increase at all timepoints. It should be noted that although the response of Id1 was not as high in EGTA treated animals, where response would have been foreseen as been higher, this could in part be due to the fact that EGTA pre-treatment predisposes the cells to have a lower starting level of Id1 mRNA (Sect. 3.2.3). BMPR-II mRNA levels were also significantly upregulated at various timepoints by the presence of BMP4 in both BMP4 only and BMP4+EGTA treatment groups. This was also seen in the levels of the receptor Smad, Smad1 in human and primate cells, in primate EGTA+BMP4 treated cells and in human and primate Snail1 and Snail2 mRNA levels.

The effects of BMP4 treatment in an intact and in an EGTA treated ALI were also examined. At an mRNA level E-cadherin did not respond with a significant change in the levels of E-Cadherin mRNA being expressed in the cells as a result of BMP4 treatment. However at various timepoints the overall level of E-Cadherin did increase over the corresponding timepoint controls. There were also two main bands detected in the E-cadherin protein analysis, a truncated 34kDa protein and a 124kDa full length protein. The levels of both increased and decreased in tandem with each other over the various timepoints analysed with no major differences noted. Co-Smad, Smad4, protein levels were analysed in BMP4 treated human ALI cells both with and without EGTA pre-treatment. The overall level in cells not receiving EGTA disruption prior to BMP4 treatment increased, whereas in EGTA pre-treated cells the levels of the Co-Smad were decreased at all timepoints except t=12hr when an increase in expression was recorded. BMPR-IA protein levels were analysed in both human and primate BMP4 treated ALI cultures, without the addition of EGTA. Levels of the protein were increased in both models for the first 24hour period before a decrease was recorded at t=48hr in both models. Id1 protein levels were also analysed and showed an increase in levels across all timepoints in primate BMP4 treated cells. Overall the protein expression trends matched the mRNA expression levels, though the fold level changes observed at mRNA levels were not replicated at protein level.

3.4 Conclusion

Allergic asthma in O_3+HDMA models in primates shows activation of the BMP pathway not seen in filtered air controls. As has been determined in this lab the BMP pathway, when activated, can play a contributory role to the progression of damage and inflammation through its effects on the airway cells and surrounds. As such the BMP pathway reveals itself as a likely contributor to the progression of disease characteristics in the allergic asthma lung. To help further assess the role of the BMP pathway in its role as an antagonist to the healthy repair to the damaged lung, it role was further evaluated by scrutinising the effect of BMP4 on both healthy and damaged version of human and primate airway cells grown in ALI. Confirmation of the pathway activation was seen by the increased levels of Id1 mRNA expression, a first responder to the onset of the activation of the BMP pathway. If the experiment was to be repeated, a more intense look at the reaction of the airway cells over the first 24hour period would be carried out, with inclusion of more timepoints and broadening the spectrum of mRNA, and most notably, protein targets analysed. The results from these experiments provided the necessary information to allow pursuit of the BMP pathway as an ideal target for the delivery of therapeutics targeting lung epithelium. As such the next step was to identify a mouse *in vivo* model that shared this characteristic BMP pathway activation seen in allergic asthma to enable *in vivo* therapeutic targeting. Other laboratory models available for use in Ireland, where Primate research is not permitted, include amongst others, rat, guinea pig, swine and ferrets. Of all these other options, ferrets provide potentially the most useful of all, generally being regarded as the most useful model animal for studying diseases of the lung outside of primates. However due to the fact that a tandem part of this project was the design and testing of a suitable delivery device for the delivery of therapeutics to small rodents, the ease of use of mice, and the wealth of available information on diseases of interest in the model favoured the use of mice in subsequent studies.

4 Establishment of a Clinically Relevant BMP Dependent Disease Model in Mice

4.1 Introduction

The studies in Chapter 3 confirmed that BMP signalling is involved in allergic airway disease in primates. However mouse models are the species of choice for proof of principle studies of therapeutic strategies. In order to evaluate in mice models the effects of modification of the BMP pathway as a potential therapeutic treatment a number of different disease models were examined. By progressing to murine *in vivo* studies it allowed the opportunity to evaluate the effects of therapeutic molecules. Before testing molecules it was vital to gain a better understanding of the two candidate disease models, emphysema, discussed here in detail, and asthma, discussed later in detail in Chapter7, in order to determine the role, if any, of the BMP pathway therein.

4.1.1 Elastase Model of Emphysema in Mice.

Emphysema, as discussed in Section 1.2.3 is a disease of the lung that results in the destruction of the lung parenchyma, causing airways to lose their structure and reducing the surface area of the lung used for gaseous exchange and increasing the resistance to airflow through the airways. Data from our lab has shown that BMP signalling is involved in maintenance of lung architecture and in regeneration after injury (Molloy et al., 2008; Masterson et al., 2010). As a result it was decided to evaluate the BMP pathways involvement, if any, in the destruction and inflammation associated with emphysema and to determine the extent of the damage induced in terms of lung structure and function. A number of different methods were to be used for this evaluation including immunofluorescence analysis of lung sections, H&E analysis combined with quantitative structural analysis of the sections and finally with analysis of the BAL fluid from harvested lungs.

Immunofluorescence analysis was carried out to gain understanding of the both the range of effects of emphysema in the mouse lung and how they pertained to the BMP pathway. As such an extensive analysis by immunofluorescence was carried out to determine the role of various marker and BMP signalling related molecules involvement with, and response to, the disease progression. The expression profiles of CC10, PCNA, pSmad1/5/8, Smad8, Smad4 and smooth muscle actin were assessed.

H&E analyses were carried out in order to qualitatively and quantitatively assess the level of damage resulting from the establishment of an emphysema model. Qualitative analysis was carried out by visual inspection and comparison of the slides for signs of inflammation and damage in the PBS control group and the Elastase treated group.

Quantitative analysis analysed the number of alveoli, length of the alveolar intersections and the number of alveolar intersections. BAL analysis was carried out by examining the neutrophil, lymphocyte and macrophage populations contained in the BAL as well as the cell quantity per BAL. Bodyweight analysis of the animals was also evaluated.

A control group of BALB/c mice that received an administration of PBS and no porcine elastase was also established as a control group for comparison.

4.2 Results

4.2.1 Elastase induced model of emphysema in mice

Animals were divided into two groups. Group1 were control animals who received PBS while Group2 animals received elastase. Elastase treatment was as detailed in Section 2.2.21.2.

4.2.1.1 H&E qualitative and Quantitative Analysis of Elastace Emphysema in BALB/c mice.

H&E analyses were carried out in order to qualitatively and quantitatively assess the level of damage resulting from the establishment of an Emphysema model. Qualitative analysis was carried out by visual inspection and comparison of the slides for signs of inflammation and damage in the PBS control group and the Elastase treated group. The PBS Group1 lung sections show healthy undamaged lung tissue sections with large number of alveoli present (Figure 4.1). In contrast to this the Group2 elastase treated animals show large vacuous regions with no alveoli or airway structure present. Inflammation however was not detected in the Elastase treated group either, as determined by histological analysis.

In relation to Quantitative analysis the number of alveoli, the length of alveolar intersections and the number of alveolar intersections were all analysed (Figure 4.2). In each of the measurements there was a significant difference between the control group and the emphysema lung group ($p < 0.001$; t-test analysis). The control lungs contained more alveoli, had shorter alveolar intersections and had a greater number of alveolar intersections ensuring better gaseous exchange and lung function than seen in the elastase treated Group2 animals. This was as expected.
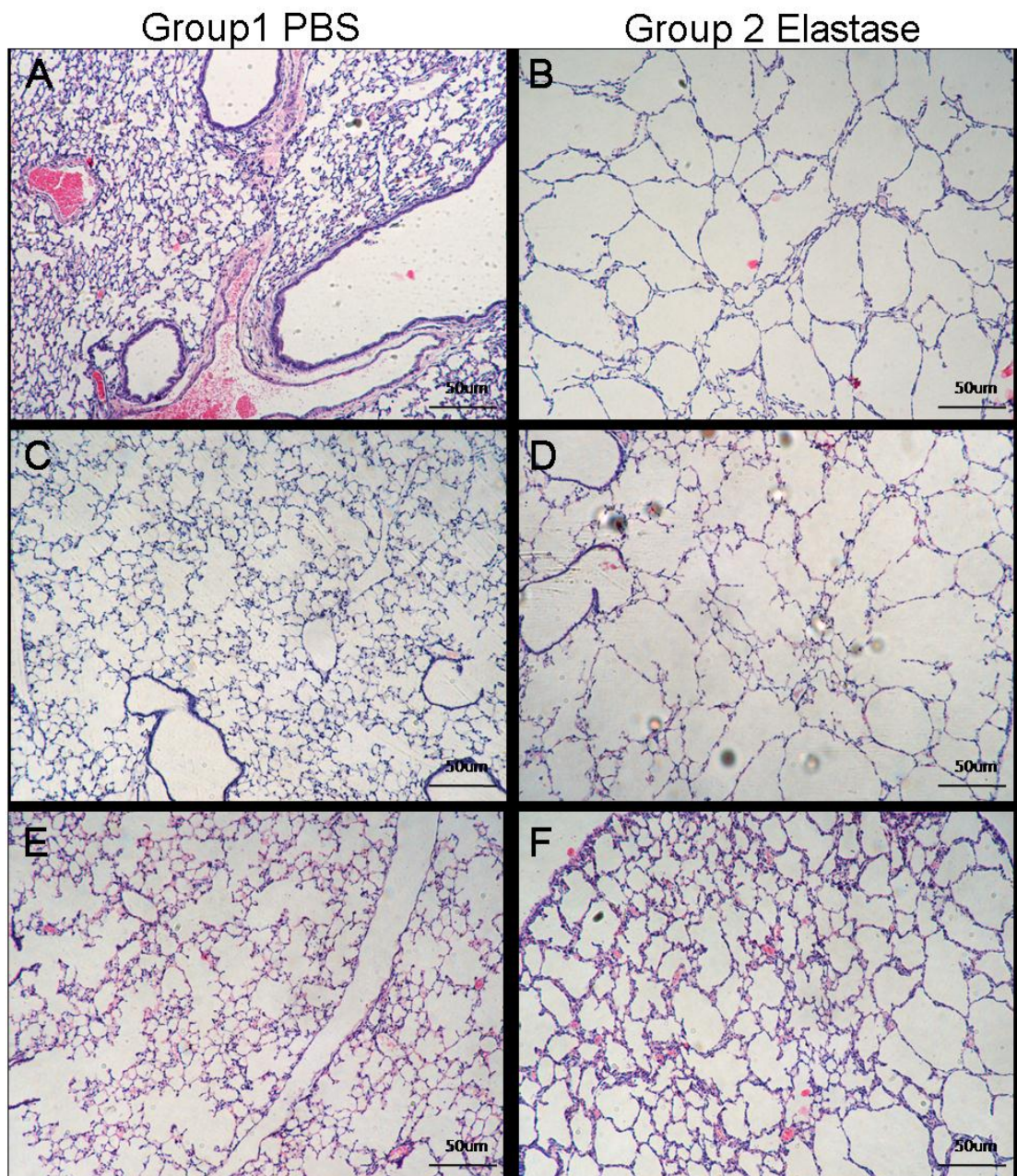
Figure 4.1 H&E histological analysis in elastase model of emphysema.

All images were taken at the same magnification. The control, Group1, animals clearly show the sections of tissue to appear healthy and normal, with large amounts of alveoli present. Group2, elastase treated, however (B, D and F) clearly show large vacous regions with no alveoli or airway structure present. Detailed analysis of the results was carried out (Figure 4.2).
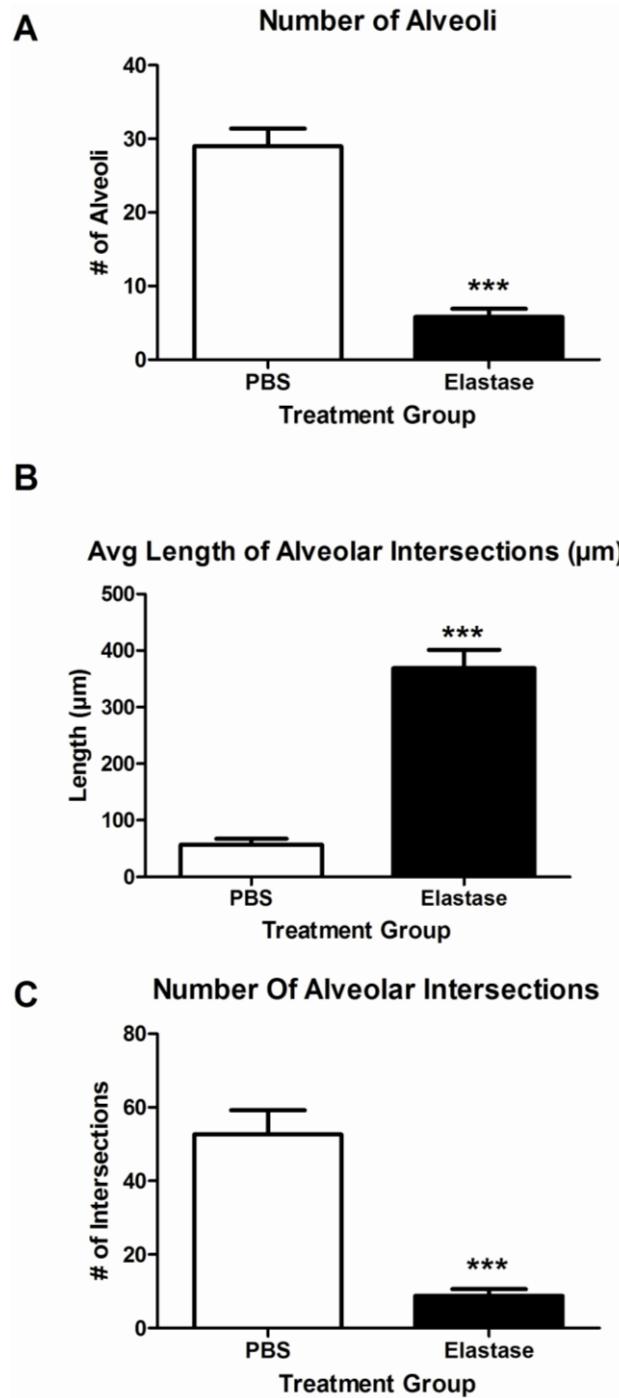
Figure 4.2 Statistical analysis from H&E histolgy sections in elastase model of emphysema

Group1 PBS (n=3) and Group2 Elastase (n=4) showed clear significant differences in all analysis carried out by histology. The PBS control animals, as was expected, contained more alveoli, shorter alveolar intersections and a greater quantity of alveolar intersections, enabling for more gaseous exchange and better lung function than in Elastase treated animals.

4.2.1.2 BAL and whole body analysis of elastase emphysema in BALB/c mice.

Cytospins were prepared from the BAL fluid of the PBS and Elastase treated animals (Figure 4.3). The ratio of macrophages to macrophages and neutrophils to neutrophils differed significantly between the groups (p<0.0001; t-test analysis). Whereas the Group1 cytospins consisted predominantly of Macrophages (77.6±5.921%) and less than 20% neutrophils (19.4±4.905%), a ratio of approximately 4:1 macrophages to neutrophils; in the Group2 Elastase model the amount this ratio was reversed with approximatly 9:1 neutrophils (90.33±84.33%) to macrophages (8.333±0.9545%) present in the BAL fluid. The number of lymphocytes in the BAL fluid analysed for both groups was not significantly different, and the population size was small, with lymphocytes making up only 3±1.414% of the cell population in the PBS treated Group1 animals and 1.333±0.494% of the Group2 Elastase treated animals.

Also analysed was the body weight of animals and the total cell population of the BAL from both treatment groups at the time of sacrifice (Figure 4.4). The bodyweight of Elastase treated Group2 animals (18.47±0.428g; n=6) was significantly less (p<0.001; t-test analysis) than that of PBS treated Control Group1 animals (22.25±0.671g; n=6). This is as expected with the Emphysema lung animals unable to thrive as well as the control group. With regards to the total cell population/ml of the BAL and the % viability of this population, no significant difference was found in either the cell number/ml (2.4923±0.265x10^5 cells/ml control Group1 vs. 3.60399±0.736x10^5 cells/ml Group2 elastase) or the viability (76±7.51 % viable control Group1 vs. 69.83±4.09% viable Elastase Group2).
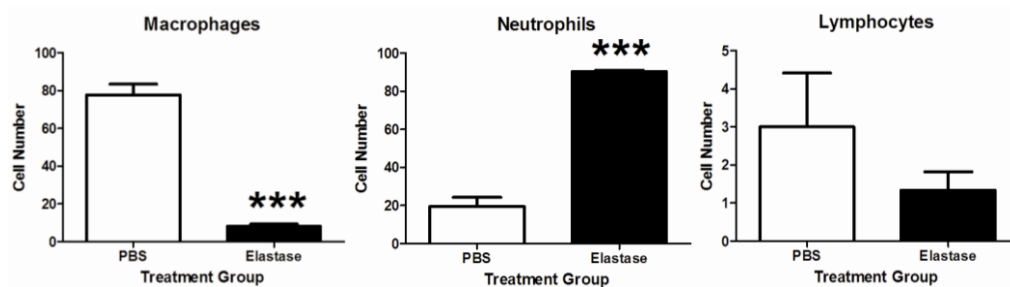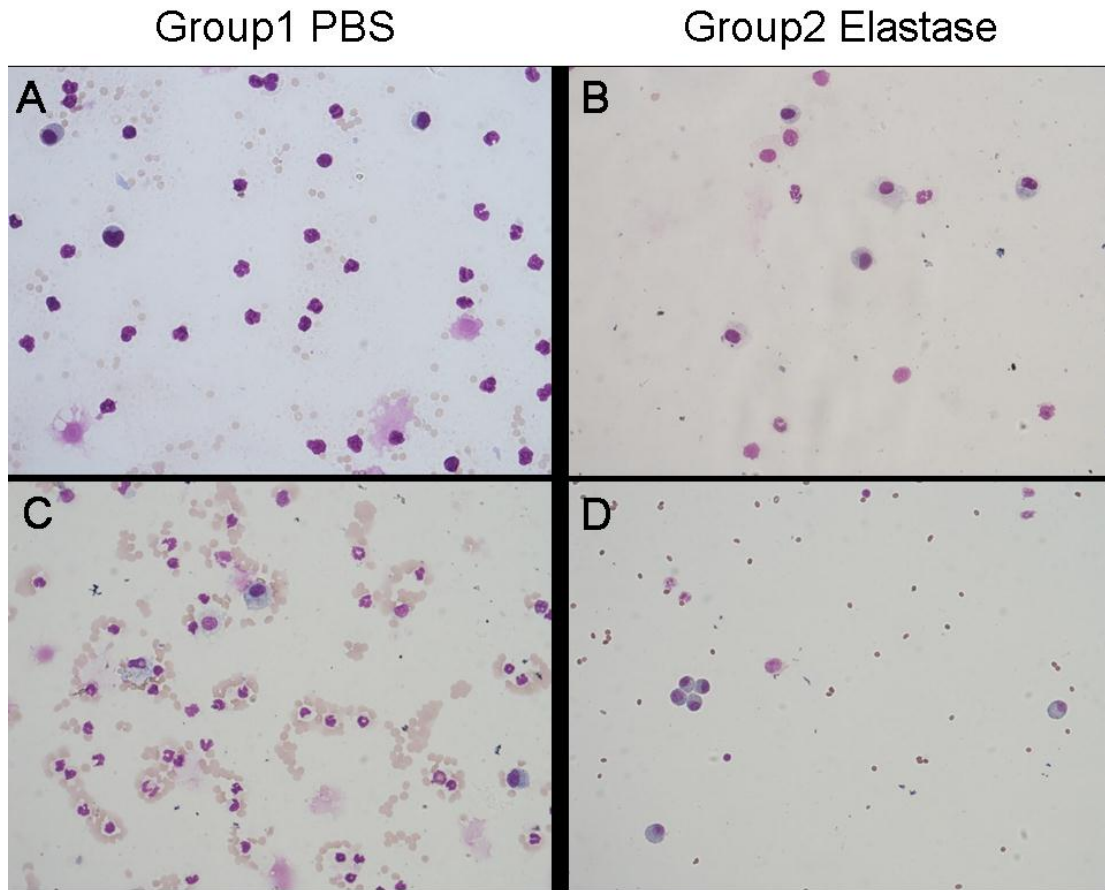
Figure 4.3 BALF Analysis In Elastase model of Emphysema

Group1 PBS, n=5; Group2 Elastase, n=6. (i) shows sample cytospins resulting from the Group1 PBS (A, C) and Group2 Elastase (B, D) treated animals. 100 sample cells were differentially counted from each animals BAL cytospin as can be seen in (ii) above. The ratio of macrophages to macrophages and neutrophils to neutrophils differed greatly significantly between the groups. Whereas the Group1 cytospins consisted predominantly of Macrophages (77.6±5.921%) and less than 20% neutrophils (19.4±4.905%), a ratio of approximately 4:1 macrophages to neutrophils; in the elastase model the amount this ratio was reversed with approximatly 9:1 neutrophils (90.33±84.33%) to macrophages (8.333±0.9545%) present in the BAL fluid.
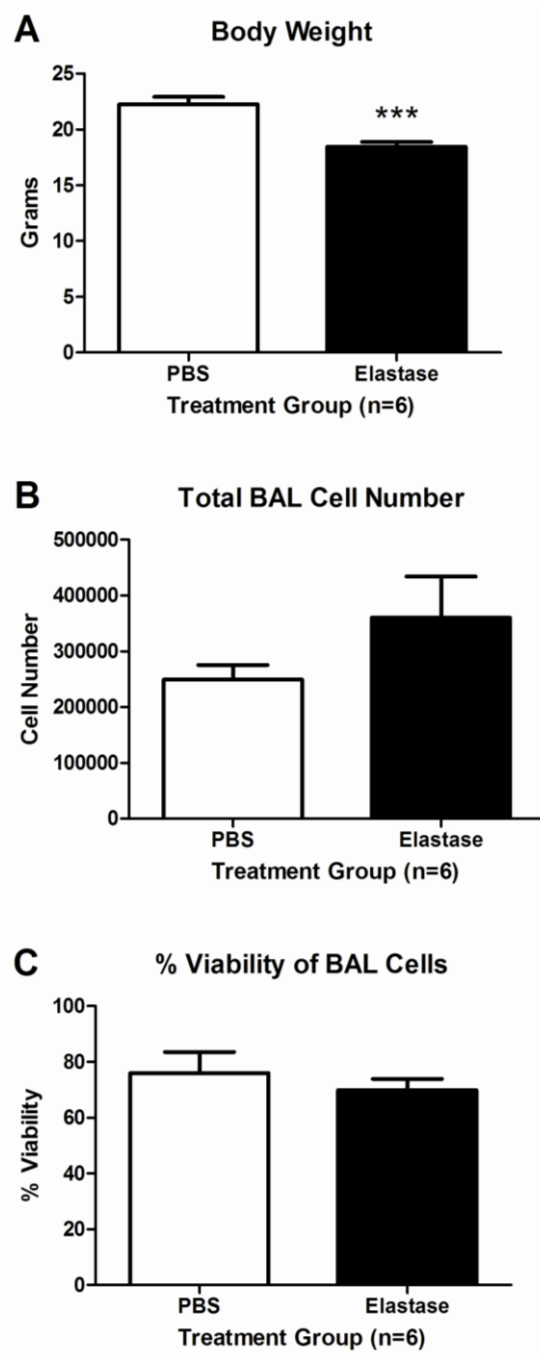
Figure 4.4 Bodyweight and BALF analysis In Elastase model of Emphysema

The bodyweight of each animal was assesed immediatly post mortem. It is of note that the emphysema model mice showed a significant decrease in body weight as a result of the elastase treatment. The total number of cells recorded in the BAL fluid of Elastase treated animals was greater than that of the PBS control group, though no significance was achieved. There was only a minor, and again, non-significant, difference noted in the viability of the cells recorded in the BAL of both groups of animals. (Group 1 PBS n=6; Group2 Elastase n=6).

4.2.1.3 Immunofluorescence analysis for BMP activity

CC10, a Clara cell secretory protein, was analysed to determine if there was a marked increase or decrease in the presence of Clara cells in the airways (Figure 4.5). An increase may indicate an increase in proliferation of the cells, and a decrease may indicate that the onset of emphysema as a result of porcine elastase treatment brought about a cessation in Clara cell activity, a potential major obstacle to repairing the airways. However in both the control and the elastase-treated airways, CC10 protein expression was abundant. There was no discernable difference in the level of expression or localisation between both groups.

PCNA is a marker of cell proliferation. In order to assess the level of regeneration in the airways the levels of PCNA between the control and treated were compared (Figure 4.6). In the control group very little PCNA activity was detected, only located in a small number of individual airway cells. There was nothing to indicate an above background level of activity of the protein. With regards to the emphysema lungs however there was a marked increase in the presence of PCNA, with a high level of abundance observed in the alveolar regions of the lungs. pSmad1/5/8 was then examined (Figure 4.7). It was one of the key indicators of the involvement of the BMP pathway as it signals active phosphorylation of the receptor Smads and their transport to the nucleas. A degree of pSmad1/5/8 activity was detected in the control animal airways, however the controls were found to be expressing more pSmad1/5/8 activity than the emphysema mice.

One of the receptor-regulated Smads, Smad8 was examined to see if there was any Smad linked response to the onset of emphysema (Figure 4.8). Smad 8 expression in the control animals' lungs was by and large non-existent, without only a small number of cells in some of the control animal alveolar regions expressing the protein. In emphysema lungs however the level of Smad8 expression was much higher, and was abundant throughout the alveolar regions. Expression was localised in the alveolar regions of the lung.

Co-Smad, Smad4, which is responsible for shepherding the R-Smads through the cytoplasm post phosphorylation was also examined (Figure 4.9). No Smad4 staining was in evidence during evaluation of the control lungs but Smad4 was detected in emphysema lungs. It was localised to the alveolar region and was highly abundant.

The final protein examined via immunofluorescence analysis was Smooth muscle actin (Figure 4.10). Due to characteristics of the disease which can affect the elasticity or compliance of the lungs it was evaluated to determine whether, after a short disease onset, any discernable difference, either increased or decreased levels of the protein,

would be observed alongside the airways. The protein was however detected in the same locality with the same level of high abundance just below the epithelium of the airways.

A full summary of observations for all analysed proteins can be seen in Table 4.1.
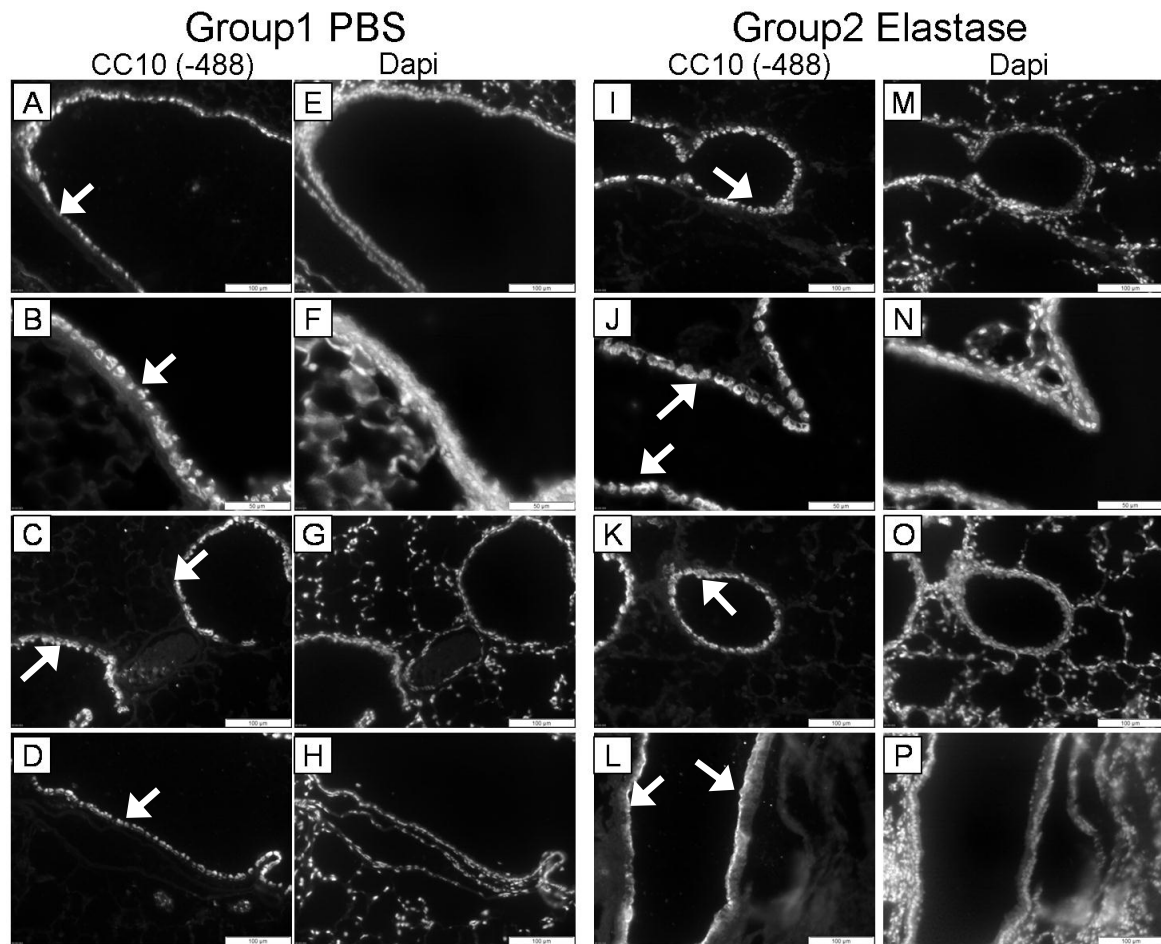
Figure 4.5 CC10 immunofluorescence in elastase model of emphysema

CC10 staining can clearly be seen lining the airways of both Group1 control animals (A, C E and G respectively) and Group2 (I, J, K and L respectively) The level of expression detected in both the PBS and Elastase treated animals was similar with no discernable difference observed
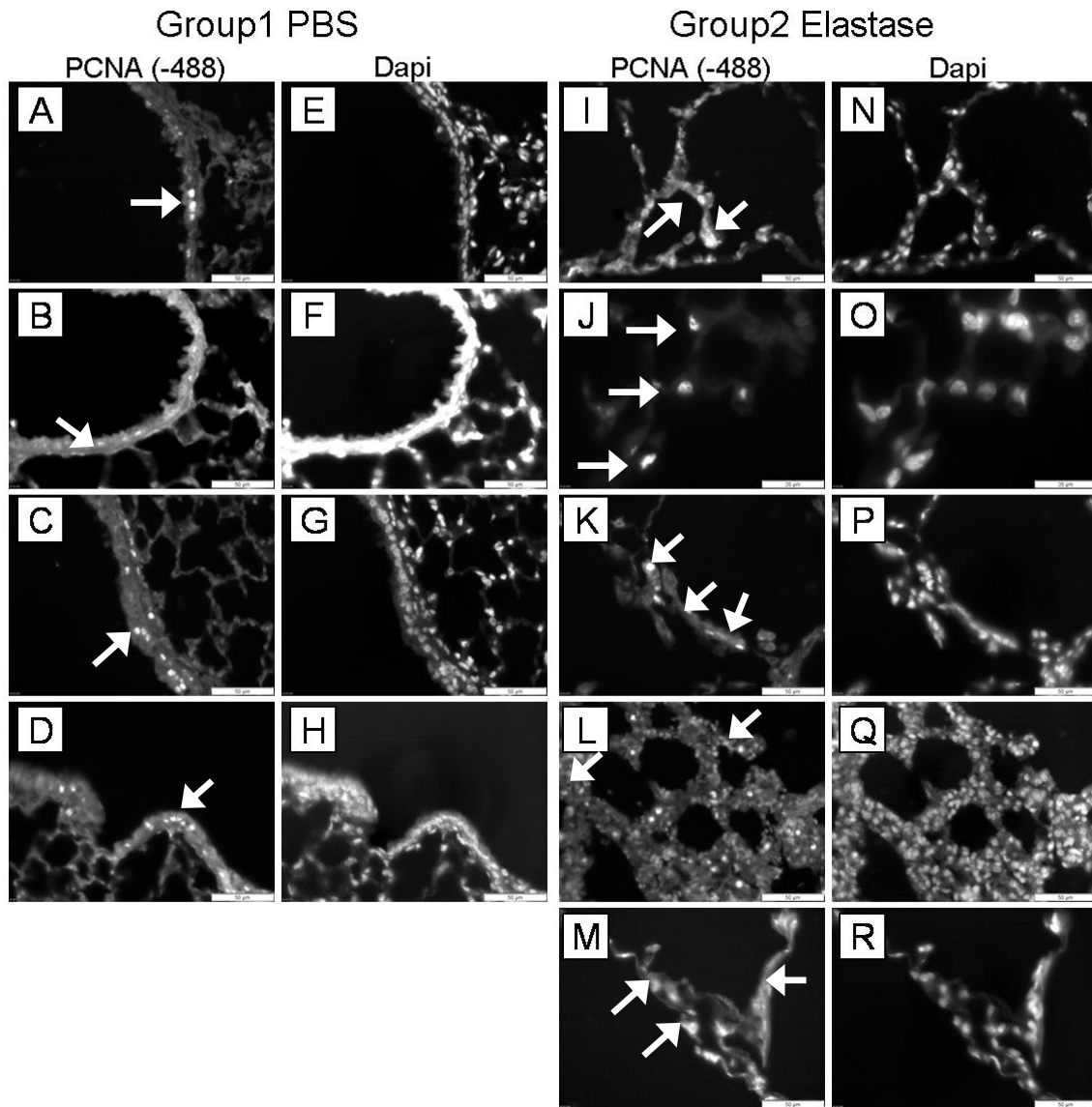
Figure 4.6 PCNA immunofluorescence in elastase model of emphysema

Group1 control animals had very little evidence of PCNA though small amounts could be deteced in parts of the airways as seen in A, B, C and D. PCNA staining was more evident in the Group2 elastase treated animals however with detection of the protein occuring throughout the alveolar regions as can be seen in I, J, K, L and M.
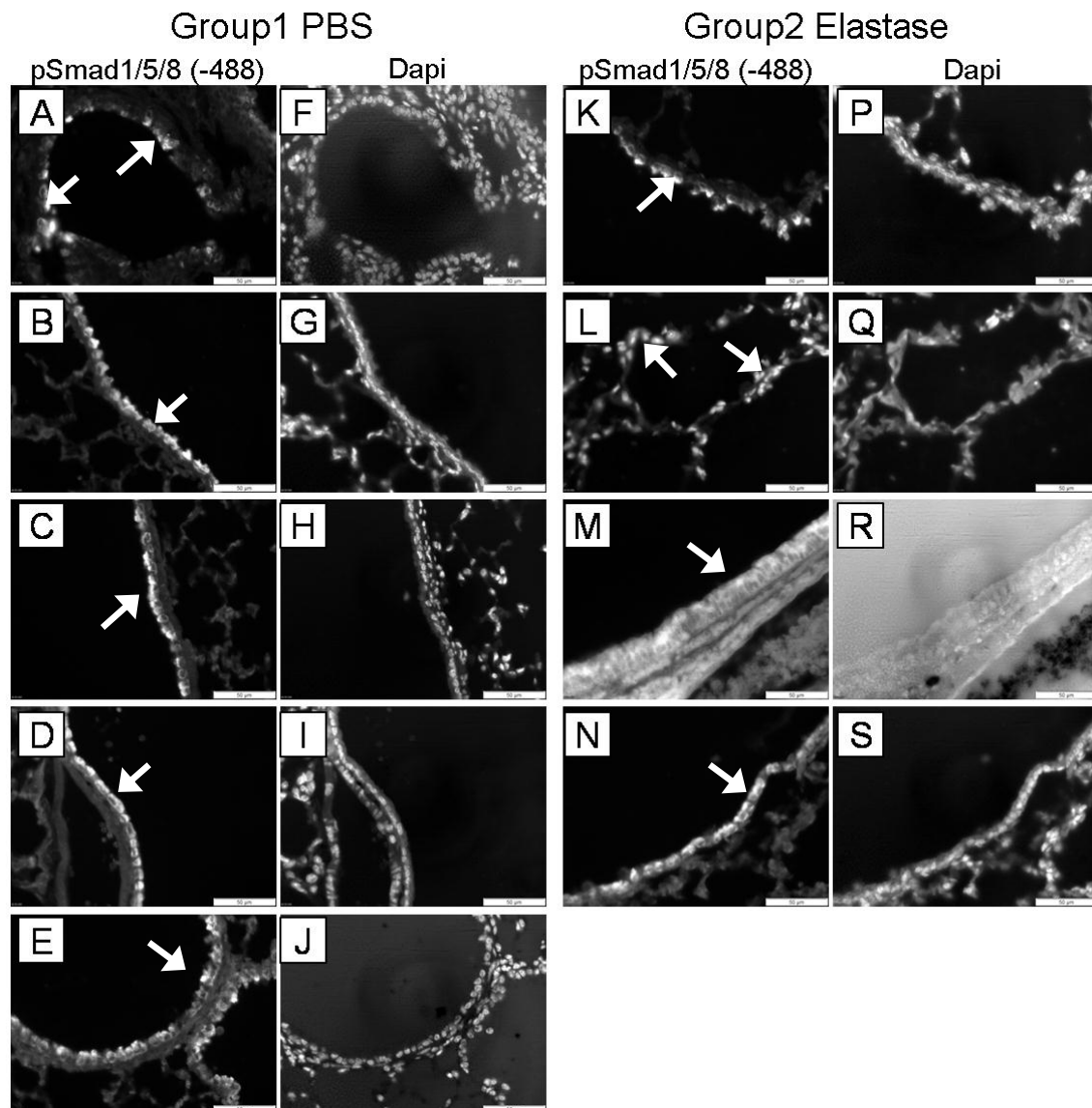
Figure 4.7 pSmad1/5/8 immunofluorescence in elastase model of emphysema

The phosphorylated Smads 1, 5 and 8 were detected in both the control, Group1, animals and in the elastase treated Group2 animals. Staining in Group1 was clearly evident, lining the airways in all of the control group animals. There was less detected however throughout the Group2 animals, where although a similar amount of airways showed some level of activation it was generally observed at a lower level than that seen in the control group.
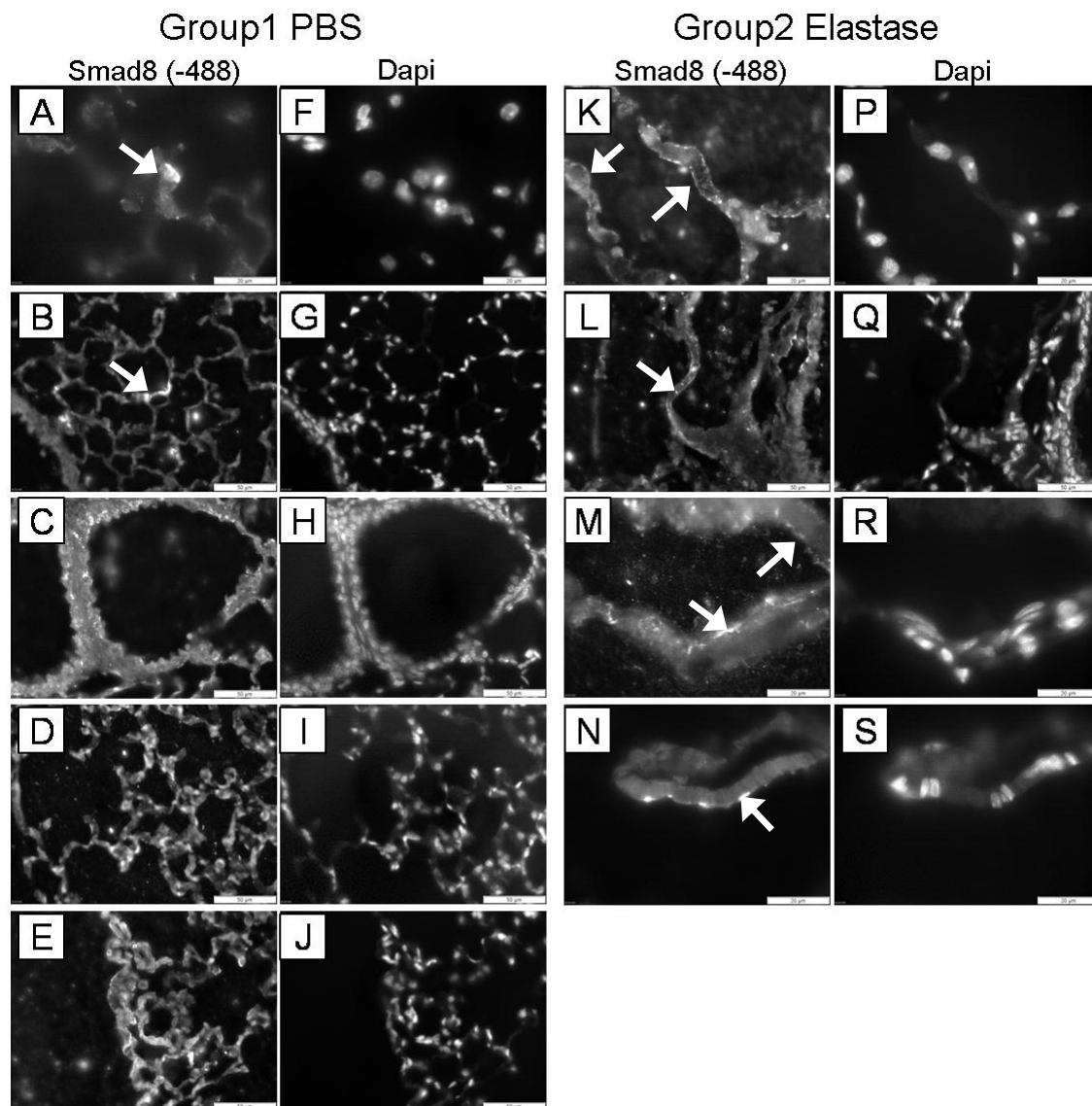
Figure 4.8 Smad8 immunofluorescence in elastase model of emphysema

Group1 PBS control mice exhibited very little Smad8 presence. A small number of individual cells were scattered through section of a number of animals, as seen in A and C. However in general the airways and alveolar regions were by and large devoid of Smad8 as can be seen in E, G and I, where the images show only tissue auto flouresence and no Smad8. Group2 elastase treated mice however showed a high presence of Smad8 throughout the alveolar regions, clearly visible along the surface of the alveolar cells in Group2 images B, D, F and H above.
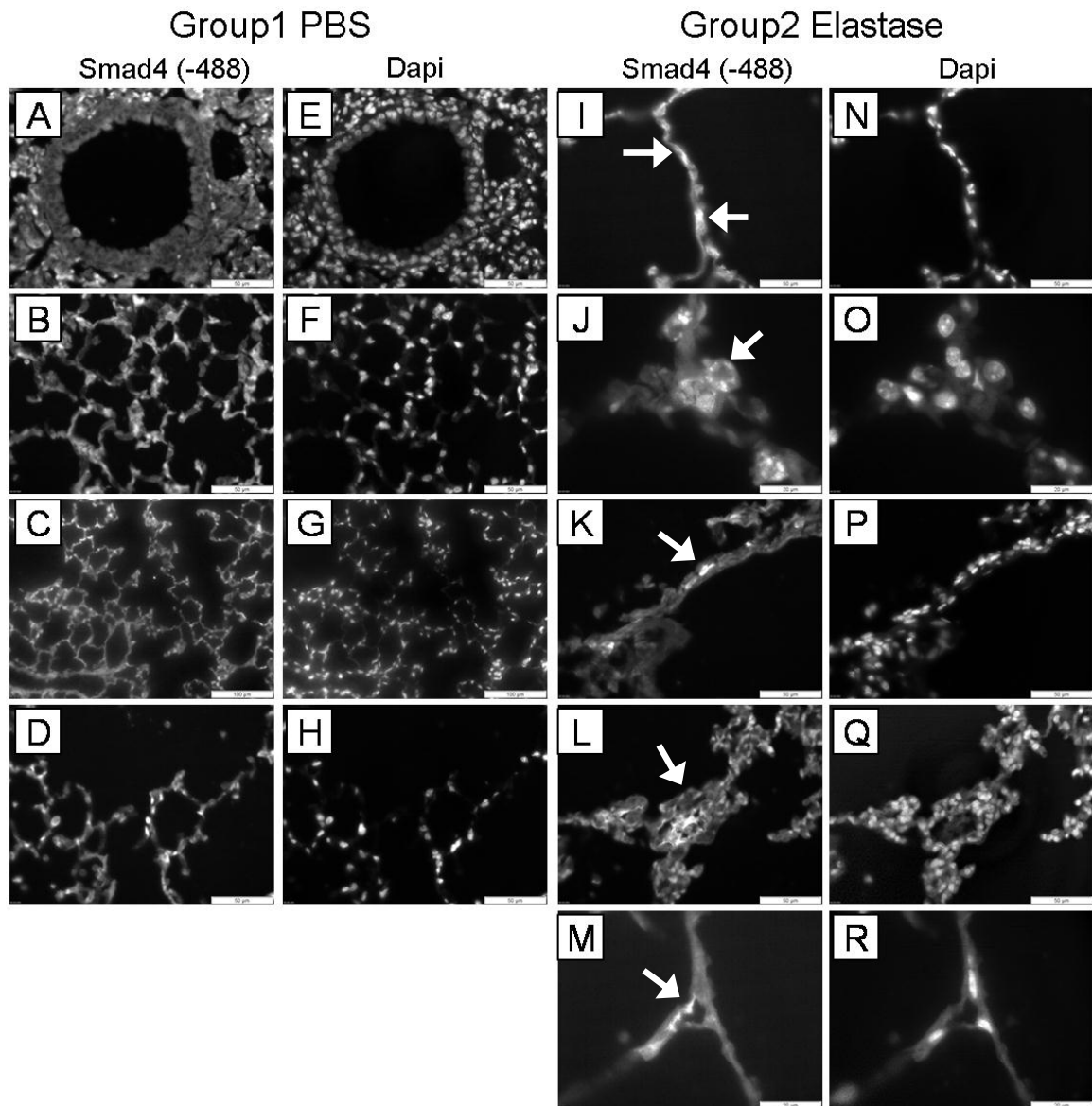
Figure 4.9 Smad4 immunofluorescence in elastase model of emphysema

No evidence of Smad4 presence was evident in Group1, control animals, in either the alveolar regions or in the airways. The only staining present in the images A, C, E and G indicates tissue autoflouresence. Smad4 staining however was abundant throughout the alveolar regions in Group2 elastase treated animals. Some tissue auto flouresence made it difficult to clearly image the Smad4 presence but in the section samples B, D, F, H and I, all bright white indicates the presence of Smad4, as indicated by the accompanying arrows.
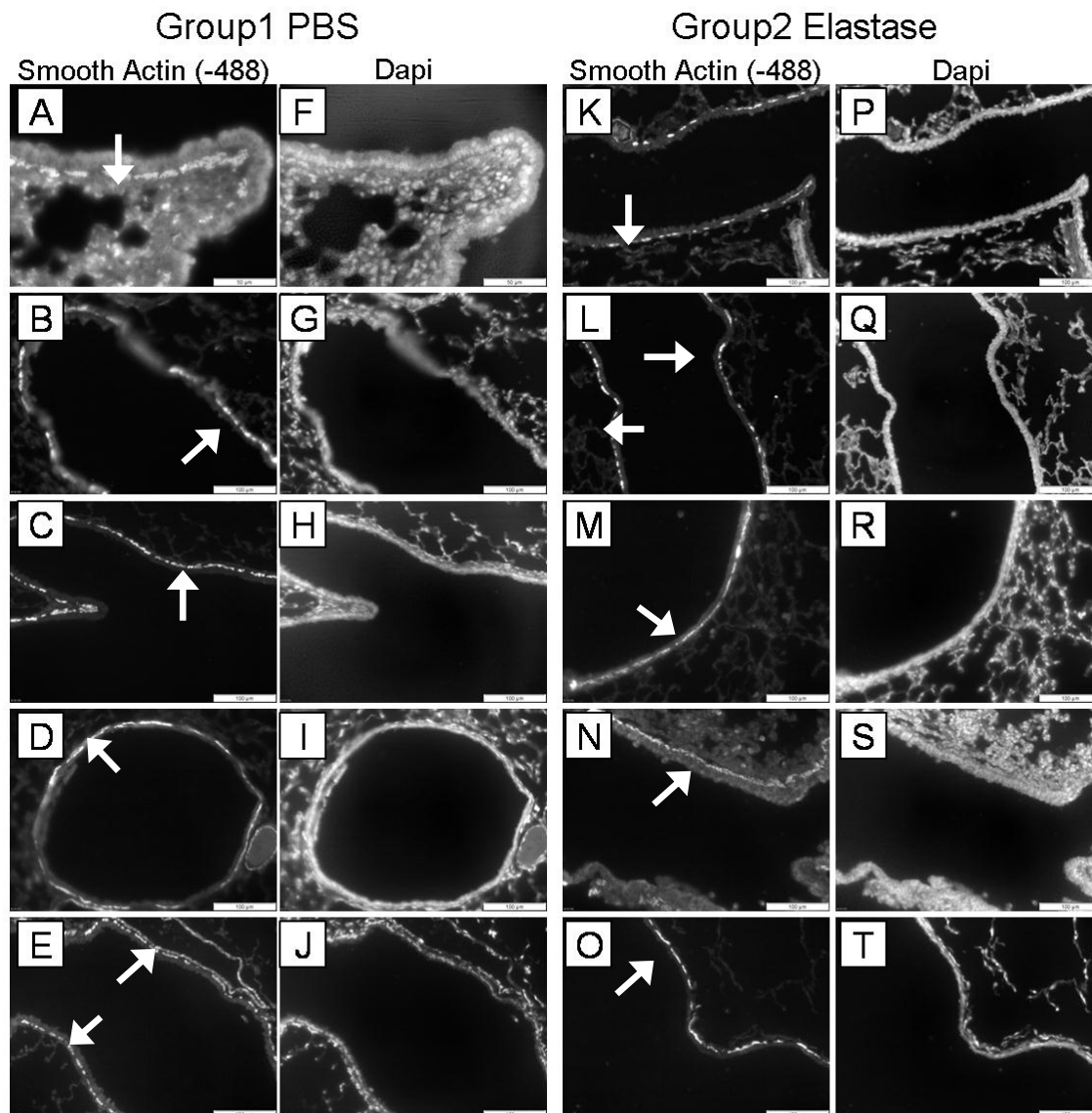
Figure 4.10 Smooth Actin immunofluorescence in elastase model of emphysema

Due to the characteristics of the disease model it was decided to also evaluate any difference which may be ocuring in musculature lining the sirways by examing smooth muscle actin presence for dysregulation, either by an increase or decrease in presence or by proliferation into the surface epithelial layer. However no difference was noted in the location or quantity of smooth actin present in either of the two groups.

	PBS Group (Group1)	Elastase Group (Group2)	Notes
CC10	Abundant in airways	Abundant in airways	No Discernable difference
PCNA	Very low levels of expression, found in some specific airway cells. No Alveolar	High level of abundance throughout Alveolar cells	Elastase animals showed a much higher level of expression of the Protein, and throughout the alveolar region, whereas almost none was detected in the PBS group
pSmad1/5/8	Detected in Airways	Detected in airways but at a lower level than PBS group	PBS group showed a higher level of activity of pSmad1/5/8 in the airways than elastase treated animals
Smad8	Very low level of expression, found in occasional alveolar cells	High abundance detected in alveolar region	Elastase treated animals displayed a much higher level of Smad8 expression throughout the alveolar region compared with the PBS control group.
Smad4	None Detected	High abundance throughout alveolar region	Elastase treated animals displayed a high level of Smad4 expression throughout the alveolar region compared with the PBS control group where none was detected.
Smooth muscle Actin	Highly abundant lining airways	Highly abundant lining airways	No Discernable difference

Table 4.1 Summary of immunofluorescence analysis in elastase induced emphysema in BALB/c mice

4.3 Discussion

4.3.1 Elastase induced model of Emphysema in Mice.

The main result from the study of emphysema in mice was that although there was an increase in the level of Co-Smad 4 and Receptor Smad 8, there was no detectable phosphorylation of the R-Smads. It is possible that the destruction of the parenchyma by the elastase also dramatically reduced the receptor number on the cells remaining in the lung, lessening the ability of any circulating BMP to trigger a reaction. It is also possible that delivery of exogenous BMP proteins may trigger an increase in BMP pathway activity that could potentially have a therapeutic effect on the lungs. In PAH, lack of a functioning BMPR-II is predominantly responsible for the disease, and it has been shown that stimulation of the cells with exogenous BMP has had a therapeutic effect. It is also possible that in emphysematous lungs, stimulation of the airway cells with exogenous BMPs such as BMP2 BMP4 or BMP7; or BMP pathway related proteins may have a therapeutic effect. Further analysis of the Emphysema model determined a number of significant differences between control lungs and emphysematous lungs that would provide solid platforms for quantitative analysis of any such treatment.

4.4 Conclusion

There are no reports of the expression of the BMP pathway in emphysema. Though a greater understanding of the disease in the *in vivo* model was attained the lack of a major involvement of the BMP pathway precluded its further use as a potential model for targeting BMP effects in disease. The model does have future potential however. Due to the fact that the BMP pathway is dormant during the onset and progression of disease in this model it may provide an ideal platform to study the effect of an induced BMP pathway in the possible repair or regeneration of the damaged tissue. However the aim of this project was to identify and target a deregulated BMP pathway in a disease model, and therefor further analysis of the Emphysema model was not initiated as part of this project.

As will be seen in Chapter 7, the OVA induced model of asthma *in vivo* shows activation of the BMP pathway, which is believed to be a contributory factor to progressive remodelling and tissue damage in the asthmatic lung. As a result the

pathway was deemed to be a more suitable target for the delivery of regulatory compounds that may facilitate a dampening of the damaging effects seen in asthma.

5 Design, Characterisation & Assessment of Aerosol Delivery Devices & Molecules

5.1 Introduction

The delivery of therapeutic molecules directly to the lung has numerous advantages over non localised systemic delivery mechanisms such as intravenous administration. In practical terms it can also be easier to get a therapeutic to the clinic when administration is local as opposed to systemic. In order to develop and test therapeutics strategies to target BMP signalling in mouse models of lung disease, it was necessary to develop a method for targeted delivery to the lung. Aerosol delivery provides a highly efficient and well developed mechanism for both local delivery of therapeutics to the airways and alveolar regions of the lung and has potential for modification to be utilised as an effective systemic mode of delivery. For therapeutic development and testing in the lab a commercially available Aerogen Aeroneb® Pro nebuliser was paired with a novel chamber device (Buxco®) for delivery to rodents and small mammals and a restraint for commercial deployment was designed and tested in house in conjunction with Buxco®.

Many different types of biological molecules are used as therapeutics including proteins (including cytokines and antibodies), siRNA, and plasmid DNA. We wished to determine if aerosolisation was feasible for the delivery of these types of molecules to mouse lungs.

5.1.1 Particle sizing and laser diffraction

Particle sizing of aerosols is vital in order to determine exactly the deposition profile and particle transport within the respiratory system of an aerosolised drug. It refers to measuring the aerodynamic size which, by definition, is the aerodynamic diameter of a particle is the diameter of a sphere with unit density of 1, having the same terminal settling velocity in still air as the particle in consideration the diameter of a sphere with a unit density (de Boer et al., 2002). It can reveal information relating to deposition patterning leading to the ability to assess absorption and uptake times and can help match an ideal nebuliser or inhaler to specific drug formulation. It is carried out primarily by two means, cascade impaction or laser diffraction. The pharmaceutical gold standard is multi stage cascade impaction in both European and US pharmacopoeias (Mitchell and Nagel, 2003). However for the reasons detailed below we pursued laser diffraction as more practical and applied means for screening the performance of both the chamber and nebulisers utilised within this thesis.

Cascade impactors are complex set ups but are favoured for a number of reasons. They measure directly the aerodynamic size and both require and facilitate the capture

and analysis of the aerosolised particles at each stage in the impactor, which correspond to airway levels in the lung. It also shows the quantity of API which is deposited at each level. However due their complexity, cascade impactors are difficult to set up and analysis is laborious and time consuming and as a result drastically reduces screening times for new formulations of drug(Marriott et al., 2006). There is also a strongly reported occurrence of inter and intra laboratory variations between same model cascade, with variation in the measurement of fine particle fractions of 5.5% to 20% in readings taken from DPIs, which it is known are even better suited to cascade impaction studies than nebulisers (Mitchell et al., 2007; Pilcer et al., 2008).

The issues with cascade impaction models have led to the optimisation of laser diffraction as a method for the characterisation of aerosols. Laser diffraction works by sending a laser through a cloud of aerosol and measuring the size of the particles it encounters. It has a number of advantages over the impaction system. It is quicker to set up and offers a higher degree of reproducibility as well as allowing for a greater number of size classes of particles to be defined for an individual aerosol cloud. This greatly improves the ability of a lab to screen different formulations and to test other parameters such as the effect of a chamber or a mouthpiece on the available aerosol for respiration, measurements which cannot be obtained using cascade impaction (Clark, 1995; Marriott et al., 2006). Laser diffraction, unlike cascade impaction is also known to be a robust system capable of very high reproducibility, and software enables automatic data recording and processing, helping eliminate any technical differences between labs (Pilcer et al., 2008).

The other main difference between the systems aside from mode of operation is that they both measure particles aerodynamic profile differently and it is not possible to directly relate a set of results from one device to another. However it has been shown that the two devices compare well when evaluating nebuliser performance on the two using the same formulation (Ziegler and Wachtel, 2005). Also data scintigraphy studies have been carried out that have enabled direct correlation between size profiles and distributions as measured by laser diffraction and corresponding deposition profiles, showing a good accord between VMD and the deposit volume in the lungs (Clark, 1995).

5.2 Chamber design and characterisation

Three nebulisers were chosen at random to generate an aerosol in the delivery chamber unit. This aerosol would then be characterised directly at the site of inhalation. This was done by connecting the chamber port directly to the Spraytech™

analyser (Figure 5.1). The aerosol was measured over a period of three different time-points (t=0min, t=5min and t=9min) to allow for the effects of reservoir level to be accurately taken into account and also to see if there was a build up of forces such as shear forces or heat which may affect aerosol production or characteristics over time. It also allowed for effects of aggregation and flow rate to be accurately taken into account. Two different flow rates were also recorded (2L/ and 4L/min) to determine if the flow rate had an adverse effect on the aerosol at the point of inhalation. An independent flow rate monitor was also used to confirm the flow rate generated by the Buxco® flow regulator. PBS was again used as the solution to generate the aerosol.

The Chamber was assessed for its ability to deliver an effective respirable dose, as determined by measuring aerosol VMD and FPF at the point of inhalation from the chamber, as can be seen in (Figure 5.1). All statistical analysis relating to VMD and FPF was determined by one-way ANOVA (repeated measures) and Tukeys multiple comparison test.

Overall the differences in VMD generated was determined to be statistically significant, $p<0.001$. The VMD achieved at the flow rate of 4L/min was significantly lower to varying degrees ($P<0.05$) than the 2L per min flow rate at all time points with the exception of the VMD recorded at 4L/min; t=9 min compared to the VMD at 2L/min; t=5 min (Figure 5.2; Table 5.1 and Table 5.2). Though not significant, the VMD was still less for the 4L/min Flow rate. There was no recorded statistically significant difference in VMD across any time point between the 4L/min flow rate and the nebuliser units on their own without the chamber. This shows that there was no significant deterioration in VMD with this chamber design under these operating conditions. The 2L/min flow rate had a significantly higher VMD across the range of measurements with the exception noted above. It also recorded a VMD statistically significantly larger than the nebuliser units alone without a chamber. This shows that a lower flow rate can cause larger molecules to present at the site of inhalation.

It was noted also that although the VMD for the 4L/min flow rate increased slowly over time, this change was not statistically significant. There was also a slight fluctuation in the VMD at the slower flow rate of 2L/min, again not statistically significant. This indicates that the time frame is less of a factor in influencing the resulting VMD of the particles than the Flow Rate.

The FPF was also assessed at the same time as the VMD, with two different flow rates and broken down into the three groupings of 1-3µm, 1-5µm and 1-7µm (Figure 5.3 and Table 5.2).

At the 4L/min flow rate there was no statistical difference across the time-points in the percentage FPF in any of these groupings with one exception. The percentage total aerosol falling within the respirable dose rage of 1-7μms was significantly less at 4L/min, t=9mins, than at t=0mins (p<0.05 Figure 5.3). However this was not significantly different to the nebulisers on their own unconnected to the chamber. At t=0 the 4L/min flow rate was generating significantly more aerosol in each measured group than the 2L/min flow rate. By t=9min this statistical difference had stopped but it can be seen that across every time-point and every particle size grouping that the greater flow rate of 4L/min resulted in a higher percentage of total aerosol being produced. It is also of note that across each time-point and all groupings the FPF generated at the 4L/min flow rate was not once significantly different than that of the nebuliser unit alone, Table 2. This was not the same for the 2L/min flow rate, giving significantly less, to varying degrees, total respirable aerosol than the no chamber alone. This mostly effected the larger grouping of 1-7μm (2l/min: t=0min, p<0.05; t=5min, p<0.01; t=9min, p<0.01) meaning that the total percentage of respirable aerosol was significantly less at all time points at the lower flow rate. The results of the FPF analysis across all readings, with the exception of the 2L/min flow rate in the FPF grouping of 1-5μm, show that an increase in time led to a trend of decreasing percentage of total aerosol available.
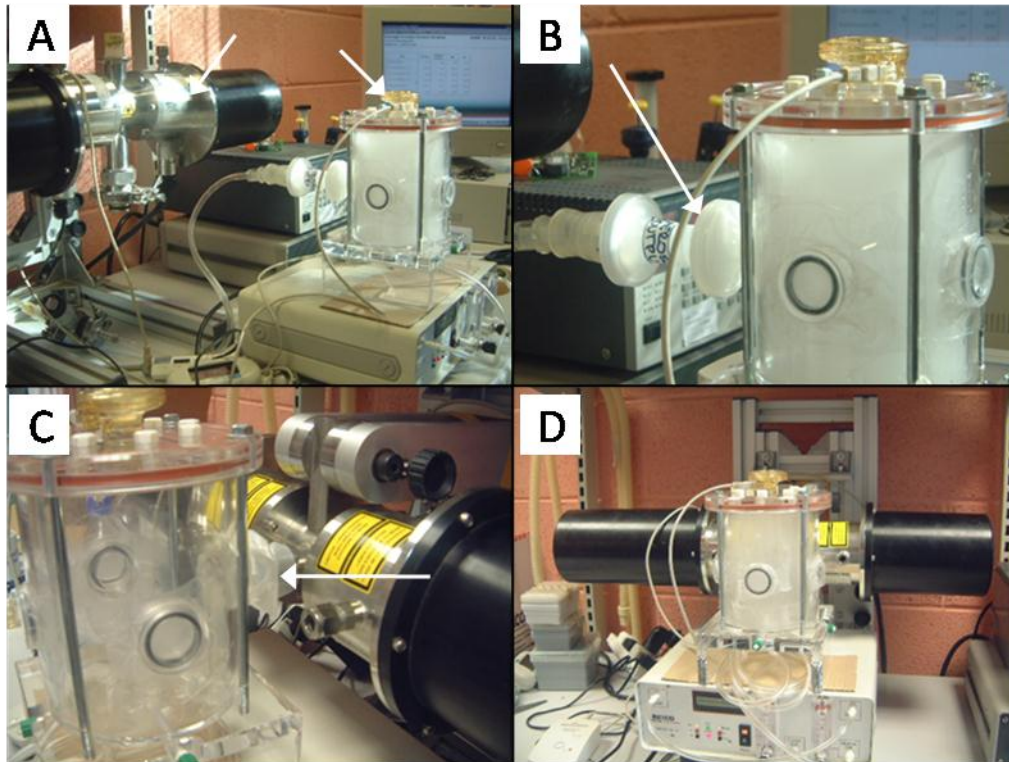
Figure 5.1 Nebuliser and chamber testing with Malvern Spraytech™

(A) shows the Nebuliser unit attached to and generating aerosol in the chamber unit. Arrows indicate the Malvern Spraytech laser and the Nubuliser head unit. Attached to chamber unit is an independent flow rate monitor as can clearly be seen indicated by arrows in (B). (C) shows the attachment of the chamber to the Malvern Spraytech™ at the point of inhalation as indicated by an arrow. (D) shows the attached nebuliser unit generating a PBS aerosol within the chamber while VMD and FPF are being assessed.

VMD Generated Through Chamber
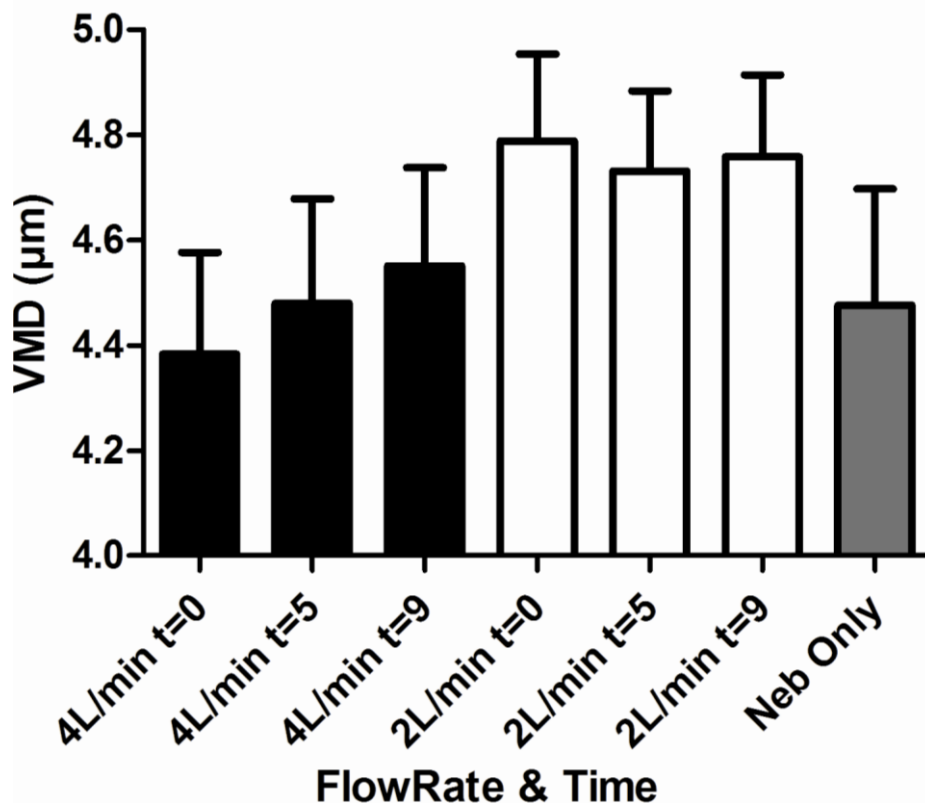
Flow Rate	Time	Average VMD	±St Err
4L/min	0mins	4.3828	0.1934
4L/min	5mins	4.48	0.1980
4L/min	9mins	4.5506	0.1862
2L/min	0mins	4.7878	0.1655
2L/min	5mins	4.7306	0.1525
2L/min	9mins	4.7583	0.1551
N/A	Neb. Only	4.4755	0.2211

**Figure 5.2 VMD generated through Chamber measured at point of inhalation**

As can be seen the 4L/min flow rate, at all timepoints, generates a smaller average VMD particles size than the slower 2L/min flow rate. Full breakdown of statistical analysis can be seen in Table 5.1.

One Way ANOVA (Repeated Measures)	Significant?	Summary†
	Yes	***
Tukeys Multiple Comparison Test	Significant?	Summary†
4L/min t=0 vs. 4L/min t=5	No	ns
4L/min t=0 vs. 4L/min t=9	No	ns
4L/min t=0 vs. 2L/min t=0	Yes	***
4L/min t=0 vs. 2L/min t=5	Yes	***
4L/min t=0 vs. 2L/min t=9	Yes	***
4L/min t=0 vs. Neb. Only	No	ns
4L/min t=5 vs. 4L/min t=9	No	ns
4L/min t=5 vs. 2L/min t=0	Yes	**
4L/min t=5 vs. 2L/min t=5	Yes	**
4L/min t=5 vs. 2L/min t=9	Yes	**
4L/min t=5 vs. Neb. Only	No	ns
4L/min t=9 vs. 2L/min t=0	Yes	*
4L/min t=9 vs. 2L/min t=5	No	ns
4L/min t=9 vs. 2L/min t=9	Yes	*
4L/min t=9 vs. Neb. Only	No	ns
2L/min t=0 vs. 2L/min t=5	No	ns
2L/min t=0 vs. 2L/min t=9	No	ns
2L/min t=0 vs. Neb. Only	Yes	**
2L/min t=5 vs. 2L/min t=9	No	ns
2L/min t=5 vs. Neb. Only	Yes	**
2L/min t=9 vs. Neb. Only	Yes	**

†Summary: ns=not significant; * = $p < 0.05$; **=$p < 0.01$; ***$p = <0.001$.

Table 5.1 Variable Mean Diameter statistical analysis

Statistical analysis was carried out by means of repeated measures ANOVA in combination with Tukeys multiple comparison posttest.
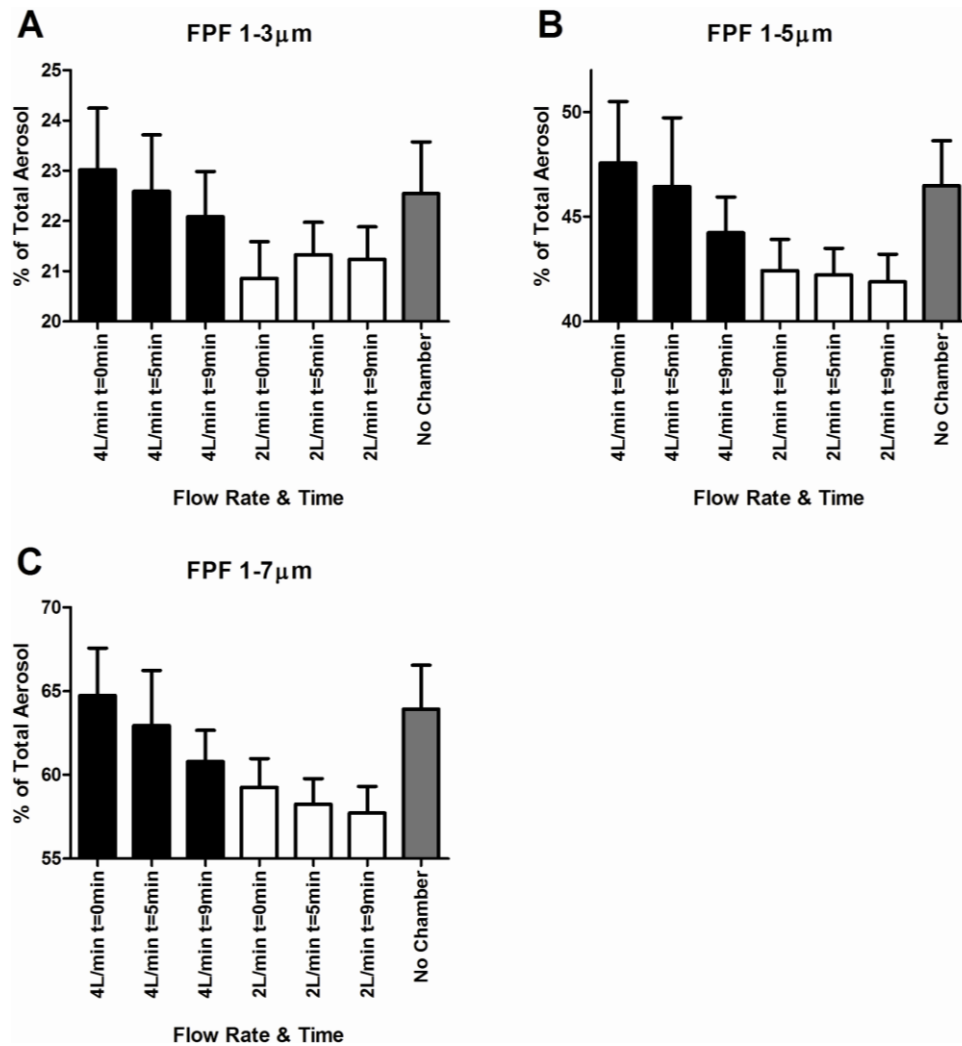
Flow Rate	Time	1-7μm		1-5μm		1-3μm	
		Average	± St. Err	Average	± St. Err	Average	± St. Err
4L/min	0mins	64.7394	2.84319	47.5711	2.92991	23.0239	1.2223
4L/min	5mins	62.9572	3.2906	46.4467	3.28397	22.5906	1.12267
4L/min	9mins	60.8089	1.86494	44.2311	1.70948	22.0872	0.89727
2L/min	0mins	59.2528	1.72251	42.4328	1.48872	20.8611	0.72892
2L/min	5mins	58.2522	1.53104	42.2291	1.2666	21.33	0.64243
2L/min	9mins	57.7244	1.5967	41.8911	1.32513	21.2411	0.64593
No Flow	0mins	63.9267	2.6246	46.4944	2.14277	22.5456	1.03108

Figure 5.3 FPF generated through Chamber measured at point of inhalation

With the 4L/min flow rate, at all timepoints, a higher percentage FPF is generated than with the slower 2L/min flow rate. Full breakdown of statistical analysis can be seen in Table 5.2.

	FPF 0-7μm		FPF 0-5μm		FPF 0-3μm	
One Way ANOVA (Repeated Measures)	Significant?	Summary†	Significant?	Summary†	Significant?	Summary†
	Yes	***	Yes	**	Yes	**
Tukeys Multiple Comparison Test	Significant?	Summary†	Significant?	Summary†	Significant?	Summary†
4L/min t=0min vs. 4L/min t=5min	No	ns	No	ns	No	ns
4L/min t=0min vs. 4L/min t=9min	Yes	*	No	ns	No	ns
4L/min t=0min vs. 2L/min t=0min	Yes	**	Yes	*	Yes	**
4L/min t=0min vs. 2L/min t=5min	Yes	***	Yes	*	Yes	*
4L/min t=0min vs. 2L/min t=9min	Yes	***	Yes	**	Yes	*
4L/min t=0min vs. No Chamber	No	ns	No	ns	No	ns
4L/min t=5min vs. 4L/min t=9min	No	ns	No	ns	No	ns
4L/min t=5min vs. 2L/min t=0min	No	ns	No	ns	Yes	*
4L/min t=5min vs. 2L/min t=5min	Yes	*	No	ns	No	ns
4L/min t=5min vs. 2L/min t=9min	Yes	**	Yes	*	No	ns
4L/min t=5min vs. No Chamber	No	ns	No	ns	No	ns
4L/min t=9min vs. 2L/min t=0min	No	ns	No	ns	No	ns
4L/min t=9min vs. 2L/min t=5min	No	ns	No	ns	No	ns
4L/min t=9min vs. 2L/min t=9min	No	ns	No	ns	No	ns
4L/min t=9min vs. No Chamber	No	ns	No	ns	No	ns
2L/min t=0min vs. 2L/min t=5min	No	ns	No	ns	No	ns
2L/min t=0min vs. 2L/min t=9min	No	ns	No	ns	No	ns
2L/min t=0min vs. No Chamber	Yes	*	No	ns	Yes	*
2L/min t=5min vs. 2L/min t=9min	No	ns	No	ns	No	ns
2L/min t=5min vs. No Chamber	Yes	**	No	ns	No	ns
2L/min t=9min vs. No Chamber	Yes	**	Yes	*	No	ns

†Summary: ns=not significant; * = p<0.05; **=p<0.01; ***p=<0.001.

Table 5.2 Fine Particle Fraction statistical analysis

Statistical analysis was carried out by means of repeated measures ANOVA in combination with Tukeys multiple comparison posttest.

5.2.1 Nebuliser design and characterisation

It was first decided to evaluate the performance of each Aerogen Aeroneb® Pro nebuliser on its own. An Aerogen nebuliser control unit with known performance characteristics was first used to ensure all measurements were being accurately recorded.

A total of 18 separate nebuliser head units were then tested to generate a profile of the performance of the nebuliser units on their own. This was done by directly attaching the nebuliser to the Spraytech™ system and recording the VMD and FPF (1-3µm, 1-5µm and 1-7µm) of each unit. The solution used for testing the aerosol generation performance was 0.9% PBS. This was due to the fact that saline was a prospective carrier solution for any future *in vivo* work, is non-volatile, and would be suitable for most foreseeable future preparations of protein and drug compound solutions for aerosolisation.

5.2.1.1 Results

The VMD of the particles formed by the nebuliser units alone, directly connected to the Malvern Spraytech™ analyser, was analysed (Figure 5.4). This showed the average VMD of the particles to be in the region of 4.43µm (±.043µm), falling inside Aerogens specified operating limits for the device. This means that 50% of the aerosol generated has a VMD of 4.43µm (±.043µm) or less as can be seen in Table 5.3.

The FPF for the individual units were all also assessed. This allows for the mapping of deposition within the lung of the particles delivered. Aerosol generated with a FPF of less than 1µm is not likely to settle in the lung after inhalation, due to its size and density it is most likely to be exhaled rather than deposit. Molecules in the range of 1-3µm are likely to target and deposit themselves in the alveolar region. Particles in the size range of 3-5µm are likely to deposit in the lower airways, and particles in the range of 5-7µm in the upper airways, with anything larger getting deposited on the back of the throat. The results of the FPF measurements show that the Aerogen Aeroneb® Pro Nebuliser unit, on its own and without a spacer or chamber influencing its aerosol production, can generate a respirable dose of 65.26% (±0.44). 22..44% (±0.43) of the aerosol generated falls within the FPF of 1-3µm, 24.65% (±0.38) within the range of 3-5µm and 18.17% (±.02) in the range of 5-7µm, (See Figure 5.5 and Table 5.4). Therefore only 34.7% (±0.756) of the aerosol produced falls outside the respirable dose limitations.
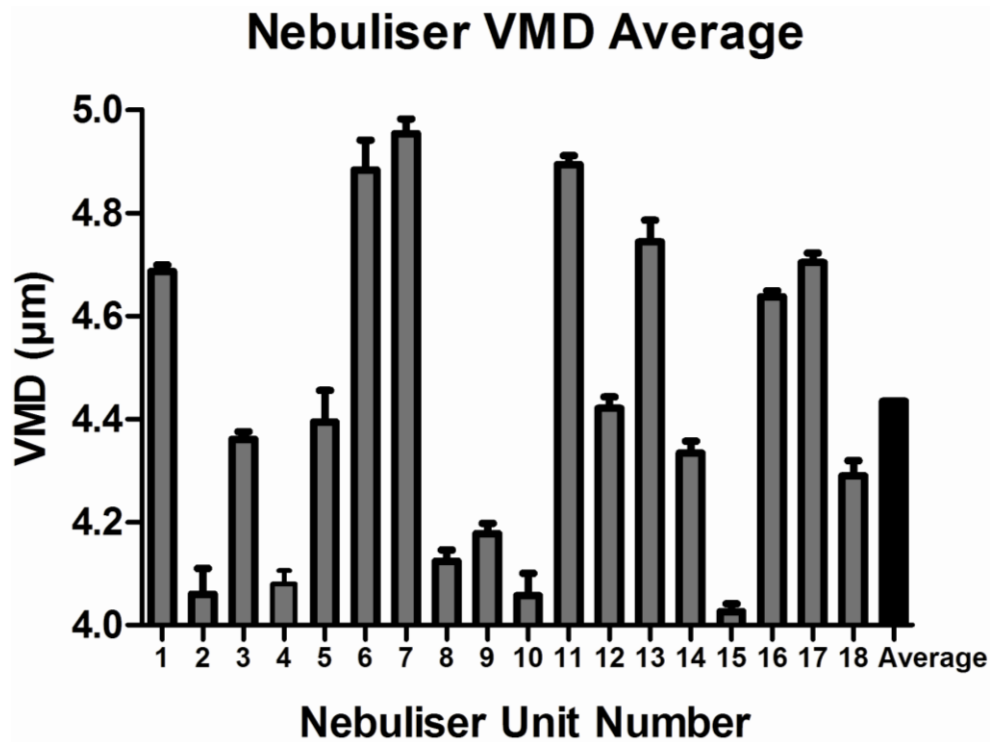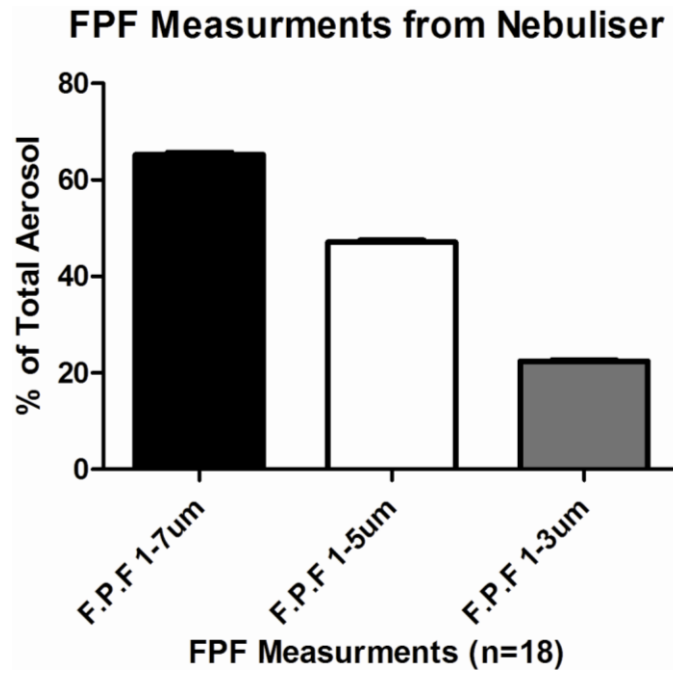
Figure 5.4 The VMD of every individual nebuliser unit was assessed (n=18)

All units fell within the operating range for the device and the average VMD generated by the devices is 4.43µm (±.043µm). Full breakdown of the behaviour of the individual nebuliser units can be seen in Table 5.3.

Neb. I.D.	VMD (μm)	+/- Standard Error (μm)
055 879 - 040	4.6867	0.01202
056 056 - 095	4.06	0.04933
055 894 - 030	4.36	0.01528
055 891 - 070	4.08	0.02517
055 879 - 144	4.3933	0.06227
055 996 - 002	4.8833	0.05783
055 894 - 005	4.9533	0.02906
055 879 - 014	4.1233	0.0219
056 065 - 100	4.1767	0.0203
056 014 - 115	4.0567	0.0433
055 923 - 143	4.8933	0.0176
056 065 - 029	4.42	0.0231
055 923 - 080	4.7433	0.0418
056 065 - 114	4.3333	0.02404
055 894 - 015	4.0267	0.01453
055 969 - 087	4.6367	0.01202
055 891 - 031	4.7033	0.01856
056 052 - 013	4.29	0.02887
Average	**4.4344**	**0.0431**

Table 5.3 Individual nebulisers VMD performance

All nebuliser units for use throughout the duration of this thesis were tested and assessed in order to ensure that nebuliser inefficiencies and discrepancies did not impact on the studies performed. This was high importance for molecular work, animal delivery and accurate characterisation of the delivery chamber.

FPF Measurments from Nebuliser

FPF Recording	% Of Total Aerosol	St. Err.
1-7µm	65.2576	0.4383
1-5µm	47.0891	0.4201
1-3µm	22.4426	0.2441

Figure 5.5 The FPF of every individual nebuliser unit was assessed (n=18).

65.25% (±SE) of the total aerosol generated fell within the 1-7µm range, 47.09% (±SE) within the 1-5µm and 22.44% (±SE) within the 1-3µm range. Full breakdown of the behaviour of the individual nebuliser units can be seen in Table 5.4.

Neb. I.D.	Percentage FPF			
	FPF 7µm+	FPF 5-7µm	FPF 3-5µm	FPF 1-3µm
055 879 - 040	37.39	18.22	23.33	21.06
056 056 - 095	34.8767	17.1367	23.5367	24.45
055 894 - 030	32.46	19.18	25.9033	22.4567
055 891 - 070	30.56	17.8567	26.8567	24.7267
055 879 - 144	36.02	17.5933	23.6	22.7867
055 996 - 002	40.13	16.8467	22.4	20.6233
055 894 - 005	38.5633	19.0933	23.0033	19.34
055 879 - 014	31.16	18.4333	26.2533	24.1533
056 065 - 100	34.4567	17.9567	23.91	23.6767
056 014 - 115	28.8233	19.0567	27.7233	24.3967
055 923 - 143	37.63	19.24	23.6133	19.5167
056 065 - 029	36.93	17.0167	23.1933	22.86
055 923 - 080	36.4567	18.9633	24.1533	20.4267
056 065 - 114	33.7167	17.9567	25.1367	23.19
055 894 - 015	29.09	18.6467	27.5967	24.6667
055 969 - 087	35.94	16.93	25.23	21.9
055 891 - 031	35.74	19.3467	24.4167	20.4967
056 052 - 013	35.42	17.56	23.78	23.24
Avg.	34.7424	18.1685	24.6465	22.4426
St. error(+/-)	0.7560	0.2037	0.3808	0.4259

Table 5.4 Individual nebulisers FPF performance.

As was done with VMD measurements, all nebuliser units for use throughout the duration of this thesis were tested and assessed in order to ensure that nebuliser inefficiencies and discrepancies did not impact on the studies performed. This was high importance for molecular work, animal delivery and accurate characterisation of the delivery chamber.

5.2.2 Restraint design and testing

Restraint design was started with a blank template rather than working on an existing model with the hope of minor modifications for improvement. The pre-existing model (Figure 5.6) that was in use had a number of design flaws that needed to be fixed and these were borne in mind during the new build. The restraint design underwent a number of prototype versions. The first prototype (Mark 1) was designed from scratch and post manufacture was tested for feasibility with a number of different aged animals of various strains and sizes. A number of areas for improvement quickly became apparent and the next prototype addressed these issues. The restraint underwent further modifications before arriving at the final prototype (Mark 2) which was put forward for selection for manufacture. Prototype plans were put forward by J.Purcell and the schematics drawn by engineers at Buxco® UK. Manufacture of the prototype units was carried out by Buxco® US on behalf of Buxco® UK. All testing was carried out in-house in N.U.I. Maynooth animal handling units under supervision of appropriately licensed and qualified individuals.

5.2.2.1 Results

In the first attempt to develop a prototype for a novel restraint one of the main features addressed was to be the design of a successful system that could safely and securely give a nose only exposure while restraining the mouse. The Mark 1 prototype was designed with the intent of having half a collar permanently mounted on the lower half of the restraint (Figure 5.7 and Figure 5.8). The top half of the restraint was then to be dropped into place, with the other half of the collar embedded in this. This collar was designed to fit around the mouse neck, preventing aerosol from travelling up the restraint. This design identified a number of problems, chiefly the following:

A neck restraint was too restrictive for dealing with large numbers of different aged or size animals

Smaller neck sizes would have to be made to measure to ensure tight fits across all sizes. As the collar would also be required to help keep the animal from moving back and forth along the chamber this would have to be relatively secure, which could be difficult to achieve without placing too much pressure on the trachea of the animal. The mouse body was to be restrained by means of an adjustable lid with Velcro attachments that could be tapered to fit any size mouse for the unit. This lid also contained an adjustable back, moveable by means of a restraining screw to help keep the animals in position and to prevent if from backing out of the nasal opening. The

floor of the restraint was raised at the nasal opening to facilitate the animals head being better positioned.

Ergonomically it was difficult for a single handler to fit an animal in the unit and restrain it effectively even when it was known that the animal fit the collar size. The floor of the device encountered the same issues as with the initial restraint with no space for the animals. The difficulty in restraining the animals while trying to fit the adjustable lid and back led to handling difficulties and further complicated efforts to ensure nose only exposure. The unit would also not allow for full nose only exposure, any aerosol delivered could potentially deposit in the eyes and was also more likely to result in ingestion of a larger amount of the aerosol.

The results of this Mark 1 prototype identified a number of key features to consider for the development of the Mark 2 prototype. The first was to develop a novel way of ensuring nose only exposure. Second was to ensure a wider range of size animals could be incorporated into the restraint. Thirdly, that the restraint was less likely to result in injury to any animal. Fourth was to increase the ergonomic handling of the unit for animal handlers. All of these considerations were also highly important in the development of a restraint that could not only be effectively used, but one that could be successfully produced and marketed.

These primary considerations led to the development of the Mark 2 Prototype (Figure 5.8, Figure 5.9 and Figure 5.10).

To ensure a nose only exposure the collar design was replaced entirely with a nose cone resembling a layered collar. This cone consisted of sheets of silicone with holes in the centre of varying diameters. This ensured an airtight seal around the nose of the animal when placed in the restraint. As it no longer impeded the windpipe and did not pressure soft tissue, this also aided in increasing the comfort of the animal. This system also allowed for a wide variety of age/size animals to be used in the same unit. It also ensured that injury to the animals was less likely to result. In order to help with the ergonomics of the system a cradle to hold the restraint was also developed, allowing the animal handler better control of the animal and its placing in the unit, with both hands free to control the animal if required. A number of other design innovations were also incorporated to help address the considerations listed above. A perforated sliding floor was incorporated into the unit. This has a number of important roles. It allows the animal to grip the floor, and this helps in the placing of the animal in the restraint. It also brings the animals head up to a higher level so that the nose cone is better positioned in relation to the restrained animal. It helps keep the animal in a more natural position when restrained compared to the common cylindrical

restraints and it allows for the circulation of air around the animal, helping to keep it cooler when restrained for long periods of time. All of this also helps obtain better measurements from the animals during experimental procedures. Another important feature design to address the above considerations was a concave plunger. This plunger has a hole in place to pass the tail through to help with restrain of the animal. This initially was a closed opening as in the structural diagrams, but was changed to be open at the bottom as can be seen in the images of the manufactured mark2 prototype. Its shape also helps keep the animal in a more natural position than could be obtained with the older plunger systems. It is easily controlled as it is on a slide which closes up behind the animal.

When tested on different animals the device produced the desired efficient seal that would ensure nose only exposure of a restrained animal. Animals of varying ages and sizes were examined in the system. A small three month old C3H mouse and a large eleven month old C3H mouse were examined closely (Figure 5.11 and Figure 5.12). Both were secured comfortably and successfully within the restraint and no animal showed any signs of distress during or after restraint. The device was also given to an animal handler with no prior knowledge of or experience with the device to assess its ergonomics and ease of use with an inexperienced user. No problems were identified and the handler was able to rapidly and successfully restrain the animals. This restraint delivers therefore, a viable and efficient restraint, designed for better handling and better animal care. It also has other potential uses. The design as is allows for easy restraint for tail bleeding animals, and a small modification to the perforated floor and base allows for restraint during I.P. injections, intramuscular injections and/or cardiac punctures, which would be sold as a separate device to allow for full integration of all the modifications. The success of the restraint can be assessed also by the decision to bring this restraint system into production by Buxco® UK. The Mark 2 device produced is a standalone unit allowing for nebulisation and delivery to a single animal. However no modification to the restraint design itself is required for the production of the prototype image, which allows for direct connection to the Novel chamber system tested here.
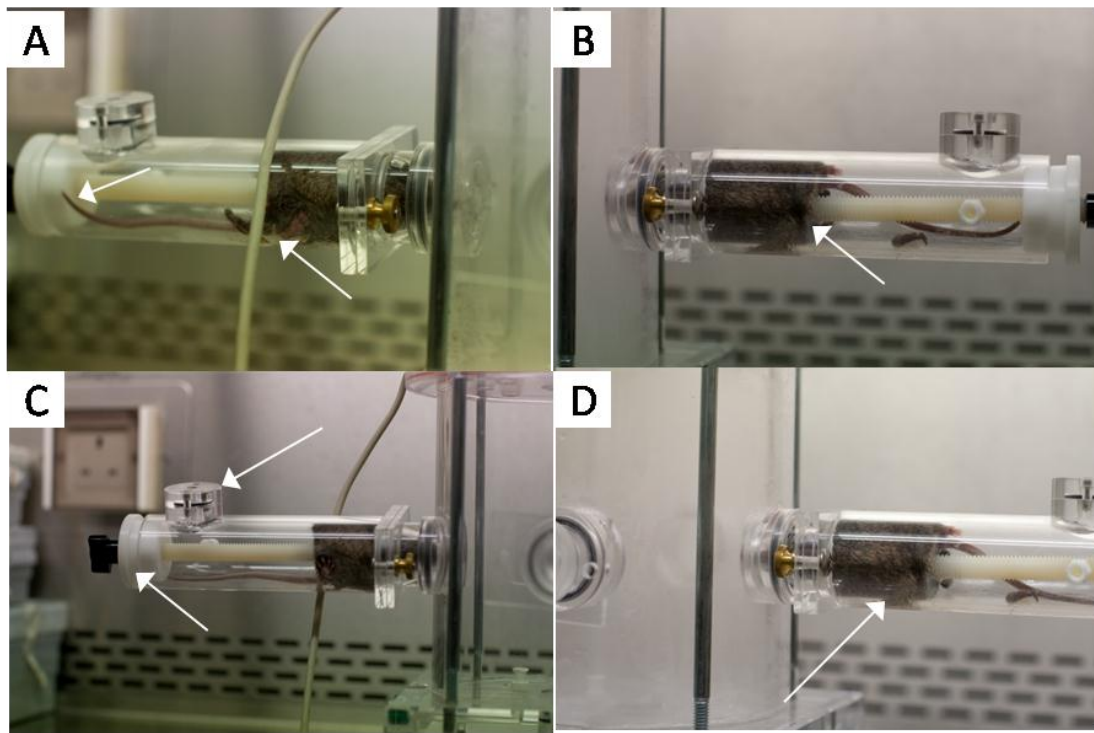
Figure 5.6 Original Restraint Device.

This shows the original device in use, A and B illustrate a number of the more common issues with this type of restraint. The tail of the animal is at risk of being trapped by the plunger device when securing in place. The animal is extremely restricted in an unnatural position. C shows the plunger with the adjustable screw for varying the length dependent on the mouse. An issue is that has to be pre set before inserting the plunger as otherwise the mouse will turn in the restraint. If this happens as the plunger is being inserted or if user error sets the screw too long, crush injuries or death can result. If the mouse manages to gain more space they have a tendency to turn, however with the screw in place this space isn't usually sufficient and suffocation can rapidly occur. In C the placement of the sensor is also indicated. D illustrates the close contact of the animal with all areas of the restraint. This prevents any dissipation of heat around the animal, restricting thoracic movement and leading to potential discomfort and distress of the animal.
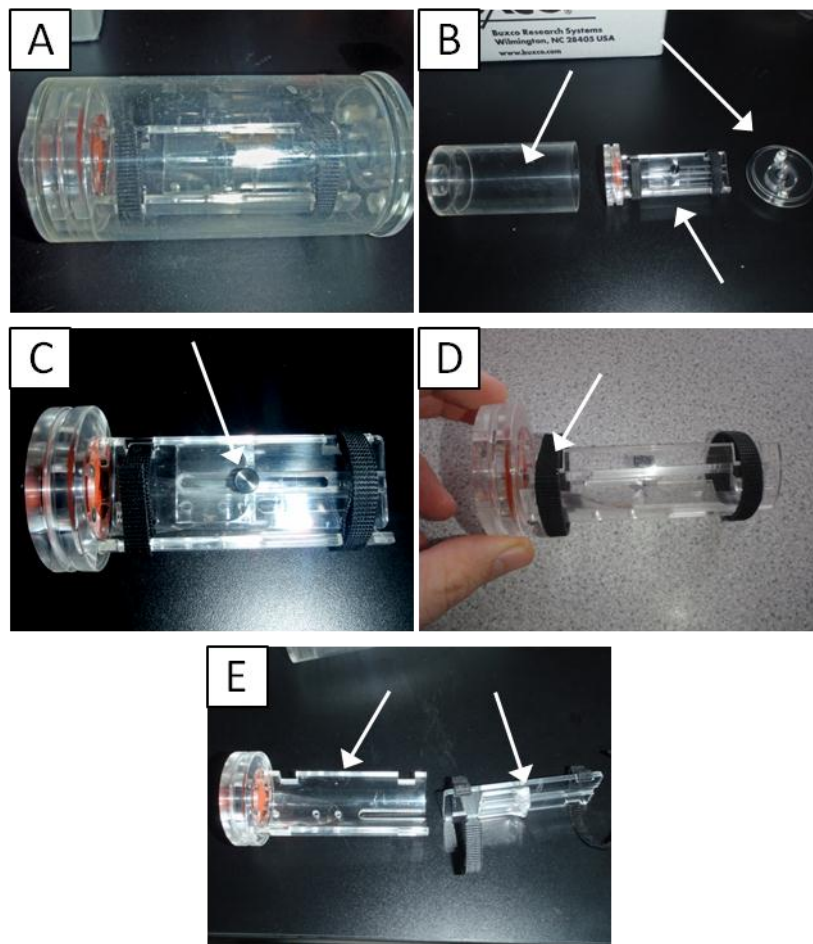
Figure 5.7 MARK 1 complete prototype

(A) Shows the complete sealed unit with the restraint inside. (B) Shows an exploded view of the full restraint. Here the enclosing chamber that attaches to the aerosol chamber, the restraint and the unit seal containing the pneumotach can be more easily seen. (C and D) Shows the restraint alone with the lid in place. Clearly identifiable are the adjustable screw for the movable back on the lid and the adjustable vecro restraints for keeping the lid in place. (E) Shows an exploded view of the restraint section with the floor unit and collar section separated from the lid.
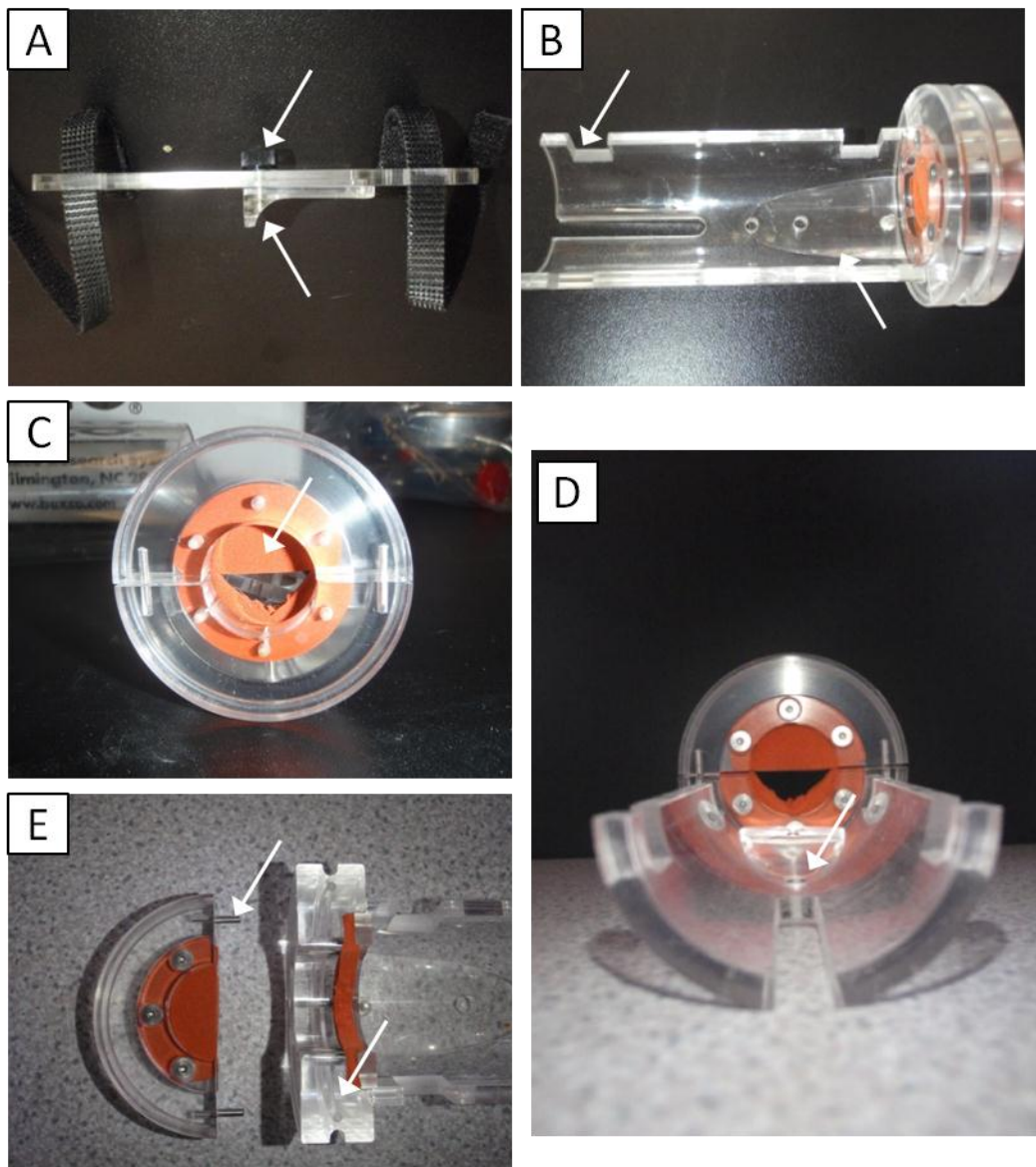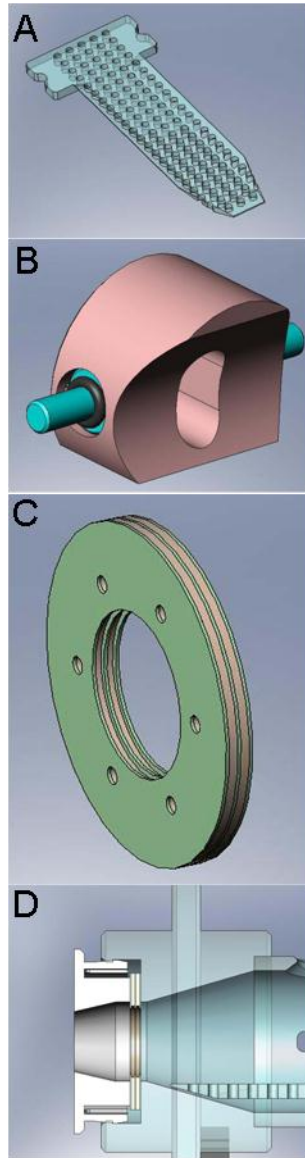
Figure 5.8 MARK 1 restraint prototype

(A) The sliding back could be moved by adjustment of the screw. However it was necessary to have already gauged the amount of space required as adjustment while handling an animal was extremely difficult to do. (B) Shows the the raised base leading to the collar to help raise the animals neck at the collar height. The particular flooring did not sufficiently deal with problems that had been common in the original restraint. (C) The collar formed a full area of contact around the neck of the animal. As can be sen here the material used for this prototype was a soft foam and could be cut to size. (E) The collar was locked into place by means of two pins to form an air tight barrier. Correct sizing of the collar was extremely important and needed to be carefully cutomised as too large a collar would result in an incomplete seal and if the collar was too tight it could asphyxiate and/or strangle the restrained animal.
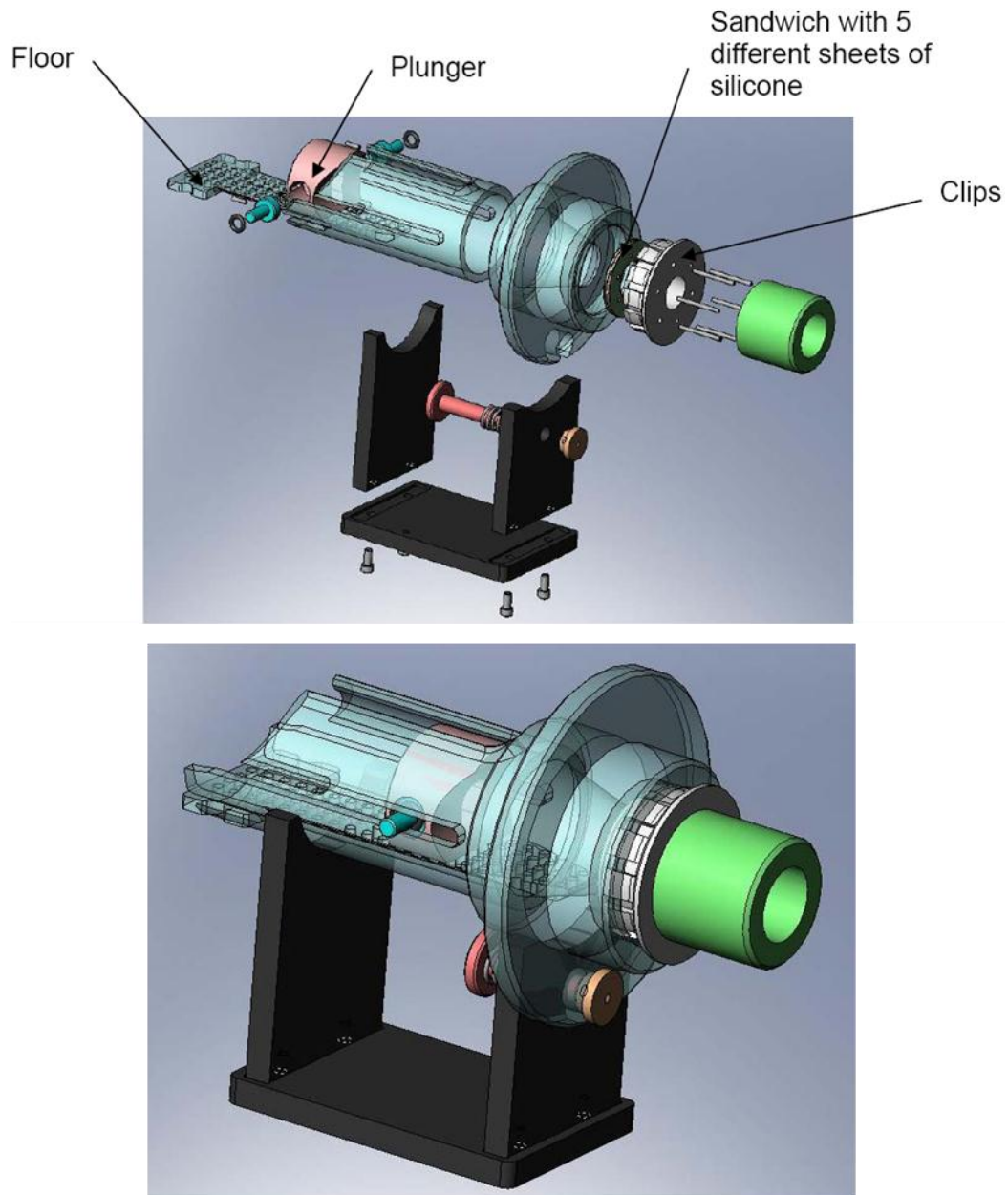
Figure 5.9 MARK 2 Production Prototype

Exploded (top) and working (bottom) views of the Mark2 restraint. Shows also in this is a cradle attachment to hold the restraint in place during animal restraint, freeing up both of the operators hands to allow easier use of the system. This diagram displays the restraint as an individual unit for attachment to a chamber device. Not seen in the diagram is the sealing tube containing the transducer that the restraint is locked into after the animal has been secured for plethysmography or delivery (Figure 5.10). Slight modification to the front of the unit allows it to be used as an individual, self-contained unit for the delivery of an aerosol to one animal at a time. This can be advantageous where drug is expensive in order to reduce the total volume of drug required or where only one or two animals are being subjected to a treatment.

Figure 5.10 Component view of MARK 2 Prototype Restraint

(A) Clearly shows the perforated flat floor. This aids in keeping the restrained animal in a more natural prone position and allows heat to dissipate from the body. It also provides the animal with grip which helps when getting the animal in position within the restraint. (B) Shows the concave nature of the plunger unit, with spring loaded stoppers on each side to keep the plunger in position. There is space for the tail to sit through so it is not trapped in the unit and also allows for restraint while tail tipping or during tail vein injection procedures. (C) shows the unique multilayered silicone 'sandwich' which surrounds the nose and (D) shows its location (Brown) in the front of the restraint.
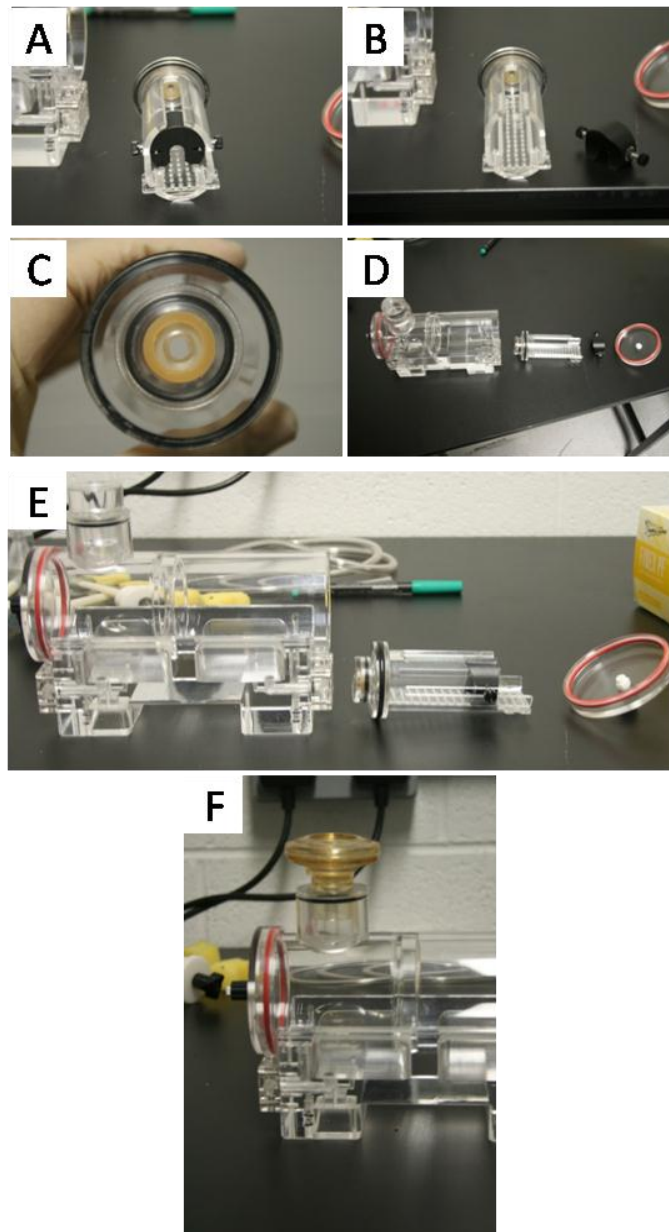
Figure 5.11 Components and completed assembly of the MARK 2 prototype

(A) Shows the back of the restraint with the sliding plunger in place, and (B) with it removed. It also clearly shows the top of the restraint unit where the scruff of the animal can be used to bring the animal up to the top of the unit. (C) Shows the location of the silicone sandwich at the top of the restraint. (D) And (E) show an exploded view of the cradle with the restraint and the rear of the seal behind. As can be seen in (E) and (F), the Mark2 prototype was modified at the front to allow for the restraint to be integrated as part of in individual aerosol delivery system. This can be easily modified for attachment to the Chamber unit characterised and helps the commercial viability of the overall restraint design by allowing incorporation in to different systems.
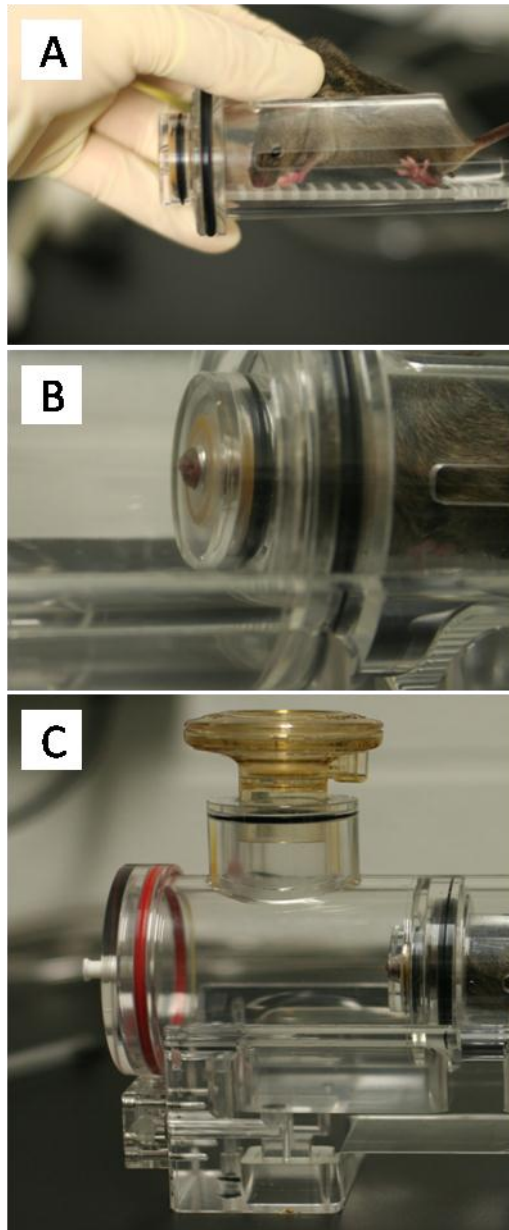
Figure 5.12 Three month old C3H mouse in restraint prototype

(A) Demonstrates the ease at which a scruffed animal can be positioned within the restraint. (B) Shows the 'nose only' nature of the restraint, with the animal in place only the tip of the nose is exposed to the aerosol. (C) Shows the unit in place as would be for delivery of aerosol to the animal.
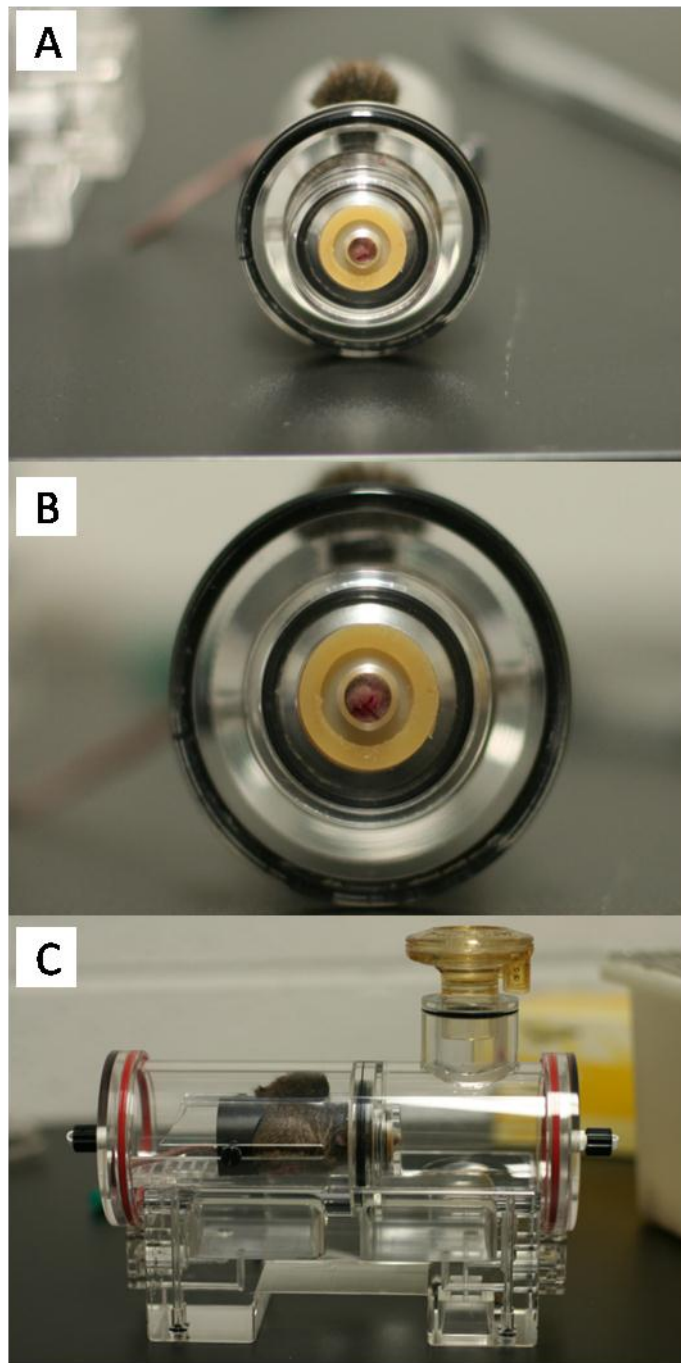
Figure 5.13 Eleven month old C3H mouse in restraint prototype

This, in combination with the 3 month old mouse, shows the unit capable of successfully restraining a wide variety of different size animals. If required for extremely young animals the restraint can easily accommodate this by simply scaling down the device until suitable.

## 5.3 Effect of nebulisation on potential therapeutic molecules

5.3.1 Effect of nebulisation on proteins.

To examine the effects of nebulisation on protein integrity and performance, a number of experiments were devised to ascertain whether or not the Aeroneb® Pro provided a feasible route for aerosol delivery of vehicle-free proteins. In order to do this the following series of experiments were devised. The main protein chosen in this experiment was BMP4, as it is a candidate for future delivery experiments.

5.3.1.1 Nebulisation of a primary antibody.

Primary antibodies, unbound and un-encapsulated, are highly susceptible to the effects of shear forces and heat. In order to determine if the Aeroneb® Pro could be suitable for the delivery of primary antibodies such as anti-BMP4 in an *in vivo* setting an α-BMP4 antibody was nebulised and then assessed for its ability to detect antigen (BMP4) in a Western blot.

The primary antibody used in this experiment produces two distinct bands under the conditions used. When densitometry (n=3) was carried out on the resulting bands it was found that the primary antibody, after nebulisation, detected 87.27% (+/-3.13) compared with 100% (+/-1.61) for the non-nebulised protein (Figure 5.14 (A, B)). This indicates again that the protein is not subject to extremes of heat or shear forces that may render it ineffective as a treatment option, preserving its epitopes intact and allowing successful interaction with the targeted protein.
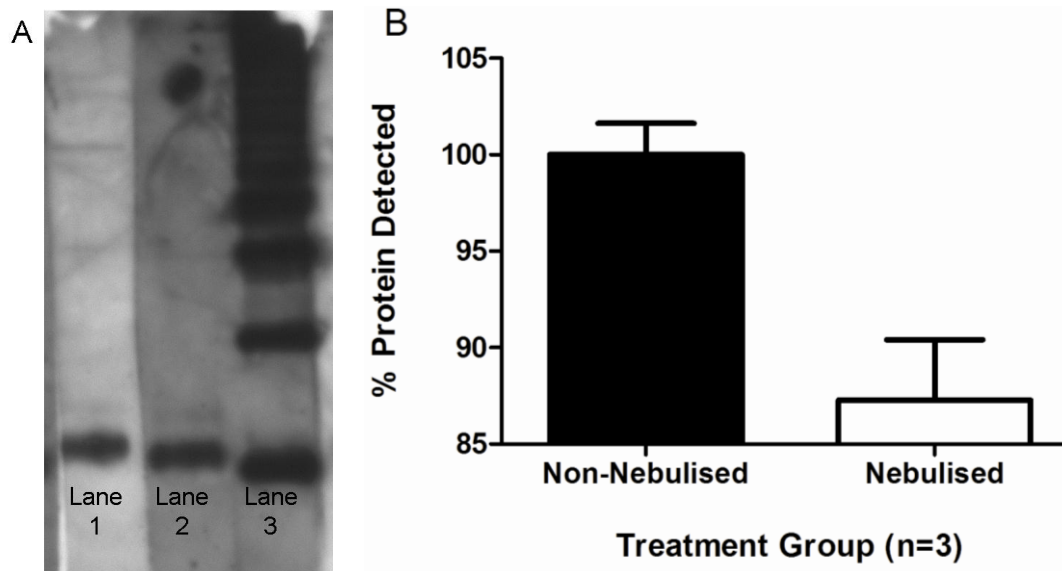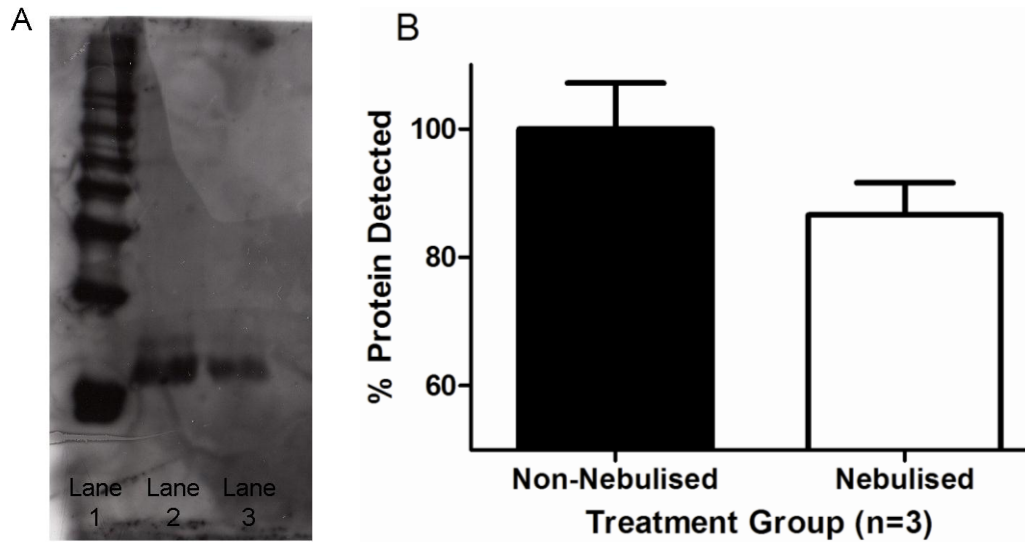
Figure 5.14 Western Blot Analysis of Nebulised α-BMP4 Antibody

1μl of BMP4 protein (10ng) was loaded onto 2 lanes of a 12% SDS-PAGE western gel. This was then immuno-blotted and divided into two strips. Primary antibody was diluted 1/500 and aliquoted into 2x1ml. One of these was stored at 4°C in a 25cm^3 tube while the other was nebulised using the Aeroneb® Pro into a chilled sterile 25cm^3 tube. Both 25cm^3 tubes were then spun @ 259g for 5 minutes, which caused the aerosolised solution to drop out of aerosol and form a solution again. The nebulised primary antibody was then used to probe one of the strips of BMP4 protein, and the non-nebulised used to probe the other.

(A) Shows a sample Western blot of the protein detection of BMP4 protein by nebulised α-BMP4 antibody (Lane1) and non-nebulised α-BMP4 antibody (Lane 2). Lane 3 shows the molecular weight marker (Magicmarker - Invitrogen). (B) Shows the results of the densitometry analysis stemming from the Western blots. With non nebulised detection being set at 100%, it can be seen that nebulised antibody was capable of detecting 87.27% (±3.13 SE) as much as the non nebulised antibody.

5.3.1.2 Nebulisation of BMP4: Effect on protein integrity

A 10ug/ml solution of BMP4 was made up to a total volume of 0.2mls. Half the solution was untreated and stored on ice while the other half was nebulised by the Aeroneb® Pro nebuliser. The solution was nebulised into an ice-cold 25cm^3 tube, which was then centrifuged at 4°C at 259g for 5 minutes, causing the aerosol to deposit at the bottom of the 25cm^3 tube. The non-nebulised protein was also centrifuged under the same conditions. A volume of 2µls, corresponding to 20ng of protein, from both the nebulised and non-nebulised. BMP4 was then loaded and run out on a 12% SDS-PAGE gel, immuno-blotted and probed using an α-BMP4 antibody. The nebulised protein was present at a rate of 86.6% (±4.99) that of the non-nebulised protein, at the same molecular weight (Figure 5.15). This resulting difference was statistically insignificant (t-test, $p < 0.05$) though the trend in the repeat experiments was consistent. This shows that the Aeroneb® Pro can be used to deliver a naked or un-encapsulated protein without grossly affecting its molecular weight or structure.

Figure 5.15 Western blot analysis of protein integrity

(A) Shows a sample Western blot of the protein detection of a non nebulised BMP4 protein by an α-BMP4 antibody (Lane 2) and nebulised BMP4 protein (Lane 3). Lane 1 shows the molecular weight marker (Magicmarker - Invitrogen). B shows the results of the densitometry analysis stemming from the Western blots. With non nebulised protein levels being set at 100%, it can be seen that nebulised protein was present at a rate of 86.6% (±4.99 SE) that of non nebulised protein.

5.3.1.3 Nebulisation of BMP4: Effect on protein function

The treatment of various cell lines and MAEC cells in our lab has shown that cells exposed to BMP4 acquire a mesenchymal like morphology (Molloy et al., 2008). This provides a quantifiable measurement for the integrity of the protein as the level of effect is dose dependent. It was determined that measuring the effect of both nebulised and non nebulised BMP4 *in vitro* would provide both a quantifiable analysis of the ability of a nebulised protein to effect change, as well as paving the way for further *in vitro* and *in vivo* delivery of proteins to aid understanding of pathway function and as possible therapeutics in different models of damage or disease.

5.3.1.3.1 BMP signalling

In order to establish that the protein was still functionally active in the cell, MLE-12 cells were exposed to both nebulised and non nebulised BMP4 and the effect on cell signalling in both was compared to that of a No Treatment control. BMPR-IA, pSmad1/5/8 and Smad4 activity levels were monitored (Figure 5.16).

At the t=20min and t=2hr timepoints, cells treated with nebulised protein and cells treated with non-nebulised protein showed a marked increase in BMPR-IA levels in both the nucleas and cytoplasm, compared to No Treatment, with no major differences noted between BMP4 treated groups. The levels of pSmad1/5/8 and Smad4 were both at higher levels in BMP4 treated cells compared to controls at the t=17hr timepoint, with Smad4 showing higher levels in the cytoplasm compared to near negative staining in the No Treatment control. pSmad1/5/8 staining was restricted to the nucleas in both the BMP4 treated cells and the No treatment control but at much more elevated levels in both the BMP4 treated cells. This correlated with the morphological assays, with both nebulised and non nebulised protein exerting the same effects, to similar extents, on the examined markers.

5.3.1.3.2 Morphology and cell number

To determine whether nebulised BMP4 retained this ability post nebulisation, MLE-12 cells were treated with 50µl BMP4 at 100ng/ml. 400uls of media per well was added in a 24well plate for 6 days with DSFM containing BMP4 protein, nebulised BMP4 protein and a no BMP4 treatment control, which was included to ensure any changes were not due to any unforeseen circumstances. Cells were seeded $4x10^3$ cells/well on Day(-1) in DSFM. On Day0 they were put in DFSM containing BMP4 protein, nebulised BMP4 protein and in the case of the control cells, just media

containing no BMP4 protein. After 6 days the cells were imaged and a cell count performed.

The morphology of MLE-12 cells in both the nebulised and non-nebulised BMP4 treatments was similar, with both looking more fibroblastic and stressed than the No Treatment control. Morphologically they were indistinguishable from each other, but both could be readily identified as being significantly different to the No Treatment control. This showed that at the same concentration and with equal volume of nebulised protein the same effect could be seen as with non-nebulised showing both were interacting with the cells to produce a morphologically equal result (Figure 5.17).

The cell count and percentage growth of the cells mirrored the morphological results (Figure 5.18). Comparing cell number 6days post treatment it can be seen that there is no significant difference between the non-nebulised and nebulised protein treatments, but that both are significantly different from the No Treatment control. It is also of note that, while not statistically significantly different from each other in terms of cell number, cells treated with Nebulised BMP4 were more significantly different from the No Treatment control than non nebulised BMP4 treated cells. With regard to the percentage growth of the cells, the No Treatment group was taken as 100% growth against which the other two treatment groups were measured It was noted that both of the BMP4 treatment groups, while not significantly different from each other, were extremely different from the No treatment control.
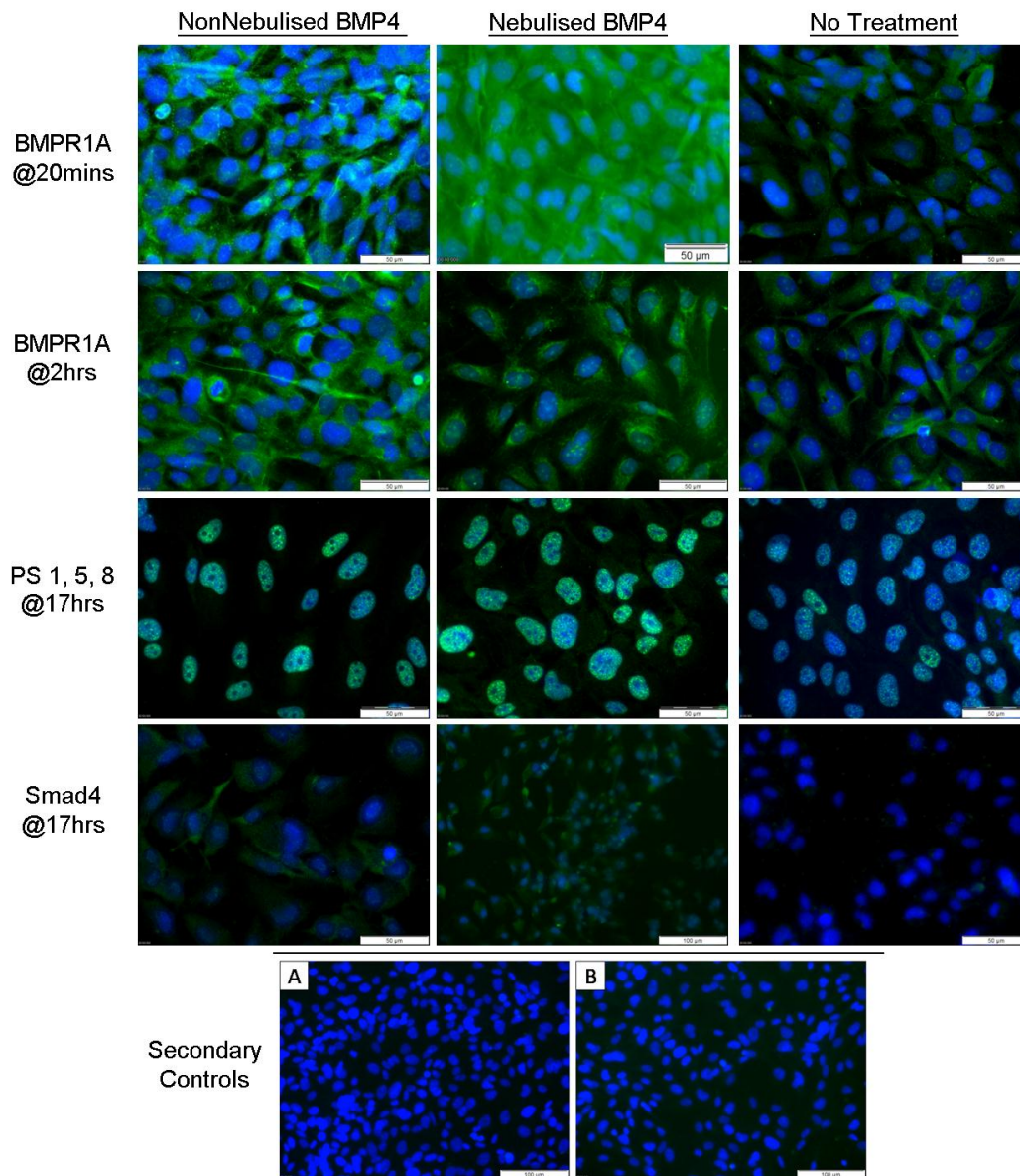
Figure 5.16 Nebulisation of BMP4, effect on pathway signalling

The activity of three different pathway related proteins, BMPR-IA, pSmad1/5/8 and Smad4 was monitored at t=20min, t=2hr and t=17hr. Cells treated with nebulised and non-nebulised protein showed a marked increase in BMPR-IA levels in both the nucleas and cytoplasm, compared to No Treatment at t=20mins and 2hrs respectively. With regards to pSmad1/5/8 and Smad4, the activity levels of both were best detected at t=17hr, when nebulised and non nebulised protein both induced a similar level of activity in the treated cells, compared to almost no level of detectable activity in the No Treatment controls. The secondary controls for BMPR-IA and pSmad1/5/8 (A) as well as Smad4 (B) are also shown.
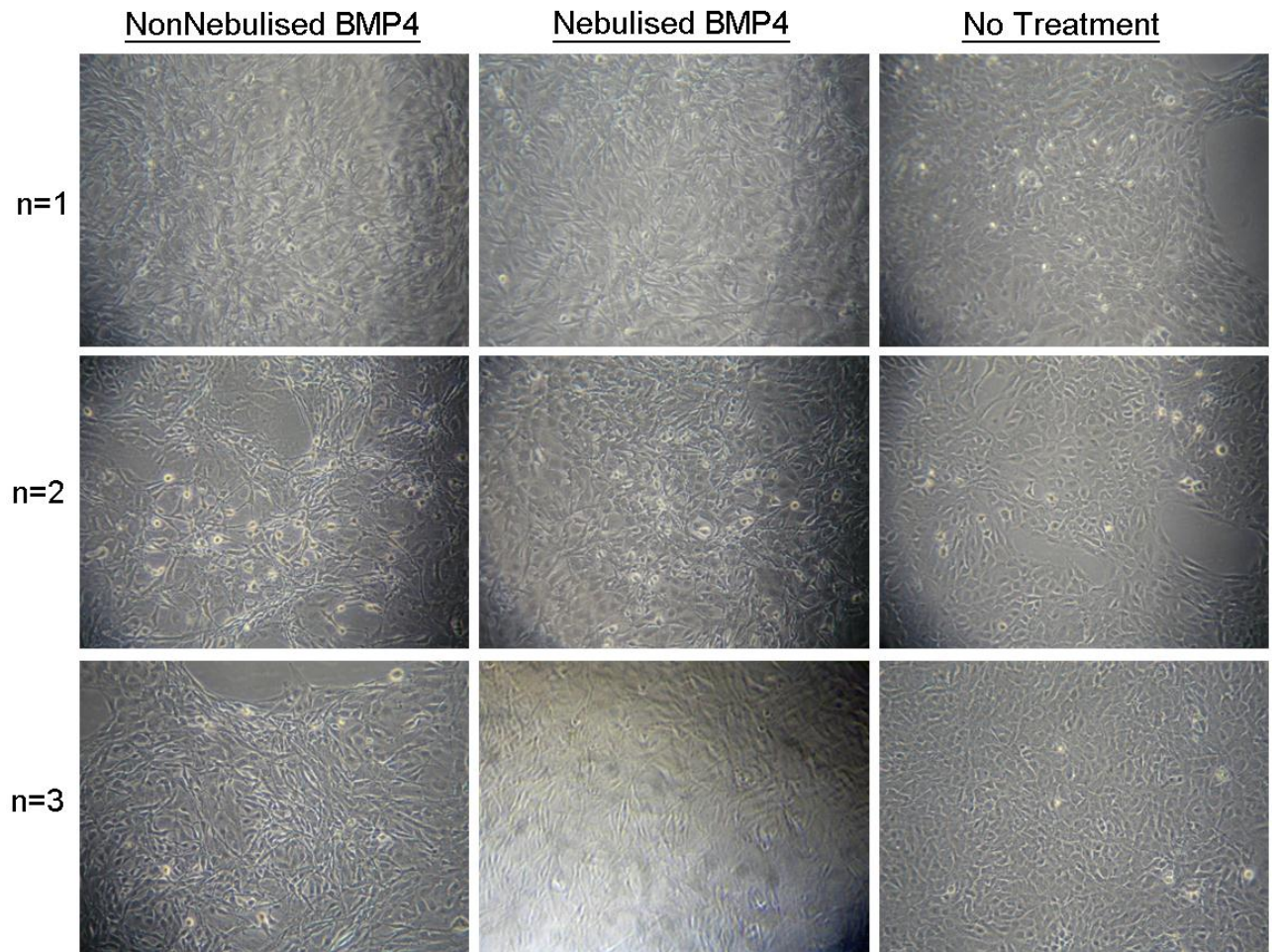
Figure 5.17 Nebulisation of BMP4, effect on cell morphology

Analysed at Day6, it can clearly be seen that both nebulised and non-nebulised BMP4 treated cells are very similar to each other but are markedly different from the No Treatment controls. Both sets of BMP4 treated cells both appear more fibroblastic and stressed than No Treatment across every repeat.
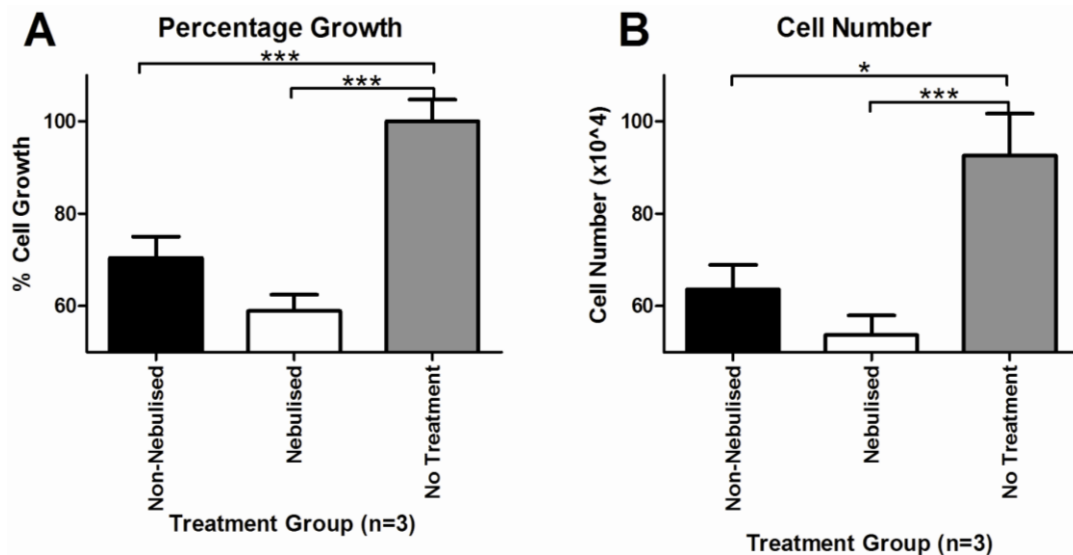
	% Cell Growth		Cell Number(x10^4)	
Treatment Group	Average	St. Err.	Average	St. Err.
Non Nebulised	65.4829	10.5229	76.8334	12.3468
Nebulised	55.3977	1.5365	65	1.8028
No Treatment	100	9.7091	117.3334	11.3920
Tukeys Multiple Comparison Test	Significant?	Summary†	Significant?	Summary†
NonNebulised vs. Nebulised	No	-	No	-
NonNebulised vs. No Treatment	Yes	***	Yes	*
Nebulised vs. No Treatment	Yes	***	Yes	***

†Summary: ns=not significant; * = p<0.05; **=p<0.01; ***p=<0.001.

Figure 5.18 The effect of nebulisation on BMP4 based cell treatment

Nebulised and non nebulised BMP4 was used to treat the MLE-12 cell line and the effects on cell growth and cell number were assessed. Nebulised BMP4 created significantly different results both in terms of percentage cell growth (A), and cell number (B). Of note was the fact that nebulised BMP4 had more of a significant effect on cell number than non-nebulised BMP4 (B).

5.3.2 Nebulisation of siRNA molecules

siRNA is a small molecule with the ability to modulate protein expression at the mRNA level when present in low concentrations. In order to assess whether or not the molecule would stay intact during nebulisation a control siRNA molecule with a fluorescent Alexa-488 tag was nebulised and then transfected into the cells. The siRNA molecule used was a control, a scrambled sequence that should not affect RNA concentration in the cell. The Alexa-488 tag is a fluorescent label attached to the siRNA molecule which enabled FACS to determine the level of transfection of the molecule into treated cells. MLE-12 cells were seeded at 70% confluency in a 24 well plate. A 0.2M solution of siRNA was prepared and split into two aliquots. One aliquot was kept chilled on ice in a sterile $25cm^3$ tube while half was nebulised using the Aeroneb® Pro nebuliser into a chilled sterile $25cm^3$ tube. Both sets of siRNA were then centrifuged at $259g$ for 5min at 4°C, causing the aerosol to condense back into liquid. Cells were then treated with either the nebulised siRNA or the non-Nebulised siRNA and a set of No Treatment cells was also included. 48hrs post transfection FACS analysis was then used to determine the level of transfection of the nebulised vs. the non-nebulised siRNA molecule by quantifying the number of cells expressing the Alexa-488 molecule and the amount of fluorescence per cell (MFI) (Figure 5.19).

79.6% (±1.65) of cells treated with nebulised siRNA were successfully transfected and expressing the Alexa-488 tag compared to 92.58% of non-nebulised siRNA. Therefore nebulised siRNA is 85% as effective as non-nebulised siRNA at being expressed in the cells. Though this is a significant difference ($P<0.01$) it shows that nebulised particles can still successfully transfect the cells. Also examined was the MFI of the cells that were analysed. In comparison to the nebulised siRNA treated cells and the No treatment cells there was a highly significant ($P<0.001$) difference compared to non-nebulised siRNA treated cells. Non-nebulised on average had a MFI of 362.839(±11.83) compared to an MFI of only 35.6% (±2.424) for the nebulised siRNA.
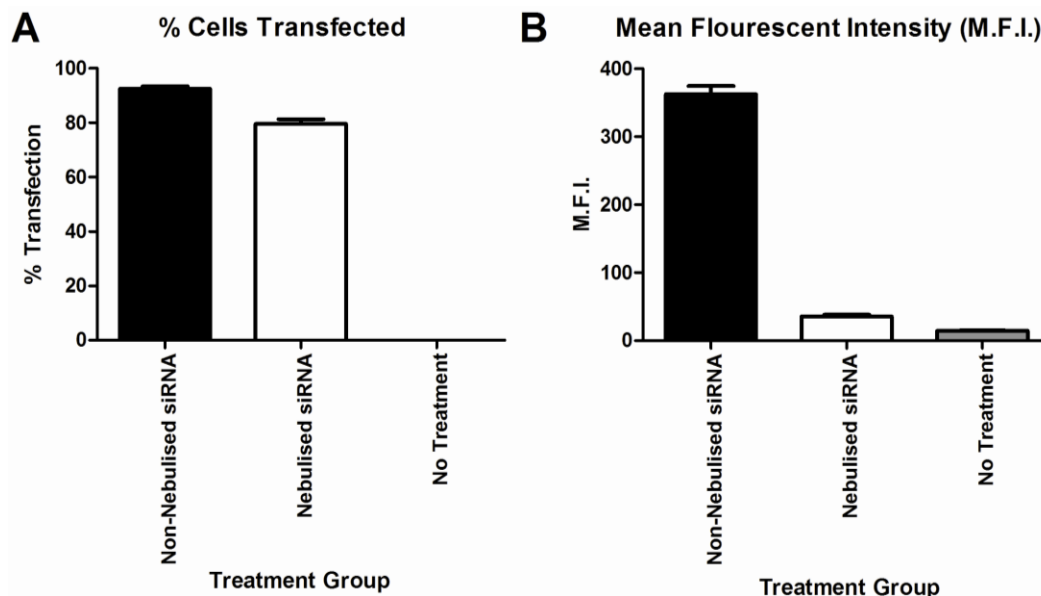
siRNA Treatment	Avg. % Cells Transfected	St. Err	Average MFI	St. Err
Non-Nebulised	92.58	0.795	362.8383	11.8314
Nebulised	79.6	1.648	35.6017	2.4243
No Treatment	0	0.095	14.4033	0.4950

Figure 5.19 FACS analysis of siRNA transfection

A and B show the percentage transfection and the MFI of cells transfected with either nebulised or non-nebulised siRNA in comparison with a No Treatment control. Though the difference in the percentage of cells transfected is quite low it can be observed that the MFI of cells transfected with nebulised siRNA is considerably lower than that of the cells transfected with the non nebulised siRNA.

5.3.3 Effect of Nebulisation on neat and complexed lipids and DNA molecules

In order to determine the effect of nebulisation on DNA and on liposomes a number of combinative experiments were devised utilising a commercially available and highly effective transfection lipid, Lipofectamine™ 2000, and Plasmid DNA encoding the fluorescent protein pMGFP.

5.3.3.1 Effect of nebulisation on lipid-DNA as quantified by Densitometry

Firstly the effect of nebulisation on the DNA component of the transfection complexes was determined. The plasmid DNA was divided equally into two aliquots. One aliquot was incubated at 4°C and the other aliquot was nebulised using the Aeroneb® Pro nebuliser. Both were then centrifuged @259g for 5mins at 4°C. All lipid and DNA, nebulised and non nebulised combinations were then drawn up, Table 5.5. This would aid in determining the effect on not just the complex itself but on the various combinations thereof. This will give information on the response of the various components to nebulisation.

All samples were then ran out on a 1.5% TBE gel and analysed by densitometry (Figure 5.20). The effect on different concentration of DNA being nebulised was also assessed where different concentrations of plasmid DNA were aerosolised and the percentage of DNA compared between the higher and lower concentrations of nebulised and non nebulised (Figure 5.21).

	Lipid And DNA Combinations
1	Optimem Only
2	Lipid Only
3	Lipid+DNA Complex (Positive Control)
4	[Lipid +DNA Complex Nebulised]
5	Lipid + [Nebulised DNA]
6	[Nebulised Lipid] + DNA
7	[Nebulised Lipid] + [Nebulised DNA] complex
8	DNA Only
9	[Nebulised DNA] only
10	[Nebulised Lipid] only

Table 5.5 Lipid and DNA combinations

The table contains all the various nebulised and non nebulised lipids+DNA combinations that were used throughout the course of the experiment.
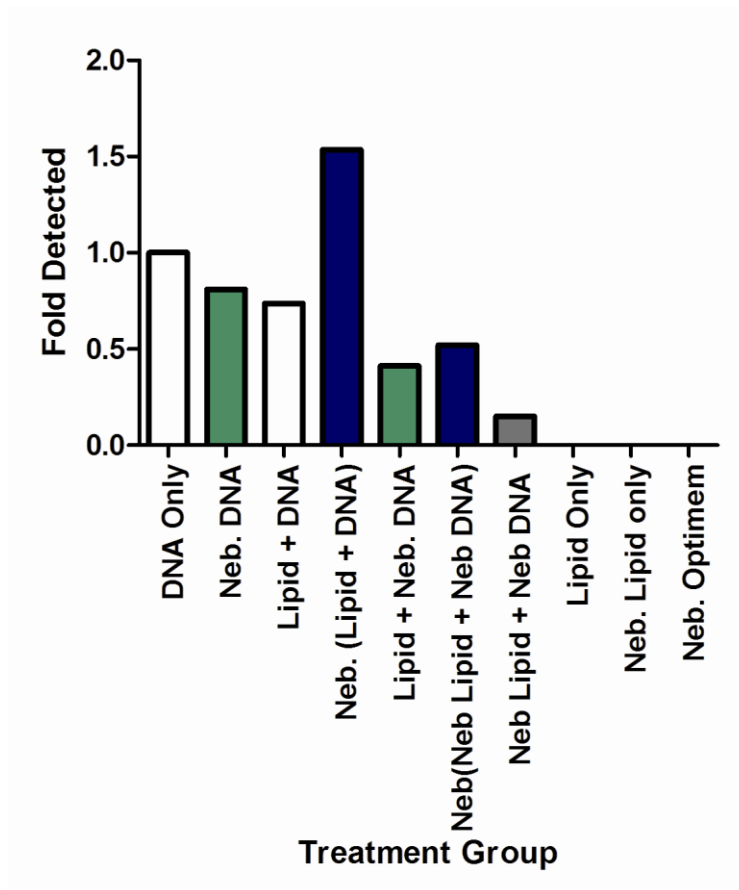
Treatment Group	Fold Detection
DNA Only	1
Neb. DNA	0.8102
Lipid + DNA	0.7380
Neb. Lipid + DNA	1.5356
Lipid + Neb. DNA	0.4124
Neb. Lipid + Neb. DNA	0.5207
Neb. (Lipid + DNA) complex	0.1501
Lipid Only	0
Neb. Lipid only	0
Neb. Optimem	0

Figure 5.20 Nebulisation of plasmid DNA and lipid combinations

Shows the effect of nebulisation on various combinations of plasmid DNA and Lipofectamine 2000. Non nebulised DNA was set as the control with detection here being set at 1 Fold and all other combinations were set against it.
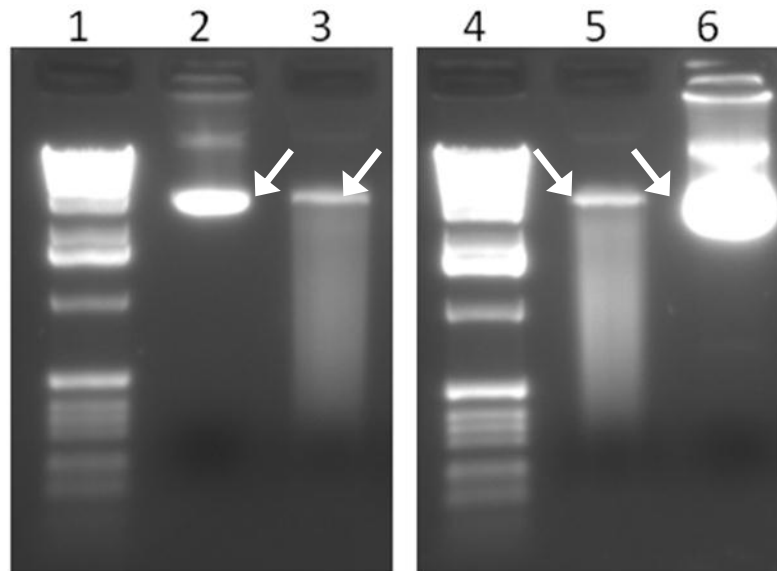
Figure 5.21 Nebulised vs non nebulised plasmid

Different concentrations of plasmid were nebulised and compared to non nebulised controls. At the main band of plasmid detection indicated in the images above, on average there was a 37.93% the amount of plasmid detected by densitometry in the aerosolised samples ran out on TBE gels compared to non nebulised controls. The higher the concentrations the more damage that was noted (42.2% vs. 33.7%).

Lane1/4: Molecular Weight Marker

Lane 2: Non aerosolised plasmid

Lane 3: Aerosolised plasmid

Lane 5: Aerosolised plasmid

Lane 6: Non aerosolised plasmid

5.3.3.2 Effect of nebulisation on lipid-DNA as analysed by FACS

It was also decided to test the effectiveness of the nebulised plasmid and lipid in an in-vitro setting to determine whether or not the DNA and liposome both remained effective and to what degree, if any, nebulisation would affect their performance. In order to do this various combinations of nebulised and non-nebulised lipid and DNA and lipid-DNA complexes were again used based on Table 5.5 above (Figure 5.22). Determination of successful transfection was carried out by FACS analysis of cells transfected with the various combinations outlaid and as per Section 2.2.12.

Various combinations of nebulised and non nebulised lipid and DNA complexes resulted in levels of successful transfection. Perhaps the two most important results of note are lipid+DNA complex which is effectively the positive control, and the nebulised (lipid+DNA) complex which is the form in which the combination is most likely to be delivered in an *in vivo* setting. The non-nebulised lipid + DNA complexes had a successful transfection rate of 33.57% ($\pm$ 1.18) of cells treated, which was not significantly different ($P < 0.05$) from the nebulised (lipid+DNA) complex transfection rate of 30.86% ($\pm 8.25\%$). This corresponds to a comparative rate of 92% for the nebulised complex. Examination of the MFI of the transfected cells shows that the difference here was also statistically insignificant, with the nebulised complex scoring 96.25% as high as the non-nebulised positive control complex. Also of note is that the nebulised lipid which was then allowed form a complex with ordinary DNA had a successful transfection percentage of 28.14% (± 1.51), or approx 84% as effective as the positive control. This was also not significantly different from the positive control. The MFI of this the (Neb. lipid) + DNA complex was 205.45, or approx 70% of that of the positive control, which was again a non significant difference. Furthermore, the nebulised DNA that was then allowed to form a complex with the non-nebulised lipid had a successful transfection rate of 10.13% (± 2.17) of cells treated. Compared to the positive control this is a significantly different result, ($P < 0.01$), yet still has a rate of transfection equivalent to 30.2% of the positive control. When the MFI of the cells is also taken into account it can be seen that there is significantly less ($P < 0.05$) fluorescence in this combination compared to the control, having a MFI index of 54.46 compared to 294.13 in the positive control, or approx 18.5% of the positive control
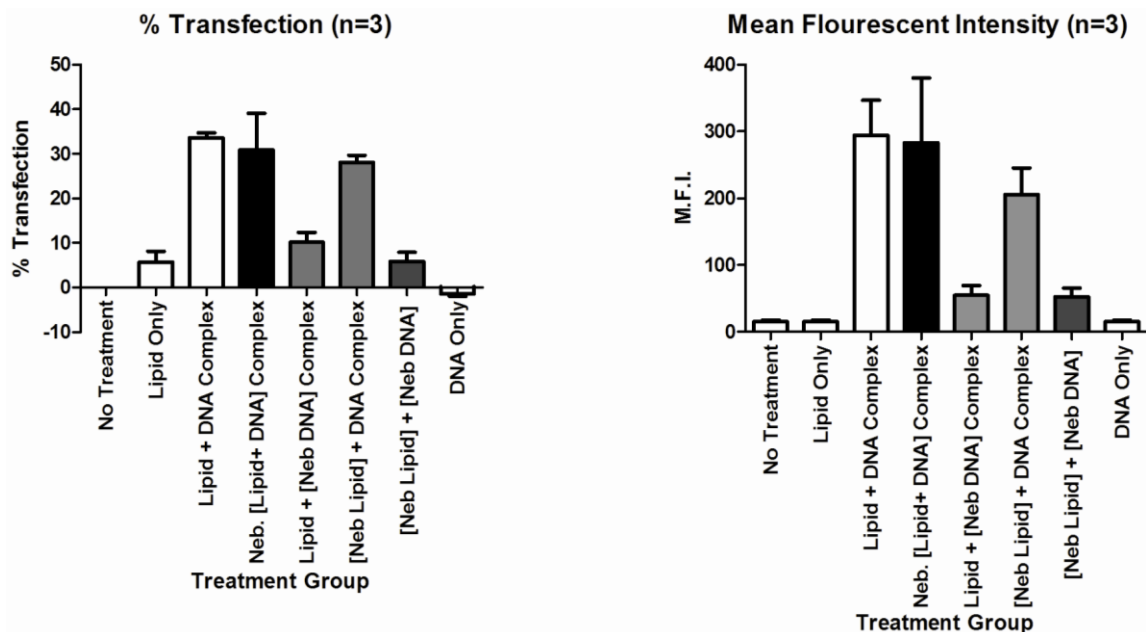
Treatment Group	% Transfection	St Err	MFI	St Err
No Treatment	0	0	15.27	2.4598
Lipid Only	5.65	2.4223	15.34	2.1425
Lipid + DNA complex	33.57	1.1799	294.13	52.8614
Neb. Lipid + DNA complex	30.86	8.2571	283.11	97.3422
Lipid + (Neb. DNA) complex	10.13	2.1702	54.46	14.5556
(Neb. Lipid) + DNA complex	28.14	1.5128	205.45	39.6093
(Neb. Lipid) +(Neb. DNA) complex	5.81	2.0731	52.64	12.7469
DNA only	-1.48	0.4938	15.16	2.4409

Figure 5.22 FACS analysis of nebulised vs. non nebulised lipid+plasmid combinations on cell transfection

Cells were treated with various combination of lipid and Plasmid mix as outlined in the Table in the above Figure. Cells were treated as per 2.2.12.7. After treatment they were analysed by FACS analysis to examine the effect of nebulisation on the ability of the various components of the combinations to transfect the cells and be successfully expressed.

	% Transfection		MFI.	
Tukeys' Multiple Comparison Test	**Significant?**	**Summary†**	**Significant?**	**Summary†**
No Treatment vs. Lipid Only	No	ns	No	ns
No Treatment vs. Lipid + DNA Complex	Yes	***	Yes	**
No Treatment vs. Neb. [Lipid+ DNA] Complex	Yes	***	Yes	**
No Treatment vs. Lipid + [Neb. DNA] Complex	No	ns	No	ns
No Treatment vs. [Neb. Lipid] + DNA Complex	Yes	***	No	ns
No Treatment vs. [Neb. Lipid] + [Neb. DNA]	No	ns	No	ns
No Treatment vs. DNA Only	No	ns	No	ns
Lipid Only vs. Lipid + DNA Complex	Yes	***	Yes	**
Lipid Only vs. Neb. [Lipid+ DNA] Complex	Yes	**	Yes	**
Lipid Only vs. Lipid + [Neb. DNA] Complex	No	ns	No	ns
Lipid Only vs. [Neb. Lipid] + DNA Complex	Yes	**	No	ns
Lipid Only vs. [Neb. Lipid] + [Neb. DNA]	No	ns	No	ns
Lipid Only vs. DNA Only	No	ns	No	ns
Lipid + DNA Complex vs. Neb. [Lipid+ DNA] Complex	No	ns	No	ns
Lipid + DNA Complex vs. Lipid + [Neb. DNA] Complex	Yes	**	Yes	*
Lipid + DNA Complex vs. [Neb. Lipid] + DNA Complex	No	ns	No	ns
Lipid + DNA Complex vs. [Neb. Lipid] + [Neb. DNA]	Yes	***	Yes	*
Lipid + DNA Complex vs. DNA Only	Yes	***	Yes	**
Neb. [Lipid+ DNA] Complex vs. Lipid + [Neb. DNA] Complex	Yes	**	Yes	*
Neb. [Lipid+ DNA] Complex vs. [Neb. Lipid] + DNA Complex	No	ns	No	ns
Neb. [Lipid+ DNA] Complex vs. [Neb. Lipid] + [Neb. DNA]	Yes	**	Yes	*
Neb. [Lipid+ DNA] Complex vs. DNA Only	Yes	***	Yes	**
Lipid + [Neb. DNA] Complex vs. [Neb. Lipid] + DNA Complex	Yes	*	No	ns
Lipid + [Neb. DNA] Complex vs. [Neb. Lipid] + [Neb. DNA]	No	ns	No	ns
Lipid + [Neb. DNA] Complex vs. DNA Only	No	ns	No	ns
[Neb. Lipid] + DNA Complex vs. [Neb. Lipid] + [Neb. DNA]	Yes	**	No	ns
[Neb. Lipid] + DNA Complex vs. DNA Only	Yes	***	No	ns
[Neb. Lipid] + [Neb. DNA] vs. DNA Only	No	ns	No	ns

†Summary: ns=not significant; * = $p<0.05$; **=$p<0.01$; ***$p=<0.001$.

Table 5.6 Statistical analysis of lipid+plasmid transfection rates

Analysis was carried out by one way ANOVA and Tukey posttest analysis.

5.3.3.3 Fluorescent detection of Nebulised Lipids and DNA.

Cells were seeded out on an 8-well chamber slide at 70% confluency per well and treated with various combinations of lipid and plasmid complexes as in Table 5.5 above. At t=48hr post treatment the cells were then viewed with fluorescent microscopy to assess the success of the transfection visually in order to complement the FACS data and to again ensure that the plasmid and liposome were fully functional post nebulisation.

All formulations of liposome and plasmid complexes, in any combination of nebulised or non-nebulised DNA and Lipid, resulted in the successful transfection of the treated cells. It was also noted that the quantity of green cells visualised appeared to match the general results observed through FACS analysis.
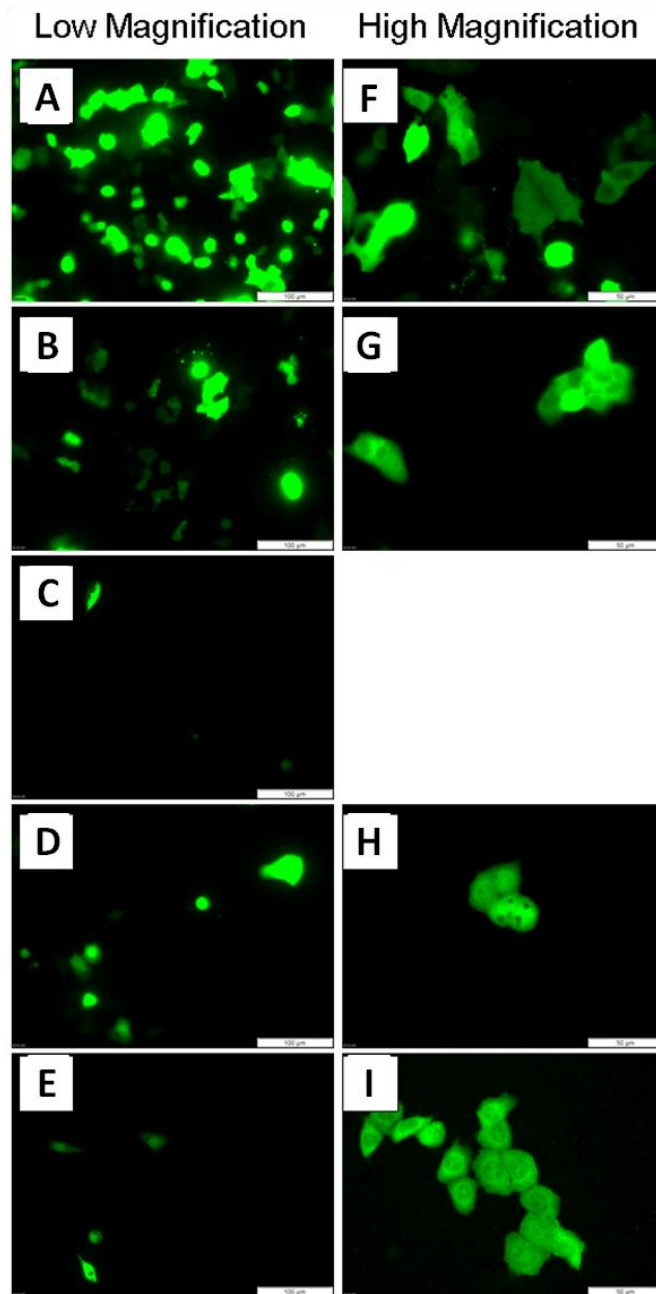
Figure 5.23 Fluorescent detection of nebulised lipids+DNA in transfected cells

A: positive control non nebulised lipid+DNA complex.

B: cells transfected with (nebulised lipid+DNAcomplex).

C: cells expressing GFP after treatment with lipid+(nebulised DNA) complex.

D: Cells transfected with (nebulised lipid)+DNA complex

E: Cells transfected with (nebulised lipid)+(nebulised DNA) complex.

F-I: Corresponding high magnification images

Any potential work *in vivo* would be best performed carrier/lipid free, to prevent loading the lung with extra chemicals and to increase likelihood of acceptance as a clinical therapeutic and regulatory body/medicine board acceptance.

5.3.4 Effect of nebulisation on cells

In order to determine if the standard issue nebuliser we had would be successful in the nebulisation of cells, a number of different cell types were attempted to be nebulised while they were in suspension. Any aerosol formed was collected in a chilled sterile 50ml^3 tube which was then centrifuged at 259g for 5mins at 4°C to collect any cells which may have been successfully nebulised. The supernatant was then removed and 1ml of media used to re-suspend any cells present. This was then added to a 24 well plate and incubated over night at 37°C in 5% CO_2. At t=24hr post treatment, the media was removed and EBAO was used to stain any remaining cells which could then be visualised by light microscopy. No cells were detected post nebulisation. Limitation is pore size, for these applications a larger pore size would be required in order to successfully evaluate the effect on and potential of nebulisation of cells.

5.4 Discussion

In this section, the Aerogen nebuliser, a novel Buxco restraint and chamber system, and potential therapeutic molecules were evaluated. While many types of biological molecules have been nebulised we are not aware of any reports describing the nebulisation of the potential therapeutic compounds tested here. It is important to note also that the system designed for the delivery of aerosolised therapeutics here is specifically designed with mice and rodents as being the end users. Particle formation and delivery can have many different requirments from those necessitated for human delivery. The main reasons for this are the structural differences between human and mouse physiology. Already mentioned in Chapter1, there are a large number of variations between human and mouse airways. Nose only chambers are the first step towards improving delivery to mice, avoiding loss of aerosol due to impaction on whole body chamber walls, prevents animals from huddling together to avoid aerosol inhalation, prevents ingestion and exposure of other mucous membranes to the aerosol (Nadithe et al., 2003). It is also vital to bear in mind that the local toxicity effects or lack thereof seen in one system, such as mice, may differ greatly from the effects seen in humans due variances in physiology and the various transport mechanisms within the lungs REFERENCE (HICKEY and Garcia-Contreras 2001;18(4):387-431)). Therefore direct scale up of delivery, in terms of drug quantity/kg body weight and targeted region of the lung, does not necessarily exist. The area of deposition can be more finely tuned in human delivery, with their larger bifurcated airways resulting in a throttling effect on the size of the aerosol droplet going deeper into the lung.

5.4.1 Nebuliser and chamber performance

By laser diffraction the average VMD of the aerosol particles generated was 4.43μm (±0.043). This roughly correlates with an MMAD as assessed by Cascade Impaction of around the range of 3μm (Chapter 5.1.1). This indicates that 50% of the aerosol generated is of this size or less, i.e. 50% of the aerosol generated is within the respirable dose limitations mentioned earlier. The FPF measurements by laser diffraction need to be adjusted also, with a FPF of 1-7μm roughly correlating to a FPF by cascade Impaction of 1-4.5μm. This is an issue with using laser diffraction over cascade impaction as a means to test the aerosol. There is no straight conversion table for the readings and both methods have both pros and cons associated with them. Cascade Impactors, and Next Generation Cascade Impactors remain the pharmacopeia standard for measuring aerosol formation. However the benefits of laser diffraction in

situations such as device qualification outweigh those provided by CI. Cascade Impactors are expensive tools with solitary uses. They are slow to set up, analyse and clean and are arguably more susceptible to erroneous measurements. In the instance used here where a large number of nebuliser units were to be analysed Laser diffraction provided the most robust and practical means of evaluation. The same can be said for the subsequent evaluation of the chamber itself. The total respirable dose available with these nebuliser units (with the VMD of 1-7µm) was an impressive 65.26%, higher than the competitive brands of nebuliser.

The Chamber design was a novel design, untested with aerosol delivery to units. Its performance was successfully characterised and resulted in an optimal VMD of 4.47µm when run at the optimised flow rate of 4L/min. The total amount of aerosol in the respirable dose range of 1-7µm at this rate was 62.83% when averaged out over time, a full 4.4 percentage points higher than that of the lower 2L/min flow rate, and only 1% lower than the nebuliser unit on its own. This shows that the chamber run under the correct conditions gives animals exposure extremely faithful and close to the nebuliser units original output. This is important as any significant variations here would mean that the chamber is having its own specific effect on the aerosol, meaning that every type of nebuliser unit connected to it would have to be individually calibrated. In this instance it can be extrapolated that the chamber would not significantly influence the Aerosol characteristics that any aerosolising unit output into the system. The main reason that there is deterioration in loyalty between nebuliser output characteristics and characteristics derived at the point of inhalation in the chamber is most likely due to collision of aerosol molecules within the chamber due to the lower flow rate. Lower flow rate increases the time spent by the aerosol in the chamber, increasing the chance that independent molecules either collide with each other or with a surface within the chamber. Collision with other molecules causes aggregation. These larger molecules are then again more likely to randomly collide with other independent aerosol droplets. This aggregation leads to the droplets falling out of aerosol and depositing and condensing at the base of the unit, unavailable for inhalation. Even if only a number of collisions occur, this will increase the average VMD, and such molecules will not be successfully respired but instead will be more likely to be ingested or deposited at the back of the throat.

5.4.2 Restraint design

The novel restraint was designed to offer a better system of restraint for animals for nose only exposure systems. It had a number of criteria to meet for various reasons.

For commercial reasons, in order to be a viable sales generating candidate, it needed to be substantially different from other devices available on the market, offering unique advantages. The restraint designed fits these requirements, with a number of unique adaptations which are strong individual commercial points. Ultimately the functionality of the design is its main selling point. This novel restraint provides a more ergonomic method for restraining small animals. It places the animals in a more natural posture and in less cramped conditions. These are important as it reduces the stress levels of the animals and also reduces the risk of animal death due to handling errors. This provides better experimental animals that can be more consistently and reliably be analysed. If a treatment results in a slight labouring of breathing, this restraint will enable these more subtle differences to be detected by plethysmography, as the animal will not be breathing in as laboured a manner just by being in the restraint. The fact that that the restraint keeps the animal orientated in a prone fashion means that it can be modified as mentioned in the results for other purposes such as tail vein injection, I.P. injections and or cardiac punctures. This should help generate more sales on the same basic model, lowering costs and increasing profit margins on the restraint. The fact that the restraint has been deemed suitable for release and mass production is testament to its design.

5.4.3 Nebulised protein

BMP4 protein and Monoclonal antibody against BMP4 were both nebulised and evaluated against non-nebulised controls. The BMP4 protein was determined to be 86.63% intact, and the primary antibody 87.27%, less than 1 percentage point in the difference. The results are consistent and show that no significant deterioration of any aspect of protein size or epitope presentation occurs due to nebulisation. In order to ensure this further analysis of the proteins performance *in vivo* post nebulisation was conducted. Both the effect on the growth of the cells, by cell number and examining morphology, and the effect on pathways in the cells by looking at proteins affected by the presence of BMP4. All assays returned an equal effect by nebulised protein in comparison to non-nebulised. In the instance of the cell count, it appeared that the nebulised protein had a greater effect than that of the non-nebulised, even though we had shown less intact protein post nebulisation. This result is due to the fact that nebulisation can break down any clumped together bits of protein. This means that instead of protein molecules being clumped together in solution they remain more dispersed throughout the solution as a result of nebulisation. This in turn would make

more protein available to interact with more receptors on the cells, triggering a greater overall effect.

The level of stability of the protein is important for a number of different reasons. If the protein was too unstable, it may be possible to modify the protein to increase stability without the need for carrier molecules. The higher the percentage stability, the more reliably consistent dose administration will remain and the cheaper the cost of drug delivery. Different drug delivery systems have different requirments, depending on the potency of the protein and the effect of delivery of degenerated protein fragments to the system. Ideally the delivery system would provide for 100% stability of the drug molecule, however, in this instance, stability of greater than 75% was deemed to be successful.

5.4.4 Nebulised siRNA

The siRNA molecule nebulised here was a control, non-functional siRNA molecule, tethered to an Alexa-488tag. The results show that the cells transfected with nebulised siRNA were successfully expressing the Alexa-488 fluorescence 85% as much as the non-nebulised protein. This difference was significant (t-test, $p<0.05$) but nonetheless showed the nebulised siRNA to be highly efficient at transfecting the cells. The MFI of the two treatment groups however differed grossly. The MFI of the nebulised siRNA was under 10% of that of the non-nebulised. This could be due to the fact that the nebulising action is damaging slightly the Alexa-488 tag, reducing its capacity to fluoresce. It may also be partly attributed again to the dispersion of the siRNA molecules by nebulisation. Instead of clumps of Alexa-488tagged siRNA been taken into cells and a large MFI being recorded, the molecules may be more dispersed, giving a more diffuse response. It is likely to be a combination of these factors creating this result.

5.4.5 Nebulised plasmid and lipid

Our results showed that approx 80% of DNA was still intact at the same mol weight post nebulisation compared to the non nebulised control. It also showed that nebulised lipid and nebulised DNA still retained their activity *in vitro* and that the aerosolised complex, the most likely form in which the treatment would be delivered, was also highly successful *in vitro*. All combinations of nebulised and non-nebulised complexes were found to be, to varying degrees, successful. This shows that both the lipid was still functioning in its capacity of delivery the Plasmid, and that Nebulised plasmid was sufficiently intact when transfected to express its reporter and this was

confirmed by both the FACS data and the visualisation of the GFP tag under Fluorescent Microscopy.

5.4.6 Nebulised cells

Nebulisation of cells has the potential to deliver cells directly to a targeted site in the lungs. The ability to nebulise cells, unlike other substances is most likely to be applied in a different fashion than the chamber system outlaid. It is more suitable to nebulisation where the subject is intubated and the cells can be guided to a specific location. There are a number of reasons why nose-only delivery may not be suitable. If the cells are too big themselves, they will not be inhaled into the lung, but will get trapped at the top of the throat, resulting predominantly in ingestion of the cells and also possibly cells migrating from or embedding in nasal or oral cavities. However the ability to nebulise cells and then deliver to a target zone via intubation has potential for targeted delivery to any region of the lung and an efficient method of dispersal in that region. Though not successful with the size nebuliser employed, there are larger nebulisers available with greater pore sizes which should be more suitable for this specific requirement.

5.5 Conclusion

The Chamber designed for the delivery of aerosol to multiple restrained animals was capable of successful aerosol delivery to the point of inhalation. The corresponding restraint designed to be used on its own or as an integrated part of the chamber delivery system provided a safe and effective nose only exposure system in which to restrain the animals for aerosol delivery and plethysmography analysis. Assessment of different therapeutic molecules, in the form of protein, siRNA, DNA and lipids, to withstand nebulisation all resulted in a positive outcome. All were found to be intact and functional post nebulisation with only low degrees of functional loss occurring. In some instances, nebulisation resulted in increased performance due to the breaking down of agglomerates during the nebulisation process. Cells were the only nebulised solution which did not successfully nebulise. This was due to the small pore size of the nebuliser unit used. Larger pore size units can be obtained on a custom basis but were not available throughout this process. Due to the fact that nebulisation was not unduly harsh on protein or DNA, it is not unfeasible that certain small cells, constrained by the ability to create large enough pores that would still produce a respirable size molecule, could be used to deliver cells to the lung *in vivo*. Critical analysis of the nebulisation process as a whole, taking into account its ease of use,

success with nebulising potential therapeutic molecules and ability to deliver directly to the site of interest shows it to be a highly capable mechanism for enabling delivery of several therapeutic molecules to mice *in vivo*. The choice of therapeutic molecule, siRNA vs. protein, for example, would therefore not be limited by delivery method. Instead our ability to assess the intended biological effect, such as upregulation of knockdown of a target, in terms of satisfactory endpoints, would determine therapeutic molecule selection.

6 Particle Bombardment and siRNA.

6.1 Introduction

The role of the BMP pathway in inflammation, damage and disease is multifaceted and complex. In addition to aerosolisation, two other techniques were investigated as potential means of effecting a therapeutic change by altering this pathway in the lung *in vivo*.

(i) Particle bombardment utilising a Bio-Rad Gene Gun is, as previously discussed (Section 1.5.3), a viable method for the inclusion of genetic material into animal cells. Our aim with the technology was to assess its potential initially as an *in vitro* tool for the delivery of DNA to both cell lines and the more difficult to transfect primary cell isolates. This work has been published (Gilbert et al., 2008). Following on from this, if the method proved successful, would be the aim to assess the potential of the underlying technology to be modified for delivery an *in vivo* system.

(ii) siRNA technology, already demonstrated to be capable of successful nebulisation of *in vivo* delivery, was further examined to determine if the technology was suitable for the project in hand. It was decided to identify, *in vitro*, targets for siRNA knockdown in order to use loss of function studies to both determine the role of various pathway components and to identify a therapeutic target. siRNA, as discussed below in Section 6.1.1 has potential uses as a therapeutic agent for both short term and long term treatments of various lung diseases. Because we have demonstrated that it is possible to aerosolise siRNA, it is a potential candidate for delivery to mouse lung *in vivo* in both healthy and disease models. Aims were to determine the potency of the technique *in vitro* and that of the siRNA molecules themselves, by determining their ability to successfully transfect different cell types and the ability to induce targeted knockdown of selected targets in these cells.

The use of plasmids and siRNA as therapeutic candidates has numerous benefits. In the case of plasmids, delivery of plasmids capable of over expressing either components or antagonists to the BMP pathway in specific targeted cells in the airways, potentially allows for long-term regulation of an aberrant pathway component. For example, in PAH where BMPR-II has been shown to be deficient, an integrated plasmid expressing copies of functional BMPR-II protein has the potential to restore the equilibrium in the pathway and reduce the effect of the disease. siRNA can be used in a somewhat similar fashion, if a BMP antagonist is being over expressed, such as Gremlin, siRNA can be used to silence the antagonist and prevent inhibition of the pathway. In instances where pathway components are being over

expressed, delivery of quick acting siRNA to the airways could limit the progress of the BMP response, reducing inflammation and subsequent damage and consequences.

6.1.1 RNA interference and short interfering RNA

RNA interference (RNAi) is an umbrella term that covers any technique that induces the post transcriptional silencing of a targeted mRNA via degradation or translational arrest (Pauls and Esté, 2004). It usually refers to the use of double stranded RNA in the degradation of mRNA. This process was first observed in plants and was initially coined as co-suppression before later work in *C.elegans* gave light to the fact that it was brought about by dsRNA and resulted in specific gene silencing. Introduction of dsRNA with exact complementarity to the target gene induces the degradation of the target molecule (Ryther et al., 2005). RNAi is know known to be a naturally occurring event that is part of an evolutionary conserved process used in the regulation of gene activity as well as a defence mechanism against viruses and foreign DNA being transcribed in cells, with many viruses having long dsRNA as a pivotal part of their replication process. If long dsRNA is introduced into cells the defence mechanism induces cellular suicide. However short interfering RNA (siRNA) duplexes of between 21 and 25 base pairs are enough to bring about specific target degradation but short enough to avoid triggering the cellular defence mechanisms (Manoharan, 2004).

siRNA molecules by nature of their structure are relatively resistant to nuclease degradation and are not overly temperature sensitive, having been shown to be capable of retaining function for up to 72hours at 37°C in calf serum. This makes siRNA suitable for cell culture and *in vivo* experimentation without the necessity for alterations or complexing. This in turn reduces the likelihood of problems associated with the use of various carrier molecules and excipients (Braasch et al., 2003). However the use of excipient or the binding or encapsulation of the molecules can increase the likelihood of the duplexes entering the target cells upon delivery. As an example the use of antibody directed delivery using a siRNA/antibody complex has been used to successfully target the siRNA molecules via a cell surface receptor to HIV or envelope virus transfected cells. This demonstrates the potential for systemic, local and cell type specific antibody mediated siRNA therapeutic delivery (Song et al., 2005a). siRNAs have been successfully targeted to the lung via intranasal delivery (Zhang et al., 2004). siRNA technology has also been used to treat SARS coronavirus (SCV), initially *in vitro* but later in Rhesus macaque primates infected with the virus via intratracheal administration. The siRNA therapeutic was seen to mediate relief

form SCV induced fever, there was a decreased viral load present in samples and there was a reduction in the level of SCV induced alveolar damage. Dosages in the range of 10-40mgs/kg were shown to not induce any siRNA related side effects or cytotoxicity. Fears of off-target effects that can be manifested in cell culture experiments (caused by the sequence used for the siRNA having complementarity to other genes) have not been reported in *in vivo* experimentation (Li et al., 2005). These type of results in a clinically relevant model of disease highlight the potential for siRNA mediated therapeutics in the targeting of lung related challenges and the potential for the short term silencing of genes associated with over responsiveness to challenge in the lungs and shortens the path from bench to bedside for siRNA inhaled therapeutics.

6.2 Particle Bombardment

6.2.1 Cell types and plasmid choice

Five different lung cell cultures were used to examine the potential of the model for successful downstream applications in an *in vivo* situation. This involved the use of three lung cell lines, primary mouse lung cells in submerged culture and primary mouse cell lungs at ALI. The cell lines used were murine LA4 and MLE-12, and human BEAS-2B.

LA4 cells are a large slowly dividing cell line that provided an excellent target for initial bombardment studies in that they provided a large target area for the individual microcarriers to hit. This then led to an obvious progression to smaller faster dividing cells to see if the success could be repeated. Moving into primary cells then afforded the opportunity to make a realistic assessment of the viability of bombardment as a treatment method, as ultimately this is where other techniques fail. Progression to ALI was a natural follow on to assess the potential of the method before looking at any potential in an *in vivo* setting

The choice of plasmid was also an important consideration as plasmids that could also be detected *in vivo* were preferable. It was decided to pursue the technique with the use of fluorescent protein encoding plasmids, cyclin-D1-GFP and later, pMGFP

6.2.2 Optimisation

Before carrying out routine particle bombardments with the Gene Gun it was important to establish a number of parameters. These parameters involved determining (i) what effect if any there was on our agent of interest from the physical

bombardment itself (i.e. if a plasmid was being compromised during the coating procedure or subject to too high shearing during the blast), (2) the amount of pressure firing the particles from the helium blast required and, (3) the shooting distance to the stage.

6.2.3 Plasmid Analysis

It was first necessary to assess what effect the process of coating the plasmid onto the microcarrier may have on plasmid integrity.

On analysis it was shown that there was no significant degradation of the super coiled or coiled lengths of DNA that had been coated onto the microcarriers, though there was a small amount more of relaxed cDNA present in sample A. Of note is that it is the coiled and supercoiled lengths of DNA which will be responsible for successful expression of the plasmid in the target cells so it is these categories that are the most important to assess on order to determine the potential of the device. The lack of plasmid present in Lane 4 (Sample B) was determined to be due to a pipetting error in removing microcarrier along with EtOH before resuspension in dH2O (Repeated separately-data not shown).

Firure 6.1 shows the supercoiled fragment of the plasmid to remain largely intact after nebulisation. Decreased quantities of the open circlular is likely due to degradation due to the fact that they are less compact than the supercoiled structures, and corresponds with an increased concentration of linear plasmid. This shows that plasmid DNA is not grossly affected by the coating procedure used in conjunction with the Au microcarriers.
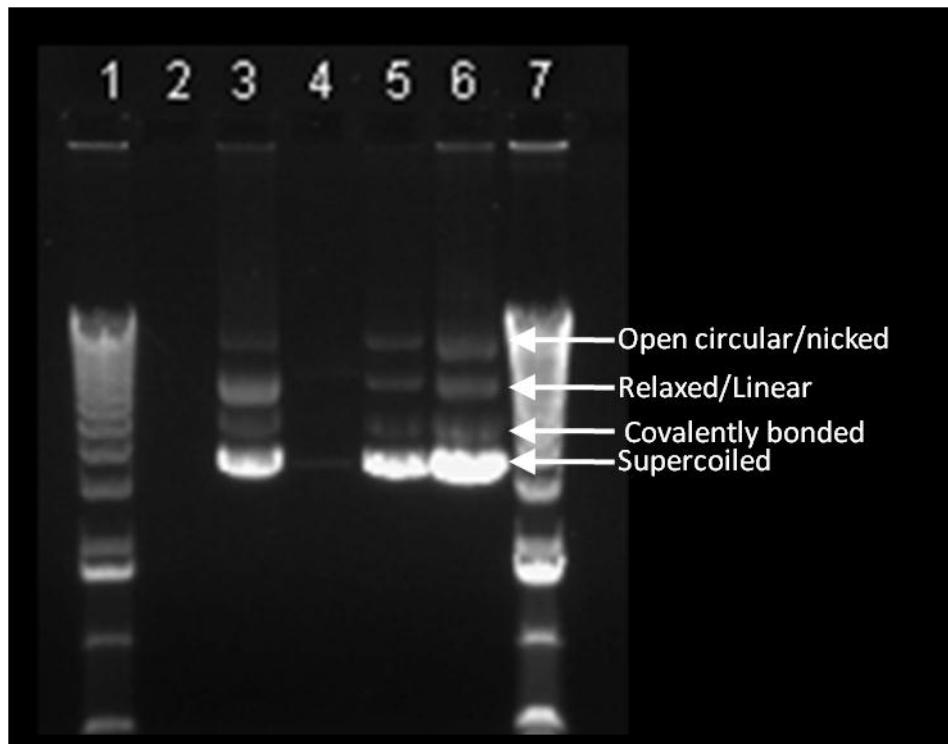
Figure 6.1 TBE gel showing plasmid recovered from Au particles against Non-coated plasmid

The plasmid, CyclinD1-GFP (50µg), was coated onto the 0.6µm gold (Au) microcarriers. Half the volume of microcarriers, suspended in EtOH, was aliquoted into a tube A, and half into tube B. Tube B was then centrifuged @650g briefly and the supernatant removed and the microcarriers were then resuspended in 30µl dH$_2$O. Two further tubes were then set up; C containing 30µl EtOH spiked with 25µg plasmid DNA and; D containing 30µl dH$_2$O spiked with 25µg plasmid DNA. DNA extraction was then carried out on all tubes. The extracted DNA was then run out on an agarose gel. The amount of super coiled, coiled and relaxed DNA in the two groups was then compared.

Lane1: Molecular Weight Ladder

Lane2: H$_2$O control

Lane3: A- DNA extracted from Au Particles coated with 25µg DNA into EtOH.

Lane4: B- DNA extracted from Au Particles coated with 25µg DNA in dH$_2$O.

Lane5: C- EtOH spiked with 25 µg DNA.

Lane6: D- dH$_2$O spiked with 25 µg DNA.

Lane7: Molecular Weight Ladder

6.2.4 Optimisation of delivery.

LA4 cells were seeded at a high confluency in order to determine the effect of blast pressure on the cells. By examining previously published work it was possible to optimise the range to three different blast pressures, 900, 1100 and 1300 psi. Cells were shot at these three pressures with microcarriers at the different level stages and then analysed for damage.

Initial experiments were carried out utilising LA4 cells coated on 10cm Petri dishes coated with serum with coverslips on the base to help the cells adhere. Cells were bombarded with 0.6um Au particles, uncoated, at 1100 psi under 15in Hg vacuum with 2mgs Au per shot. It was noted that the cells would not adhere to the Petri dishes but showed an affinity for the glass coverslips. This initial experiment was to examine whether the cells could tolerate the procedure prior to proceeding with transfection with a plasmid. The cells were re-fed with fresh media immediately post bombardment and viewed under a light microscope where cell death of approximately 50% was noted. This indicated that although harsh, the procedure had potential as other parameters were modifiable in order to reduce the damage inflicted on the cells.

The next set of experiments utilised LA4 cells again. Cells were seeded on glass cover slips in Petri dishes at approx 50% confluency. This time a range of parameters, including pressure (900, 1100 and 1300 psi) and shooting distance (1st and 2nd stage) were varied and examined. Plasmid DNA was also used to coat the particles at two different concentrations (0.5ug and 5ug per shot) in order to ensure whatever effect it would have on the Au particles would be included as too much DNA can lead to agglomeration of the Au particles. All cells were shot once.

The experiment resulted in successful transfection of the cell line after 24 hours with plasmid cycD1-GFP but the stresses on the cells were noted (Figure 6.2). It was especially noted that in this particular case that LA4 cells did not tolerate the procedure well, with a high rate of cell death, and due to the slow growing rate, took a long time to recover from the effects of the bombardment. A number of the cells were left for a period of 20 days in order to allow them to divide and see if transfection was transient or could be observed in the cells after this period of time (Figure 6.3). This showed that cells were still expressing the plasmid almost three weeks post transfection.

At this point, in line with literature recommendations, the size of the Au particle utilised was changed from 0.6um (more commonly utilized in the transfection of

plants) to 1.6um, which had previously been shown to be successful in the transfection of mammalian cells (Heiser, 2004).

The first test under this scenario was to check LDH levels of cells between control cells which were exposed to vacuum and pressure blast but no microcarriers, with cells bombarded with microcarriers at both the 1st and 2nd stage. It was noted that there was no significant difference in LDH levels between the control and the bombarded cells, indicating that neither the first or second stage greatly enhanced the survivability of the cells post bombardment and that the bombardment itself didn't greatly increase the LDH output of the microcarrier bombarded cells vs. control cells. It is worth noting however that any cells that may have been physically removed from the Petri dishes during bombardment or which may have had their integrity seriously disrupted may have been removed from the Petri dish during a procedural step where bombarded cells were briefly rinsed in media which was removed, removing their capacity to affect the LDH assay.
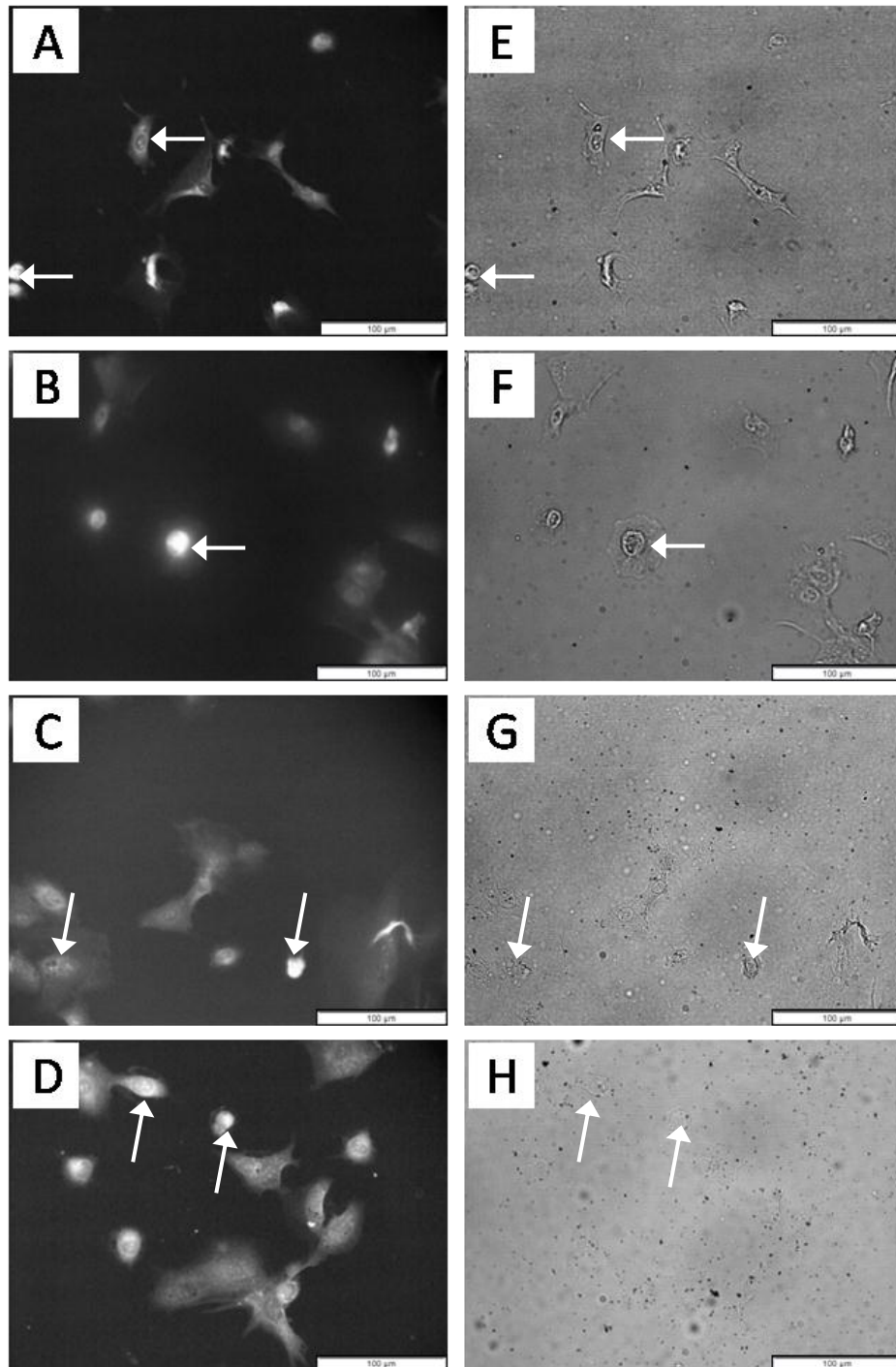
Figure 6.2 LA4 cells bombarded with CycD1-GFP coated microcarriers

Cells were analysed by Fluorescence microscopy 24hr post bombardment;
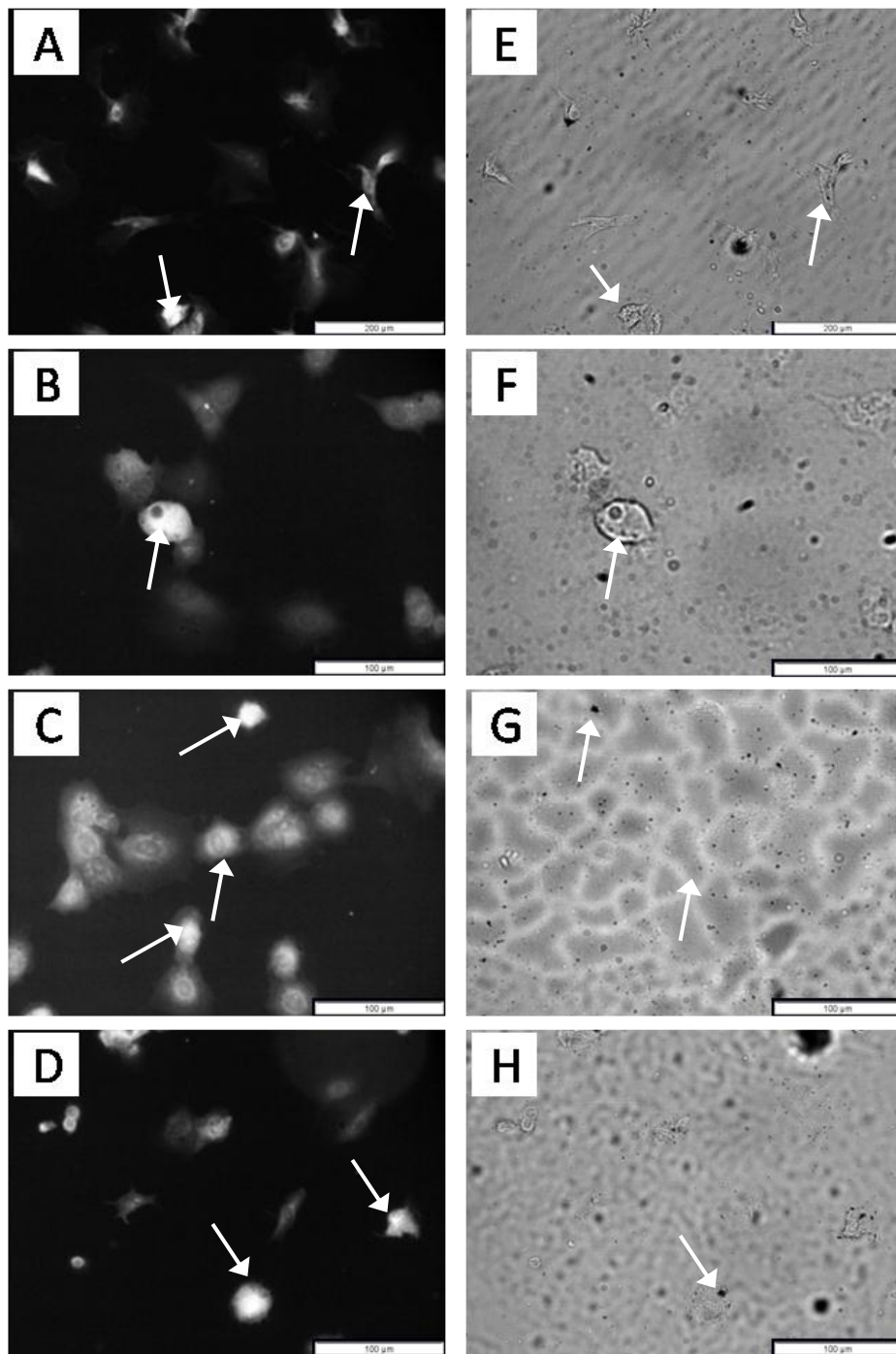
A: 900 psi 4cm shooting distance 0.5µg plasmid DNA

B: 1100 psi 4 cm shooting distance 0.5µg plasmid DNA

C: 900 psi 3cm shooting distance 5µg plasmid DNA

D: 1100 psi 3cm shooting distance 5µg plasmid DNA

E-H: Show corresponding brightfield images.

Arrows indicate fluorescing cells (A-D) and gold particles (E-H).

Figure 6.3 LA4 cells bombarded with CycD1-GFP coated Au particles

Cells were analysed by Fluorescence microscopy 20 days post bombardment;

A: 900 psi 4cm shooting distance 5µg plasmid DNA

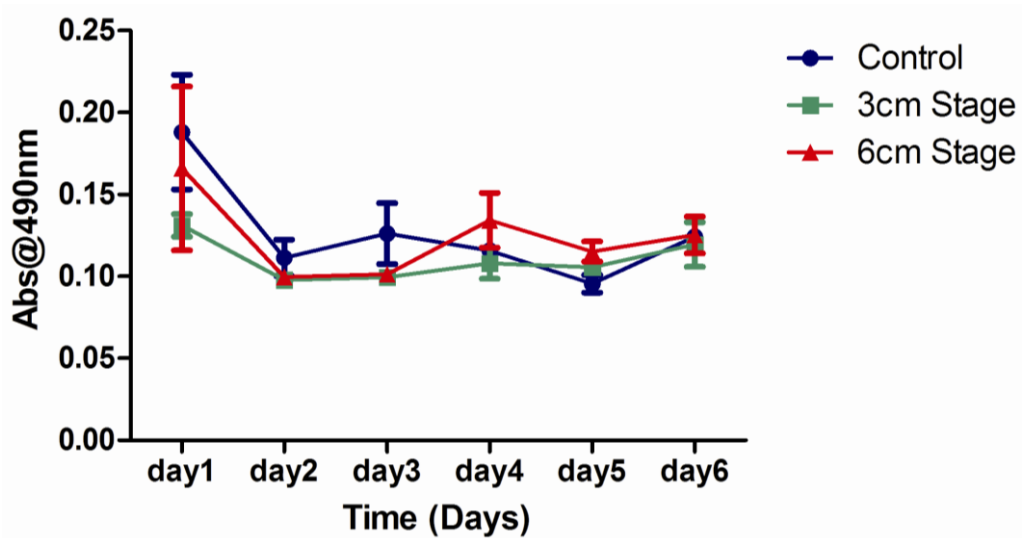B: 1100 psi 4 cm shooting distance 5µg plasmid DNA

C: 1350 psi 3cm shooting distance 5µg plasmid DNA

D: 1350 psi 4cm shooting distance 5µg plasmid DNA

E-H: Show corresponding brightfield images.

Arrows indicate fluorescing cells (A-D) and gold particles (E-H).

**Figure 6.4 LDH assay carried out on cells for 6days post bombardment**

There was no significant difference between control cells which were not bombarded and cells bombarded at either the 3cm or 6cm shooting distance with regards to LDH levels.

6.2.5 Modification of coating and particle preparation, analysis in BEAS-2B cell line.

Due to the slow growing nature of LA4 cells it was then decided to further refine the technique, now that it had been shown to work, in a smaller but faster growing human cell line, BEAS-2B. Also the plasmid used so far was cycD1-GFP, which as previously explained, is reliant on being switched on during the D1 stage of the cell cycle. This mitigates some of the advantage of using a technique such as particle bombardment in the instance where you want your plasmid of choice universally expressed at all times in all cells. Therefore it was decided to utilize a different plasmid, pMGFP, which is a GFP plasmid made containing a CytoMegloVirus (CMV) promoter. The GFP is different to the GFP used in the CyclinD1-GFP plasmid and is known as Monster GFP and is more brightly luminescent under fluorescent light than cycD1 GFP. It is a constitutively expressed reporter plasmid encoding also for GFP, but of a different and brighter variety than that found in the cycD1-GFP plasmid.

Both the cell type and new plasmid were tested together to examine feasibility initially and the protocol adapted to include other literature cited recommendations (Hagio, 1998), Section 2.2.13.

BEAS-2B cells were tested under 900psi with different shooting distances, differing numbers of shots and differing times of analysis. Results showed that the new coating technique and new plasmid were both effective (Figure 6.5). By t=24hr post transfection the cells were clearly expressing the GFP plasmid and it could be seen that one shot of bombardment was effective, with two shots resulting in much more cell damage. It also showed that a 24hour period was sufficient for detectable plasmid expression. Compared to the previously employed plasmid, cycD1-GFP, the pMGFP plasmid proved to be visually easier to detect and far brighter upon viewing.
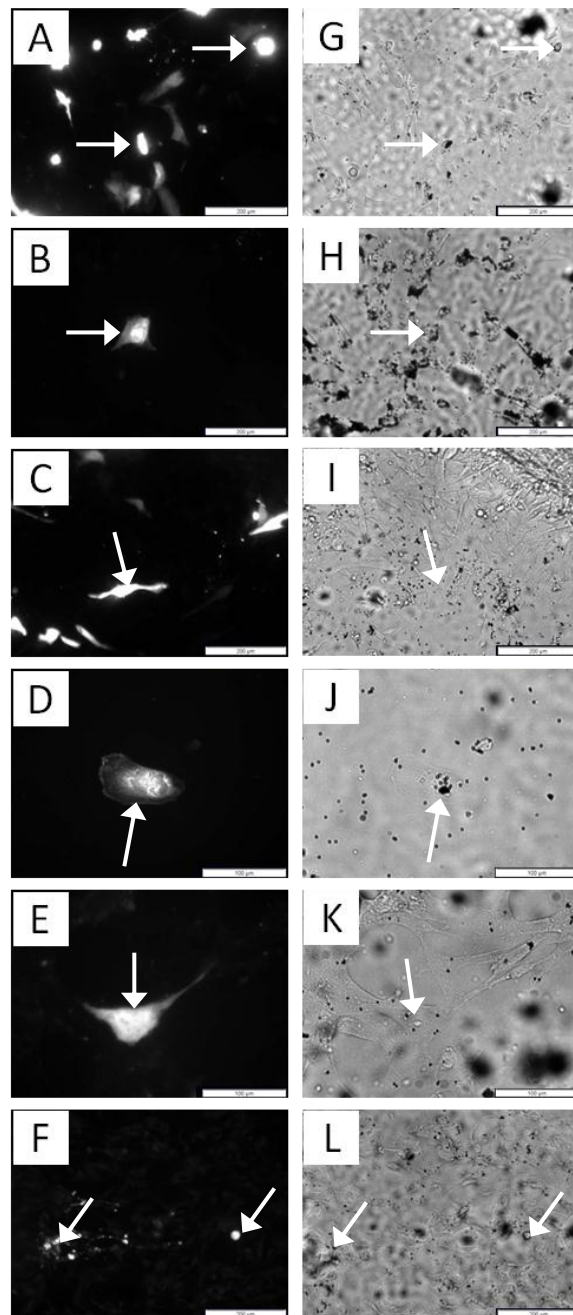
Figure 6.5 BEAS-2B cells transfected with the pMGFP plasmid

Cells seeded with 1×10^7 cells 24hr before treatment on Fibronectin coated coverslips.

A: 900psi; 1 shot 5µg DNA coated Au; shooting distance 3cm; Imaged 24hours later.

B: 900psi; 1 shot 5µg DNA coated Au; shooting distance 3cm; Imaged 96hours later.

C: 900psi; 1 shot 5µg DNA coated Au; shooting distance 4cm; Imaged 24hours later.

D: 900psi; 1 shot 5µg DNA coated Au; shooting distance 4cm; Imaged 24hours later.

E: 900psi; 2 shot 5µg DNA coated Au; shooting distance 3cm; Imaged 24hours later.

F: 900psi; 2 shot 5µg DNA coated Au; shooting distance 4cm; Imaged 24hours later.

G-L: Show corresponding brightfield images.

Arrows indicate Fluoresence (A-F) and gold particles (G-L).

6.2.6 Validation of technique in different cell types

BEAS-2B, MLE-12 and MAEC lung cells were then seeded for bombardment under the optimised conditions. Bombardment was carried out in 35 mm^2 tissue culture dishes. Cells were approximately 90% confluent. The target area of the gene gun was estimated to be approximately 20% of the surface area of the dish. As it was not possible to isolate this specific area for FACS analysis the percentage transfected and viability reported is of the entire population of cells in the Petri dish, not just cells which actually received particles from the bombardment process. Cells were then analysed for GFP expression by both FACS analysis and fluorescence microscopy.

The FACS analysis gave the ability to monitor the percentage of cells transfected and helped determine the percentage viability of the cells post bombardment (Figure 6.7 and Figure 6.8). The percentages of cells transfected per cell type were as follows: BEAS-2B cells 5.74 ($\pm$ 3.5) % transfected; MLE-12 cells 7.11 ($\pm$ 3.2) % and; MAEC cells 5.04 ($\pm$ 3.6) %.

The viability of the cells was also analysed. Because the MAECs were bombarded twice, the procedure was relatively harsh on these cells with only 58.98 ($\pm$ 9.15) % of cells remaining viable at t=24hr post bombardment, which was significantly different from the control. The treatment was less damaging to MLE-12 (86.13$\pm$4.166) and BEAS-2B cells (88.94$\pm$4.42% viable).

Fluorescence microscopy then confirmed the FACS data with pMGFP clearly visible in bombarded cells as indicated (Figure 6.9). Au particles are also clearly visible in the transfected cells. Control cells showed no green or auto-fluorescent cells.

MAECs were also grown in ALI prior to being subjected to bombardment. The method resulted in transfection of the cells but had a number of inherent difficulties. Establishment of the ALI takes place on a 6 well insert in order to allow a large enough target area to be exposed to the blast. The more regular 24well inserts used in these applications are too deep and narrow to allow use in bombardment and are also very difficult to correctly align in the chamber outside of a plate which could not fit due to space limitations. The 6well inserts have a large surface area, and are shallower making them more appropriate. However the bases of the inserts were constantly damaged by the technique, resulting in the cells having to be returned to submerged culture and losing their ALI status. Consequently it was decided not to pursue this method further. Of note however is that the trial of the method on the cells did return transfected cells when examined 24hours post bombardment when returned to submerged culture (Data not shown).
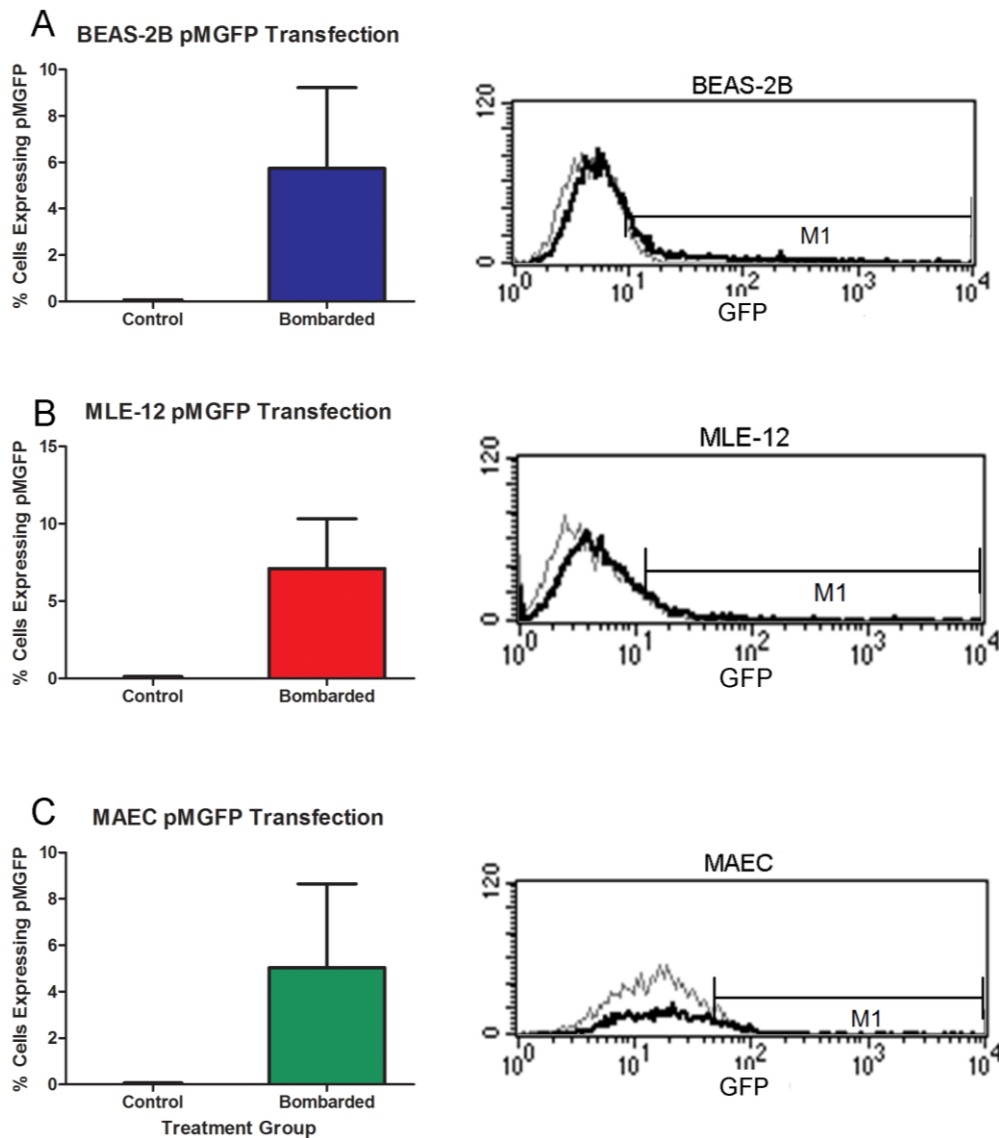
Figure 6.7 Transfection of cells was quantified by FACS analysis

MLE-12 cells were shot once with 900psi pressure on the 3cm stage, returned to a submerged culture state with fresh media and then analysed at t=48hr post treatment. BEAS-2B cells were shot once with 900psi pressure on the 3cm stage, returned to a submerged culture state with fresh media and then analysed at t=48hr post treatment. MAEC cells were shot twice with 900psi pressure on the 3 cm stage, returned to a submerged culture state with fresh media and then analysed at t=48hr post treatment. Shooting the MAEC cells twice decreased the viability of the overall population of cells significantly but also greatly increased the percentage of cells successfully transfected with the plasmid compared to one shot (data not shown). Cells were then analysed for GFP expression by FACS analysis. The percentages of cells transfected per cell type were as follows: BEAS-2B cells (A) 5.74 ($\pm$ 3.5) % transfected; MLE-12 cells (B) 7.11 ($\pm$ 3.2) % and; MAEC cells (C) 5.04 ($\pm$ 3.6) %.Also shown is a sample FACS fluorescence graph showing treated populations (black line) and control populations (grey line).
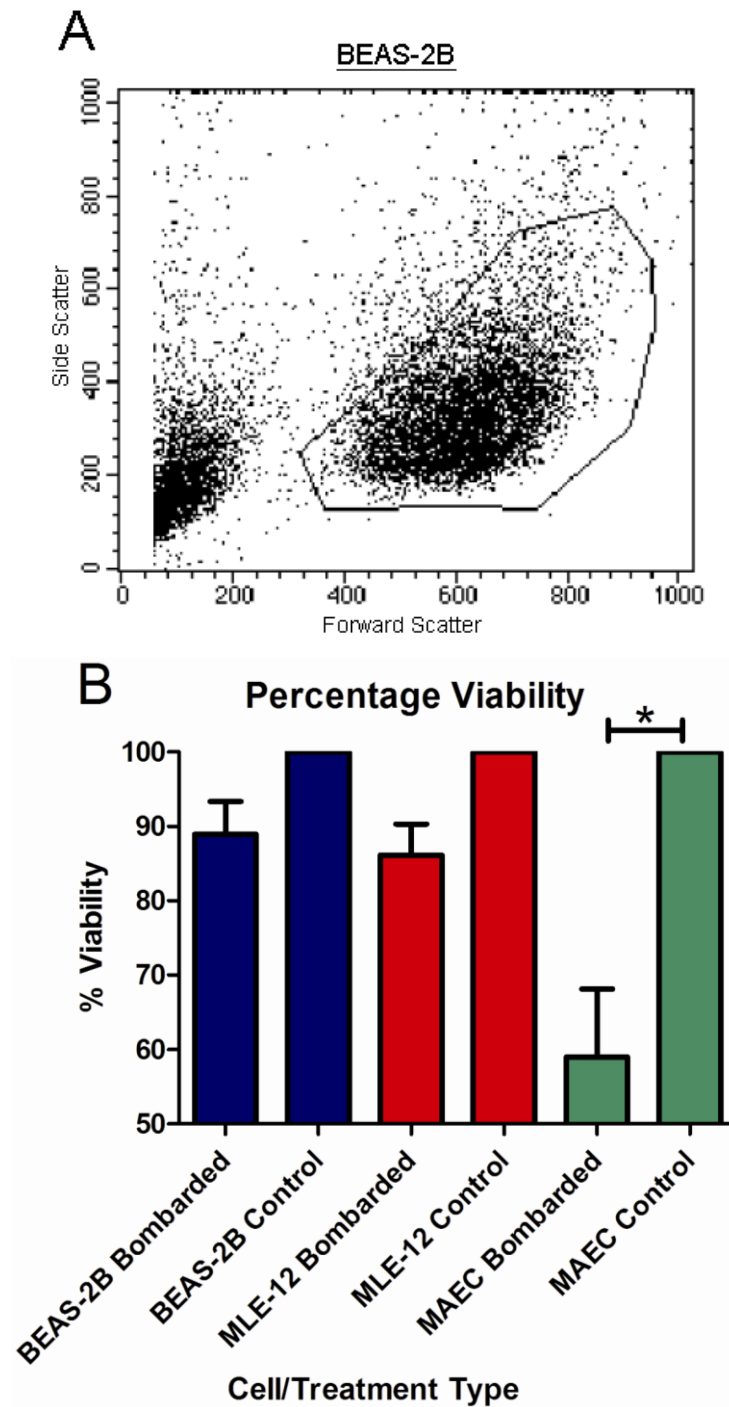
Figure 6.8 Viability of cells post bombardment

The control cells of each experiment were gated as shown in the Scatter plot (A) and this gate was applied to the bombarded cells to determine the percentage viability and the percentage of viable transfected cells. The percentage viability was then analysed for each cell type (B). One shot from the gene gun did not significantly affect viability of the BEAS-2B or MLE-12 cell populations. However, the MAECs were bombarded twice in order to increase the efficaciousness of the technique, but at a significant cost to the viability of the overall cell population (t-test analysis, $p < 0.05$).
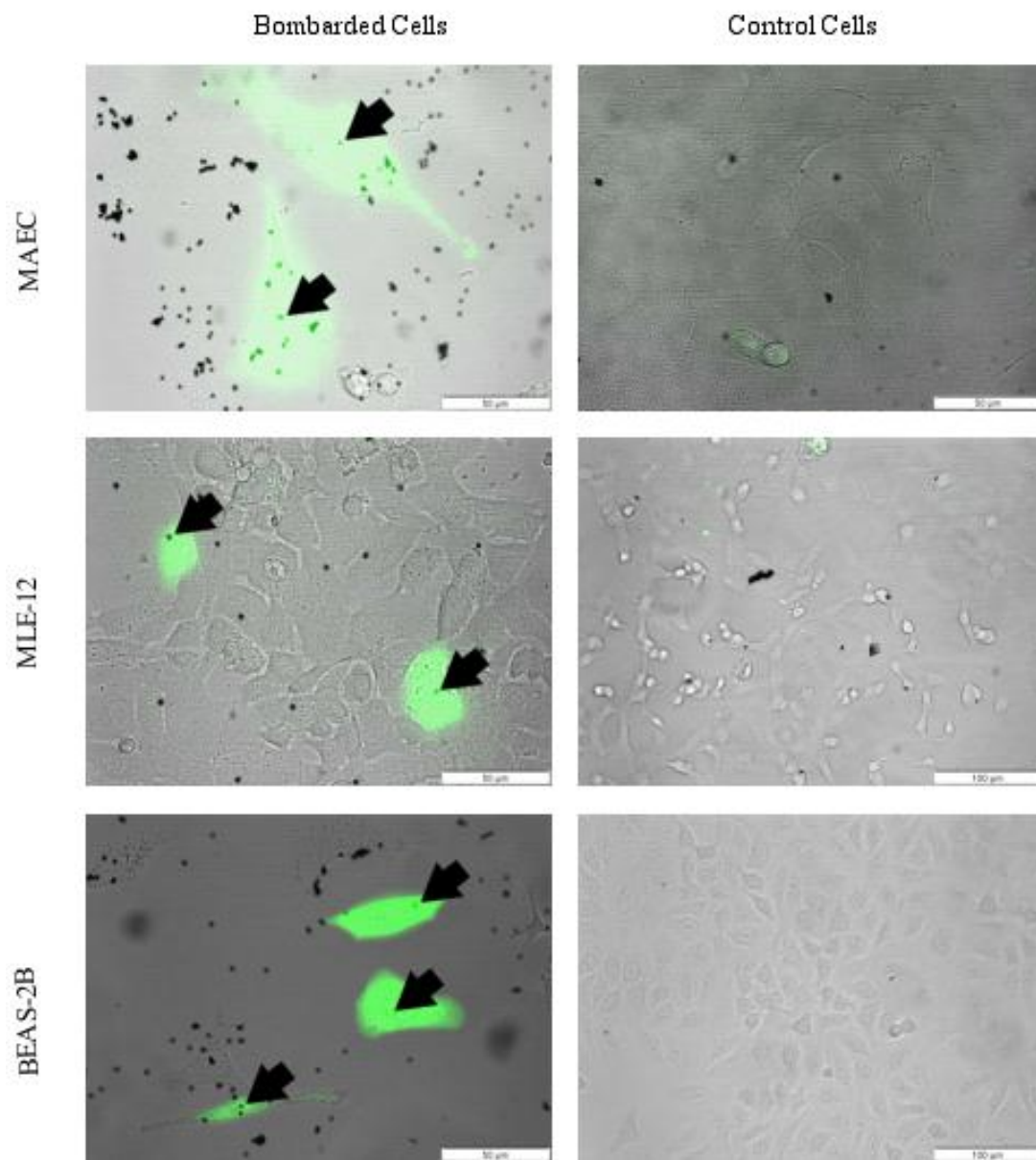
Figure 6.9 Fluorescence microscopy confirmation of GFP expression.

Fluorescence microscopy confirmed visually the expression of the GFP expressing pMGFP plasmid in the different cell types. Also clearly visible in the cells are the plasmid coated gold particles.

6.3 siRNA

The first step before delivering siRNA *in vivo* was to determine the ability of siRNA to down regulate gene expression *in vitro* in characterised cell lines. This began by examining E-cadherin knockdown in the A549 cell line and progressed to knockdown of BMPR-II in BEAS-2B cells and the identification of a successful housekeeper candidate. It was envisaged that knockdown of E-cadherin may lead to further information in the role of BMP4 in remodelling and that the knockdown of BMPR-II may, by removing the primary binding site of action for BMP4 after insult, prevent or stop a cycle of inflammation and damage *in vivo*.

6.3.1 siRNA in the targeting of E-cadherin in A549 cells.

6.3.1.1 Transfection efficiency of siRNA

In order to determine if the siRNA molecules could be successfully delivered to the A549 cell line it was first decided to test the capability of the transfection reagent to carry the siRNA into the cells. To do this, cells were set up in 24 well tissue culture flasks and transfected with negative control siRNA molecule (Sect.2.2.19). This negative control siRNA was a sequence of nucleotides that was scrambled and tested to ensure it has no known homology to any mammalian genes. This negative control siRNA also had an Alexa-488 tag attached to allow visualisation of the molecule by fluorescence microscopy and detection by FACS. The uptake of siRNA into the cells was recorded at t=24hr and t=48hr periods. FACS analysis demonstrated that in excess of 90% of the cells (91.45±.099% averaged over a 24 and 48 hour period) were successfully transfected with the Alexa-488 tagged negative control siRNA (Figure 6.10). A549 cells were then transfected with E-cadherin siRNAs along with a full set of treatment controls. These included (i) scrambled siRNA negative control, (ii) a positive control siRNA targeting MAPK1- a validated siRNA shown to knockdown the levels of expression of MAPK1 in human and mouse *in vitro* and (iii) a transfection reagent only control. Cells were examined by bright field microscopy 24 hours post treatment to determine if any morphological difference could be observed between the different treatments and to observe the health of the cells in response to the Hiperfect transfection reagent. The different treatments showed no discernable morphological differences or effects from exposure to transfection reagent (Figure 6.11(A-E)). Fluorescence microscopy also confirmed the successful uptake of siRNA into the cells as was seen with FACS analysis (Figure 6.11 (F)).

6.3.1.2 Quantitative analysis of E-cadherin knockdown by QPCR

E-cadherin knockdown was attempted using two separate siRNA molecules targeting separate regions of the E-cadherin gene. QPCR was then used to determine the success of the housekeeper and the level of E-cadherin knockdown achieved. Analysis of the housekeeper used in this experiment, β-Actin, showed that the level of the expression detected varied over the course of the treatments. As can be seen in Figure 6.12, the housekeeper standard curve was successful (Figure 6.12 (A) with an R^2 value of 0.9991. An R^2 value in excess of 0.95 would have been acceptable). The melting curve analysis of the products also verifies the specificity of the reaction (Figure 6.12 (B)). The melting temperature for a particular primer pair should all be the same. The shape and position of the melting curve are a function of the GC/AT ratio, length and sequence. As a result it can be successfully employed in the distinguishing of amplified products separated by less than 2°C in melting temperature. This means in practice that different melting temperature curves will result where there are primer dimers, mis-priming or contamination (Ririe et al., 1997). As sybr-green does not differentiate DNAs Tm (melting Temperature), the melting curve acts as an important quality control. However the cycle thresholds (CTs) of the different treatments varied considerably amongst the various treatments and controls (Figure 6.12 (C)). The CT is defined as the PCR cycle at which the fluorescent signal of the reporter dye crosses an arbitrarily placed threshold. By presenting data as the CT, one ensures that the PCR is in the exponential phase of amplification. The numerical value of the CT is inversely related to the amount of amplicon in the reaction (i.e., the lower the CT, the greater the amount of amplicon) (Schmittgen and Livak, 2008).

Compared to the No Treatment control (20.42±0.157) both the non-silencing siRNA (22.13±0.321) and the Hiperfect only control (22.63±0.066), differed by greater than 1.5 CT from the No Treatment control showing that both the Hiperfect alone and in the presence of siRNA was inducing a significant change in the level of the β-actin housekeeper. Both E-cadherin siRNA(1) (23.5±0.047) and E-cadherin siRNA (2) (32.44±0.082) differed greatly from the No Treatment control, with the E-cadherin siRNA(2) also differing significantly from the non-silencing siRNA control.

This was further confirmed by the analysis of the Genomic Equivalents (GEs), where large variation occurred across the different treatments (No treatment 6530±738.9; Non-silencing siRNA 2076±426.2; Hiperfect only 1405±63.76; E-cadherin siRNA (1) 775.1±25.1; E-cadherin siRNA (2) 1.635±0.09) (Figure 6.12 (D)).

One-Way ANOVA and Tukey posttest analysis was also carried out on both CTs and GEs, also showing the differences to be statistically significant, $p<0.0001$, a full breakdown of which can be seen in Table 6.1.

Definitive analysis of the knockdown, if any, of E-cadherin in the cells could not be reliably constructed.

6.3.1.3 Immunofluorescence analysis of E-cadherin knockdown

Immunofluorescence analysis was carried out on the cells, examining both the level of E-cadherin expression and any changes in localisation. However no changes in the either the abundance or localisation of the expression in cells was noted in any of the treatment groups (Data not shown).
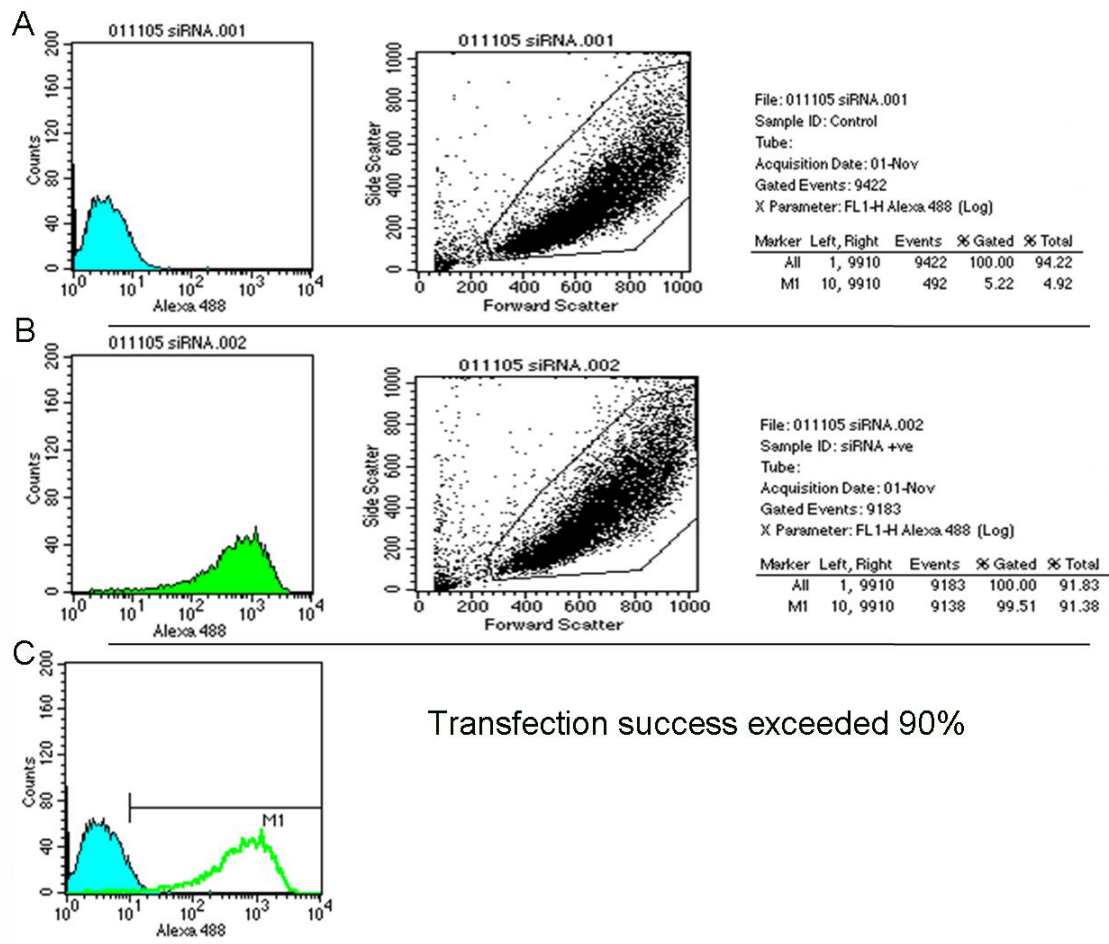
Figure 6.10 FACS analysis of siRNA transfection efficiency Transfection efficiency of siRNA using Hiperfect transfection reagent-determined by FACS analysis to give 91.45±0,099% transfection averaged over a 24hr and 48hr period. (A) The acquisition graph and scatter plot of normal non transfected A549 cells. (B) The acquisition graph and scatter plot of the A549 cells transfected with a negative control -488 siRNA. (C) The shift in populations from non-488 expressing (A) to -488 expressing (B).
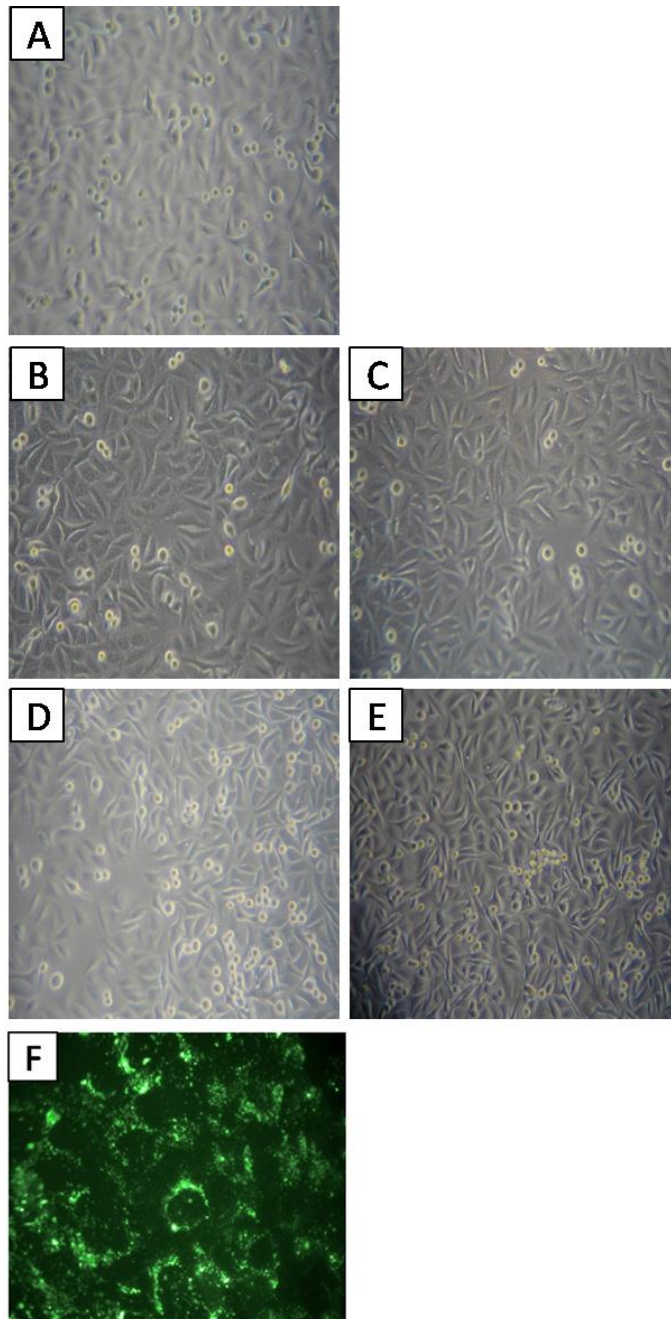
Figure 6.11 Brightfield and Fluorescent analysis of siRNA transfection
Images A-E inclusive shows the lack of morphological effect on the transfection on A549 cells undergoing various siRNA treatments. (A) Untreated cells, (B) Hiperfect treated cells, (C) positive control (MAPK1) treated cells, (D) and (E) are both treated with siRNA targeting E-cadherin. No major morphological change was visible with any of the cells, indicating that neither the Hiperfect nor Hiperfect/siRNA combination was having a deleterious effect on the cells. (F) Cells expressing a large amount of 488 tagged siRNA, mostly clustered in and around the cell nuclei, following successful transfection and imaged using fluorescent microscopy.
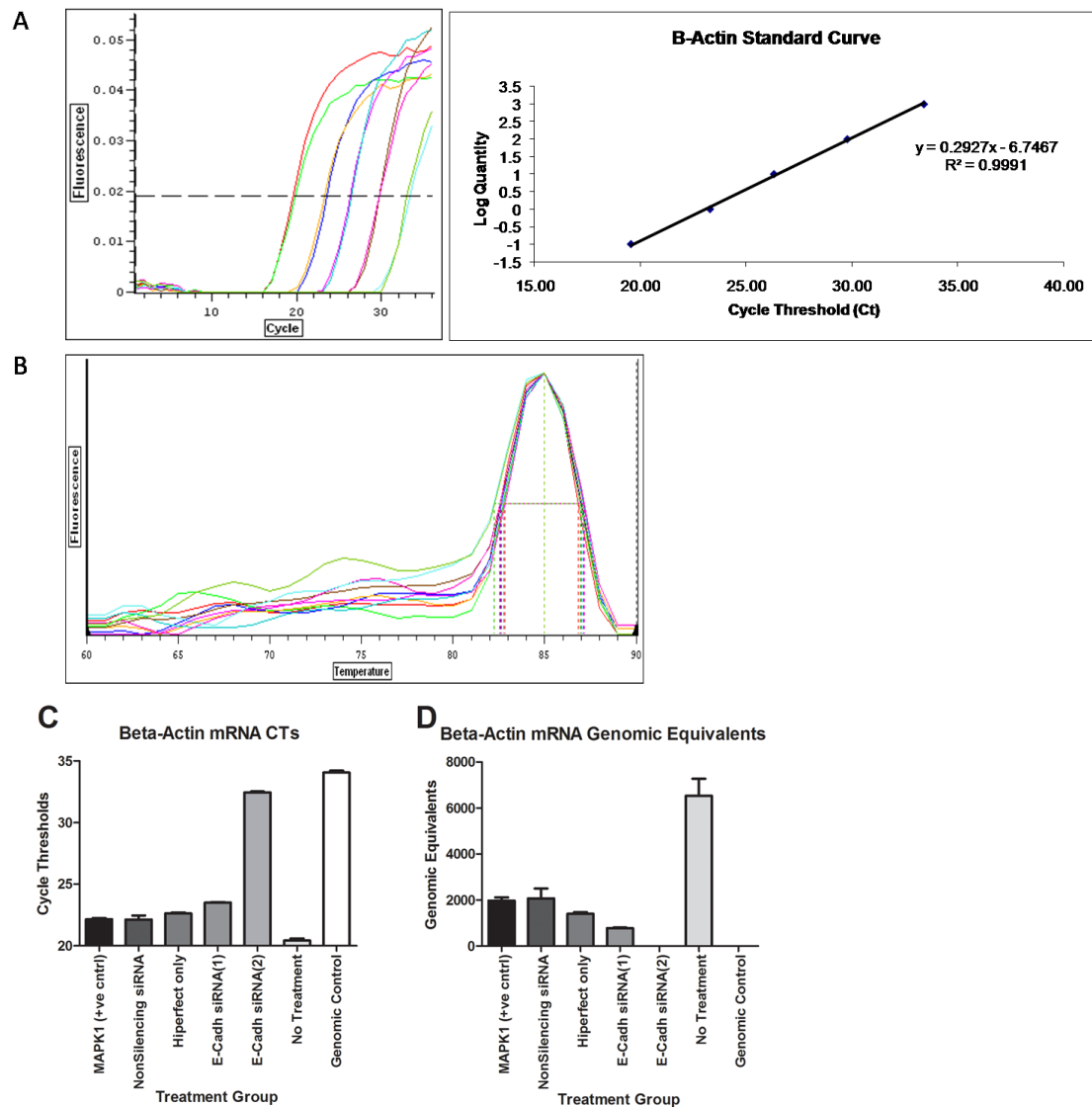
Figure 6.12 QPCR analysis of β-Actin housekeeper gene (A) shows the CTs of the different concentrations of the β-Actin housekeeper, with the CTs appearing as expected, approximately every 1.5-2CTs, and the resulting standard curve showing a high performance standard curve (R^2=0.9991). A melting curve (B) was also carried out to further analyse the performance of the housekeeper. It showed a successful melting performance curve, with all the curves melting together at 85°C, indicating no impurities or performance issues with the standards or the primers. The CTs of the β-Actin (C) between the No Treatment controls and the various treatments were however variable to an unacceptable level (>1.5 CTs difference for the Housekeeper shows a change in housekeeper due to treatment, therefore cannot be used as a housekeeper). This difference in behaviour can also be seen in the difference in the genomic equivalents across the different groups (D).

One Way ANOVA	Cycle Threshold		Genomic Equivalents	
	Yes P<0.0001	***	Yes P<0.0001	***
Tukey's Multiple Comparison Test	**Significant? P < 0.05?**	**Summary**	**Significant? P < 0.05?**	**Summary**
MAPK1 (+ve cntrl) vs NonSilencing siRNA	No	ns	No	ns
MAPK1 (+ve cntrl) vs. Hiperfect only	No	ns	No	ns
MAPK1 (+ve cntrl) vs. E-Cadh siRNA(1)	Yes	***	No	ns
MAPK1 (+ve cntrl) vs. E-Cadh siRNA(2)	Yes	***	Yes	*
MAPK1 (+ve cntrl) vs. No Treatment	Yes	***	Yes	***
Non-Silencing siRNA vs. Hiperfect only	No	ns	No	ns
Non-Silencing siRNA vs. E-Cadh siRNA(1)	Yes	***	No	ns
Non-Silencing siRNA vs. E-Cadh siRNA(2)	Yes	***	Yes	*
Non-Silencing siRNA vs. No Treatment	Yes	***	Yes	***
Hiperfect only vs. E-Cadh siRNA(1)	Yes	*	No	ns
Hiperfect only vs. E-Cadh siRNA(2)	Yes	***	No	ns
Hiperfect only vs. No Treatment	Yes	***	Yes	***
E-Cadh siRNA(1) vs. E-Cadh siRNA(2)	Yes	***	No	ns
E-Cadh siRNA(1) vs. No Treatment	Yes	***	Yes	***
E-Cadh siRNA(2) vs. No Treatment	Yes	***	Yes	***

Table 6.1 One-Way ANOVA and Tukey post-test analysis of CT and GE.

One-Way ANOVA and Tukey post-test statistical analysis of CT and GE differences between the differing control groups. The Genomic control was not included in this analysis.

6.3.2 siRNA knockdown of BMPR-II in MLE cells.

6.3.2.1 QPCR analysis of BMPR-II expression silencing

The MLE cell line was used to analyse the ability of siRNA to knockdown the expression of BMPR-II *in vitro*. A number of candidate housekeepers were examined (Table 6.2) before selection of 18S. It was found to be the most consistent over all treatment types and standard deviation from the average CT never exceeded 1.5 CTs. For attaining BMPR-II knockdown, two siRNAs targeting BMPR-II were used. Cells were harvested at the appropriate timepoints, t=12hr and t=24hr, and RNA was isolated. Determination of percentage knockdown was completed by comparing the expression level in every treatment group to the negative control siRNA at the 12 and 24 hour timepoints by using the ΔCT method ($2^{-\Delta\Delta C_T}$= [(C_T gene of Interest- C_T Internal control) sample A]-[(C_T gene of Interest- C_T Internal control) sample B] where sample B is the control) (Figure 6.13 (A)). It is acknowledged that presenting data as a fold increase or decrease as derived by ΔC_T analysis can be more relevant that commenting on the copy number variation of a gene (Livak and Schmittgen, 2001). The results here showed that although most of the siRNA treatments targeting BMPR-II showed knockdown at t=12hr and t=24hr timepoints, the level of BMPR-II expression in the No treatment cells appeared lower which would not be expected. As a result it was decided to look at comparing the expression of BMPR-II in all the treatment groups to the No Treatment controls (Figure 6.13 (B)). Results showed that the levels of BMPR-II in all treated cells were higher than in the No Treatment cells across all treatment groups and in many cases multi-fold increases were apparent, Table 6.3(B). Initial comparison to the scrambled siRNA control had shown that same treatment to have resulted in a knock down in expression of BMPR-II in the case of a number of different combinations of siRNA treatment including BMPR-II_1 20 24 (BMPR-II siRNA; siRNA molecule 1; 20nM; analysed at t=24hr); BMPR-II_1 50 24; Pooled siRNA at t=12hr and t=24hr and all no treatment cells against the different combinations of niegative control siRNA at t=12hr and t=24hr (Figure 6.13 (A) and Table 6.3(A)).

MAPK1, the positive control knockdown, used as a positive control to determine if the transfection procedure worked showed successful knockdown at different concentrations at all timepoints with A) 20nM siRNA effecting a -0.07±0.72 fold decrease at t=12hr and -1.825±0.81 fold decrease at t=24 and; B) 50nM siRNA effecting a -0.428±169 fold decrease at t=12hr and a -0.298±0.18 fold decrease at t=24hr (Figure 6.14).

6.3.2.2 Western blotting analysis of silencing of BMPR-II

In order to validate the level of silencing seen by QPCR a second method of analysis, preferably quantitative, is required. In this instance it was decided to try confirming the knockdown achieved at an mRNA level by looking for knockdown at a protein level in the treated cells by means of Western Blotting. A number of commercially available antibodies successfully bind to BMPR-II in immunofluorescence studies and a number claim to successfully bind to murine BMPR-II by western blotting. Ideally one antibody that could do both would be used, allowing confirmation quantitatively by Western Blotting and visually by immunofluorescence. A number of commercially available antibodies were assessed for their ability to detect BMPR-II by western blotting; however none proved successful (Data not shown). The only limited success was the detection of a 37kDa isoform of the BMPR-II protein by Abgents BMPR-II antibody (Abgent AP2006a). It successfully detected the isoform in two different mouse cell lines, LA4 and MLE, in primary isolates, MAEC cells, and in human A549 cells (Figure 6.15). The band detected was confirmed to be an isoform of the BMPR-II antibody through correspondence with the antibody manufacturer. However this antibody could not be successfully employed as for the purposes required it couldn't validate silencing of the full length protein by siRNA.

Housekeeper Candidate	Pass/Fail
Beta-Actin	Fail
GAPDH	Fail
MTAP	Fail
PLUNC	Fail
SAPA1	Fail
18S rRNA	Pass

Table 6.2 Candidate Housekeepers

Ribosomal 18Swas the onlyhouse keeper which could be successfully employed as an internal control for the purposes of analysis the differences in expression levels in the genes of interest.
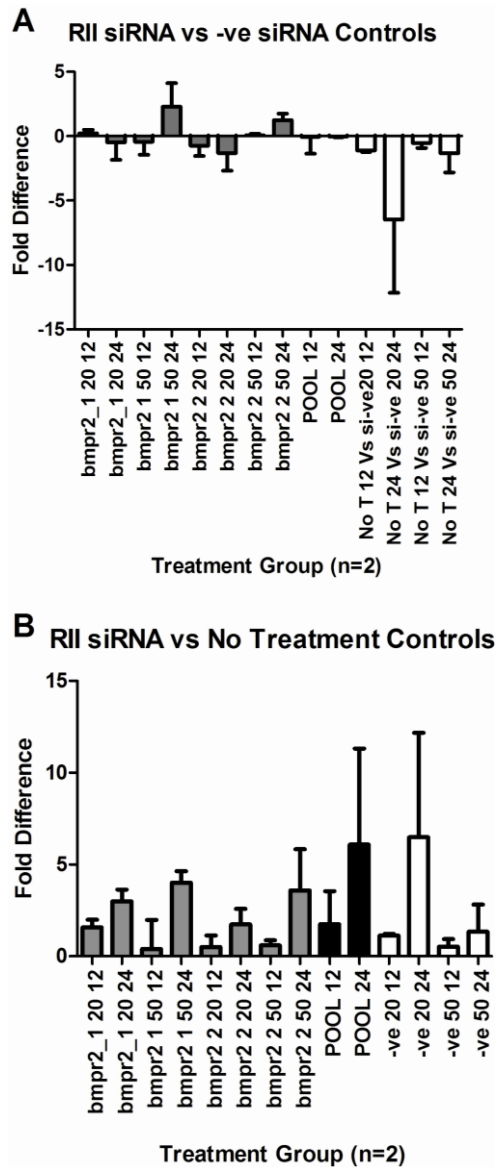
Figure 6.13 BMPR-II mRNA levels after siRNA treatment
(A) shows the level of BMPR-II fold differences, determined using the ΔCT method, in the various treatments compared to the negative siRNA control treatment. This is regarded as the best indicator of behaviour of the siRNA effectiveness. However comparison to the No Treatment cells in A shows that cells that received no treatment whatsoever had a lower level of BMPR-II than any treated with BMPR-II siRNA. In order to further examine this it was decided to also look at the effect of the siRNA molecules in all treatments by comparing them to the No Treatment cells as controls (B), where it can be seen, post treatment, that all the treatments actually resulted in an increase in the amount of BMPR-II mRNA. This indicates that the Hiperfect transfection reagent, the siRNA molecule, or a combination of the two, in and of themselves, have an impact on the BMPR-II mRNA expression levels in the cells.

(A) BMPR-II mRNA compared to -ve control siRNA			(B) BMPR-II mRNA compared to No Treatment Control		
Treatment	Fold Difference	S.E	Treatment	Fold Difference	S.E
bmpr2_1 20 12	0.2323	0.2578	bmpr2_1 20 12	1.581	0.413
bmpr2_1 20 24	-0.4832	1.362	bmpr2_1 20 24	2.999	0.6275
bmpr2 1 50 12	-0.4446	0.9893	bmpr2 1 50 12	0.3998	1.58
bmpr2 1 50 24	2.293	1.82	bmpr2 1 50 24	4.011	0.6232
bmpr2 2 20 12	-0.7426	0.8048	bmpr2 2 20 12	0.4941	0.6399
bmpr2 2 20 24	-1.314	1.366	bmpr2 2 20 24	1.732	0.8457
bmpr2 2 50 12	0.0747	0.1057	bmpr2 2 50 12	0.5944	0.2765
bmpr2 2 50 24	1.261	0.4761	bmpr2 2 50 24	3.587	2.238
POOL 12	-0.0477	1.311	POOL 12	1.743	1.805
POOL 24	-0.0219	0.0468	POOL 24	6.079	5.24
No T 12 Vs si-ve20 12	-1.116	0.107	-ve 20 12	1.116	0.107
No T 24 Vs si-ve 20 24	-6.48	5.686	-ve 20 24	6.48	5.686
No T 12 Vs si-ve 50 12	-0.5227	0.4062	-ve 50 12	0.5227	0.4062
No T 24 Vs si-ve 50 24	-1.329	1.494	-ve 50 24	1.329	1.494

Table 6.3 Fold Difference in BMPR-II expression levels compared to –ve siRNA control and No Treatment control.
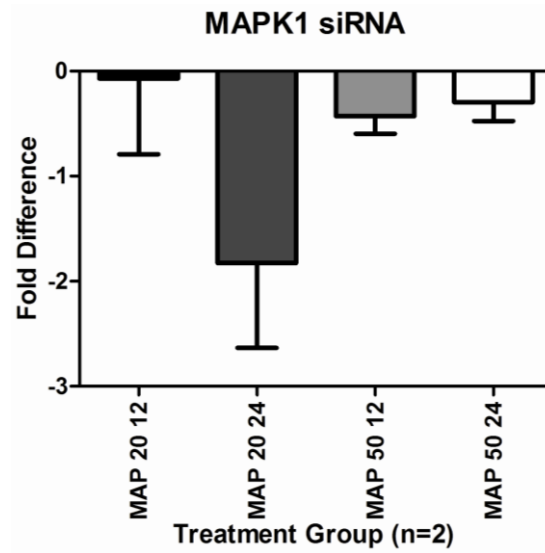
Figure 6.14 MAPK1 siRNA positive control expression levels
MAPK1 was used as a positive control in the experiments. This shows that at a concentration of 20nM, the MAPK1 siRNA successfully achieved an almost 2 fold knockdown of the target RNA compared to the negative control siRNA.
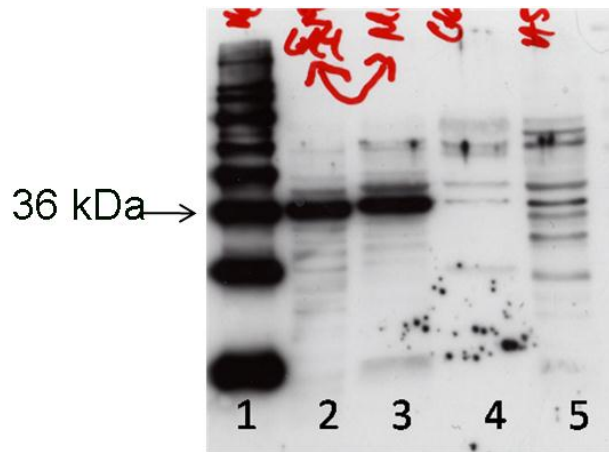
Figure 6.15 Western blot analysis of a BMPR-II antibody Of the range of commercially available BMPR-II antibodies tested, only one antibody was capable of protein detection by Western (Abgent AP2006a). The western blot above shows the antibody detecting a BMPR-II protein band at approx. 37kDa in 4 different cell types (Lane 1= Magic Marker MWL, 2=MLE protein sample, 3=LA4 protein sample, 4= MAEC protein sample, 5= A549 protein sample). The full length of the BMPR-II protein is approx 70-80kDa in mice. The antibody generated (rabbit polyclonal) was detecting heart lysate BMPR-II in mice at approx 115kDa. However as seen above the only band reliably detected across species with a strong signal to noise ratio and in different cell types was at approx 37kDa. In conjunction with the antibody manufacturer, Abgent, it was determined to be a 37kDa isoform of the full length BMPR-II protein.

6.4 Discussion:

6.4.1 Particle Bombardment

As a method for the transfection of cells, particle bombardment was successful and we reported for the first time the successful transfection of primary mouse airway epithelial cells using this method. However limitations are evident and refining of the device would be required for in-vivo work. Comparison work in our lab with various lipofection techniques and with the use of viral vectors (Gilbert et al., 2008) showed that with cell lines there exists a set of conditions returning higher transfection ratios with increased viability levels over that achieved by particle bombardment. However particle-mediated gene transfer was more efficient in MAECs than AAV5, Lipofectamine 2000 and SuperFect. Lentivirus pseudotyped with the vesicular stomatitis virus glycoprotein was the most efficient gene transfer method for both MAECs and BEAS-2B cells while AAV6 was most efficient for MLE-12 cells.

Physical methods of gene delivery can circumvent many of the disadvantages associated with viral and non-viral methods such as immunogenicity, potential for oncogene activation and requirements for dividing cells and expression of specific receptors. The experimental procedure is relatively harsh on the cells and parameters require optimisation to minimise cell damage. Cells exposed to vacuum for prolonged periods become stressed, hypoxic and may die. The helium blast used to transfer the particles also has a blast effect on the cells. The spread of particles before impact must also be accounted for. When the microparticles are launched at the target site, they have to cover a distance of at least 3cm before impact with the cells making it difficult to specifically target areas on the culture dish and only a proportion of the dish can be targeted. Only a subpopulation of total population harvested from the dishes for analysis after bombardment were actually targeted and extrapolation of the data would show a 5x increase in the level of cells transfected if only targeted cells were counted (hypothetically giving MLE-12 35.55% transfected; BEAS-2B 28.7% transfection; MAEC 25.2% transfected of the targeted cells). While cell damage was minimal with MLE-12 cells and BEAS-2B cells, the procedure was lethal in almost 50% of MAECs. Further optimisation of experimental parameters may reduce the extent of cell damage. In tandem with a complimentary technique, such as FACS Cell Sorting where a small population of successfully transfected cells can be isolated from a larger, un-transfected, population, lower transfection rates are not so debilitating to the technique and would allow for the study of highly pure populations of transfected

cell lines over many generations. Although this may not be feasible for primary cells where their defining primary characteristics may be lost, in other difficult to transfect cell lines this would be possible for as long as the plasmid stayed successfully integrated in the genome. In the case of primary cells it would allow for analysis of protein and RNA from a purified population of plasmid transfected cells, where it is known that the plasmid has been successfully integrated and expressed in the cell. This brought the use of the gene gun device to its peak set of uses in the lab, for rapid testing of a plasmid and for successful transfection of a difficult cell type and was routinely used to rapidly test newly designed plasmids in conjunction with other steps such as restriction digests. However it also reveals its limitations. Although there are other variations of the Gene Gun available it has a number of inherent drawbacks.

Although inert materials can be used as microcarriers, in an ideal transfection no external substances bar the material of interest itself would be introduced into the cell, lowering cost, speeding up the process, removing any unforeseen cellular responses to the materials and speeding up the regulatory process for the approvement of a potential therapy. The mechanism doesn't allow for targeting of discreet internal areas of interest in an *in vivo* scenario, there are devices which do not require a vacuum in which to work but also have other constraints. Ideally a device would be small enough to be intubated or delivered via a scope into an animal with the ability to specifically target a precise area. This would allow for dedicated bombardment of a particular cell type, a cancer cluster or a particular membrane or epithelial layer.

6.4.2 siRNA

siRNA undoubtedly has potential for potent *in vivo* applications, as seen by the fact that different siRNA molecules are currently or have already undergone clinical trials (Section 6.1.1). They have the potential for targeting at the RNA level inflammatory triggers, receptors or products, thereby eliminating an adverse reaction and can either by transient or long-term in their activity. However in our hands and on the pathway targeted siRNA technology proved to be an unwieldy and time-consuming technique to successfully affect a high rate of detectable targeted knockdown. Added to this the inherent difficulties involved in not only getting the product successfully into the correct region of the lungs but doing so and monitoring cell uptake and localised cell effect while overcoming cell uptake problems without the use of a stabilising transfection reagent such as Hiperfect, and it was decided that for the goals of this project that protein delivery may be a more successful avenue to follow. If a

transfection reagent were to be used for *in vivo* delivery to a damaged system, the issues of extra burden and unintended innate reactions after repeat delivery were likely to become major obstacles. Other issues with siRNA such as off-target effects, as encountered in the hunt to identify a successful housekeeper for *in vitro* studies lead to a concern that while the delivery would be localised, off target effects induced in the lung such as cytokine production or cessation of such, could lead to other systemic or localised problems that may be difficult to detect under the auspices of this study.

6.5 Conclusion

Particle bombardment proved to be a useful tool for the *in vitro* analysis of plasmid integration into cell lines and difficult to transfect primary cells. As a potential tool however for the delivery of DNA *in vivo*, technical difficulties with adaptation for *in vivo* use were beyond the scope of this project and there were associated issues with the delivery of a carrier substance and the effect of burdening the lungs with multiple loads. This work led to a separate successful project on physical delivery of therapeutics to lung *in vivo* (O'Dea et al- unpublished data). siRNA was also examined, and although it lends itself as a tool for *in vivo* delivery, difficulty in executing targeted knockdown in an *in vitro* setting meant that it would be more difficult to not only effect knockdown *in vivo* with the various physical barriers that the siRNA would encounter but also assessing its efficaciousness and the ideal of not having to use a transfection reagent for delivery *in vivo* meant that it was ruled out for progression to *in vivo* work. Both of these decisions, relating to both particle bombardment and siRNA, were also taken with the knowledge that tests on protein, both for its suitability and potential in an *in vivo* setting meant that *in vivo* work would focus on aerosol delivery of protein compounds to the lung.

7 *Ex Vivo* and *In Vivo* Assessment of Aerosolised Protein Therapeutics

7.1 Introduction

Current progress in this project identifies aerosolised proteins as being the most likely strategy to efficiently and quantifiably be able to induce a therapeutic effect in an *in vivo* situation. As shown in Chapter5, protein molecules are capable of withstanding nebulisation intact and functional. Building on the effects seen induced by BMP4 treatment in ALI (Chapter3) and in MAECS (Chapter5), and having determined that OVA induced damage was a suitable model for assessing the effect of potential BMP pathway modulators, I then proceeded with delivery of potential protein therapeutics firstly to an *ex vivo* model, followed by delivery *in vivo* to a healthy model and finally into a diseased model lung of OVA induced asthma.

With the overall aim being to assess both the potential therapeutics for effect and the mechanism of delivery for capability a series of steps were identified. Firstly ex-vivo analysis of the therapeutics instilled into isolated healthy lungs was evaluated to determine if any particular adverse reaction to the treatments was observed in the airway cells or lung parenchyma and structure. Following on from this direct aerosol delivery to

A healthy *in vivo* lung model was to be evaluated for both safety and efficacy. Analysis was to be preformed at t=4hr after delivery with careful monitoring of the animals for the duration in case of adverse reactions.

Building on this the model, progress to a longer multiday analysis of the safety of delivery in a healthy model, before;

Culminating in a multi-day analysis on the safety and efficacy of delivery in an OVA induced model of allergic asthma in BALB/c mice.

The aims were to evaluate the success of the aerosol delivery mechanism, the ability of the potential therapeutics to induce a response and to evaluate the type of response induced. BMP4 was delivered to see if it could specifically induce inflammationand pathway activation; α-BMP4 and α-BMPR-II were delivered as potential therapeutics and EGF was delivered as a control protein to ensure that the effects seen were not non specific responses to the presence of protein in the aerosol.

7.1.1 Plethysmography

During restraint testing and also during the delivery of therapeutics plethysmography was used in order to assess lung function of the subject animals. Plethysmography can be carried out on animals using various methods, from unrestrained, to restrained to anaesthetised and tracheotomized animals. Two of the major and most common

measurements of lung function that provide information on bronchoconstriction derived from plethysmography from conscious subject plethysmography are EF50 and Penh. EF50 is the measurement taken from conscious restrained animals, with physical parameters and dimensions. Penh utilises conscious unrestrained animals, but has no actual physiological parameter or unit measurement (Hoymann, 2007).

In spite of its popularity, Penh is widely condemned as a "nonsense variable", as observed differences in Penh provide no information on airway conditions due to the fact the baseline measurements do not contain any information about the airways, As such fold differences in Penh are essentially meaningless (Mitzner and Tankersley, 2003). While some studies have shown correlations with differences in pulmonary resistances, others have shown no such correlation to exist and have shown Penh to be primarily related to breathing patterns as opposed to bronchoconstrictions, and these can vary greatly between different species under different models of disease and damage (Hantos and Brusasco, 2002; Bates et al., 2004). It has also been concluded that unless lung volume and tidal volume are accurately recorded and measured, which is not possible with an unrestrained animal, Penh is not suitable as a means of evaluating bronchoconstriction in animals. It has been strongly advised that in the absence of other means of conformation of airway response to a treatment that Penh should not be accepted in publication as a method of evaluating airway reactivity or responsiveness unless there is sufficient independent confirmation of the results (Bates et al., 2004).

EF50, using restrained conscious animals however, provides a mechanism of evaluation that correlates well with invasive measurements, which are regarded as the gold standard for pulmonary function analysis in mouse models (Vanoirbeek et al., 2010). EF50 is measured in ml/sec and it is a physiological based measurement defined as the tidal flow at the midpoint of expiratory tidal volume, which is an indicator of the degree of bronchoconstriction in animal. Restrained plethysmography data has been shown to be capable of monitoring the bronchoconstriction in drug safety studies and in asthma models showing late airway responsiveness or early allergic response to inhaled allergens, or critically of interest in our studies, to show the effect of therapeutics on pulmonary endpoints and is particularly well suited to animals that are exposed to inhalation treatment (Hoymann, 2007). EF50, though not as exact as invasive forced recordings, is regarded as being especially appropriate for the studies involving the screening of respiratory effect in large numbers of animals such as used in our studies (Hoymann, 2007). The use of invasive measurements on anaesthetised unconscious animals offers more detailed and exact measurements but

is far more demanding time wise and technically, is unsuitable for use in studies with large animal numbers involved and doesn't provide data from an animal in a condition that is any way natural. Restrained plethysmography also allows for repeat analysis as often as desired of an animal over a given timeframe, meaning that response to a treatment or therapeutics can be mapped out over hours days or months in individual animals. As a result it was decided for the purposes of this study to evaluate lung function using restrained conscious animals and EF50 measurements as a means of determining bronchoconstriction and other parameters to different treatments and therapeutics. The breakdown of the other parameters is as follows

- Frequency: respiratory rate or breaths per minute.

- Tidal Volume: Tidal volume is the lung volume representing the normal volume of air displaced between normal inhalation and exhalation when extra effort is not applied.

- Total Volume: Total volume refers to the total volume of air displaced over the period that data was recorded-in this instance over a period of twenty minutes.

- Minute Volume: refers to the average volume of air displaced over the period of One Minute.

- Inspiratory time (TI): Inspiratory time is the time over which the tidal volume is delivered.

- Expiratory time (TE): Expiratory time is the time over which the tidal volume is exhaled.

- Relaxation time: Time between end of exhalation and start of inhalation.

- Peak Inspiratory Flow (PIF): This is the maximal flow (or speed) achieved during inspiration, measured in ml/sec.

- Peak expiratory flow (PEF): This is the maximal flow (or speed) achieved during expiration, measured in ml/sec.

- EF50: Tidal mid-expiratory flow.

- End Inspiratory pause (EIP): Time between the end of inspiration and the onset of expiration.

- dV: Change in lung volume.

The derivation of EF50 from the breathing pattern of an animal is clearly defined in Figure 7.1 (A, B), along with a breakdown of the various other measurements recorded over the duration of the experiments.
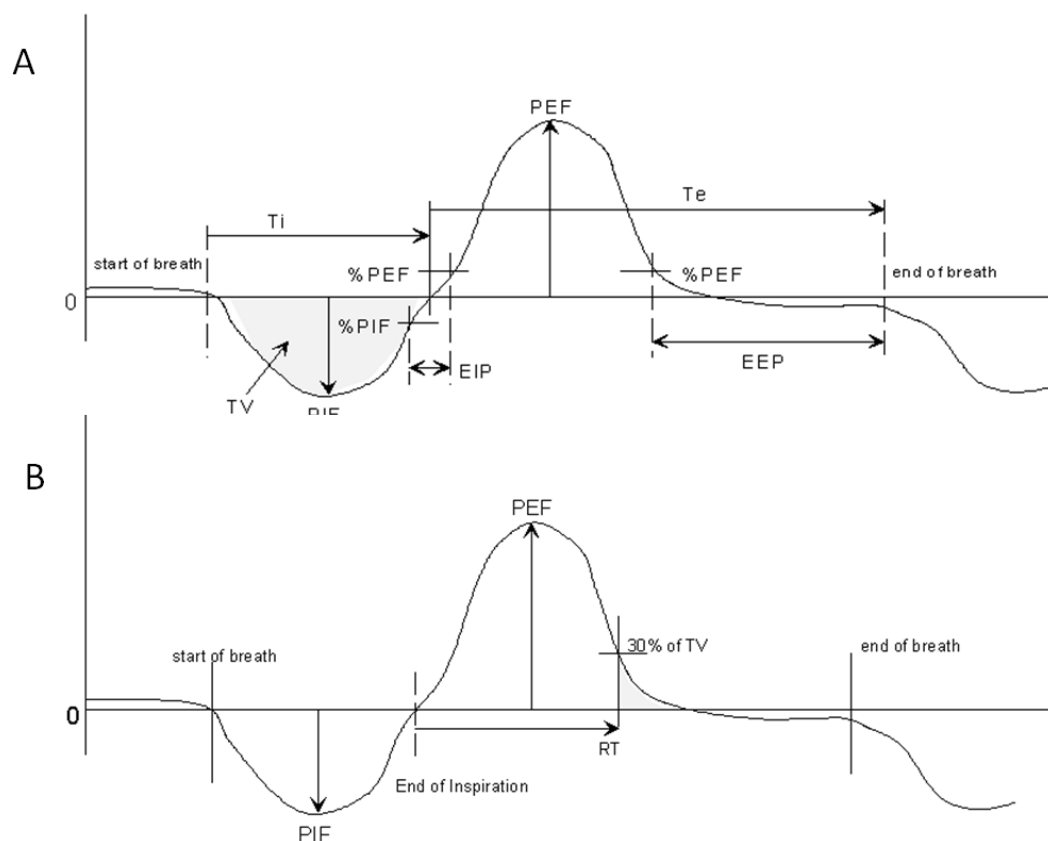
Figure 7.1 The derivation of measurements from a breath profile using restrained plethysmography

(A) Shows the derivation of parameters from a complete breath, with (B) clearly showing the derivation of the relaxation time (Rt). The breakdown of the measurements is as follows; f is the frequency of breathing and is recorded in breaths per minute (BPM); TV is Tidal Volume (ml) and is the volume of air per breath; AV is Accumulated Volume (ml) and refers to the volume of breath over the experiment duration, MV is the Minute Volume (ml/min) and is the total volume recorded per minute; Ti is Inspiratory Time (sec); Te is Expiratory Time (sec); PIF is Peak Inspiratory Flow (ml/s); PEF is the Peak Expiratory Flow ml/s; RT is the Relaxation Time in each individual breath (sec); EIP refers to the End Inspiratory Pause (ms) in each breath; EEP is the End Expiratory Pause (ms) in each breath; dV is the Delta/difference in volume of the lung as measured over the time of the experiment; EF50 is the flow at the point 50% of TV is expired (ml/sec); Rinx is the Rejection Index and records the error occurring in data collection. Graphs reproduced from Biosystems XA user manual (Buxco, 2005).

7.1.2 *Ex vivo* analysis

Ex vivo experimentation was designed to examine the effect of a known BMP pathway antagonist, BMP4, along with a number of controls. In total three different substances were delivered to isolated healthy mouse lungs from C3H mice. These included

Human recombinant BMP4 protein in order to assess its effect on the BMP pathway;

PBS as a vehicle control;

EGF, epidermal growth factor, as a control, it is a functional protein that is not related to the BMP pathway and its inclusion was designed to ensure that any reaction assessed in the lung as a result of BMP4 delivery was as a result of its pathway stimulation and not as a innate immune response to an exogenous protein.

Immunofluorescence analysis of the treated lungs was then carried out to evaluate the level of expression of phosphorylated Smad activity, an indicator of BMP pathway activation, in response to the instilled solutions.

7.1.3 Short term analysis *in vivo* in a healthy lung model

Short term analysis was carried out in order to assess the effect of both the delivery process and the potential therapeutics in a healthy lung model. This consisted of delivery via aerosol of BMP4, PBS, EGF and also HamsF12, with animals being sacrificed 4 hours post administration. The aim was to see if in a healthy lung the controls or BMP4 induced an immediate response to the delivery of any of the substances. This would help determine (i) if aerosol delivery was being effective and (ii) if the BMP4 protein was activating the pathway as we had shown in the lab *in vitro* (Section 5.3.1.3) and (iii) if there were adverse effects on the lungs. It would also help monitor animals for any adverse reactions. In order to fulfil these assessments analysis carried out included plethysmography to analyses lung function and breathing, immunofluorescence and H&E analysis of lung sections, total BAL protein analysis and rt-PCR of whole lung mRNA.

7.1.4 Longterm analysis *in vivo* post delivery to healthy lung

Building on the information gained from the short term study, delivery to a healthy model was carried out via aerosolisation of BMP4, EGF and PBS. The aim was to identify any changes that may occur over a longer time period following exposure to BMP4 and the controls. As such the time line for analysis was extended with delivery occurring at t=0hr and analysis taking place at t=24hr, t=48hr and t=72hr. Analysis

carried out was by means of plethysmography, H&E analysis of lung sections, bodyweight analysis and BAL analysis.

7.1.5 Longterm analysis *in vivo* post delivery to OVA treated lung

7.1.5.1 OVA induced Asthma in Mice

OVA-induced asthma in mice is a well established mechanism for the study of the effects of asthma in mouse lung, as discussed in detail in Section 1.2.2. The verification of model establishment here was carried out by IgE analysis of serum derived from facial bleeds from a subsection of randomly chosen animals from each treatment group. In total two treatment groups were established and utilised for this study, an OVA treated group and a PBS sham control group which received PBS *in lieu* of OVA or OVA+Alum at all the treatment times.

Immunofluorescence analysis of the expression profiles for CC10, pSmad1/5/8 and Smooth Actin was executed in order to ascertain the role and level of activation of the BMP pathway.

The OVA model of asthma using BALB/c mice was induced by a combination of intravenously administered OVA+Alum (i.v.) and intranasal (i.n.) administration of OVA as detailed in Section 2.2.21.1

7.1.5.2 Analysis *in vivo* post delivery to OVA treated lung- Long term

OVA induced allergic asthma was induced in BALB/c mice. The animals were then exposed to a number of different potential therapeutic molecules related to the BMP pathway. In total four different substances were delivered to the diseased lung. These were PBS, BMP4, anti BMP4 antibody and anti BMPR-II antibody.

PBS was utilised as a vehicle control. BMP4 has been shown *in vitro* and *in vivo* to induce a response via the BMP pathway. Analysis here was to determine what effect the delivery of exogenous BMP would have on the disease progression. Anti BMP4 antibody was delivered in order to bind and reduce the activity level of endogenous BMP4, to determine if endogenous BMP4 was having an effect on the disease progression. Anti BMPR-II antibody was delivered to evaluate the role of the BMP receptor in disease progression and to determine, as was previously hypothesised, that temporary inactivation by means of a blocking antibody may provide a means to reduce the level of activity of the BMP pathway and lessen the effect of the OVA induced allergic asthma.

7.2 Results

7.2.1 *Ex vivo* analysis of BMP pathway

Ex vivo set up with exposure to the different solutions limited to four hours before fixation. PBS, BMP4 (2.5µg/10ml PBS) and EGF (2.5µg/10ml PBS) were nebulised, collected and instilled into the cannulated lungs and incubated for t=4hr at 37°C. Immunofluorescence analysis of the lungs was carried to evaluate the level of expression of phosphorylated Smad activity, an indicator of BMP pathway activation in response to the instilled therapeutics. pSmad1/5/8 expression and localisation in the different lung sections was examined (Figure 7.2). Only the BMP4 treatment induced a BMP pathway response, with immunofluorescence analysis showing no phosphorylated Smad activity in any of the other lungs examined. This indicates successful pathway stimulation with the 2.5µg/10ml of BMP4 solution that had been nebulised.
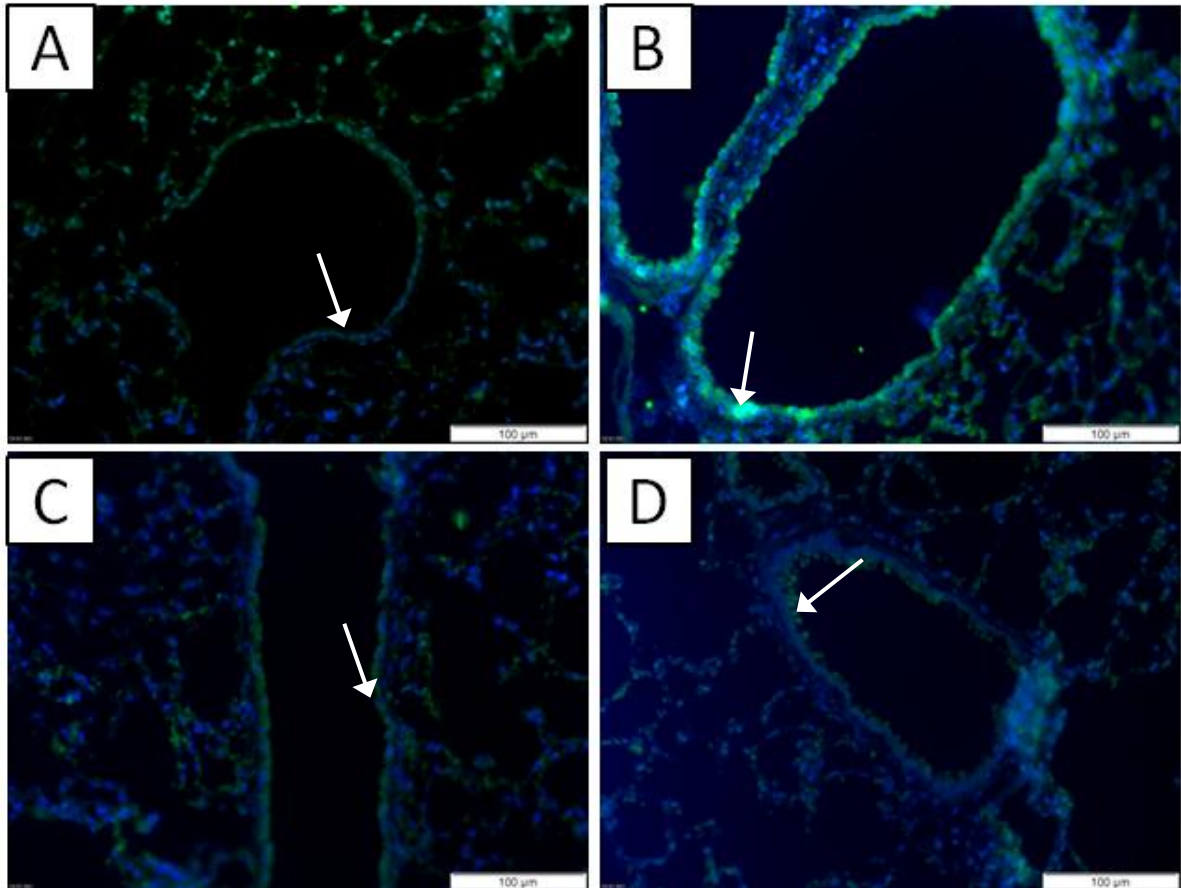
Figure 7.2 pSmad1/5/8 expression analysis on *ex vivo* mouse lung model

pSmad1/5/8 expression analysis on *ex vivo* mouse lung model treated with PBS (A), BMP4 (B) and EGF (C) respectively. As can clearly be seen in these images there was no major response by the lungs after incubation for t=4hr at 37°C with either PBS or EGF treatments. However BMP4 treatment illicited a response by the BMP pathway as illustrated by an increase in the amont of pSmad1/5/8 detected in the some of the airways as shown. The secondary control showed no fluorescence as expected (D). (Arrows indicate airways Green =Alexa-488, Blue =Dapi nuclear stain).

7.2.2 *In vivo* analysis of the BMP pathway

As mentioned the *in vivo* assessment of aerosolised therapeutics was carried out in three distinct stages:

Short term assessment of a single delivery to healthy animals, with sacrifice and assessment to take place at t=4hr post aerosol administration.

Single delivery via aerosol into healthy animals with longer assessment phases at t=24hr, t=48hr and t=72hr (Day1, Day2 and Day3) respectively.

Single delivery via aerosol (PBS alone or 2.5µg of BMP4 or EGF in 10mls PBS) into asthmatic lungs (BALB/c mice with OVA induced allergic asthma) with assessment phases at t=24hr, t=72hr and t=120hr (Day1, Day3 and Day5) respectively.

7.2.2.1   Short term assessment of in-vivo delivery of aerosolised proteins to C3H Mice (t=4hr).

6-8 week old mice had their lung function analysed by plethysmography to establish baseline readings. They were exposed to an aerosol of PBS, BMP4, EGF or HamsF12 1hour post plethysmography recordings. PBS was delivered as a vehicle control. BMP4 (2.5µg/10ml PBS) was delivered in order to assess its effect on the BMP4 pathway. EGF, epithelial growth factor, was delivered as a functional protein control (2.5µg/10ml PBS). HamsF12 was also delivered as a control solution. At t=4hr the animals again had the lung function analysed by plethysmography and immediately after were sacrificed.

In order to fully evaluate the effects, if any, that the different aerosolised compounds had on the lung the following analysis was carried out;

- Plethysmography analysis to determine the effect on respiration lung function.
- Lungs were paraffin embedded for immunofluorescence and H&E analysis to examine specific protein responses to the treatment and to evaluate any inflammatory response
- Whole lung RNA was isolated for rtPCR analysis for different genes linked to various pathways that would reflect BMP pathway response.
- BAL fluid protein levels were analysed to assess seepage of protein into the alveolar spaces.

7.2.2.1.1 *Plethysmography analysis*

Plethysmography was carried out on all animals as per Chapter2 immediately prior to exposure the delivery of aerosol at t=0hr. It was then repeated with each animal at

t=4hr, immediately after which animals were sacrificed. The difference in measurements at t=0hr and t=4hr were then analysed and graphed (Figure 7.3, Figure 7.4 and Figure 7.5). Overall significant differences between treatments were observed in the Accumulated and Minute volume measurements (Figure 7.3 (C+D)), and in the peak expiratory flow (PEF) rate, Relaxation time (Rt) and EF50 measurements (Figure 7.4 (B, C, D)), as determined by one-way ANOVA (Table 7.3).

Closer analysis of the results shows that the frequency of breathing (f) was most reduced in the BMP4 treated animals (-16.13±11bpm), though not by a statistically significant amount. BMP4 animals overall had a more decreased tidal volume (Tv) (-0.04±0.01mls), accumulated volume (Av) (-286±48mls) and minute volume (Mv) (12.95±2.03mls/sec) compared to their t=0hr measurements than all other treatments (Figure 7.3 (B, C, D)). The means were significantly different in regards to Av and Tv, as assessed by one way ANOVA (Av=*, $p<0.05$; Tv=**, $p<0.01$) and Tukey multiple comparison test analysis also showed that with regard to Av and Mv, BMP4 and HamsF12 groups also differed very significantly (**, $p<0.01$). A full breakdown of statistical analysis can be seen in Table 7.1.

No major changes were noted in inspiratory time (Ti) measurements (Figure 7.3 (E)). The only group that showed a small increase at t=4hr was the PBS group (+0.002178±0.002456sec) whereas all other treatment groups showed a slight decrease on average, though this was not statistically significant. The expiratory time (Te) however, although not having a statistically significant difference recorded does show a noticeable increase in the Te required by BMP4 treated animals (+0.0207±0.012sec) compared to all other treatment groups (PBS +0.00266±0.00364sec; EGF -0.00466±0.0104sec; HamsF12 -0.003742±0.00592sec) (Figure 7.3 (F)). This is indicative of a possible airway response to BMP4 treatment and correlates with the significant differences observed in the volume measurements recorded by the various treatment groups.

The difference in all treatment groups was statistically significant in regard to PIF overall by one way ANOVA analysis ($p<0.05$), and Tukey post test analysis showed statistically significant differences between BMP4 and HamsF12 treated animals (Δ=0.6811, $p<0.05$) (Figure 7.4 (A)). BMP4 treated animals showed a marked decrease in PIF post treatment at t=4hr compared to all other treatment groups, greater than 0.4ml/sec (-0.4507±0.0723ml/sec). The same overall pattern was seen in PEF (Figure 7.4 (B)). Here again animals that had BMP4 delivered to the airways showed the greatest decrease in PEF rate, greater than 0.4ml/sec (-0.4563±0.1296mls/sec).

Tukey posttest analysis showed a statistically significant difference between HamsF12 and BMP4 treated animals (Δ=0.6644 mls/sec, p<0.05).

Rt analysis showed a significant difference due to treatments as determined by one way ANOVA (p<0.05) (Figure 7.4 (C)). BMP4 treated animals (+0.0154±0.0051sec) had a significantly increased (p<0.05) Rt compared to both EGF (-0.00399±0.0048sec) and HamsF12 (-0.0232±0.003sec) treated animals. Although not statistically different from the PBS treatment group there was a marked difference between BMP4 and PBS treated animal groups with PBS showing on average a slight decrease (-0.0019±0.0035sec) in Rt at t=4hr in common with the decrease observed in EGF and HamsF12 treated animals.

Analysis of EF50, which decreases in response to bronchoconstriction, showed the greatest decrease in BMP4 treated animals (0.5609±0.1243mls/sec) and Tukey posttest analysis showed a significant difference between BMP4 treated animals and those treated with HamsF12 (p<0.05) (Figure 7.4 (D)).

EIP varied across the treatment groups with no individual treatment resulting in a significant difference although PBS animals on average were the only group to increase the pause, though only slightly (0.2655±0.2586ms) (Figure 7.4 (E)). EEP showed a reversed trend with PBS treated animals the only group to show a slight decrease in pause (Figure 7.4 (F)). Of note here, though not statistically significant, is the greatly increased EEP in BMP4 treated animals. While the difference in all other treatment groups comes to within 0.1ms of the pre-treatment recordings, BMP4 treated animals averaged an almost 1.0ms increase in EEP (+0.9841±0.8212ms).

The change in lung volume (dV) shows the increased or decreased capacity of the lungs of the treated animals after treatment (Figure 7.5 (A)). Although the differences were not significant is of note that only BMP4 treated animals showed a decreased capacity (-0.000874±0.000713mls) after treatment with all other groups averaging differing levels of slightly improved capacity.

7.2.2.1.2 rt-PCR analysis of whole lung RNA

One complete set of lungs from each treatment group was used from each group (n=1) to provide a quick snapshot of the level of mRNA of different proteins linked to the BMP pathway after treatment. The markers used were BMPR-II, CC10 and Smad3. GAPDH was used as a control. The levels of expression were compared to that of the PBS treatment group. BMP4 treatment of the animals was the only treatment to result in an increase in the levels of BMPR-II, CC10 and Smad3 expression (Figure 7.6 (A, B, C)). All other treatment options, compared to PBS, resulted in a decreased level of

mRNA. However it is of note that only an n=1 was available for this data, providing only a snap shot and not a detailed analysis of the levels of expression of these markers in the lung.

### 7.2.2.1.3 Immunofluorescence analysis (n=2)

With regards to analysis of the expression levels of CC10 protein in the different treatment groups, PBS (A), EGF(C) and HamsF12 (D) treated animals all showed a high level of CC10 expression compared to the BMP4 treatment group (B), which showed a lower level of CC10 expression (Figure 7.7 (i)). In relation to the immunofluorescence analysis of BMPR-II expression in PBS and BMP4 treatment groups, it was noted that the level of detection of BMPR-II in PBS treated animals exceeded that seen in BMP4 treated animals (Figure 7.7 (ii)). The expression profile of pSmad1/5/8 throughout the airways was assessed (Figure 7.8). While pSmad1/5/8 activity was observed in all treatment groups it was detected at much higher levels in the airways of BMP4 treated animals.

7.2.2.1.4 H&E analysis (n=2)

H&E analysis was carried out to determine if any physiological differences could be noticed between the PBS and BMP4 treatment groups. However no discernable differences could be seen between either treatment groups in terms of inflammation or phenotype (Figure 7.9).

7.2.2.1.5 BAL Fluid Protein concentration (n=2)

Though no statistically significant differences were present it was noted that BMP4 treated animals on average had elevated levels of protein present in the BAL than any other treatment group (1.65mgs/ml in BMP4 treated animals versus 1.15mgs/ml in EGF and HamsF12 treated animals, and 1.35mgs.ml in EGF treated animals which equates to an increase in protein levels of 43.5% compared to PBS and Hams F12 groups, and 22.2% increase compared to EGF levels).
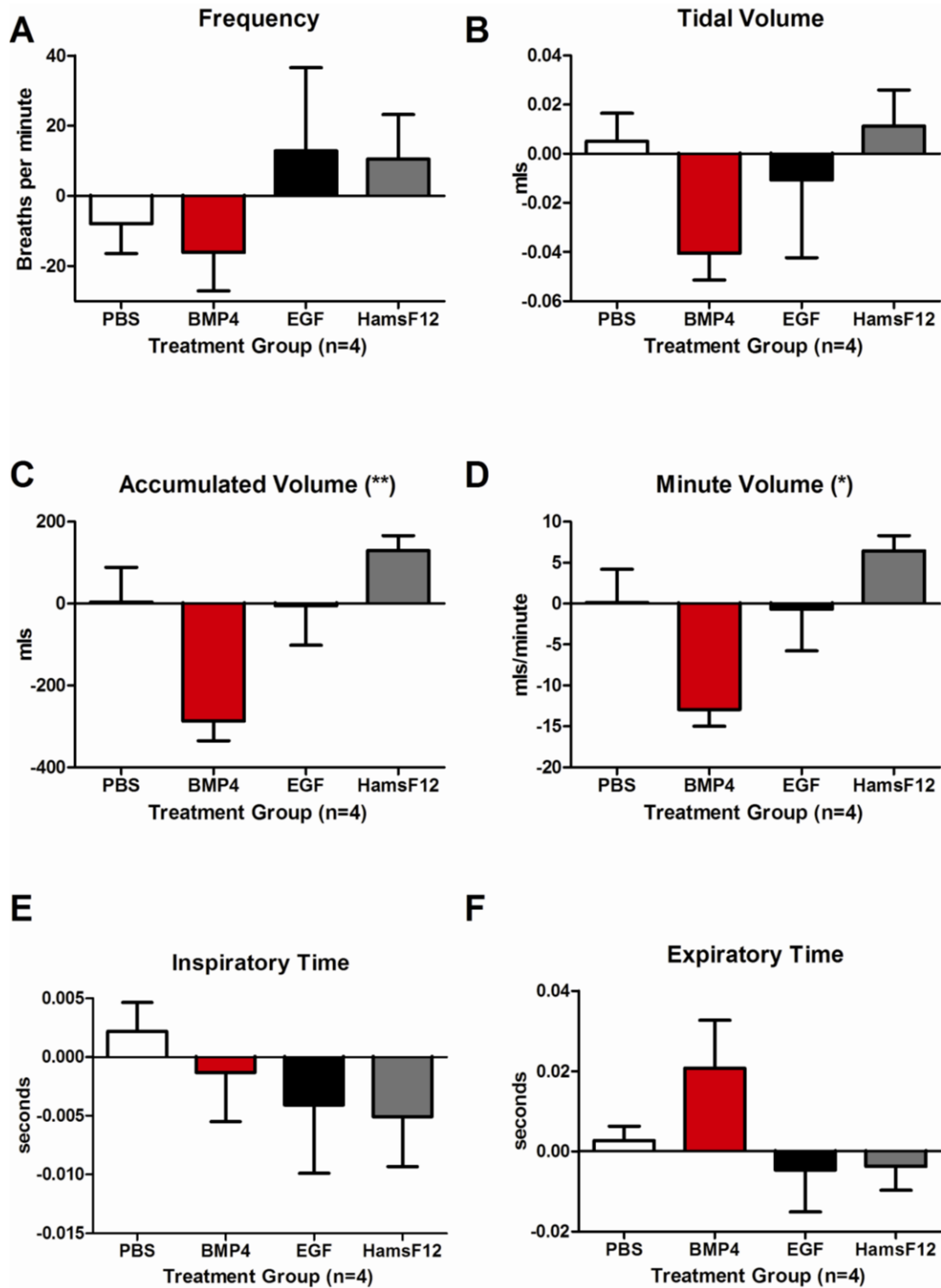
Figure 7.3 Plethysmography results on different treatments on C3H mice carried out over a t=4hr period (n=4)

Treatment was administered at t=0hr, 1 hour post initial plethysmography readings. Plethysmography was repeated on the treatment groups immediately prior to harvest at t=4hr. Statistical analysis was carried out by one way ANOVA and a full set of statistical breakdown can be seen in Table 7.1.
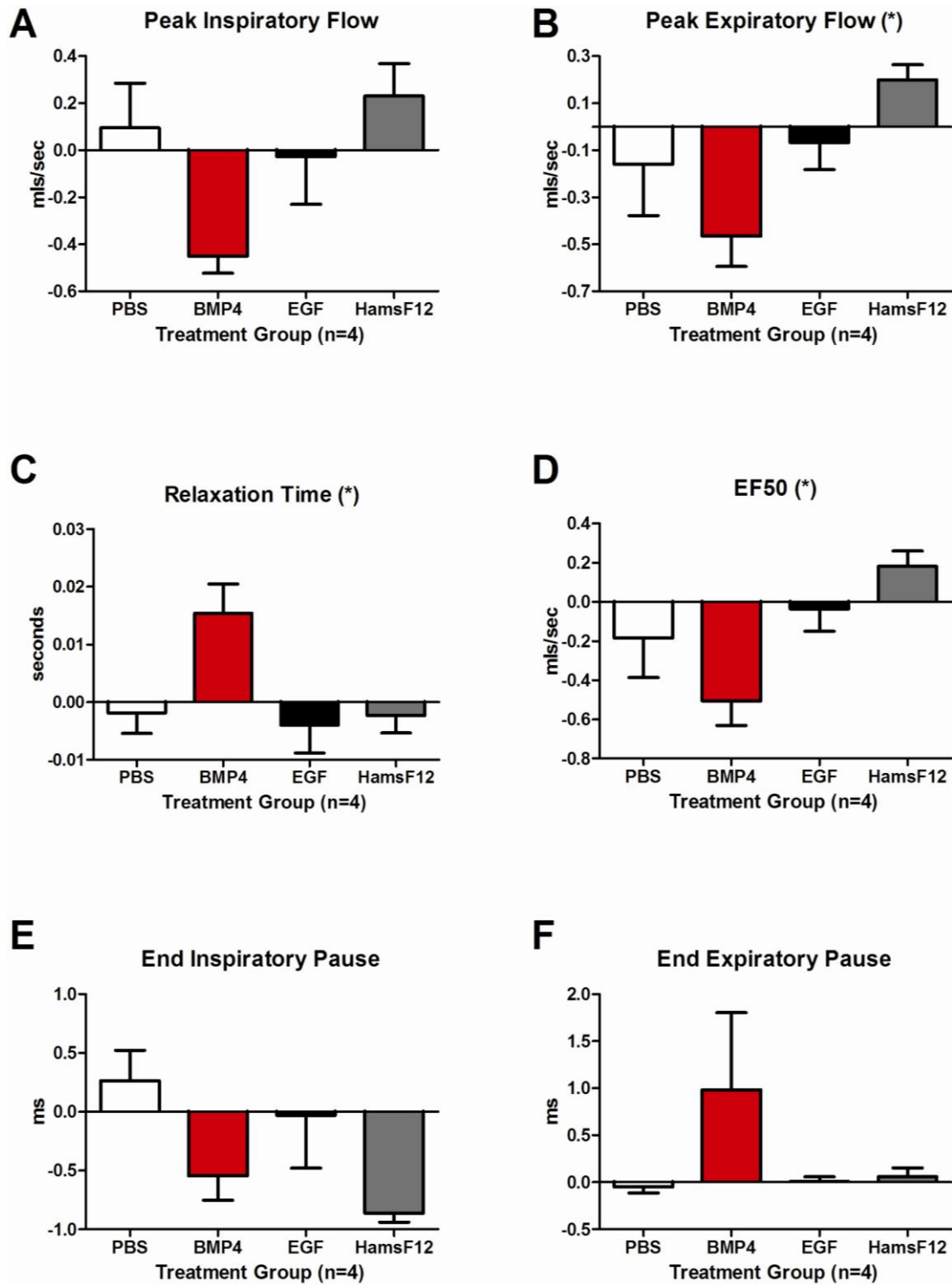
Figure 7.4 Plethysmography results on different treatments on C3H mice carried out over a t=4hr period (n=4)

Treatment was administered at t=0hr, 1 hour post initial plethysmography readings. Plethysmography was repeated on the treatment groups immediately prior to harvest at t=4hr. Statistical analysis was carried out by one way ANOVA and a full set of statistical breakdown can be seen in Table 7.1.
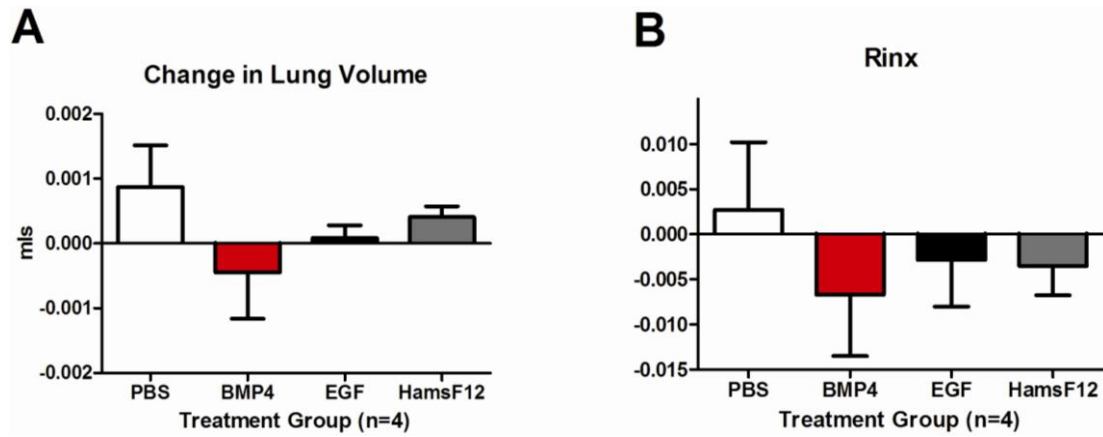
Figure 7.5 Plethysmography results on different treatments on C3H mice carried out over a t=4hr period (n=4)

Treatment was administered at t=0hr, 1 hour post initial plethysmography readings. Plethysmography was repeated on the treatment groups immediately prior to harvest at t=4hr. Statistical analysis was carried out by one-way ANOVA and a full set of statistical breakdown can be seen in Table 7.1.

Measurement	One-Way ANOVA Analysis	Tukey Multi-comparison Test
Frequency (f)	-	-
Tidal Volume (Tv)	-	-
Accumulated Volume (Av)	** $p<0.01$	BMP4 vs. HamsF12 **$p<0.01$
Minute Volume (Mv)	* $p<0.05$	BMP4 vs. HamsF12 **$p<0.01$
Inspiratory Time (Ti)	-	-
Expiratory Time (Te)	-	-
Peak Inspiratory Flow (PIF)	* $p<0.05$	BMP4 vs. HamsF12 *$p<0.05$
Peak Expiratory Flow (PEF)	-	BMP4 vs. HamsF12 *$p<0.05$
Relaxation Time (Rt)	* $p<0.05$	BMP4 vs. HamsF12 * $p<0.05$ BMP4 vs. EGF * $p<0.05$
EF50	* $p<0.05$	BMP4 vs. HamsF12 *$p<0.05$
End Inspiratory Pause (EIP)	-	-
End Expiratory Pause (EEP)	-	-
Change in Lung Volume (dV)	-	-
Rinx	-	-

Table 7.1 Statistical analysis of plethysmography results

Statistical analysis was carried out by one-way ANOVA and Tukey posttest analysis.
Statistical significance with regards to one way ANOVA was observed in
Av, Mv, PIF, Rt and EF50.
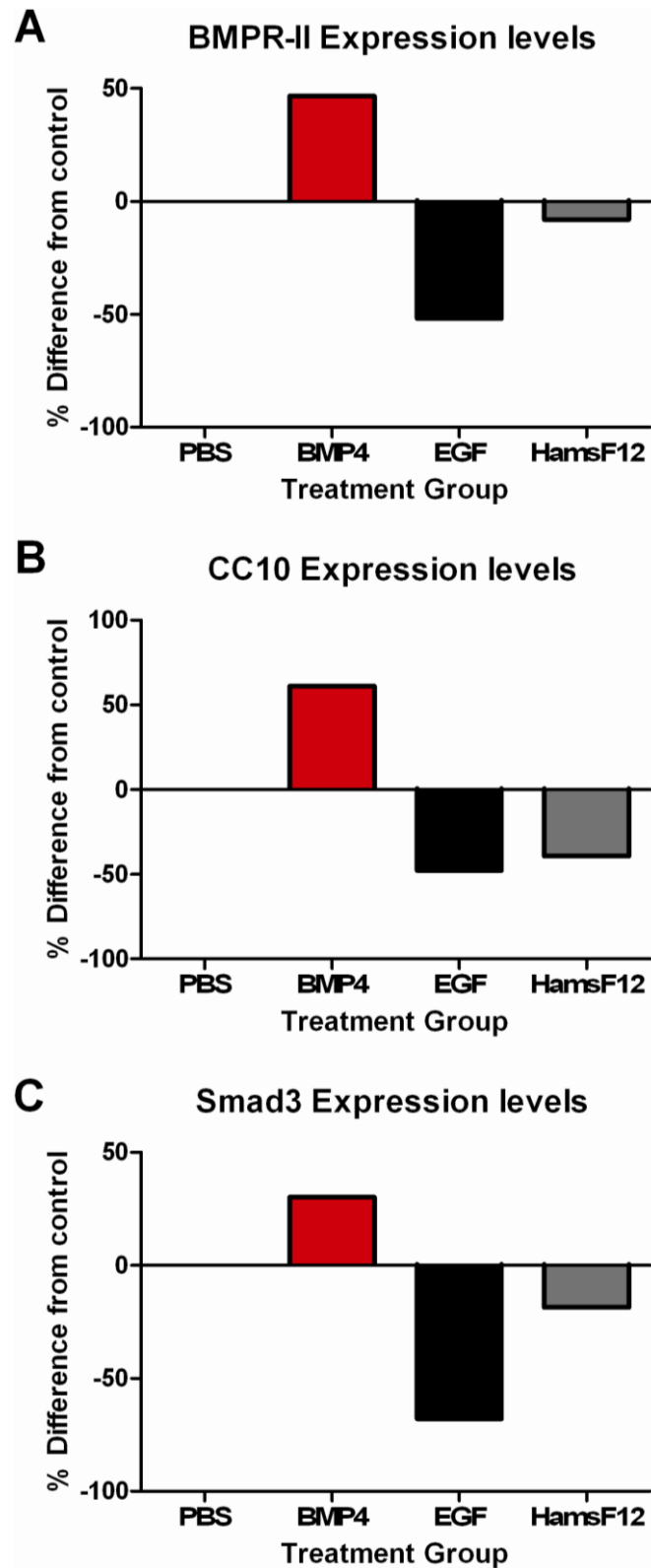
Figure 7.6 rtPCR analysis of whole lung mRNA analysed by densitometry

Whole lung RNA was isolated from each of the treatment. Using GAPDH as a control, the levels of BMPR-II, CC10 and Smad3 mRNA were analysed via rt-PCR densitometry and the percentage expression in each was compared as a percentage to the level expressed in the PBS treated animals (n=1).

(i) CC10 *in vivo*

(ii) BMPR-II *in vivo*
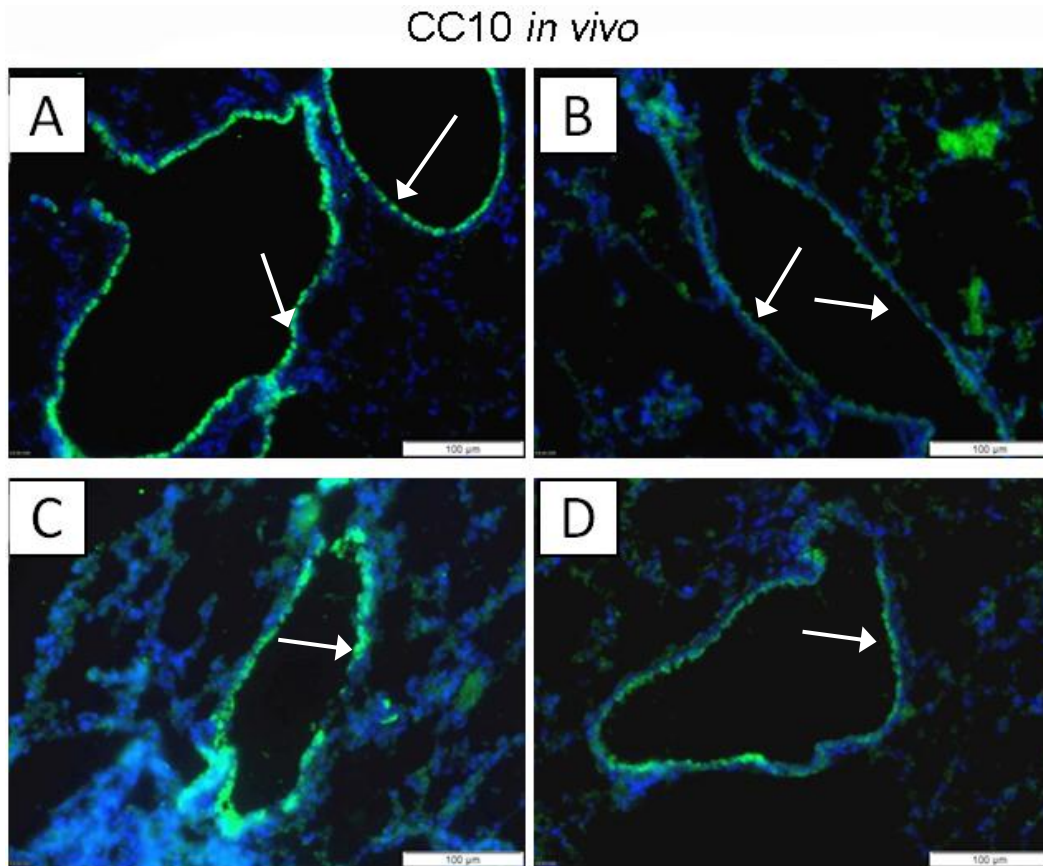
Figure 7.7 Immunofluorescence analysis of CC10 and BMPR-II protein expression in the lung
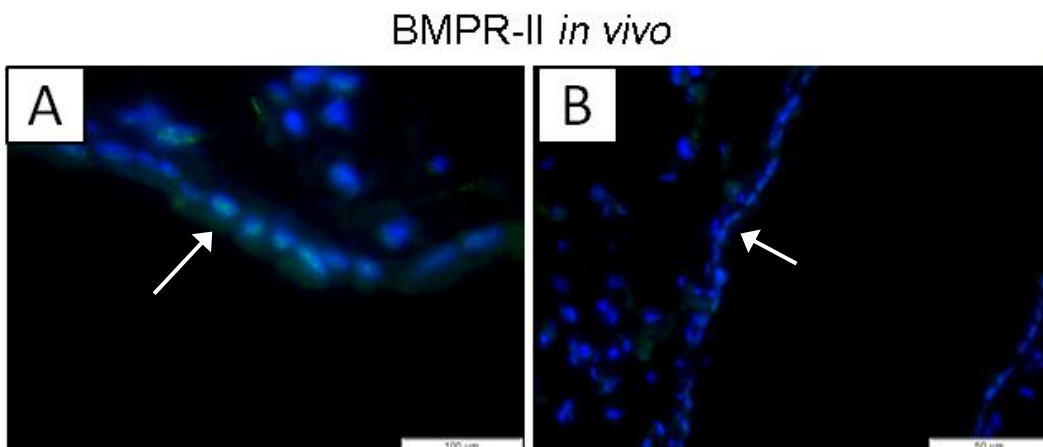
(i) Shows the expression of CC10 in each of the treatment groups. PBS treated (A), EGF treated (C) and HamsF12 (D) treated all showed a high level of expression of CC10 protein in the airways. Though staining was also present in BMP4 treated lung (B) it was not as strongly expressed as it was in the other treatment groups.

(ii) shows the expression of BMPR-II in PBS (A) and BMP4 (B) treatment groups. It is of note that the level of expression in PBS treated animals exceeded the level of expression in BMP4 treated animals. (Arrows indicate airways Green =Alexa-488, Blue =Dapi nuclear stain).

pSmad1/5/8 *in vivo*
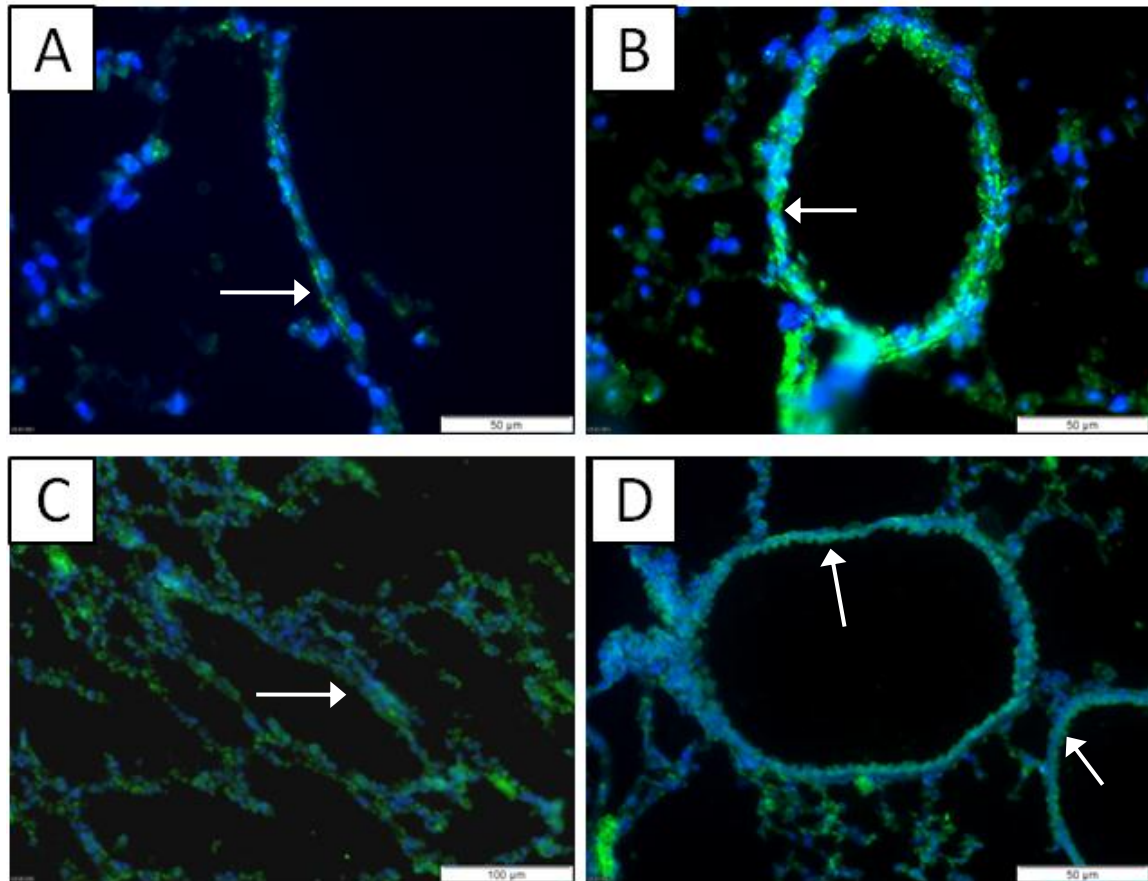
Figure 7.8 Immunofluorescence analysis of pSMAD1/5/8 protein expression in the lung

pSmad1/5/8 expression levels in PBS (A), BMP4 (B), EGF (C) and HAMS F12 treated C3H mice. While the presence of pSmad1/5/8 was detected in all groups of animals, it was expressed at a noticeably higher level in the BMP4 treated mice, as can be seen in (B) above. (Arrows indicate airways Green =Alexa-488, Blue =Dapi nuclear stain).
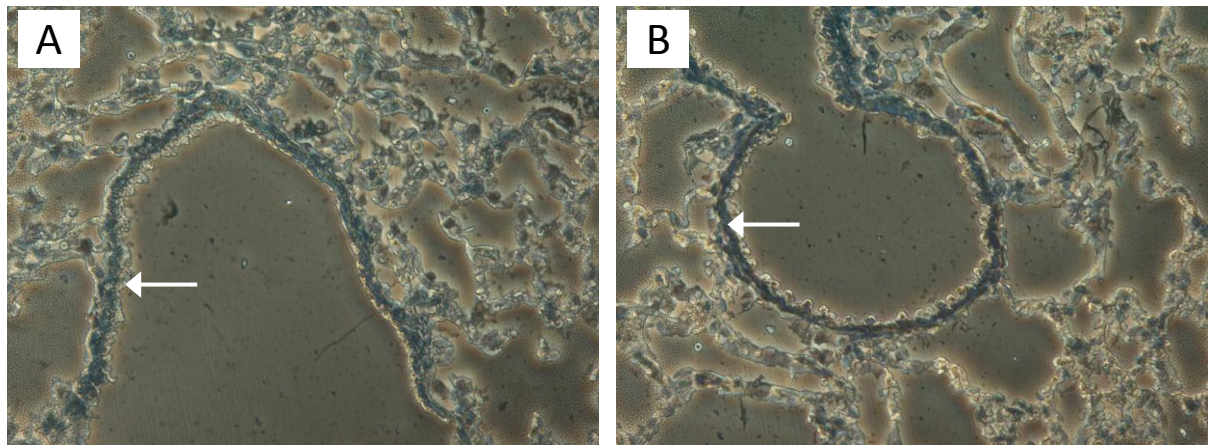
Figure 7.9: H&E staining of PBS and BMP4 treated animals.

H&E analysis showed no major change in airway morphology between the treatment groups. As in evidence above in PBS treated (A) and BMP4 (B) treated neither set of airways were showing any contrasting features, both displaying intact airways and no inflammation (20x magnification. Arrows indicate airways).

BAL Fluid Protein Concentration
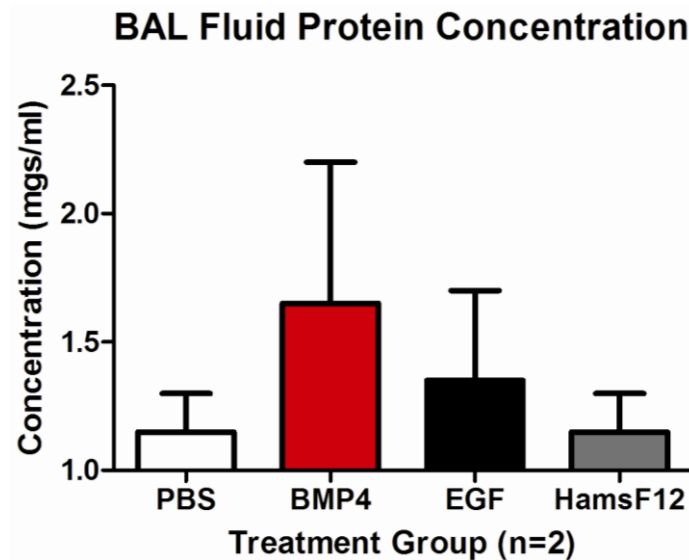
Figure 7.10 BAL fluid protein levels

As was expected, PBS treated animals showed the lowest levels of protein in the BAL fluid along with HamsF12. BMP4 treated mice had the highest protein levels, approximately 0.5mgs/ml higher than either the PBS or HamsF12 treatment groups, with EGF falling in between the PBS and BMP4 treatments. However due to the small n numbers (n=2) and large error bars the difference was not reported as statistically significant. Statistical significance was determined by one-way ANOVA analysis.

7.2.2.2 Three Day assessment of in-vivo delivery of aerosolised proteins.

6-8 week old C3H mice were exposed to an aerosol of BMP4, PBS and EGF over a twenty minute period at t=0hr as per protocol (Section 2.2.22). Animals were then harvested at t=24hr, t=48hr and t=72hr timepoints, referred to from here in as Day1 Day2 and Day3 timepoints.

7.2.2.2.1 *Plethysmography analysis*

Plethysmography was carried out on all animals immediately prior to aerosol exposure at t=0hr and again immediately prior to endpoint harvest on Day1, Day3 and Day5 respectively. The differences in measurements between t=0hr and harvest were determined and the data was then analysed and graphed (Figure 7.11, Figure 7.12 and Figure 7.13). Statistical analysis was carried out by Two Way ANOVA with Bonferroni post test analysis. It is of note that no significant difference ($p<0.05$) was observed across any of the three day timepoints between any of the treatments either by two-way ANOVA analysis or by way of the Bonferroni post test analysis (statistical data not shown). The measurement data was scrutinised to determine if any notable, if not statistically significant, results could be observed. The frequency data showed no exceptional behaviour by any treatment group (Figure 7.11 (A)). The volume analysis appear to indicate that Day1 and Day2 post treatment, BMP4 treated animals were, by volume, inhaling less air into their lungs than compared to other treatment groups, though still showed an increase over t=0hr recordings for both (Figure 7.11 (B, C, D)). The only exception to this was in Accumulated volume where on Day1 the BMP4 treatment group had a lower Av than when measured prior to treatment commencing. All other groups across all timepoints showed an increased Av. The Ti and Te did not show any particular pattern associated with BMP4 treatment (Figure 7.11 (E, F)). EGF treated animals however all showed a decreased Ti post treatment, the effect of which appeared to decrease over time from Day1 to Day3.

It was noticed that BMP4 treated animals displayed an increasing PIF as time after treatment increase whereas EGF and PBS treated animals appeared to just decrease their PIF back towards levels of t=0hr after treatment (Figure 7.12 (A)). Perhaps of more significance is the fact that the PEF of all BMP4 animals was below that of the pre-treatment measurements at all timepoints, getting closer to approaching their respective t=0hr base line as the time post treatment increased (Figure 7.12 (B)). Neither PBS nor EGF treated animal established such a pattern. Rt showed no emerging patterns from analysis between treatment groups across the different

timepoints (Figure 7.12 (C)). EF50 however again reflects pattern seen elsewhere (Figure 7.12 (D)). While neither PBS or EGF treatment group establishes a clear pattern post treatment, all animals which were treated with BMP4 showed a decreased EF50, which remained lower throughout the three day period and did not look to be approaching the t=0hr baseline. EIP and EEP also did not establish any clear patterns of response to any treatment (Figure 7.12 (E) and Figure 7.12 (F)).

In regards to the change in lung volume between initial t=0hr and harvest day, the PBS group establishes no clear pattern. Both EGF and BMP4 treatment groups however show a decrease in lung volume post treatment (Figure 7.13 (A)). With respect to BMP4 it appears to be rapidly approaching the established baseline by Day3, whereas with the EGF treated animals, it appears, while taking note of the standard errors, to be decreasing further as the timepoints lengthen.

7.2.2.2.2 Bodyweight and BAL analysis

The bodyweight of each individual animal was noted at time of death to see if delivery of any of the aerosol treatment had noticeable effect on the bodyweight of the animals. However in statistical analysis of the results no statistical differences were detected with respect to weight loss or weight gain between the different groups (Figure 7.14 (A)). The concentration of cells in the BAL was also recorded and analysed but here again no statistically different results were noted between treatment groups (Figure 7.14 (B)). The only pattern noticeable was an increase over the three day period of the concentration of cells in the BAL of EGF treated animals and the noticalbe decrease in the cell number in the Bal of BMP4 treated animals on Day3 and Day5.

7.2.2.2.3 H&E analysis

H&E analysis was carried out on sections of lung from Day1 harvested treatment groups (Section 2.2.17.1 & 2.2.17.2) to determine if any inflammation or damage resulted in response to the treatments (Figure 7.15). However no differences were noted between any of the 3 treatment groups.
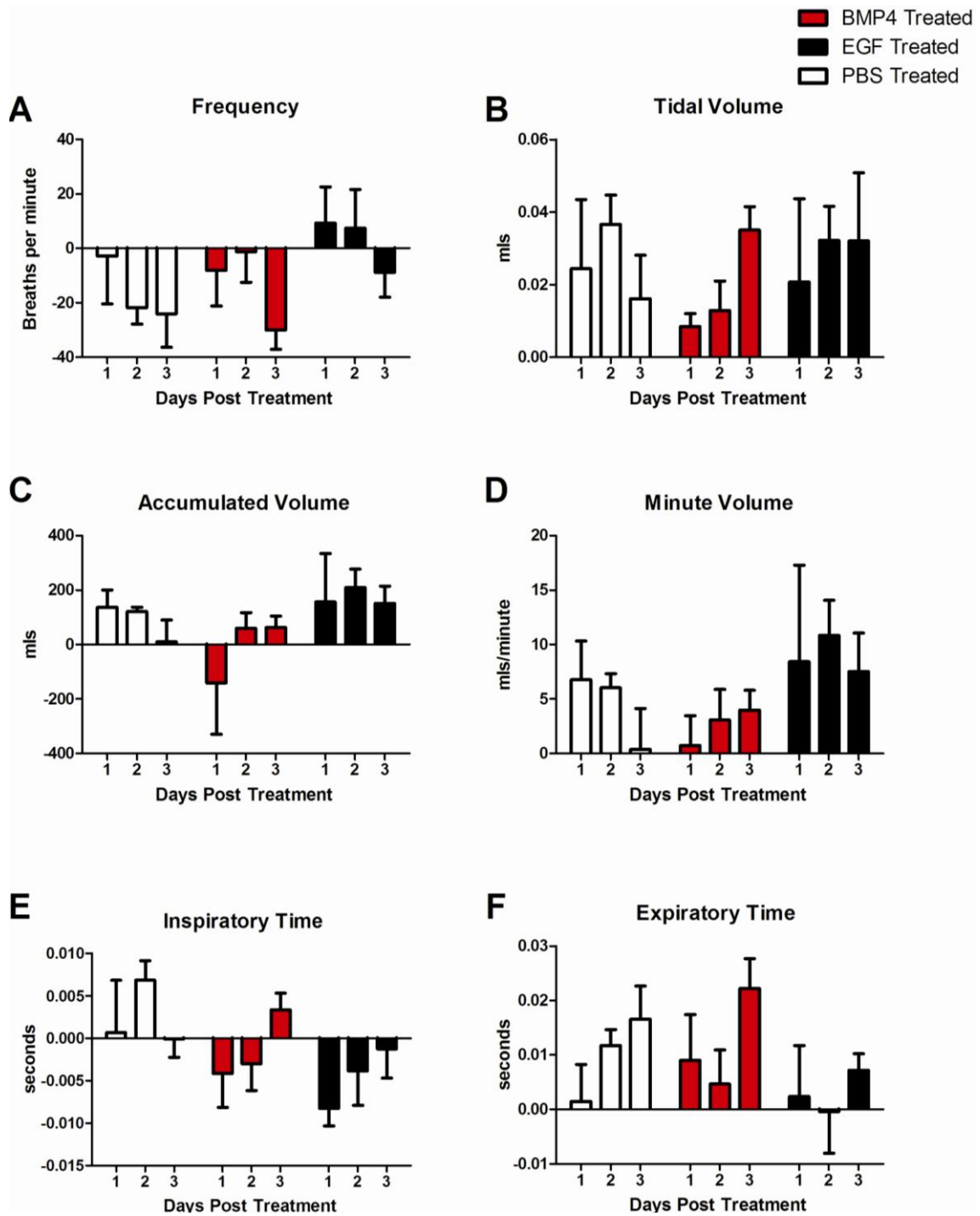
Figure 7.11 Plethysmography results on different treatments on C3H mice carried out over a 3 day period (n=4†)

Treatment was administered at t=0hr, 1 hour post initial plethysmography readings. Plethysmography was repeated on the treatment groups immediately prior to harvest at t=24hr (Day1), t=48hr (Day2) and t=72hr (Day3). An explanation of all measurements can be found in Section 7.1.1.

†PBS day3 n=3, EGF day1 n=3.
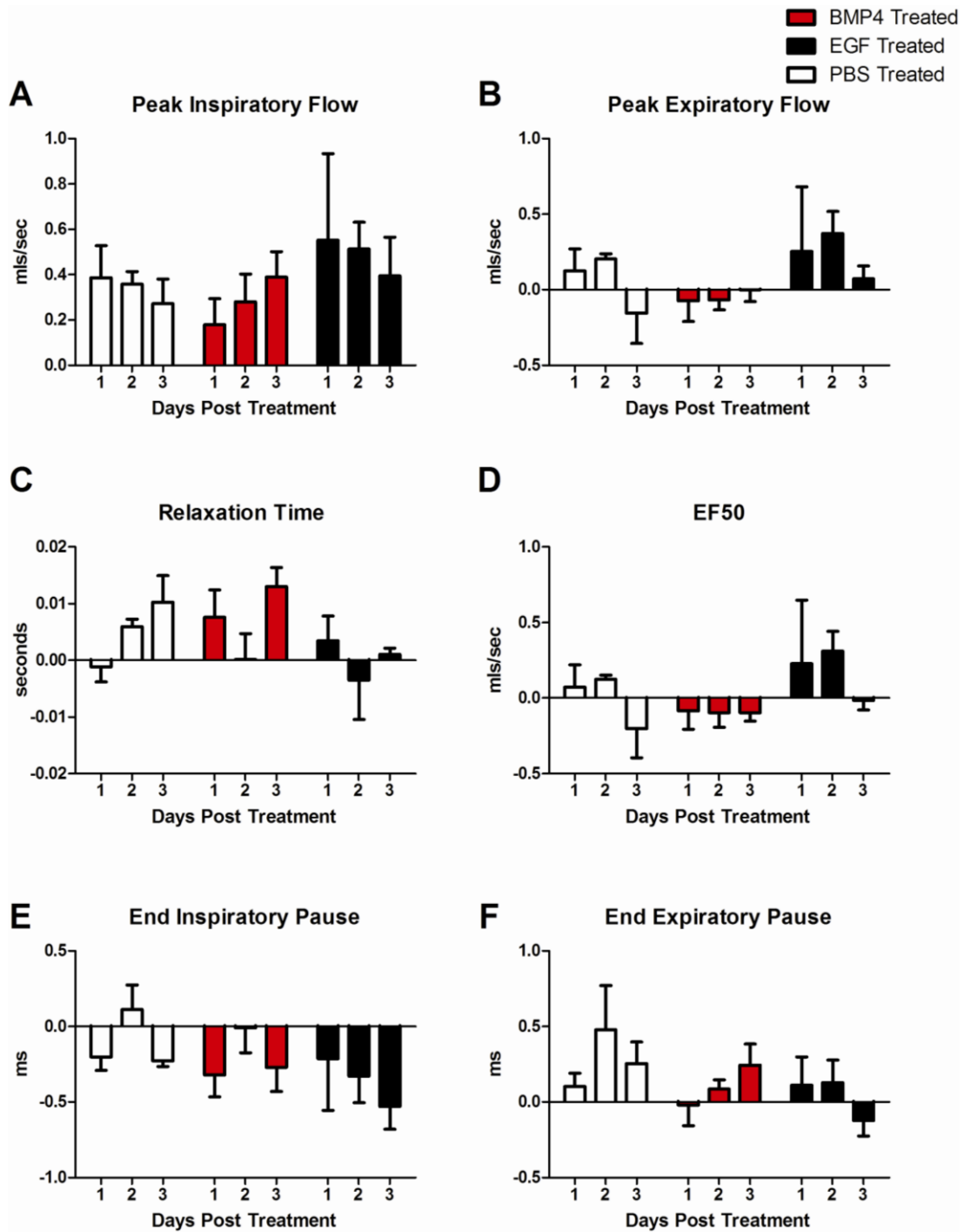
Figure 7.12 Plethysmography results on different treatments on C3H mice carried out over a 3 day period (n=4†)

Treatment was administered at t=0hr, 1 hour post initial plethysmography readings. Plethysmography was repeated on the treatment groups immediately prior to harvest at t=24hr (Day1), t=48hr (Day2) and t=72hr (Day3). An explanation of all measurements can be found in Section7.1.1.

†PBS day3 n=3, EGF day1 n=3.

Figure 7.13: Plethysmography results on different treatments on C3H mice carried out over a 3 day period (n=4†)

Treatment was administered at t=0hr, 1 hour post initial plethysmography readings. Plethysmography was repeated on the treatment groups immediately prior to harvest at t=24hr (Day1), t=48hr (Day2) and t=72hr (Day3). An explanation of all measurements can be found in Section 7.1.1.
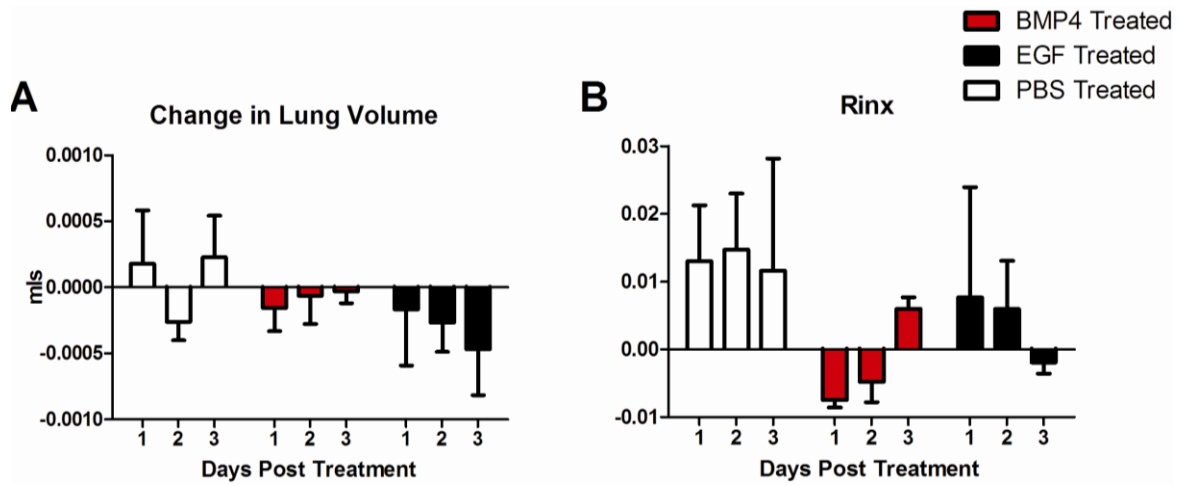
†PBS day3 n=3, EGF day1 n=3.
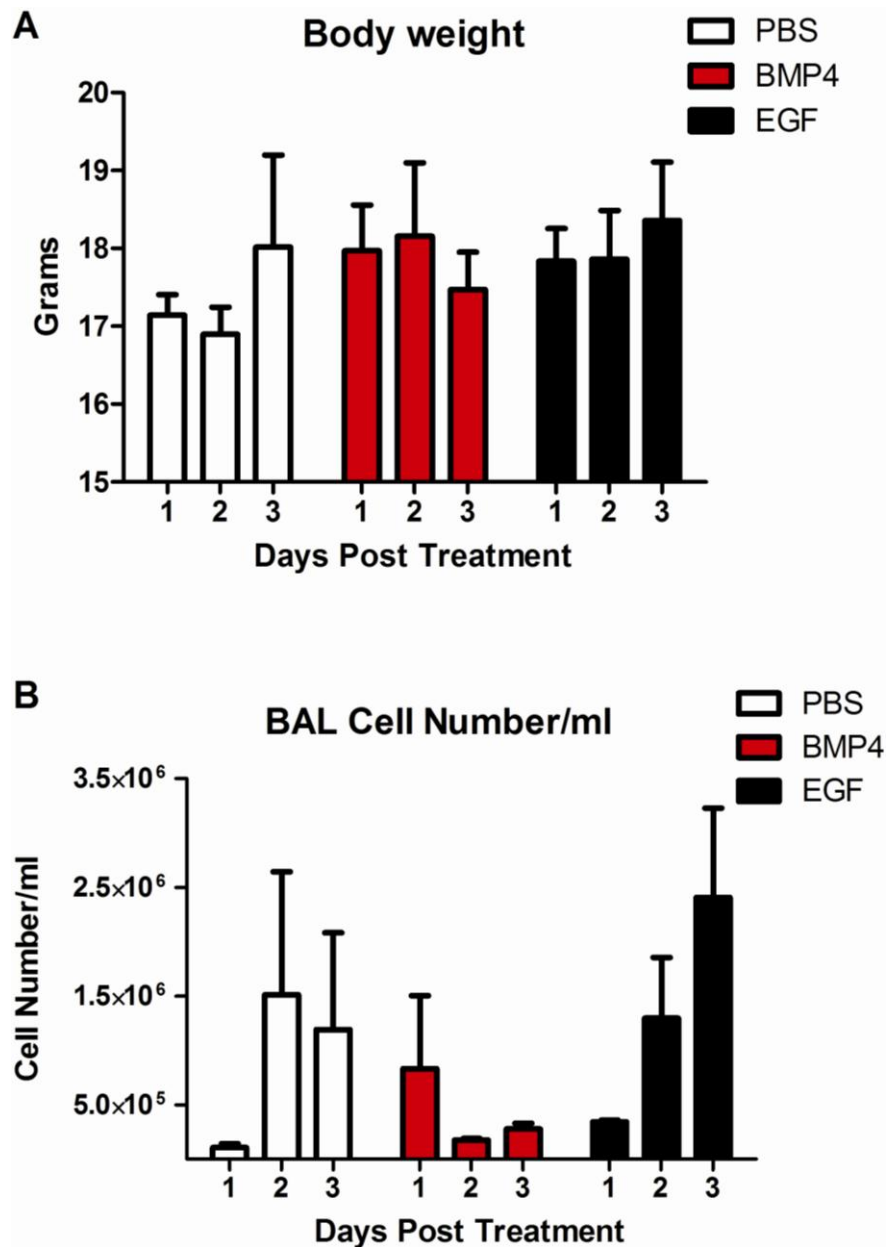
Figure 7.14: Bodyweight and Cell concentration of BAL Fluid

Body weight analysis (A) of the different treatments showed that no treatment resulted in a statistically significant difference in bodyweight of the animals over a 72 hour period as determined by two ways ANOVA and Bonferroni post-test comparing each treatment type individually. Cell concentration in the BAL fluid (B) of the treated animals over a 3day period, analysed the same way, was also found to produce no statistically significant different results. No steady pattern was observed over the 3day post treatment period in PBS or BMP4 treated animals. The only patterns that emerged were a steady increase in the cell concentration in the BAL fluid of EGF treated animals over the time frame and on Day2 and Day3 BMP4 treated animals recorded noticeably less cells in their BAL fluid than any other treatment group.
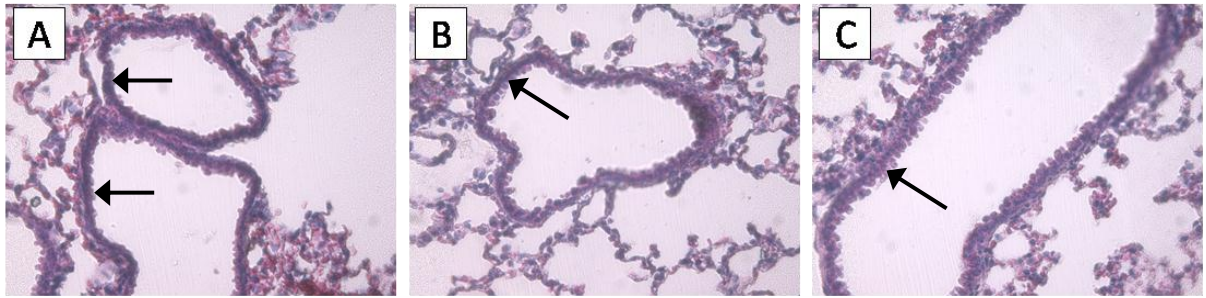
Figure 7.15: H&E analysis of the treatment groups at t=24hr (Day 1)

A snap shot analysis was carried out to determine if any of the treatments had a detectable inflammatory effect on the epithelium 24 hours after exposure to the aerosol treatment. However no damage was detected in any treatment group (n=2) with PBS treated (A), BMP4 treated (B) and EGF treated (C) lungs all showing lungs healthy in appearance (Arrows indicate airways).

7.2.2.3 OVA induced model of Asthma in Mice- Model Establishment and targeted delivery of potential therapeutics

7.2.2.3.1 OVA induced Model of Asthma in ice

7.2.2.3.1.1 Immunofluorescence analysis of OVA induced Asthma in Mice.

Immunofluorescence analysis of the expression profiles for CC10, pSmad1/5/8 and Smooth Actin was executed on PBS treated control animals and OVA treated allergic Asthma model animals (Figure 7.16 and Figure 7.17). Immunofluorescence analysis of CC10 expression determined that while both groups of animals expressed CC10, the expression levels were higher in the Group2 OVA treated animals (Figure 7.16). Localisation of expression was consistent between both groups and confined to the airways. pSmad1/5/8 analysis showed a much greater expression of pSmad1/5/8 in Group2 OVA treated animals throughout the airways, compared to only low level and sporadic fluorescence detected in Group1 PBS treated animals (Figure 7.17 (A)). Increased pSmad1/5/8 activity is linked to activation of the BMP pathway with BMP binding to the receptors triggering phosphorylation of the Receptor Smads Smad1, Smad5 and Smad8. Smooth muscle actin showed no difference in expression levels or localisation between the two groups (Data not shown).

7.2.2.3.2 Five Day assessment of in-vivo delivery of aerosolised proteins to OVA induced models of asthma.

Animals were treated with OVA as described in Chapter2 to establish an OVA model of asthma in 6-8week old BALB/c mice. One group of control animals also had the OVA model of asthma established and one control group of animals acted as a sham control, receiving PBS instead of OVA. In total, four groups of animals were treated with OVA to establish the asthma model before being treated by aerosol with PBS, BMP4 (2.5µg/10ml PBS), α-BMP4 Antibody (2.5µg/10ml PBS) and α-BMPR-II antibody (2.5µg/10ml PBS) respectively, at t=0hr, 24 hours after the last OVA administration. Data was collected and animals sacrificed from each treatment group at t=24hr, t=72hr and t=120hr, referred to as Day1, Day3 and Day5 from this point forward. The OVA and PBS control animals, which received no aerosol treatment, had plethysmography analysis carried out on Day0 and all other analysis was carried out on Day5 along with the remaining treatment group animals.

7.2.2.3.3 Plethysmography analysis of Treatment Groups

Statistical analysis of the plethysmography data was carried out by two-way ANOVA and Bonferroni post-test analysis and is detailed in Table 7.3. In brief, two-way ANOVA determined that the type of treatment administered to the animals caused a significant difference in lung function with regards to frequency, Te, and Rt (Figure 7.18 (A), Figure 7.18 (F), and Figure 7.19 (C)).

With respect to plethysmography data on frequency, it was observed that the frequency of breathing in BMP4 treated animals was below that of the animals the same animals at t=0hr at all three timepoints (Day1 -9.16±5.69bpm; Day2 -11.48±10.84bpm; Day5 -15.52±0.14bpm) (Figure 7.18 (A)). This differed to the response of PBS treated animals (increased bpm on Day1 and Day3) and notably, to that of α-BMP4 treated animals (increased bpm at all timepoints) which both showed an increased frequency of breathing post administration off the respective aerosols. Also of note, α-BMPR-II treatment, with the exception of Day3, showed the same pattern of decreased frequency over the analysis timeframe as BMP4 treated animals. The tidal volume of all animals analysed increased over the analysis timeframe and no particular difference was noted between treatment groups (Figure 7.18 (B)). With respect to the accumulated volume, all animals increased their Av compared to their t=0hr timepoints (Figure 7.18 (C)). However at Day1 the BMP4 treatment group has a noticeably less improved Av than the other treatment groups. The exact same pattern was noted in the Minute volumes of the different treatment groups (Figure 7.18 (D)). The Ti shows no statistically significant differences across the groups (Figure 7.18 (E)). At Day1 all groups irrespective of treatment group appear to respond in a similar fashion. However on Day3 the Ti of BMP4 treated animals, though still shorter that the t=0hr measurement, is not anywhere as short as seen in any other treatment group, PBS, α-BMP4 and α-BMPR-II inclusive. On Day5 it is the only treatment group to have an increased Ti (+0.0021±0.0007sec) compared to its t=0hr measurements. Te showed a statistically relevant difference between treatment groups (Figure 7.18 (F)). On Day1 and Day3 the PBS treatment group shows a decreased Te whereas BMP4 treated animals show an increased Te across the same timepoints. Both treatment groups show an increased Te on Day5 however. Also of note is the response of the animals treated with α-BMP4, which directly contrasts that of BMP4 treated animals. Whereas BMP4 treated animals show an increase Te over all timepoints, α-BMP4 treated animal show a decreased Te over all timepoints. It is also noted that the α-BMPR-II treatment resulted in a similar profile of Te to BMP4 treated animals and contrasted with that of α-BMP4 and of PBS treatment groups over Day1 and Day3. The differences in the α-BMPR-II animals were not as consistent over time as with BMP4 and α-BMP4 treated animals.

With regard to PIF, it is of note that the flow rate increase from t=0hr in BMP4 treated animals at Day1 was approximately half that of all other treatment groups (Figure 7.19 (A)). The other pattern of note is the contrasting nature of the profiles of the BMP4 and α-BMP4 treatment groups. PEF shows no major differences over the

entire 5 day period, the only difference of note being with PBS treatment animals on Day5 (Figure 7.19 (B)). Of note on Day1 however is the fact that BMP4 treated animals show less than half the increase in flow rate compared to any other treatment group at the same time point. Rt showed a significant difference across the different groups as a result of treatment (Table 7.3) (Figure 7.19 (C)). BMP4 treated animals' show a markedly different profile to PBS treated animals on Day1 and Day5, and to α-BMP4 treated animals across all timepoints. BMP4 treated animals show an increase in Rt whereas PBS and α-BMP4 treated animals show a decline in Rt relative to t=0hr measurements. Animals treated with α-BMPR-II showed a similar profile to BMP4 treated animals. EF50 also shows an interesting set of results (Figure 7.18 (D)). The EF50 profile (-note: an increase in EF50 indicates a decrease in bronchoconstriction) shows that EF50 in all treatment groups at all times, with the exception of PBS treated animals on Day5, showed an increase in flow rate compared to their respective t=0hr measurements. The EF50 profile of BMP4 and α-BMPR-II treatment groups are very similar, whereas at Day1 and Day3 the improvement in EF50 is notably better in the PBS and α-BMP4 treatment groups. EIP shows BMP4 treated animals to have, on Day3 and Day5, noticeably longer EIP than any other treatment groups (Figure 7.19 (E)). EEP however shows no particular differences between any treatment groups with no distinguishing patterns emerging (Figure 7.19 (F)). The change in lung volume on Day1 shows BMP4 treated animals to be the only treatment group to record a decrease in lung volume compared to t=0hr (Figure 7.20 (A)). All other groups show an increase in lung volume on Day1. With respect to all treatment groups it approaches the baseline measurement of t=0hrs at Day5 with the exception of the α-BMP4 antibody treatment group where it drops below the baseline measurement by Day5.

7.2.2.3.4 *Plethysmography analysis of control groups*

At t=0hr plethysmography analysis was carried out on the control groups alongside all the treatment groups as per protocol (Section 2.2.16). This was performed in order to assess the effect that OVA induced asthma brought about in lung function compared to healthy animals. OVA treatment resulted in a number of statistically significant differences between the control groups (Figure 7.21) (Table 7.3). Statistically significant differences were noted in Tv, Av, Mv, PEF and EIP.

7.2.2.3.5 *Immunofluorescence analysis of treatment and control groups*

The expression profile of four different proteins was analysed by immunofluorescence in sections from lungs harvested in response to the different treatments of PBS, BMP4, α-BMP4 and α-BMPR-II (Section 2.2.6 & 2.2.17). The protein expressions examined were PCNA, pSmad1/5/8, Smad4 and Smad8. Smad8 was not detected in any sections analysed so data was not included. A full breakdown of immunofluorescence analysis results can be seen in Table 7.5.

PCNA: PCNA expression, where detected, was localised to the alveolar regions of the lungs (Figure 7.22 and Figure 7.23).

With regards to PBS treated animals, PCNA was not detected in the alveolar region on Day1 and moderate levels of expression were detected in the alveolar region on Day3. Day5 was not determined. BMP4 treated animals showed no expression on Day1 in common with PBS treated animals, and on Day3 had a moderate level of PCNA expression. By Day5 the level of abundance of PCNA expression in the alveolar region was significant. PCNA expression in α-BMP4 treated lungs was at a moderate level in the alveolar region on Day1, higher than what was detected in either of the PBS or BMP4 treated animals. On Day3 the level of expression was significant in the alveolar region, and again far higher than what was detected in any of the other treatment groups including that of α-BMPR-II. Day5 was not determined. α-BMPR-II treated animals were non-determined on Day1. On Day3 the lungs expressed very low levels of PCNA and by Day5 this was had increased to a moderate level of expression resembling the levels seen in the BMP4 and PBS lungs on Day3.

pSmad1/5/8: pSmad1/5/8 protein expression, where detected, was located in the airways of the lungs and not in the alveolar regions (Figure 7.24 and Figure 7.25).

In PBS treated animals the level of pSmad1/5/8 detected in the airways on Day1 was very low, and by Day3 the level detected had increased to a moderate level of abundance/expression. In BMP4 treated animals, pSmad1/5/8 expression was detected at all three timepoints. At the available comparable timepoints of Day1 and Day3, the amounts of pSmad1/5/8 detected in BMP4 treated animals was higher than that of the PBS control group. On Day1 the level detected was low, but by Day3 the level detected escalated to high. On Day5 the level had reduced in comparison to Day3 and a low level of expression was recorded. α-BMP4 treated animals displayed levels of expression on par with what was recorded in BMP4 treated animals, with a low-moderate level of expression on Day1 and a moderate level of expression recorded on Day3. α-BMPR-II treatment on Day3 recorded a moderate level of expression, similar to what was observed in PBS treated animals on Day3. On Day5, as seen in BMP4

treated animals the level of expression dropped and only a small amount of protein was detected.

Smad4: Where expressed, Smad4 was found to be located predominantly in the alveolar region, though airway expression was also recorded in certain samples (Figure 7.26 and Figure 7.27).

On Day1 in the PBS treatment group no Smad4 was detected in the lungs. On Day3 a moderate level of expression was recorded in the alveolar region. BMP4 treated animals expressed, consistently throughout the timepoints against all other treatment groups, the highest level of the Co-Smad, Smad4, expression. On Day1 and Day5 the level of expression was high and the localisation of the Smad4 protein was in the alveolar regions of the lungs. On Day3 the level of expression was again high in the alveolar region but there was additional low level expression occurring tin the airways. α-BMP4 treated animals also had a high level of expression on Day1 on Smad4 in the alveolar region of the lungs. On Day3 the level detected was lower and recorded as moderate, but there was additional low level expression recorded in the airways of lungs from this treatment group. Day5 was not determined. α-BMPR-II was not determined on Day1 but Day3 revealed in a moderate level of expression in the alveolar region and, in common with BMP4 and α-BMP4 treatment groups, a small level of Smad4 expression was detected in the alveolar region. By Day5 the expression was restricted to the alveolar region once more and the level of expression was moderate, in contrast to the high level detected in BMP4 treated animals.

Immunofluorescence analysis was also used to evaluate the differences in protein expression of PCNA, pSmad1/5/8, Smad4 and Smad8 in the control groups- OVA only and PBS sham control-these animals received no aerosol treatments. These lungs were harvested at the same time as lungs from the Day5 treatment group.

pSmad1/5/8 expression in the OVA lungs was low but higher than in the PBS treated animal where only trace amounts of the protein were detected (Figure 7.28 (i)).Where detected, the protein was located in the airways and none was found to be expressed in the alveolar regions. PCNA expression was very low in the PBS treated animals in general. Localisation was restricted to the alveolar regions near the extremities of the lungs, and was not found in the central regions. OVA treated animals however expressed a high level of PCNA protein. Localisation was in the alveolar regions and spread throughout the entire lung, not just the outer regions as seen in the PBS animals (Figure 7.28 (ii)).

Smad4 analysis showed no expression of the protein in the PBS treated animals. OVA lungs expressed high levels of the Co-Smad protein, with localisation restricted to the alveolar regions of the lungs (Figure 7.29 (i)). The Receptor Smad, Smad8, was also analysed. In this instance Smad8 was detected at a moderate level in the airways of the OVA lungs. PBS control lungs showed no expression of Smad8 (Figure 7.29 (ii)). A summary of the data is available in Table 7.5.

7.2.2.3.6 Bodyweight and BAL analysis

Bodyweight of every animal from the aerosol treated OVA groups was recorded immediately after sacrifice. Two-way ANOVA and Bonferroni posttest analysis were carried out to determine any significant differences as a result of treatment type. No significant differences were found in bodyweight analysis (Figure 7.30 (A)). The percentage of viable cells in the different treatment groups BAL fluid was analysed and no statistical difference here was noted between any of the groups, nor was any statistical difference noted in the cell concentration of the BAL fluid. Although it was noted that α-BMP4 treated animals, especially at Day1, but also on Day3, had a greater cell concentration in the BAL than any other treatment type. Body weight analysis and cell concentration of the OVA and PBS control animal treatment groups were also recorded. With regard to bodyweight there was a very significant difference as a result of OVA treatment in the body weight of the animals ($p<0.005$) (Figure 7.31 (A)). No statistical difference was noted between the differing cell concentration averages recorded in the BAL fluid of both treatment groups but it was noted that as expected, the OVA treated animals showed a higher cell concentration average than that of the PBS control group (Figure 7.31 (B)).

7.2.2.3.7 Cytospin analysis

Cytospins were prepared from the BAL fluid of treated groups of animals on Days 1, 3 and 5. Visual comparison of the cytospins showed no major change in the profile of cells expressed in the BAL fluids in the different treatment groups, as can be seen in Figure 7.32.

7.2.2.3.8 Western blot analysis of whole lung protein

After BAL was harvested lungs were snap frozen in liquid Nitrogen and stored at -80°C. Later the lungs were then homogenised and the protein isolated as per Section 2.2.18. Protein concentration was determined by Bradford assay and 20μg protein from each sample was loaded per lane in 12% SDS page gels (Section 2.2.8). Actin

was used as housekeeper and the protein blots were probed for the presence of Actin and the proteins of interest, Smad4 and pSmad1/5/8, as can be seen in Figure 7.32 (A, B, C). Densitometry was carried out on the detected bands and the results graphed as per Figure 7.33 (D and E). The results were analysed by one-way ANOVA and a full breakdown of statistical results can be seen in Table 7.6.

pSmad1/5/8 statistical analysis showed that treatment had an extremely significant effect on the levels of the protein in the different treatment groups ($p<0.001$). It was noted that every timepoint BMP4 treated animals showed a higher level of pSmad1/5/8 expression than any other treatment group. At Day1 and Day5 α-BMP4 treated animals showed a greater than half fold decrease in the level of expression than PBS treated animals. α-BMPR-II treated animals consistently expressed the least amount of pSmad1/5/8 compared to all other groups at all timepoints.

In relation to Smad4 expression, although treatment resulted in a significant effect across all treatment groups ($p<0.05$), no individual treatment group over the course of the experiment a distinct pattern of increased or decreased expression relative to the PBS control.

pSmad1/5/8 was also analysed in the control OVA and PBS groups as can be seen in Figure 7.34. T-test analysis was performed on the results but no significant difference was noted between the two groups. It was noted however that the OVA control group, as was anticipated, showed on average a higher, though not statistically significant, level of pSmad1/5/8 than the PBS control group.
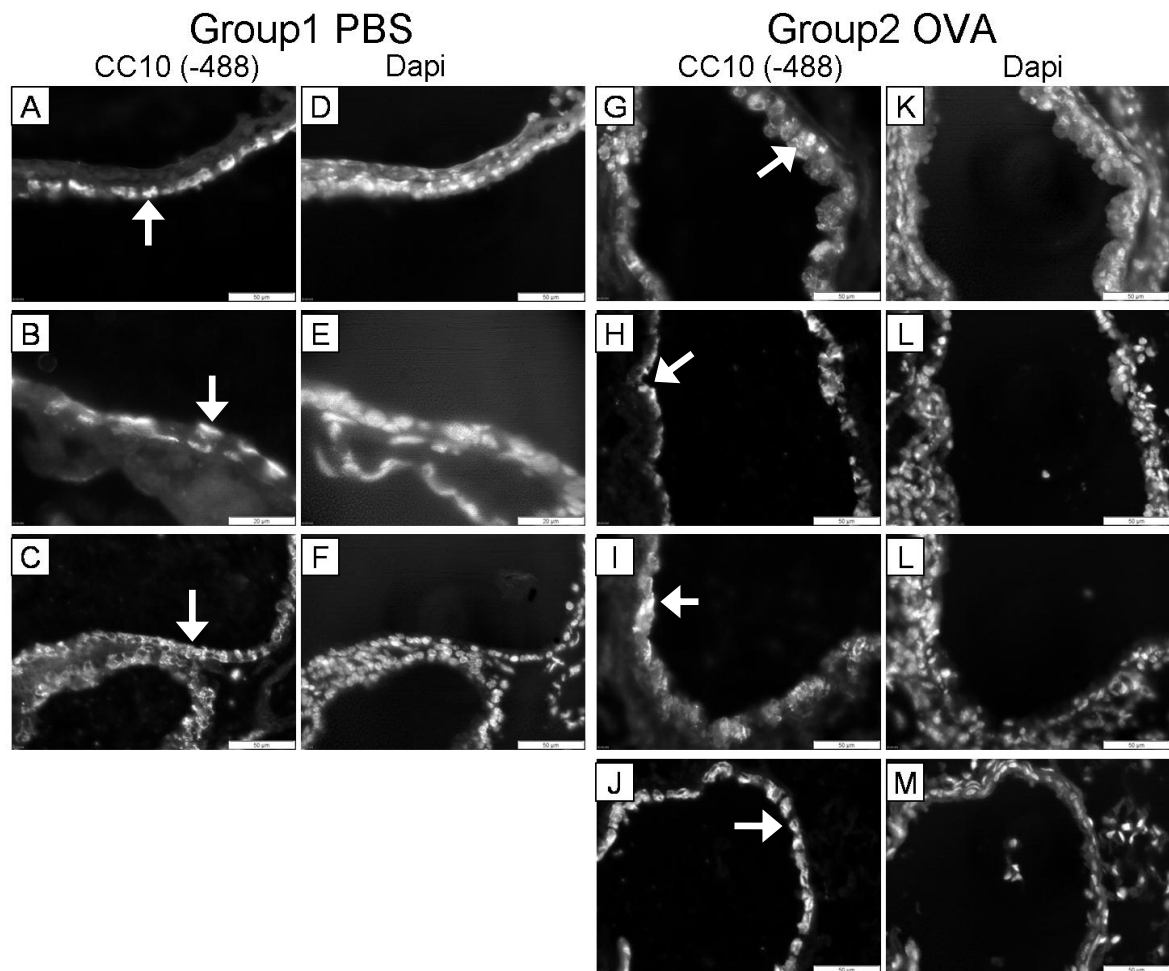
Figure 7.16 CC10 immunofluorescence in OVA model of Asthma

CC10 staining was observed in the airways of both Control and OVA exposed animals. However it was detected at a higher level in Group2, the OVA exposed asthma model, though this difference was not quantifiable.
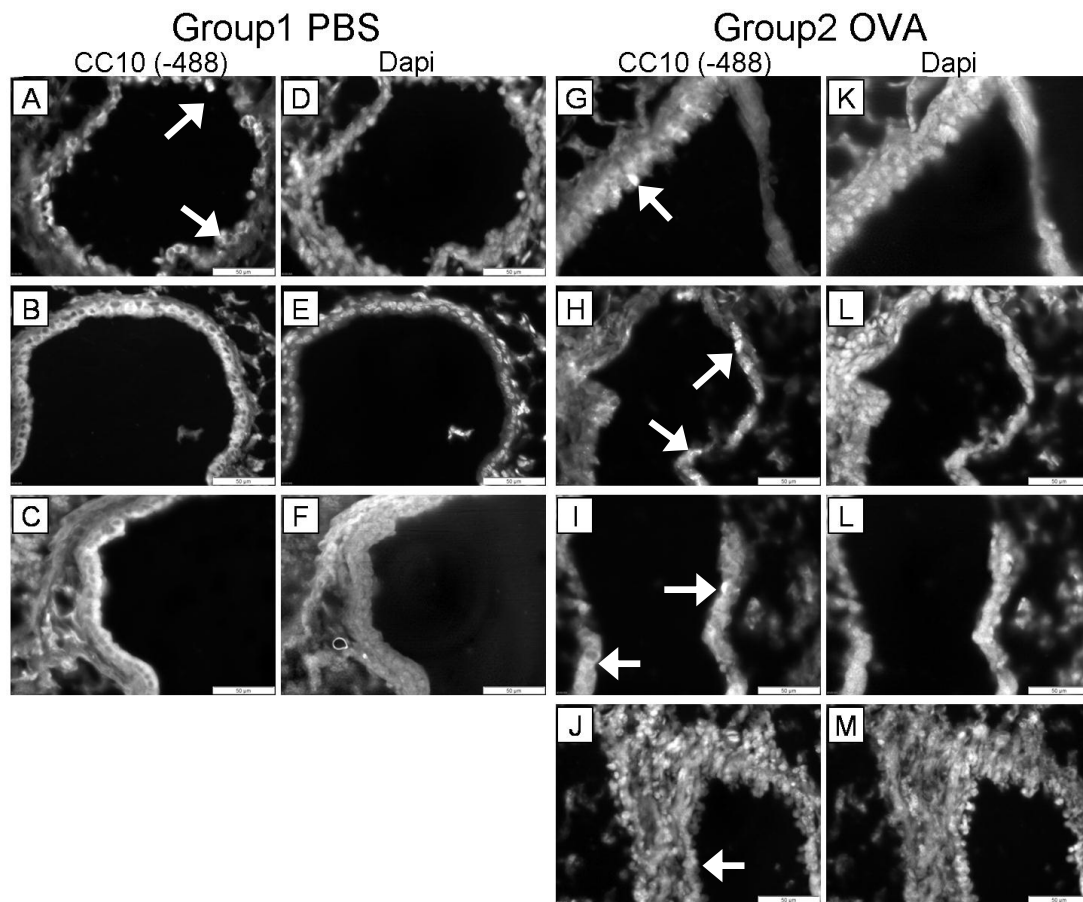
Figure 7.17 pSmad1/5/8 immunofluorescence n OVA model of Asthma

pSmad1/5/8 was more evident in Group2 OVA treated animals than in Group1 controls. Occasionally airways in Group1 animals displayed small amounts of localised phosphorylated Smads, though in general, as seen in B and C, no pSmad1/5/8 was detected in Group1 animals and the staining in evidence here was tissue autoflouresence. Group2 animals however displayed an abundant amount of pSmad1/5/8 staining in the airways as can clearly be seen in G, H, I and J above, indicated by the bright white in the airways. Arrows also indicate areas of fuorescence, the duller white seen in the alveolar regions is auto-fluorescence.
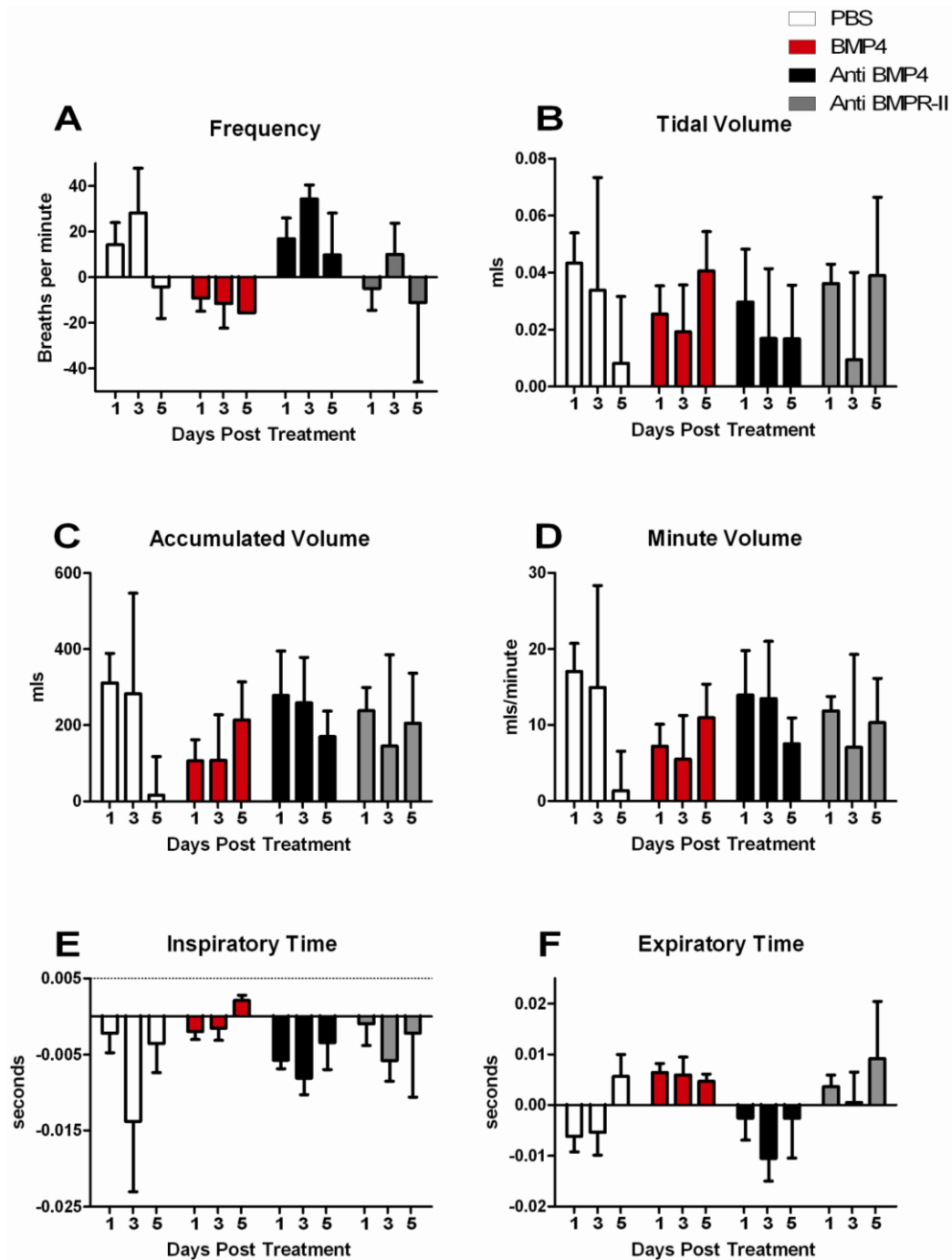
Figure 7.18 Plethysmography results on different treatments on OVA induced Asthma BALB-C mice carried out over a 5 day period (n=4†)

Treatment was administered at t=0hr, 1hr post initial plethysmography readings. Plethysmography was repeated on the treatment groups immediately prior to harvest at t=24hr, t=72hr and t=120hr. Statistical analysis was carried out by twoway ANOVA and a full statistical breakdown can be seen in Table 7.2.Graphs show the difference in readings between t=0hr and time of harvest, Day1, 3 or 5 respectively. *†PBS day1 n=3, BMP4 day5 n=3, α-BMPR-II day5 n=3.*
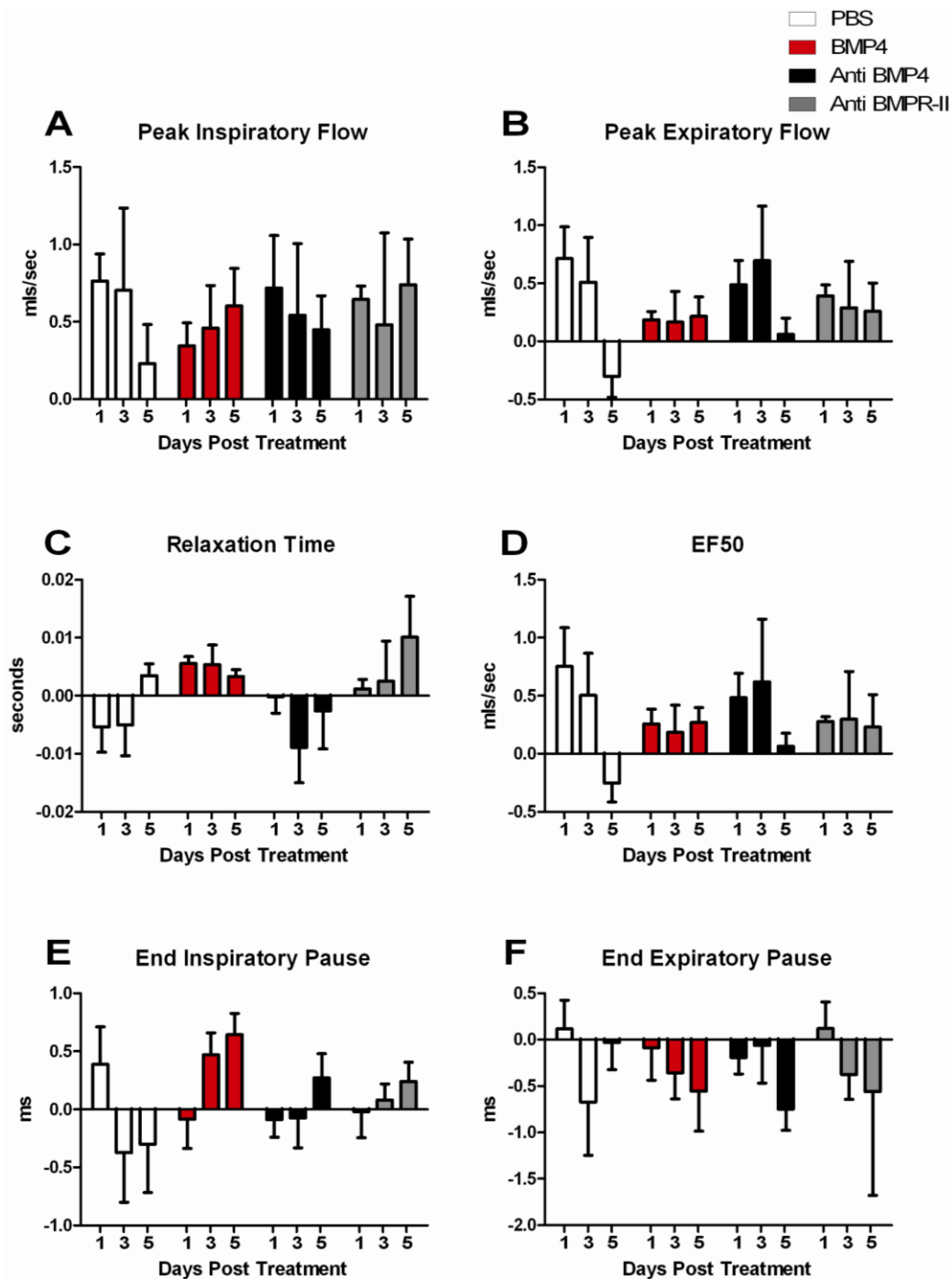
Figure 7.19 Plethysmography results on different treatments on OVA induced Asthma BALB-C mice carried out over a 5 day period (n=4†)

Treatment was administered at t=0hr, 1 hour post initial plethysmography readings. Plethysmography was repeated on the treatment groups immediately prior to harvest at t=24hr, t=72hr and t=120hr. Statistical analysis was carried out by two-way ANOVA and a full statistical breakdown can be seen in Table 7.2. Graphs show the difference in readings between t=0hr and time of harvest, Day1, 3 or 5 respectively. *†PBS day1 n=3, BMP4 day5 n=3, α-BMPR-II day5 n=3.*
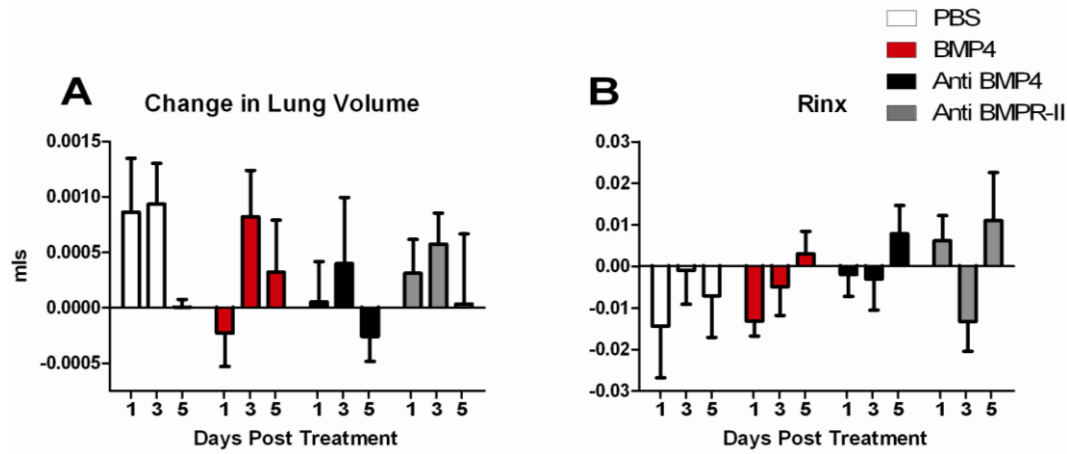
Figure 7.20 Plethysmography results on different treatments on OVA induced Asthma BALB-C mice carried out over a 5 day period (n=4†)

Treatment was administered at t=0hr, 1 hour post initial plethysmography readings. Plethysmography was repeated on the treatment groups immediately prior to harvest at t=24hr, t=72hr and t=120hr. Statistical analysis was carried out by two-way ANOVA and a full statistical breakdown can be seen in Table 7.2. Graphs show the difference in readings between t=0hr and time of harvest, Day1, 3 or 5 respectively. *†PBS day1 n=3, BMP4 day5 n=3, α-BMPR-II day5 n=3.*

Measurement	Two-Way ANOVA Analysis			Bonferroni Post Test
	Interaction	**Treatment**	**Time**	**_**
Frequency (f)	-	*	-	-
Tidal Volume (Tv)	-	-	-	-
Accumulated Volume (Av)	-	-	-	-
Minute Volume (Mv)	-	-	-	-
Inspiratory Time (Ti)	-	-	-	-
Expiratory Time (Te)	-	*	-	-
Peak Inspiratory Flow (PEF)	-	-	-	-
Peak Expiratory Flow (PIF)	-	-	-	-
Relaxation Time (Rt)	-	*	-	-
EF50	-	-	-	-
End Inspiratory Pause (EIP)	-	-	-	-
End Expiratory Pause (EEP)	-	-	-	-
Change in Lung Volume (dV)	-	-	-	-
Rinx	-	-	-	-

Table 7.2 Plethysmography analysis of Treatment Groups

Analysis was carried out by two way ANOVA with Bonferroni post test analysis on plethysmography data from OVA induced allergic asthma lungs exposed to an aerosol of either PBS, BMP4, αBMP4 antibody or αBMPR-II antibody. Two-way ANOVA revealed significant differences in f, Tv, Te and Rt between different treatment groups overall- ie there was a significant difference between PBS vs. BMP4 vs. α-BMP4 vs. αBMPR-II overall . Bonferroni posttest analysis between individual treatments, ie, BMP4 treated vs. Anti- BMP4 etc., did not show any further significant differences between individual treatment types.
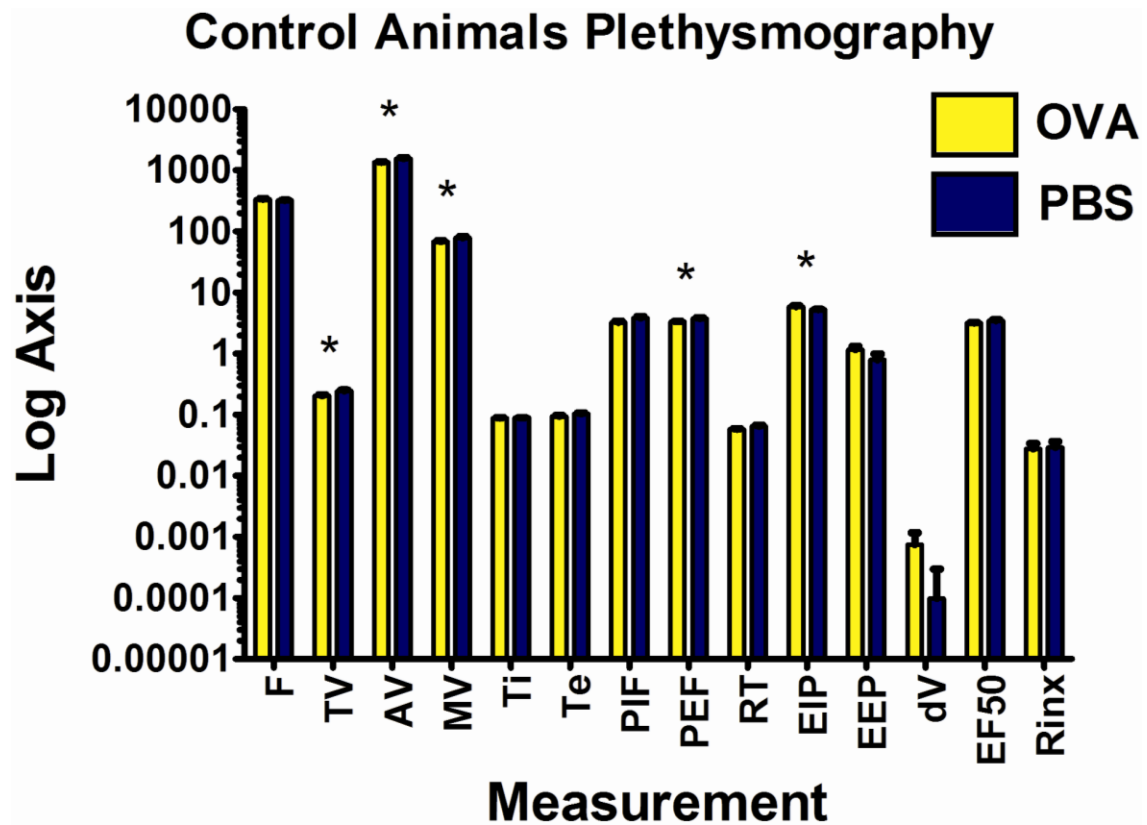
Figure 7.21 Plethysmography results on OVA induced Asthma BALB-C mice
Plethysmography carried out after completion of OVA treatment and immediately prior to treatments commencing (n=4 for OVA and PBS groups). Statistical analysis was carried out by t-test between all readouts and a full set of statistical breakdown can be seen in Table 7.3. An explanation of all measurements can be found in Section 7.1.1.

Measurement	T-Test Analysis
Frequency (f)	-
Tidal Volume (Tv)	*
Accumulated Volume (Av)	*
Minute Volume (Mv)	*
Inspiratory Time (Ti)	-
Expiratory Time (Te)	-
Peak Inspiratory Flow (PIF)	-
Peak Expiratory Flow (PEF)	*
Relaxation Time (Rt)	-
EF50	-
End Inspiratory Pause (EIP)	*
End Expiratory Pause (EEP)	-
Change in Lung Volume (dV)	-
Rinx	-

Table 7.3 Plethysmography analysis of Control Groups

Statistical analysis was carried out by way of t-test in order to determine if the onset of OVA induced asthma in the lung could, without challenge, be successfully detected by plethysmography. This showed that a number of measurements were statistically different between the two groups, including Tv, Av, Mv, PEF and EIP.
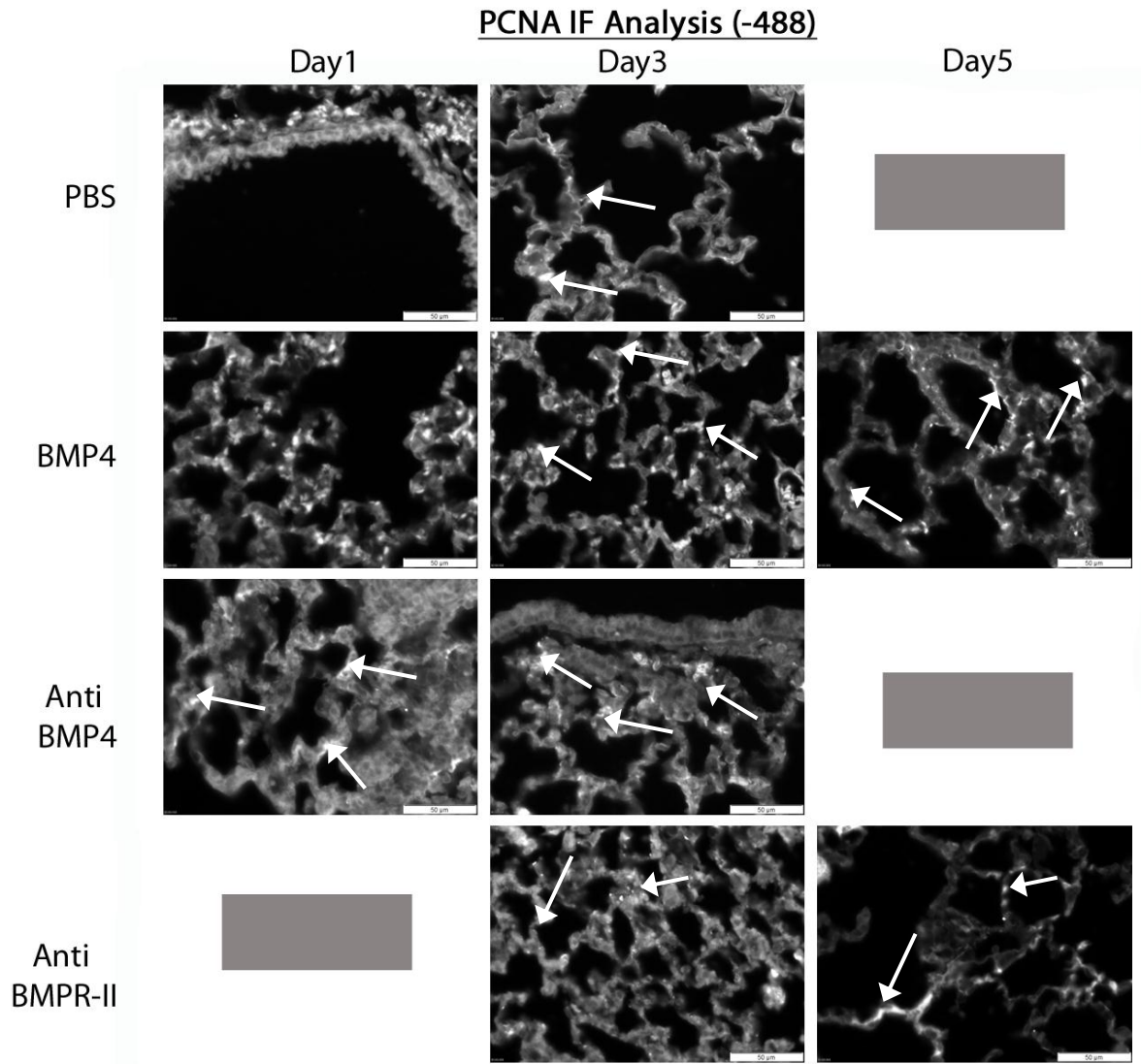
Figure 7.22 PCNA expression levels in aerosol exposed OVA lung

(see overleaf for Figure Legend)

Figure 7.22 PCNA expression levels in aerosol exposed OVA lung

PCNA expression levels in OVA animals treated with aerosolised: PBS, BMP4, αBMP4 and α-BMPR-II.

Day1: PCNA was not detected in PBS or BMP4 treated animals at a significant level, with the airways showing only Auto-fluorescence and predominantly no PCNA (sporadic trace amounts were found) in evidence in the Alveoli. PCNA staining was apparent α-BMP4 treated animals however. PCNA was detected in PBS and BMP4 treated animals at a moderate level compared to other sections examined, with staining restricted to the alveolar regions.

Day3: No staining was apparent in the airways. PCNA staining in α-BMP4 treated animals was significant when compared to other sections examined, with an abundance of staining apparent in the alveolar regions of the lungs. Staining was also visible in the α-BMPR-II animals; however it was at a lower level than that seen in any of the other treatment groups examined.

Day5: staining restricted to the alveolar regions. No staining was apparent in the airways. Compared to other sections in the treatment groups examined, PCNA was moderately abundant in the α-BMPR-II treated animals, but highly abundant in the BMP4 treated animals.

Arrows indicate some areas of actual PCNA fluorescence where present.
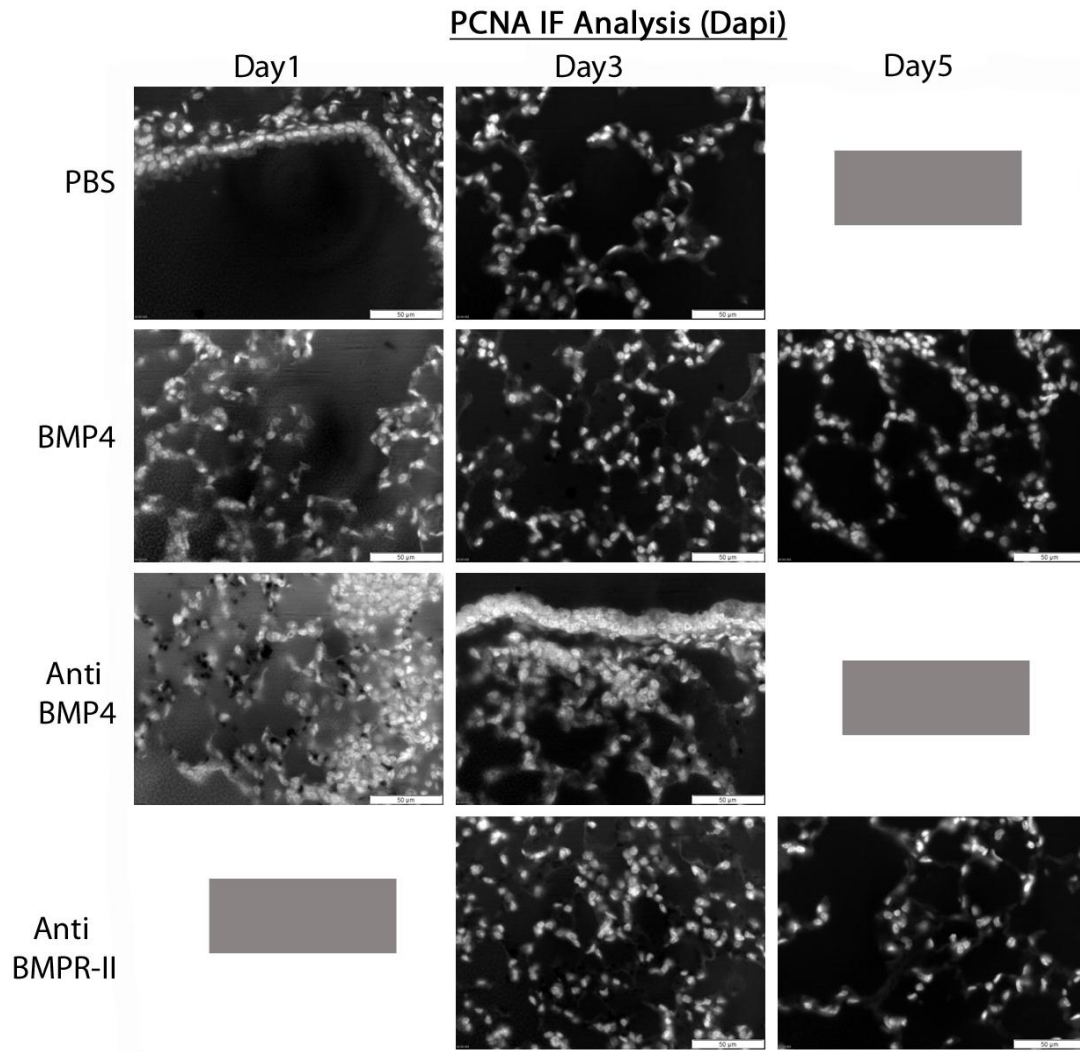
Figure 7.23 Dapi counterstain for PCNA expression levels in aerosol exposed OVA lung

Dapi counterstain to PCNA expression analysis (Figure 7.22) PCNA expression levels in OVA animals treated with aerosolised: PBS, BMP4, αBMP4 and α-BMPR-II (Figure 7.22).
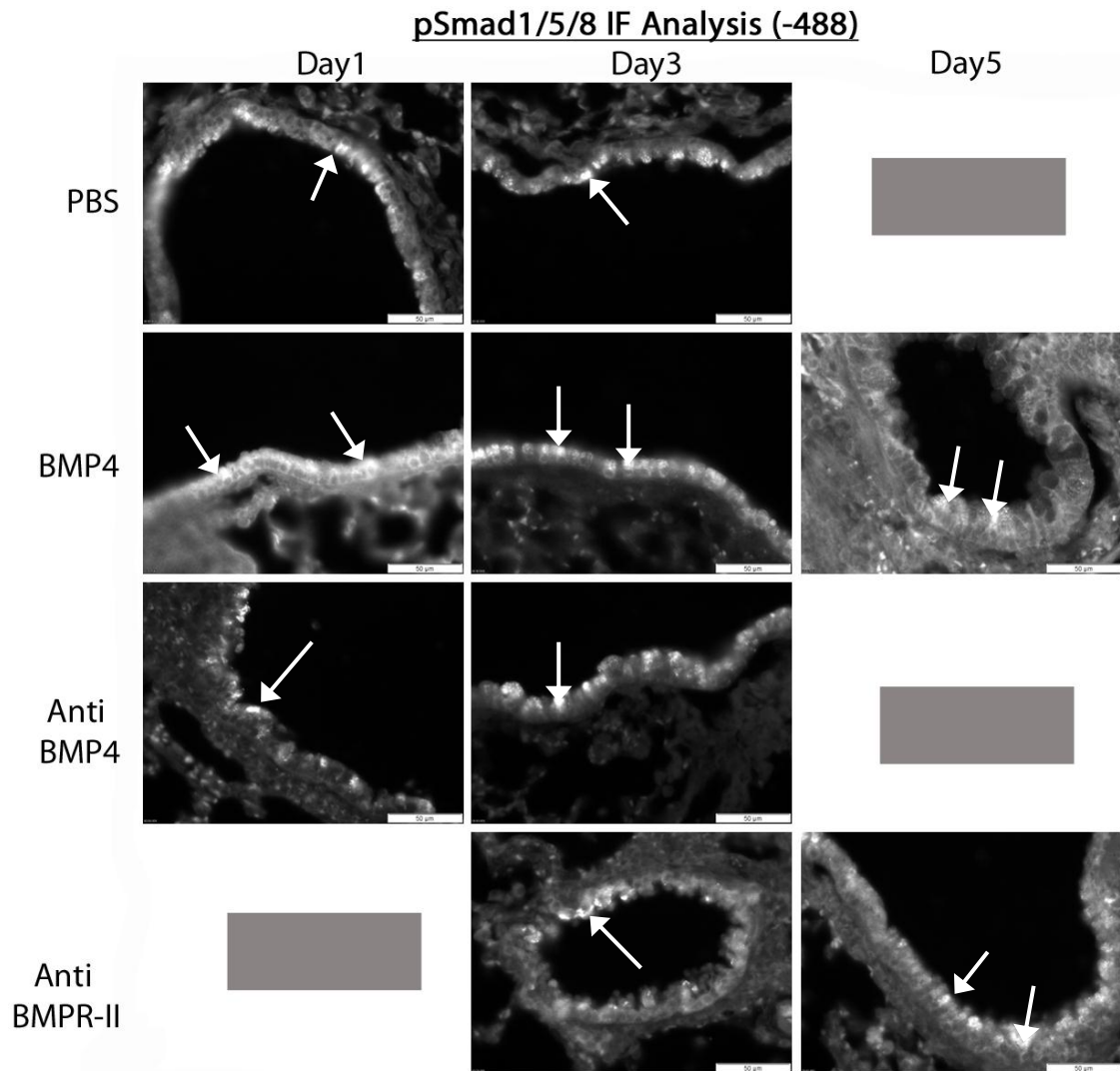
Figure 7.24 pSmad1/5/8 expression levels in aerosol exposed OVA lung

pSmad1/5/8 expression levels in OVA animals treated with aerosolised: PBS, BMP4, αBMP4 and α-BMPR-II.

Day1: By comparing all treatment groups the levels of staining in Day1 treatment groups can be described as very low in PBS treated animals, low in BMP4 treated animals, though more than seen in PBS treated. pSmad1/5/8 staining was slightly more abundant again in animals treated with α-BMP4.

Day3: pSmad1/5/8 was detected in all treatment groups. It was least abundant in α-BMP4 treated animals and most abundant in BMP4 treated animals. Both PBS and α-BMPR-II treated groups of animals had moderate levels of pSmad1/5/8 present, though not to the same level as seen in BMP4 treated animals.

Day5: pSmad1/5/8 was detected in both BMP4 (A) and α-BMPR-II (B) treated. Compared to other sections in the treatment groups examined, pSmad1/5/8 was detected at a low level in both the BMP4 (A) and α-BMPR-II (B) treated animals. Arrows indicate some areas of actual pSmad1/5/8 fluorescence where present.
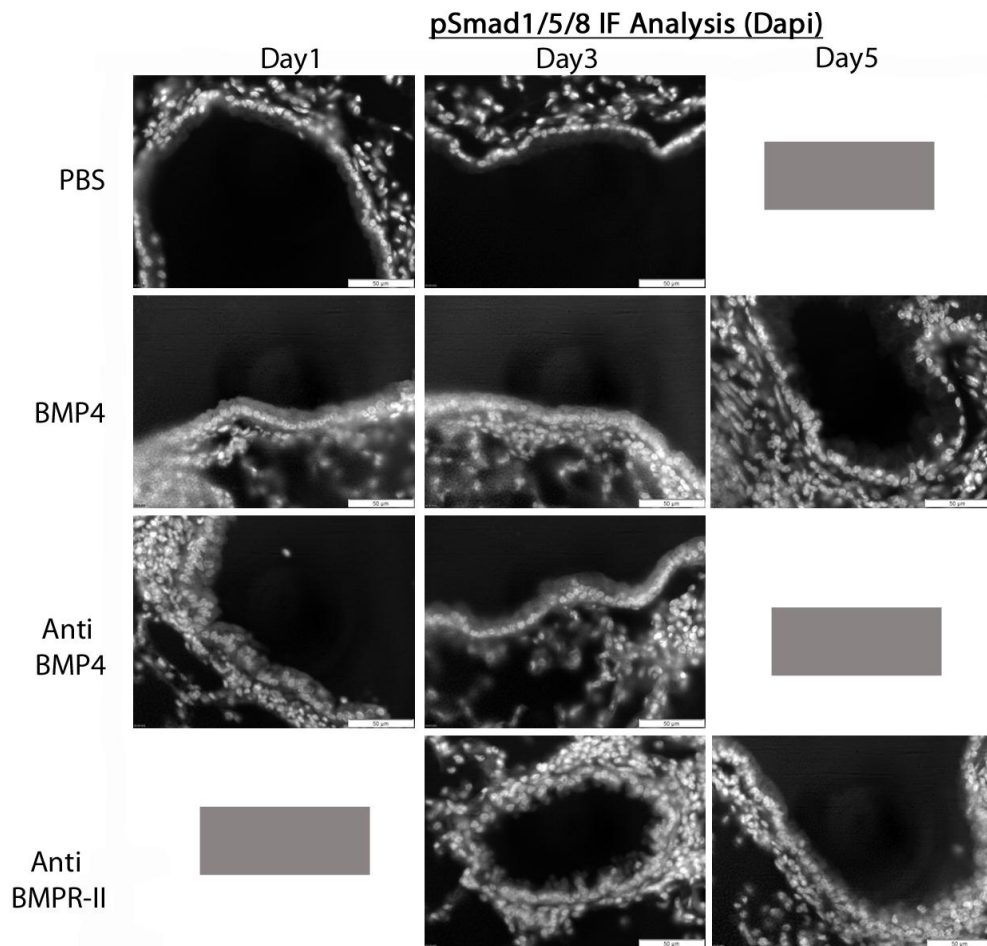
Figure 7.25 Dapi counterstain for pSmad1/5/8 expression levels in aerosol exposed OVA lung

Dapi counterstain to pSmad1/5/8 expression levels in OVA animals treated with aerosolised: PBS, BMP4, αBMP4 and α-BMPR-II (Figure 7.24).
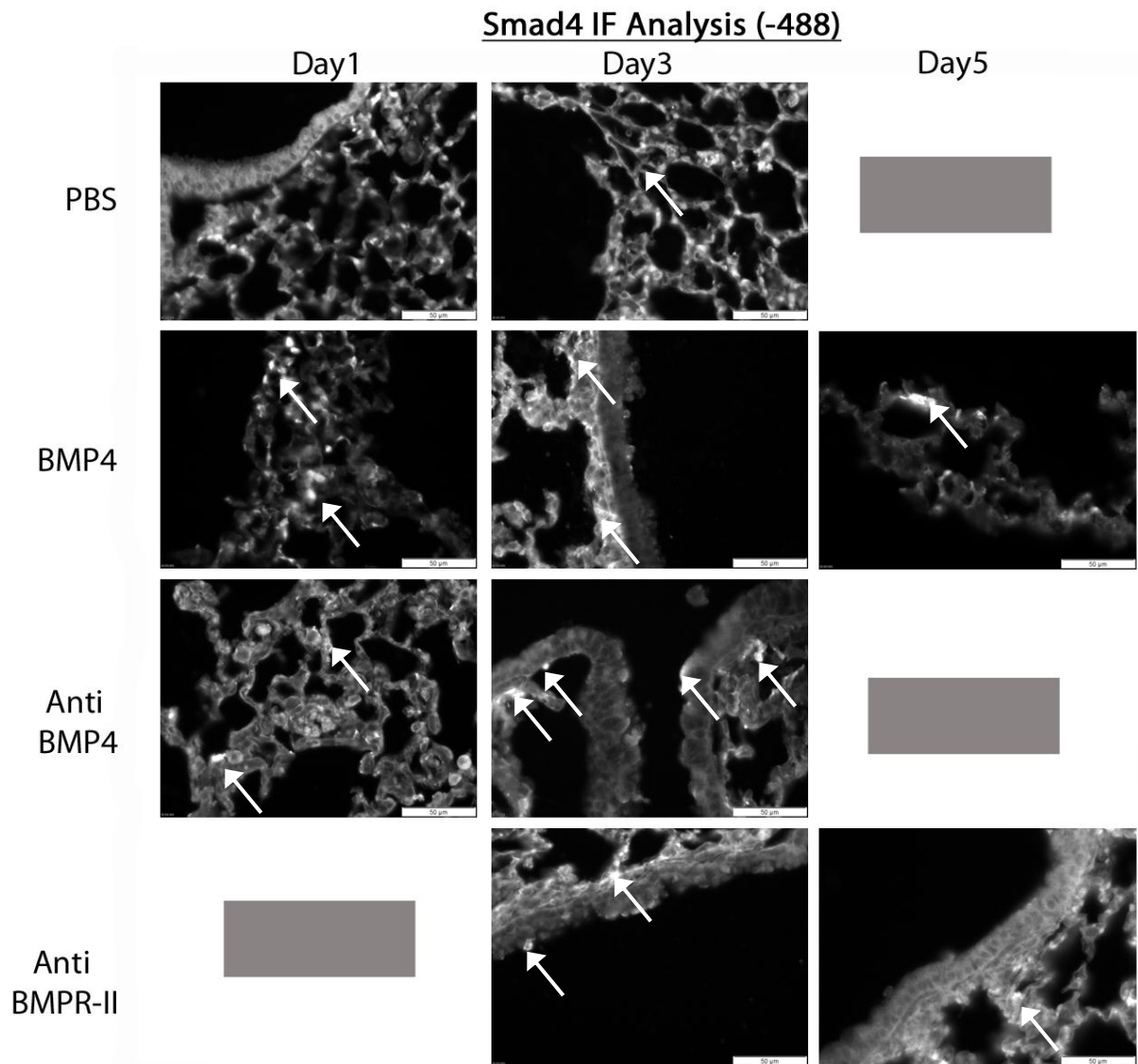
Figure 7.26 Smad4 expression levels in aerosol exposed OVA lung

Day1: Levels of Smad4 in Day 1 treatment groups can be described as not present in PBS treated animals, detected at high levels in BMP4 treated animals and detected at high levels in α-BMP4 treated animals, though not as high as in BMP4 treated lungs. Staining was evident in the alveolar regions of examined lungs, not airways.

Day3: Smad4 detected in all treatment groups. In the PBS treatment group Smad4 appeared only in the alveolar region and at a moderate level of abundance. In BMP4, α-BMP4 and α-BMPR-II treatment groups Smad4 was detected at very low levels in airways, located sporadically in some airways in individual cells. In alveolar regions of these treatment groups, Smad4 was detected at high levels in BMP4 treated animals and at lower, moderate levels in α-BMP4 and α-BMPR-II treated animals.

Day5: Smad4 was detected in both BMP4 and α-BMPR-II treated. Compared to other sections in the treatment groups examined, Smad4 was detected at a high level in BMP4 treatment group and at a moderate level in α-BMPR-II treated animals.

Arrows indicate some areas of actual Smad4 fluorescence where present.

Figure 7.27 Dapi counterstain for Smad4 expression levels in aerosol exposed OVA lung

Dapi counterstain to Smad4 expression levels in OVA animals treated with aerosolised: PBS, BMP4, αBMP4 and α-BMPR-II (Figure 7.26).

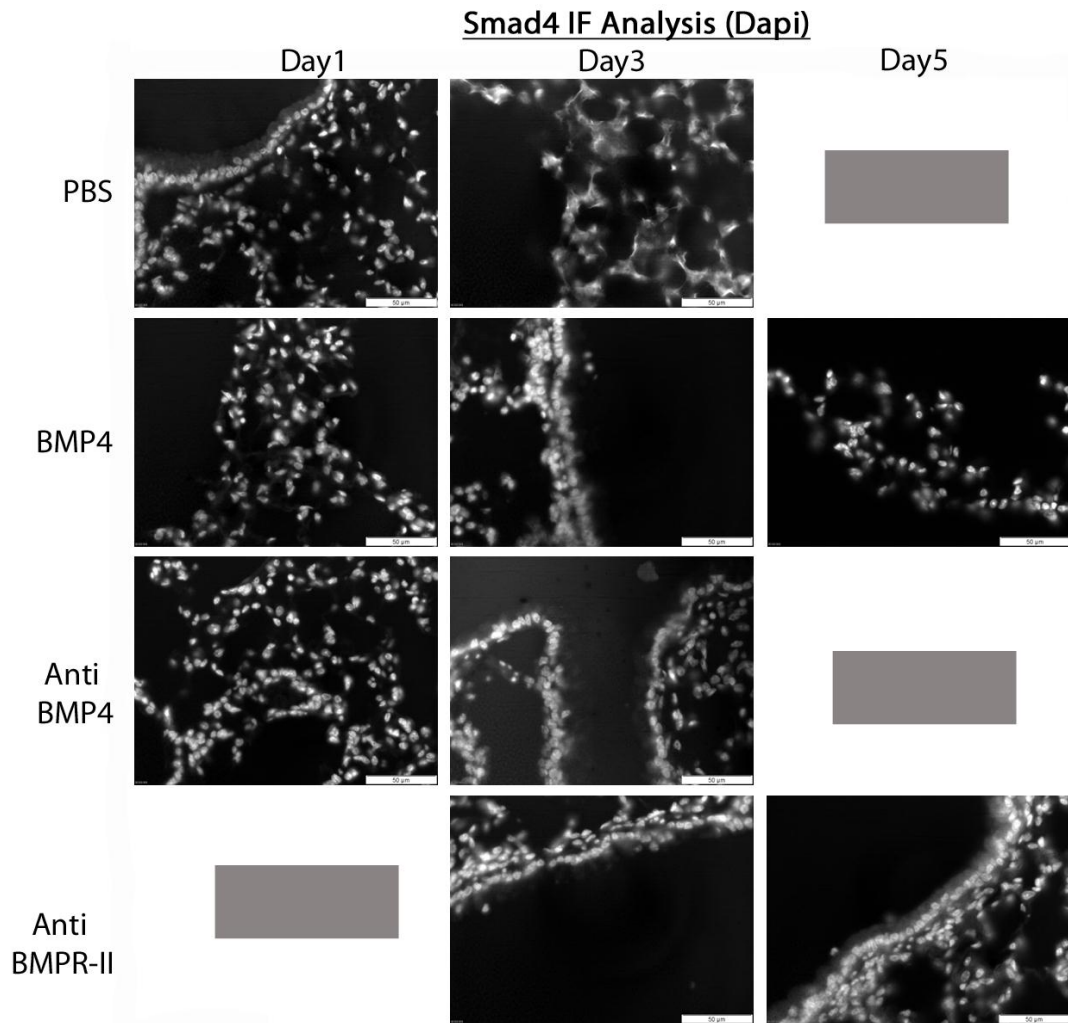|	**Day1**	**Day3**	**Day5**
PCNA			
PBS	Not detected	Moderate level of expression-Alveolar	Not Determined
BMP4	Not detected	Moderate level of expression- Alveolar	High level of abundance/expression-Alveolar
α-BMP4	Moderate alveolar expression	High level of abundance/expression-Alveolar	Not Determined
α-BMPR-II	Not Determined	Very low level of expression- Alveolar	Moderate level of expression- Alveolar
pSmad1/5/8			
PBS	Very low level of expression- Airway	Moderate Airway expression	Not Determined
BMP4	Low level of expression- Airway	High level of abundance/expression-Airway	Low level of expression- Airway
α-BMP4	Low/moderate level of expression-Airway	High level of abundance/expression-Airway	Not Determined
α-BMPR-II	Not Determined	Moderate level of expression-Airway	Low level of expression- Airway
Smad4			
PBS	Not detected	Moderate alveolar expression	Not Determined
BMP4	Highest level of abundance/expression-Alveolar	Highest level of abundance/expression-Alveolar. Small amount of airway expression detected.	High level of abundance/expression-Alveolar
α-BMP4	High level of abundance/expression-Alveolar	Moderate level of expression- Alveolar. Small amount of airway expression detected.	Not Determined
α-BMPR-II	Not Determined	Moderate level of expression- Alveolar. Small amount of airway expression detected.	Moderate level of expression- Alveolar

Table 7.4 Immunofluorescence analysis of OVA induced asthmatic BALB/c mice after exposure to potential therapeutics

Samples which could not be analysed were marked as 'Not Determined'.

Figure 7.28 Day5 pSmad1/5/8 and PCNA protein expression analysis of the OVA treated control versus the PBS control group

(i) Day5 pSmad1/5/8 protein expression; PBS control group showed almost no pSmad1/5/8 expression in airways-predominantly auto-fluorescence is shown in (B). Very low levels of protein were seen in OVA model (A). Corresponding Dapi images can be seen in C, D.

(ii) Day5 PCNA protein expression; Very little PCNA was in evidence in PBS control group, with only small amounts of PCNA being detected in the extremities of the lung region as indicated in B. The OVA group however had a high level of expression of PCNA throughout all the alveolar regions of all lungs examined (A). Corresponding Dapi images can be seen in C, D. Arrows indicate detected protein.

Figure 7.29 Day5 Smad4 and Smad8 protein expression analysis of the OVA treated control versus the PBS control group

(i) Day5 Smad4 protein expression; No Smad4 protein was in evidence in the PBS control group, as indicated in B. The OVA group however had a high level of expression of Smad4 throughout all the alveolar regions of all lungs examined (A). Corresponding Dapi images can be seen in C and D.

(ii) Day5 Smad8 protein expression; PBS control group showed no Smad8 protein expression in the airways or alveoli; predominantly auto-fluorescence is shown in B. A moderate level of expression was seen in the OVA model (A) however, located in the airways. Corresponding Dapi images can be seen in C and D.

Arrows indicate detected protein.

Treatment Group	OVA	PBS
Protein Analysed		
PCNA	High level of abundance/expression-Alveolar	Very low level of expression- Alveolar-Only at edge of lungs
pSmad1/5/8	Low level of expression-Airway	Very low level of expression- Airway
Smad4	High level of abundance/expression-Alveolar	Not detected
Smad8	Moderate level of expression-Alveolar	Not detected

Table 7.5 Immunofluorescence analysis of Control groups

OVA induced asthma in lungs resulted in increased levels of PCNA and pSMAD1/5/8 in the lungs compared to PBS control animals. OVA lungs also contained high levels of Smad4 and moderate levels of Smad8 where neither protein was detected to any noticeable level in PBS control animals as determined by immunofluorescence analysis.
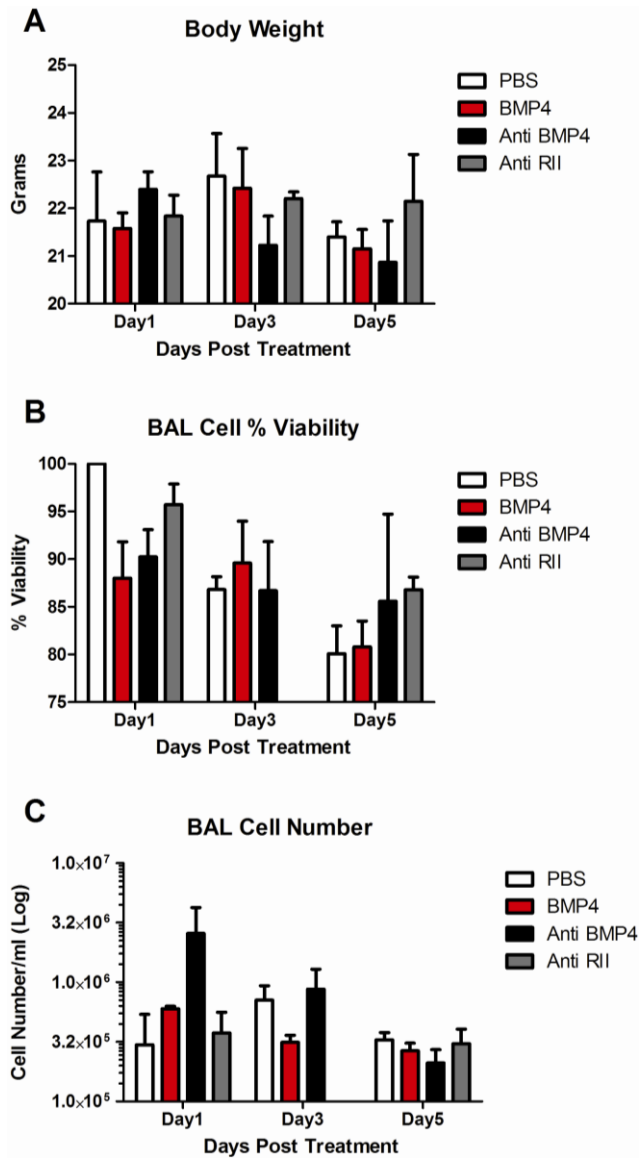
Figure 7.30 Body weight (n=4†) and BAL fluid (n=3‡) analysis results

No significant difference was observed in bodyweights between the treated groups or within the individual treatments when analysed by two-way ANOVA and Bonferroni post-tests. No pattern was evident either showing that in OVA treated animals no treatment resulted in a statistically significant weight gain or weight loss. Due to missing values two ways ANOVA could not be used to analyse Cell % viability or cell number. No patterns were evident in the % viability of the cells present in the BAL also. With regards to cell number however it appeared that, although not statistically significant, α BMP4 resulted in a greater influx of cells into the BAL fluid over the first 3 days before returning to a level closer to that of the other treatments by day5.

† Body weight: PBS Day1 n=3; α-BMP4 Day5 n=3; α-BMPR-II day3 n=3.

‡BAL fluid analysis: PBS day1 n=2; α-BMP4 Day1, 3, 5 n=2; α-BMPR-II Day3 Data not available.
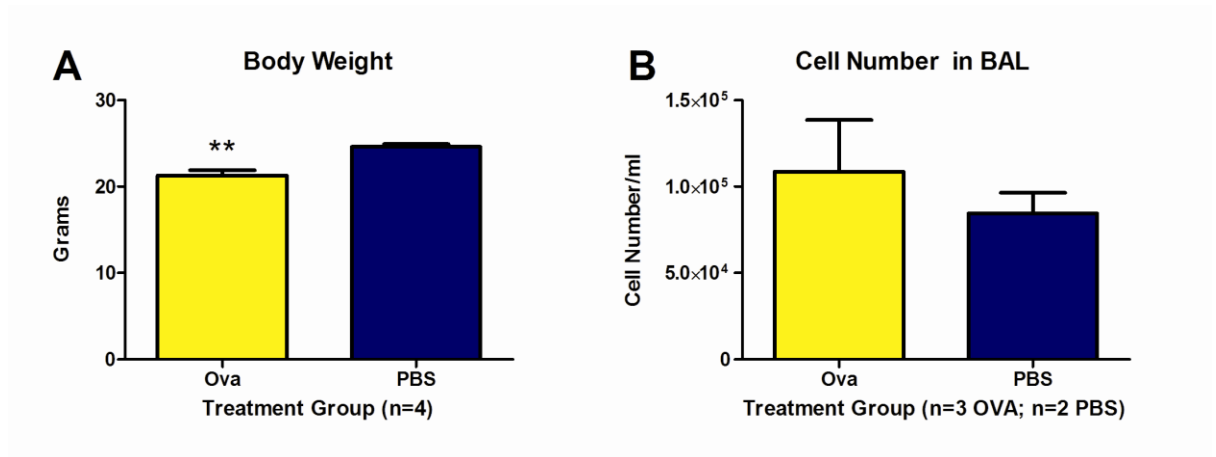
Figure 7.31 Analysis of the Bodyweight of the OVA group vs. the PBS control group

There was a significant difference (p<0.005) in body weight between the two groups of animals (A). No significant difference was found in the cell concentration in the BAL fluid (B).
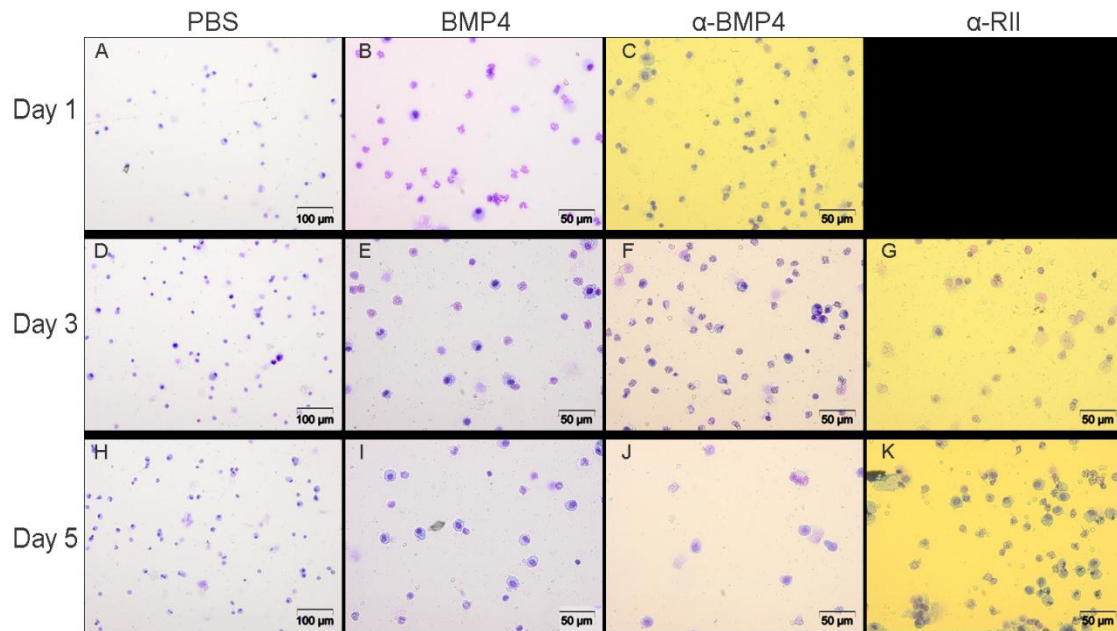
Figure 7.32 Cytospin images form OVA induced asthmatic lungs after aerosol delivery of potential therapeutics

Cytospins were taken from the BAL fluid of the 4 different treatment groups over days 1, 3 and 5. No data was available for Day1 α-BMPR-II. No major differences in cell populations were observed in the Cytospins.
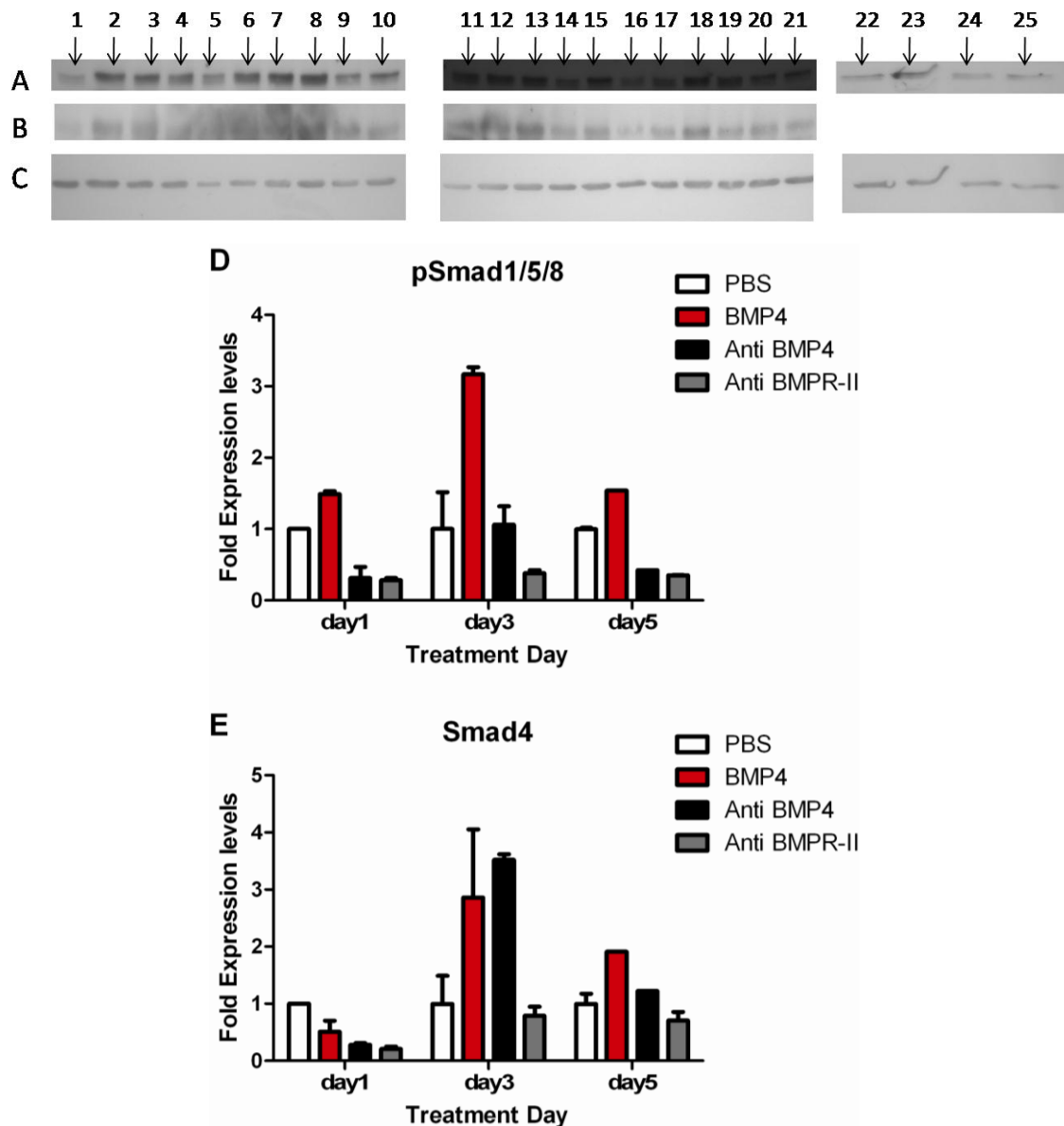
Figure 7.33 Actin, Smad4 and pSmad1/5/8 Western Blots and densitometry results from whole lung protein analysis (n=2†)

All lanes were loaded with equal amounts of whole lung protein (20µg/lane). Actin was used as housekeeper, against which the expression levels of the target proteins were measured. Lungs treated with PBS were then used as the standard against which levels of the target proteins were measured against from the other treatment groups. The image above shows Actin (A), Smad4 (B) and pSmad1/5/8 (C) western blots. The graphs below show the fold expression levels of pSmad1/5/8 (D) and Smad4 (E) in each of the treatment groups at the three different timepoints. As analysed by two-way ANOVA the treatments were responsible for extremely significant ($p < 0.0001$) differences in the fold expression levels of pSmad1/5/8 across the different treatment groups, and a significant effect ($p < 0.05$) on Smad4 expression. Full statistical analysis can be seen in Table 7.6. Numbers 1-25 indicate corresponding individual samples. †PBS Day1 n=1; BMP4 Day5 n=1; α-BMP4 Day5 n=1.

	Two-Way ANOVA Analysis			Bonferroni Post Test	
	Interaction	Treatment	Time		
pSmad1/5/8	*	***	**	Day3 PBS vs. BMP4	***p<0.001
				Day1 BMP4 vs. α-BMP4	** p<0.01
				Day3 BMP4 vs. α-BMP4	***p<0.001
				Day1 BMP4 vs. α-BMPR-II	** p<0.01
				Day3 BMP4 vs. α-BMPR-II	***p<0.001
				Day5 BMP4 vs. α-BMPR-II	* p<0.05
Smad4	-	*	**	Day3 PBS vs. BMP4	* p<0.05
				Day3 PBS vs. α-BMP4	** p<0.01
				Day3 BMP4 vs. α-BMPR-II	* p<0.05
				Day3 αBMP4 vs. α-BMPR-II	** p<0.01

Table 7.6 Western blot analysis of whole lung protein

Western blotting in combination with densitometry revealed a significant level of difference between treatments by way of two-way ANOVA analysis and further specific differences could be seen by way of Bonferroni posttest analysis.
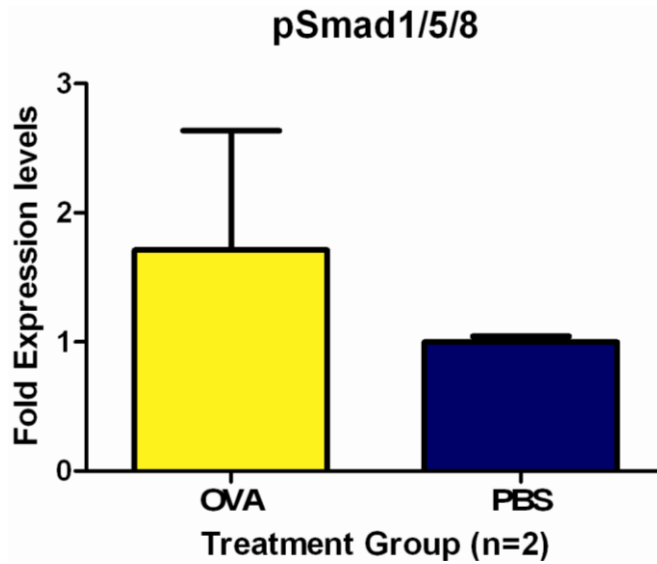
Figure 7.34 pSmad1/5/8 expression levels in control animals.

pSmad1/5/8 expression levels were not significantly different, as determined by t-test analysis. A greater amount of pSmad1/5/8 was found in the OVA treated animals compared to the PBS control animals as would be expected, though this was not statistically significant.

7.3 Discussion

7.3.1 *Ex vivo* analysis

Ex vivo analysis was established to determine the scale of effect, if any, the delivery of exogenous BMP4 ligand would have on the murine lung. In order to ensure that the delivery process, the model itself or the presence of extra protein irregardless of type or structure was not responsible for the activation of the target BMP pathway PBS and EGF were delivered as a vehicle and protein control respectively alongside the BMP4 ligand. The analysis of the lungs by immunofluorescence revealed pathway activation as a result of BMP4 delivery as seen by the phosphorylation of pSmad1/5/8. This result validated the progression of the delivery process into an aerosol delivery to an *in vivo* model and demonstrates the potential for *ex vivo* analysis as an intermediate step for the progression from *in vitro* to *in vivo* assessment of therapeutics.

7.3.2 *In vivo* analysis

Short-term *in vivo* delivery of aerosolised proteins to C3H mice.

The short time frame for analysis allowed a view of the early onset reaction *in vivo* to the delivery of aerosolised therapeutics. Plethysmography data obtained from the test subjects showed that BMP4 delivery provided a unique profile in comparison to the treatment controls, most notably in regard to the Av, Te, PIF, Rt and EEP. Taken together these results showed that the aerosol delivery of BMP4 induced a negative effect in the lungs of healthy mice when examined 4hr post delivery. As expected excess BMP4 ligand in a healthy lung was detrimental to the performance of the lung, and, extrapolated, bad for the overall health of the animal. Before and after analysis of lung function showed that BMP4 treated animals were the only subject group to suffer from decreased lung volume as a result of the treatment administered. rtPCR analysis of whole lung RNA showed that BMP4 treatment resulted in an increase in BMPR-II mRNA. This correlates with data obtained by others (Section 1.2.4) showing that delivery of BMP4 ligand could induce the increased expression of BMPR-II in the lung. This offers a potential treatment for PAH where loss of functional BMPR-II expression has detrimental effects on the lungs. An observed increase in CC10 expression correlates with an increase in activity by Clara cells as a result of the BMP4 treatment.

In contrast both HamsF12 and EGF treated animals both trended in the opposite direction to BMP4 indicating that the results were ligand specific and not related to either the delivery process or a non specific reaction to the presence of protein in the

lung. While this rtPCR data is on its own inconclusive (n=1) the trends relay the expected effects and support the further analysis of the effects of BMP4 delivery *in vivo* over a longer timeframe. Analysis of the lungs by immunofluorescence revealed that CC10 expression and BMPR-II expression was lower in BMP4 treated animals. This is a mirror of the observed results in rtPCR data. However in conjunction with that data it would appear to suggest that 4hr post exposure to BMP4 ligand there is a temporary decrease in the level of available CC10 and BMPR-II. This is combined with a major increase in the level of activity of the BMP pathway as determined by immunofluorescence detection of pSmad1/5/8 which is directly attributable to the delivery of the exogenous BMP4. There for the decrease in available BMPR-II for binding could be due to the fact that much of the available BMPR-II molecules were already bound by endogenous BMP ligands and CC10 protein may have been depleted and the increase in mRNA levels would support this.

H&E analysis determined that no major structural insult resulted from either the aerosol delivery process or the delivery of the BMP4 molecule. BAL analysis also determined that BMP4 treatment resulted in the greatest presence of protein in the BAL, again showing a physiologically relevant difference resulting from specific ligand inhalation.

This study determined that the inhalation of BMP4 could activate the BMP pathway *in vivo* in the mouse lung and at the given concentration was sufficient to induce effect without stimulating a non specific inflammatory response. It also validated the delivery process, demonstrating that the nebulisation and delivery of a naked protein could be successfully carried out to mice *in vivo*.

7.3.3   3 Day assessment of *in vivo* delivery of aerosolised proteins to C3H mice.

Building on the observations from the short time course experiment it was decided to determine how the delivery of a single dose of BMP4 ligand at a single concentration may effect the lungs of healthy mice at t=24hr, t=48hr and t=72hr post delivery. Plethysmography analysis of the animals determined no significant differences across control and treated animals as a result of the different treatments. This could be due to the fact that the differences observed in the short time course experiments may have subsided by the time analysis began. However BMP4 treated animals showed some distinct, if not statistically significant, profiles with regard to lung function analysis by plethysmography. Noticeably they displayed a decreased lung volume capacity at t=24hr compared to t=0hr measurements. BMP4 treated animals also displayed

increasing PIF after treatment compared to the decrease observed in EGF and PBS treated animals. Notably PEF of all BMP4 animals was below that of the pre-treatment recordings at all timepoints and EF50 also established a distinct profile resulting from BMP4 treatment. The individual components of the plethysmography data taken together shows that aerosolised delivery of BMP4 has a distinct physiological effect on the respiratory function of healthy animals that does not result from the delivery process alone-as attested by the delivery of PBS- orby the presence of any protein in the aerosol as determined by the delivery of the EGF control. Bodyweight and BAL analysis of the treated animals did not reveal much distinct patterning resulting from the delivery of the different aerosol combinations, though in the BAL analysis a slight steady increase in the cell number detected in the BAL was observed over the 3 days post treatment whereas the BAL of BMP4 animals at t=48hr and t=72hr contained noticeably less cells compared to the other treatment groups. This shows again that the delivered protein was initiating a distinct cellular effect in the lungs providing a treatment specific result. H&E analysis confirmed that in healthy lungs the treatment with different aerosols at the concentrations used had no effect on the structure of the lungs and no inflammation or destruction of the airways was evident as a result of the treatment. These results showed that in healthy mice BMP4 delivery at the physiologically relevant delivery concentrations used had no major inflammatory or negative effect on lung function or structure. However it did have a distinct effect, though not statistically significant, in regards to both lung function and BAL fluid cell content. In a healthy model where tight junctions and lung clearance mechanisms are intact with normal functional BMP signalling occurring, the effect of a once off physiologically relevant dose of BMP4 would not have been expected to result in a different outcome. It does however validate the progression of analysis into a diseased lung where tight junctions and clearance mechanisms are less effective and where deregulated BMP signalling is expected to be occurring.

7.3.4 Establishment of an OVA model of disease and a 5 Day assessment of *in vivo* delivery of aerosolised proteins to an OVA induced model of asthma in BALB/c mice.

7.3.4.1 Establishment of OVA induced model of Asthma in BALB/c mice.

Immunofluorescence evaluation of the OVA lung showed BMP pathway activation as seen by the greatly increased activity of the phosphorylated receptor Smads 1, 5 and

8. This indicates that the BMP pathway is potentially contributing to the inflammatory damage and remodelling characteristic of allergic asthma. As such it provides an ideal platform model for the evaluation of potential therapeutics selected to interfere with this pathway via direct delivery of proteins to the affected cells via aerosolisation. Immunofluorescence analysis in combination with other markers of inflammation and damage should then enable effective determination of the success of potential therapeutics in limiting either the effects of, or activation of, this pathway.

7.3.4.2 5 Day assessment of *in vivo* delivery of aerosolised proteins to an OVA induced model of asthma in BALB/c mice.

In this study the effect of BMP4 was analysed in an inflammation based model of lung disease in mice-OVA induced Asthma. The effect of BMP4 and the other BMP related antibodies were assessed in terms of lung function, pathway responses, bodyweight and BAL analysis and by Western Blot analysis of whole lung protein in the exposed animals. PBS was delivered as a delivery control, BMP4 as an active signalling ligand, α-BMP4 antibody as was delivered to determine if it may decrease the effects occurring in the model by binding to endogenous BMP4 present in the lungs and α-BMPR-II was delivered with the expectation that it may bind to any expressed BMPR-II molecules that were available, preventing or diminishing the capacity of endogenous BMP signalling to promote further pathway activation in the damage model.

Plethysmography analysis showed that different treatments did result in statistically significant different lung function profiles with regard to Frequency, Expiration Time, and Relaxation Time. However the last treatment with OVA occurred 24 hours before the exposure of the animal model to any treatment. Therefore it should be noted that where an improvement in lung function is observed across all groups the level of improvement, particularly on Day1, may be a very important indicator as animals lung function may be recovering from the last exposure to OVA anyhow. Therefore the degree of recovery is important.

Of note especially is the decreased total lung volume in animals treated with BMP4 ligand on Day1 post treatment, where it showed that increased BMP4 signalling exacerbated the damage seen in the lungs, whereas α-BMP4 and notably α-BMPR-II antibodies showed a profile more in line with that seen in the PBS control animals. Most notably, over all the lung function measurements analysed is the fact that, with faint exception α-BMP4 and the control PBS treated animals shared the best lung

function profiles. Interestingly, BMP4 and α-BMPR-II, one activating the pathway and one possibly inhibiting its activation, show similar distinct responses in a number of areas of lung function such as Te, PEF, Rt, f and EIP. This could show that BMP4 treatment stimulates the increased inflammatory response occurring as a result of OVA treatment. α-BMPR-II effects may be due to the fact that non specific blocking of the BMP pathway is resulting in actuation of non canonical signalling pathways that are eliciting a similar response to circulating ligand or that pathway in activation is causing a response in other pathways to damage occurring in the OVA lungs. It may also demonstrate that inhibition of the pathway prevents negative feedback mechanisms from inhibiting the effects of endogenous BMP4 involvement.

Immunofluorescence analysis of lung sections from treated animals was analysed at the relevant timepoints for PCNA, pSmad1/5/8 and Smad4. With relation to BMP4 treatment it is of note that most timepoints and analysis determined BMP4 to have induced an effect distinct from that observed with the other treatments. α-BMP4 treatment generally resulted in slightly higher or lower levels of expression compared to BMP4. This may be due to two main reasons; the first is that the α-BMP4 antibody is binding a small amount of the endogenous protein before becoming saturated and results in a similar response but to a different level of severity. The second, alternative reason is that the α-BMP4 antibody is binding a significant amount of the endogenous BMP4 upon delivery, resulting in activation of a feedback mechanism stimulating further secretion of the ligand which would again result in the slightly different profile of the immunofluorescence targets analysed at the different timepoints. Sequential exposure to the α-BMP4 antibody at different doses and at multiple timepoints could help further elucidate the response observed.

The results from the treatment with α-BMPR-II were also noteworthy, resulting in much less BMP pathway related activation along with less of a response from PCNA compared to all other treatment groups. This was especially notable in comparison to lungs in receipt of BMP4 aerosol where the greatest observable differences occurred at Day3 and Day5. Overall the data suggests that delivery of α-BMPR-II antibody successfully binds the receptor *in vivo* and can reduce the effects of BMP signalling in an inflammation model of disease. However two highly important timepoints required for full analysis, PBS treated animals on Day5 and α-BMPR-II antibody treated animals on Day1, were non determinable and would need to be re examined in more detail.

BAL and bodyweight analysis of the animals undergoing the various treatments failed to show any marked differences between the treatment groups. Whole lung protein

analysis however did shed further light on the study. With regard to pSmad1/5/8 expression levels in the lung, total protein levels in the BMP4 treatment group were the highest detected showing that in an OVA induced model of inflammation in the lung, exogenous BMP4 will further stimulate the pSmad1/5/8 response. Of regard also is the fact that in relation to the quantity of both pSmad1/5/8 and Smad4, α-BMPR-II antibody treated animals expressed less than all other treatment groups, including that of the PBS control group. This shows that α-BMPR-II antibody delivery may curtail the Smad response in an inflammation damaged lung.

7.4 Conclusion.

The last treatment with OVA occurred 24 hours before exposure to any treatment. Therefore it should be noted that where an improvement in lung function is observed across all groups the level of improvement, particularly on Day1, may be a very important indicator as animals lung function may be recovering from the last exposure to OVA anyhow. Therefore the degree of recovery is important. In comparing the OVA only with no Treatment on Day 5 to the 2 available timepoint comparisons, BMP4 and α-BMPR-II treated animals it can be seen that BMP4 treatment appeared to correlate closely with the OVA animal whereas α-BMPR-II exhibited less pathway activity. This could mean that BMP4 activity kept the level of activity of the pathway activated, whereas α-BMPR-II decreased the level of activity. Given that there was an effect observed on the level of activity of the protein pathways as determined by immunofluorescence and by the analysis provided through plethysmography and in order to gain a better understanding of the effect of the aerosolised protein treatments a number of different experimental additions would be recommended for inclusion on the results gained from this experiment. The timepoints would be shortened to a t=4hr, t=24hr and t=48hr and t=72hr to get a better picture of the more immediate response.

 Also a multiple dosing regime of the therapeutics would be introduced, both throughout OVA administration to determine if the onset of damage was lessened and also after OVA administration to see if the effects were reversible. In addition the strength of the dosages would also be modified to determine if a dosage threshold needs to be crossed in order for a successful reversion to a healthy phenotype. Methacholine challenge would also be introduced into future studies to help obtain a more complete picture of the level of effect of the potential therapeutics on the level of damage and recovery repair occurring in different treatment groups across different timepoints.

We showed through progressive modelling that the BMP pathway is capable of being targeted for activation through aerosol delivery of recombinant human BMP4 protein. It was shown to be antagonistic to the recovery of the lung in the dosages applied under both normal and inflamed conditions. That it is effective in stimulating an effect on the pathway may be of benefit in other models of lung disease such as PAH where it may help increase the levels of functional BMPR-II expression or in diseases such as emphysema where the pathway was shown to be quiescent in mouse models and where BMP pathway stimulation may encourage proliferation of cells and regrowth of

damaged tissue and cells. Delivery of α-BMPR-II antibody was also shown, in a model of OVA induced lung inflammation, to be of possible therapeutic benefit. However in combination with studies in healthy animals it is of note that general inhibition of the pathway by blocking the BMPR-II functional epitope may have unforseen consequences related to other signalling cascades and would need to be more closely examined in any future work.

The entire process related to the delivery of the various treatments to the animals *in vivo* also showed the capabilities of the Aeroneb Pro system in conjunction with the novel chamber developed by Buxco for the delivery of naked protein *in vivo* that retained their functionality and activity, and their capability to induce specific reactions in target pathways.

8 Conclusions & future directions

Our studies here have demonstrated the BMP pathway is activated in an *in vivo* primate model of allergic asthma. Further to this we were able to show in both human and primate ALI studies involving primary airway cells that BMP4 ligand can induce pathology in cultured cells. In order to develop a system for more detailed examination of the involvement of the BMP pathway in disease pathology and to determine a method for modulation of the effects, it was necessary to establish a working lab model in mice that would facilitate such work. This led to the establishment of an OVA induced model of lung inflammation which showed BMP pathway involvement, and also led to the confirmation of the lack of BMP pathway activity in elastase induced emphysematous lung.

Once pathway activation had been confirmed in the murine model, the next progression was to establish a means of evaluating the role of BMP4 in the pathology and to develop a means for targeted delivery of therapeutics that may prevent pathology from progressing and potentially restore a healthy lung phenotype in the damage model. A number of different mechanisms for achieving therapeutic effect were analysed. DNA therapies based on particle bombardment were determined to have an *in vitro* applicability in the delivery of plasmid encoding DNA to cells in culture, but device limitations precluded the use of the method *in vivo*. However this work led to the progression of a separate study in the lab which has resulted in the development of direct delivery device suitable for *in vivo* applications capable of delivering DNA and protein based therapeutics directly to specific regions of the lung. For the study here, aerosol delivery was determined to be the best mechanism for the delivery of potential therapeutics to the lung. To this end a novel chamber device was fully characterised and a new model restraint was developed in order to improve delivery of any potential therapeutics to mouse models. Different therapies based around siRNA, DNA and protein were then examined for robustness and suitability. While all were determined to be suitable for aerosolisation, protein based therapeutics offered the most robust potentially most clinically relevant means of developing a therapeutic for interfering with the BMP pathways activation and for being measurable for effect. The potential was first examined using aerosolised BMP4 ligand *in vitro* on cell cultures where it was shown to stimulate pathway activation, before progression to *ex vivo* healthy lungs, and then *in vivo* to healthy animals, where aerosolised BMP4 was shown to induce a ligand specific effect in the lungs. Building on this it was decided to determine what effect exogenous BMP4 would have on the established OVA damage model that had already shown BMP pathway involvement in its pathology. Because we had shown not only ligand but functional antibodies to

retain functionality after nebulisation, it was decided to target the damage model not only with ligand but with antibodies against various BMP pathway components including endogenous BMP4 and against BMPR-II. It was shown that all the delivered proteins had specific effects on the measurement of lung functionality as well as different measurements of disease progression, showing aerosol delivery of BMP pathway targeting drugs to be a potentially viable mechanism for interfering with and regulating BMP pathway involvement in disease.

Future experimentation should include the multiple delivery of different dosage concentrations of BMP pathway related proteins and antibodies to various models of lung disease, not only in disease models showing pathway involvement such as OVA induced asthma, but including models such as elastase induced emphysema to see if pathway activation may promote a healing phenotype. Further analysis of downstream affects and of the mRNA profiles of specific cell types such as Clara cells that are subject to these treatments would be of great benefit to the progression of the understanding of the involvement and effect of the various treatments in the different models of disease. ALI interface studies using cells derived from genetically derived models of lung disease would also allow screening for a fundamental understanding of the pathways involvement in a wide variety of different diseases.

Another potentially interesting future focus would be for the use of a nebuliser capable for the aerosolisation of small cells. This could allow for the delivery of genetically modified cells to damaged lungs that are programmed to release certain cytokines or receptors to encourage regeneration and healthy restoration of the damaged lung.

Creating a Translational Framework for Drug Development and Delivery

6	GMP Therapeutic Production Facility (REMEDI)	→	Beaumont Hospital Clinical Research Facility- Dr. Costello
5	Pre-clinical Studies	Establishment of a Pre-clinical studies facility	Medical Device Development
4	Proof of Principle	Therapeutic Molecule Delivery Characterisation	
3	Target Validation	*In vivo* studies/ ALI work/ Primate research	
2	Key Platform Technologies	Disease models/ Culture models/ Chamber and restraint testing and development/ Nebulisation/ Particle Bombardment	
1	Basic Research	Differentiation Pathways- *in vitro* analysis in cell lines and primary cultures	

Figure 8.1 Thesis Contribution

In total, this thesis provided a measurable contribution towards the building of a dedicated approach to the identification of strategies to target the BMP signalling pathway in lung disease, all the way through from basic research in cell lines up to and including the identification of partners for both medical device development and for GMP certified therapeutic production. Key targets and potential treatment areas were identified in specific diseases and potential targets other airway diseases identified as being potentially successful targets for follow on work.

8.1 Publications

Gilbert, J. L., J. Purcell, et al. (2008). "Comparative evaluation of viral, nonviral and physical methods of gene delivery to normal and transformed lung epithelial cells." Anticancer Drugs **19**(8): 783-788.

Few studies have directly compared the efficiencies of gene delivery methods that target normal lung cells versus lung tumor cells. We report the first study directly comparing the efficiency and toxicity of viral [adeno-associated virus (AAV2, 5, 6) and lentivirus], nonviral (Effectene, SuperFect and Lipofectamine 2000) and physical [particle-mediated gene transfer (PMGT)] methods of gene delivery in normal mouse lung cells and in mouse adenocarcinoma cells. Lentivirus pseudotyped with the vesicular stomatitis virus glycoprotein was the most efficient gene transfer method for normal mouse airway epithelial cells [25.95 (+/-3.57) %] whereas AAV6 was most efficient for MLE-12 adenocarcinoma cells [68.2 (+/-3.2) %]. PMGT was more efficient in normal mouse airway epithelial cells than AAV5, Lipofectamine 2000 and SuperFect. AAV5 displayed the lowest transfection efficiency at less than 10% in both cell types. PMGT was the only method that resulted in significant toxicity. In summary, for all of the gene delivery methods examined here, lung tumor cells were transfected more easily than normal lung cells. Lipofectamine 2000 is potentially highly selective for lung tumor cells whereas AAV6 and lentivirus vesicular stomatitis virus glycoprotein may be useful for gene delivery strategies that require targeting of both normal and tumor cells.

9 Bibliography

Adi, S., Adi, H., Tang, P., Traini, D., Chan, H.-k. and Young, P. M. (2008) 'Microparticle corrugation, adhesion and inhalation aerosol efficiency', *European Journal of Pharmaceutical Sciences* 35(1-2): 12-18.

Aneja, M. K., Geiger, J. P., Himmel, A. and Rudolph, C. (2009) 'Targeted gene delivery to the lung', *Expert Opin Drug Deliv* 6(6): 567-83.

Avdalovic, M. V., Putney, L. F., Schelegle, E. S., Miller, L., Usachenko, J. L., Tyler, N. K., Plopper, C. G., Gershwin, L. J. and Hyde, D. M. (2006) 'Vascular remodeling is airway generation-specific in a primate model of chronic asthma', *Am J Respir Crit Care Med* 174(10): 1069-76.

Balemans, W. and Van Hul, W. (2002) 'Extracellular regulation of BMP signaling in vertebrates: A cocktail of modulators', *Developmental Biology* 250(2): 231-250.

Bates, J., Irvin, C., Brusasco, V., Drazen, J., Fredberg, J., Loring, S., Eidelman, D., Ludwig, M., Macklem, P., Martin, J. et al. (2004) 'The use and misuse of Penh in animal models of lung disease', *Am J Respir Cell Mol Biol* 31(3): 373-4.

Beck-Broichsitter, M., Gauss, J., Packhaeuser, C. B., Lahnstein, K., Schmehl, T., Seeger, W., Kissel, T. and Gessler, T. (2009) 'Pulmonary drug delivery with aerosolizable nanoparticles in an ex vivo lung model', *Int J Pharm* 367(1-2): 169-78.

Benezra, R., Davis, R. L., Lockshon, D., Turner, D. L. and Weintraub, H. (1990) 'The protein Id: a negative regulator of helix-loop-helix DNA binding proteins', *Cell* 61(1): 49-59.

Beppu, H., Ichinose, F., Kawai, N., Jones, R. C., Yu, P. B., Zapol, W. M., Miyazono, K., Li, E. and Bloch, K. D. (2004) 'BMPR-II heterozygous mice have mild pulmonary hypertension and an impaired pulmonary vascular remodeling response to prolonged hypoxia', *Am J Physiol Lung Cell Mol Physiol* 287(6): L1241-7.

Bitonti, A. J., Dumont, J. A., Low, S. C., Peters, R. T., Kropp, K. E., Palombella, V. J., Stattel, J. M., Lu, Y., Tan, C. A., Song, J. J. et al. (2004) 'Pulmonary delivery of an erythropoietin Fc fusion protein in non-human primates through an immunoglobulin transport pathway', *Proc Natl Acad Sci U S A* 101(26): 9763-8.

Bivas-Benita, M., Ottenhoff, T. H., Junginger, H. E. and Borchard, G. (2005) 'Pulmonary DNA vaccination: concepts, possibilities and perspectives', *J Control Release* 107(1): 1-29.

Bloom, B., Cohen, R. A. and Freeman, G. (2009) 'Summary health statistics for U.S. children: National Health Interview Survey, 2007', *Vital Health Stat 10*(239): 1-80.

Boers, J. E., Ambergen, A. W. and Thunnissen, F. B. (1999) 'Number and proliferation of clara cells in normal human airway epithelium', *Am J Respir Crit Care Med* 159(5 Pt 1): 1585-91.

Braasch, D. A., Jensen, S., Liu, Y., Kaur, K., Arar, K., White, M. A. and Corey, D. R. (2003) 'RNA interference in mammalian cells by chemically-modified RNA', *Biochemistry* 42(26): 7967-75.

Brandenberger, C., Rothen-Rutishauser, B., Muhlfeld, C., Schmid, O., Ferron, G. A., Maier, K. L., Gehr, P. and Lenz, A. G. (2010) 'Effects and uptake of gold nanoparticles deposited at the air-liquid interface of a human epithelial airway model', *Toxicol Appl Pharmacol* 242(1): 56-65.

Brodie, T. and Adalat, S. (2006) 'Unilateral fixed dilated pupil in a well child', *Arch Dis Child* 91(12): 961.

Brown, J., Mellis, C. M. and Wood, R. E. (1985) 'Edetate sodium aerosol in Pseudomonas lung infection in cystic fibrosis', *Am J Dis Child* 139(8): 836-9.

Buckley, S., Shi, W., Driscoll, B., Ferrario, A., Anderson, K. and Warburton, D. (2004) 'BMP4 signaling induces senescence and modulates the oncogenic phenotype of A549 lung adenocarcinoma cells', *Am J Physiol Lung Cell Mol Physiol* 286(1): L81-6.

Buxco (2005) 'BioSystem XA for Windows User Manual Analyser Reference', *Buxco Biosystem XA User manual*.

Campuzano, S. (2001) 'Emc, a negative HLH regulator with multiple functions in Drosophila development', *Oncogene* 20(58): 8299-307.

Chatburn, R. L. and McPeck, M. (2007) 'A new system for understanding nebulizer performance', *Respir Care* 52(8): 1037-50.

Chrystyn, H. (2007) 'The Diskus: a review of its position among dry powder inhaler devices', *Int J Clin Pract* 61(6): 1022-36.

Chu, Q., St George, J. A., Lukason, M., Cheng, S. H., Scheule, R. K. and Eastman, S. J. (2001) 'EGTA enhancement of adenovirus-mediated gene transfer to mouse tracheal epithelium in vivo', *Hum Gene Ther* 12(5): 455-67.

Chu, Q., Tousignant, J. D., Fang, S., Jiang, C., Chen, L. H., Cheng, S. H., Scheule, R. K. and Eastman, S. J. (1999) 'Binding and uptake of cationic lipid:pDNA complexes by polarized airway epithelial cells', *Hum Gene Ther* 10(1): 25-36.

Clark, A. R. (1995) 'The Use of Laser Diffraction for the Evaluation of the Aerosol Clouds Generated by Medical Nebulizers', *International Journal of Pharmaceutics* 115(1): 69-78.

Coles, S. J., Judge, J. and Reid, L. (1982) 'Differential-Effects of Calcium-Ions on Glycoconjugate Secretion by Canine Tracheal Explants', *Chest* 81(5): S34-S36.

Coppe, J. P., Smith, A. P. and Desprez, P. Y. (2003) 'Id proteins in epithelial cells', *Exp Cell Res* 285(1): 131-45.

Cowley, E. A., Govindaraju, K., Guilbault, C., Radzioch, D. and Eidelman, D. H. (2000) 'Airway surface liquid composition in mice', *Am J Physiol Lung Cell Mol Physiol* 278(6): L1213-20.

Coyne, C. B., Kelly, M. M., Boucher, R. C. and Johnson, L. G. (2000) 'Enhanced epithelial gene transfer by modulation of tight junctions with sodium caprate', *Am J Respir Cell Mol Biol* 23(5): 602-9.

Crapo, J. D., Barry, B. E., Gehr, P., Bachofen, M. and Weibel, E. R. (1982) 'Cell Number and Cell Characteristics of the Normal Human-Lung', *American Review of Respiratory Disease* 126(2): 332-337.

Cryan, S. A. (2005) 'Carrier-based strategies for targeting protein and peptide drugs to the lungs', *AAPS J* 7(1): E20-41.

Danesh, S. M., Villasenor, A., Chong, D., Soukup, C. and Cleaver, O. (2009) 'BMP and BMP receptor expression during murine organogenesis', *Gene Expr Patterns* 9(5): 255-65.

Davies, R. J. and Morrell, N. W. (2008) 'Molecular mechanisms of pulmonary arterial hypertension: role of mutations in the bone morphogenetic protein type II receptor', *Chest* 134(6): 1271-7.

de Boer, A. H., Gjaltema, D., Hagedoorn, P. and Frijlink, H. W. (2002) 'Characterization of inhalation aerosols: a critical evaluation of cascade impactor analysis and laser diffraction technique', *Int J Pharm* 249(1-2): 219-31.

de Vries, T. W., Rottier, B. L., Gjaltema, D., Hagedoorn, P., Frijlink, H. W. and de Boer, A. H. (2009) 'Comparative in vitro evaluation of four corticosteroid metered dose inhalers: Consistency of delivered dose and particle size distribution', *Respir Med* 103(8): 1167-73.

Deed, R. W., Armitage, S. and Norton, J. D. (1996) 'Nuclear localization and regulation of Id protein through an E protein-mediated chaperone mechanism', *J Biol Chem* 271(39): 23603-6.

Denker, B. M. and Nigam, S. K. (1998) 'Molecular structure and assembly of the tight junction', *Am J Physiol* 274(1 Pt 2): F1-9.

Derynck, R. and Zhang, Y. E. (2003) 'Smad-dependent and Smad-independent pathways in TGF-beta family signalling', *Nature* 425(6958): 577-84.

Di, K., Wong, Y. C. and Wang, X. (2007) 'Id-1 promotes TGF-beta1-induced cell motility through HSP27 activation and disassembly of adherens junction in prostate epithelial cells', *Exp Cell Res* 313(19): 3983-99.

Eblaghie, M. C., Reedy, M., Oliver, T., Mishina, Y. and Hogan, B. L. (2006) 'Evidence that autocrine signaling through Bmpr1a regulates the proliferation, survival and morphogenetic behavior of distal lung epithelial cells', *Dev Biol* 291(1): 67-82.

Eimon, P. M. and Harland, R. M. (1999) 'In Xenopus embryos, BMP heterodimers are not required for mesoderm induction, but BMP activity is necessary for dorsal/ventral patterning', *Dev Biol* 216(1): 29-40.

Elhissi, A. M., Faizi, M., Naji, W. F., Gill, H. S. and Taylor, K. M. (2007) 'Physical stability and aerosol properties of liposomes delivered using an air-jet nebulizer and a novel micropump device with large mesh apertures', *Int J Pharm* 334(1-2): 62-70.

Epstein, M. M. (2006) 'Are mouse models of allergic asthma useful for testing novel therapeutics?', *Exp Toxicol Pathol* 57 Suppl 2: 41-4.

Fanucchi, M. V., Plopper, C. G., Evans, M. J., Hyde, D. M., Van Winkle, L. S., Gershwin, L. J. and Schelegle, E. S. (2006) 'Cyclic exposure to ozone alters distal airway development in infant rhesus monkeys', *Am J Physiol Lung Cell Mol Physiol* 291(4): L644-50.

Farrell, P. M. (2008) 'The prevalence of cystic fibrosis in the European Union', *J Cyst Fibros* 7(5): 450-3.

Fong, S., Debs, R. J. and Desprez, P. Y. (2004) 'Id genes and proteins as promising targets in cancer therapy', *Trends Mol Med* 10(8): 387-92.

Fujita, M., Ye, Q., Ouchi, H., Nakashima, N., Hamada, N., Hagimoto, N., Kuwano, K., Mason, R. J. and Nakanishi, Y. (2004) 'Retinoic acid fails to reverse emphysema in adult mouse models', *Thorax* 59(3): 224-30.

Geller, D. E. (2005) 'Comparing clinical features of the nebulizer, metered-dose inhaler, and dry powder inhaler', *Respir Care* 50(10): 1313-21; discussion 1321-2.

Ghazanfari, T., Elhissi, A. M., Ding, Z. and Taylor, K. M. (2007) 'The influence of fluid physicochemical properties on vibrating-mesh nebulization', *Int J Pharm* 339(1-2): 103-11.

Ghosh-Choudhury, N., Woodruff, K., Qi, W., Celeste, A., Abboud, S. L. and Ghosh Choudhury, G. (2000) 'Bone morphogenetic protein-2 blocks MDA MB 231 human breast cancer cell proliferation by inhibiting cyclin-dependent kinase-mediated retinoblastoma protein phosphorylation', *Biochem Biophys Res Commun* 272(3): 705-11.

Gibbs, R. A. Rogers, J. Katze, M. G. Bumgarner, R. Weinstock, G. M. Mardis, E. R. Remington, K. A. Strausberg, R. L. Venter, J. C. Wilson, R. K. et al. (2007) 'Evolutionary and biomedical insights from the rhesus macaque genome', *Science* 316(5822): 222-34.

Gilbert, J. L., Purcell, J., Strappe, P., McCabe, M., O'Brien, T. and O'Dea, S. (2008) 'Comparative evaluation of viral, nonviral and physical methods of gene delivery to normal and transformed lung epithelial cells', *Anticancer Drugs* 19(8): 783-8.

Gordon, K. J. and Blobe, G. C. (2008) 'Role of transforming growth factor-beta superfamily signaling pathways in human disease', *Biochim Biophys Acta* 1782(4): 197-228.

Hagio, T. (1998) 'Optimizing the particle bombardment method for efficient genetic transformation', *Jarq-Japan Agricultural Research Quarterly* 32(4): 239-247.

Hantos, Z. and Brusasco, V. (2002) 'Assessment of respiratory mechanics in small animals: the simpler the better?', *J Appl Physiol* 93(4): 1196-7.

Harkema, J. R., Carey, S. A. and Wagner, J. G. (2006) 'The nose revisited: A brief review of the comparative structure, function, and toxicologic pathology of the nasal epithelium', *Toxicologic Pathology* 34(3): 252-269.

Hassel, S., Eichner, A., Yakymovych, M., Hellman, U., Knaus, P. and Souchelnytskyi, S. (2004) 'Proteins associated with type II bone morphogenetic protein receptor (BMPR-II) and identified by two-dimensional gel electrophoresis and mass spectrometry', *Proteomics* 4(5): 1346-58.

Heijerman, H., Westerman, E., Conway, S., Touw, D. and Doring, G. (2009) 'Inhaled medication and inhalation devices for lung disease in patients with cystic fibrosis: A European consensus', *J Cyst Fibros* 8(5): 295-315.

Heinemann, L. (2008) 'The failure of exubera: are we beating a dead horse?', *J Diabetes Sci Technol* 2(3): 518-29.

Heinemann, L. (2010) 'New ways of insulin delivery', *Int J Clin Pract Suppl*(166): 29-40.

Heiser, W. C. (2004) 'Delivery of DNA to cells in culture using particle bombardment', *Methods Mol Biol* 245: 175-84.

Heldin, C. H., Miyazono, K. and ten Dijke, P. (1997) 'TGF-beta signalling from cell membrane to nucleus through SMAD proteins', *Nature* 390(6659): 465-71.

Herpin, A. and Cunningham, C. (2007) 'Cross-talk between the bone morphogenetic protein pathway and other major signaling pathways results in tightly regulated cell-specific outcomes', *FEBS J* 274(12): 2977-85.

Hess, D. R. (2008) 'Aerosol delivery devices in the treatment of asthma', *Respir Care* 53(6): 699-723; discussion 723-5.

Heubner W, D. J. S., Laquer E (1924) 'Über inhalation von insulin. ', *Klin Wochenschr*(51): 2342–2343.

Hillman, K. M. and Twigley, A. (1984) 'Aerosol EDTA to eliminate respiratory-tract pseudomonas', *Lancet* 2(8394): 99.

Hindi, K. M., Ditto, A. J., Panzner, M. J., Medvetz, D. A., Han, D. S., Hovis, C. E., Hilliard, J. K., Taylor, J. B., Yun, Y. H., Cannon, C. L. et al. (2009) 'The antimicrobial efficacy of sustained release silver-carbene complex-loaded L-tyrosine polyphosphate nanoparticles: characterization, in vitro and in vivo studies', *Biomaterials* 30(22): 3771-9.

Hogan, B. L. (1996) 'Bone morphogenetic proteins in development', *Curr Opin Genet Dev* 6(4): 432-8.

Hollnagel, A., Oehlmann, V., Heymer, J., Ruther, U. and Nordheim, A. (1999) 'Id genes are direct targets of bone morphogenetic protein induction in embryonic stem cells', *J Biol Chem* 274(28): 19838-45.

Houghton, A. M., Mouded, M. and Shapiro, S. D. (2008) 'Common origins of lung cancer and COPD', *Nat Med* 14(10): 1023-4.

Hoymann, H. G. (2007) 'Invasive and noninvasive lung function measurements in rodents', *J Pharmacol Toxicol Methods* 55(1): 16-26.

Hyatt, B. A., Shangguan, X. and Shannon, J. M. (2002) 'BMP4 modulates fibroblast growth factor-mediated induction of proximal and distal lung differentiation in mouse embryonic tracheal epithelium in mesenchyme-free culture', *Dev Dyn* 225(2): 153-65.

J.B. Fink, D. S. a. J. P. (2001) 'Comparison of a nebulizer using a novel aerosol generator with a standard ultrasonic nebulizer designed for use during mechanical ventilation', *American Thoracic Society 97th International Conference San Francisco, CA*.

Jakiela, B., Brockman-Schneider, R., Amineva, S., Lee, W. M. and Gern, J. E. (2008) 'Basal cells of differentiated bronchial epithelium are more susceptible to rhinovirus infection', *Am J Respir Cell Mol Biol* 38(5): 517-23.

Johnson, J. C., Waldrep, J. C., Guo, J. and Dhand, R. (2008) 'Aerosol delivery of recombinant human DNase I: in vitro comparison of a vibrating-mesh nebulizer with a jet nebulizer', *Respir Care* 53(12): 1703-8.

Johnson, L. G., Mewshaw, J. P., Ni, H., Friedmann, T., Boucher, R. C. and Olsen, J. C. (1998) 'Effect of host modification and age on airway epithelial gene transfer mediated by a murine leukemia virus-derived vector', *J Virol* 72(11): 8861-72.

Johnson, L. G., Vanhook, M. K., Coyne, C. B., Haykal-Coates, N. and Gavett, S. H. (2003) 'Safety and efficiency of modulating paracellular permeability to enhance airway epithelial gene transfer in vivo', *Hum Gene Ther* 14(8): 729-47.

Karaulanov, E., Knochel, W. and Niehrs, C. (2004) 'Transcriptional regulation of BMP4 synexpression in transgenic Xenopus', *EMBO J* 23(4): 844-56.

Kariyawasam, H. H., Xanthou, G., Barkans, J., Aizen, M., Kay, A. B. and Robinson, D. S. (2008) 'Basal expression of bone morphogenetic protein receptor is reduced in mild asthma', *Am J Respir Crit Care Med* 177(10): 1074-81.

Katoh, Y. and Katoh, M. (2008) 'Hedgehog signaling, epithelial-to-mesenchymal transition and miRNA (review)', *Int J Mol Med* 22(3): 271-5.

Kendall, M., Mitchell, T. J., Costigan, G., Armitage, M., Lenzo, J. C., Thomas, J. A., von Garnier, C., Zosky, G. R., Turner, D. J., Stumbles, P. A. et al. (2006) 'Downregulation of IgE antibody and allergic responses in the lung by epidermal biolistic microparticle delivery', *J Allergy Clin Immunol* 117(2): 275-82.

Klein, T. M., Wolf, E. D., Wu, R. and Sanford, J. C. (1987) 'High-Velocity Microprojectiles for Delivering Nucleic-Acids into Living Cells', *Nature* 327(6117): 70-73.

Kobinger, G. P., Weiner, D. J., Yu, Q. C. and Wilson, J. M. (2001) 'Filovirus-pseudotyped lentiviral vector can efficiently and stably transduce airway epithelia in vivo', *Nat Biotechnol* 19(3): 225-30.

Koli, K., Myllarniemi, M., Vuorinen, K., Salmenkivi, K., Ryynanen, M. J., Kinnula, V. L. and Keski-Oja, J. (2006) 'Bone morphogenetic protein-4 inhibitor gremlin is overexpressed in idiopathic pulmonary fibrosis', *Am J Pathol* 169(1): 61-71.

Kreda, S. M., Pickles, R. J., Lazarowski, E. R. and Boucher, R. C. (2000) 'G-protein-coupled receptors as targets for gene transfer vectors using natural small-molecule ligands', *Nat Biotechnol* 18(6): 635-40.

Kretzschmar, M. and Massague, J. (1998) 'SMADs: mediators and regulators of TGF-beta signaling', *Curr Opin Genet Dev* 8(1): 103-11.

Kumar, R. K. and Foster, P. S. (2002) 'Modeling allergic asthma in mice: pitfalls and opportunities', *Am J Respir Cell Mol Biol* 27(3): 267-72.

Lambrecht, B. N. and Hammad, H. (2003) 'Taking our breath away: dendritic cells in the pathogenesis of asthma', *Nat Rev Immunol* 3(12): 994-1003.

Langlands, K., Down, G. A. and Kealey, T. (2000) 'Id proteins are dynamically expressed in normal epidermis and dysregulated in squamous cell carcinoma', *Cancer Res* 60(21): 5929-33.

Legssyer, R., Huaux, F., Lebacq, J., Delos, M., Marbaix, E., Lebecque, P., Lison, D., Scholte, B. J., Wallemacq, P. and Leal, T. (2006) 'Azithromycin reduces spontaneous and induced inflammation in DeltaF508 cystic fibrosis mice', *Respir Res* 7: 134.

Lentz, Y. K., Worden, L. R., Anchordoquy, T. J. and Lengsfeld, C. S. (2005) 'Effect of jet nebulization on DNA: identifying the dominant degradation mechanism and mitigation methods', *Journal of Aerosol Science* 36(8): 973-990.

Lenzer, J. (2006) 'Inhaled insulin is approved in Europe and United States', *BMJ* 332(7537): 321.

Li, B. J., Tang, Q., Cheng, D., Qin, C., Xie, F. Y., Wei, Q., Xu, J., Liu, Y., Zheng, B. J., Woodle, M. C. et al. (2005) 'Using siRNA in prophylactic and therapeutic regimens against SARS coronavirus in Rhesus macaque', *Nat Med* 11(9): 944-51.

Lian, W. N., Chang, C. H., Chen, Y. J., Dao, R. L., Luo, Y. C., Chien, J. Y., Hsieh, S. L. and Lin, C. H. (2007) 'Intracellular delivery can be achieved by bombarding cells or tissues with accelerated molecules or bacteria without the need for carrier particles', *Exp Cell Res* 313(1): 53-64.

Liu, J., Shi, W. and Warburton, D. (2000) 'A cysteine residue in the helix-loop-helix domain of Id2 is critical for homodimerization and function', *Biochem Biophys Res Commun* 273(3): 1042-7.

Liu, Y., Martindale, J. L., Gorospe, M. and Holbrook, N. J. (1996) 'Regulation of p21WAF1/CIP1 expression through mitogen-activated protein kinase signaling pathway', *Cancer Res* 56(1): 31-5.

Livak, K. J. and Schmittgen, T. D. (2001) 'Analysis of Relative Gene Expression Data Using Real-Time Quantitative PCR and the 2-[Delta][Delta]CT Method', *Methods* 25(4): 402-408.

Lucey, E. C., Keane, J., Kuang, P. P., Snider, G. L. and Goldstein, R. H. (2002) 'Severity of elastase-induced emphysema is decreased in tumor necrosis factor-alpha and interleukin-1beta receptor-deficient mice', *Lab Invest* 82(1): 79-85.

Luthje, L., Raupach, T., Michels, H., Unsold, B., Hasenfuss, G., Kogler, H. and Andreas, S. (2009) 'Exercise intolerance and systemic manifestations of pulmonary emphysema in a mouse model', *Respir Res* 10: 7.

MacNeish, C. F., Meisner, D., Thibert, R., Kelemen, S., Vadas, E. B. and Coates, A. L. (1997) 'A comparison of pulmonary availability between Ventolin (albuterol) nebules and Ventolin (albuterol) Respirator Solution', *Chest* 111(1): 204-8.

Manoharan, M. (2004) 'RNA interference and chemically modified small interfering RNAs', *Curr Opin Chem Biol* 8(6): 570-9.

Marriott, C., MacRitchie, H. B., Zeng, X. M. and Martin, G. P. (2006) 'Development of a laser diffraction method for the determination of the particle size of aerosolised powder formulations', *Int J Pharm* 326(1-2): 39-49.

Martinez-Palomo, A., Meza, I., Beaty, G. and Cereijido, M. (1980) 'Experimental modulation of occluding junctions in a cultured transporting epithelium', *J Cell Biol* 87(3 Pt 1): 736-45.

Martonen, T. B., Smyth, H. D., Isaacs, K. K. and Burton, R. T. (2005) 'Issues in drug delivery: concepts and practice', *Respir Care* 50(9): 1228-52.

Massague, J. (1998) 'TGF-beta signal transduction', *Annu Rev Biochem* 67: 753-91.

Massari, M. E. and Murre, C. (2000) 'Helix-loop-helix proteins: regulators of transcription in eucaryotic organisms', *Mol Cell Biol* 20(2): 429-40.

Masterson, J. and O'Dea, S. (2007) 'Posttranslational truncation of E-cadherin and significance for tumour progression', *Cells Tissues Organs* 185(1-3): 175-9.

Masterson, J. C., Molloy, E. L., Gilbert, J. L., McCormack, N., Adams, A. and O'Dea, S. (2010) 'Bone morphogenetic protein signalling in airway epithelial cells during regeneration', *Cell Signal*.

McCray, P. B., Jr., Zabner, J., Jia, H. P., Welsh, M. J. and Thorne, P. S. (1999) 'Efficient killing of inhaled bacteria in DeltaF508 mice: role of airway surface liquid composition', *Am J Physiol* 277(1 Pt 1): L183-90.

McKay, K. O. and Hogg, J. C. (2002) 'The contribution of airway structure to early childhood asthma', *Med J Aust* 177 Suppl: S45-7.

Mills, P. R., Davies, R. J. and Devalia, J. L. (1999) 'Airway epithelial cells, cytokines, and pollutants', *Am J Respir Crit Care Med* 160(5 Pt 2): S38-43.

Mitchell, J., Newman, S. and Chan, H. K. (2007) 'In vitro and in vivo aspects of cascade impactor tests and inhaler performance: a review', *AAPS PharmSciTech* 8(4): E110.

Mitchell, J. P. and Nagel, M. W. (2003) 'Cascade impactors for the size characterization of aerosols from medical inhalers: their uses and limitations', *J Aerosol Med* 16(4): 341-77.

Mitzner, W. and Tankersley, C. (2003) 'Interpreting Penh in mice', *J Appl Physiol* 94(2): 828-31; author reply 831-2.

Miyazono, K., Kamiya, Y. and Morikawa, M. (2010) 'Bone morphogenetic protein receptors and signal transduction', *J Biochem* 147(1): 35-51.

Molloy, E. L., Adams, A., Moore, J. B., Masterson, J. C., Madrigal-Estebas, L., Mahon, B. P. and O'Dea, S. (2008) 'BMP4 induces an epithelial-mesenchymal transition-like response in adult airway epithelial cells', *Growth Factors* 26(1): 12-22.

Morrell, N. W. (2006) 'Pulmonary hypertension due to BMPR2 mutation: a new paradigm for tissue remodeling?', *Proc Am Thorac Soc* 3(8): 680-6.

Myles, C., Sorscher, E. and Matalon, S. (2002) 'Enhancement of adenovirus-mediated gene transfer in lungs and epithelial cells by EGTA', *Chest* 121(3 Suppl): 35S.

Nadithe, V., Rahamatalla, M., Finlay, W. H., Mercer, J. R. and Samuel, J. (2003) 'Evaluation of nose-only aerosol inhalation chamber and comparison of experimental results with mathematical simulation of aerosol deposition in mouse lungs', *J Pharm Sci* 92(5): 1066-76.

Nickoloff, B. J., Chaturvedi, V., Bacon, P., Qin, J. Z., Denning, M. F. and Diaz, M. O. (2000) 'Id-1 delays senescence but does not immortalize keratinocytes', *J Biol Chem* 275(36): 27501-4.

Norton, J. D., Deed, R. W., Craggs, G. and Sablitzky, F. (1998) 'Id helix-loop-helix proteins in cell growth and differentiation', *Trends Cell Biol* 8(2): 58-65.

O'Connor, T. (2008) Ireland Needs Healthier Airways and Lungs-the Evidence Irish Thoracic Society.

Ortega, A., Domingo, J. L., Gomez, M. and Corbella, J. (1989) 'Treatment of experimental acute uranium poisoning by chelating agents', *Pharmacol Toxicol* 64(3): 247-51.

Park, C., Lavine, K., Mishina, Y., Deng, C. X., Ornitz, D. M. and Choi, K. (2006) 'Bone morphogenetic protein receptor 1A signaling is dispensable for hematopoietic development but essential for vessel and atrioventricular endocardial cushion formation', *Development* 133(17): 3473-84.

Patton, J. S., Fishburn, C. S. and Weers, J. G. (2004) 'The lungs as a portal of entry for systemic drug delivery', *Proc Am Thorac Soc* 1(4): 338-44.

Pauls, E. and Esté, J. A. (2004) 'RNA interference as a tool for target validation', *Drug Discovery Today: Technologies* 1(2): 135-140.

Phalen, R. F., Oldham, M. J. and Wolff, R. K. (2008) 'The relevance of animal models for aerosol studies', *J Aerosol Med Pulm Drug Deliv* 21(1): 113-24.

Pickles, R. J., McCarty, D., Matsui, H., Hart, P. J., Randell, S. H. and Boucher, R. C. (1998) 'Limited entry of adenovirus vectors into well-differentiated airway epithelium is responsible for inefficient gene transfer', *J Virol* 72(7): 6014-23.

Pilcer, G., Vanderbist, F. and Amighi, K. (2008) 'Correlations between cascade impactor analysis and laser diffraction techniques for the determination of the particle size of aerosolised powder formulations', *Int J Pharm* 358(1-2): 75-81.

Pinkerton, K. E. and Joad, J. P. (2000) 'The mammalian respiratory system and critical windows of exposure for children's health', *Environ Health Perspect* 108 Suppl 3: 457-62.

Plopper, C., St George, J., Cardoso, W., Wu, R., Pinkerton, K. and Buckpitt, A. (1992) 'Development of airway epithelium. Patterns of expression for markers of differentiation', *Chest* 101(3 Suppl): 2S-5S.

Plopper, C. G. and Hyde, D. M. (2008) 'The non-human primate as a model for studying COPD and asthma', *Pulm Pharmacol Ther* 21(5): 755-66.

Ririe, K. M., Rasmussen, R. P. and Wittwer, C. T. (1997) 'Product Differentiation by Analysis of DNA Melting Curves during the Polymerase Chain Reaction', *Analytical Biochemistry* 245(2): 154-160.

Rogers, C. S., Abraham, W. M., Brogden, K. A., Engelhardt, J. F., Fisher, J. T., McCray, P. B., Jr., McLennan, G., Meyerholz, D. K., Namati, E., Ostedgaard, L. S. et al. (2008) 'The porcine lung as a potential model for cystic fibrosis', *Am J Physiol Lung Cell Mol Physiol* 295(2): L240-63.

Rosendahl, A., Pardali, E., Speletas, M., Ten Dijke, P., Heldin, C. H. and Sideras, P. (2002) 'Activation of bone morphogenetic protein/Smad signaling in bronchial epithelial cells during airway inflammation', *Am J Respir Cell Mol Biol* 27(2): 160-9.

Rubin, L. J. (1997) 'Primary pulmonary hypertension', *N Engl J Med* 336(2): 111-7.

Ruzinova, M. B. and Benezra, R. (2003) 'Id proteins in development, cell cycle and cancer', *Trends Cell Biol* 13(8): 410-8.

Ryther, R. C., Flynt, A. S., Phillips, J. A., 3rd and Patton, J. G. (2005) 'siRNA therapeutics: big potential from small RNAs', *Gene Ther* 12(1): 5-11.

Sabet, M., Miller, C. E., Nolan, T. G., Senekeo-Effenberger, K., Dudley, M. N. and Griffith, D. C. (2009) 'Efficacy of aerosol MP-376, a levofloxacin inhalation solution, in models of mouse lung infection due to Pseudomonas aeruginosa', *Antimicrob Agents Chemother* 53(9): 3923-8.

Schaefer, B. M., Koch, J., Wirzbach, A. and Kramer, M. D. (2001) 'Expression of the helix-loop-helix protein ID1 in keratinocytes is upregulated by loss of cell-matrix contact', *Exp Cell Res* 266(2): 250-9.

Schelegle, E. S., Gershwin, L. J., Miller, L. A., Fanucchi, M. V., Van Winkle, L. S., Gerriets, J. P., Walby, W. F., Omlor, A. M., Buckpitt, A. R., Tarkington, B. K. et al. (2001) 'Allergic asthma induced in rhesus monkeys by house dust mite (Dermatophagoides farinae)', *Am J Pathol* 158(1): 333-41.

Schelegle, E. S., Miller, L. A., Gershwin, L. J., Fanucchi, M. V., Van Winkle, L. S., Gerriets, J. E., Walby, W. F., Mitchell, V., Tarkington, B. K., Wong, V. J. et al. (2003) 'Repeated episodes of ozone inhalation amplifies the effects of allergen sensitization and inhalation on airway immune and structural development in Rhesus monkeys', *Toxicol Appl Pharmacol* 191(1): 74-85.

Schell, J. and Van Montagu, M. (1977) 'The Ti-plasmid of Agrobacterium tumefaciens, a natural vector for the introduction of nif genes in plants?', *Basic Life Sci* 9: 159-79.

Schmidt, C. R., Gi, Y. J., Patel, T. A., Coffey, R. J., Beauchamp, R. D. and Pearson, A. S. (2005) 'E-cadherin is regulated by the transcriptional repressor SLUG during Ras-mediated transformation of intestinal epithelial cells', *Surgery* 138(2): 306-12.

Schmittgen, T. D. and Livak, K. J. (2008) 'Analyzing real-time PCR data by the comparative C(T) method', *Nat Protoc* 3(6): 1101-8.

Selam, J. L. (2008) 'Inhaled insulin: promises and concerns', *J Diabetes Sci Technol* 2(2): 311-5.

Shannon, J. M. and Hyatt, B. A. (2004) 'Epithelial-mesenchymal interactions in the developing lung', *Annu Rev Physiol* 66: 625-45.

Shefi, O., Simonnet, C., Baker, M. W., Glass, J. R., Macagno, E. R. and Groisman, A. (2006) 'Microtargeted gene silencing and ectopic expression in live embryos using biolistic delivery with a pneumatic capillary gun', *J Neurosci* 26(23): 6119-23.

Shen, S. C. (2010) 'A new cymbal-shaped high power microactuator for nebulizer application', *Microelectronic Engineering* 87(2): 89-97.

Shi, C., Zhu, Y., Ran, X., Wang, M., Su, Y. and Cheng, T. (2006) 'Therapeutic potential of chitosan and its derivatives in regenerative medicine', *J Surg Res* 133(2): 185-92.

Shi, W., Chen, H., Sun, J., Chen, C., Zhao, J., Wang, Y. L., Anderson, K. D. and Warburton, D. (2004) 'Overexpression of Smurf1 negatively regulates mouse embryonic lung branching morphogenesis by specifically reducing Smad1 and Smad5 proteins', *Am J Physiol Lung Cell Mol Physiol* 286(2): L293-300.

Shi, W., Xu, J. and Warburton, D. (2009) 'Development, repair and fibrosis: what is common and why it matters', *Respirology* 14(5): 656-65.

Siekmeier, R. and Scheuch, G. (2008) 'Inhaled insulin--does it become reality?', *J Physiol Pharmacol* 59 Suppl 6: 81-113.

Sikder, H. A., Devlin, M. K., Dunlap, S., Ryu, B. and Alani, R. M. (2003) 'Id proteins in cell growth and tumorigenesis', *Cancer Cell* 3(6): 525-30.

Snider, G. L., Ciccolella, D. E., Morris, S. M., Stone, P. J. and Lucey, E. C. (1991) 'Putative role of neutrophil elastase in the pathogenesis of emphysema', *Ann N Y Acad Sci* 624: 45-59.

Song, E., Zhu, P., Lee, S. K., Chowdhury, D., Kussman, S., Dykxhoorn, D. M., Feng, Y., Palliser, D., Weiner, D. B., Shankar, P. et al. (2005a) 'Antibody mediated in vivo delivery of small interfering RNAs via cell-surface receptors', *Nat Biotechnol* 23(6): 709-17.

Song, L., Yan, W., Chen, X., Deng, C. X., Wang, Q. and Jiao, K. (2007) 'Myocardial smad4 is essential for cardiogenesis in mouse embryos', *Circ Res* 101(3): 277-85.

Song, Y., Jones, J. E., Beppu, H., Keaney, J. F., Jr., Loscalzo, J. and Zhang, Y. Y. (2005b) 'Increased susceptibility to pulmonary hypertension in heterozygous BMPR2-mutant mice', *Circulation* 112(4): 553-62.

Steinman, R. A., Hoffman, B., Iro, A., Guillouf, C., Liebermann, D. A. and el-Houseini, M. E. (1994) 'Induction of p21 (WAF-1/CIP1) during differentiation', *Oncogene* 9(11): 3389-96.

Stewart, D. J. (2005) 'Bone morphogenetic protein receptor-2 and pulmonary arterial hypertension: unraveling a riddle inside an enigma?', *Circ Res* 96(10): 1033-5.

Su, D., Zhu, S., Han, X., Feng, Y., Huang, H., Ren, G., Pan, L., Zhang, Y., Lu, J. and Huang, B. (2009) 'BMP4-Smad signaling pathway mediates adriamycin-induced premature senescence in lung cancer cells', *J Biol Chem* 284(18): 12153-64.

Tang, J., Gordon, G. M., Nickoloff, B. J. and Foreman, K. E. (2002) 'The helix-loop-helix protein id-1 delays onset of replicative senescence in human endothelial cells', *Lab Invest* 82(8): 1073-9.

Taraseviciene-Stewart, L. and Voelkel, N. F. (2008) 'Molecular pathogenesis of emphysema', *J Clin Invest* 118(2): 394-402.

Teichert-Kuliszewska, K., Kutryk, M. J., Kuliszewski, M. A., Karoubi, G., Courtman, D. W., Zucco, L., Granton, J. and Stewart, D. J. (2006) 'Bone morphogenetic protein receptor-2 signaling promotes pulmonary arterial endothelial cell survival: implications for loss-of-function mutations in the pathogenesis of pulmonary hypertension', *Circ Res* 98(2): 209-17.

ten Dijke, P., Korchynskyi, O., Valdimarsdottir, G. and Goumans, M. J. (2003) 'Controlling cell fate by bone morphogenetic protein receptors', *Mol Cell Endocrinol* 211(1-2): 105-13.

Tsuji, T., Ibaragi, S., Shima, K., Hu, M. G., Katsurano, M., Sasaki, A. and Hu, G. F. (2008) 'Epithelial-mesenchymal transition induced by growth suppressor p12CDK2-AP1 promotes tumor cell local invasion but suppresses distant colony growth', *Cancer Res* 68(24): 10377-86.

Urist, M. R. (1965) 'Bone: formation by autoinduction', *Science* 150(698): 893-9.

Vanoirbeek, J. A., Rinaldi, M., De Vooght, V., Haenen, S., Bobic, S., Gayan-Ramirez, G., Hoet, P. H., Verbeken, E., Decramer, M., Nemery, B. et al. (2010) 'Noninvasive and invasive pulmonary function in mouse models of obstructive and restrictive respiratory diseases', *Am J Respir Cell Mol Biol* 42(1): 96-104.

Virchow, J. C., Crompton, G. K., Dal Negro, R., Pedersen, S., Magnan, A., Seidenberg, J. and Barnes, P. J. (2008) 'Importance of inhaler devices in the management of airway disease', *Respir Med* 102(1): 10-9.

Wagner, D. H., Ramanathan, S., Taylor, M. L., Brown, A. B., Wobker, M. E. S. and Prior, M. W. (2009) 'The thermodynamics of high shear blending', *Powder Technology* 193(2): 195-199.

Walters, R. W., Grunst, T., Bergelson, J. M., Finberg, R. W., Welsh, M. J. and Zabner, J. (1999) 'Basolateral localization of fiber receptors limits adenovirus infection from the apical surface of airway epithelia', *J Biol Chem* 274(15): 10219-26.

Warburton, D. and Bellusci, S. (2004) 'The molecular genetics of lung morphogenesis and injury repair', *Paediatr Respir Rev* 5 Suppl A: S283-7.

Ward, C., Forrest, I. A., Murphy, D. M., Johnson, G. E., Robertson, H., Cawston, T. E., Fisher, A. J., Dark, J. H., Lordan, J. L., Kirby, J. A. et al. (2005) 'Phenotype of airway epithelial cells suggests epithelial to mesenchymal cell transition in clinically stable lung transplant recipients', *Thorax* 60(10): 865-71.

Weaver, M., Dunn, N. R. and Hogan, B. L. (2000) 'Bmp4 and Fgf10 play opposing roles during lung bud morphogenesis', *Development* 127(12): 2695-704.

West, J., Fagan, K., Steudel, W., Fouty, B., Lane, K., Harral, J., Hoedt-Miller, M., Tada, Y., Ozimek, J., Tuder, R. et al. (2004) 'Pulmonary hypertension in transgenic mice expressing a dominant-negative BMPRII gene in smooth muscle', *Circ Res* 94(8): 1109-14.

Williams, R. S., Johnston, S. A., Riedy, M., Devit, M. J., Mcelligott, S. G. and Sanford, J. C. (1991) 'Introduction of Foreign Genes into Tissues of Living Mice by DNA-Coated Microprojectiles', *Proceedings of the National Academy of Sciences of the United States of America* 88(7): 2726-2730.

Wozney, J. M., Rosen, V., Celeste, A. J., Mitsock, L. M., Whitters, M. J., Kriz, R. W., Hewick, R. M. and Wang, E. A. (1988) 'Novel regulators of bone formation: molecular clones and activities', *Science* 242(4885): 1528-34.

Wrana, J. L. and Attisano, L. (2000) 'The Smad pathway', *Cytokine Growth Factor Rev* 11(1-2): 5-13.

Yang, X., Castilla, L. H., Xu, X., Li, C., Gotay, J., Weinstein, M., Liu, P. P. and Deng, C. X. (1999) 'Angiogenesis defects and mesenchymal apoptosis in mice lacking SMAD5', *Development* 126(8): 1571-80.

Yokota, Y. (2001) 'Id and development', *Oncogene* 20(58): 8290-8.

Yu, P. B., Beppu, H., Kawai, N., Li, E. and Bloch, K. D. (2005) 'Bone morphogenetic protein (BMP) type II receptor deletion reveals BMP ligand-specific gain of signaling in pulmonary artery smooth muscle cells', *J Biol Chem* 280(26): 24443-50.

Zelenin, A. V., Alimov, A. A., Titomirov, A. V., Kazansky, A. V., Gorodetsky, S. I. and Kolesnikov, V. A. (1991) 'High-velocity mechanical DNA transfer of the chloramphenicolacetyl transferase gene into rodent liver, kidney and mammary gland cells in organ explants and in vivo', *FEBS Lett* 280(1): 94-6.

Zelenin, A. V., Alimov, A. A., Zelenina, I. A., Semenova, M. L., Rodova, M. A., Chernov, B. K. and Kolesnikov, V. A. (1993) 'Transfer of foreign DNA into the cells of developing mouse embryos by microprojectile bombardment', *FEBS Lett* 315(1): 29-32.

Zelenin, A. V., Titomirov, A. V. and Kolesnikov, V. A. (1989) 'Genetic transformation of mouse cultured cells with the help of high-velocity mechanical DNA injection', *FEBS Lett* 244(1): 65-7.

Zhang, X., Shan, P., Jiang, D., Noble, P. W., Abraham, N. G., Kappas, A. and Lee, P. J. (2004) 'Small interfering RNA targeting heme oxygenase-1 enhances ischemia-reperfusion-induced lung apoptosis', *J Biol Chem* 279(11): 10677-84.

Zhu, N. L., Li, C., Huang, H. H., Sebald, M., Londhe, V. A., Heisterkamp, N., Warburton, D., Bellusci, S. and Minoo, P. (2007) 'TNF-alpha represses transcription of human Bone Morphogenetic Protein-4 in lung epithelial cells', *Gene* 393(1-2): 70-80.

Ziegler, J. and Wachtel, H. (2005) 'Comparison of cascade impaction and laser diffraction for particle size distribution measurements', *J Aerosol Med* 18(3): 311-24.